25th Annual Meeting of the

American Society of Biomechanics

University of California - San Diego
San Diego, California
August 8 - 11, 2001

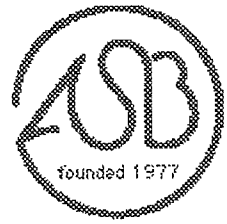

25th Annual Meeting of the

American Society of Biomechanics

University of California - San Diego
San Diego, California
August 8 - 11, 2001

Course Objectives/Statement of Need

- Apply rigorous engineering principles to medicine, biology and biophysics.
- Practice both muscle physiological and molecular biological methods.
- Facilitate strong interactions between scientists from the biological and medical disciplines, engineers and others.
- Foster informed discussion on the mechanics of the widest possible variety of biological systems and organisms.

Target Audience

This course is designed for research scientists, physicians, engineers and others.

UCSD Office of Continuing Medical Education Mission Statement

The University of California, San Diego Health Science's mission is to serve by discovery, education, healing and promoting well being. Our goal is to be a preeminent academic health science community valued locally, nationally, and internationally for excellence and innovation in all missions. (UCSD Health Sciences Vision, 1998)

The mission of the UCSD Office of Continuing Medical Education is to research, develop and provide quality postgraduate medical education that maintains, develops or increases knowledge, skills, and professional performance of physicians and health care providers who serve patients, the public and the profession.

The content of the educational program is determined by rigorous assessment of educational need and includes surveys, program feedback, expert faculty assessment, literature review, medical practice, chart review, and new medical knowledge. Educational goals and objectives are established for each activity. The target audience is program specific and may include physicians and other health care providers locally, regionally, nationally and internationally. Educational formats are based on the course goals, objectives and target audience; they include departmental grand rounds/case conferences, specialized mini-residencies, home-study programs, state of the art postgraduate medical conferences, scientific symposia, review courses, procedure training and workshops, computer based training and tele-education programs. Programs are reviewed for academic excellence by the Associate Dean for Continuing Medical Education's Advisory Committee comprised of physicians from the medical school and community. Programs are evaluated to determine if the objectives are met; if the format/content/relevance are appropriate; on the effectiveness of the faculty; and to provide needs assessment for future planning. UCSD Office of Continuing Medical Education jointly sponsors programs with reputable organizations if they meet the ACCME guidelines.

The CME Office is reviewed by the Vice Chancellor for Health Sciences annually and ongoing assessment is used to identify better policies and procedures for meeting the needs of our constituents.

Faculty Disclosures

Verbal disclosures will be made at the conference.

ACKNOWLEDGEMENTS

We would like to offer very special thanks to the following companies and organizations for their support of this conference. Their financial support makes this conference possible; their products and services add to the educational value of our program.

We encourage you to take this opportunity to meet and share your ideas and experiences with the exhibit representatives.

ADVANCED TISSUE SCIENCES

AMTI

CIR SYSTEMS, INC.
GaitRite Division

NORAXON USA, INC.

PEAK PERFORMANCE TECHNOLOGIES, INC.

QUALISYS, INC.

RUN TECHNOLOGIES

SIMEX USA

TEXSCAN, INC.

WHITAKER FOUNDATION

WHITAKER INSTUTE FOR
BIOMEDICAL ENGINEERING (UCSD)

American Society of Biomechanics 2001
Program Schedule
Thursday, August 09, 2001

American Society of Biomechanics 2001
Program Schedule
Thursday, August 09, 2001

American Society of Biomechanics 2001
Program Schedule
Saturday, August 11 2001

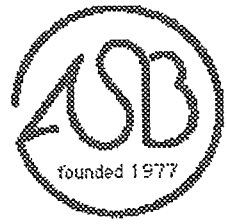

KEYNOTE

Jan Fridén, M.D., PhD

"Mechanical Considerations in the Design of Surgical Reconstructive Procedures"

Thursday August 9, 2001
0800 to 0855

MECHANICAL CONSIDERATIONS IN THE DESIGN OF SURGICAL RECONSTRUCTIVE PROCEDURES

Jan Fridén
Department of Hand Surgery
Sahlgrenska University Hospital, Göteborg, Sweden

INTRODUCTION. Tendon transfers are commonly used to restore arm and hand function after injury to the main motor nerves or after spinal cord injury. Traditional principles used to choose the length at which the transferred muscle should be attached are relatively vague and have not been thoroughly examined (1). Since surgeons use passive tension to indicate the "length" at which a muscle should be attached during tendon transfer, misunderstanding of the sarcomere length-passive tension relationship can result in severe overstretch of the muscle, and thus, poor function. The focus of our studies was to measure muscle sarcomere length and passive tension during tendon transfer surgery. It is hypothesized that a significant functional improvement will be realized when muscles are reattached during tendon transfer procedures at the appropriate length and tension. In addition, since many of these transfers involve spastic muscles and no adequate animal model exists to study spasticity, preliminary length-tension data on spastic wrist flexor muscles will be discussed.

MATERIALS AND METHODS. A laser diffraction device that permits direct measurement of sarcomere length in human muscles during surgery was developed (2,3). The use of this device has enabled us to understand the normal function of human upper extremity muscles and to provide specific recommendations regarding optimal surgical reattachment of muscle during reconstructive surgery. The basic device consists of a low power laser beam that transilluminates a small muscle fiber bundle. The striation pattern within the muscle results in a diffraction pattern that can be measured with photodetectors.

RESULTS AND DISCUSSION. To date, we have published intraoperative sarcomere length data from six studies involving 47 subjects. Thirty-five of these cases involved surgical tendon transfers:

- Patients (n=5) undergoing tendon transfer of the flexor carpi ulnaris (FCU) to the extensor digitorum communis (EDC) secondary to acute radial nerve palsy (4).
- Patients (n=5) undergoing tendon transfer of the FCU to the combined wrist extensors (ECRB and ECRL) secondary to radial nerve palsy (6).
- Patients (n=22) undergoing tendon transfers about the wrist, primarily involving the flexor carpi ulnaris (n=15), but also including the ECRL (n=4), and brachioradialis (n=3) secondary to tetraplegia (7).
- Patients (n=3) undergoing tendon transfer of FCU to ECRB or EDC to correct for wrist flexion contracture secondary to spasticity (8).

We have found that upper extremity muscles have operating ranges that vary between synergists (5) and antagonists (9). In contrast to other *in vivo* studies of muscle function that seem to indicate an architectural and biochemical optimization for power production (10,11) our data suggest that upper extremity muscles are designed to provide optimal control of joint position and stability. In the study of spastic muscles we found that spastic FCU muscles had

extremely long sarcomere lengths with the wrist fully flexed and the slope of the FCU sarcomere length-joint angle relationship was essentially normal (8). This suggests that serial sarcomere number (and therefore muscle fiber length) is unchanged in spite of the dramatic absolute sarcomere length change.

In addition, we have demonstrated that it is possible to stretch muscles intraoperatively to such lengths that they no longer have sufficient myofilament overlap to perform the desired function (Fig. 1).

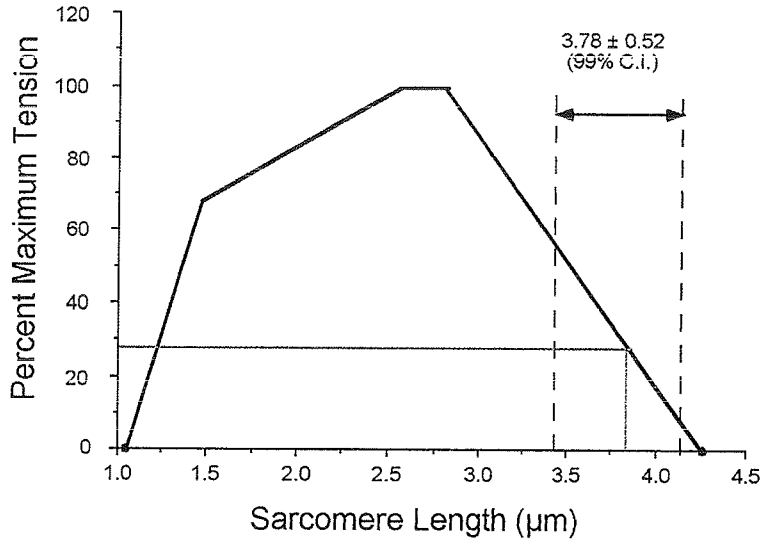

Fig. 1: Relationship between predicted muscle force (percent of maximum isometric force) and intraoperative sarcomere lengths obtained after various tendon transfers. Dashed vertical lines represent 99% confidence interval for the average post-transfer sarcomere lengths. Dotted lines represent average sarcomere length and corresponding predicted force. Note that transferred muscles were predicted to generate only about 25% of maximum active force.

However, the extent to which this problem can be measured and controlled intraoperatively remains to be determined. In addition, the extent to which skeletal muscles will adapt to such chronic length changes is not know but preliminary data suggest (12) that muscle adaptation may not result in optimized function as has been assumed based on extrapolation of studies in rodent muscle (13).

LITERATURE REFERENCES

1. Brand and Hollister (1993) Clinical Mechanics of the Hand.
2. Lieber *et al.* (1994) J. Neurophysiol. **71**:874.
3. Fridén and Lieber (1994) J Hand Surg. (Am) **19A**:269.
4. Lieber *et al.* (1996) J. Hand Surg. (Am.) **21A**:612.
5. Lieber *et al.* (1997) J. Exp. Biol. **200**:19.
6. Lieber and Fridén (1997) J. Biomech. Eng. **119**:386.
7. Fridén and Lieber (1998) J. Hand Surg. (Am.) **23A**:105.
8. Lieber and Fridén (2001) Muscle&Nerve (in press)
9. Loren *et al.* (1996) J. Biomech. **29**:331.
10. Lutz and Rome (1994) Science **263**:370.
11. Rome *et al.* (1988) Nature **335**:824.
12. Fridén *et al.* (2000) J. Hand Surg. (Am.) **25A**:138.
13. Williams and Goldspink (1978) J. Anat. **127**:459.

KEYNOTE

Geert Schmid-Schoenbein, PhD

Friday August 10, 2001
0800 to 0855

Fluid Shear Stress as a Control Mechanism in Tissue Injury.

Geert W. Schmid-Schönbein, Shunichi Fukuda, Peter Marschel
Department of Bioengineering and
Whitaker Institute for Biomedical Engineering
University of California San Diego
La Jolla, California

In the majority of cardiovascular complications a key reaction is the development of an 'inflammatory reaction'. In inflammation, circulating leukocytes become activated and adhere to vascular endothelium, they migrate into the tissue and participate in parenchymal cell dysfunction, apoptosis and even necrosis. An important requirement for inflammation is *cell activation.* Cell activation can be detected in circulating leukocytes, platelets, and under experimental conditions also in endothelial cells in form of cytoskeletal mechanical parameters, a shift in membrane adhesion molecules (e.g. selectins, integrins), degranulation of cytoplasmic granules or production of reactive oxygen species. Among several mechanisms that may lead to cell activation, increasing evidence suggests that fluid mechanical shear may play a central role. Fluid shear stress (of the order of 1 dyn/cm^2) applied to freshly collected leukocytes leads to rapid actin degranulation, pseudopod retraction and down-regulation of membrane integrins. In contrast, reduction of the fluid shear in the microcirculation leads in many leukocytes to development of pseudopods, attachment to the endothelium, spreading and migration across the endothelium. Thus application of physiological fluid shear stress is a requirement to prevent early forms of inflammation. Application of *normal* stress is less effective in downregulation of leukocytes than fluid *shear* stress. Recently, we also uncovered mechanisms that lead to abolishment of the fluid shear response by depletion of the second messenger cGMP from the cytoplasm and attachment via β_1 integrin. The mechanisms that serve to enhance the fluid shear response and to block it are a key to understanding trigger mechanisms that lead to cardiovascular complications.

Supported by NIH Grants HL10881 and HL43026.

KEYNOTE

James A. Spudich, PhD

Saturday August 11, 2001
0800 to 0855

Single Molecule Mechanics and the Myosin Family of Molecular Motors

James A. Spudich, Departments of Biochemistry and Developmental Biology, Stanford University School of Medicine, Stanford, CA 94305.

General:

We use a multifaceted approach to unravel the mechanism by which molecular motors transduce the chemical energy of ATP hydrolysis into mechanical motion. Work in my laboratory has focused on the myosin family of molecular motors, enzymes that generate the force and motions that underlie muscle contraction, cytokinesis in nonmuscle cells, cell movement, and membrane translocations in cells. We have established both *in vitro* motility assays and a cell system for functional and molecular genetic analyses of myosin. Using the cellular slime mold *Dictyostelium*, we provided genetic proof that myosin is required for cytokinesis of cells in suspension, changes in cell shape during morphogenesis, and capping of cell surface receptors. We also designed and developed *in vitro* assays for ATP-dependent movement of purified myosin on filaments reconstituted from purified actin. This assay has been extended to the single molecule level, using a dual beam laser trap microscope developed in collaboration with Steve Chu. We are measuring directly the interaction of single myosin molecules with single actin filaments, examining both conventional myosin (myosin-II), found in muscle and in the contractile ring of dividing cells, and nonconventional myosins such as myosin-V (in collaboration with Drs. Mark Mooseker, Richard Cheney, and Lee Sweeney), found in nerve cells and other cells where membrane translocations are required.

Recent work:

It has long been hypothesized that the molecular motor myosin acts by binding to actin and swinging its light-chain binding region through a large angle to provide a ~10-nm step in motion coupled to changes in the nucleotide state at the active site. Direct dynamic measurements to date, however, have largely failed to reveal changes of that magnitude. We used a cysteine engineering approach to create a high resolution FRET-based sensor that reports a very large ~70-degree nucleotide dependent angle change of the light-chain binding region. The combination of steady-state and time-resolved (with Zygmunt Gryczynski and Joseph Lakowicz, Univ Maryland) fluorescence resonance energy transfer measurements unexpectedly reveals two distinct prestroke states, one of which has not yet been detected in crystallographic studies. The measurements also show that bound Mg.ADP.Pi, and not bound Mg.ATP, induces the myosin to adopt the prestroke states.

It is thought that Switch II of myosin, kinesin and G-proteins plays a critical role in relating the nucleotide state to the protein conformation. We examined S456L myosin-II from *Dictyostelium*, a mutant of the Switch II region, whose mechanical activity is uncoupled from the chemical energy of ATP hydrolysis so that actin filament gliding velocities are only one-tenth that of wild type. The mutant myosin exhibits an extended strongly-bound state time and a shorter step size, which together account for the decrease in *in vitro* velocity.

Myosin-V is a molecular motor from brain that moves processively along its actin track. With Mark Mooseker (Yale) and Richard Cheney (Univ North Carolina), we employed a feedback-enhanced optical trap to examine the stepping kinetics of this

movement. By analyzing the distribution of time periods separating discrete ~36-nm mechanical steps, we characterized the number and duration of rate-limiting biochemical transitions preceding each such step. Based on this, we propose a model for myosin-V processivity involving a tightly coupled motor whose cycle time is limited by ADP release. In collaboration with Lee Sweeney (Univ Pennsylvania), we are characterizing a number of mutant forms of myosin-V, expressed in Baculovirus, as well as myosin-VI, a fascinating motor that moves in the opposite direction along an actin filament from all the other known myosins.

BORELLI AWARD

Felix Zajac

"Understanding Muscle Coordination of the Human Leg with Dynamic Simulations"

Saturday, August 11, 2001
1100 to 1200

Understanding Muscle Coordination of the Human leg with Dynamic Simulations

Felix E. Zajac[1,2]

[1] Rehabilitation R&D Center, VA Palo Alto Health Care System, Palo Alto, CA USA
[2] Mechanical Engineering and Functional Restoration Departments,
Stanford University, Stanford, CA, USA
E-mail: zajac@rrdmail.stanford.edu

INTRODUCTION

Movement of our body requires muscles to coordinate force and power generation so the body segments can accelerate or decelerate, consonant with the task being executed. It is with extreme pleasure, in honor of Giovanni Borelli, considered to be the father of modern biomechanics, to be able to convey the work of my collaborators and me. Specifically, how dynamic simulations of human lower limb tasks have assisted in elucidating muscle coordination principles during standing posture, jumping, seated pedaling, and walking.

METHODS

The generation of dynamic simulations begins with a multi-step modeling process. We use simple models, if appropriate; otherwise more complex models, depending on the specific question under study. Rigid body segments are used to represent the body mass distribution. Joints are modeled as hinges or ball-and-sockets whenever possible (e.g., ankle, hip; cf. knee). Joints superior to the hip have been ignored (i.e., head-arms-trunk is one segment). Currently, the dynamic equations of motion (EOM) of the articulated body are generated by commercial software.

Muscles are modeled with force-length-velocity and activation (excitation-contraction) dynamical properties with one excitation signal (cf. EMG signal). Elasticity in-series with the muscle fibers is accounted for by a "tendon" model. Musculotendon paths are modeled by straight-line sequences with intermediate via points to allow wrapping over anatomical structures (to emulate appropriate muscle moment arms). In seated pedaling the feet are assumed to be rigidly attached to the pedals and the hips stationary. In the other tasks, the ground-foot interface has undergone an evolution. Currently, viscoelastic elements represent this interface. To facilitate musculoskeletal model development, a computer-graphics user-interactive interface was created and integrated with the EOM software.

Muscle excitations are found using optimization algorithms. Either some task performance criterion (e.g., maximum height in jumping; maximum speed in pedaling) or the replication of experimental data is maximized (e.g., submaximal effort pedaling; walking). Simulation data are analyzed to find the contributions of individual muscles to the acceleration and power of the segments.

RESULTS AND DISCUSSION

In standing, FES feedback controllers were designed to excite leg muscles to maintain upright posture subject to extreme perturbations, such as what might occur during arm movements. Simulation analysis of standing posture showed that hamstrings and gastrocnemius muscle strength limit postural mobility.

To jump high, we found that uniarticular hip, knee, and ankle extensor muscles produce the energy required, with most of it delivered to the trunk. Biarticular muscles (i.e., hamstrings, rectus femoris, gastrocnemius) fine-tune the coordination. Countermovement causes upwards propulsion to be stronger because decelerating downward body motion gives muscles time so that high force is produced from the outset of upward body motion.

In pedaling, power delivery to the crank occurs, in large part, by muscle synergies. A muscle synergy is defined as co-excited muscles executing different body segmental energetic functions so energy can be delivered to the crank. A hip (and somewhat a knee)/ankle extensor synergy during leg extension and a hip (knee)/ankle flexor synergy during leg flexion have been identified. The uniarticular hip (and somewhat the knee) muscles produce energy but, because of their limited ability to accelerate the crank, deliver energy to the leg instead. The ankle muscles produce relatively little energy but, by developing high (isometric) force, transfer leg energy to the crank by decelerating the leg and accelerating the crank. Thus the hip and knee uniarticular muscles work synergistically with the ankle muscles to provide crank propulsion. Hamstrings produce energy and deliver it directly to the crank near the limb extension-to-flexion transition to diminish the ongoing crank deceleration. Rectus femoris has a similar, though less effective role at the opposite transition. In backwards pedaling, the transitions where these biarticular muscles accelerate the crank reverse.

In walking, ankle plantar flexor muscles have a prominent role in stance, but soleus (SOL) and gastrocnemius (GAS) often have different segmental energetic functions. In the beginning of stance, both eccentric SOL and GAS, while storing energy in their tendons and hindering trunk forward progression, provide trunk support. In midstance, however, near isometric SOL and GAS have different segmental energetic functions. GAS transfers energy from the trunk to the leg, and SOL the opposite, enabling them to work in synergy to support the body and maintain its forward momentum. In late stance, though both SOL and GAS are concentric, SOL delivers the energy it produces and the energy stored in its elastic structures to the trunk, whereas GAS delivers its energy to the leg to assist swing initiation.

In the very beginning of stance, the eccentric quadriceps (vasti muscles particularly), not only provide support of the trunk but also forward progression of the trunk. More energy is transferred from the leg to the trunk by the quadriceps than dissipated by their muscle fibers. Thus the role of quadriceps as an accelerator of the trunk seems to be comparable to its role as a brake of the leg.

SUMMARY

Dynamic simulations provide invaluable data to understand muscle coordination. Dissection of the acceleration and power of individual body segments into individual muscle (and gravity and inertia) contributions, made possible with simulations, shows how muscles work together to execute the specific motor task.

ACKNOWLEDGEMENTS

Supported by the Rehabilitation R&D Service, Department of Veterans Affairs, and NIH grant NS17662. Thanks to all my collaborators. References to be provided at the Borelli Lecture.

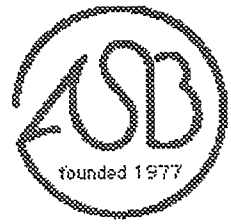

MICROSTRAIN AWARD

Karen Reed

"Design and Evaluation of a Cryogenic Probe to Induce Osteonecrosis in a Precise Location"

Friday, August 10, 2001
1400 to 1530

DESIGN AND EVALUATION OF A CRYOGENIC PROBE TO INDUCE OSTEONECROSIS IN A PRECISE LOCATION

Karen L. Reed[1], Thomas D. Brown[2,1], Michael G. Conzemius[3]
[1]Departments of Biomedical Engineering and [2]Orthopaedic Surgery
University of Iowa, Iowa City, IA
[3]Veterinary Teaching Hospital
Iowa State University, Ames, IA
Email: karen-reed@uiowa.edu

INTRODUCTION

Approximately 25,000 new cases of femoral head osteonecrosis (ON) present each year in the U.S. To better understand the pathology and improve treatment of this disorder, animal models used by other research groups have included dogs, horses, goats, and rabbits. Recently, we hypothesized that the emu *(Dromaius novaehollandiae)*, a large, bipedal, flightless bird native to Australia, would be more biomechanically similar to humans. Results from a pilot series of 38 birds showed that after ON is induced with liquid nitrogen injection into the femoral head, lameness ensues in 12-16 weeks, due to bony collapse (Conzemius, 2000). However, pilot series lesion size was too large, and was difficult to control. To improve lesion localization in this model, a C-arm fluoroscope is now being used during the surgery for more precise cryo-insult delivery. And, an improved, closed-circulation liquid nitrogen probe has been developed. A finite element (FE) model and physical bench simulations have proven helpful to further refine the freeze protocol.

METHODS

A closed-circulation cryogenic probe (Figure 1) was developed in tandem with an FE model of the probe's heat transfer characteristics in cancellous bone. Primary considerations in the probe design were appropriate size for the emu, no direct liquid nitrogen/tissue contact, no freezing of non-targeted tissue, durable, autoclavable. To this end, the closed-circulation probe was designed, built, and tested. Several key features of this probe include its small-diameter (3 mm), actively heated shaft, and thermally isolated tip. The tip and shaft are separated by a small layer of Ultem® (polyetherimide) (GE Plastics, Pittsfield, MA). This plastic has a very low thermal conductivity (k=0.13 W/m*K) compared to the shaft material (stainless steel, k=12.49 W/m*K). This prevents the tip from becoming warm as a result of shaft heat conduction.

A finite element model of this probe was developed, using Patran 9.0 for pre-processing (HKS, Pawtucket, RI), and ABAQUS 5.8 for analysis (MSC, Los Angeles, CA). More specifically, a probe surrounded by an "infinite" field of a 1% agarose-water gel (whose thermal conductivity is similar to that of cancellous bone) was constructed. Boundary conditions for this model are fixed temperatures on the probe tip and shaft, and emu body-temperature (303 K) at distant points. This model provides a 2D longitudinal section of the temperature fields, which were modeled before the

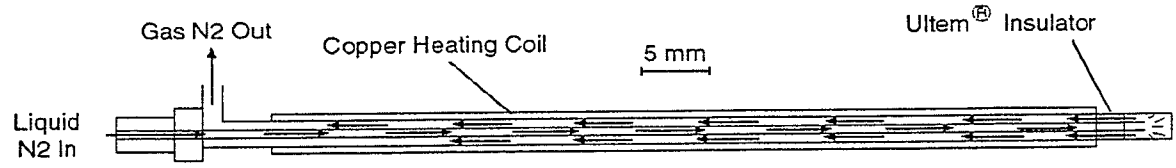

Figure 1: Schematic of final cryogenic probe

probe was built. The predicted temperature fields were used in the probe design process. The experimental probe testing setup consisted of 5 type T thermocouples, embedded in the agarose gel at locations ranging from 0 mm to 12 mm from the cryogenic probe (Figure 2). Data were collected using LabVIEW (National Instruments, Austin, TX).

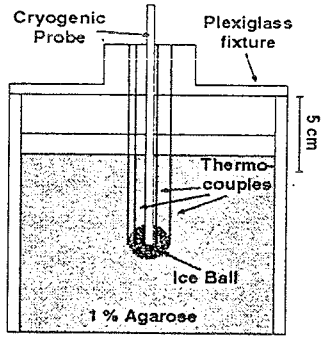

Figure 2: Schematic of bench testing set-up

RESULTS

Bench-top testing of the probe embedded in agarose showed a tip temperature decreasing exponentially to an average of –45 °C over 300 seconds, with shaft minimum of 0 °C and a maximum of 30 °C. When boundary conditions of the FE model were set to these temperatures, a steady-state ice ball 26 mm in diameter was formed after 385 seconds (Figure 3). Steady state was defined as no temperature change of greater than 0.02 degrees/second.

Due to unsteadiness in the nitrogen delivery system, the bench-top probe had a slower freezing rate than that of the FE model. Several trials showed that an ice ball of 8 mm in diameter could be consistently produced at just under 100 seconds, and a diameter of 20 mm was reached at roughly 500 seconds (Figure 4). Visual observation confirmed that the experimental ice ball was nearly spherical in shape, and was situated at the tip of the cryogenic probe.

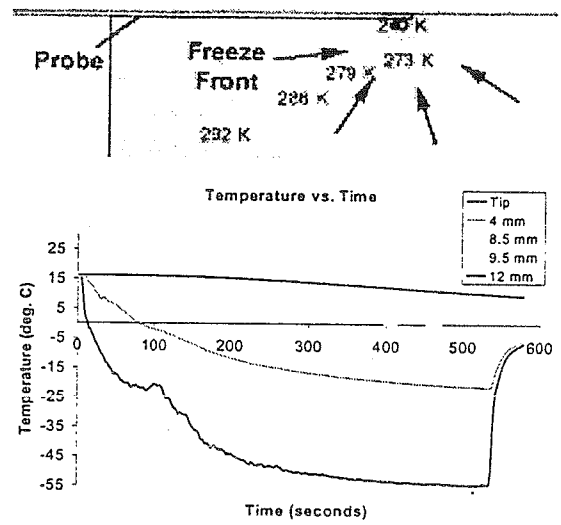

Figures 3 and 4: (3) Steady-state temperature field from FE model (4) Temperature/Time curve generated from bench-top freeze experiments showing temperature at probe tip (Tip) and at several radii.

DISCUSSION

The copper heating coil surrounding the probe actively prevents tissue along the shaft from freezing. Power input to the coil is manually adjusted during probe operation, to compensate for changes in nitrogen flow, with the average input being 17 Watts (17 V, 1 A). A thermocouple is mounted at the probe tip to actively monitor temperature during surgery. The entire probe is coated in an autoclavable epoxy to protect and strengthen all components, and seal any leaks.

SUMMARY

An actively heated cryogenic probe was developed and evaluated for purposes of inducing local osteonecrosis. Additionally, a finite element model of the probe's heat transfer characteristics was developed to aid in probe design.

AKNOWLEDGEMENTS

NSF Graduate Research Fellowship and NIH Grant #46601

REFERENCES

Conzemius et al. *ORS Proceedings* (2000) p. 206

CLINICAL BIOMECHANICS AWARD

Tom Brown

"A Database of Living-Subject Motion to Examine Both Posterior and Anterior Dislocation of Total Hip Replacements"

Friday, August 10, 2001
1400 to 1530

A DATABASE OF LIVING-SUBJECT MOTION TO EXAMINE BOTH POSTERIOR AND ANTERIOR DISLOCATION OF TOTAL HIP REPLACEMENTS

M.E. Nadzadi [2], D.R. Pedersen [1], H.J. Yack [3], J.J. Callaghan [1,2], and T.D. Brown [1,2]

[1] Departments of Orthopaedic Surgery and [2] Biomedical Engineering, and [3] Physical Therapy Graduate Program, University of Iowa, Iowa City, IA
E-mail: tom-brown@uiowa.edu

INTRODUCTION

Dislocation in total hip arthroplasty remains the second leading cause of implant failure, with primary failure rates between 2 and 11%, and roughly double that rate for revisions. Several maneuvers have been identified as being responsible. Included in this list are erectly seated leg crossing, bending over in a chair to tie one's shoes, or rising out of a low seated position. Most current thinking on dislocations has been shaped by retrospective clinical reports, although several laboratory models have recently emerged to begin addressing direct causality.

Although that research has led to a greater understanding of dislocation mechanics, such data are specific to just one maneuver. It also is important to address anterior dislocations (about 20% of cases). To this end, we report the development of a motion database for seven dislocation-prone maneuvers, and we explore these motions in terms of their leading to dislocation of a THA finite element model.

METHODS

Ten (5 male, 5 female) THA-aged normal (i.e., non-THA-implanted) subjects (49.7 ± 4.97, range 44 to 59 y.o.) performing a series of dislocation prone maneuvers were monitored by an optoelectronic motion tracking system and force plate recordings. A total of seven maneuvers were repeatedly recorded for each patient over several days, resulting in nearly 400 separate trials. Five of these maneuvers are prone to posterior dislocations (SSL, SSN, STOOP, TIE, XLG)*, and two are for anterior dislocation-prone maneuvers (PIVOT and ROLL). A 47-muscle kinetic model (Brand, 1982) was used to estimate the physiologic joint load in the pelvic reference frame, as a function of hip clinical angles. Figure 1 represents a typical data set as a function of the captured motion frame number.

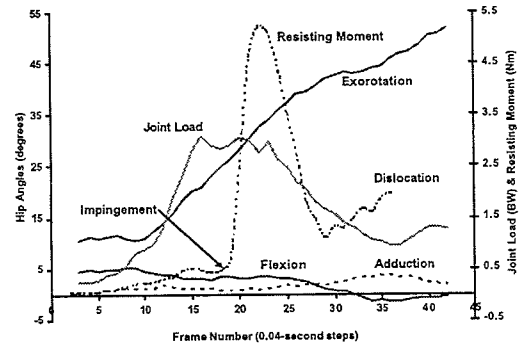

Figure 1: Optoelectronically determined Cardan angles, joint loading, and FEA-computed resisting moment, for a PIVOT maneuver.

A series of three-dimensional FE models of a widely used titanium-backed total hip implant system** were developed from manufacturer IGES files, using Patran 8.5 pre-processing. Following an established formulation (Scifert, 1998), a non-linear, large displacement contact analysis was performed with ABAQUS 5.8. The cup backing and liner were modeled with 3920 continuum elements, while the proximal third of the femoral component was modeled

with 4238 rigid-body Bezier surface elements. The polyethylene liner was characterized by a 4th-order constitutive model relating von Mises stress to tangent modulus (Cripton, 1993).

RESULTS AND DISCUSSION

We have recorded several cases of impingement leading to a computed lever-out dislocation event for each maneuver. These results are of particular importance for the two maneuvers that result in an anterior dislocation. This is the first time (to our knowledge) that an anterior dislocation has been simulated experimentally or computationally. This will allow additional research in the area of optimal design and placement to best avoid a dislocation. Additionally, the present data represent the first formal kinetically based study of dislocations from other than primarily hip flexion events such as leg crossing (Sahni, 1998).

In a few instances in our FE series, the femoral head subluxed and dislocated without an impingement/lever-out. This "shear-out" of the head was due to a combination of component orientation and prescribed joint load magnitude and direction, (Figure 2).

SUMMARY

Seven maneuvers of ADL have been optoelectronically recorded for computational studies of THA dislocation, using THA-aged living subjects. Included in this data set are two maneuvers that result in an anterior dislocation. This opens the way for a much richer picture of the spectrum of dislocation challenges which THA implants must meet. Specifically, current empirical criteria for optimal surgical placement of the acetabular component can be deterministically refined. The revised criteria can then be applied in conjunction with recent accuracy improvements of surgical navigational systems, to reduce clinical dislocation rates. Additionally, a non-impingement/lever-out mode of dislocation has been demonstrated.

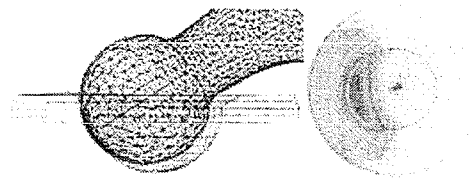

Figure 2: (L) Close-up view illustrating impingement-free subluxation, and (R) von Mises stress pattern in the liner (deformations NOT magnified).

* SSL = sit-to-stand from low chair; SSN = sit-to-stand from normal chair; STOOP = stand and reach for right foot with left hand; TIE = bend over in a seated position to tie a shoe; XLG = seated leg crossing; PIVOT = pivoting to produce femoral extension and exorotation; ROLL = rolling over while lying on back

** Endurance femoral stem, 22mm modular head, and Duraloc 22-52 acetabular shell, DePuy, Inc.

REFERENCES

Brand, R.A. et al. (1982). *J. Biomech Engineering*, **104**, 304-310.

Cripton, P.A. (1993). MS Thesis, Queen's University, Kingston, Ontario.

Sahni, I.K. et al. (1998). *44th Annual Meeting of ORS*, 195.

Scifert, C.F. et al. (1998). *CORR*, **355**, 152-162.

ACKNOWLEDGEMENTS

Financial support provided by a VA Merit Grant, and DePuy, Inc. Assistance from Ms. Ruchika Wahi, Mr. Jason Wilken, Mr. Mike Squire, and Ms. Hannah Lundberg.

CLINICAL BIOMECHANICS AWARD

Scott Hazelwood

"Abductor Muscle Impairment and Recovery May Affect Bone Loss Around Hip Implant Stems"

Friday, August 10, 2001
1400 to 1530

ABDUCTOR MUSCLE IMPAIRMENT AND RECOVERY MAY AFFECT BONE LOSS AROUND HIP IMPLANT STEMS

Scott Hazelwood and Yoshihiko Mizumoto

Orthopaedic Research Laboratories, University of California Davis, Sacramento, CA 95817
e-mail: sjhazelwood@ucdavis.edu

INTRODUCTION

Abductor muscle strength reduction after total hip arthroplasty may lead to functional impairment, such as limping and reduced walking speed (Murray et al., 1975; Vaz et al., 1993), and also may contribute to bone loss of the femur (Burr, 1997). Depending on the surgical approach used (anterolateral, direct lateral, posterior, etc.), as much as 50% of the abductor function may be lost following the insertion of the implant (Vaz et al., 1993). The recovery period for the abductor muscles varies greatly and may last up to two years after surgery (Horwitz et al., 1993; Minns et al., 1993; Murray et al., 1981). We used a bone remodeling simulation to study the effects of the reduction and recovery of the abductor muscle force on femoral bone loss following hip replacement surgery.

METHODS

An adaptation simulation based on bone remodeling stimuli of damage and disuse was used for this study (Hazelwood and Castillo, 2000). The mechanical stimulus for remodeling was assumed to be proportional to the product of the strain range (s) raised to a power and the loading rate (R_L) from n different activities:

$$\Phi = \sum_{i=1}^{n} s_i^q R_{Li}$$

Damage in the bone matrix was assumed to accumulate at a rate proportional to Φ. The principal strain with the largest magnitude was used as the strain quantity, s, for this simulation. Disuse was assumed for values of Φ below an equilibrium mechanical stimulus.

The damage removal rate was calculated from existing damage, basic multicellular unit (BMU) activation frequency (f_a), and the area of bone removed by each BMU. A removal specificity factor was included to spatially associate removal with damage. Daily f_a values were calculated from the amount of disuse, existing damage, and the surface area available for remodeling. The number of resorbing and refilling BMUs active each day were calculated from the f_a history over the remodeling period: 25 days for resorption, 5 days for reversal, and 64 days for refilling. Daily density changes were then calculated from the net amount of bone removed or added by each resorbing or refilling BMU, respectively. A mechanism was included to allow for less than complete refilling on trabecular surfaces in disuse. Elastic modulus–density relationships were determined from empirical data for both cortical and trabecular bone.

A two-dimensional finite element model (linearly elastic, isotropic), consisting of 4216 4-node quadrilateral elements, was created from a radiograph of a representative femur. A bony side plate was added to the model to account for the out-of-plane cortical bone (Weinans et al., 1992). Three load cases, each consisting of joint reaction and abductor muscle forces, were used to simulate the daily loading history for normal activity (Carter et al., 1989): single-leg stance was applied for 3000cpd while the abduction and adduction load conditions were each applied for 500cpd. The bone adaptation algorithm was integrated into the analysis through a UMAT subroutine and the simulation was run using ABAQUS 5.8 (HKS, Pawtucket, RI) until the density distribution achieved steady state.

The steady-state results of the femur model were used as the pre-surgical condition. Hip replacement surgery was simulated by adding

a conventional press-fit prosthesis and reducing the abductor muscle force to 50% or 70% of normal. The abductor muscle strength was allowed to recover to 100% in a linear fashion over either 400 days or 800 days for each simulation, and bone loss was analyzed after simulating remodeling of the femur for 2000 days.

RESULTS AND DISCUSSION

A reduction in the initial abductor muscle function to 50% of normal after hip replacement surgery produced increases in femoral bone loss in the seven Gruen zones surrounding the implant stem (Table 1). Increasing the recovery period of the abductor muscles also produced increases in predicted bone loss in the regions examined, especially in the proximal/lateral region (P/L, zone 1). In this region, bone loss during an 800 day recovery period increased by 19% compared to a recovery period of 400 days for a 50% reduction in initial muscle force. Femoral bone loss was generally greater in the proximal and medial regions than the distal and lateral ones, and was found to be largest in the proximal/medial zone (P/M, zone 7). In this region, only slight affects in femoral bone loss were observed following changes in the reduction and recovery of the abductor muscle function.

Table 1. Simulated Femoral Bone Loss (%) in 7 Gruen Zones after 2000 Days for 50%, 70%, and 100% Abductor Muscle Function

		400 day recovery		800 day recovery	
zone	100%	50%	70%	50%	70%
1 (P/L)	33.1	38.2	35.1	45.3	38.4
2 (M/L)	31.3	36.6	33.2	42.6	36.8
3 (D/L)	27.5	31.7	30.4	35.9	34.3
4*	3.7	6.1	6.5	7.1	7.6
5 (D/M)	33.7	39.1	37.3	43.2	41.1
6 (M/M)	38.4	43.2	39.2	48.8	43.3
7 (P/M)	61.7	64.4	63.1	67.6	64.8

*zone 4 is distal to the implant stem
P/L=proximal/lateral, M/L=mid/ lateral, D/L=distal/lateral, D/M=distal/medial, M/M=mid/ medial, P/M=proximal/medial

SUMMARY

Many factors contribute to the bone loss of the femur following hip replacement surgery: bone quality, implant material and design, patient weight and activity level, duration of implantation, etc. In this study, it was found that the reduction and recovery in the strength of the abductor muscle force following hip replacement surgery also affects bone loss around implant stems. With several options available to surgeons for exposing the hip during surgery, these results imply that a surgical approach which maintains most of the abductor muscle function would not only improve patient functionality, but also would reduce the amount of femoral bone lost in the period following implantation. In addition, patients who undergo hip surgery usually participate in a rehabilitation program that emphasizes strengthening of the abductor muscles. Our results suggest that if such a program were designed to allow for the quickest feasible recovery of the muscle function, then subsequent bone loss following surgery may be significantly reduced.

ACKNOWLEDGMENTS

Support provided by NIH grant AR41644.

REFERENCES

Burr D.B. (1997). *J Bone Min Res*, 12:1547-1551.
Carter D.R. et al. (1989). *J Biomech*, 22:231-244.
Hazelwood S.J., Castillo A.B. (2000). *Proceedings of ASB*, 245-246.
Horwitz B.R. et al. (1993). *Clin Orthop*, 291:154-163.
Minns R.J. et al. (1993). *J Arthroplasty*, 8:625-627.
Murray M.P. et al. (1975). *J Bone Joint Surg*, 57A:337-342.
Murray M.P. et al. (1981). *Clin Orthop*, 157:119-124.
Vaz M.D. et al. (1993). *J Orthop Sports Physical Therapy*, 18:526-531.
Weinans H. et al. (1992). *J Orthop Res*, 10:845-853.

JOURNAL OF BIOMECHANICS AWARD

Richard Lieber

"Structural and Functional Roles of Desmin in Mouse Skeletal Muscle Under Conditions of Passive Loading"

Friday, August 10, 2001
1400 to 1530

STRUCTURAL AND FUNCTIONAL ROLES OF DESMIN IN MOUSE SKELETAL MUSCLE UNDER CONDITIONS OF PASSIVE LOADING

Sameer B. Shah[1], Jan Fridén[2], Yassemi Capetanaki[3], and Richard L. Lieber[1]

[1]Departments of Bioengineering and Orthopaedics, U.C. San Diego, La Jolla, CA
[2]Department of Hand Surgery, Sahlgrenska University Hospital, Göteborg, Sweden
[3]Department of Cell Biology, Baylor College of Medicine, Houston, TX
email: rlieber@ucsd.edu

INTRODUCTION

Desmin is the primary intermediate filament in the skeletal muscle cytoskeletal system. Early experiments have established that intermediate filaments provide transverse and longitudinal linkages between Z-disks in adjacent myofibrils (Wang and Ramirez-Mitchell, 1983). In addition, desmin also appears to connect sarcomeres to the sarcolemmal membrane at the costameric complexes, and the nucleus to the plasma membrane (for review, see Capetanaki and Milner, 1998).

Based on the prevalence of desmin connections, it has been suggested that desmin plays a role in radial and longitudinal force transmission through the fiber. Such a role, in addition to influencing the passive and active mechanical properties of a muscle, could have significant implications in a mechanical signal transduction pathway, from the inside to the outside of a cell, or *vice versa.*

This study compared wild-type (+/+) and desmin-null (*des -/-*) mouse extensor digitorum longus (EDL) muscles to further characterize structural and functional roles of desmin under passive loading conditions. A novel experimental system was designed to image, in real-time, the positions of representative proteins within a single skinned fiber during stretch, while simultaneously measuring force and sarcomere length (SL). In addition, electron microscopy (EM) was used to assess in greater detail inter-myofibrillar interactions at varying passive strains.

METHODS

Membrane-sarcolemma interactions

Single skinned fibers from the 5th toe of +/+ and *des -/-* mouse EDL muscles were dissected, and mounted in relaxing solution between two rigid posts. One post was attached to a force transducer (Aurora Sci., 405-A), and the other to a rotational bearing (Newport, MT-RS). Fiber/post position was controlled using XYZ-translational stages. The fiber was double-labeled fluorescently for α-actinin (a Z-disk protein) and talin (a costameric protein). The apparatus was then integrated into a laser scanning confocal microscopy system (Zeiss, Axiovert 100M) for imaging of the fiber during stretch.

Upon preconditioning, passive tension was measured at varying fiber strains. Sarcomere length was estimated using average regional α-actinin periodicity. Cross-sectional area was calculated using phase-contrast images of the fiber, and used to calculate stress. Stiffness/modulus and the periodicities of the talin label and α-actinin label (adjacent to the membrane) were compared between +/+ and *des -/-* fibers. Differences between genotypes in Z-disk curvature due to strain were also assessed.

Myofibril-myofibril interactions

+/+ and *des -/-* EDL 5th toe muscles were fixed for EM at varying muscle strains. Images of randomly sampled deep and superficial regions (5 each) from each muscle were digitized. SL (5 SL per image) and average longitudinal displacement between adjacent Z-disks (all Z-disks per image) were obtained.

RESULTS AND DISCUSSION

Membrane-sarcolemma interactions

Sample images and periodicity analysis of one wild-type fiber at slack length and ~100% stretch are given in **Figure 1**. It is observed that costameres and Z-disks adjacent to the membrane were coupled even at high strains. A phase shift and/or differences in the periodicities of talin and α-actinin labels are expected in the *des -/-* at high strains. Differences in periodicity were detected to a resolution of 100 nm.

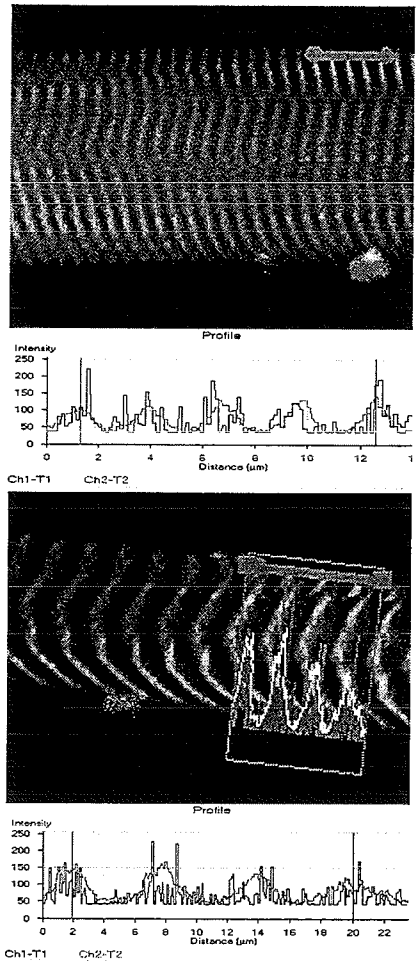

Figure 1: *Sample images/profiles in a wild-type fiber of in-phase talin (red/Ch1-T1) and α-actinin (green/Ch2-T2) periodicities at slack SL (top) and >100% stretch (bottom).*

Passive tension in single mouse fibers

Wild-type fibers display typical viscoelastic properties such as stress-relaxation and hysteresis. Fibers were consistently stretched by more than 100% before fracture. It is expected that due to increased "sliding" of myofibrils with respect to each other (**Figure 2**) and the membrane, *des -/-* fibers may reflect greater compliance.

Myofibril-myofibril interactions

Longitudinal displacement of Z-disks vs. sarcomere length is plotted in **Figure 2**. While adjacent +/+ Z-disks remain coupled at high strains, dramatic separations are observed between adjacent *des -/-* Z-disks. Decoupling in the absence of a significant intermediate filament system could lead to the expected differences in passive mechanical properties between wild-type and desmin-null muscle fibers.

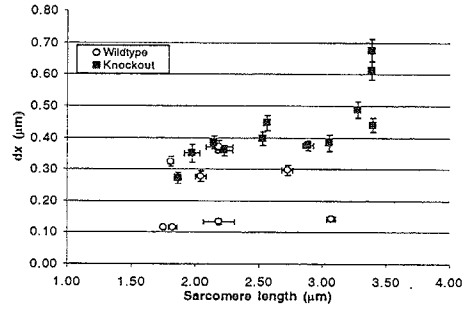

Figure 2: *Longitudinal displacement of adjacent Z-disks vs. Sarcomere length*

REFERENCES

Capetanaki, Y. and Milner, D. (1998). *Subcellular Biochemistry: Intermediate Filaments.* edited by Herrmann and Harris, Plenum Press. **31**: 463-495.

Wang, K., Ramirez-Mitchell, R. (1983). *J. Cell Biol.* **96**, 562-570.

ACKNOWLEDGEMENTS

The authors thank Kimberly Jordan for excellent technical assistance, and the Dept. of Veterans Affairs, and NIH grant 40050 for financial support.

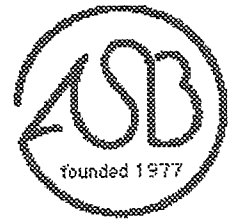

JOURNAL OF BIOMECHANICS AWARD

Sundar Srinivasan

"The Potent Osteogenic Potential of Rest-Inserted Loading: Role of Fluid Flow as an Underlying Modality"

Friday, August 10, 2001
1400 to 1530

THE POTENT OSTEOGENIC POTENTIAL OF REST-INSERTED LOADING: ROLE OF FLUID FLOW AS AN UNDERLYING MODALITY

Sundar Srinivasan and Ted S. Gross, Orthopaedics and Sports Medicine, University of Washington, Seattle, WA, USA, E-mail: sundars@u.washington.edu

INTRODUCTION: Bone response to repetitive mechanical stimuli is rapidly saturated (Rubin and Lanyon 1984). To investigate response saturation, in part, we developed an analytical model of canalicular fluid flow in bone (Srinivasan and Gross 2000). We found that fluid flow and related stimulation of bone cells is markedly reduced (nearly 50%; due to viscous inertial effects) beyond the first load cycle of a repetitive loading regimen (Fig 1). If this occurred *in vivo*, the percentage of bone surface (and therefore the percentage of bone cells) exposed to stimuli above threshold levels (for bone cell activation) could be dramatically reduced. We propose that insertion of rest between load cycles could overcome inertial effects, reproduce the maximal fluid flows during each and every load cycle and thereby enhance bone cell activation. Here, we indirectly test this proposal by examining the ability of rest inserted loading to enhance bone modeling response in two *in vivo* models.

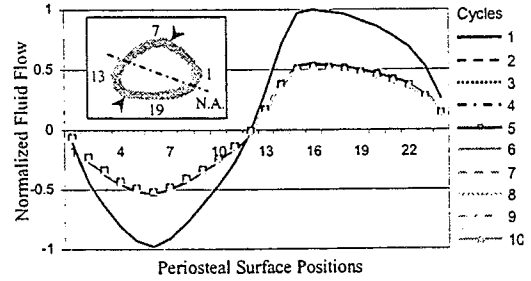

Fig 1: Fluid flows around mid-diaphyseal cortex are maximal during the first load cycle (1) with markedly reduced profiles during subsequent cycles (2-10). Inset illustrates the numbering scheme with neutral axis and sites of peak flow noted.

METHODS: *Surgical Avian Ulna Model:* The left ulnae of a group of adult male turkeys (n=4, 1.5 Yrs) underwent a 1-Hz, 800 με peak strain, 100 cycle/d, 1-wk loading protocol wherein bending loads were applied to the left ulna via transcortical pins ('repetitive'). The second group (n=4) was different only in that a 10-s rest (or unloaded) interval was inserted between each of 100 load cycles ('rest-inserted'). Mid-diaphyseal osteoblastic activation was assessed via Calcein (day 5) incorporation and peak strains estimated via beam theory. *Non-Invasive Murine Tibia Model:* The right tibia of three groups of adolescent female C57BL/6J mice were subject to mechanical loading utilizing the noninvasive murine tibia loading device (Gross et al. In Review). The first group (n=7) underwent a 1-Hz, 0.25 N, 100 cycles/d, 1-wk loading protocol followed by three weeks of normal cage activity ('low-mag'). The second group (n=6) underwent an identical protocol but at double the loading magnitude (0.5 N; 'high-mag'). The last group (n=7) underwent a similar protocol as the 'low-mag' group but: 1) the tibia was loaded for only 10 cycles/d, and 2) a 10-s rest interval was inserted between each of the 10 load cycles ('rest-inserted'). Mid-diaphyseal bone formation was determined via Calcein labels (days 5, 26) and peak strains estimated via FE and beam theory estimates.

RESULTS: *Surgical Avian Ulna Model:* Peak strains induced in the repetitive and rest-inserted groups were not significantly different (820 ± 50 με, 830 ± 60 με, p=0.40). While low-magnitude repetitive loading did not induce periosteal osteoblastic activation significantly different from control (3.8 ± 1.5% vs 1.6 ± 1.1%, p= 0.14), rest-inserted loading enhanced

osteoblastic activation 10-fold versus controls (21.9 ± 4.5%) and 6-fold versus the repetitive loading group ($p < 0.01$; Fig 2).

Non-Invasive Murine Tibia Model: While peak strains induced at the tibia mid-diaphysis in the low-mag and rest-inserted groups were not significantly different (643 ± 5, 648 ± 32 με; p=0.44), strains induced in the high-mag group were significantly increased (1332 ± 50 με, $p < 0.0001$). Low-magnitude loading did not increase bone formation rate (BFR) vs control bones (0.04 ± 0.04 vs 0.08 ± 0.02 $\mu m^3/\mu m^2/d$, $p = 0.22$). In contrast, the high-magnitude (0.3 ± 0.1 $\mu m^3/\mu m^2/d$, $p < 0.01$) and rest-inserted loading (0.37 ± 0.1 $\mu m^3/\mu m^2/d$, $p < 0.001$) significantly increased BFR (Fig 3).

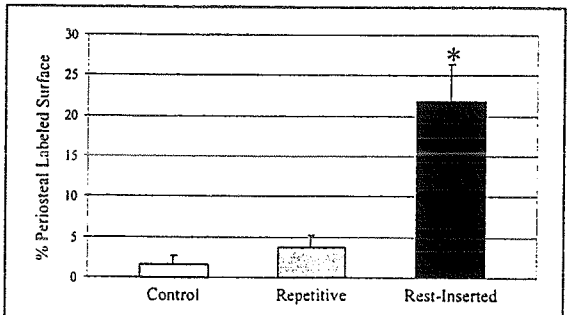

Fig 2: While periosteal activation induced by repetitive loading was not different from controls, insertion of a 10-s rest between load cycles significantly (*) enhanced osteoblastic activity.

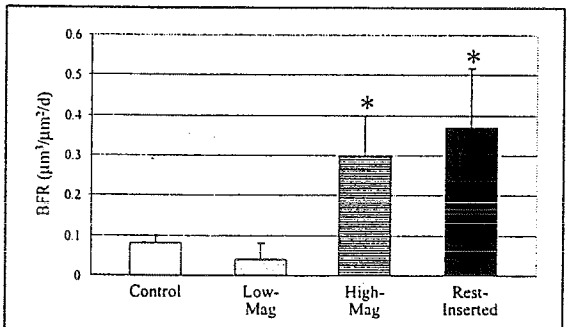

Fig 3: Low-magnitude loading does not alter BFR compared to control. In contrast, both high-magnitude and rest-inserted loading significantly (*) increased BFR by greater than 3- and 4-fold, respectively, versus controls.

DISCUSSION: Data in two *in vivo* models demonstrate that insertion of a 10-s rest between load cycles, per se, dramatically enhances osteoblastic activation and bone formation. These results are surprising considering that the peak strains induced by comparative repetitive and rest-inserted protocols were identical (in both the avian ulna and murine tibia). Of note however, for a given magnitude of bone tissue strains, the induced fluid flows could be markedly diminished (by 50%) beyond the first cycle of repetitive loading. In contrast, insertion of a 10-s rest between load cycles could overcome inertial effects, maximize fluid flows and stimulate cells over a greater percentage of the bone surface. The enhanced activation of bone surface in the avian ulna via simple insertion of rest between load cycles supports this possibility. Specific to the murine tibia model, the 'high-mag' loading induces strains double those in the 'rest-inserted' group. Doubling strain magnitudes ('high-mag') increases fluid flow related stimulation of bone cells; nevertheless, the repetitive nature of the waveform diminishes fluid flows by one-half beyond the first load cycle. In effect, flow magnitudes induced during cycles 2-100 of the 'high-mag' protocol could be similar to flow magnitudes induced during all 100 cycles of rest-inserted loading. The equivalent bone formation induced in the murine tibia by both the 'rest-inserted' and 'high-mag' protocols additionally suggests that the osteogenic benefit of rest inserted loading arises via the modality of increased fluid flow related stimulation of bone.

REFERENCES:

Gross TS, et al. (In Review). *J. Bone Mineral Research.*

Rubin C and Lanyon L (1984). *J. Bone Joint Surgery,* **66A**, 397-402.

Srinivasan S and Gross TS (2000). *Medical Engineering and Physics,* **22**, 127-33.

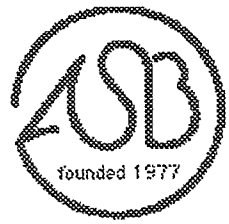

- PARALLEL SESSION -

Symposium

In Vivo Muscle Function in Humans

Thursday, August 9, 2001
0900 to 1030

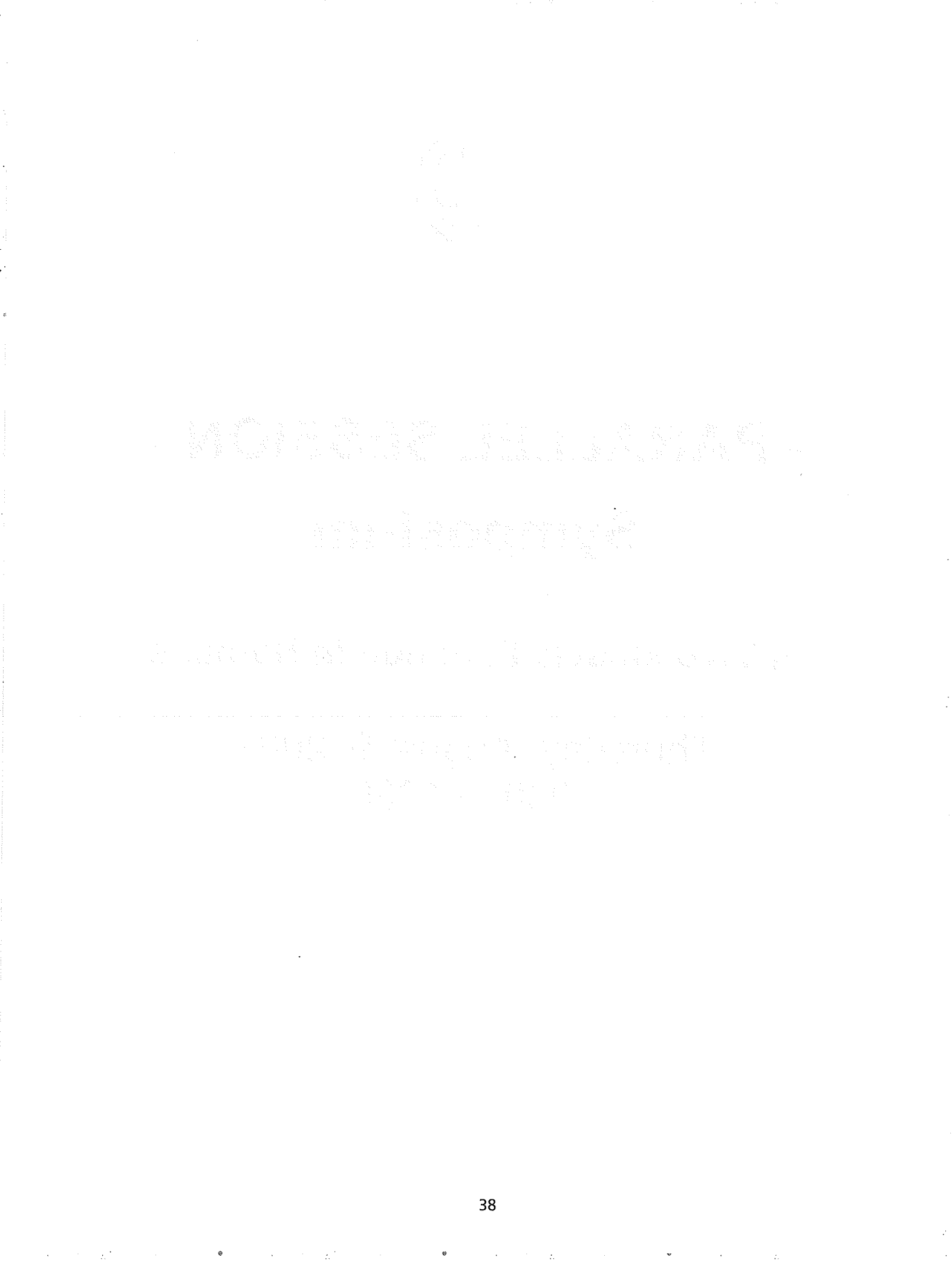

CHANGES IN MUSCLE MECHANICAL ADVANTAGE OF HUMAN RUNNERS DURING SPRINT ACCELERATION

Gwyneth Card, Peter G. Weyand and Andrew A. Biewener

Concord Field Station, Harvard University, Bedford MA USA
E-mail: card@fas.harvard.edu

INTRODUCTION

Previous studies of muscle mechanical advantage relative to ground reaction force (G_{RF}) mechanical advantage, defined as the ratio: $R/r = \int F_m / \int G_{RF}$ or 'EMA' (Fig. 1), have shown that EMA decreases (i.e. mass-specific muscle force decreases) with increasing size when compared broadly across different sized mammalian runners (mouse to horse; Biewener, 1989), that EMA remains constant across steady speeds within a gait, and that differences in EMA between avian bipeds and mammalian quadrupeds of similar size helps to explain their metabolic cost for generating muscle force to support body weight (Roberts et al., 1998).

In this study we examine how muscle mechanical advantage varies during sprint acceleration in human runners, testing the hypothesis that shifts in limb posture during progressive steps of a sprint are matched to changes in the direction of G_{RF} during limb support to maintain a constant limb mechanical advantage at the hip, knee and ankle joints overall.

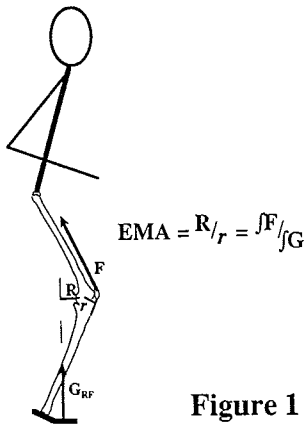

Figure 1

METHODS

Nine runners (5 male/4 female) sprinted from a four-point start (with > 90% of body weight supported over the primary propulsive limb) beginning on a Kistler 9203 force platform and preceding the platform at specific distances to record the fore-aft and vertical ground reaction forces for steps 1, 3, 5, and steady speed (> step 13) of maximal sprints over the force platform. A MacReflex (Qualysis) infrared camera was used to record joint positions of the lower limb and trunk at 60 Hz. Joint coordinate data were smoothed using a four-order digital Butterworth filter (17 Hz 3db cut-off) and referenced to the platform and the location of G_{RF} application in order to calculate the external moments acting at the hip, knee and ankle joints. All signal processing and computations were performed in Matlab. EMA was defined as $\int F_m / \int G_{RF}$ measured over the entire period of ground contact. By focusing on how muscle forces are influenced by limb posture and G_{RF}, EMA ignores inertial and gravitational moments, which are likely important at the hip and knee.

RESULTS AND DISCUSSION

A significant decline in EMA were observed at the hip for step 1 ($p<0.001$) and step 3 ($p<0.005$) compared with step 5 and steady speed (Fig. 2A). No significant change in

EMA however was observed at the knee and ankle joints during different steps of a sprint (Fig. 2B&C). When summed for all three joints, a significant decline ($p < 0.001$) in whole limb EMA (Fig. 2D) was only observed from step 1 to step 3; remaining constant from step 3 to steady speed running.

Consequently, these results partially support our hypothesis that shifts in limb posture during a sprint help to maintain consistent muscle force generating requirements at different limb joints as an individual accelerates during a sprint. However, the decline in limb EMA observed from step 1 to 3 results from the decline in hip extensor EMA. This likely reflects the 'crouched' posture that the runners adopted when beginning a sprint, which greatly increases the hip flexor moment during steps 1 and 3.

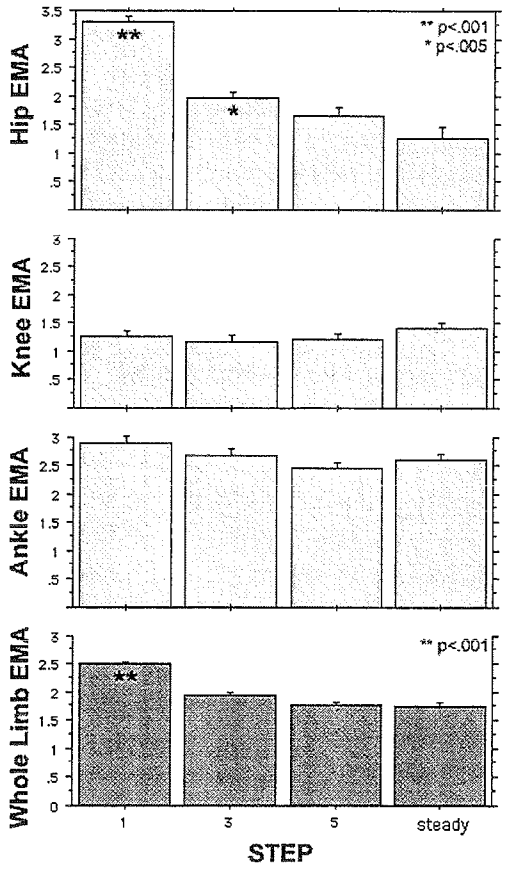

Figure 2. Changes in effective muscle mechanical advantage (EMA = $\int F_m / \int G_{RF}$) of major lower extremity muscle extensor groups as a function of step number during sprinting trials. Whole limb EMA represents the average of the hip, knee and ankle values.

The increase in hip flexor moment reflects the large horizontal component of G_{RF} (net horizontal impulse = 0.60 vertical impulse at step 1 and 0.32 vertical impulse at step 3) and large amount of positive mechanical work (Cavagna et al. 1971) that occurs as a runner accelerates early in a sprint.. The large hip extensor force contributes to increased mechanical power developed at the hip, which is likely transmitted to more distal limb joints in a temporally coordinated manner (Jacobs et al. 1992), in order to facilitate more rapid acceleration of a sprinter.

REFERENCES

Biewener, A. A. (1989). *Science* **245**:45-48.

Cavagna, G. A., L. Komarek & S. Mazzoleni (1971). *J. Physiol.* **217**:709-721.

Jacobs, R. & G. J. Van Ingen-Schenau (1992). *J. Biomech.* **25**:953-965.

Roberts, T. J., M. S. Chen & C. R. Taylor (1998). *J. Exp. Biol.* **201**:2753-2762.

(supported by NSF Grant IBN 9723699)

IN VIVO ESTIMATION OF HUMAN ACHILLES TENDON MOMENT ARM BASED ON ULTRASONOGRAPHY

Yasuo Kawakami[1], Keiko Nakai[1], Constantinos N. Maganaris[2],
Toshiaki Oda[1], Kentaro Chino[1], and Tetsuo Fukunaga[1]

[1]Department of Life Science, University of Tokyo, Japan
[2]Department of Sport and Exercise Science, Manchester Metropolitan University, UK
E-mail: kawakami@idaten.c.u-tokyo.ac.jp

INTRODUCTION

Recent studies have attempted estimation of moment arm (the distance between joint center of rotation and muscle line of action) for in vivo human muscles, by two-dimensional morphometrics using X-ray or MRI (Marshall et al. 1990; Rugg et al. 1990) and tendon travels using ultrasound (Ito et al. 2000; Maganaris et al. 2000). The latter method overcomes the uncertainty of determining joint center of rotation inherent in the former method, and can take a functional aspect of muscles into consideration. However, the major drawback of this method is a possible error of tendinous movement determination due to concurrent occurrence of tendon elongation (Maganaris et al. 2000). Here we propose a novel approach to take advantage of this tendon elongation for moment arm estimation.

METHODS

The relationship between joint moment (M), moment arm (r), and muscle force (F) is expressed as

$$M = rF$$

If we assume constant moment arms at different muscle force levels, then

$$\Delta M = r\Delta F$$

The elongation of tendinous tissues (ΔL) is a function of muscle force, i.e.

$$\Delta F = k\Delta L$$

where k is stiffness of the tendinous tissues at a linear region of the length-force curve where tendon elongation is linearly related to applied force. It thus follows that

$$\Delta M = rk\Delta L$$

$$\therefore \quad r = \frac{\Delta M}{k\Delta L}$$

Consequently, the moment arm is a linear function of the ratio of changes in muscle force and tendon length. Therefore, once we obtain this ratio for different joint positions, we can estimate the relative moment arms for those positions.

We applied this procedure to human Achilles tendon moment arm estimation in vivo. Subjects were six healthy men (23-46 yr, 172 ± 4 cm, 67 ± 8 kg, means ± SD). The subject lay prone with the knees fully extended, and the right foot was secured to a foot plate of an electrical myometer with the ankle joint set either at -15, 0, 15, and 30° (0°: anatomical position, positive values for plantar flexion). At each ankle position, the subject performed constant-level, submaximal and maximal plantar flexions isometrically. The torque levels were selected so that they were scattered over the whole range of torque from rest to maximal voluntary contraction. During contraction, B-mode real-time ultrasonogram (Aloka, Japan) was obtained for the distal attachment site of the gastrocnemius muscle fibers onto the Achilles tendon. At each ankle position, the attachment site moved proximally as the torque level increased, which was regarded as elongation of the Achilles

tendon. From the relationships between Achilles tendon elongation and torque at four ankle positions (Fig. 1), the linear regions were determined and slopes (torque / elongation) over these regions were calculated, and values relative to that of 0° were obtained. The absolute moment arm at 0° was derived from the length change of the whole gastrocnemius muscle-tendon unit (determined by 3D ultrasonogram, Aloka, Japan) for an angle change of 15° arc around 0°, from which, absolute moment arms at other positions were estimated.

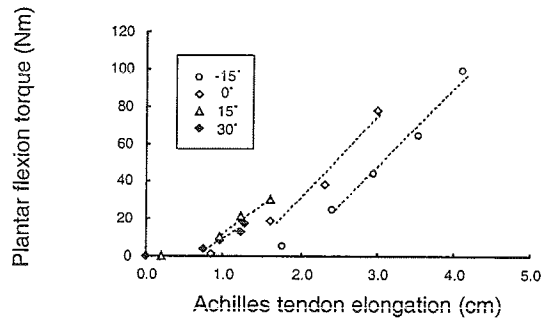

Figure 1: The relationship between Achilles tendon elongation and plantar flexion torque at four ankle positions. Example from one subject.

RESULTS AND DISCUSSION

Moment arms varied from 2.3 ± 0.7 to 4.1 ± 0.9 cm, and peaked at 0° (Fig. 2). These values were slightly smaller than, and the changes with respect to ankle positions were different from, those reported previously using MRI morphometrics (Rugg et al. 1990). These results might be related to the possible error in determination of joint center in the previous study, since the present values were similar (both for absolute values and their variations for ankle joint positions) to the measurements on cadaver specimens using the tendon travel method (Spoor et al. 1990). However, the present method might also have sources of errors inherent in the assumptions. For example, the moment arm can increase by muscle contraction (Ito et al. 2000; Maganaris et al. 2000) although we assumed constant moment arms at different torque levels. The contribution of other muscles than the gastrocnemius to plantar flexion torque might change at different ankle positions, as pointed out by Kawakami et al. (2000). These concerns should be clarified in further studies.

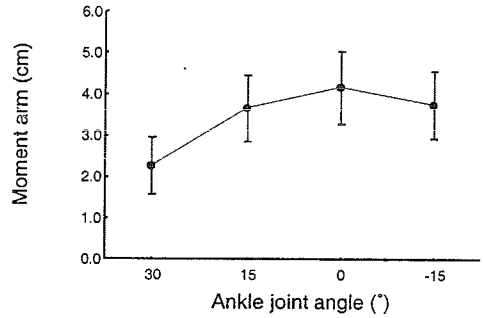

Figure 2: Estimated moment arms at four ankle positions. Means and SD from six subjects.

Muscle force estimation from joint moment relies greatly on the accuracy of moment arms. Considering anatomical variations, in vivo determination of moment arms as proposed in this study should be done for each individual.

REFERENCES

Ito, M. et al. (2000). J. Biomech., **33**, 215-218.

Kawakami, Y. et al. (2000). In: Skeletal Muscle Mechanics. John Wiley & Sons.

Maganaris, C.N. (2000). J. Biomech. **33**, 375-379.

Marshall, R.N. et al. (1990). Eur. J. Appl. Physiol., **61**, 263-270.

Rugg, S.G. et al. (1990). J. Biomech., **23**, 495-501.

Spoor, C.W. et al. (1990). J. Biomech., **23**, 1247-1259.

CHANGES IN *IN VIVO* APONEUROTIC DIMENSIONS UPON HUMAN MUSCLE CONTRACTION

Constantinos N. Maganaris

Active Life Span Research, Manchester Metropolitan University, Alsager ST7 2HL, UK, E-mail: C.N.Maganaris@mmu.ac.uk

INTRODUCTION

In modelling-based studies of muscle performance, the aponeurotic portion of tendon has often been treated as a rigid element (e.g. Huijing & Woittiez, 1985). In vitro experiments, however, have shown that aponeuroses posses elastic properties (e.g. Scott & Loeb, 1995). Aponeurotic deformations during muscle contraction have so far been measured after epimysial removal (e.g. Scott & Loeb, 1995). This procedure decreases the muscle force and pressure elicited during contraction (Garfin *et al.* 1981), thus indicating that *in vitro*-based aponeurotic deformations may not represent *in vivo* conditions. In the present study, changes in the resting-state dimensions of the central aponeurosis of the human tibialis anterior (TA) muscle during contraction were estimated *in vivo*.

METHODS

Measurements were taken in seven healthy men (age 23±4 years, height 172±3 cm, body mass 73.5±3 kg; mean±SD) at an ankle angle of 30° of plantarflexion, at rest and during isometric dorsiflexion maximum voluntary contractions (MVC) elicited against the footplate of a dynamometer (Lido, Loredan Biomedical, Davis). At each contraction state, the TA aponeurosis' length, the aponeurosis' width along its length and the aponeurosis' entire area were estimated *in vivo* using B-mode ultrasonography (Esaote Biomedica, Florence). Sagittal-plane scans over the myo-tendinous junction and the aponeurosis' proximal end were taken, and the distance between the echoes of these reference markers over the skin was assumed to be the aponeurosis' length. Axial-plane scans were taken every 1 cm along the aponeurosis' length to measure, by means of digitization, aponeurotic widths. The aponeurotic areas between the axial-plane scans were estimated and summed up to take the aponeurosis' entire area. Differences between resting-state and MVC-state dimensions were tested using a Student's *t*-test.

RESULTS AND DISCUSSION

All aponeurotic dimensions examined increased in the transition from rest to MVC. The aponeurosis' length increased from 165±6 to 177±6 mm (7%, $P<0.05$), the aponeurosis' width increased by between 8 and 21% (from 8.7±1 to 9.4±1.2 mm, and from 20.4±2 to 24.4±2 mm, respectively, $P<0.05$), and the aponeurosis' entire area increased from 2,327±197 to 2,715±202 mm^2 (17%, $P<0.05$). The aponeurotic lengthening in the experiment would be associated with the traction imposed by the contracting muscle. The aponeurotic widening may be associated with a medio-lateral fibre curvature due to intra-muscular pressure rise during contraction.

SUMMARY

The present results indicate that the TA aponeurosis behaves as a compliant

material during *in vivo* muscle contraction.
The methodology employed here allows cross-sectional and longitudinal design investigations, circumventing the problems associated with fascial removal under *in vitro* experimental conditions.

REFERENCES

Garfin, S. R., Tipton, C. M., Mubarak, S. J., Woo, S. L.-Y., Hargens, A. R. & Akeson, W. H. (1981). *J. Appl. Physiol.* **51**, 317-320.
Huijing, P. A. & Woittiez, R. D. (1985). *Neth. J. Zool.* **35**, 521-525.
Scott, S. H. & Loeb, G. E. (1995). *J. Morphol.* **224**, 73-86.

MUSCLE FIBER BEHAVIOR DURING DROP JUMP IN HUMAN

Tetsuo Fukunaga, Sadao Kurokawa, Senshi Fukashiro, and Yasuo Kawakami

Department of Life Science, University of Tokyo,
Komaba 3-8-1, Meguro, Tokyo, Japan
E-mail: fukunaga@idaten.c.u-tokyo.ac.jp

INTRODUCTION

Many human movements such as jumping and running involve muscle actions in which a concentric phase is immediately preceded by an eccentric phases. This is generally referred to as stretch-shortening cycle exercise (SSC). It is generally observed that mechanical power output and efficiency are enhanced in SSC, which has been attributed to some mechanisms, one of which is the storage of elastic energy during pre-stretch and its release. However no research has so far been done to determine in vivo behavior of muscle fibers and tendinous tissues in human movements during SSC. The purpose of the present study is to determine the in vivo behavior of muscle-tendon complex during drop jump by means of real-time ultrasonography and to discuss the functional role of contractile (muscle fibers) and elastic elements (tendinous tissues).

METHODS

Subjects. Eight healthy male subjects (age 23 ± 5 yr, height 1.72 ± 9.9 m, and body mass 68 ± 11 kg) participated in this study. All subjects gave their informed consent to participate in the experiment.

Experimental protocol. Subjects with bare feet performed several drop jumps (DJ) from a height of 0.2 m, keeping with their arms akimbo. During DJ kinematic, kinetic and ultrasonographic data as well as electromyograms from lower leg muscles were obtained simultaneously. The behavior of muscle fascicles (fiber) and tendinous tissues of gastrocnemius medialis were observed by means of real time ultrasonic apparatus (SSD-2000, Aloka, Japan) using electronic linear array probe of 7.5 MHz. The probe was carefully fixed onto the tissue surface with a specially designed tool and elastic tape to prevent oscillation, which may occur during jumping. The length of fiber was measured as the length of the echo that runs diagonally from the superficial to the deep along the fascicle. The fascicle angle (pennation) was obtained as the angle between the deep aponeurosis and the line drawn tangentially to the fascicles. During DJ the ultrasonic images of the MG were stored consecutively in the cine-memory of the ultrasonic apparatus set to operate at 40 frames/sec. The instantaneous length of MTC for MG was obtained from the equations developed by Grieve et al (1978). The length of tendinous structures was calculated

from following equation,

$$L_t = L_{mtc} - L_f \cdot \cos\theta$$

where L_f, θ, and L_{mtc} are fiber length, fiber angle and MTC length, respectively.

The force exerted by MG was calculated by the plantar flexion torque and moment arm, under the assumption of that the MG force was equivalent to the relative physiological cross-sectional area of MG to the total plantar flexor area (i.e. 15.4 % by Fukunaga et al 1996). Net joint torque around the ankle and knee were calculated using inverse-dynamics (Winter, 1990).

RESULTS

After touchdown of feet onto the force platform, the downward displacement of mass center of body (MCB) was turned toward upward before 100ms of toe off. During MCB downward-phase, the L_{mtc} increased by 4%, L_f decreased from 43 to 35 mm and L_t increased from 370 to 400 mm. After the MCB turned upward (upward-phase) the L_{mtc} decreased by 7 %, while the L_f kept approximately constant of 35 mm accompanying with decreasing of the L_t by 6.5 %. The fascicle angle changed due to changing L_f. Mechanical work during downward-phase were calculated positive 2.6 J for fascicle and negative 7.6 J for tendinous tissue. During upward-phase the fascicle exerted positive work of 1.9 J and the tendinous tissue performed positive work of 5.8 J.

DISCUSSION

Higher performance in DJ has been explained by the enhancement of mechanical work due to storage and reutilization of elastic energy (Komi, 1992). In the present study during downward-phase the tendinous structures stored elastic energy (equivalent to 66 % of total work of MTC) and remaining work of 34 % was originated from concentric contraction of muscle fiber. In the following upward-phase 76 % of the total mechanical work done by MTC was accounted from reutilize the elastic energy in tendinous tissue. The present results demonstrated that the explosive power during DJ is due to mainly rapid recoil of tendinous structures, allowing the quasi-isometric contraction of muscle fibers.

REFERENCES

Fukunaga, T. et al. (1996). J. Appl. Physiol., 80,158-165,1996

Grieve D. et al. (1978). Biomechanics VI-A, 405-412.

Komi, P. (1992). Strength and Power in Sport, Blackwell, pp169-179.

Kurokawa, S. (2001). J. Appl. Physiol., in press

Winter, D.A. (1990). Biomechanics and motor control of human movement.

RELATIVE MOTION OF THE RECTUS FEMORIS AND VASTUS INTERMEDIUS DURING KNEE EXTENSION

Deanna Asakawa[1,3], Silvia Blemker[1], Garry Gold[2,3], and Scott Delp[1]

Departments of [1]Mechanical Engineering and [2]Radiology, Stanford University
[3]Diagnostic Radiology Center, Palo Alto VA Health Care System, Palo Alto, California
Email: djasakawa@stanford.edu Web: www.stanford.edu/group/nmbl

INTRODUCTION

The long-term goal of our work is to understand the function of the rectus femoris muscle before and after surgical transfer of its distal tendon. In this surgery, the tendon of the rectus femoris is detached from the patella and reattached behind the knee. The surgery is performed in persons with cerebral palsy who walk with stiff-knee gait, and is thought to convert the muscle from a knee extensor to a knee flexor to assist in knee flexion during walking (Perry, 1987). However, stimulation of the muscle after surgery has revealed that it does not generate a knee flexion moment (Riewald and Delp, 1997). It is possible that scar tissue formed after surgery adheres the rectus femoris to the vastus intermedius and does not allow independent motion of the two muscles. Consequently, the ability of the rectus femoris to transmit force to its tendon and generate knee flexion could be compromised.

As a first step, we examined the relative motions of the rectus femoris and vastus intermedius in subjects with no surgical history. These two muscles share a common distal tendon, but the proximal regions are separated by a fascial plane. We hypothesized that in the absence of scar tissue the rectus femoris and vastus intermedius slide relative to one another during extension of the knee. Futhermore, because the rectus femoris inserts more anteriorly on the patella, we expected this muscle to displace more than the vastus intermedius. The purpose of this study was to test these hypotheses by measuring the displacements of the rectus femoris and the vastus intermedius muscles during knee extension in unimpaired subjects.

METHODS

We used cine phase-contrast magnetic resonance imaging (cine-PC MRI), a dynamic imaging technique, to capture muscle tissue velocity *in vivo* (Pelc et al., 1991; Pappas, 2000). One magnitude image and three velocity images (x, y, and z directions) are acquired for each time frame in a cine-PC MRI movie. Cine-PC MR images of the lower limb were acquired from 3 unimpaired subjects (age: 25-32 yrs, height: 5' 5" - 5'6", 2 female, 1 male) with a 1.5T GE scanner. The subjects were positioned supine with the thigh supported in 40° of hip flexion. Subjects were imaged as they actively moved their knee through 100 repeated cycles of knee extension/flexion from approximately 65° of flexion to near full extension at a rate of 35 cycles/min. A second set of images was acquired as the investigator moved the subject's relaxed leg. All images were acquired in the sagittal plane with a 17ms TR, 36 x 27 cm field of view, and 256x128 matrix with 24 time frames representing a complete motion cycle.

The displacement of square regions of interest in the mid-thigh portion of the rectus femoris (RF) and the vastus intermedius (VI) muscles (Fig. 1) were calculated by integrating the velocity image data (Zhu et al., 1996). We compared the displacements in RF to displacements in VI to assess the relative motion of these muscles.

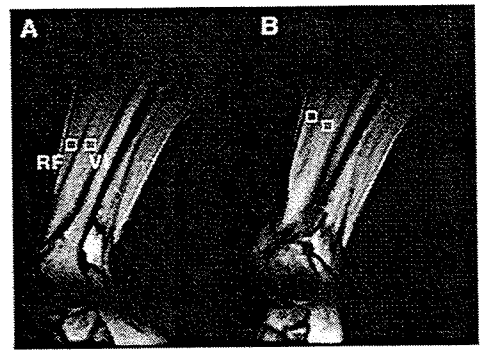

Figure 1. Sagittal plane cine-PC MR images of the thigh. Positions of 1-cm square tissue regions (white boxes) depict displacement of RF relative to VI during active extension from maximum flexion (A) to maximum extension (B).

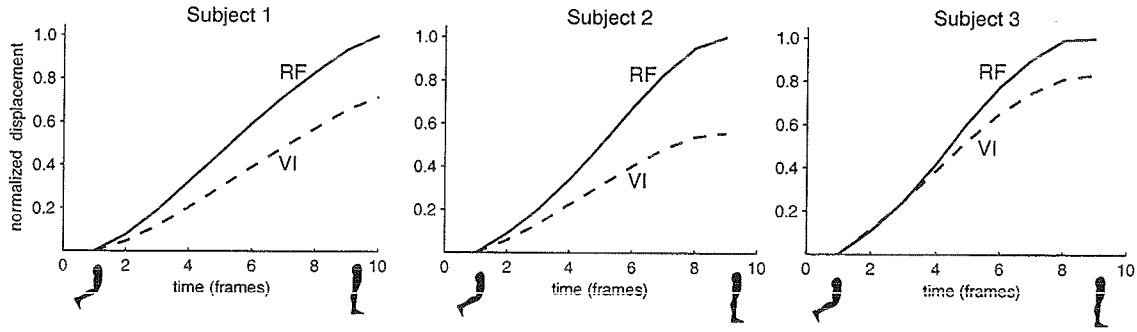

Figure 2. Displacements of the regions of interest within the rectus femoris (RF) and vastus intermedius (VI). Time frame 1 represents approximately 65° of knee flexion and time frame 10 represents the maximum knee extension achieved by the subjects. Displacements were normalized by peak RF displacement during active knee extension.

RESULTS

Displacements of the regions of interest were greater in the RF than in the VI (Figure 2). The maximum displacements of the RF during active extension were 2.1 cm (subject 1), 2.6 cm (subject 2), and 2.4 cm (subject 3). The VI displaced 17-44% less than the RF. When the subjects were moved by the investigator, the displacement trends were similar to the active case, with slightly reduced displacements. The maximum displacements of the regions of interest in RF for the passive motion case were 1.9 cm (subject 1), 2.0 cm (subject 2), and 2.2 cm (subject 3). The VI displaced 21-47% less than the RF when the investigator moved the limb.

DISCUSSION

The results of our study indicate that the rectus femoris slides relative to the vastus intermedius. Therefore, we believe that the fascia between the muscles allows the relative motion of these muscles in unimpaired subjects. The displacements of the regions of interest within the rectus femoris were greater than the displacements of the regions of interest within the vastus intermedius; this is consistent with the observation that the rectus femoris has a larger moment arm (Buford et al., 1997).

This study demonstrates that we can quantitatively assess the relative motions of muscles *in vivo* using dynamic MR imaging. In the future we will use cine-PC MRI to measure the relative displacements of the rectus femoris and vastus intermedius in subjects with cerebral palsy after rectus femoris transfer surgery. If the rectus femoris is functioning as a knee flexor after transfer, it will move in the opposite direction of the vastus intermedius. We plan to quantify rectus femoris displacement to determine if scarring of the fascial plane restricts relative motion of the rectus femoris and vastus intermedius. This work will evaluate how adhesive scar tissue affects the function of rectus femoris after surgery.

REFERENCES

Buford, WL et al. (1997). *IEEE Trans Rehab Med,* **5**, 367-79.

Pappas, GP (2001). Ph.D. Dissertation, Stanford University.

Pelc, NJ et al. (1991). *Mag Res Quarterly*, **7**, 227-54.

Perry, J (1987). *Dev Med Child Neurol*, **29**, 153-8.

Riewald, SR, Delp, SL (1997). *Dev Med Child Neurol*, **39**, 99-105.

Zhu, Y et al. (1996). *Magn Res Med*, **35**, 471-80.

ACKNOWLEDGEMENTS

We are thankful to George Pappas, John Drace, and Doug Schwandt. Funding provided by NIH Grant HD38962 and Graduate Fellowships from the Whitaker Foundation and the NSF.

FORCE ENHANCEMENT FOLLOWING STRETCH DURING HUMAN VOLUNTARY CONTRACTIONS

Hae-Dong Lee, Walter Herzog and Tim Leonard

Human Performance Laboratory, University of Calgary, Calgary, AB, Canada
E-mail: lee@kin.ucalgary.ca Web: www.kin.ucalgary.ca

INTRODUCTION

When an active muscle is stretched to a new length and held, the isometric force produced at the new length is greater than the isometric force at the corresponding length without preceding stretch (Abbott & Aubert, 1952). This property is referred to as force enhancement following muscle stretch (FE) (Herzog & Leonard, 1997).

FE has been well accepted and observed in various muscle or fibre preparations (Edman et al., 1978; de Ruiter et al., 2000; Morgan et al, 2000) using electrical stimulation. However, the mechanism responsible for FE is not well understood, and FE has never been reported for *in vivo* human voluntary contractions.

The purpose of this study was to investigate FE in *in vivo* human skeletal muscle during *voluntary contractions*.

METHODS

Effect of muscle stretch on force production was investigated for the adductor pollicis (n = 12) of the left hand of twelve volunteer subjects during electrically induced and voluntarily elicited contractions. Once muscle force reached the steady-state isometric force at the initial length, stretches of varying amplitude (10, 20 and 30 degree) and speed (10, 20 and 60 degree/s) were applied and held at the new length until the final steady-state isometric force was reached. The isometric force following stretch, and the passive force after deactivation of the muscle, were measured using a custom-built apparatus, and were compared with the corresponding purely isometric contractions.

We also investigated FE in *in situ* cat soleus (n = 8) for electrical stimulation. Once the isometric force at the initial length was achieved, muscles were stretched to a new length under various contractile conditions (i.e., 3, 6, and 9 mm stretch amplitude and 3, 9, and 27 mm/s stretch speed) and held at the final length until a steady-state force was reached. The isometric force following stretch and the passive force after deactivation of the muscle were measured.

RESULTS AND DISCUSSION

For human adductor pollicis, FE was observed during electrically induced and voluntary contractions, regardless of stretch conditions. During electrically induced contractions, FE increased with increasing amplitudes of stretch (Fig. 1) but was independent of stretch speed. For voluntary contractions, FE was independent of stretch amplitude (Fig. 2) and stretch speed. FE during voluntary contractions (12.0 ± 8.7 %) was smaller and more variable than FE obtained from electrical stimulation (14.9 ± 3.5 %). The passive force after active stretching of the muscle was greater (Fig. 1) than

the passive force obtained after isometric contractions.

The same results were obtained in cat soleus. FE was increased with increasing amplitude of stretch (Fig. 3) but was independent of stretch speed. The passive force enhancement was more pronounced in cat soleus than human adductor pollicis. This result may be caused by stretching the soleus in the mid-part of the descending limb of the force-length relationship, whereas the adductor pollicis tests were performed at about optimal length.

The results of this study suggest that FE is an actual property of *in vivo* human skeletal muscle during voluntary contraction. Furthermore, they indicate that passive elastic elements play an important role in producing FE, as had been speculated by Edman and Tsuchiya (1996). Unfortunately, this study cannot provide direct evidence for the origin of the passive FE. However, the giant molecular spring titin seems the most likely candidate. Future studies will need to address this issue.

REFERENCES

Abbott & Aubert (1952). *J. Physiology* 117, 77-86.

De Ruiter et al. (2000). *J. Physiology* 526.3, 671-681.

Edman et al. (1978). *J. Physiology*, 281, 139-155.

Edman & Tsuchiya (1996). *J. Physiololgy*, 490.1,191-205.

Herzog & Leonard (1997). *J. Biomechanics* 30(9), 865-872.

Morgan et al. (2000). *J. Physiology*. 522.3, 503-513

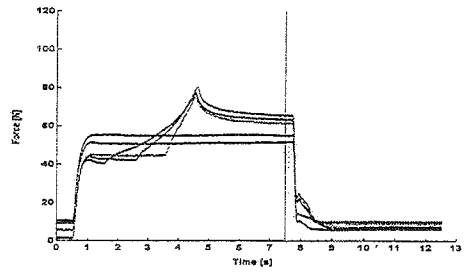

Figure 1. Force-time curves from electrically induced adductor pollicis for isometric reference contractions and stretches of 10, 20 and 30 deg.

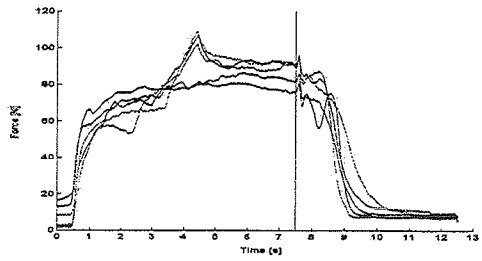

Figure 2. Force-time curves from voluntarily elicited adductor pollicis for isometric reference contractions and stretches of 10, 20 and 30 deg.

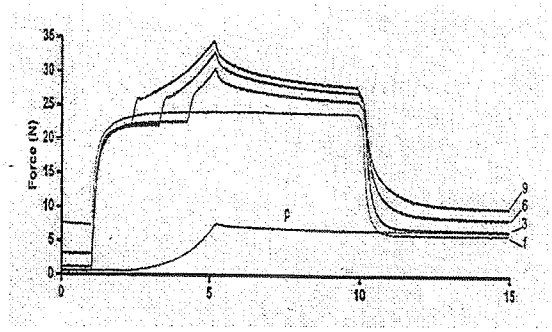

Figure 3. Force-time curves of cat soleus for an isometric reference contraction and stretch of 3, 6 and 9 mm on the descending limb of the F-L relationship. A passive stretch (p) is also shown.

ACKNOWLEDGEMENTS

The Natural Sciences and Engineering Research Council of Canada (NSERC)

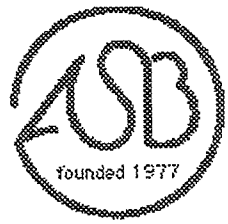

- PARALLEL SESSION -

Spine Biomechanics

Thursday, August 9, 2001
0900 to 1030

EFFECT OF SPECIMEN LENGTH FOR IN VITRO SPINAL MECHANICS TESTING

Duncan J. Kerr and James P. Dickey

Human Biology and Nutr. Sci., University of Guelph, Guelph, Ontario, CANADA
E-mail: jdickey@uoguelph.ca Web: www.uoguelph.ca/hb+ns/dickey.htm

INTRODUCTION

In vitro testing is an essential approach for studying spinal mechanics. Anatomical studies show that structures such as the supraspinous and longitudinal ligaments contain collagen fibers that span several spinal levels (Adams, 1995). Many researchers use functional spinal units (two adjacent vertebrae and all intervening tissue) for mechanical testing, however the effect of cutting the structures that span several levels has not been tested. The purpose of this study was to directly compare the effect of specimen length (number of vertebral levels) on in vitro spinal mechanics. This study focuses on the mechanical contribution of the posterior spinal ligaments.

METHODS

Thirteen porcine thoracolumbar spines were used in this experiment (L2-L5). Pure flexion-extension moments were applied using a spine testing apparatus (Dickey, 1998; Lysack et al., 2000). This machine applied continous cycles of moment between approximately 3 Nm of extension and 13 Nm of flexion. Two-dimensional kinematics were collected using reflective markers and videotape using a Peak5 system (Peak Performance Technologies, Engelwood, CO). This two-dimensional analysis is justified as the segmental motion in flexion-extension has been shown to be planar (Dickey, 1998). Loads were transduced using a six-axis load cell (JR3, 45E15A-E24E, Multi-Axis Load Cell Technologies, Woodland, CA). These loads were transformed into the spinal coordinate system to reflect the forces and moments acting at the L3/L4 segment of the spine (Cholewicki et al, 1996).

The testing involved performing five cycle of loading between 3Nm of extension and 13 Nm of flexion; analysis was perfomed on the data extracted from the fifth loading cycle.

Three loading conditions were performed on each lumbar specimen. The motion and loads for the L3-L4 levels were evaluated in all conditions. The first laoding condition (Long-Intact) involved testing the intact multi segment spine (L2-L5). The second condition (Long-Cut) involved cutting the supraspinous ligament at the L1/L2 and L4/L5 levels, while maintaining the multi segment spine. The third testing condition (FSU) involved cutting the specimen down to a L3-L4 functional spinal unit.

Moment-Angle curves were generated for each test, and the laxity zone (Tencer et al., 1995), stiffness, and range of motion parameters (Wilke et al., 1998) were extracted. Repeated measures one-way analysis of variance tests were performed to assess the statistical significance of observed differences.

RESULTS

We observed significant systematic differences in the mechanics of the L3/L4 motion segment when it was tested as part of a multi segment specimen compared to a functional spinal unit (Figure 1).

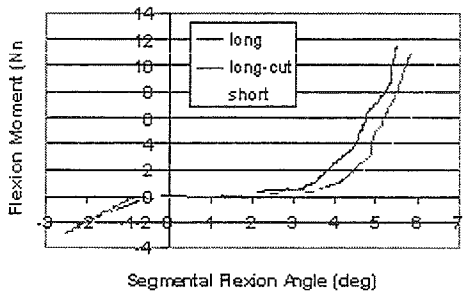

Figure 1: Moment-Angle curves for the three experimental conditions for a representative specimen.

The range of motion and laxity zones were significantly increased in the long-cut and FSU conditions compared to the long-intact condition (Figure 2).

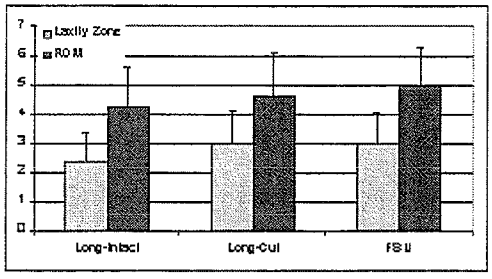

Figure 2: Laxity zone and range of motion for the three experimental conditions. The FSU and Long-Cut conditions are significantly different than the Long-Intact condition ($p<0.01$).

There were no statistically significant differences in stiffness between any of the conditions.

DISCUSSION

A number of researchers have stated that the mechanical integrity of the spine is disrupted when functional spinal units are tested (Adams, 1995; Wilke et al., 1998), yet few studies have quantified this effect. Kettler et al (2000) report that there are significant differences in both the flexion and extension ROM between the multisegment spine and the FSU. They analyzed the motion segments at the extreme ends of their multi segment constructs, which may be appropriate for assessing spinal implant mechanics. However, the boundary conditions for these levels were compromised, and accordingly their tests on multi segment spines does not represent physiologic spinal loading. The current study clearly illustrates that the mechanics of functional spinal units do not represent the mechanics of motion segments within the more physiologically appropriate multi segment spinal constructs. Accordingly, extreme caution should be used when using functional spinal units to assess spinal mechanics.

REFERENCES

Adams, M.A. (1995) *Spine* **20**:2151-6.

Cholewicki, J. et al. (1996) *Spine* **21**:2421-8.

Dickey, J.P. (1998) Ph.D. Thesis, Mechanical Engineering, Queen's University, Kingston, Ontario, Canada.

Kettler, A. et al. (2000) *Spine* **25**:543-50.

Lysack, J.T. et al. (2000) *J Biomech* **33**:765-70.

Tencer, A.F. et al. (1995) *Spine* **20**:2408-14.

Wilke, H.J. et al. (1998) *Eur Spine J* **7**:148-54.

ACKNOWLEDGEMENTS

Special thanks to Dr Jack Callaghan, Dr John Runciman and Mr Kevin Gillespie.

COMPRESSIVE BIOMECHANICS OF DEVELOPING SPINAL TISSUES

David Nuckley[1,2], Suzanne Hertsted[2], Jarrod Carter[2], Sohail Mirza[2], and Randal Ching[2]

[1]Department of Bioengineering and [2]Department of Orthopaedics and Sports Medicine
Applied Biomechanics Laboratory, Harborview Medical Center, Seattle, WA
E-mail: dnuckley@u.washington.edu

INTRODUCTION

Spinal column development, a dynamic interplay of cellular, chemical, and mechanical stimuli, involves morphologic changes that confer distinct mechanical properties to the hard and soft tissues of the spine (Ogden, 1994). These changes in tissue properties manifest epidemiologically as distinct spinal injury patterns throughout maturation (McGrory et al., 1993). The dearth of basic tissue mechanics data for the developing spine precludes the generation of injury prevention or management schemes to mitigate the devastating consequences associated with pediatric spinal injuries.

Our investigation into the developmental biomechanics of the spine utilizes the cadaveric baboon *(Papio anubis)* spine, an anatomic and kinematic analog to the human cadaveric spine, as our model. Using this model we evaluated the compressive mechanics of maturing hard (vertebrae) and soft (intervertebral) tissues in an attempt to understand the functional biomechanics of the spine throughout development. This basic science appreciation of developmental biomechanics will empower efforts to model, minimize, and manage pediatric spinal column injuries.

METHODS

Twenty, fresh cadaveric baboon cervical thoracic spines were obtained through the Washington Regional Primate Research Center. These specimens ranged in human equivalent age from 2.5 to 30-years based upon radiographic assessment of their skeletal maturity (Kuhns, 1998).

Specimen Preparation. Each specimen was dissected free of all musculature and then further dissected into functional spinal units: Occiput-C2, C3-4, C5-6, C7-T1 and an isolated vertebral body: T9. The functional spinal unit preparations involved the wiring of each vertebra and its fixation in poly-methylmethacrylate. Each vertebral body was dissected free of its posterior elements and fixed 1-mm deep into dental plaster for even load distribution.

Experimental Procedure. Compressive inputs were provided by a MTS (Model 858 Bionix, MTS Corp., Eden Prairie, MN) servohydraulic testing system at 0.5-mm/sec. Each specimen (functional spinal unit and vertebral body) was loaded 5 cycles to 40% body weight and the stiffness data was recorded on the final cycle. An inferiorly mounted six-axis load cell measured the force/moment response and the displacement was recorded using an LVDT. These data were collected at 200-Hz using LabVIEW (National Instruments, Austin, TX) data acquisition software.

Data Analysis. Specimen stiffness was computed as the slope of the linear portion of the load-displacement curve. A two-way ANOVA was used to make comparisons between soft (intervertebral) and hard (vertebral) tissue stiffness measures and to examine differences between functional spinal unit levels.

RESULTS

The compressive mechanics of the maturing spine reveals significant increases in stiffness with skeletal development for both

the functional spinal units ($p = 0.003$) and individual vertebral bodies ($p = 0.009$). Further, these values for the hard and soft tissues of the spine were found to be statistically different for a similar developmental age ($p < 0.001$). Figure 1 demonstrates the function whereby stiffness varies with skeletal development for both the hard and soft tissues.

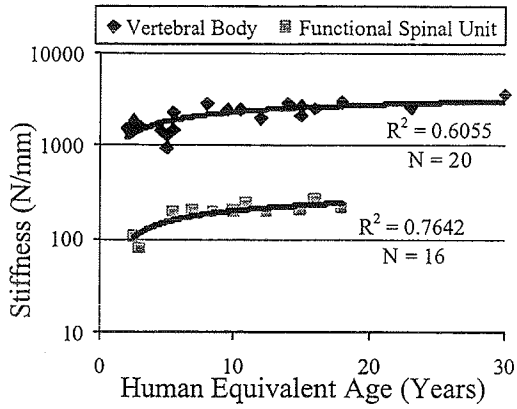

Figure 1: Compressive Stiffness as a Function of Development. The vertebral and functional spinal unit stiffness plots reveal similar exponential fits demonstrating magnitude differences between maturing hard and soft tissues of the spine.

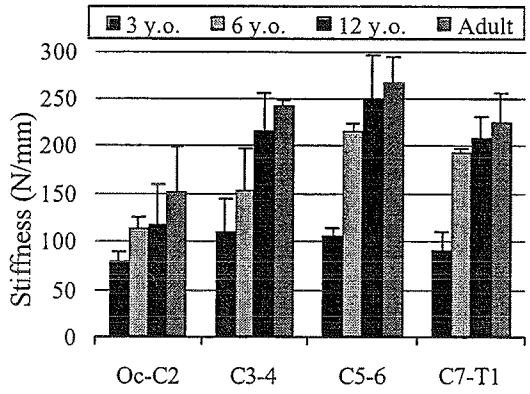

Figure 2: Functional Spinal Unit Compressive Stiffness by Development and Spinal Level. The data were grouped by age for this comparison. (N=4 for each group)

Level-specific differences in the compressive stiffness were discovered (Figure 2). A significant difference between the compressive stiffness of the Occiput-C2 level and each of the other levels exists ($p<0.028$). These results reveal changes in compressive mechanics between hard and soft tissues and between spinal levels all occurring throughout spinal development.

DISCUSSION

The compressive mechanical properties of spinal hard and soft tissues were measured and correlated with spinal development. These data clearly demonstrate age-related differences in the spinal biomechanics as well as tissue related differences. Moreover, level-specific differences were exhibited indicating differing mechancial properties along the length of the spine throughout development. Ultimately, these data will support tissue level modeling efforts aimed at effectively protecting children from spinal injuries and aide in the management of pediatric spinal column trauma.

REFERENCES

Kuhns L. (1998) *Imaging of Spinal Trauma in Children: An Atlas and Text.* Hamilton: B.C. Decker Inc.

McGrory BJ, et al. (1993). Acute fractures and dislocations of the cervical spine in children and adolescents. *J. Bone Joint Surg [Am],* 75, 988-95.

Ogden J. (1994) *Development and Maturation of the Axial Skeleton. In: Weinstein, The Pediatric Spine: Principles and Practice.* New York:Raven Press.

ACKNOWLEDGEMENTS

This research was supported by the National Highway Traffic Safety Administration and the National Center for Injury Prevention and Control (Centers for Disease Control).

BIOMECHANICAL ANALYSIS OF ANTERIOR SPINAL INSTRUMENTATION CONSTRUCTS FOR LUMBAR FUSIONS

Andrew Mahar[1], Kevin Fricka[2], Peter Newton [1,2]

[1]Orthopedic Biomechanics Research Center, Children's Hospital – SD, San Diego, CA, USA
[2]Department of Orthopaedics, University of California – SD, San Diego, CA, USA
Email: amahar@chsd.org

INTRODUCTION

Corrective surgery for scoliosis with anterior instrumentation can be accomplished with different constructs: single rod, single rod with interbody cages and dual rods. These varying constructs are most often used in the lumbar spine to generate a fusion mass while retaining the natural lordosis of the lumbar region (Sweet, 1999). In a pediatric population or in smaller adults, two screws cannot often be implanted into a single vertebral body due to the body's limited size. Previous work has compared the rigidity of one rod versus two rods (Kaneda, 1996) but no information exists directly comparing the stability of a single rod augmented with an interbody cage against a dual rod construct (Glazer, 1997). This study was initiated to determine stiffness differences in extension, lateral bending and axial torsion between 4 possible lumbar constructs: a single rod (Group 1), a single rod plus interbody cages (Group 2), two rods (Group 3) and two rods plus interbody cages (Group 4).

METHODS

Eight bovine lumbar spines from L1 to L6 were harvested from twelve week old calves. Muscular tissue was removed from each specimen while keeping ligamentous structures intact. Each specimen was randomly assigned a device order using 5mm Moss-Miami anterior instrumentation (DePuy, Warsaw, IN). Full discectomies and end plate removal were performed at the L2-3, L3-4 and L4-5 disc spaces. An MTS machine (Eden Prairie, MN) applied non-destructive, eccentric bending moments. The flexion/extension and right/left lateral bending testing protocol consisted of an axial preload of 5 N and an applied bending moment of 5.2 Nm. Eccentric bending moments were applied in displacement control at 5 mm/s with a static lever arm of 12 cm and a maximal force cutoff of 44 N. The torsion testing protocol consisted of an axial preload of 5 N and an applied ± 2 Nm torsional moment applied in torsional control at 0.4 Nm/s (Ashman, 1989). Data from the machine were sampled at 10Hz for the force, displacement, angle and torque channels. Construct stiffness (Nm/deg) for each load condition was compared using a two-way ANOVA combined with Tukey's *post-hoc* correction to compare the one rod/cages with two rods/no cages constructs.

RESULTS/DISCUSSION

Stiffness data for each group and loading condition is shown in Table 1. For flexion, extension and torsion, as more instrumentation was placed in the spine, there was a trend toward greater stiffness. For the lateral bending conditions, there was no significant difference between groups.

The addition of cages to the rod systems increased construct stiffness in flexion ($p=0.04$), but not in all other loading conditions (Figure 1).

Figure 1: Flexion stiffness for each group.

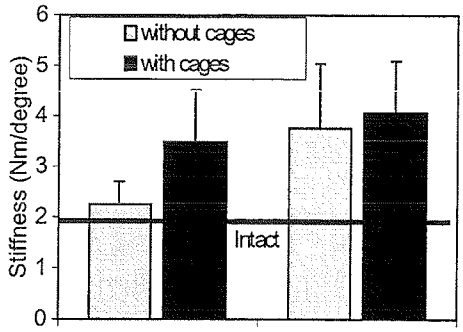

The two rod system was significantly stiffer than a single rod in flexion ($p=0.01$), extension ($p=0.03$), and torsion ($p=0.02$), but not in lateral bending. When comparing one rod/cages and two rods/no cages there was no statistically significant difference in stiffness for any condition.

Dual rods provided significantly higher construct stiffness than a single rod. The use of interbody cages resulted in significantly higher construct stiffness in flexion than when cages were not used. There was no difference in stiffness when comparing one rod/cages vs. two rods/no cages for any condition. Single rod/cage constructs have the advantage of decreased operative time, are not limited by vertebral body dimensions and maintain lateral plane correction because the cages prevent anterior collapse of the spine.

Table 1: Overall Construct Stiffness Data (Nm/°)

	Flexion	Extension	Right Lateral Bending	Left Lateral Bending	Axial Torsion
1 rod/no cages	2.26 + 0.44	1.83 + 0.31	1.72 + 0.36	2.67 + 0.67	0.78 + 0.20
1 rod with cages	3.49 + 1.02	2.11 + 0.28	2.05 + 0.92	2.60 + 0.58	0.95 + 0.37
2 rods/no cages	3.76 + 1.03	2.58 + 0.86	1.97 + 0.83	3.22 + 1.14	1.14 + 0.29
2 rods with cages	4.07 + 1.03	2.65 + 1.21	1.80 + 0.52	2.75 + 0.63	1.19 + 0.42

SUMMARY

The primary purpose of this study was to compare the performance of one rod plus cages versus two rods without cages during physiologic loading. Since these constructs performed the same in each condition, it is possible to use a single rod and cage to maintain lumbar lordosis and provide equal fusion possibilities as that of the two rod system.

REFERENCES

Ashman RB, et al. (1989) *J Spinal Disord*, **2**, 274-81.

Glazer PA, et al. (1997) *Spine*, **22**, 171-82.

Kaneda K, et al. (1996) *Spine* **21**, 1250-61; discussion 61-2.

Sweet FA, et al. (1999) *Spine* **24**, 1655-62.

ACKNOWLEDGEMENT

This research was financially supported by the Children's Hospital Orthopedic Research Foundation.

VERTEBRAL KINEMATIC DESCRIPTIONS BASED ON IN VIVO MEASUREMENT OF SURFACE MARKER MOTIONS

Xudong Zhang, Jinjun Xiong, and Angela Bishop
Biomechanics and Ergonomics Laboratory, University of Illinois, Urbana, IL, USA
E-mail: xudong@uiuc.edu Web: www.staff.uiuc.edu/~xudong

INTRODUCTION

Among various techniques and systems for acquiring spinal kinematic data (Gracovertsky et al., 1995; Lundberg, 1996; Marras et al., 1992), the most direct non-invasive in vivo measurement still relies on the use of skin-surface markers or sensors. Markers as skin-based rigid posts have been devised to estimate lumbarsacral orientation (Anderson et al., 1986; Chen et al., 1997) and external spinal profile (Bryant et al., 1989). Spherical markers may also be directly adhered to the skin over spinous processes to attain gross spinal kinematic information (Gram & Hasan, 1999). However, a more elaborate assessment of the kinematics of individual vertebrae, through measuring the surface marker motions, has been difficult. This is due mainly to, besides other challenges (Lundberg, 1996), the fact that the small separation between spinous processes poses a limit on the size of or the distance between markers (or sensors). This limit would be even more stringent for dynamic situations when marker interference becomes more probable. Recent advances in instrumentation technology have enabled considerable improvement on the accuracy and resolution of the motion measurement systems. For instance, an evaluation of contemporary motion measurement systems (Richards, 1999) showed that a millimeter level of resolution (minimal discriminable inter-marker distance) is achievable by some of the newest opto-electronic systems. Such technological advancement can be fully exploited to better capture and understand the kinematic characteristics of the human spine.

The purpose of this study was to explore the feasibility of quantifying vertebral kinematics by in vivo measurement of skin-surface marker movements. We proposed a novel method to derive, from measured surface marker trajectories, the centers of rotation for individual vertebrae during two-handed symmetric lifting.

METHODS

Ten adult subjects (5 m, 5 f) participated in an experiment in which they lifted a 15-lb box from the floor up to a chest-height shelf, at a self-preferred pace and in a sagittally symmetric manner. Reflective spherical markers were placed over subjects' surface landmarks corresponding to major body joints (e.g., shoulders, elbows, hips, and knees) and seven spinal processes (C7, T7, L1-L5). Only the ones illustrated in Fig. 1a were relevant and thus analyzed in the current study. Note the markers in the lumbar spine region were 9 mm in diameter, and the rest were 25 mm. The marker placement was conducted under the guidance of an experienced physical therapist. A five-camera Vicon 250 system

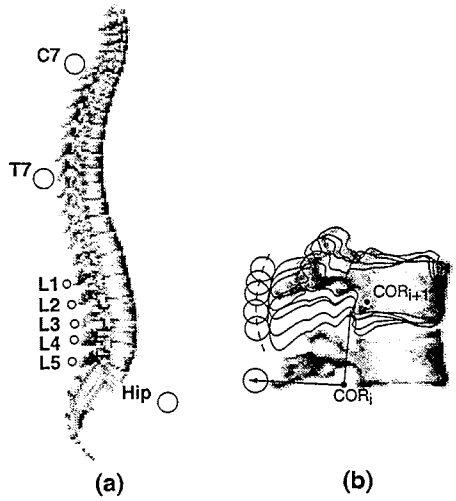

Figure 1: Illustrations of (a) marker placement scheme, and (b) vertebral center of rotation derivation based on a minimum marker set.

was employed to capture the motions at a frequency of 120 Hz. The acquired 3D marker location data were projected onto the mid-sagittal plane and thus simplified as 2D data, while the bisection of two greater trochanter markers was used to represent the hip joint (Fig. 1a). The derivation of vertebra center of rotation (COR) locations was based on the assumption that a vertebral segment follows a circular trajectory with respect to a local reference frame affixed to its adjacent segment(s). Given that there was only one marker attached to each presumably rigid vertebral segment, construction of a local frame was made possible by utilizing the COR coordinates pre-determined for the lower adjacent segment (Fig. 1b). This procedure was repeated recursively in the "bottom-up" direction, with the initial frame constructed from known coordinates of the L5 and hip markers. An optimization routine was created to identify the circle that best fit a marker trajectory expressed in the respective local coordinate system, by minimizing the fitting error:

$$e(a,b,r) = \frac{1}{n}\sum_{i=1}^{n}(\sqrt{(x_i-a)^2+(y_i-b)^2}-r)^2$$

where x_i and y_i $(i = 1...n)$ are the marker coordinates in the local frame, (a, b) is the center of the circle, and r the radius. Algorithm determining the a, b, and r of the maximum-likelihood circle (Rorres & Romano, 1997) was implemented numerically based on the Nelder-Mead simplex search (1965).

RESULTS AND DISCUSSION

Table 1 presents a sample of the results from this study. The initial inter-marker distance (d) values provide a reality-check of the marker placement and a reference for the derived centers of rotation. Except for the upper thoracic (C7-T7) segment, the COR locations (not presented) and r values seem plausible; the latter varied in a reasonable range across subjects, and had very small within-subject trial-to-trial variabilities. The assumed circularity of marker trajectories, and adequacy of the proposed analysis method, are supported by favorable e/r ratios for all but the C7-T7 segment.

SUMMARY

This work has demonstrated the viability of using in vivo measurement of spinal surface marker motions and novel analytical means to quantify vertebral kinematics. Such capability will facilitate investigating the biomechanics of human spine, particularly the lumbar spine, in a more discerning yet non-invasive manner.

REFERENCES

Anderson, C.K. et al. (1986). *Spine*, **11**, 456-462.

Bryant, J.T. et al. (1989). *Spine*, **14**, 258-265.

Chen, Y.L., Lee, Y.H. (1997). *Clinical Biomechanics*, **12**, 185-189.

Gracovertsky, S. et al. (1995). *Spine*, **20**, 1036-1046.

Gram, M.C., Hasan, Z. (1999). *Spine*, **24**, 169-177.

Lundberg, A. (1996). *Human Movement Science*, **15**, 411-422.

Marras, W.A. et al. (1992). United States Patent #5094249.

Nelder, J.A., Mead, R. (1965). *Computer Jounral*, **7**, 308-313.

Richards, J.G. (1999). *Human Movement Science*, **18**, 589-602.

Rorres, C., Ramano, D.G. (1997). *SIAM Review*, **39**, 745-754.

Table 1: Mean (±S.D.) values for d—the initial inter-marker distance while subjects assuming an upright standing posture, r—the derived marker-COR distance or radius of fitted marker trajectory, and e/r—normalized fitting error.

	C7	T7	L1	L2	L3	L4	L5
d	192±8	174±11	27±2	23±2	22±2	22±2	
r	636±307.9	329±165	68.5±38.4	58.9±31.9	46.3±21.6	22.8±7.0	
e/r	.15±.098	.05±.037	.01±.007	.02±.007	.04±.035	.07±.034	

AN *IN-VIVO* ASSESSMENT OF PANJABI'S THEORY OF SPINAL INSTABILITY USING EMG

Sheri P. Silfies and Andrew R. Karduna
Rehabilitation Sciences, MCP Hahnemann University, Philadelphia, PA, USA
email: silfies@drexel.edu

INTRODUCTION

Researchers have proposed that the muscular system plays an essential role in spinal stability, demonstrating that muscle coactivation is necessary to stabilize the healthy spine around a neutral spine position (Panjabi, 1992; Cholewicki and McGill, 1996; Cholewicki et al., 1997). Panjabi further hypothesized that spinal instability, which results in a compromise of the passive support system, requires compensation by trunk musculature to maintain spinal stability (Panjabi, 1992). The purpose of this study was to test Panjabi's theory by investigating trunk muscle activity levels around the neutral spine position in patients with clinical lumbar instability and healthy adults.

MATERIALS AND METHODS

Subjects-Ten subjects (6 female, 4 male, age 29-48) were studied with IRB approval. Five healthy controls were matched on the basis of age and gender to five subjects diagnosed with lumbar segmental instability. Segmental instability was defined as disc degenerative changes on MRI and corresponding positive discography. Additionally, these patients had pain that was limiting function, a pain history greater than seven months and segmental instability at two or more lumbar levels. The healthy subjects had no history of low back pain that limited function or required medical intervention.

Electromyography (EMG)- Pre-amplified surface electrodes (Motion Control, Inc., Salt Lake City, UT) were applied bilaterally over five trunk muscles: internal oblique/transverse abdominus, external oblique, rectus abdominus, lumbar multifidus and lumbar erector spinae group. Data were collected at 1248 Hz, amplified and bandpass filtered (10-750 Hz). Standardized submaximal reference contractions were collected for normalization of EMG amplitude values.

Kinematics- An electromagnetic tracking device (Polhemus 3Space Fastrak, Colchester, VT) was used to collect three dimensional trunk kinematics. A receiver was placed over the L1 spinous process using double-sided tape. Anatomical axes were derived from calibration of the subject in a relaxed standing posture. Trunk angle was referenced to the global reference frame.

Figure 1: Reaching activity mid-range.

Protocol- Subjects performed three repetitions of active forward reaching with their arms maintained at 90°of flexion (Figure 1). EMG and kinematic data were collected simultaneously using LabVIEW 5.1 (National Instruments, Austin, TX). Reaching was performed with no weight and while holding a 10-pound sandbag.

Data Analysis- EMG data corresponding to the neutral position (0° trunk flexion) were processed using an RMS filter and normalized to the previously collect reference contractions (DeLuca, 1997). The data were averaged over all three trials of forward trunk motion. Descriptive statistics were used to identify trends and statistical significance was assessed with t-tests.

RESULTS

In both conditions, four out of five muscles in the instability group demonstrated higher levels of muscle activation at the neutral spine position (Figure 2). Despite the small subject pool and high variability within the instability group the three abdominal muscle groups approached significance. All muscles dramatically increased activity between the no load and 10-pound condition (Figure 3). However, only the erector spinae muscles in the instability group demonstrates a significant increases in activation level ($p \leq 0.05$).

DISCUSSION

Results of this study are consistent with pervious *in-vivo* research on healthy subjects reporting a baseline level of muscle coactivation around a neutral spine position and greater levels of coactivation with increasing loads. (Cholewicki, et al., 1997) It is acknowledged that muscle activation levels reported here are higher than previous research, however, secondary to the low back pain group, normalization was performed using standardized submaximal contractions. These data are consistent with biomechanical models that have predicted increased trunk muscle coactivation secondary to passive subsystem damage (Cholewicki and McGill, 1996). The trends in these data support Panjabi's theory that greater muscle coactivation may occur in subjects with clinical lumbar instability. Additional subjects will be tested using this protocol and may provide evidence to support specific muscle activation patterns or recruitment strategies that would assist with rehabilitation of low back pain patients diagnosed with segmental instability.

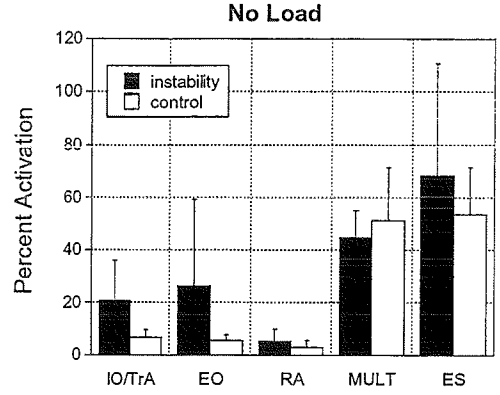

Figure 2: Normalized group mean (SD) for each muscle, right side only, at the neutral spine position in the no load condition.

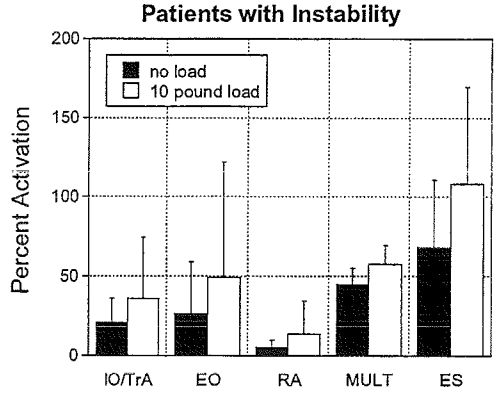

Figure 3: Instability group mean (SD) for each muscle, right side only, no load vs.10-pound condition.

REFERENCES

Cholewicki, J., McGill, S.M. (1996). *Clin Biomech,* **11**, 1-15.

Cholewicki, J. et al. (1997). *Spine* **22**, 2207-2212.

DeLuca, C.J. (1997). *J Appl Biomech,* ***13***,135-63.

Panjabi, M.M. (1992). *J Spinal Disord,* **4**, 383-97.

EFFECT OF LIFTING SPEED ON THE BIOMECHANICAL BEHAVIOR OF THE LUMBAR SPINAL MOTION SEGMENT

Raghu N Natarajan[1] and Gunnar BJ Andersson[1]

[1]Department of Orthopedic Surgery, Rush-Presbyterian-St.Luke's Medical Center, 1653 West Congress Parkway, Chicago, Illinois 60612, E-mail: rnataraj@rush.edu

INTRODUCTION

Epidemiological studies suggest that repetitive lifting is of importance in the development of back injuries including, disc injuries. None of the cadaveric studies or model studies existing in literature reflects the type of repetitive loading that causes disc failures. Clearly, in-vitro studies are limited when it comes to understanding the relationship that exist between the large number of parameters needed to describe a single loading and how the disc tissue break down over the course of many years of exposure. An improved understanding of these complex relationships can best be achieved by finite element modeling. With the help of a poro-elastic finite element model of a lumbar disc, biomechanical responses due to a slow (1 lift per minute) as well as a fast lifting activity (3 lift per minute) are studied here. The hypotheses of the current study are that (1) during initial stages of lifting, the disc stiffness decreases during both slow and fast lifting activity and (2) the rate of decrease in disc stiffness is faster during fast lifting activity.

MATERIALS & METHODS

A three-dimensional finite element model (L3-L4) (1), was modified to include poro-elastic components. Permeability and porosity values for the nucleus, annulus, endplate, cancellous bone and cortical bone were taken from the literature (2). The drained elastic modulus and Poisson's ratios for all the disc components were also taken from the literature (2). Initial disc pressure used in the subsequent analyses was obtained by applying a compressive load of 400 N on to the motion segment with a boundary condition preventing fluid from flowing out of the disc. This resulted in an internal disc pressure of 0.8 MPa.

The model was validated for dynamic loading conditions (3) in which a compressive preload of 400 N and a peak-to-peak compressive load of 430 N was applied cyclically for 30 loading cycles at three frequencies, 0.01 Hz, 0.1 Hz and 1.0 Hz. The dynamic stiffness of the disc calculated from the finite element results followed a similar trend and fell within one standard deviation of the experimental results.

Load acting on the lumbar motion segment during each lift was simulated in the finite element model by applying maximum compression force of 1000 N combined with a maximum flexion moment of 10 Nm. Time taken to perform each lift was assumed as 3 seconds. During first half of the lifting period the load reached the maximum while during the second half the motion segment was unloaded. Between two lifts (57 seconds for 1 lift per minute and 17 seconds for 3 lift per minute) the disc carried the upper body weight (400N) only. The study was conducted over 100 lifts. The loads were applied to the superior surface of L3 while the inferior surface of L4 was fixed in all degrees of freedom.

RESULTS

During initial 60 lifts both disc compression stiffness (Figure 1) and disc flexion stiffness (Figure 2) decreased non-linearly as the number of lifts increased. Maximum decrease in stiffness occurred in compression (of the order of 40%) while the corresponding decrease in flexion stiffness

was only of the order of 15%. After the initial 60 lifts, rate of decrease in both compression and flexion stiffnesses were very small (1% over the rest 40 lifts).

During the initial 60 lifts, rate of decrease in disc compression stiffness remained same as the lifting progressed both during slow and fast lifting activity (44%). On the other hand for the same period, rate of decrease in disc flexion stiffness was higher during fast lifting activity. One lift per minute reduced the flexion stiffness by 15% while three lifts per minute reduced the flexion stiffness by a larger amount (18%).

After the initial 60-lift period, rate of decrease in compression stiffness was slightly higher during fast lifting activity while the rate of decrease in flexion stiffness remained same in both slow and fast lifting activity.

DISCUSSION

A non-linear, poro-elastic finite element model including fluid flow between the disc and the surrounding tissues showed that the disc became flexible rapidly during initial lifting period suggesting that the spine is more susceptible to injury during this period. Fluid is forced out of the nucleus with each loading cycle thereby reducing the volume of the fluid inside the disc each time the load is applied. This loss of fluid volume in the nucleus allows for an increased amount of deformations with each load application thus explaining why the disc stiffness reduces rapidly. During the initial lifting phase, percent reduction in the disc compression stiffness was twice as much as the reduction in flexion stiffness. This result leads to the conclusion that the disc is vulnerable more under compression than under flexion.

The current study showed that the lifting speed had no effect on rate of decrease in compression stiffness while higher lifting speed induced larger reduction in flexion stiffness as lifting progressed. This leads to the conclusion that if lifting involves flexion, higher speed of lift should be avoided from injury point of view.

REFERENCES

(1) Natarajan RN and Andersson GBJ, (1999), Spine: 24:1873-1881

(2) Argoubi M and Shirazi-Adl, (1996), J. of Biomechanics: 29:1331-1339

(3) Siping L et al., (1995), J. of Biomechanics: 28(7):779-790

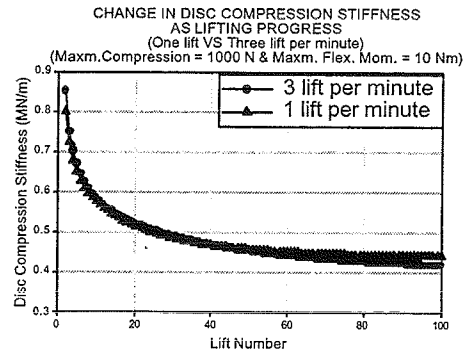

Figure 1: Disc compression stiffness decreased non-linearly over the first 60 lifts during both slow and fast lifting modes. Subsequent to this, rate of decrease in disc stiffness was very small.

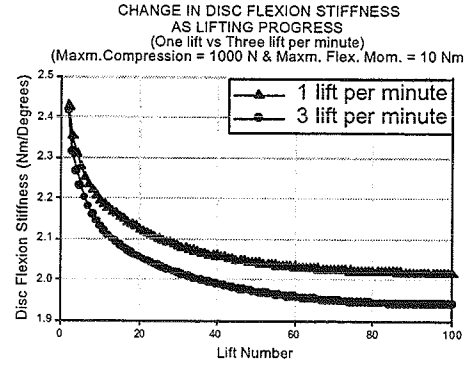

Figure (2) The rate of decrease in disc flexion stiffness was higher during fast lifting activity. Subsequent to the initial 60 lifts, rate of decrease in disc stiffness was very small during both fast and slow lifting modes.

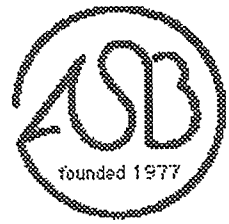

- PARALLEL SESSION -

Symposium

In Vivo Muscle Function in Animals

Thursday, August 9, 2001
1100 to 1230

Tendon Force Transducers: Their Use in Musculoskeletal Biomechanics and Neural Control

Robert J. Gregor

Department of Health and Performance Sciences and Center for Human Movement Studies
Georgia Institute of Technology, Atlanta, GA, USA

INTRODUCTION

Tendon force transducers have been used in research involving musculoskeletal biomechanics and the neural control of movement for over thirty years. Investigators interested in the use of different skeletal muscle fiber types and whole muscle, bi-articular vs. uni-articular muscles and their selection by the nervous system in the control of movement, and changes in muscle structure and function as a result of selected interventions, e.g. compensatory hypertrophy or reinnervation, would like to know the nature of the forces produced by the muscles under study. Knowledge of such forces, in-vivo, has also been used to evaluate force/emg relationships and selected muscle models related to force prediction during selected forms of movement.

As a measurement tool tendon force transducers are commonly used in conjunction with muscle length measurement systems and emg to more completely evaluate muscle performance. Synchronization of these measurements with motion capture data, e.g. video, in an effort to understand the role of the neuromuscular system during different movement forms, is common.

The purpose of this presentation will be to place this system of measurement in perspective as it relates to biomechanical, neurophysiological and physiological questions. The advantages and disadvantages of such a system will be discussed and specific reference made to locomotion in the adult cat.

METHODS

Tendon force transducers were used in two sets of experiments, one set designed to compare the force-velocity properties of the cat soleus muscle in-vivo and in-situ and a second set to evaluate the performance of the same muscle during slope walking in the adult cat. In the first set motion capture provided kinematic data during level treadmill locomotion at increased speed while synchronized data from tendon force transducers provided muscle force data during the same trials. Terminal experiments were conducted to evaluate the in-situ force/velocity properties of the same muscle.

The second series of experiments focused on movement control and slope walking as a perturbation to the neuromuscular system in the adult cat. A series of slopes varying from a –75% slope to a +75% slope, in increments of 25%, was used. High speed video provided kinematic data, a force platform concealed in the walkway floor provided ground reaction forces and center of pressure data, and tendon force transducers and implanted patch emg electrodes provided data on soleus muscle output. Slopes were randomized within and across four cats and each cat walked at a self-selected comfortable speed. Data were collected over a two-week period of time.

RESULTS

Data on soleus output during level treadmill locomotion indicate force; mechanical work and power increased as treadmill speed increased. These increases were greater at the faster treadmill speed, in-vivo, then would be predicted from the in-situ force/velocity relationship of the same muscle. Muscle-tendon unit lengths increased markedly as treadmill speed increased, as did lengthening velocities during the yield phase in early stance. Soleus output appeared to be enhanced during the shorting action of the muscle in late stance by the stretch imposed on the muscle during early stance.

Data on slope walking, to date, are mixed regarding soleus output. Plantar flexor moments increase as upslope intensity increases but soleus peak forces appear to decline. In a separate cat, soleus emg appeared to increase as upslope intensity increased. Data are considered preliminary and reasons for this possible discrepancy will be discussed.

During downslope walking the soleus muscle plays a major role in controlling ankle joint kinetics. The moment at the ankle appears to decline as downslope intensity increases but soleus peak force does not. The muscle undergoes a significant amount of stretch during early stance but contributes considerably more than other plantar flexors during the entire stance phase.

Ongoing experiments will be discussed related to slope walking.

REFERENCES

Fowler, E.G. et al. (1993) J. Biomechanics, **26**, 465-483.

Gregor, R.J. et al. (1988) J. Biomechanics, **21**, 721-732.

Gregor, R.J. et al. (1999) Proceedings XVIIth ISB Congress, Calgary, Alberta, Canada, pg. 367.

Smith, D.W. et al. (1997) Society for Neuroscience Abstr., **23**, 760.

INSIGHTS INTO MUSCLE FUNCTION FROM MINIMALLY INVASIVE RECORDING

[1,3]John A. Hodgson, [1,2,3]V. Reggie Edgerton, [3]Roland R. Roy
Departments of [1]Physiological Science and [2]Neurobiology, and [3]The Brain Research Institute, UCLA, Los Angeles, CA 90095-1606 USA.
Email: jhodgson@ucla.edu.

INTRODUCTION

The development of implantable tendon force transducers capable of measuring in-vivo tendon force supplemented available electromyogram (EMG) (Engberg & Lundberg, 1969) and length measurements (Goslow et al., 1973) settled much of the speculation about how muscle operated and allowed researchers to focus more on the function of muscles. At the same time, an interest in spaceflight, where microgravity results in much lower levels of muscle loading than on Earth, stimulated even further interest in the role of muscle force in physiological function. Over time, the perception of muscle has evolved from that of a contractile tissue tugging on tendons to that of a complex organ system with sensory (Abelew et al., 2000) and endocrine roles (McCall et al., 2000) in addition to its role as a sophisticated biomechanical engine, all of which are extremely responsive to changes in environmental conditions.

Interest in muscle force measurement has covered many species and a sampling of many muscles operating under a variety of conditions (Biewener & Roberts, 2000; Binding et al., 2000; Gregor & Abelew, 1994 ; Shadwick et al., 1999). In order to better understand the conditions that may play an important role in a muscle's response to environmental factors, it is also important to study the conditions under which muscles are most commonly used.

EMGs recorded continuously over a day or more suggest widely differing levels of activity across species and between the different muscles of individual subjects (Alford et al., 1987; Blewett & Elder, 1993; Hensbergen & Kernell, 1998). Rat muscle appear to be highly active for prolonged periods of time whereas cat muscles exhibit much shorter periods of activation. Postural muscles such as the soleus (Sol), possessing a substantial population of 'slow' twitch fibers are more active than other muscles with a mixed fiber type population. We have recently concluded a similar study of EMG activity and medial gastrocnemius (MG) tendon force in the caged Rhesus monkeys.

METHODS

EMG electrodes were implanted in the Sol, MG, tibialis anterior (TA) and vastus lateralis (VL) muscles of 8 Rhesus monkeys. Tendon force transducers (Konigsberg Instruments, Pasadena, CA) were placed on the MG tendon. Telemetered EMG and force data were recorded continuously over 24-hour periods between 1 and 4 months after implantation. Additional recordings were made during bipedal and quadrupedal treadmill locomotion.

RESULTS AND DISCUSSION

Results from 8 animals show that the Sol muscle was the most active muscle but that it was active for less than 4 hours (average 2.5 hours) in a 24-hour period. TA, active for an average of 1 hour per day, was the least active muscle. The distributions of

EMG amplitudes suggest that activation levels sufficient to recruit all motor units occurred for only a few seconds per day and force recordings from MG suggest that such activation levels would be accompanied by forces close to a maximal tetanic contraction. The distributions of EMG amplitudes during locomotion differed from those observed over a 24-hour period, suggesting that behaviors other than locomotion contributed a majority of the overall daily muscle activity.

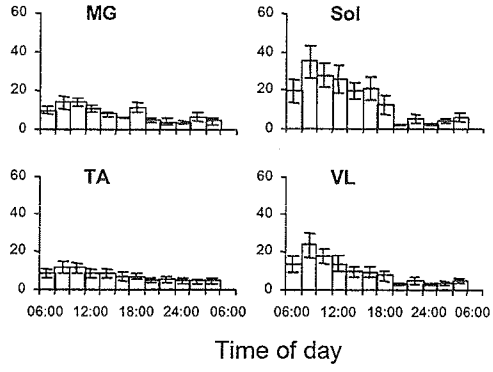

Figure 1. Average ± SD durations of EMG activity from 8 Rhesus monkeys measured during 2-hour periods throughout a day.

Comparisons of EMG activity and force levels in quadrupedal and bipedal locomotion suggest that minimal adjustments were necessary to achieve bipedal stepping. Plantarflexors EMG levels and MG force were slightly higher in bipedal stepping, probably as a consequence of greater loading on the hindlimbs. Thes findings suggest that the evolution of bipedal locomotion did not require major alterations of motor control strategies.

The growing recognition that brief periods of muscle loading are the norm and that such stimuli are sufficient to activate protein synthesis pathways (Baldwin & Haddad, 2001) has broadened the search for the mechanisms linking biomechanical events and muscle gene expression, particularly when faced with the notion that some muscle fibers may rarely become active. The distribution of strain within muscles and muscle compartments (Fukunaga et al., 2001) is one poorly understood area that may link passive and active portions of a muscle. We will demonstrate how recent developments in velocity cine phase contrast MRI provide an opportunity to track the motions of intramuscular tissues and thus the distribution of strain within calf muscles during repetitive movements (Drace & Pelc, 1994; see also A.M. Lia et al., these proceedings).

REFERENCES

Abelew, T.A. et al. (2000) *J. Neurophysiol.*, **84**, 2709-2714.

Alford, E.K. et al., (1987) *Exp. Neurol.* **96**, 635-649.

Baldwin, K.M. & Haddad, F. (2001) *J. Appl. Physiol.* **90**, 345-357,

Binding, P. et al. (2000) *J. Biomech.* **33**, 1423-1432.

Biewener, A.A. & Roberts, T.J. (2000) *Exerc. Sports Sci. Rev.* **28**, 99-107.

Blewett, C. & Elder, G.C. (1993) *J. Appl. Physiol.* **74**, 2057-2066.

Drace J.E. & Pelc N.J. (1994) *J. Magn. Reson. Imaging.* **4**, 773-778.

Engberg & Lundberg (1969) *Acta Physiol. Scand.* **75**, 614-630.

Fukunaga, T. et al. (2001) *Proc. R. Soc. Lond. B Biol. Sci.* **268**, 229-233.

Goslow et al. (1973) *J. Morph.* **141**, 1-41.

Gregor, R.J. & Abelew, T.A. (1994) *Med. Sci. Sports Exerc.* **26**, 1359-1372.

Hensbergen, E. & Kernell, D. (1998) *Muscle Nerve* **21**, 345-351.

McCall, G.E et al., (2000) *J. Appl. Physiol.* **89**, 1137-1141.

Shadwick, R.E. et al. (1999) *J. Exp. Biol.*, **202**, 2139-2150.

PATTERNS OF STRAIN AND ACTIVATION IN PROXIMAL LIMB MUSCLES OF THE RAT: DO FASCICLES CHANGE LENGTH SUBSTANTIALLY WHEN ACTIVE?

Gary B. Gillis and Andrew A. Biewener
Concord Field Station, Harvard University, Bedford, MA, USA
E-mail: ggillis@oeb.harvard.edu

INTRODUCTION

Direct measurements of muscle strain in the ankle extensors of running turkeys and hopping wallabies have shown that fascicles shorten little (< 6%) when actively generating force during stance (Roberts *et al.*, 1997; Biewener *et al.*, 1998). It has been proposed that vertebrate limb muscles, more generally, may function nearly isometrically during locomotion, producing little mechanical work, but economizing force production (Taylor, 1994). However, studies of ankle extensors in cats suggest otherwise, with fascicles changing length more substantially and producing positive work and power (e.g., Prilutsky *et al.*, 1996). Because turkeys, wallabies, and cats comprise a small range of vertebrates and ankle extensors constitute only a fraction of a limb's total musculature; it is important to examine strain patterns in more proximal muscles and in other vertebrate groups. In this study we examine strain and activation in hip and knee extensors of rats to test more broadly the hypothesis that major limb muscles may be active nearly isometrically during locomotion. In addition, we compare functional patterns among different gaits to assess how these more proximal muscles respond to changing locomotor demands.

METHODS

To examine patterns of muscle strain and activation, finewire bipolar electrodes and pairs of sonomicrometry crystals were implanted unilaterally into the cranial aspect of the biceps femoris and into the central region of the vastus lateralis. Following surgeries, rats were allowed to recover and then exercised on a small treadmill over a range of speeds to elicit walking, trotting, and galloping gaits. Strain and/or activity were recorded from each muscle from a total of four rats. Data from 3-5 step cycles were analyzed for each locomotor trial. Variables characterizing the timing and magnitude of electromyographic activity and strain were determined for each stride, and averaged over each trial. Using the mean trial values, analyses of variance were performed to examine the effects of gait on the parameters characterizing activation and length-change.

RESULTS AND DISCUSSION

The cranial portion of the biceps femoris actively shortens during the stance phase, regardless of gait (Fig. 1). Total shortening strain, however, varies significantly among gaits ($P < 0.01$), ranging from $23 \pm 3\%$ during slow walking, to a maximum of $27 \pm 5\%$ at a fast trot.

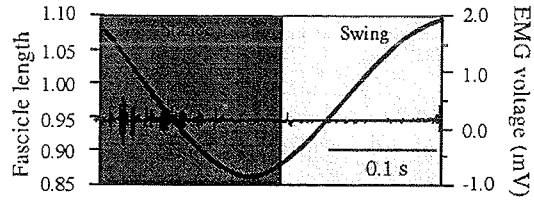

Figure 1: Representative patterns of strain and activation in the biceps femoris during trotting.

Upon shifting to a gallop, strains decrease and shortening velocities become less consistent, with some periods of little length change. Furthermore, during galloping, which is an asymmetrical gait, levels of fascicle strain differ, on average, between the hindlimb that makes ground contact first (12 ± 5%) versus second (19 ± 6%).

The vastus lateralis typically actively lengthens during the first half of stance (8-16%, depending on gait), and exhibits little shortening in the remainder of stance (Fig. 2).

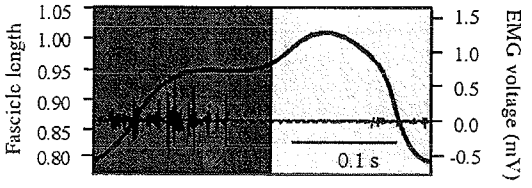

Figure 2: Representative patterns of strain and activation in the vastus lateralis during trotting.

The one exception to this pattern is the vastus of the leading hindlimb during galloping. In this case, the fascicles do shorten substantially in the second half of stance (mean = 10 ± 2%) and the timing of EMG activity is phase-delayed such that this shortening occurs while the fascicles are active.

Thus, patterns of muscle activation and/or strain differ among gaits and between muscles, and even between contralateral hindlimbs during the same gait (galloping). Further, our results also show that these two proximal muscles of the rat exhibit substantial ranges of strain during activation, countering the hypothesis that limb muscles operate nearly isometrically when active during stance. Finally, comparisons with strain patterns of similar muscles in horses suggest that differences in animal size (and corresponding shifts in limb configuration) may influence the functional roles of homologous muscles.

REFERENCES

Biewener, A.A. , Konieczynski, D. D. and Baudinette, R. V. (1998). *J. exp. Biol.*, **201,** 1681-1694.

Prilutsky, B. I., Herzog, W. and Allinger, T. L. (1996). *J. exp. Biol.*, **199**, 801-814.

Roberts, T. J., Marsh, R. L., Weyand, P. G. and Taylor, C. R. (1997). *Science*, **275,** 1113-1115.

Taylor, C.R. (1994). In *Comparative Vertebrate Exercise Physiology* (ed. J. H. Jones), pp. 181-215.

CAN MUSCLES PRODUCE MORE MECHANICAL WORK THAN THEIR FIBRES?

W. Herzog and T.R. Leonard

The University of Calgary, 2500 University Drive N.W., Calgary, AB, Canada, T2N 1N4
E-mail: walter@kin.ucalgary.ca

INTRODUCTION

The answer to the question posed in the title is, NO! or is it? The contractile elements that reside in a muscle are the fibres. Fibres are known to produce tensional force along their long axis. There are no other (known) contractile elements in muscle, therefore the work produced by all fibres of a muscle should be equal or smaller than the work performed by the entire muscle.

In recent investigations, we, and others, made two observations that made us rethink the idea of mechanical work production in whole muscle and fibres: first, during normal cat locomotion, shortening of soleus (S) and medial gastrocnemius (MG) fibres were about 70% and 40% of the corresponding shortening of the muscle (Carvalho et al., submitted); second, the resultant force on the cat MG aponeurosis was in the direction of the collagen fibres of the aponeuroses, not in the muscle fibre direction, as has typically been assumed (e.g. Huijing, 1985). Both these observations suggest that mechanical work production of whole muscle might not come exclusively from fibre shortening, but possibly also from other sources, such as muscle deformation.

PURPOSE

The purpose of this study was to measure the forces, muscle lengths, and fibre lengths in cat S and MG during unrestrained locomotion, and to calculate from these measurements the mechanical work produced by muscles and fibres.

METHODS

Cat S and MG forces were measured using buckle-type tendon transducers (e.g. Walmsley et al., 1978; Herzog and Leonard, 1991). Muscle lengths were determined post-sacrifice using a tendon travel approach and using the digitized time histories of knee and ankle angles obtained from high speed video records. Fibre lengths were measured from a fibre in the mid-belly of S and MG using sonomicrometry (Roberts et al., 1997). Mechanical work of muscles and fibres was calculated by integrating the force-length data of the muscles and fibres, respectively. Four cats were tested while walking and trotting on a motor-driven treadmill on a level, 10E uphill and 10E downhill slope.

RESULTS

Typically, but not always, the mechanical work performed per step cycle was greater for the entire muscle than the corresponding fibres. This result was observed because during the positive work production phase (muscle and/or fibre shortening), the amount of shortening of the whole muscle exceeded that of the corresponding fibres (e.g. Figures 1 and 2). For example, for level trotting at 1.4 m/s, the average work per step cycle was about 0.020 and 0.045J for the MG.

DISCUSSION

It has been a basic rule of muscle mechanics that the mechanical work produced by all fibres is equal or greater than the mechanical work produced by the muscle. This notion was based on the idea that only fibre shortening produces mechanical work, and that this work is, at best, transmitted without loss to the attachment points of the muscle at the bone. Since the aponeuroses and tendons in series with the fibres are not perfectly elastic, there should actually be a loss of mechanical work of about 7%.

The results of this study suggest that a substantial amount of work might be produced by whole muscle that is not associated with shortening of the muscle fibres. A candidate for this extra work production is muscle deformation. It is quite perceivable, and initial calculations suggest that it is also possible, that the reorientation of fibres during muscle contraction can provide mechanical work for the whole muscle that is not reflected by fibre shortening. The idea of muscle deformation being an important part of whole muscle work production needs thorough investigation.

REFERENCES

Carvalho, W., Leonard, T.R., Herzog, W. Structural changes and functional properties of unipennate skeletal muscle during isometric contractions. *J Applied Physiol* (submitted June 2000).

Herzog, W., Leonard, T.R., (1991). *J of Biomech* 24S, 31-39.

Huijing, P.A. (1985). *Acta Anat.* 123:101-107.

Roberts, T.J., Marsh, R.L., Weyand, P.G.,Taylor, C.R., (1997). *Science* 275, 1113-1115.

Walmsley, B., Hodgson, J.A., Burke, R.E., (1978). *J Neurophysiol* 41, 1203-1215.

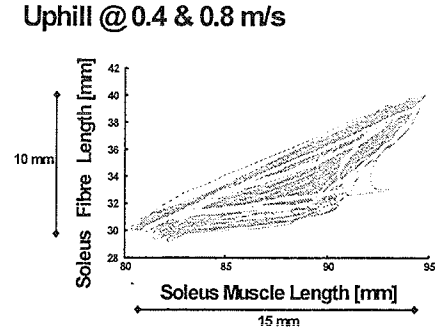

Figure 1: Soleus fibre vs. muscle length changes for approximately 20 consecutive step cycles during uphill walking

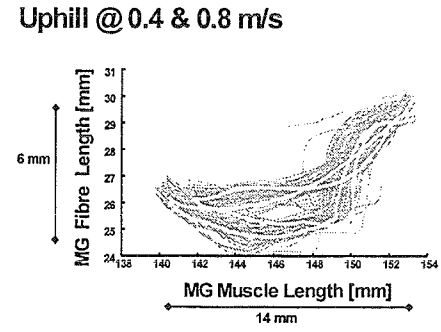

Figure 2: MG fibre vs. muscle length changes for approximately 20 consecutive step cycles during uphill walking

ACKNOWLEDGMENTS

NSERC of Canada

CONSIDERATION OF ONE- AND TWO-JOINT MUSCLE FUNCTION BASED ON DIRECT MEASUREMENT OF *IN VIVO* MUSCLE FORCES

Motoshi Kaya, Tim Leonard, and Walter Herzog

Human Performance Laboratory, University of Calgary, Calgary, Alberta, CANADA
E-mail: motoshi@kin.ucalgary.ca

INTRODUCTION

It has been proposed that one- and two-joint muscles perform distinctly different functions: one-joint muscles have been associated with positive joint power generation, irrespective of the required net joint moment; while two-joint muscles have been said to cause appropriate distribution of net joint moments to control the direction of external forces (Ingen Schenau *et al.*, 1992). In Ingen Schenau's studies, muscle force patterns were estimated by EMG rather than by direct measurement of the forces. Therefore, the purpose of this study was to determine the proposed function of one- and two-joint muscles based on direct measurement of *in vivo* cat ankle extensor forces during level and downslope walking.

METHODS

Four adult male cats were trained to perform level and 30 degree downslope walking. The forces in the two-joint muscle, medial gastrocnemius (MG), and the one-joint muscle, soleus (SO), were individually measured using buckle type force transducers (Walmsley *et al.*, 1978). EMG activities of these muscles were measured using indwelling, bipolar fine wire electrodes. The hind limb kinematics and ground reaction forces (GRF) were measured using high-speed cameras and force platforms. The muscle-tendon length changes were estimated by kinematics and muscle geometry measurement including, the origin-insertion location, and the instantaneous moment arm.

Results

Typically, SO produced greater forces than MG during the stance phase of level and downslope walking (Fig. 1 a). For level walking, SO and MG produced forces over the entire stance phase and the ankle extensor moment was extensor (Fig. 1 b). For downslope walking, MG forces became virtually zero around the middle of stance when the ankle moment changed from extensor to flexor (Fig. 1 b), while SO produced force during the entire stance phase. SO and MG initially lengthened (level: up to 30% of stance phase, downslope: up to 60 %), followed by shortening (Fig. 1 c).

DISCUSSION

For level walking, the net ankle moment was always extensor during stance, while for downslope walking, the ankle moment changed from extensor to flexor at about 50 % of stance. The differences in MG force patterns for level and downslope walking seem to correspond to the change in ankle moment (Fig. 1 a). Therefore, MG force appears to parallel the required ankle joint moment. Since the direction of ankle joint moment (flexor/extensor) also represents the direction of the external GRF relative to the ankle joint center, MG might primarily control the direction of GRF, consistent with the function of two-joint

muscles proposed by Ingen Schenau *et al.* (1992). During stance, MG lengthened, followed by shortening, and thus MG produced positive and negative power. Therefore, MG force seems to be independent of joint power.

In contrast to MG, SO produced force during the entire stance phase in downslope walking when ankle extensor and ankle flexor moments were required (Fig 1 b). Thus, SO force seems to be independent of the net joint moment requirements. Moreover, SO reached its peak force in the first half of stance, when SO was lengthening, and SO produced negative power. This suggests that SO force production is not consistent with the function of one-joint muscles proposed by Ingen Schenau *et al.* (1992) who stated that one-joint muscles are primarily activated to produce positive power. From our results, it appears that SO is a stabilizer of the ankle and prevents a collapse of the ankle during stance.

In one animal, SO forces were zero, presumably because of pain or damage to SO. In this animal, MG forces persisted throughout the entire stance phase in level and downslope walking (Fig 1 d). In this case, MG appeared to take over the lost function of SO in the late stance phase of downslope walking.

CONCLUSION

Based on the results of this study, we conclude that the function of one-joint muscles proposed by Ingen Schenau *et al.* (1992) is not correct and cat SO is not a power producer but an ankle stabilizer. SO produced force independent of the net joint moment and joint power requirements. The function of two-joint muscles proposed by Ingen Schenau *et al.* (1992) appears correct for MG. MG force production was tightly linked to the direction of the external GRF, and therefore, the net ankle moment (Fig. 1 a, b). MG primarily functions as an ankle moment generator, and MG can take over the function of SO, if SO function is lost.

REFERENCE

Ingen Schenau, G. J. V. *et al.*, (1992) *Neuroscience*, **46**, 197-207.

Walmsley B. *et al.* (1978) *Neurophysiol.*, **43**, 612-620.

ACKNOWLEDGEMENTS

AHFMR and NSERC of Canada

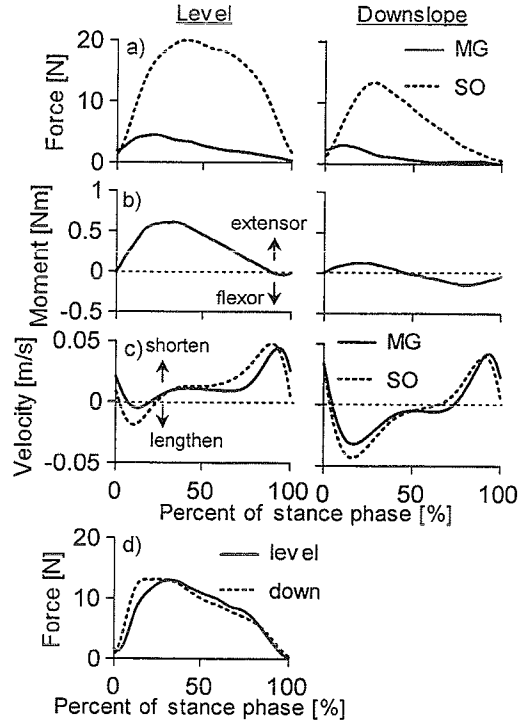

Figure 1: Mean curve of a) MG/SO force, b) ankle moment, c) MG/SO contraction velocity (cat #2), and d) MG force (cat#3).

IN VIVO MUSCLE FUNCTION IN HIGH PERFORMANCE FISHES

Robert E Shadwick[1] and Douglas A. Syme[2]

[1] Scripps Institution of Oceanography, University of California, San Diego, CA, USA
[2] Department of Biological Sciences, University of Calgary, Calgary, Alberta, CANADA
E-mail: rshadwick@ucsd.ed

INTRODUCTION

Axial locomotor muscle in most fishes consists of a series of nested cone-shaped myotomes that run along the sides of the body. These muscle blocks are linked by connective tissue to the skin and backbone. Typically, muscle shortening results in local bending, whether it be superficial red (aerobic) fibers that power steady cruise swimming, or deep white (glycolytic) myotomal fibers powering burst swimming. Progression of a wave of muscle activation and contraction along the body yields a travelling wave of bending. Muscle strain amplitude increases from anterior to posterior in direct correlation to the increasing amplitude of body bending.

An exception to this pattern is found in the tunas and lamnid sharks (e.g. great white and mako), where the bulk of red fibers are located deep within the myotomal mass, which has been shifted anteriorly to create a more streamlined body. This specialized location of red muscle presents a potential dilema. Shifting the aerobic muscle mass anteriorly and internally should hinder its ability to contribute power to swimming, yet these animals are regarded as being highly adapted for continuous locomotion. There is little body bending in the region where the bulk of the red muscle resides, and the nearness of this muscle to the neutral axis of bending should further limit its strain amplitude and power output. Here we address this issue by using *in vivo* and *in vitro* methods to analyze muscle function.

METHODS

We measured *in vivo* muscle strain in yellowfin tunas (*Thunnus albacares*) while they swam in a large water tunnel treadmill. Fish were implanted with three pairs of 2 mm diameter sonomicrometer crystals. placed in three locations: in the superficial and deep red muscle at the longitudinal midpoint of the animal (0.5 BL, BL = body length), and in the superficial red muscle at 0.7 BL. Simultaneously, the fish were videotaped from above. Sequences of images of the fish were digitized, and polynomial functions were fit to the body midline for each frame. From these functions we calculated local curvature of the body and the corresponding local muscle strain, based on simple beam theoery. The fish averaged 42.3 cm in BL (S.E. = 1.1) and had an average mass of 1297g. (S.E. = 157). Once recovered from anesthesia, fish swam at a mean speed of 1.85 BL/s (S.E. = 0.04),

Mechanical work and power were measured on excised blocks of red muscle using the work loop (e,g, Altringham and Johnson 1990). Briefly, the muscle was subjected to sinusoidal length oscillations (strain) centered about l_o. The muscle was stimulated phasically during the strain cycle such that it developed force primarily during muscle shortening and was relaxed during lengthening. Muscle work and power were measured over a range of cycle frequencies, strains and stimulus duty cycles and phases that encompassed and/or equaled the

physiological conditions measured from swimming fish (Knower, 1998; Shadwick et al., 1999). These included cycle frequencies of 1-12 Hz and strains of ±5.5%, ±2.75% and ±8%. Stimulus duty cycle and phase were systematically altered to maximize the net work produced by the muscle; in all cases the physiological values were included the values tested.

RESULTS AND DISCUSSION

Sonomicrometry measured strain in superficial red muscle is matched in amplitude and phase to strain calculated from midline curvature (Fig.1). However, the internal red muscle contracts independently of the more peripheral red muscle. Contrary to being strain limited, the internal red muscle produces large strain amplitudes and greater power all along the body, without causing large local bending. This is the defining difference between the thunniform design and all others. Internal red muscle strains based on curvature are predicted to be ±2.5-3%, whereas those measured with sonomicrometry (±5.5 - 6%) are double the amplitude expected if the myotomes were acting as a homogeneous beam, and may even be larger than peripheral red muscle strain at the same longitudinal position. Work-loop tests show that the power produced by red muscle at the measured strain is indeed twice that produced at the smaller calculated strain. Most importantly, cyclic length changes in the internal red muscle of tunas are significantly out of phase with changes in local bending. For example, at a midpoint along the body length, deep red muscle shortening is 30-50° later in time than local body bending, which means the muscle shortening is synchronous with midline bending several cm more posterior (Fig.1). Thus, the internal placement of tuna red muscle appears to provide a performance enhancement not seen in other teleost fishes, one that should increase power output and focus muscle action to the more posterior thrust-producing caudal region. The internal and anterior location of red muscle in the mako shark suggests a parallel mechanical function to tunas which is currently under investigation.

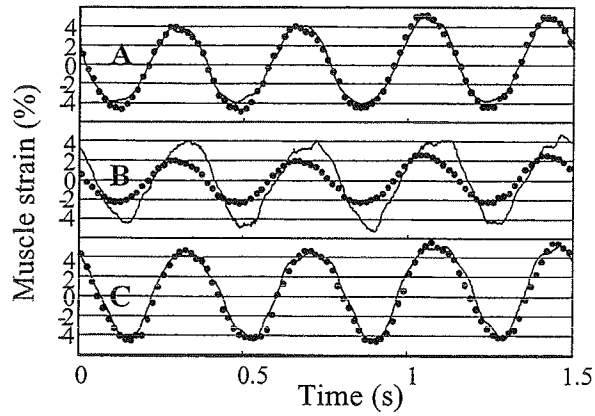

Figure. 1. Comparison of muscle strain calculated from midline curvature (symbols) *vs.* that measured by sonomicrometry (line) for a yellowfin tuna swimming at 2BL/sec. **A**. Superficial red muscle strain at 0.5 BL, showing close agreement between the two methods. **B**. Internal red muscle strain at 0.5BL. Note that the measured strain here is larger and phase-delayed compared with the predicted strain. **C**. Superficial red muscle strain at 0.7BL. Strain here is approximately in phase with strain of internal red muscle at 0.5BL.

REFERENCES

Altringham, J.D. and Johnston, I.A. (1990). *J. Exp. Biol.* **148**, 395-402.

Shadwick, R.E. et al., (1999). *J.Exp. Biol.* **202**, 2139-2150.

Knower, T. (1998). Ph.D. thesis, University of California, SanDiego.

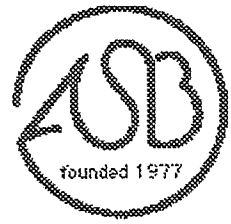

- PARALLEL SESSION -

Finite Element Simulations

Thursday, August 9, 2001
1100 to 1230

FULL WALKING CYCLE SIMULATION OF A ROTATING PLATFORM TKR

Jason K Otto[2], John J. Callaghan[1,2], and Thomas D. Brown[1,2]

Depts. of [1]Orthopaedic Surgery and [2]Biomedical Engineering, University of Iowa, Iowa City, IA
E-mail: tom-brown@uiowa.edu

INTRODUCTION

Although mobile bearing total knee replacements are growing in popularity, little is known about the mechanics (i.e., motion, contact stresses, wear) at the "mobile" (backside) interface. The objective of this study was to develop a physically realistic, multi-contact-interface finite element (FE) model of a rotating platform total knee, for the purpose of studying the mechanics at the "mobile" interface under a standardized walking cycle.

METHODS

A 3-D FE model of a rotating platform total knee* was meshed with the PATRAN 8.5 pre-processor (Fig 1). ABAQUS 5.8 was used to perform a nonlinear, large-displacement contact analysis. Since the CoCr elastic modulus (220 GPa) is over 300 times higher than that for UHMWPE, the femoral component and tibial tray were modeled as rigid surfaces (3062 and 3707 3-noded triangular elements, respectively). The PE insert (7390 8-noded hexagonal elements) was treated as a nonlinear deformable body, with a Poisson ratio of 0.45 and a tangent elastic modulus governed by a 4th-order constitutive relationship with von Mises stress (σ): $E(\sigma) = 634.92 - 12.31\sigma - 3.61\sigma^2 + 0.199\sigma^3 - 0.00283\sigma^4$ MPa (Cripton, 1993).

Unlike FE models with prescribed bearing surface traction, this model used multiple-surface contact interactions ("bearing" = femoral component/PE and "mobile" = tibial tray/PE interfaces), which permitted a realistic load transfer analysis. An experimentally derived dynamic friction coefficient of 0.089 was used at the interfaces. The femoral component was given varus/valgus rotational, and full translational freedom. The tibial tray was only free to axially rotate. The PE insert, by contrast, had complete translational and rotational freedom, constrained only by contact with the femoral and tibial components.

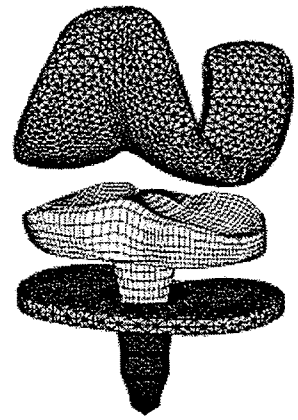

Fig 1: FE model of a rotating platform TKR.

Waveforms from the proposed ISO standard #14243-1 were used as input for the FE model. The standard includes force-controlled axial load, axial torque, and A/P force waveforms, and also a displacement-controlled flexion waveform (Fig 2). These waveforms were discretized into 100 piecewise linear segments, each increment being an FE analysis step. In addition, linear soft tissue constraints of 30 N/mm A/P, and 0.6 N-m/deg rotational displacement were used. Lastly, a medially biased condylar load allocation was achieved by moving the concentrated axial load 4.9 mm medially.

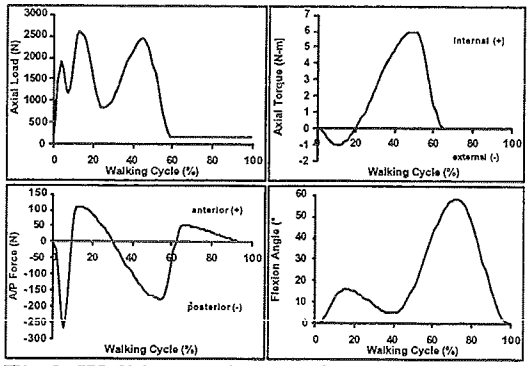

Fig 2. Walking cycle waveforms.

RESULTS AND DISCUSSION

During surgery, the tibial tray is implanted with a 10° posterior slope, and the femoral component is flexed 5°. Therefore, flexion angles used here are 15° less than clinical flexion angles. As flexion angle increased (as seen in most of the swing phase), the contact stress distributions shifted posteriorly. When this posterior shift of contact was coupled with a nontrivial level of anterior force, the posterior edge of the PE insert acted as a fulcrum, lifting the anterior edge off of the tibial tray.

Peak von Mises contact stresses in the PE insert rarely exceeded 12 MPa. These stresses were considerably lower than those measured in fixed bearing total knees, which can be 20 MPa or more (Szivek *et al.*, 1996). Contact stresses developed in the post were low (<5 MPa). Although this may change when the tibial tray is placed at 10° of posterior slope.

The amount of torque required to overcome friction at the "mobile" interface is proportional to the axial load (Otto *et al.*, 2000). There was very little axial rotation of the tibial tray during the first 30% (first half of stance phase) of the gait cycle (Fig 3). This was caused by the high axial loads and small axial torques during this period. Conversely, the end of stance phase was marked by significant tibial tray rotation. Normal kinematic total ROM for endo/exorotation is generally considered to be approximately 13° (Kabada *et al.*, 1990). This implant has a total ROM of just over 6°. Changes in normal kinematics may have adverse consequences in terms of accelerated wear and/or loosening.

Solution of the finite element model was sensitive to the soft tissue constraint constants. A previous model used constraints of 0.27 N-m/deg rotational and 20 N/mm A/P displacement. The decrease in constraint caused the tibial tray to internally rotate nearly 11°, which caused the solution to diverge and end before completion.

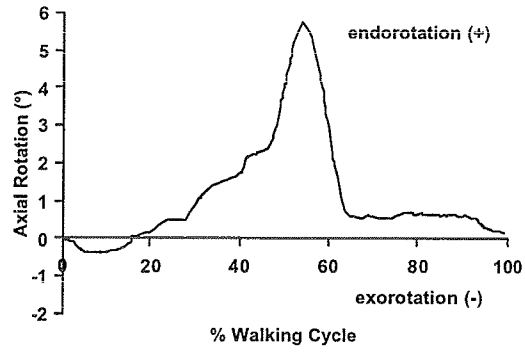

Fig 3. Axial rotation of the tibial tray.

REFERENCES

Cripton, P.A. (1993). *Thesis*, Queen's Univ.
Kabada, M. *et al.* (1990). *JOR*, 383-92.
Otto, J.K. *et al.* (2000). *Proc of ASB*, 181-2.
Szivek *et al.* (1996). *JOA*, 952-63.

ACKNOWLEDGEMENTS

DePuy, Inc provided financial support. Andrew Dooris, Mark Nadzadi, and Nicole Grosland provided key technical help.

*LCS Standard, DePuy, Inc. Femoral component: Std/Left; tibial tray: MBT, size 3; polyethylene insert: Std, 6.0 mm thick.

STRAIN ANALYSIS OF THE PROXIMAL FEMUR AFTER RETROGRADE FEMORAL NAILING: A 3 DIMENSIONAL FINITE ELEMENT STUDY

R. Neiman,[1] S.J. Hazelwood,[2] D.J. Hak[1]

[1]Department of Orthopaedic Surgery, University of California Davis Medical Center, Sacramento, CA 95817

[2]Orthopaedic Research Laboratories, University of California Davis, Sacramento, CA 95817

E-mail: sjhazelwood@ucdavis.edu

INTRODUCTION

Retrograde femoral nailing for femoral shaft fractures has been used in its present form since approximately 1995. A rod is placed into the medullary canal through an entry site in the knee, extending into the subtrochanteric region of the proximal femur. Little is known regarding the implant's effect on strain in the proximal femur. Report of fracture at the tip of the nail has occurred in shorter retrograde nails that end in the mid-diaphysis (Leibner et al., 1999). Other implanted devices which end in the subtrochanteric region, such as femoral neck pins and short antegrade intramedullary nails, have a well-established history of increased fracture risk (Andrew and Thorogood, 1984). This study examines strain changes incurred in the proximal femur before and after retrograde nailing, using a three dimensional finite element model.

METHODS

A three dimensional solid model of a commercially available synthetic femur (Sawbones, Pacific Research Laboratories, Vashon, WA, USA) was constructed using public domain surface geometries for *The Standardized Femur* (Viceconti, 1997). A mesh of 8 node hexahedral elements, with intervals of 3mm, was constructed for cortical and cancellous bone from the femoral head to the distal femoral metaphysis (31,600 elements). An intramedullary retrograde rod was modeled to fit the inner curvature of the femur with a constant 11mm diameter. Material properties were modeled as linear, elastic, isotropic, and homogeneous. The elastic modulus was defined as 14,200 MPa for cortical bone (McNamara et al., 1997), 1500 MPa for cancellous bone (Duda et al., 1998), and 200,000 MPa for the stainless steel rod (manufacturer); Poisson's ratio was 0.3 for all materials. A femoral shaft fracture was simulated by creating a segmental defect at the mid-diaphysis. The distal end was fully constrained.

Axial Loading: The femur was loaded in a simulated single limb stance with the femur positioned in 25° adduction (Sim et al., 1995) and a load of 2000N distributed over the femoral head. An abductor force of 1240N was applied on the greater trochanter at 40° from the long axis of the femur (McNamara et al., 1997). The maximum (tensile) and minimum (compressive) principal strains were recorded laterally and medially in the intact femur and for nails with the proximal tip ending 2cm above the lesser trochanter (LT), at the LT, and 4cm below the LT.

Torsional Loading: A moment of 20 N-M was applied about the z axis, centered proximally around the long axis of the femur. Maximum shear strain was recorded at the same locations as for axial loading.

RESULTS AND DISCUSSION

Axial Loading: In the intact femur (no rod in place), minimum principal strains recorded along the medial proximal femur ranged from 2100 to 3300 με, with the highest strains immediately below the LT. Laterally, maximum principal strains ranged from 2100 to 2700 με, also with the highest strains just below the LT. For all nail lengths, strains decreased by less than 5% proximal to the tip of the nail (Figure 1). With the tip at 4cm below the LT, strains distal to the nail decreased up to 15% medially and 20% laterally. With the tip at the LT, strains distal to the nail decreased 12 to 15% medially and up to 27% laterally. With the tip of the nail

2cm above the LT, medial and lateral strains decreased more than for the other two nail lengths. Distal to the nail, medial strains decreased 8% at the LT and 10-15% 4cm below the LT, while laterally the strains decreased by 34% near the LT and equilibrated to a 20% decrease further distally.

Torsional Loading: All nail placements behaved similarly for medial shear strain (Figure 2). At 4cm below LT, minimal decrease in shear strain was observed (2 to 5% in all cases). At the LT, strains were increased by 17 to 18% compared to the intact femur for all nail positions. Shear strains increased by 34% for all nails at 2cm above LT. Lateral shear strains demonstrated similar behavior for all nails except in the region between 2cm above the LT and 4cm below the LT. In this region, progressively higher strains were observed as the nail was made shorter (Figure 2).

SUMMARY

Varying the length of a retrograde femoral nail alters the strain distribution in the proximal femur in this 3-D finite element model. During axial loads, progressively more stress shielding was observed, especially laterally, when the length of the nail was increased. The shortest nail had the least alteration in strain compared to the intact femur. In torsion, progressively higher shear strain was observed laterally at the LT and below for progressively shorter nails. Placing the tip of the nail more proximal may potentially protect the femur from fractures in the subtrochanteric region, but it will also predispose this region to stress shielding, which could be deleterious over time.

ACKNOWLEDGMENTS

Supported in part by NIH grant AR41644.

REFERENCES

Andrew T.A., Thorogood M. (1984). *Injury* **16**, 169-177.
Duda G.N. et al. (1998). *J Biomech*, **31**, 841-846.
Leibner E. et al. (1999). *Am J Ortho*, **28**, 53-55.
McNamara B. et al. (1997). *J Biomech*, **30**, 621-630.
Sim E. et al. (1995). Injury, **26**, 445-449.
Viceconti M. (1998). *ISB Finite Element Repository*, www.cineca.it/hosted/LTM-IOR/back2net/stand_fem/stand_fem.html

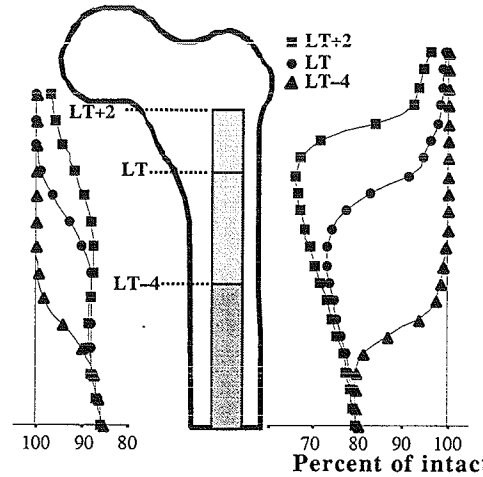

Figure 1: Axial load with minimum (medial) and maximum (lateral) principal strains along the proximal femur plotted as percent of intact (refer to RESULTS section).

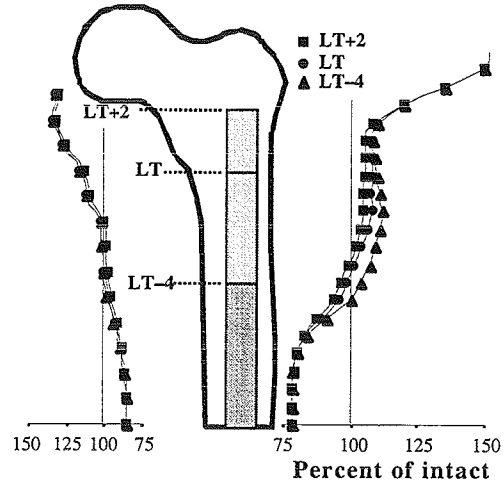

Figure 2: Torsional load of the femur with maximum shear strain plotted as percent of intact (refer to RESULTS section).

3-D FINITE ELEMENT ANALYSIS OF A HUMAN KNEE JOINT IN FLEXION

K. Moglo, A. Shirazi-Adl

Department of Mechanical Engineering Ecole Polytechnique, Montreal, Quebec, Canada
E-mail: moglo@meca.polymtl.ca

INTRODUCTION

The human knee joint is a multi-body complex system that experiences relatively large loads and displacements during normal daily activities. The joint stability is provided by its articular surfaces, menisci, ligaments and muscles. An injury to a component influences the joint normal kinematics/kinetics with liklihood to initiate/accelerate joint instability and degeneration. In this work, a validated nonlinear 3-D model of the human knee joint (Benjaballah et al, 1997 and 1998) is further refined and applied to the analysis of the tibiofemoral joint in passive flexion. Attention is focused on the global motions, ligament forces and load transmission. The effect of changes in ligament initial strain on the response is also investigated.

METHODS

The FE model (Fig. 1) of the tibiofemoral joint consists of two rigid bony structures (tibia, femur), articular cartilage layers, menisci, and four principal ligaments (collaterals and cruciates). The tibial articular cartilage layers were refined into two layers along the depth. For meniscal tissue, a non homogeneous composite model of a matrix of ground substance reinforced by a network of radial and circumferential collagen fibres was considered. Ligaments were each modelled by a number of uniaxial elements with nonlinear stress-strain curves and initial strains; 6 elements for AM/PL bundles of ACL, 6 for AL/PM of PCL and 3 for LCL. To account for the wrapping of the MCL around the proximal medial tibial edge and its peripheral attachment to the medial meniscus, the MCL was modelled by 5 uniaxial elements for proximal part, 10 elements for the attachment to the meniscus and 5 wrapping elements for the distal part. The mechanical properties remained nearly the same as before.

For the loading in this study, femoral flexion was prescribed while coupled femoral medial-lateral, posterior-anterior and distal-proximal translations were set free. Tibial coupled varus-valgus and external-internal rotations were also left free. Remaining degrees-of-freedom at femur/tibia were constrained. The joint nonlinear analysis was carried out in two steps; ligaments pre-strains were applied resulting in initial strains in ACL, PCL, LCL and MCL of respectively –0.7%, -25%, 1% and 0%. Subsequently, the femur was flexed to 90°.

RESULTS

Displacements of the primary bony nodes (Fig. 2) show the femoral rollback and screw-home mechanism (tibial internal rotation). The tibial rotation, however, reverses at larger flexion rotations. As for ligament forces (Fig. 3), all ligaments were nearly inactive in the first third of the applied rotation whereas the forces increased at rotations beyond 40°; specially in ACL and PCL reaching values beyond 100N at the final rotation of 90°. The computed forces transferred by medial and lateral plateaus (Table 1) at both covered (via menisci) and not-covered (cartilage-cartilage) regions demonstrate that the axial component of the load is transferred mainly

through the lateral compartment, particularly through the lateral meniscus.

DISCUSSION

A detailed 3-D model of the human knee joint is used in this study to compute the global response, ligament forces and load transmission in passive flexion. The results are in general agreement with measurements. The ACL and PCL ligaments exhibit a clear coupling in that, for example, an increase in PCL initial strain would increase the tensile forces in both ACL and PCL and decrease the tibial internal rotation to become external at smaller flexion angles and vice versa. As the flexion angle increases, so do the forces in ligaments, specially cruciates, which in turn compress the articualr surfaces resulting in compression forces on both covered and not-covered areas. This developed nonlinear model is currently used to investigate joint pathomechanics in various loading combinations and pathologic conditions.

ACKNOWLEDGEMENT

The work is supported by the NSERC (Canada) and FCAR (Quebec).

REFERENCES

Bendjaballah, M.Z. et al. (1997). Clin Biomech , **12**, 139-148.

Bendjaballah, M.Z. et al. (1998). Clin Biomech , **13**, 625-633.

	MEDIAL		LATERAL	
Flexion °	Covered	Not-covered	Covered	Not-covered
0	0.9	0	9.73	0.25
30	0	0	9.32	0.2
60	22.38	22.43	67.23	0
90	58.83	56.71	95.98	36.7

Table1. Total axial contact forces (N) on the medial and lateral plateaus.

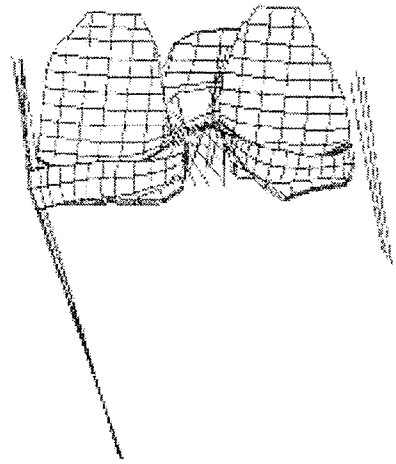

Fig. 1 A typical posterior view of the model; bony structures are not shown.

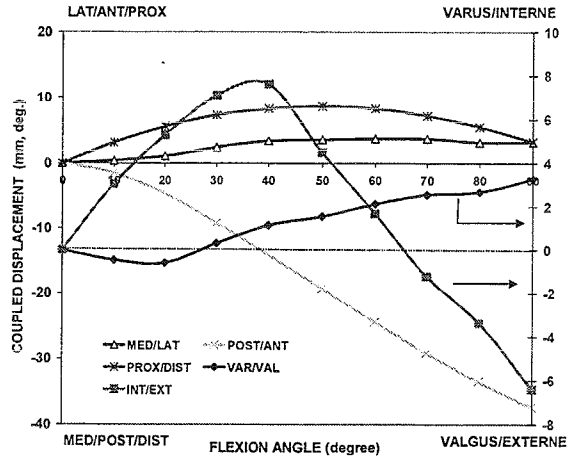

Fig. 2 Predicted coupled displacements.

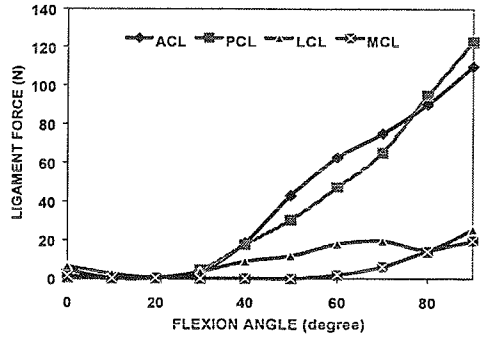

Fig. 3 Predicted total ligament tensile forces.

A NONLINEAR FINITE ELEMENT MODEL OF THE HUMAN EYE FOR LARGE DEFORMATION LOADING

Erik D. Power[1], Joel D. Stitzel[1], Robert L. West[1], Ian P. Herring[2], and Stefan M. Duma[1]
[1]Impact Biomechanics Laboratory, Mechanical Engineering Dept., Virginia Tech
[2]College of Veterinary Medicine, Virginia Tech
Email: duma@vt.edu URL: www.ibl.vt.edu

INTRODUCTION

Blunt impact to the eye can cause a large range of ocular injuries. Among men, fights account for 18% of ocular injuries, while sporting activities account for 11% (Wong *et al.*, 2000). The military sector of the population is also experiencing a large number of eye injuries. One would predict that eye injuries would account for less than 1% of all injuries since the ocular surface area is approximately only 0.27% of the total body surface area. However, in Operation Desert Storm, the incidence of ocular injury was 13% of the total combat injuries (Heier *et al.*, 1993). Debris and fragments sent into the face are usually responsible. This study presents the methods used to develop a finite element (FE) model of the human eye to simulate blunt impacts. This model is designed to handle the large deformation induced by a blunt impact and is suitable for investigating the associated ocular injuries.

METHODS

The outer shell of the eye is formed by the cornea and sclera (Figure 1). The varying thickness of each was incorporated into the model. Inside the shell lies the lens, held in place by the ciliary body and zonules. The ciliary body and zonules were modeled as a single structure. Anterior to the lens is the aqueous humor and posterior is the vitreous. The globe is surrounded by fatty tissue and encased by the bony orbit.

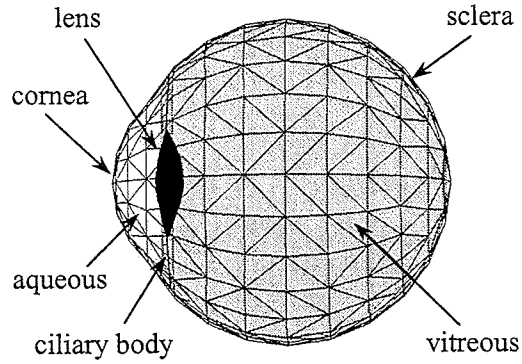

Figure 1. The meshed globe and internal structures.

For this study, the bony orbit was approximated as a pyramid (Sauerland, 1994). The six muscles that control eye movement were also modeled (Figure 2).

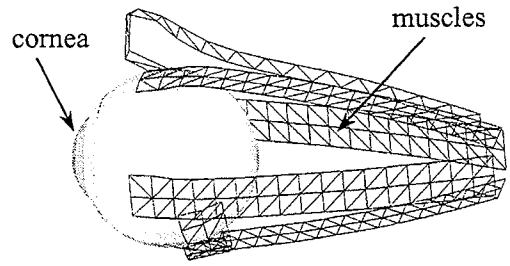

Figure 2. Extraocular muscles attached to the sclera (fatty tissue not shown).

The nonlinear stress-strain behavior of the cornea and sclera, up to rupture, was taken from a study by Uchio *et al* (1999)(Table 1). The bony orbit and lens were assumed to be rigid. All six muscles and the ciliary body were assigned a tensile strength of 20 MPa. This initial approximation is supported by the

tensile strength reported for collagen and the large amount of collagen in these structures. The aqueous, vitreous, and fatty tissue were modeled similar to soft human tissue with a Young's modulus of 47 kPa and a Poisson's ratio of 0.49 (Todd and Thacker, 1994). All densities were approximated between those known for water and collagen.

Table 1. Summary of material properties.

Structure	E (MPa)	ν	ρ (kg/m^3)
Cornea	Nonlinear	NA	1400
Sclera	Nonlinear	NA	1400
Lens	Rigid	NA	315
Ciliary body	20	0.40	1600
Aqueous	0.037	0.49	999
Vitreous	0.042	0.49	999
Six muscles	20	0.40	1600
Fatty tissue	0.047	0.49	999
Orbit	Rigid	NA	NA

Meshing was performed using I-DEAS and Hypermesh software programs. Triangular elements yielded better computational stability than quadrilateral elements. Therefore, triangular membrane elements were used to mesh the cornea and sclera. Thus they do not possess bending rigidity but instead behave like the membrane of a water balloon. Solid elements were used to model the aqueous, vitreous, and fatty tissue. Only the passive strength of the muscles and ciliary body was simulated in this study. Therefore, they were modeled with tension-only membrane elements. In total, 1256 elements and 1172 nodes were used to construct the eye model.

RESULTS AND DISCUSSION

The finite element eye was imported into MADYMO to simulate dynamic impacts with rigid blunt objects. MADYMO was chosen because of its airbag and dummy models and the ability to perform both multibody and finite element calculations. The extraocular muscles were allowed to move freely within the fatty tissue (Figure 3). Under impact loading, the fatty tissue acted as a dampening material while the cornea and anterior chamber experienced a large amount of compression. The model also remained stable under this loading.

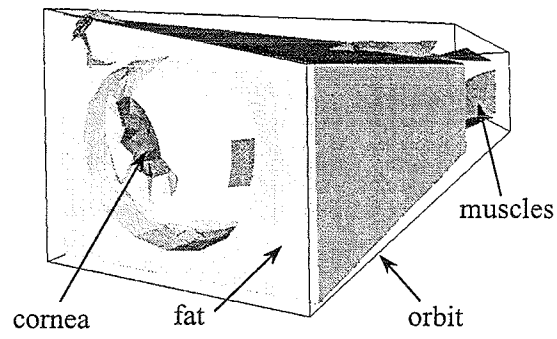

Figure 3. Globe being impacted with a blunt object.

Several assumptions were made in the formulation of this model. All anisotropic and viscoelastic behavior was neglected. However, this model can still provide valuable insight into the ocular injuries associated with blunt trauma. With modeling of the surgical incisions, it could be used to study the additional risks associated with vision correction procedures (RK, LASIK, etc.). Finally, more accurate material and geometric properties of the orbit could be incorporated to investigate blowout fractures or other orbital injuries.

REFERENCES

Heier JS *et al. Arch Ophthal* 1993;111:795-8.

Sauerland, EK. Grant's dissector. Williams & Wilkins, Baltimore, MD, 1994.

Todd BA, Thacker JG. *J Rehabil Res Dev* 1994;31(2):111-9.

Uchio E, Ohno S, *et al. Br J Ophthal* 1999;83:1106-11.

Wong TY, Smith GS, *et al. Am J of Ophthal* 2000 May;129(5):645-650.

NUMERICAL MODELLING OF THE INDENTATION OF THIN CORNEAS

C.J. Fyfe[1] and T.A. Newson[1]

[1]Department of Civil Engineering, University of Dundee, Scotland, DD1 4HN, United Kingdom.
[email: t.a.newson@dundee.ac.uk]

INTRODUCTION

The cornea performs two major functions: to protect the inner contents of the eye and to refract light. To do so, the cornea must maintain its strength and transparency. The main structural component of the cornea is the stroma, which provides most of the cornea's strength, and helps give the eye its shape. The refractive power of the cornea is determined by its index of refraction and by its radius of curvature, and accounts for over two-thirds of the optical power of the eye.

The topography of the cornea is predominantly dependent upon the material stiffness properties and thickness of the cornea. Corneal diseases can affect corneal thickness and stiffness, e.g. keratoconus, and can lead to changes in topography, causing visual impairment. There is also a need to understand the effects of corneal thinning in myopic cornea, in response to photorefractive surgery, where the cornea is artificially thinned with a laser to improve the optical properties of the eye. Hence an understanding of the biomechanical behaviour of the cornea is vital for the development of predictive tools to aid clinical management of patients.

Corneas with reduced thickness and stiffness will affect the accuracy of the indentor techniques used for estimating intraocular pressure (IOP), which are part of the process of diagnosis for disease states such as glaucoma. It is accepted in clinical practice that applanation tonometry (which uses a cylindrical indentor) becomes unreliable following photorefractive keratectomy and is unreliable in keratoconic subjects.

The overall aim of this research is the development of finite element models of the cornea, to assess the effects of photorefractive surgery and corneal thinning disease on the accuracy of clinical indentor techniques. This work is described below.

METHODS

Numerical analysis of thin corneas has been carried out using finite element analysis of axisymmetric models, subject to indentation. Two approaches were adopted: (1) where the pressure due to an indentor was applied as a boundary condition and (2) where the indentor was explicitly modelled. The thickness and stiffness of corneal models were varied for different intraocular pressures, above and below normal physiological levels. The resulting changes to corneal topography and thickness were then compared. Simple linear elastic material behaviour was assumed for both the cornea and indentor.

Calibration exercises were conducted to compare finite element predictions with clinical observations. An example is shown in Figure 1, which is a simulation of an applanation tonometer test on a cornea. A cylindrical indenter is pushed into the cornea and applanates the eye, leading to local deformation. The undeformed and deformed meshes are shown in Figure 1.

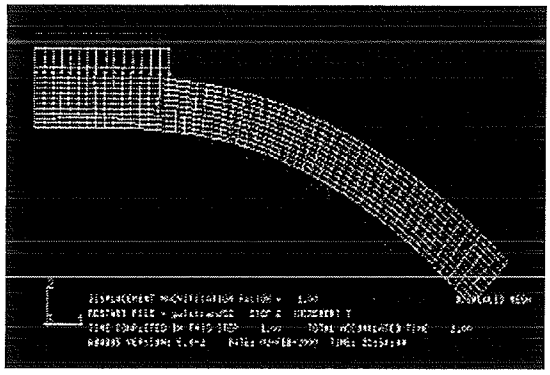

Figure 1: Finite element simulation of a Goldmann tonometer test showing undeformed and applanated eye

RESULTS AND DISCUSSION

Finite element analysis was carried out to assess the variation in predicted intraocular pressure (IOPG) from applanation tonometry compared to the true intraocular pressure (IOPT) as specified by the model boundary conditions, for various pressures, material thickness and stiffness. This variation can be expressed using the modification factor (K) below (after Orssengo and Pye, 1999):

$$K = \frac{IOPG}{IOPT} \qquad (1)$$

A plot of central corneal thickness versus correction factor (K), for an applied (true) intraocular pressure of 15 mmHg (2.5 kN/m^2) using a uniformly distributed load (to simulate the indentor) and a fully explicit model of the indentor is shown in Figure 2. This is compared with data from a review of the clinical literature produced by Doughty and Zaman (2000). This data represents the average correction of measured intraocular pressure from applanation tonometry required for healthy eyes with a 10% change in central corneal thickness. The shaded region shown in Figure 2, shows the data which represents the maximum and minimum corrections required. The results indicate that the finite element analysis shows a strong correlation to the clinical studies. In addition, the prediction where the indentor is modelled explicitly produces better results, which can be attributed to the effects of the linear interface between the cornea and indentor. Further improvements of the corneal model (e.g. non-linear elasticity) would provide better correlation with the data.

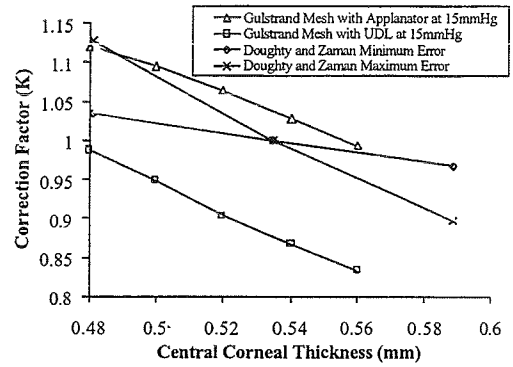

Figure 2 : Comparison of correction required to find true IOP from applanation tonometry for numerical and clinical data

SUMMARY

It has been shown that the biomechanics of the thin corneas can be represented reasonably accurately with a finite element models and compare favourably with clinical data. With further development this may provide a simple method of correcting tonometry readings for thin corneas to help improve clinical management of patients.

REFERENCES

Doughty, M.J. and Zaman, M.L., (2000) Human Corneal Thickness and Its Impact on Intraocular Pressure Measures. A Review and Meta-analysis Approach. *Surv Ophthalmol.* 44. 367-408.

Orssengo, G.J., Pye, D.C. (1999) Determination of the True Intraocular Pressure and Modulus of Elasticity of the Human Cornea *in vivo*. *Bul. Math. Biol.* 61, 551-572.

FREE VIBRATION OF A FINGERTIP: FINITE ELEMENT ANALYSIS

John Z. Wu, Subhash Rakheja, Ren G. Dong, Aaron W. Schopper, and W. Paul Smutz
National Institute for Occupational Safety and Health, Morgantown, WV, USA
E-mail: jwu@cdc.gov

INTRODUCTION

An extended occupational exposure to hand-transmitted vibration, arising from the operation of hand-held power tools, has been associated with the development of an array of vascular, sensorineural and musculoskeletal disorders. The vibrotactile perception threshold (VPT) measurement technique is widely used to diagnose the sensory neuropathy of the hand induced by an extended exposure to vibrations. The measured values of VPT have been reported to depend on the contact force, vibration frequency and magnitude, and the temperature of the finger skin [1]. Although the measured values of VPT responses of fingertips have been widely spread, no attempts have been made to develop adequate analytical models to study the mechanics of tactile sensation. This study proposes a finite element model of a human fingertip to study its responses to impinged vibration.

METHOD

A two-dimensional finite element (FE) model of a fingertip is developed to study its deformation-dependent vibration responses. The model is composed of linearly elastic bone and nail, and nonlinearly elastic and visco-elastic soft tissue. The fingertip was assumed to be symmetric (Fig. 1). The skin tissue is assumed to be in contact with a linearly elastic, smooth steel plate, representing the vibrotactile probe. The dimensions of the fingertip model are assumed to be representative of the index finger of a male subject. The material parameters of the soft tissues, bone, and nail are taken from the published experimental data [2,3]. The fingertip tissue is subjected to varying levels of static deformations and contact force by displacing the contact plate vertically. At $t=0$, the plate is considered to be in contact with the fingertip skin surface with negligible resultant contact force. The contact plate is then displaced upwards to achieve a predetermined value of the tissue deformation (Δ) within a ramping period of Tc (=1s). The FE simulation is performed to determine the free-vibration characteristics of the fingertip corresponding to different tissue deformation levels (Δ =1.5, 2.0, 2.5, and 3.0 mm).

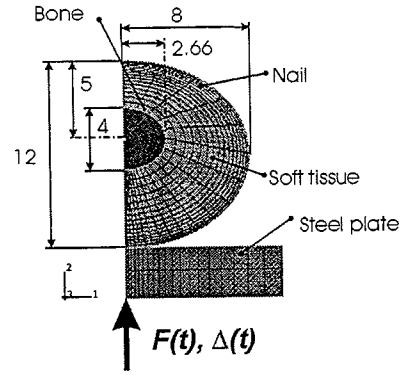

Figure 1: Finite element model of a fingertip

RESULTS

The modal analysis of the fingertip model was performed using the tangential stiffness of the tissue corresponding to the maximum deformation at $t=Tc$. The free vibration analysis of the fingertip model, as expected, resulted in a large number of natural modes. Considering that most power tools generate dominant vibration in the frequency range of 25-320 Hz [4,5], the first ten eigen-frequencies of the fingertip model were extracted corresponding to each static deformation. Fig. 2 illustrates the variations in the modal frequencies as a function of the static tissue deformation. The natural frequencies corresponding to the extracted modes lie in the 40 Hz to 320 Hz frequency range. The eigenfrequencies corresponding to the selected modes increase considerably with increase in the magnitude of the tissue compression or pre-load. The eigen-frequency corresponding to a specific mode

- PARALLEL SESSION -

Musculoskeletal Biomechanics

Thursday, August 9, 2001
1400 to 1530

LOWER EXTREMITY STRENGTH REQUIREMENTS IN YOUNG AND OLDER FEMALE ADULTS DURING LOCOMOTOR ACTIVITIES OF DAILY LIVING

Sicco A. Bus [1], Brandi S. Row [1,2], Noriaki Okita [1,6], and Peter R. Cavanagh [1-6]

[1]The Center for Locomotion Studies and Departments of [2]Kinesiology, [3]Biobehavioral Health, [4]Medicine, [5]Orthopaedics & Rehabilitation, and [6]Bioengineering, Penn State University, University Park, PA and The Penn State University College of Medicine, Hershey, PA
Email: celos@psu.edu Web: www.celos.psu.edu

INTRODUCTION

A comparison of joint moments with measured strength has demonstrated the relative difficulty of sit-to-stand (STS) tasks for older adults (Alexander et al., 1997). Such an analysis remains to be performed for various other locomotor activities of daily living (LADLs). Thus, the purpose of the present study was to compare maximum measured dynamometric strength with the calculated 3D lower extremity joint moments required to perform overground walking (OGW), sit-to-stand (STS), stair ascent (SA), and stair descent (SD) in healthy young and older adults.

METHODS

Eleven young [age: 24.2 (2.6) yrs, body mass (BM): 63.4 (7.2) kg, height: 165.0 (2.9) cm: mean (st. dev.)] and 10 active healthy older females [age: 73.5 (2.6) yrs, BM: 65.6 (10.8) kg, height: 158.3 (4.6) cm] were studied. VICON 370 (Oxford Metrics, U.K.) was used to collect 3D kinematics of the left lower extremity. Five trials of SA and SD were collected at 0.65 m/s on a 7-step staircase instrumented with a portable force platform (type 9286, Kistler Instrument Corp, NY). Five trials of OGW (1.35 m/s) and STS (rise time: 1.8s, chair height: 43 cm) were collected on a 10m runway equipped with a Kistler force platform (type 9287A). Net joint moments were calculated using the MARey package (Cavanagh et al., 2001). Maximum voluntary contractions (MVC) in the sagittal plane were assessed for the hip, knee, and ankle and for hip ab/adduction with a Biodex dynamometer (System 2, Biodex Med Sys, NY). The muscle contraction modes tested were isometric, 30°/s and 90°/s concentric, and 60°/s eccentric. All strength tests demonstrated good repeatability. For each subject in each activity, the strength requirement (%MVC) was expressed as the ratio of peak calculated joint moments to peak measured dynamometric torques (at the most appropriate contraction mode and joint angular velocity). Analysis of variance with Bonferroni corrections compared the differences in strength requirements between activities, and t-tests compared differences between age groups for each activity (Minitab 12, Minitab Inc, PA).

RESULTS

Older adults required a significantly higher fraction of measured MVC in the lower extremity musculature than young subjects to perform the majority of the LADLs studied (Table 1, Figure 1). The most significant age differences were found in the hip abductors (ABD) during all LADLs. The most demanding LADL was not the same for each muscle group. SA was most demanding for knee EXT and ankle PF whereas the hip EXT group was challenged the most during OGW. There were no significant differences in the demands placed upon the hip ABD during these LADLs, with the exception that SD was more demanding than OGW for the young.

DISCUSSION

Although STS is commonly used to assess the functional level in older adults, at the chair height used here it was one of the least challenging of the LADLs studied for the lower extremity musculature. Stair ascent required a substantial portion of the maximum available strength for both young and older adults, and should be considered in future analyses of strength and functional ability in older individuals. Similarly, the striking age differences in hip abductor requirements for all LADLs suggest that this muscle group should be considered in a functional assessment of older adults. The difficulties in comparing maximum measured strength and calculated joint moments are demonstrated by the finding that several LADLs were predicted to require more than 100% of the MVC at the ankle joint. Some requirements also seem unreasonably large at other joints. This is clearly an artifact of the different approaches to estimation of the two quantities and deserves further study.

Table 1. Required strength [mean (st. dev) in %MVC] for young and older adults

	Ankle	Knee	Hip	
LADL	PF	EXT	EXT	ABD
	Young			
SD	78.3 $^{b\,\dagger}$ (26.7)	55.0 † (26.5)	22.6 $^{\dagger\,\ddagger}$ (12.0)	74.7 $^{a\,\dagger}$ (15.8)
SA	179.1 $^{\dagger\,\ddagger}$ (56.0)	78.5 $^{b\,\dagger\,\ddagger}$ (16.1)	59.0 † (22.1)	65.8 ^{a} (17.8)
STS	29.2 $^{b\,\dagger}$ (10.0)	38.8 $^{a\,\ddagger}$ (6.9)	45.6 $^{b\,\ddagger}$ (10.1)	-
OGW	114.2 $^{b\,\ddagger}$ (29.4)	18.0 $^{b\,\dagger\,\ddagger}$ (8.6)	83.5 $^{\dagger\,\ddagger}$ (16.9)	57.1 $^{a\,\dagger}$ (18.1)
	Older			
SD	132.8 $^{b\,\dagger}$ (53.9)	68.8 † (21.8)	32.5 † (16.7)	100.3 ^{a} (17.3)
SA	232.4 † (79.0)	88.1 $^{b\,\dagger\,\ddagger}$ (16.7)	87.5 $^{\dagger\,\ddagger}$ (27.5)	86.1 ^{a} (13.9)
STS	43.8 $^{b\,\dagger\,\ddagger}$ (17.7)	52.1 $^{a\,\ddagger}$ (8.5)	57.9 $^{b\,\ddagger}$ (14.0)	-
OGW	176.4 $^{b\,\ddagger}$ (71.8)	29.6 $^{b\,\dagger\,\ddagger}$ (10.6)	105.1 $^{\dagger\,\ddagger}$ (31.3)	92.5 ^{a} (23.0)

Age difference within an activity ^{a} $p<0.01$, ^{b} $p<0.05$;
Activity difference within an age group $^{\dagger\,\ddagger\,*}$ $p<0.01$

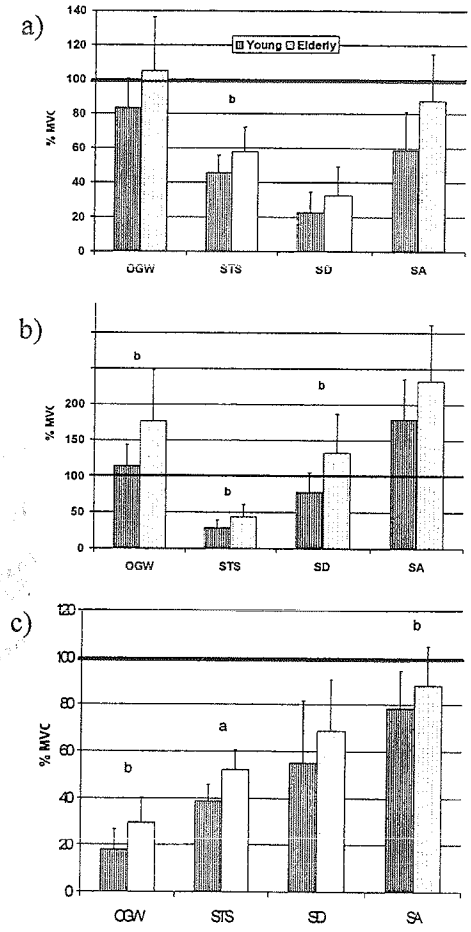

Figure 1. Required strength (%MVC) during LADLs in young and older adults for a) Hip EXT, (b) Ankle PF, and (c) Knee EXT. Solid line is 100% MVC.

REFERENCES

Alexander, N.B. et al. (1997). Musc Nerve, **5** (Suppl):S56-9.

Cavanagh, P.R. et al. (2001). ISB 2001.

ACKNOWLEDGEMENTS

This research was supported by NIH grants AG14073 and M01 RR10732. Mary Becker played an important role in recruitment and data collection. The authors would also like to thank Steve Piazza and Steve Arnold for their contributions to this project.

MODIFICATION IN INITIAL SEGMENT CONDITIONS REDISTRIBUTES MECHANICAL DEMAND DURING SIT-TO-STAND TASKS

Witaya Mathiyakom, Jill L. McNitt-Gray, Phillip S. Requejo, and Kathleen E. Costa
Biomechanics Research Laboratory, Department of Kinesiology,
University of Southern California, Los Angeles, CA 90089
E-mail: mathiyak@usc.edu

INTRODUCTION

The inability to rise from a chair limits an individual's functional mobility and restricts the activities available for those undergoing rehabilitation. Previous experimental and modeling studies suggest successful performance of sit-to-stand (STS) tasks involves total body momentum control, lower extremity strength, and multijoint coordination (Gross et al., 1998; Riley et al, 1997; Pai and Rogers, 1991). To facilitate performance of a sit-to-stand (STS) task, clinicians commonly move the position of the patient's total body center of mass (TBCM) closer to the base of support, as a means of simplifying the task at the total body level. The relocation of the TBCM relative to the feet, however, requires reorientation of the lower extremity segments relative to the reaction force. Modifications in the initial segment position however, may induce modifications in the mechanical demand imposed on the lower extremity during the STS task and as a result, increase the difficulty of the task at the joint level.

This study tests the hypothesis that modifications in initial segment positions will redistribute the mechanical demand imposed on the lower extremity during the performance STS tasks. Large variations in peak net joint moments (NJM) during STS tasks between subjects and studies suggest the distribution of load across the lower extremity may vary between subjects (Gross et al., 1998; Pai and Rogers, 1991). Therefore, between task differences in ankle, knee, and hip NJMs will be compared within subject.

METHODS

Eight normal subjects (4 women and 4 men) performed STS tasks with four different initial positions (Figure 1) using their self-selected strategies. These four initial positions are representative of those patient populations may use to accommodate limitations in lower extremity joint range of motion. Ground reaction force (1200 Hz) and sagittal plane kinematics (60 Hz) were collected simultaneously during the STS tasks. Each coordinate of the body landmarks (deLeva, 1996) were digitized, filtered using a fourth order Butterworth Filter (Saito & Yokoi, 1982) with cut-off frequencies determined using a method based on Jackson (1979). Kinematic and reaction force data were synchronized at seat departure. Net joint forces (NJF) and moments (NJM) for the ankle, knee, and hip were determined using Newtonian mechanics. Total body momentum and lower extremity NJMs at seat departure were compared between task within subject ($p<0.05$).

RESULTS AND DISCUSSION

Task specific differences in initial shank and thigh segment positions resulted in significant differences in mechanical demand imposed on the lower extremity (Figure 1). During weight acceptance, between task differences in ankle NJMs were attributed to more posterior center of pressure locations during Tasks 1 & 3 as

compared to Tasks 2 & 4. Orientation of the ankle posterior to the knee (Task 2 & 4) resulted in knee extensor NJMs that were twice the magnitude of those performed with the shank in the vertical position (Tasks 1 & 3). The magnitude of the hip extensor NJM was dependent on the angle of the thigh relative to the knee and hip NJF and the magnitude of the knee NJM. Subjects electing to increase total body momentum at seat departure experienced relatively larger reaction forces at seat departure. These relative increases in reaction forces accentuated the magnitude of the moments created by the NJFs about the shank (Task 2 & 4) and thigh (Task 3 & 4), and as a result, amplified the differences mechanical demand imposed on the knee and hip.

The results of this study indicate the mechanical demand imposed on the lower extremity can be redistributed by selectively reorienting initial shank and thigh positions. The NJMs determined for each task provide quantitative basis for clinicians to identify initial STS conditions that complement the capacity of a patient's muculoskeletal system. For example, patients unable to modify their initial segment positions (e.g. patients with limited ankle doriflexion or knee flexion due to osteoarthritis or a total knee replacement) may need to rise from a chair with ankle, knee, and hip angles at 90 degrees (Figure 1, Task 1). To prepare the patient to successfully perform this movement, the patient will need to generate and control momentum at the total body level and control the reaction force at the lower extremity level with a relatively large hip extensor NJM. If patient is unable to perform this movement, a specific exercise program to improve total body momentum control and hip net joint moment and power generation can be prescribed. In addition, knowledge of the mechanical demand imposed by this set of STS tasks may also provide the mechanical basis for an assessment tool to determine momentum control, loading preferences and/or avoidance strategies utilized by individual patients.

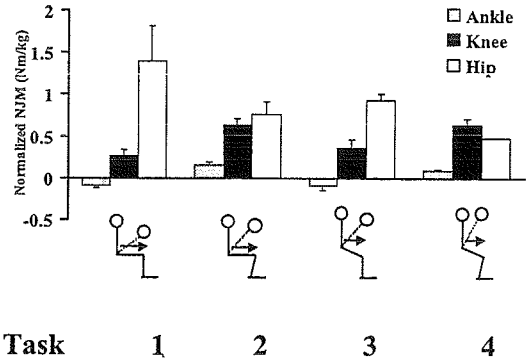

Figure 1. Differences in net joint moments (NJM) between sit-to-stand tasks (1-4) with different initial shank and thigh segment orientations for an exemplar subject with no significant differences in TBCM horizontal velocity at seat departure. Between task differences in trunk position at seat departure is represented with a dotted line.

REFERENCES

de Leva, P. (1996). *J Biomech,* 29, 1223-1230.

Gross, M., et al. (1998). *Gait Posture,* 8, 175-185.

Jackson, K. (1979). *IEEE Trans Biomed. Eng,* 26, 122-124.

Pai, Y. & M. W. Rogers, M. (1991). *Arch Phys Med Rehabil,* 72, 881-885.

Riley, P., et al. (1997) *IEEE Trans Rehabil Eng,* 5, 353-359.

Saito, S., & Yokoi, T. (1982). *Bull. of Hlth & Sport Sci,* U of Tsukuba, 5, 201-206.

IN VIVO AND NON-INVASIVE PATELLAR TRACKING

Amanda Fang Lin [1,2] and Li-Qun Zhang [1-4]

[1]Sensory-Motor Performance Program, Rehabilitation Institute of Chicago
Departments of [2]Physical Medicine & Rehabilitation, [3]Orthopaedic Surgery, and
[4]Biomedical Engineering, Northwestern University Chicago, Illinois
Email: l-zhang@northwestern.edu

INTRODUCTION

Patellofemoral pain (PFP) syndrome is one of the most common physical abnormalities involving the knee in sports-related injuries, and it is closely related to patellar malalignment and abnormal tracking. Patellar tracking was generally evaluated using cadaveric specimens, and in some cases, *in vivo* and invasive measurement was obtained[2,3]. The purpose of this study was to evaluate 3-D patellar tracking *in vivo* and noninvasively on human subjects.

METHODS

Nineteen knees from 11 subjects with no prior history of knee injuries were evaluated in the study. The subject was seated upright with the femur clamped at the medial and lateral condyles. Active markers were placed at the patella (through a small clamp), femur, and tibia to measure the patellar and leg movement[4]. Three-dimensional patellar tracking and tibial movement were studied during voluntary knee extension in the range of 15° to 0° flexion and during selective activation of the vastus medialis longus (VML), vastus medialis oblique (VMO), and vastus lateralis (VL) at 20° and 0° flexion combined with tibial axial rotation of −10° (external), 0°, and 10° (internal). Patellar tracking was described in a coordinate system with the origin located at the center of the patella. For the right patella, the x, y and z axes pointed medially, proximally, and anteriorly, respectively. The patellar rotations about the x, y and z axes were defined as flexion/extension, mediolateral tilt, and mediolateral rotation, respectively. Patellar shift along and rotation about each axis were used to calculate the direction of translation (DOT) and direction of rotation (DOR). The DOT was defined as $DOT_x=T_x/T$, $DOT_y=T_y/T$, and $DOT_z=T_z/T$ with $T=\sqrt{T_x^2+T_y^2+T_z^2}$. The DOR was calculated in a similar way.

RESULTS AND DISCUSSION

When the subjects voluntarily extended the knee from 15° flexion to full knee extension, the patella was extended about 8° and laterally tilted 2° (Fig. 1). At the same time, the patella shifted laterally 3mm, proximally 10mm, and anteriorly 3mm. Shortly before the knee reached full extension, the patella stopped lateral tilt and lateral rotation.

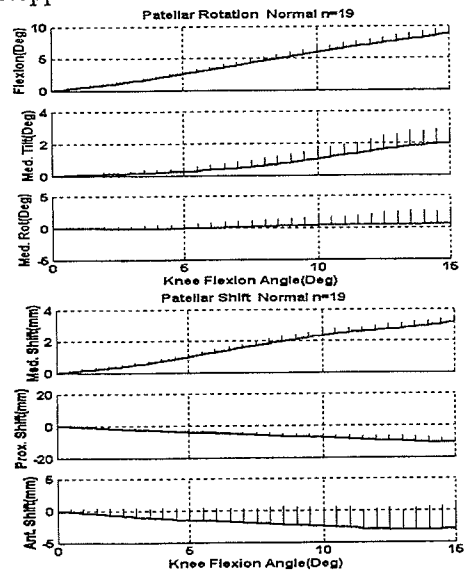

Fig. 1. Six DOF patellar tracking during voluntary knee extension from 15° knee flexion to full knee extension. The zero position corresponded to patellar position at full knee extension. The positive direction of each DOF is given for the ordinate.

Selective activation of different quadriceps components generated quite different patellar tracking (Fig. 2). Selective contraction of the VL mainly pulled the patella proximally at full knee extension. In contrast, contraction of the VMO mainly pulled the patella in the medial direction (Fig. 2). Both the VMO and VL extended the patella, while the VMO also generated considerable medial tilt of the patella. Compared with patellar tracking at more flexed knee positions, the patella was moved in a larger range of motion at full knee extension by comparable quadriceps contractions. From full knee extension to

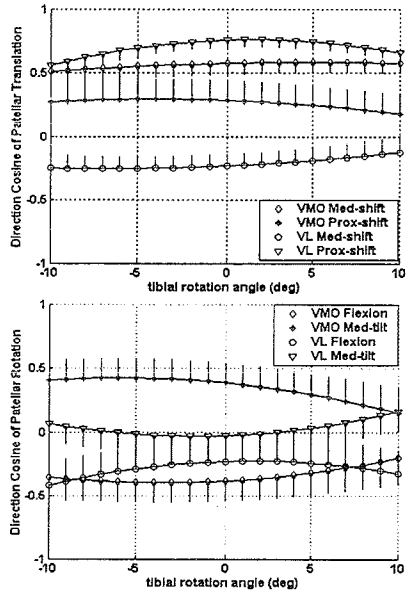

Fig 2. Patellar DOT (top) and DOR (bottom) generated by contraction of the VMO and VL at various tibial axial rotation positions. The knee was at full extension. Results are shown in mean ± SE.

20° knee flexion, the VMO's main action changed from patellar extension to flexion, especially when the tibia was internally rotated. Unlike the VMO, the main action of the VML in patellar tracking did not change much between 20° knee flexion and full knee extension, and it maintained its main actions of patellar extension, medial tilt, and proximal shift. At full knee extension, none of the three heads of superficial quadriceps components changed its main action with different tibial axial rotations. At 20° knee flexion, the VMO and VML changed their main actions considerably, mostly in the rotations of the patella.

The results were in general consistent with in vitro and in vivo data reported previously[2-4]. In addition, we found that the DOR and DOT in patellar tracking could be altered by activating different portions of a quadriceps component.

The noninvasive fixation of the patellar clamp used in this study restricted the technique to the more extended knee position. However, this is happens to be the range where the patellar malalignment and abnormal tracking tend to be more significant. It is also the range difficult to apply the radiographic methods.

SUMMARY

The above study provides us a tool to evaluate patellar tracking in vivo and noninvasively during voluntary knee extension and during selective activation of individual head of quadriceps. Furthermore, patellar tracking was evaluated at various knee flexion and tibia rotation angles. Further work is being carried out to compare patellar tracking between normal and patellar malaligned subjects.

REFERENCES

1. Fulkerson, J.P. (1997). *Disorders of the Patellofemoral Joint.* Williams & Wilkins
2. Koh, T.J., et al.(1992). *J Biomech*,**25**, 637-643.
3. Heegaard, J., et al.(1994). *Clin Orthop Res*, 299:235-243.
4. Wang, G., et al.(1998). 3rd N. Am. Congress on Biomechanics, Waterloo, Canada, Aug. 513-514.

ACKNOWLEDGEMENTS

The study was supported by NIH (LZ).

EFFECTS OF FATIGUE ON THE REGULATION OF LEG SPRING STIFFNESS

Gregory M. Harron[1], Peter F. Vint[1], and Julie A. Kraus[2]
[1]Research Integrations, Inc., Tempe, AZ
[2]University of North Carolina at Greensboro, Greensboro, NC
E-mail: Greg.Harron@ResearchIntegrations.com

INTRODUCTION

As a greater understanding of the role of leg spring stiffness in locomotion has been realized, research in this area has begun to shift toward the underlying mechanisms that control leg stiffness. Leg stiffness adjustments can be accomplished either by changes in the torsional stiffness of the various leg joints or by changes in the leg geometry at ground contact (Farley & Morgenroth, 1999). Examining the effects of muscle fatigue on leg spring stiffness, leg geometry, and torsional joint stiffness during hopping may help to further explain the role of active muscle force in the regulation of leg spring stiffness.

Landing in a more extended knee position can result in reductions in muscle activity about the knee (Farley et al., 1998). Possible reasons for the decrease in muscle activity include a decreased ground reaction force (GRF) moment about the knee and more force distribution to bone in the landing phase (Farley et al., 1998). Under fatigued conditions, it seems reasonable that a more extended landing position would be implemented to decrease the demands of the active musculature.

Torsional joint stiffness values are dependent upon a number of factors, including muscle activation, reflexes, joint moment, and the angular position of the joint (Farley et al., 1998; Horita et al., 1996). Fatiguing the muscles surrounding a joint may cause changes in any of the above mechanisms involved in joint stiffness regulation.

The purpose of this study was to determine if knee flexor and/or knee extensor muscle fatigue results in changes in hip, knee, and ankle joint stiffness or changes in leg geometry when hopping at a preferred hopping height and frequency.

METHODS

Thirty subjects (mean age 22.6 ± 2.8 years; mean body weight 147.6 ± 29.6 lbs.) were divided evenly into the following three fatigue condition groups: knee extensor fatigue, knee flexor fatigue, and combined knee extensor and knee flexor fatigue. The fatigue protocol consisted of three maximum effort bouts of continuous concentric exertions performed on an isokinetic dynamometer. Each bout was terminated when the subject failed to produce 40% of MVC (maximum voluntary contraction) force for 5 consecutive exertions. All subjects performed two-legged hopping in place at their preferred hopping height and preferred hopping frequency before and after completion of the appropriate fatigue protocol. GRF and sagittal plane kinematic data were collected for all hopping trials at 960 and 60 Hz, respectively.

RESULTS AND DISCUSSION

Across all subjects, the fatigue protocol resulted in a reduction in knee flexion and/or knee extension MVC force of 19.5% following the fatigued hopping trials. However, subjects were able to maintain spring-like characteristics as they hopped. Specifically, for both non-

fatigued and fatigued hoppers, the peak GRF during ground contact typically occurred when the body center of mass was at its lowest point. Subjects maintained similar leg spring stiffness values for pre-fatigued and fatigued hopping trials (Table 1).

The various leg joints maintained torsional spring-like properties with the peak joint moment coinciding with the point of maximal joint flexion under all conditions. There were no significant differences for ankle, knee, or hip joint stiffness values between pre-fatigued and fatigued hopping trials (Table 1).

Limb geometry at landing and at the low point of the ground contact phase was similar for the ankle and knee when comparing pre-fatigued and fatigued hops. The hip joint maintained a slightly more flexed position at landing and at the low point of the hop for fatigued hopping trials. However, the magnitude of these differences was very small (0.030 radians and 0.027 radians for the landing and low point, respectively).

Maximum effort concentric fatigue about the knee presented only small changes in the overall hopping technique. The muscle fatigue protocol may have caused changes to the stiffness of muscle fibers without affecting joint stiffness. Muscle stiffness has been shown to decrease under fatigue (Avela & Komi, 1998), however, the more compliant tendon is typically the limiting factor in the overall combined muscle-tendon stiffness (Alexander, 1997). Therefore, if the fatigued muscles were still able to generate sufficient tension to utilize the elastic properties of the tendon (through near isometric activity for this hopping movement), no major differences in joint stiffness should have resulted. The efficient use of elastic tendon properties in this spring-like movement may have eliminated the need for a major compensatory movement strategy.

REFERENCES

Alexander, R., McN. (1997). *J. Appl. Physiol.*, **82**, 13-14.

Avela, J., Komi, P.V. (1998). *Muscle & Nerve*, **21**, 1224-1227.

Blickhan, R. (1989). *J. Biomech.*, **22**, 1217-1227.

Farley, C.T. et al. (1998). *J. Appl. Physiol.*, **85**, 1044-1055.

Farley, C.T., Morgenroth, D.C. (1999). *J. Biomech.*, **32**, 267-273.

Horita, T. et al. (1996). *Eur. J. Appl. Physiol.*, **73**,393-403.

Table 1: Stiffness data for normal and fatigue hopping trials for all groups (mean ± SD).

	Knee Extensor Group		Knee Flexor Group		Knee Flex/Ext Group	
Stiffness	Normal	Fatigue	Normal	Fatigue	Normal	Fatigue
Leg ($kN \cdot m^{-1}$)	18.8 ± 5.0	18.5 ± 4.9	16.9 ± 4.3	17.6 ± 4.4	13.9 ± 2.9	14.3 ± 3.5
Ankle ($N \cdot m\ rad^{-1}$)	558 ± 196	561 ± 186	491 ± 165	514 ± 141	397 ± 117	417 ± 187
Knee ($N \cdot m\ rad^{-1}$)	552 ± 263	584 ± 282	541 ± 174	508 ± 151	470 ± 146	448 ± 86
Hip ($N \cdot m\ rad^{-1}$)	84 ± 508	322 ± 554	223 ± 459	251 ± 634	−121 ± 575	168 ± 540

SIMULATING ANATOMICAL VARIATIONS IN THE THUMB: EFFECT ON MAXIMAL FORCE AND MUSCLE ACTIVATION

F.J. Valero-Cuevas[1,2], J.D. Towles[3,4], M.E. Johanson[3]

[1]Neuromuscular Biomechanics Laboratory, Cornell University, Ithaca, New York, U.S.A.
[2]Department of Biomechanics, The Hospital for Special Surgery, New York, New York, U.S.A.
[3]RR&D Center, VA Palo Alto Health Care System, Palo Alto, CA, U.S.A.
[4]Mechanical Engineering Department, Stanford University, Stanford, California, U.S.A.
E-mail fv24@cornell.edu Web: http://www.mae.cornell.edu/valero

INTRODUCTION

Impairment of the thumb following neuro-musculo-skeletal conditions (e.g., peripheral neuropathies, osteoarthritis) can severely diminish manipulation ability. Treatments to restore effective key and opposition pinch focus on restoring thumbtip forces. Ideally, treatment outcomes should be consistent across individuals despite anatomical variations (e.g., in thumb size). In practice, outcomes can vary greatly. In preparation to study the variability of key and opposition pinch outcomes, we now explore the effect of anatomical variations on maximal unimpaired thumbtip forces, and the muscle activation patterns that achieve them.

METHODS

Thumbtip force magnitude and EMG from all thumb muscles were simultaneously recorded during maximal voluntary contractions of the thumb in standardized key and opposition postures. Subjects produced thumbtip force against a smooth dynamometer in directions perpendicular and collinear to the distal phalanx in key and opposition postures. Metallic beads embedded on a thimble (Figure 1) defined a low-friction contact to ensure thumbtip force was well directed, or else the bead would slip *(Valero-Cuevas et al., 1998)*. Subjects rested their forearm in a trough and wrapped their fingers around a vertical dowel (Figure 1). We recorded fine-wire EMG from the eight muscles of the thumb: flexors pollicis longus (FPL) and brevis (FPB), extensors pollicis longus (EPL) and brevis (EPB), abductors pollicis longus (APL) and brevis (APB), opponens pollicis (OPP), and adductor pollicis (ADD). Seven subjects (mean age 26 yrs.) signed an IRB-approved consent form. Thumbtip force magnitude was displayed as a trace on a computer screen with visual targets encouraging subjects to maximize force within 10 s. Each muscle s activation for maximal force was the mean of its full-wave rectified, filtered and normalized EMG in a 750 ms window centered on maximal force (Figure 2).

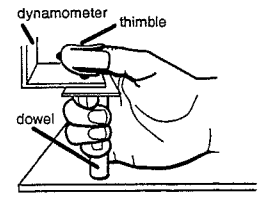

Figure 1. Producing thumbtip force in standardized key posture. For opposition posture, the thumb is abducted 45° and the dynamometer contacts the other bead.

A computer model of the thumb in *Mathematica* language predicted the unique muscle activation pattern that maximized thumbtip force in two directions (perpendicular and collinear to the distal phalanx) for two postures (key and opposition, Figure 1). Five pin-joints articulate a fixed trapezium, a metacarpal bone and two phalanges; eight isometric Hill-type models simulated the thumb muscles. Cadaver studies provided muscle architecture parameters *(Jacobson et al., 1992; Lieber et al., 1992)* and moment arms *(Smutz et al., 1998)*. Phalanx lengths and

joint angles were those measured in the experimental subjects. The effects of anatomical variations on maximal thumbtip force and muscle activation were predicted for 10,000 iterations of a Montecarlo simulation *(Hughes and An, 1997)*. At each iteration, moment arms, maximal muscle force, phalanx lengths and joint angles were randomly varied within 3 standard errors of their experimental mean as a Gaussian distribution.

RESULTS

The maximal measured thumbtip forces for key and opposition postures were 47.4–19.3 N and 46.7–22.5 N, respectively, compared to 17.8–12.2 and 14.65–16.3 N predicted by the Montecarlo simulation.

In 13 of 16 comparisons, the 75 percentile of predicted activation (white boxes in Figure 2) overlapped or included the 75 percentile of EMG values (gray boxes). In three comparisons (arrows in Figure 2), predicted activation and EMG boxes did not overlap.

DISCUSSION

Perhaps because parameter co-variance was not modeled (i.e., larger hands may be associated with stronger muscles), the predicted coefficient of variance of force (SD as % of mean) and distribution of activation were greater than those measured. The model s underestimation of thumbtip force by a factor of 2 supports the notion that finger models based on physiological cross sectional areas measured in cadavers are not representative of the strength of young adults *(Valero-Cuevas et al., 1998)*. Our representation of ADD in key posture, and of FPB and EPL in opposition posture, may require modification because their predicted activation was consistently lower than measured values.

The overlap in measured and predicted

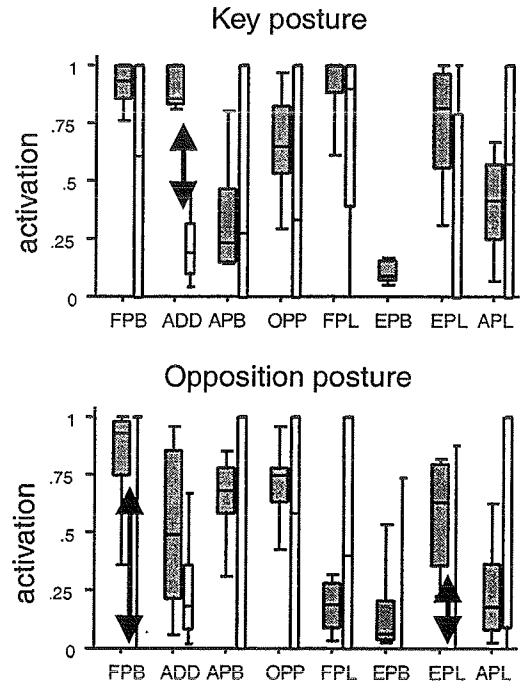

Figure 2. Box plot distribution of muscle activation range: EMG (gray) and Montecarlo simulations (white).

activation range in 13 of 16 comparisons suggests our representation of these muscles can approximate well their biomechanical action. The predicted range of activation for each muscle reflects the sensitivity of its recruitment to anatomical variations, which can be high (APL), low (EPB) or depend on posture or force direction (FPL).

REFERENCES

Hughes, R. E. and An, K. N. (1997). *Medical and Biological Engineering and Computing* **35**, 544-548.

Jacobson, M. D. et al (1992). *Journal of Hand Surgery (American)* **17**, 804-809.

Lieber, R. L. et al (1992). *Journal of Hand Surgery (American)* **17**, 787-798.

Smutz, W. P. et al (1998). *Journal of Biomechanics* **31**, 565-570.

Valero-Cuevas, F. J. et al (1998). *Journal of Biomechanics* **31**, 693-703.

ACKNOWLEDGEMENTS

Whitaker Foundation. VA RR&D Service.

DO ULNAR INSERTIONS OF THE TFCC AFFECT DRUJ STABILITY?

PG Neale, RA Berger, T Nakamura, J-R Haugstvedt, ME Hahn, K-N An

Biomechancs Laboratory, Division of Orthopedic Research, Mayo Clinic, Rochester, MN, USA
E-mail: an.kainan@mayo.edu

INTRODUCTION

Clinical problems at the distal radioulnar joint (DRUJ) are frequently due to a compromise of one of the many stabilizing soft tissues surrounding the joint. Disruption of one or more of these structures affects stability, however it is not known how each structure specifically contributes. Previous work determined that the radioulnar ligaments (RUL) in the triangular fibrocartilage complex (TFCC) are the most important structures in maintaining joint stability (Stuart, 1999). However, the anatomy of the RUL shows that they converge from separate radial origins to attach as a conjoined ligament to the ulna in two locations: the fovea at the base of the ulnar styloid process, and along the length of the ulnar styloid process itself (Ishii 1998; Nakamura 1996). Disruption of the foveal or styloid attachments of the RUL may lead to a different instability pattern than disruption of an isolated ligament attachment from the radius. No study has been performed to assess the importance of these attachments, particularly as they relate to dynamic stability of the DRUJ.

In an attempt to quantify dynamic instability at the DRUJ, our laboratory has adopted the use of an Instability Index (Neale, 2000). This method uses the intersection of vectors created from bony landmarks to calculate the instability (Figure 1). This method can incorporate the effects of instability due to both translation and rotation at the joint.

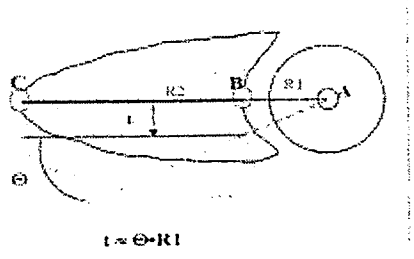

Figure 1: Definition of the instability index.

The purpose of this study was to further establish the Instability Index as a reliable means to quantify bony motion, and to use the Instability Index to quantify the role of the ulnar insertions of the TFCC in a human cadaveric study.

METHODS

Human cadaveric forearms, transected at the mid-humerus level, with soft tissues around the wrist and elbow were prepared. Three pronators (PQ, PT, FCU) and three supinators (supinator, biceps, ECU) were preserved and controlled by air actuators, with the line of action determined for each. The specimens were mounted on a custom forearm simulator which prescribed passive pronation-supination motion regulated by a PC controlled motor. 3Space Fastrak electromagnetic sensors (Polhemus, Inc., Colchester, VT) were attached to the radius, ulna, and metacarpals to measure the relative motion of these bones. Three muscle loading conditions were simulated: unloaded, assisting the motion, and resisting the motion.

Repeatability study: 17 specimens were prepared. Four trials were collected for each condition. The Instability Index was calculated throughout the range of motion. The intraclass correlation coefficient (ICC) was calculated at 6 positions throughout the range of motion.

Dynamic cadaveric study: 12 human cadaveric forearms were prepared and

loaded as described above. The specimens were tested in the intact state, and then after sequential cutting of the ulnar insertions of the TFCC (at ulnar fovea and styloid). The Instability Index was calculated throughout the range of motion. Results were statistically compared with a two-factor ANOVA.

RESULTS

Repeatability study: The ICC determined that the Instability Index, as measured using the dynamic simulator, was a highly repeatable means of measuring instability. The ICC for both the assistive and unloaded specimens was greater than 0.998 throughout the full range of motion. Under resistive loading, the ICC was only slightly lower, with an average of 0.989 during pronation and 0.956 during supination.

Dynamic cadaveric study:
No differences were noted between the instability created with each of the two ligaments sectioned in the unloaded muscle condition. However, once the muscles were loaded, statistical differences were observed. Sectioning the ulnar fovea had the largest effect on the instability at the joint. This difference was largest under assistive loading in the supination area of the range of motion (Figure 2), however, similar trends were observed under resistive loading as well

DISCUSSION

The Instability Index has proven to be a highly repeatable means of measuring instability in the DRUJ. This method provides added benefits to the more traditional means of calculating the changes in kinematics, namely using Euler angles and screw displacement axes, as this method mathematically accounts for changes in both rotation and translation between the bones—

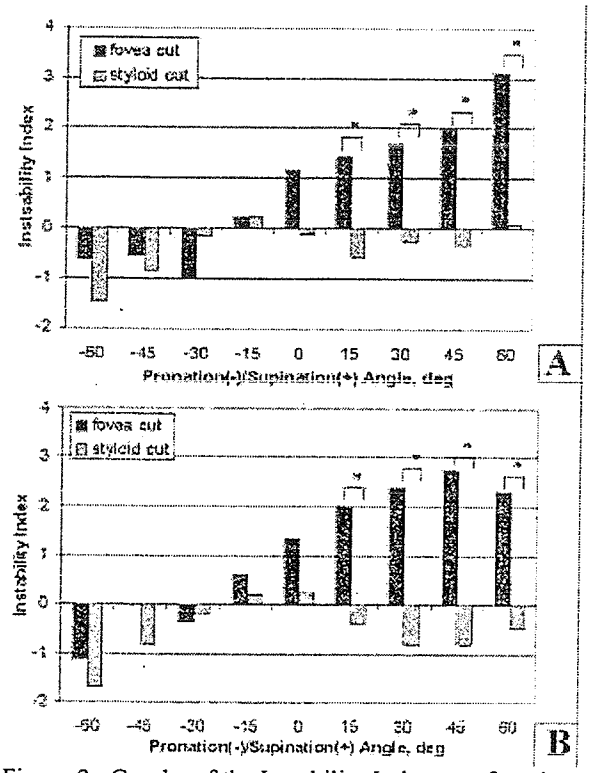

Figure 2. Graphs of the Instability Index as a function of sectioning foveal and styloid insertions of the TFCC in pronation (A) and supination (B).

a varying phenomena which is frequently seen at the DRUJ.

The fovea insertion of the TFCC appears to have the largest effect on the stability of the DRUJ, and this effect is exacerbated in the supination region of motion, where the joint is typically more stabile. In the pronation region, where joint laxity tends to be highest clinically, sectioning of either insertion individually does not substantially create additional instability.

REFERENCES

Ishii SI et al. (1998). J Hand Surg. **23A**, 977-985.

Nakamura T et al (1996). J Hand Surg. **21B**. 581-586.

Neale, PG et al. (2000). Proceedings of ASB 2000, 157-158.

Stuart, P et al (1999). J Hand Surg. **25A**, 689-99.

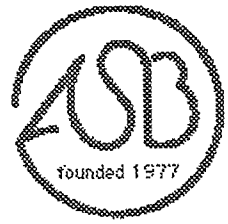

- PARALLEL SESSION -

Locomotion (Running)

Thursday, August 9, 2001
1400 to 1530

IMPACT FORCES DURING RUNNING IN A NOVEL SPRING BOOT

Jason Vance and John A. Mercer

Department of Kinesiology, University of Nevada, Las Vegas
E-mail: vance@nevada.edu Web: http://www.unlv.edu/faculty/jmercer

INTRODUCTION

It has been reported that runners generally select a running style that optimizes oxygen cost of running but not impact magnitude (Hamill et al., 1995). Since impact magnitudes have been hypothesized to be related to running overuse injuries (Hreljac et al., 2000), it seems reasonable to suspect that if the impact magnitude can be reduced, the risk of overuse injuries could be reduced. Recently, a spring-boot (SB, Kangoo, Inc.) has been developed for general exercise use. Based on boot construction, a purpose of the SB is to reduce impact magnitudes during activities such as running. Since runners can change their running style (e.g. change stride length), and since running style affects impact attenuation (Hamill et al., 1995), it is not known if impact magnitudes are attenuated during SB running. Therefore, the purpose of this study was to determine if impact magnitudes are affected while running with SBs.

METHODS

Seven healthy subjects (age: 23±2.5 years, height:168±8 cm, mass: 62±11 kg; male: n=4, female: n=3) were recruited from a university population. Informed consent was obtained prior to data collection. Subjects ran at three different velocities (2.2, 3.1, and 4.0 $m \cdot s^{-1}$) during two shoe conditions: 1) running shoes (RS, laboratory shoe); 2) Spring Boot (SB, Kangoo, Inc.). Order of shoe and velocity conditions was counterbalanced among subjects. All running trials were completed along a 20m runway with the right foot contacting a force plate (Kistler) mounted in the middle of the runway. GRF data were collected (1000Hz) for five acceptable trials for each shoe-speed condition. An acceptable trial was defined as the right foot entirely contacting the force platform with no obvious modification of stride (e.g., lunge or stutter-step), and velocity within ±5% of the target velocity. Velocity was monitored using sensors placed 3m before and 2m after the center of the force platform. Prior to testing, ample time was allowed for subjects to become comfortable with SB running. Impact magnitude (F1), active force peak (F2), average vertical force (F_{avg}), and contact time were each analyzed using repeated measures ANOVA with linear contrast follow-up testing (SPSS, version 10.1).

RESULTS AND DISCUSSION

An impact peak was observed in 15% of the trials during SB running, compared to 96% of the trials during RS running. Table 1 reports the percent of trials in which F1 was observed per condition.

Table 1: Percent of trials that impact peak was observed.

	Velocity (m/s)			
Condition	**2.2**	**3.1**	**4.0**	**Total**
RS	89%	100%	100%	96%
SB	3%	6%	37%	15%

Mean for F1 was not calculated across subjects since only a small number of trials contained an impact peak. However, one subject who had at least one F1 per

condition, F1 magnitude ranged from 1.0-1.6 BW during RS and 1.5-2.0 BW during SB running. This suggests that for this user, impacts were not attenuated but for the majority subjects F1 was attenuated. The observation that frequency of F1 occurrence increased as velocity increased indicates that the effectiveness of the boots to attenuate impact peak was related to velocity.

F2 increased linearly across velocity for both RS and SB conditions (Figure 1, $p<0.05$) with F2 increasing 0.28 BW/m·s^{-1} during RS but only 0.17 BW/m·s^{-1} during SB. However, F2 was not different between shoes collapsing across velocity ($p>0.05$).

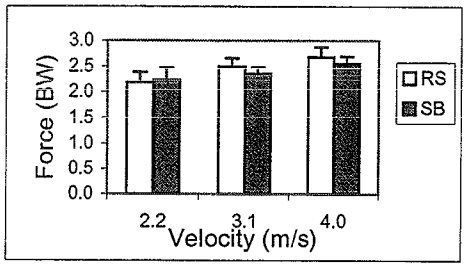

Figure 1: F2 during SB and NS running.

F_{avg} increased linearly across velocity during RS (0.20 BW/m·s^{-1}) and SB (0.13 BW/m·s^{-1}) running (Figure 2, $p<0.05$). The F_{avg} increase during RS was similar to the 0.21 BW/m·s^{-1} increase across similar velocities reported by Munro et al. (1987). Mean F_{avg} was 6% greater during SB than RS across velocity (Figure 2, $p<0.05$).

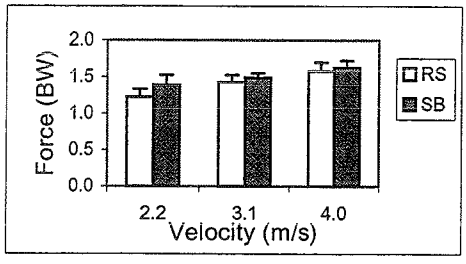

Figure 2: F_{avg} during SB and RS running.

Contact time was not different between RS and SB running ($p>0.05$) but did decrease linearly across velocity for both conditions ($p<0.05$). There is evidence indicating that runners adjust lower extremity stiffness to surface stiffness. Ferris et al. (1999) reported that runners adjusted lower extremity stiffness inversely proportional to the surface stiffness. They also reported that contact time and peak forces were similar during running across surfaces with different stiffness when runners adjusted lower extremity stiffness to the surface. Hardin et al. (2000) also reported that lower extremity stiffness was modified to surface-shoe changes. In the present study, the similarity in contact time and F2 between shoes across velocity suggests that subjects adjusted lower extremity stiffness to SB stiffness.

SUMMARY

Running with SB reduced the frequency of occurrence of F1 compared to RS, but F2, F_{avg} and contact time remained similar between conditions across velocities tested. It is suggested that subjects were able to adjust lower extremity stiffness to the novel spring surface with the impact cost of running reduced.

REFERENCES

Ferris, D.P. et al (1999). *J. Biomech.*, **32**, 787-794

Hamill, J. et al (1995). *Hum. Movt. Sci.*, **14**, 45-60

Hardin, E.C. et al. (2000). *Proceedings of 24th Annual Meeting of ASB.*

Hreljac, A. et al (2000). *Med. Sci. Sp. Ex.*, **32**, 1531-1666

Monroe, C.F. et al (1987). *J. Biomech.*, **20**, 147-155

ACKNOWLEDGEMENTS

The authors would like to thank Kangoo, Inc. for providing SB for testing.

AN EXAMINATION OF GROUND REACTION FORCES IN RUNNERS WITH VARIOUS DEGREES OF PRONATION

Joanna B. Morley[1], Nick Stergiou[2], Tracy Dierks[2], Daniel Blanke[2], and Jeffrey A. French[2]
[1]Peak Performance Technologies, Inc., Englewood, Colorado
[2]HPER Biomechanics Lab, University of Nebraska at Omaha, Omaha, Nebraska
Email: nstergio@unomaha.edu Web: www.unocoe.unomaha.edu/hper/hper.htm

INTRODUCTION

Few studies have examined the kinetic differences between normal runners and runners exhibiting overpronation, and an even smaller proportion of these studies have included measurements of medio-lateral ground reaction forces (MLGRF; Freychat et al., 1996; Messier et al., 1991; Williams et al., 1987). The relationship between M-L GRFs and patterns of pronation is of considerable interest because of their commonality of side-to-side movement. The use of MLGRF to analyze various running characteristics, however, has been limited due to the lack of established reliable standards. The purpose of this study was to examine possible relationships between MLGRF and different degrees of pronation during running. A barefoot condition was also incorporated to observe possible interactions between changes in forces and movement patterns.

PROCEDURES

Thirty subjects (17 males and 13 females) ran at a self-selected pace with and without their normal athletic shoes. Frontal kinematic (Peak Performance video system; 60 Hz) and kinetic (Kistler force platform; 960 Hz) data were collected for 10 trials per condition. Following data analysis, the subjects were divided into three equal groups based upon their peak eversion values: the underpronation (U; 3-8.9 deg), the normal-pronation (N; 9-12.9 deg), and the overpronation (O; 13-18 deg) groups. The lower limit for the overpronation group was based on Clarke et al. (1984). The kinematic parameters analyzed were the maximum eversion (ME) and the time to maximum eversion (TME). The kinetic parameters analyzed were the peak medial MLGRF (PM), the peak lateral MLGRF (PL), their respective times of occurrence (TPM and TPL), the absolute difference between PM and PL (AD), the impulses associated with the PM and the PL (IPM and IPL) and the total medial and lateral impulses (ITM and ITL). Two by three mixed ANOVAs [(shoe X subject) X pronation group], with shoe as the repeated factor were performed on the subject means for each dependent variable. A one-way ANOVA was performed on group means for average speed of running trials to confirm that groups performed similarly under testing conditions.

RESULTS AND DISCUSSION

The mean running speed for all subjects was 3.41 m/s, and it was found that speeds were not significantly different among groups. The barefoot condition resulted in decreased eversion values across all groups (Table 1). A possible explanation for this phenomenon is modifications to running technique and increased plantarflexion which is associated with supination. Furthermore, the barefoot condition resulted in larger MLGRF peaks. This result may imply that the shoe functions to decrease these forces and improve side-side stability. No significant differences were found for all force

parameters expect AD. Messier et al. (1991) found that TPL was a significant discriminator between controls and a group that exhibited patellofemoral pain and increased pronation. Our results did not support such a claim. Based upon relative times of occurrence, it can be observed that peak medial GRF are more closely associated to peak eversion than peak lateral GRF. This was found to be more evident in the barefoot condition. Lastly and as indicated by the high standard deviations in Table 1, the MLGRF plots were characterized by large amounts of variability.

SUMMARY

It was concluded that the amount of eversion had no effect on the magnitude of MLGRF. The barefoot condition was found to have a significant effect on selected kinematic and kinetic variables. The results obtained from associations of MLGRF and footwear revealed that shoes provided increased stability to the foot. The large variability related to individual subject data made it difficult to formulate any solid conclusions indicative of reliable MLGRF standards. Thus, further research must be performed in this area before knowledge gained can be used for practical applications.

REFERENCES

Clarke, T.E. et al (1984). In E.C. Frederick (Ed.), *Sport Shoes and Playing Surface.* Human Kinetics Publ., 166-189.

Freychat, P. et al. (1996). *Med. Sci. Sports Exerc.*, **28**, 225-232.

Messier, S.P., Pittala, K.A. (1988). *Med. Sci. Sports Exerc.*, **20**, 501-505.

Williams, K.R. et al. (1987). *Int. J. Sports Med.*, **8**, 107-118.

Table 1: Parameters evaluated for both conditions (mean ± SD). Timing parameters are expressed in % of stance, impulses in Nsec, MP in degrees, and PM and PL in BW.

	Shoe Condition			Barefoot Condition		
	Under	Normal	Over	Under	Normal	Under
ME	$6.7^{N,O} \pm 2.1$	$10.3^{O,*} \pm 0.9$	$14.8^{*} \pm 1.5$	$6.3^{O} \pm 2.6$	$6.7^{*} \pm 1.7$	$9.2^{*} \pm 3.2$
TME	$38.6^{*} \pm 7.1$	$40.6^{*} \pm 10.9$	$36.9^{*} \pm 8.3$	$25.0^{*} \pm 11.5$	$23.8^{*} \pm 10.2$	$27.2^{*} \pm 8.4$
PM	0.10 ± 0.03	0.13 ± 0.05	0.10 ± 0.04	0.10 ± 0.03	0.14 ± 0.05	0.11 ± 0.03
TPM	$32.9^{*} \pm 10.4$	28.7 ± 11.2	23.9 ± 13.7	$24.0^{*} \pm 13.1$	22.4 ± 7.9	21.9 ± 10.8
PL	0.11 ± 0.06	$0.09^{*} \pm 0.02$	0.11 ± 0.05	0.12 ± 0.03	$0.13^{*} \pm 0.04$	0.12 ± 0.03
TPL	$22.5^{*} \pm 20.3$	$17.7^{*} \pm 6.2$	$20.0^{*} \pm 14.9$	$12.9^{*} \pm 12.2$	$7.23^{*} \pm 3.4$	$9.72^{*} \pm 9.0$
AD	$0.20^{N} \pm 0.05$	$0.23^{O,*} \pm 0.06$	0.21 ± 0.05	0.22 ± 0.04	$0.27^{*} \pm 0.08$	0.24 ± 0.05
IPM	$4.75^{*} \pm 3.5$	5.61 ± 3.7	3.67 ± 3.2	$3.36^{*} \pm 1.9$	4.81 ± 3.3	3.47 ± 2.3
IPL	1.25 ± 0.8	1.11 ± 0.5	$2.85^{*} \pm 3.8$	1.35 ± 0.8	1.04 ± 0.7	$1.43^{*} \pm 0.7$
ITM	5.52 ± 3.5	6.65 ± 3.8	4.25 ± 3.4	4.29 ± 2.3	6.16 ± 3.6	4.37 ± 2.1
ITL	2.27 ± 1.7	1.86 ± 1.0	4.96 ± 3.8	2.54 ± 1.47	2.07 ± 1.0	3.71 ± 2.6

* Indicates significant differences ($P<0.05$) for the same group between conditions.
^{N,O,U} Indicate significant differences ($P<0.05$) for the same condition between groups.

CHANGES IN RUNNING LEG MECHANICS DUE TO MUSCLE SORENESS

Darren Dutto[1] and Turi Braun[2]
[1]Biomechanics Laboratory and [2]Human Performance Laboratory,
California State Polytechnic University, Pomona, CA, USA
E-mail: ddutto@csupomona.edu

INTRODUCTION

Downhill running can produce muscle soreness/damage. Delayed onset muscle soreness has been found to alter leg kinematics 2 days following a 30-min downhill run (Hamill, et al.1991; Braun & Dutto, 2001). In particular, observed maximum knee flexion during stance tends to decrease with muscle soreness. For a given running velocity, stride rate tends to increase with soreness (Braun & Dutto, 2001)

Stride rate changes at constant speed are associated with changes in stiffness properties of the leg (Farley & Gonzalez, 1996). Leg stiffness can be determined using kinematics (Li, 1999). The purpose of this study was to determine leg stiffness prior to and after a downhill run.

METHODS

Seven, well-trained runners (m = 73 ± 6 kg; VO_2 peak = 59.8 ± 8.1 ml/kg/min) were recruited to 4 runs at various conditions of intensity and grade. During the first test session, VO_2 peak was measured. The second test consisted of three level runs at speeds corresponding to 65%, 75%, and 85% of VO_2 Peak. Each run lasted for 5-min, with 5-min between runs. During the third testing session, the subject ran at a 10% downhill grade for 30-min at approximately 70% of VO_2 peak. The fourth test, exactly 48 hours post downhill run, was the same as the second testing session.

During the second and fourth testing sessions, reflective spheres were secured on the subject's left leg at points representing the hip, knee, and ankle joints. For each 5 min test run, 10 sec of data were recorded at 120 Hz after 2.5 minutes. From the 10 sec of data, 13-15 consecutive strides were identified. From each stride, the stance period was found. Knee angle and angular velocity were calculated from the kinematic data.

For each stance period, three phases were identified, and leg stiffness estimated for each phase (Li, 1999). Phase 1 represented the period from foot contact to maximum knee flexion velocity. Phase 2 lasted from the end of phase 1 to the point of maximum knee flexion. Phase 3 was from the end of phase 2 to toe-off. For each phase, knee rotational stiffness was determined using the equation:

$$\mathbf{k_R} = \mathbf{I}\frac{\omega^2}{\theta^2},$$

where I is ml^2. For a given subject, m is body mass and l is the distance from the hip to the knee joint. As illustrated by Li (1999), in the plot (θ^2, ω^2) (Figure 1), the slope represents k/I.

Leg stiffness was estimated from knee rotational stiffness for each phase using the equation,

$$\mathbf{k_L} = \frac{\mathbf{k_R}}{\mathbf{l^2 \sin \Delta\theta}},$$

where $\Delta\theta$ is the change in knee angle for a given time interval.

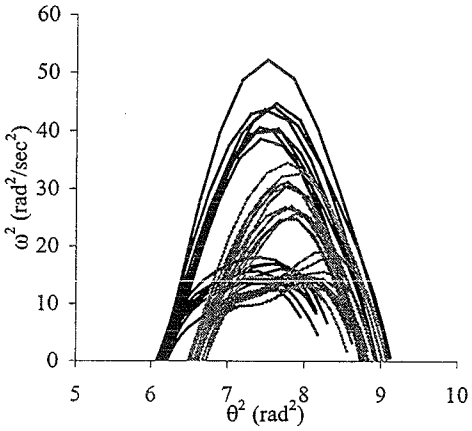

Figure 1: Stance phase knee kinematics. Dark curves represent pre- and light curves post- downhill run.

RESULTS AND DISCUSSION

Figure 1 shows the plot (θ^2, ω^2) for one subject pre- and post- downhill run at the speed corresponding to 65% VO_2 peak. For this subject, definite changes in leg kinematics are observed. Leg stiffness increased 28% during phase 1 and decreased 2% and 10% during phases 2 and 3 relative to the pre-downhill session.

Table 1: Percent change in leg stiffness. (Range of percent change)

Effort	Phase 1	Phase 2	Phase 3
65%	20 (-5 - 82)	1 (-11 - 15)	1 (-29 - 34)
75%	13 (-13 - 72)	5 (-22 - 50)	0 (-16 - 15)
85%	9 (-16 - 32)	-1 (-25 - 20)	-4 (-13 - 17)

Table 1 gives the average percent change in leg stiffness from pre to post across all subjects. Statistical comparisons have not been run due to differences in running speeds between individuals. The greatest differences generally occurred during phase 1 of the stance phase, with a large degree of variability, as denoted by the observed ranges. Generally, leg stiffness increased with muscle soreness, particularly during phase 1, the initial impact phase. Most subjects (6 of 7) experienced increased leg stiffness during phase 1 at the 65% speed, as seen in Figure 2.

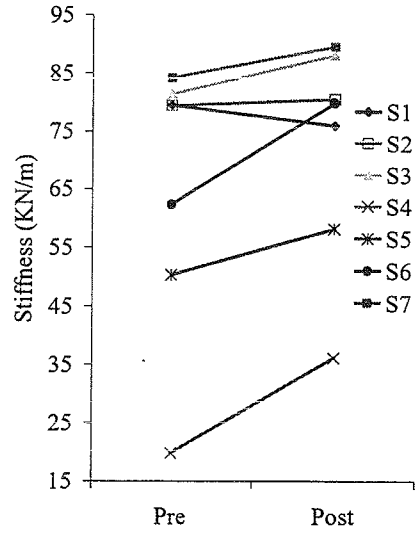

Figure 2: Change in leg stiffness during phase 1 at 65% of VO_2 peak.

It is unknown what affect increased leg stiffness has for the runner. Increased stiffness during impact (phase 1) may relate to increased accelerations on the body that must be absorbed, possibly increasing the risk of injury. Increased stiffness may reflect a strategy that balances minimization of pain with increased lower limb loading.

REFERENCES

Braun, W.A. & Dutto, D.J. (2001). *Proceedings of the ACSM.*

Farley, C. & Gonzalez, O. (1996). *J Biomech*, **29**, 181-186.

Hamill, et al. (1991). *Int J Sport Biomech*, 7, 125-137.

Li, L. (1999). *ASME: Proc of the Intl Mech Eng Congress and Expo, Nashville, Tenn.*, 299-300.

LOWER EXTREMITY JOINT POWER WHEN RUNNING OVER OBSTACLES

Alan Hreljac[1], Nick Stergiou[2], and Shane Scholten[2]

[1]Kinesiology and Health Science Department, California State University, Sacramento
[2]HPER Biomechanics Laboratory, University of Nebraska at Omaha
E-Mail: ahreljac@hhs4.hhs.csus.edu

INTRODUCTION

Running over obstacles of sufficient height requires a change in landing strategy from a heelstrike (HS) to a forefoot (FF) strike pattern (Stergiou et al., in press). Energy absorption and shock attenuation have been shown to be superior in a FF landing compared to a HS landing in both running (Hamill et al., 2000) and jumping (Kovács et al., 1999). The relative contribution of the ankle joint to energy absorption was found to be greater in a FF jump landing compared to a HS landing (Kovács et al., 1999). During the propulsive phase of running, it has been suggested (Hamill et al., 2000) that the ankle is a better energy generator following a FF landing than following a HS landing, while the energy generation contribution from the knee is similar in both conditions. In the extension phase of a jump following a FF landing, the ankle also has been reported (Bobbert et al., 1987) to be the primary power generator, but in contrast to the running situation, the knee was found to be the primary energy generator following a HS landing (Kovács et al., 1999). As landing strategy changes when running over obstacles of increasing height, it would likely become necessary to modify joint power absorption and generation patterns, although it is not clear in which way these modifications would occur. The purpose of this study was to compare ankle and knee joint power patterns between level running and running over obstacles at the height at which landing strategy changed from a HS pattern to a FF striking pattern.

METHODS

Ten subjects (4 males, 6 females) ran at their preferred speed down a 25 m runway over a balsa wood obstacle, landing with their right (dominant) foot on a floor mounted force platform. Seven obstacle height conditions (level, and heights ranging from 10% to 22.5% of standing height in 2.5% increments) were tested. Sagittal plane kinematics (180 Hz) of relevant markers were recorded and synchronized with ground reaction force data (900 Hz). After smoothing, using a fourth order, zero lag Butterworth filter, ankle and knee joint angular velocities, moments, and powers were calculated. The height at which no initial plantarflexion occurred was defined as the transition height (TH). Joint powers were normalized by dividing by body mass before comparing peak power absorption and generation values at the ankle and knee between level running (H0), the height prior to TH (H1), and TH using a repeated measures MANOVA ($p = 0.05$).

RESULTS AND DISCUSSION

The average TH was 14.5 ± 2.5 % of standing height, similar to that reported by Stergiou et al. (in press). Peak power

absorption at the ankle, and peak power generation at the knee were both significantly greater at TH than at H0 and H1 (Table 1). There were no significant differences noted between height conditions in peak power generation at the ankle, and peak power absorption at the knee (Table 1).

Table 1: Peak ankle and knee power absorption (Abs) and generation (Gen) at various heights (W/kg ± 1 SD).

Phase	Height	Ankle	Knee
Abs	H0	6.8 ± 1.6	25.8 ± 5.9
	H1	8.9 ± 3.0	29.0 ± 9.0
	TH[1]	16.9 ± 8.6	27.0 ± 9.2
Gen	H0	15.3 ± 2.5	4.1 ± 1.3
	H1	17.4 ± 2.4	3.9 ± 1.5
	TH[2]	17.5 ± 2.3	7.3 ± 4.3

[1]TH > (H0 = H1) at ankle
[2]TH > (H0 = H1) at knee

The knee was the primary power absorber during the landing phase for all obstacle height conditions, regardless of landing strategy. The relative contribution of the ankle joint to power absorption increased significantly at the transition height, at which time the landing strategy changed from a HS pattern to a FF strike pattern.

Although hip power was not calculated in this study, joint power absorption contributions appeared to shift distally when landing strategy changed from a HS to a FF pattern, while joint power generation contributions shifted proximally at this transition. These observations are in agreement with results from a jumping study (Kovács et al., 1999) which did include hip power.

The increased compliance of the ankle when landing in a FF strike pattern (Hamill et al., 2000) likely leads to an increase in the power absorption ability of the ankle at landing without reducing the power generation during the propulsive phase. It is likely that the ankle increases stiffness prior to pushoff, although this change of stiffness would incur an energetic cost. Similarly, the increase in power generation at the knee when using the FF landing strategy would also incur an energetic cost. Thus, a strategy of HS landing would probably be retained over obstacles until a switch became a necessity to maintain speed or prevent injury.

SUMMARY

When running over low obstacles, joint energetic patterns at the ankle and knee are similar to patterns observed during level running. At these low obstacle heights, landing strategy remains similar to that demonstrated during level running. At the height where the landing strategy changes from a HS to a FF strike pattern, peak power absorption and generation at the knee and ankle change substantially, resembling patterns found when landing from a jump.

REFERENCES

Bobbert, M. F. et al. (1987). *Med. Sci. Sports Exerc.*, **19**, 332-338.

Hamill, J. et al. (2000). *Proceeding of XIth CSB Congress*, 47.

Kovács, I. et al. (1999). *Med. Sci. Sports Exerc.*, **31**, 708-716.

Stergiou, N. et al. (in press). *Gait Posture.*

REDISTRIBUTION OF JOINT WORK DURING ACCELERATION AND DECELERATION IN AN AVIAN BIPED

Monica A. Daley and Andrew A. Biewener

Concord Field Station, Harvard University, Bedford MA USA
E-mail: mdaley@oeb.harvard.edu

INTRODUCTION

The nature of muscle force generation in relation to length change (muscle work) is key to understanding the roles of different muscles within the limb. Recent research has shown that the gastrocnemius muscle in the turkey is able to produce force economically during steady running by contracting with little length change, but can contribute significantly to positive work by shortening during incline running (Roberts et al., 1997). Direct measurement of *in vivo* muscular work however is only possible in a few muscles for which direct recordings of muscle force and length change are possible. Moreover, the role of more proximal muscle groups at the hip and knee, which have been shown to be important for power generation or absorption in human jumping and running (e.g., Bobbert et al., 1986; Pandy & Zajac, 1991; Winter, 1983), raises the question of how different muscle groups contribute to mechanical work versus economical force transmission during steady versus non-steady locomotion.

In order to assess more broadly how muscle work versus isometric force transmission is distributed within the limb of a running animal, we examine the external work performed at each joint in the hindlimb of the guinea fowl (*Numida meleagris*) during steady running, acceleration and deceleration. By comparing the external joint work performed under these different locomotor conditions, we seek to evaluate how various muscle groups within a limb contribute to weight support and mechanical work, and how these roles may vary to accommodate variable conditions of locomotor movement.

METHODS

We obtained horizontal fore-aft, vertical, and center of pressure ground reaction force (G_{RF}) recordings from four guinea fowl (1.58 ± 0.11 kg) as they ran across a Kistler 9203 force platform over a range of speeds. A Redlake high-speed digital video system was used to track skin-marked limb joint positions at 250Hz. Coordinate data were then smoothed using a fourth-order digital Butterworth filter with a 35 Hz 3db cutoff before calculating joint angular velocities (ω) and external moments (M). All calculations were carried out in Matlab. [Ongoing work will incorporate segmental and gravitational moments in our analysis.] Measurements of joint power ($M \times \omega$) were integrated over the stance phase of the step cycle to obtain the net external joint work performed during support.

External power and net work at each joint were compared under three conditions: steady running, acceleration, and deceleration. Trials were considered steady if the change in velocity during the single step was less than 3% of the animal's initial velocity as it reached the force plate.

RESULTS AND DISCUSSION

We found that each joint contributes differently to mechanical work under steady running conditions (Fig. 1). The hip performs net positive work, the ankle and knee perform nearly equal amounts of positive and negative work, resulting in little

net work, and the tarsometatarsophalangeal (TMP) joint absorbs energy.

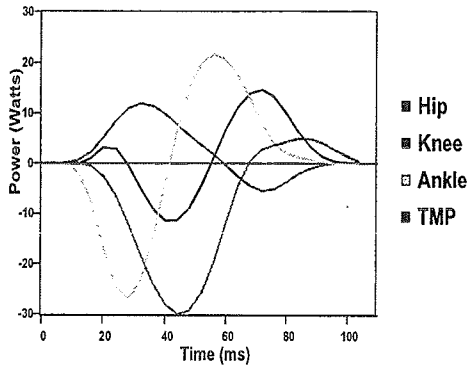

Figure 1. External joint power at each joint in the hindlimb during the support phase of a single steady run.

During acceleration (+5.1 ± 2.8 % Δvel) and deceleration (-5.0±1.3% Δvel) the net mechanical work for the limb as a whole shifts as expected to being more positive or negative, respectively. However, the shift in mechanical work is not the same at each joint (Fig. 2). In particular, we found that the increase in whole limb positive work during acceleration was achieved primarily by a decrease ($p=0.028$) in the net energy absorbed by the TMP joint, together with an increase ($p=0.07$) in positive work performed by the ankle.

In contrast, the increase in energy absorption during deceleration was mainly achieved by negative joint work performed at the knee and ankle, for which energy absorption was significantly greater than during steady running ($p<0.0001$) (Fig. 2). The hip also contributed by reducing its net positive work during deceleration ($p=0.07$). Finally, the TMP joint actually absorbed less energy during deceleration than during steady running (Fig. 2).

These results indicate that changes in whole limb external joint power and work are achieved by differing contributions from individual limb joints for steady versus non-steady locomotor movement. Although the relatively low values of external work observed at the knee and ankle joints during steady running are consistent with isometric contraction and economical force transmission of the quadriceps and ankle extensors, the positive work performed at the hip and negative work at the TMP joint, indicate that substantial modulation of recruitment to control fascicle shortening or lengthening is important to the mechanics of steady, as well as non-steady running.

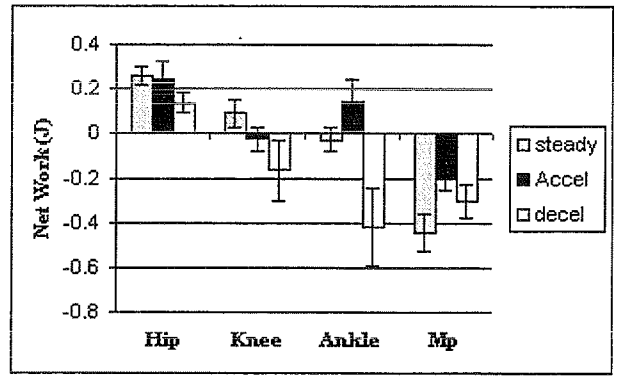

Figure 2. Mean net joint work during the support period for all trials for the four birds (±SEM).

REFERENCES

Bobbert, M. F., P. A. Huijing, et al. (1986). *J. Biomech.* **19**: 899-906.

Pandy, M. G. and F. E. Zajac (1991). *J.Biomech.* **24**: 1-10.

Roberts, T. J. et al.(1997). *Science* **275**:1113-1115.

Winter, D. A. (1983). *J. Biomech.* **16**: 91-97.

LEG STIFFNESS ADJUSTMENT FOR RUNNING ON ALTERNATING SURFACE STIFFNESSES

C.A. Shigeoka[1] and C.T. Farley[2]
[1] Dept. of Integrative Biology, University of California, Berkeley, CA, USA
[2] Locomotion Lab, University of Colorado, Boulder, CO, USA
Email: cassies@socrates.berkeley.edu

Introduction

This study investigated whether runners separately control their contralateral legs to accommodate changing terrain. Walking animals have the capacity to control their left and right limbs to move at different speeds when they are on split treadmill belts (Dietz et al., 1994; Forssberg et al., 1980). However, the independent control of contralateral limbs in faster gaits like running has yet to be examined.

Running can be modeled with a "leg spring" representing leg behavior and a point mass equal to body mass (Fig. 1; McMahon and Cheng, 1990). Runners can adjust their center of mass (COM) dynamics by changing leg stiffness and/or leg angle at touchdown. To accommodate an expected, single transition in surface stiffness, runners alter leg stiffness for the first step on the new surface (Ferris et al., 1998, 1999).

We tested the hypothesis that runners completely adjust leg stiffness from step-to-step on surfaces with expected, alternating hard and soft sections. We predicted that runners would use different left and right leg stiffness values, corresponding to those used for a continuous hard or soft surface.

Methods

Ten subjects ran at 3.7 m/s on: (1) an alternating surface spaced so that one limb always hit a soft rubber surface (k_{surf} = 16.0 kN/m) and the other hit a hard rubber surface (k_{surf} = 368.7 kN/m), (2) a continuous track of the hard surface, and (3) a continuous track of the soft surface. Surface damping was negliglible (Ferris et al., 1998). After subjects practiced running on each surface, we measured the ground reaction force and kinematics (200 Hz) for two steps. Statistical differences were assessed with a repeated-measures ANOVA.

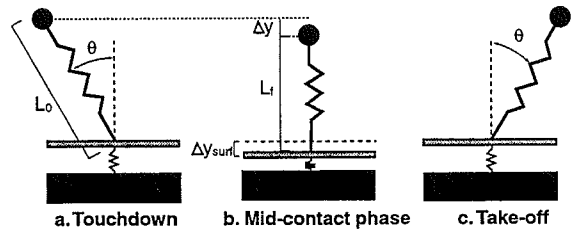

Fig. 1. Spring-mass model. Leg compression (ΔL) is the difference between the starting (L_0) and minimum (L_f) leg lengths. Vertical displacement of the COM (Δy) depends on the runner's COM displacement relative to the surface (Δy_{person}, not shown) and surface compression (Δy_{surf}, where $\Delta y_{surf} = F_{peak}/k_{surf}$).

We calculated leg stiffness (k_{leg}) by dividing the peak ground reaction force by leg compression (ΔL). Leg compression was determined from:

$$\Delta L = \Delta y - \Delta y_{surf} + L_0(1 - \cos\theta) \quad (1).$$

The vertical displacement of the COM was calculated by integration of the force platform data (Cavagna, 1975). We calculated θ (Fig. 1) from running speed (u), ground contact time (t_c) and L_0:

$$\theta = \sin^{-1}(ut_c/2L_0) \quad (2).$$

Results and Discussion

On the alternating surface, runners used a 2.2-fold greater leg stiffness for the leg hitting the soft sections than for the leg hitting the hard sections of the alternating surface (Table 1). On a given surface stiffness, runners used the same leg stiffness on continuous and alternating surface configurations.

Due to leg stiffness modulation, COM vertical displacement was only 1.4 cm greater on the soft surface than on the hard surface, despite the 8.8 cm increase in surface compression (Fig. 2, Table 1).

	Continuous Hard Surface	Alternating Hard Surface	Continuous Soft Surface	Alternating Soft Surface	p-values surface	p-values configuration
F_{peak} (N)	1385 (57)	1313 (53)	1413 (69)	1457 (62)	0.001	0.511
Δy (cm)	5.1 (0.2)	4.7 (0.2)	6.0 (0.3)	6.6 (0.3)	<0.001	0.691
Δy (cm)	0.0 (0.3)	0.4 (0.0)	8.8 (0.4)	9.1 (0.4)	<0.001	0.315
Δy_{person} (cm)	5.1 (0.4)	4.4 (0.2)	-2.8 (0.4)	-2.5 (0.3)	<0.001	0.421
ΔL (cm)	13.8 (0.5)	14.5 (0.6)	7.8 (0.6)	7.4 (0.7)	<0.001	0.653
θ (deg)	25.4 (0.7)	27.0 (0.6)	27.6 (0.4)	26.7 (0.5)	0.066	0.509
k_{leg} (kN/m)	10.3 (0.8)	9.3 (0.6)	20.3 (2.7)	22.6 (3.2)	< 0.001	0.699

Table 1. *Each value is the mean (SEM). P-values compare the hard vs. soft "surface" and the alternating vs. continuous surface "configuration". Positive values indicate downward movement for the first half of the contact phase for Δy, Δy_{surf}, and Δy_{person}.*

Surprisingly, on the soft surface, COM vertical displacement was less than surface compression, indicating that the COM moved upward relative to the surface during the first half of the contact phase ($\Delta y_{person} < 0$ in Table 1; Figs. 2C-D). This pattern occurred because the small leg compression was more than offset by the effect of the leg rotating over the stance foot. Thus, the stiff stance leg resulted in very little leg compression, producing a smaller vertical displacement of the COM than the surface.

This study examined leg stiffness adjustment for a 25% softer surface than used in previous studies (Ferris et al., 1998, 1999). On our soft surface, leg stiffness values were 1.5- to 2-fold greater than those measured in previous running studies (Ferris et al., 1998; Farley & Gonzalez, 1996). However, the observed leg stiffness adjustment was not quite sufficient to maintain the same COM dynamics as on a hard surface. Runners may not be able to make their legs so stiff.

These findings support our hypothesis that runners fully adjust leg stiffness step-to-step for changes in surface stiffness. Independent control of the stiffness of each leg likely helps runners negotiate the variable terrain encountered in the natural world.

Acknowledgements

Supported by NSF grant (ECS-9873474) and NIH grant (AR44008) to C.T.F.

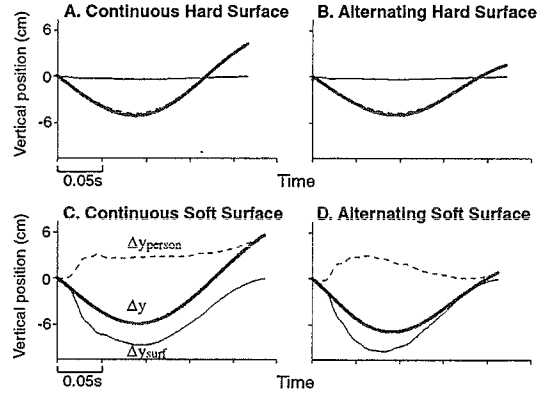

Fig. 2. *The vertical displacement of the COM (——; Δy) is determined by the vertical displacement of the runner's COM relative to the surface (- - - -; Δy_{person}) and the compression of the surface (——; Δy_{surf}). A single ground contact phase is shown in each panel.*

References

Cavagna, G. A. (1975). *J. Appl. Physiol.* **39**: 174-179.

Dietz, V., W. Zijlstra, et al. (1994) *Exp. Brain Res.* **101**: 513-520.

Farley, C. T. and O. Gonzalez (1996). *J. Biomech.* **29**: 181-186.

Ferris, D. P., K. Liang, et al. (1999) *J. Biomech.* **32**: 787-794.

Ferris, D. P., M. Louie, et al. (1998) *Proc. Royal Soc. Lond.* **265**: 989-994.

Forssberg, H., S. Grillner, et al. (1980) *Acta Physiol. Scand.* **108**: 283-295.

McMahon, T. A. and G. C. Cheng (1990). *J. Biomech.* **23 (suppl. 1)**: 65-78.

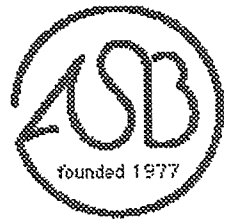

- PARALLEL SESSION -

Symposium

Isokinetic Testing

Friday, August 10, 2001
0900 to 1030

MEASURING MUSCLE FATIGUE AND GENDER DIFFERENCES WITH ISOKINETIC CONTRACTIONS

Danny M. Pincivero[1], William S. Gear[2], Robert L. Sterner[3]

[1]Human Performance and Fatigue Laboratory, Department of Physical Therapy, Eastern Washington University, Cheney, WA, USA
[2]Kinesiology Department, California Lutheran University, Thousand Oaks, CA, USA
[3]Department of Health and Human Performance, University of Toledo, Toledo, OH, USA
E-mail: dpincivero@mail.ewu.edu

INTRODUCTION

Muscle fatigue has been defined as "any reduction in the force generating capacity of the total neuromuscular system regardless of the force required in any given situation" (Bigland-Ritchie and Woods, 1984). A reliable muscle fatigue measure has subtly emerged during maximal effort isokinetic contractions that has been able to highlight gender differences in quadriceps and hamstring torque generating ability. The objectives of this presentation are to: I) discuss and contrast different methods of documenting muscle fatigue during isokinetic contractions (Pincivero et al, 2001), II) demonstrate the relationship between isokinetic peak torque generating ability and muscle fatigue (Pincivero et al, 2000a), and III) examine gender differences in quadriceps and hamstring torque and muscle fatigue (Pincivero et al, 2000b).

METHODS

I) 16 healthy male (n=8) and female (n=8) volunteers participated. Each subject performed 30 maximal, concentric repetitions (Biodex System II) at a pre-set angular velocity of 180 deg•s^{-1} for both dominant and non-dominant legs. Quadriceps work was evaluated between an range of 10 and 60 deg flexion, for each repetition. Quadriceps muscle fatigue was calculated through an index (work performed last 5 repetitions / work performed first 5 repetitions x 100%) and the slope (β) across the 30 repetitions. The subjects participated in 2 test sessions separated by 1-2 weeks. Intraclass correlation coefficients (ICC) and standard errors of measurements (SEM) were calculated for each fatigue measure on both legs.

II) 16 healthy male and 16 healthy female volunteers participated. Subjects performed 30 reciprocal, concentric maximal knee extension and flexion contractions at a pre-set angular velocity of 180 deg•sec^{-1}. Values for quadriceps work (N•m) were calculated for each repetition between a windowed range of motion of 10 degrees and 60 degrees of flexion. Values for quadriceps work were then normalized to body mass (N•m•kg^{-1}). The rate of quadriceps fatigue was calculated as the decline in work output by the slope (β) across the 30 repetitions. The relationship between peak quadriceps work and the associated slope was examined by regression analysis for males and females, separately, and differences in these relationships were calculated using Fisher's Z-transformation.

III) 20 healthy female and 17 healthy male volunteers participated. Subjects performed 4 sets of 30 reciprocal maximal effort isokinetic contractions for the dominant leg

at 180 deg•s^{-1}. Subjects were randomly assigned to a short (1 min) or long (5 min) inter-set rest interval. Quadriceps and hamstring peak torque (PT), total work (TW), and average power (AP) were calculated for each set.

RESULTS AND DISCUSSION

I) The findings demonstrated moderate to high ICC's for the non-dominant leg (0.78 – 0.92) and high ICC's for the slope and y-intercept for the dominant leg (0.82 and 0.89, respectively). The fatigue index for the dominant leg was found to be low (0.26).

II) The results demonstrated that peak quadriceps work, normalized to body mass, was significantly higher ($t_{30} = 4.82$, $p<0.05$) in males (1.35 ± 0.17 N•m•kg^{-1}) than females (1.10 ± 0.11 N•m•kg^{-1}). Males also showed a significantly greater reduction in work output over 30 repetitions than females ($t_{30} = -5.45$, $p<0.05$), as demonstrated by the β values (males: $\beta = -1.70 \pm 0.47$; females: $\beta = -0.92 \pm 0.32$). The relationship between peak quadriceps work and the rate of work decline (β) was found to be statistically significant in both males ($r = 0.86$, $p<0.05$) and females ($r = 0.69$, $p<0.05$), and was higher in males (r^2 95% C.I.: 0.57 – 0.95) than females (r^2 95% C.I.: 0.30 – 0.89).

III) Males displayed a significantly greater reduction for quadriceps PT, TW and AP across sets 1-2 with a 1 min rest interval, as compared to the other groups (Figure1). Males in both groups displayed a significantly greater reduction in hamstring PT, TW, and AP than the females across sets 1-3 (Figure 2).

SUMMARY

These studies demonstrate that muscle fatigue can be reliably documented by the slope, and suggest that males possess greater susceptibility to muscle fatigue than females. It is speculated that this greater rate of fatigue in males may be explained by the significantly greater relationship to normalized peak torque generating capacity.

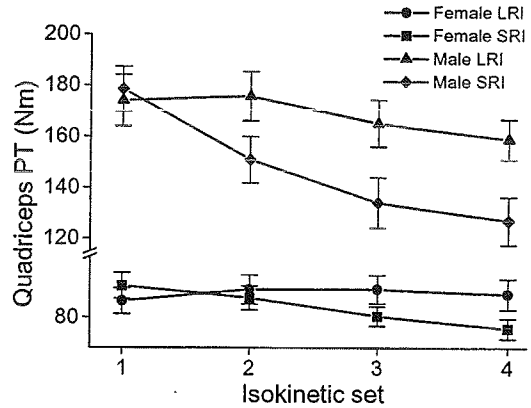

Figure 1: Mean ($\pm$ SD) quadriceps PT across 4 sets of 30 isokinetic contractions.

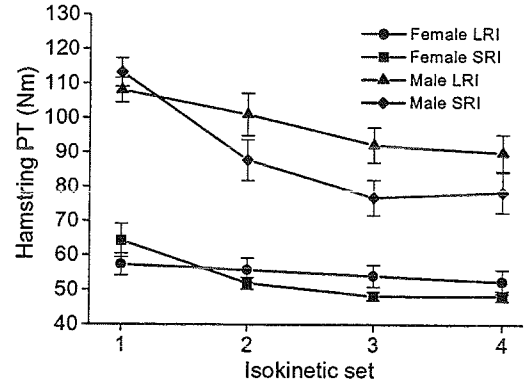

Figure 2: Mean ($\pm$ SD) hamstring PT across 4 sets of 30 isokinetic contractions.

REFERENCES

Bigland-Ritchie, B, Woods, J.J. (1984). *Muscle Nerve*, 7, 691-699.

Pincivero, D.M., et al (2000a). *J Strength Cond Res*, **14**, 202-206.

Pincivero, D.M., et al (2000b). *Can J Appl Physiol*, **25**, 398.

Pincivero, D.M., et al. (2001). *Med Sci Sports Exerc*, **33**, 334-338.

How do you know female [illegible]?

MECHANOMYOGRAPHIC AND ELECTROMYOGRAPHIC RESPONSES TO ISOKINETIC MUSCLE ACTIONS

Kyle T. Ebersole[1], Terry J. Housh[2], Tammy K. Evetovich[3], and Joel T. Cramer[2]

[1]Department of Human Kinetics, University of Wisconsin-Milwaukee, Milwaukee, WI, USA
[2]Department of Health & Human Performance, University of Nebraska, Lincoln, NE, USA
[3]Division of HPLS, Wayne State College, Wayne, NE, USA
E-mail: ebersole@uwm.edu

INTRODUCTION

Mechanomyography (MMG) records and quantifies the low frequency lateral oscillations of active skeletal muscle fibers. It has been suggested that MMG is the mechanical counterpart of the motor unit electrical activity as measured by electromyography (EMG). Thus, simultaneous measurements of MMG and EMG may provide insight into the mechanical and electrical components of muscle function. MMG has been used to discriminate between muscle fiber types, monitor strength training, and identify changes in force production and muscle action velocity. Clinically, MMG may be useful for examining muscle diseases and controlling external prostheses. Simultaneous measurements of MMG and EMG have been used to monitor the dissociation between the electrical and mechanical events (excitation-contraction coupling) that occurs with fatigue and examine factors related to electromechanical delay. Most previous studies have examined the MMG responses to isometric muscle actions, however, little is known about the MMG response to isokinetic muscle actions. Recently, we have examined the MMG and EMG responses of the superficial muscles of the quadriceps femoris during maximal concentric and eccentric isokinetic muscle actions as well as passive leg extension movements at velocities ranging from 30-300 $^{\circ} s^{-1}$.

METHODS

Isokinetic Measurements
Isokinetic muscle actions were performed on a calibrated Cybex 6000 dynamometer. Peak torque (PT) and mean power (MP) were calculated by the Cybex 6000 software.

MMG Measurements
The MMG signals were detected by piezoelectric crystal contact sensors (HP 21050A) placed between the active EMG electrodes on the vastus lateralis (VL), rectus femoris (RF), and vastus medialis (VM). A stabilizing ring, double-sided foam tape, and microporous tape were used to ensure consistent contact pressure of the MMG sensor.

EMG Measurements
A bipolar surface electrode (Quinton Quick Prep silver-silver chloride) arrangement was placed over the muscle belly of the RF, VL, and VM muscles of the dominant leg. For all EMG measurements, the reference electrodes were placed over the iliac crest. Interelectrode impedance for each muscle was kept below 2000 Ohms by shaving the area and careful skin abrasion. The EMG signals were preamplified (gain 1000X) using a differential amplifier (EMG 100, Biopac Systems Inc).

Signal Processing
The raw MMG and EMG signals were stored on a personal computer. The

sampling frequency was 1000 points per second for all signals. The MMG and EMG signals were bandpasss filtered from 5-150 Hz and 10-500 Hz, respectively, by software (Acqknowledge III, Biopac Systems, Inc.).

RESULTS AND DISCUSSION

Concentric Muscle Actions (Ebersole et al. 2000, 2001; Cramer et al. 2001; Evetovich et al. 1997)

There were velocity-related dissociations between PT, MP, and MMG amplitude. As expected, PT decreased across velocities ranging from 60 to 300 ° s^{-1}. MMG amplitude and MP, however, increased up to 240 ° s^{-1} and then decreased from 240 to 300 ° s^{-1}. Thus, MMG amplitude may be more closely related to MP than PT during maximal, concentric, isokinetic muscle actions. EMG amplitude increased up to 240° s^{-1} for the VL, remained unchanged across velocities for the RF, and increased up to 300 ° s^{-1} for the VM. These findings suggest that the velocity-related increases in MMG amplitude were due to decreases in muscle stiffness, increases in the rate of actin-myosin cycling, and/or limb movement.

Eccentric Muscle Actions (Cramer et al. 2001)

During eccentric muscle actions ranging from 60 to 180° s^{-1}, there was no change in PT, but increases in MP and MMG amplitude. The EMG amplitude remained unchanged from 60-120° s^{-1}, but decreased from 120-180° s^{-1}. Thus, as with concentric muscle actions, MMG amplitude may be more closely related to MP than PT. The dissociation between MMG and EMG from 120 to 180° s^{-1} suggests that during maximal eccentric muscle actions, changes in the recruitment patterns (slow vs. fast-twitch) may have resulted in decreased muscle stiffness, thereby, increasing MMG amplitude.

Passive Leg Extension Movements (Ebersole et al. 2001)

When the leg was passively moved through leg extension at velocities of 30, 90, and 150° s^{-1}, the EMG amplitude was not different from those values recorded at rest. The MMG amplitude, however, increased with an increase in velocity. These findings suggest that limb movement, independent of muscle activation, may account for a portion of the velocity-related increase in MMG amplitude during isokinetic muscle actions. It is possible that during isokinetic muscle actions, the MMG amplitude is influenced by factors such as turbulences of the intracellular and extracellular fluid mediums and/or cross-talk from the hamstring muscles.

REFERENCES

Cramer et al. (2001). To be presented at NSCA's annual convention, Spokane, WA.

Cramer et al. (2000). *Muscle Nerve,* 23, 1826-1831.

Ebersole et al. (2000). *Isok. Exer. Sci.,* 8, 1-8.

Ebersole et al. (2000). *Electromyogr. Clin. Neurophysiol.*, 40, 49-55.

Evetovich et al. (1997). *Eur. J. Appl. Phys.*, 75, 166-169.

ISOKINETIC EXERCISES AND KNEE JOINT FORCES DURING ISOKINETIC KNEE EXTENSIONS

John W. Chow

Department of Exercise and Sport Sciences, University of Florida, Gainesville, FL 32611
E-mail: jchow@hhp.ufl.edu Web: www.hhp.ufl.edu\ess

ISOKINETIC EXERCISES

The term "isokinetic" was introduced in the late 1960s when the Cybex I dynamometer was developed (Hislop and Perrine, 1967):

> ... the concept of isokinetic exercise is control of the speed of muscular performance. In order to achieve this kind of performance, it is necessary to provide an external means of holding the speed of body movements to constant rates irrespective of the magnitude of forces generated by the participating muscles. (p. 116)

Although not explicitly stated, these authors used "isokinetic" to describe a type of muscular contraction characterized by the *constant angular velocity* of the body segment.

The resistance provided by the isokinetic dynamometer matches the force exerted on the attachment arm by the user throughout the range of motion of an exercise, making it theoretically possible for the muscles to exert a continual maximal force throughout the full range of motion (Fleck & Kraemer, 1997). In general, isokinetic exercises are very safe to perform and demand little coordination. As a result, isokinetic exercises and testings are commonly used in clinical settings for the strengthening of muscles and the evaluation of strength, respectively.

Despite the advantages of isokinetic exercises, several issues must be considered when using strength data collected from isokinetic dynamometers for research and diagnostic purposes.

- Torque "overshoot" and "oscillation" may occur before the constant angular velocity is attained and deceleration occurs toward the end of the contraction (Osternig et al., 1982; Sapega, 1982).
- The duration of constant angular velocity decreases as the preset angular velocity increases (Chow et al., 1997; Herzog, 1988; Osternig et al., 1983). This phenomenon is primarily due to the fact that, under the same experimental condition, longer time (or angular distance) is needed to accelerate a body segment to a higher angular velocity.
- Errors in torque measurements occur when the gravitational and inertial effects are not considered (Chow et al., 1997; Herzog, 1988; Winter et al., 1981). The feature of gravity-correction is available in most modern isokinetic dynamometers.
- Mixed results on the within-day, inter-day, inter-machine reliability (or reproducibility) of strength data have been reported for different exercises (e.g., Madsen, 1996; Pincivero et al., 1997; Wyse et al., 1994).

Clinicians and researchers are all aware of the fact that there are limitations in isokinetic dynamometers. It should be emphasized that recognizing the limitations does not diminish the valuable contributions isokinetic dynamometers can make to our understanding of muscular function, but rather enhances the clarity of interpretation

KNEE JOINT FORCES DURING ISOKINETIC KNEE EXTENSIONS

Isokinetic knee extensions are commonly used in knee rehabilitation after treatments and surgeries. Knee joint forces during isokinetic knee extensions have been reported in four studies.

In a study by Nisell et al. (1989), eight male subjects performed knee extensions at two speeds (30 and 180 °/s). Inertial effects

were neglected in the force analysis. The axial component (compressive force parallel to the longitudinal axis of the shank) of the tibiofemoral joint force was found to be the *same* magnitude as the patellar ligament force throughout the knee extension range of motion. The maximum tibiofemoral axial forces were nine times the body weight (9 BW) and 5 BW for 30 and 180 °/s, respectively. Peak tibiofemoral shear forces of 1.0 and 0.7 BW were recorded for 30 and 180 °/s, respectively.

Based on strength data collected from five male subjects at isokinetic speeds of 60 and 180 °/s and musculoskeletal parameters reported in the literature, Kaufman et al. (1991) predicted muscle forces using an optimization technique and also reported knee joint forces. The peak patellofemoral joint force, and peak tibiofemoral axial and shear forces were estimated to be 5.1, 4.0, 0.5 BW, respectively, during isokinetic knee extensions performed at 60°/s. They found minimum reductions in various knee joint forces when the speed increased from 60 to 180 °/s. This contradicts the findings of Nisell et al. (1989) unless most of the decrease in knee joint forces from 30 and 180 °/s observed by Nisell et al. occurred between 30 and 60 °/s.

Using a biomechanical model of the knee joint developed from direct radiographic measurements of the subjects, Baltzopoulos (1995) tested five males at four isokinetic knee extension speeds—30, 90, 150, and 210 °/s. The average peak tibiofemoral axial forces for these four speeds (from slow to fast) were found to be 7.4, 6.6, 5.8, and 5.7 BW, respectively. The corresponding tibiofemoral shear forces were 0.9, 0.8, 0.7, and 0.8 BW, respectively. The results supported the findings of Nisell et al. (1989) except that the tibiofemoral shear force seemed to be relatively insensitive to the isokinetic speed.

In a case study, Chow (1999) tested a female subject at preset angular speeds ranging from 25 to 400 °/s. Gravitational and inertial effects were included in determining the resultant knee torque. A combination of knee torque and geometry of the knee (obtained from knee radiographs) was used to determine the different knee joint forces. All knee joint forces were found to decrease with increasing isokinetic speed. The presence of tibiofemoral shears force indicated that the ACL was loaded throughout the range of motion.

It is apparent that there are inconsistences in the findings of these four studies. The differences are probably due to the differences in technique for determining knee joint forces, geometric data of the knee joint, and isokinetic dynamometer used for strength tests, and small sample sizes. It is noteworthy that a total of 20 subjects were tested in these previous studies and only one female was involved. Clinicians and researchers should interpret all these results with caution. More studies are needed before any conclusion is made.

REFERENCES

Baltzopoulos, V. (1995). *Clin Biomech* **10**, 208-214.

Chow, J.W. (1999). *Clin Biomech* **14**, 329-338.

Chow et al. (1997). *Med Sci Sports Exer* **29**, 794-803.

Fleck, S.J., Kraemer, W.J. (1997). *Designing resistance training programs*. Human Kinetics. (pp. 28-33)

Herzog, W.H. (1988). *J Biomech* 21, 5-12.

Hislop, H.J., Perrine, J.J. (1967). *Phys Ther* **47**, 114-117.

Kaufman et al. (1991). *Am J Sports Med* **19**, 305-316.

Nisell et al. (1989). *Am J Sports Med* **17**, 49-54.

Madsen, O.R. (1996). *Spine* **21**, 2770-2776.

Osternig et al. (1982). *Res Q Exer Sport* **53**, 252-256.

Osternig et al. (1983). *Biomechanics VIII-A*, 251-257.

Sapega et al. (1982). *Med Sci Sports Exer* **14**, 368-375.

Pincivero et al. (1997). *Int J Sports Med* **18**, 113-117.

Winter et al. (1981). *Eur J Appl Physiol* **46**, 397-408.

Wyse et al. (1994). *Br J Sports Med* **28**, 167-170.

MOTOR OUTPUT VARIABILITY DURING ISOMETRIC, CONCENTRIC, AND ECCENTRIC CONTRACTIONS IN YOUNG AND OLD ADULTS

Evangelos A. Christou

Department of Kinesiology and Applied Physiology, University of Colorado, Boulder
Email: echristo@colorado.edu Web: www.Colorado.EDU/kines/Lab/NCM.html

INTRODUCTION

Rapid eccentric contractions of the quadriceps have been shown to produce a more variable motor outcome than isometric and concentric contractions (Christou & Carlton, 1999, 2000). These findings provide additional support to the hypothesis that the central nervous system may control gradation of muscle force differently for eccentric contractions (Enoka, 1996). Several studies suggest that when old adults perform isometric or slow anisometric contractions they produce more variable movements compared with young adults (Laidlaw et al., 2000). These differences between young and old adults as a function of contraction type, however, have not been examined during rapid tasks. The aim of this study was to compare the ability of young and old adults to control motor output during rapid isometric, concentric and eccentric contractions of the knee extensor muscle group.

PROCEDURES

Twenty-four young (25.3 ± 2.8 years) and 24 old (73.3 ± 5.5 years) healthy and active individuals with no history of previous knee pathology were recruited for this study. A KIN-COM 500H isokinetic dynamometer was used to to provide a constant velocity of 25°/s throughout the range of motion (ROM) and assess force production and motor output variability during a knee extension task. Each participant attended three testing sessions and performed knee extensions through a 10° ROM (90-100° of knee flexion, isometric at 90°). Six different parabolas were displayed on the monitor of the dynamometer based on maximum voluntary contraction (MVC) (20, 35, 50, 65, 80 and 90% MVC) and with a time to peak force of 200ms. Each participant was instructed to match the parabola by controlling the knee extension force. To familiarize the participants with the targeted parabolas, thirty practice trials were given for each target prior to the data collection. In addition to verbal feedback, the first half of the practice trials received visual feedback. The remainder of the practice trials and the test trials were given visual feedback only after the trial was completed. All target parabolas were randomly assigned for each subject and were counterbalanced in order across subjects. A rest period of 120 seconds was given between data collection trials. Means, standard deviations (SD) and coefficient of variations (CV) for variability in peak force (PF), impulse (IMP), time to peak force (TPF) and impulse duration (ID) were computed (Figure1) from forty trials per contraction at each %MVC.

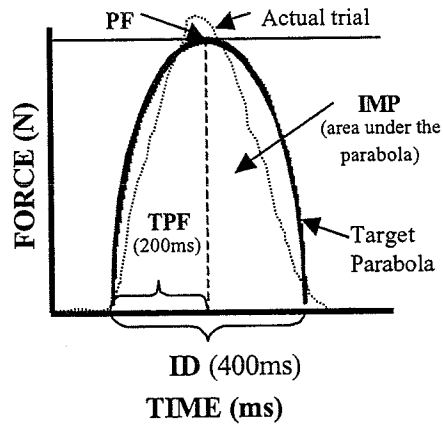

Figure 1. Illustration of the task and parameters computed for analysis.

RESULTS AND DISCUSSION

Subjects produced similar MVC forces for the three contractions ($p>0.05$), and young subjects produced greater MVC forces than old subjects ($p<0.05$). The SD of PF and IMP was greater for young than old subjects because of the higher absolute forces

produced by young subjects. Results in this abstract are presented as the CV, a measure of variability that normalizes SD to the amount of force or time produced.

The CV for PF and IMP revealed significant differences between the three contractions and two age groups ($p<0.01$). Eccentric contractions had a more variable outcome compared with isometric and concentric contractions and old adults were more variable than young adults. For both PF and IMP the interactions for age x %MVC (Figure 1 for PF) and contraction x %MVC (Figure 2 for IMP) were significant ($p<0.01$). Old adults were more variable than young adults particularly at the low forces; whereas the motor output was more variable during low and high levels of force for eccentric contractions. The age x contraction and the three-way interaction were not significant ($p>0.05$).

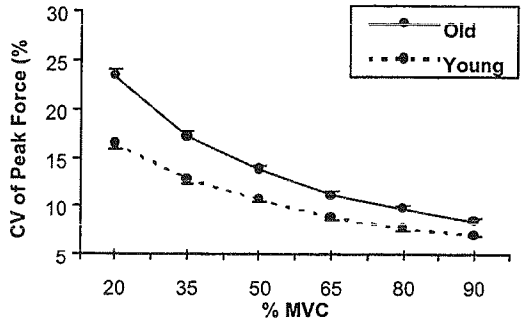

Figure 1. Old adults exhibit greater CV for PF than young adults, particularly at low forces.

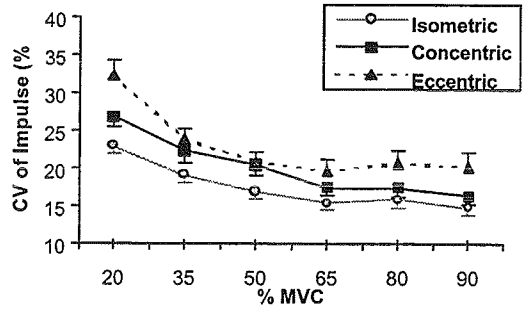

Figure 2. The CV for Impulse was greater during low and high %MVC for eccentric than concentric and isometric contractions.

The CV for TPF and ID revealed significant differences between the three contractions, however, only TPF revealed differences between the two age groups ($p<0.01$). In general, eccentric contractions were more variable compared with isometric and concentric contractions, and old adults were more variable than young adults. For both TPF and ID, the interaction for age x %MVC was significant ($p<0.01$). Old adults were more variable than young adults, particularly at the low forces. For TPF, furthermore, the contraction x %MVC, age x contraction, and the three-way interaction among age, contraction and % MVC were significant ($p<0.05$). Old adults were more variable than young adults during low forces; however, these differences were greater during eccentric contractions. For ID the contraction x %MVC, age x contraction, and the three-way interaction were not significant ($p>0.05$).

The results of this study provide further evidence that control of the motor output is different for eccentric compared with concentric and isometric contractions. In addition, these results support and extend previous research (Laidlaw et al., 2000) indicating that old adults are less consistent than young adults, particularly during eccentric contractions.

SUMMARY

The CV of the motor output was found to be greater for eccentric than concentric and isometric contractions, and old adults were more variable than young adults.

REFERENCES

Christou, E.A., & Carlton, L.G. (1999). *ASB Proceedings*, 122-123.

Christou, E.A., & Carlton, L.G. (2000). *ASB Proceedings*, 137-138.

Enoka, R.M. (1996). *Journal of Applied Physiology*, **81**, 6, 2339-2346.

Laidlaw, D.H., Bilodeau, M., Enoka, R.M. (2000). *Muscle and Nerve* **23**, 600-612.

ISOKINETIC STRENGTH IN THE ELDERLY

Michelle M. Porter, PhD

Faculty of Physical Education & Recreation Studies, University of Manitoba, Winnipeg
portermm@ms.umanitoba.ca

INTRODUCTION

Isokinetic dynamometers provide a means of measuring many of the changes that occur in muscular fitness with aging and training. These changes include, but are not limited to: strength, endurance, passive resistance of joints, as well as contractile speed.

One aspect of isokinetic testing that has particularly expanded our knowledge of changes in neuromuscular performance with aging is the ability to test eccentric (ECC) actions. Although much research on strength changes with aging has found declines, there is now evidence that ECC strength may be relatively preserved in physically active individuals in some muscle groups.

The purposes of the studies described below were to determine: 1) whether ECC strength changes with age in the plantar and dorsiflexors (Porter and Vandervoort, 1997a); 2) to what extent changes in passive resistance of the joint as well as rate of torque development (RTD) may contribute to a preservation of ECC strength (Porter and Vandervoort, 1997a); 3) how will concentric (CON) and eccentric resistance training on an isokinetic dynamometer affect CON and ECC strength of the plantar and dorsiflexors, along with RTD, and passive resistance of the plantar flexors (Porter and Vandervoort, 1997b).

METHODS

I. Sixteen older (OW; age = 67 ± 4 years) and sixteen younger women (YW; age = 27 ± 4 years) participated in a study to examine strength, passive resistance and RTD (Porter and Vandervoort, 1997a). All subjects were healthy and recreationally physically active.

All testing was conducted on a KINCOM 500H isokinetic dynamometer. In order to test the plantar and dorsiflexors in a position similar to a standing posture a stand was constructed to allow subjects to perform the test in an upright position. Strength (Porter et al, 1996a) and passive resistive torque (Porter et al, 1996b) were found to be reliable in this position.

Passive resistive torque of the plantar flexors was measured at 6°/s, from 10° of plantar flexion (PF) to 10° of dorsiflexion (DF). Biofeedback was provided to allow subjects to move passively without activating the muscles around the ankle.

CON and ECC peak torque (PT) were measured from contractions performed at 30 °/s, from 20° PF to 10° DF. Rate of torque development (RTD) was determined from these contractions, and torque-angle curves were also examined for age group differences.

II. Training of the plantar and dorsiflexors was also performed on the KINCOM in a standing position with a group of 15 OW (age = 68 ± 5 years) (Porter and Vandervoort, 1997b). All of the above tests were performed before and after the 8 weeks of training, in both the standing and supine positions. Training was conducted 2 days per week, with 3 sets of 8 repetitions being done. The dorsiflexors were trained eccentrically at over 85% of ECC PT (or about 150% of CON PT). The plantar flexors were trained concentrically at over 85% of CON PT.

- PARALLEL SESSION -

Motor Control

Friday, August 10, 2001
0900 to 1030

CONTROL STRATEGIES FOR MANIPULATING MASS-SPRING OBJECTS

Jonathan B. Dingwell, Christopher D. Mah, and Ferdinando Mussa-Ivaldi

Sensory Motor Performance Program, Rehabilitation Institute of Chicago, Chicago, IL
Email: j-dingwell@northwestern.edu Web: http://manip.smpp.northwestern.edu/dingwell/

INTRODUCTION

When planning and executing reaching movements, the CNS must account for the mechanical properties of the arm. It is believed that this is accomplished through the use of an internal model of arm dynamics that adapts when the physical properties of the arm are consistently altered, such as when making reaching movements in external force fields (Lackner and Dizio 1994; Shadmehr and Mussa-Ivaldi 1994) or when lifting rigid objects (Bock 1990). However, it is not known if model-based strategies are used to control dynamical systems outside the body; i.e. those that add new degrees-of-freedom (DOF) to the mechanical system being controlled (i.e. the arm). Examples of such tasks include carrying a cup of coffee, or controlling an external prosthesis.

To perform such tasks, humans could use knowledge of the object dynamics learned through their interactions. Alternatively, they might employ a less model-dependent strategy, such as slowing down or globally increasing arm stiffness to enforce a specific kinematic trajectory for the hand. We tested for evidence of these alternative hypotheses.

METHODS

Six young healthy subjects (3M & 3F; age = 30.7 ± 4.6 yrs) held the handle of a robotic manipulandum (Fig. 1A). Subjects made reaching movements (Fig. 1B) with their dominant arm while the robot produced forces that simulated a mass-on-a-spring (Fig. 1C) defined by the equation of motion:

$$\begin{bmatrix} \dot{q}_1 \\ \dot{q}_2 \end{bmatrix} = \begin{bmatrix} 0 & 1 \\ -K/M & 0 \end{bmatrix} \cdot \begin{bmatrix} q_1 \\ q_2 \end{bmatrix} + \begin{bmatrix} 0 \\ K/M \end{bmatrix} \cdot u \qquad (1)$$

where M = mass, K = stiffness, q_1 and q_2, were the y-position and y-velocity of the mass, respectively. The control input u was the y-position of the handle (Fig. 1C). Subjects performed 600 trials and were instructed to bring both their hand and the mass to rest ($dy/dt \leq 0.02$ m/s) within the target zone within 0.8 ± 0.2s. Trials exceeding 2.5s were terminated automatically.

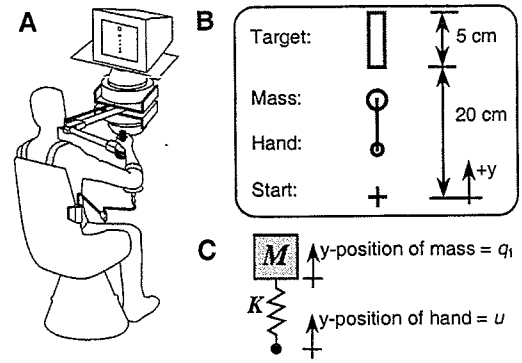

Fig. 1: A: 2-DOF robotic manipulandum. B: 1D reaching task. C: Mass-spring object.

Subjects learned to perform the task with an object of M = 3 kg and K = 120 Nm^{-1}. Exponential fits to movement time data were used to quantify learning rates ($T = a \cdot e^{bN} + c$ where T = Movement time & N = Trial #). If subjects simply slowed down until the mass-spring object effectively behaved like a simple mass, no learning would be observed.

The object's dynamics depended only on K/M (Eq. 1). Thus, all objects with the same K/M will exhibit the same output ($[q_1, q_2]$) for the same input (u). If subjects enforced a pre-defined u, by implementing a high-stiffness position controller, unexpectedly replacing the learned object with an object having the same K/M should not significantly affect task performance.

The last 120 trials included 12 "catch trials" where the K/M = (120 Nm^{-1} / 3 kg) object was unexpectedly replaced with either a K/M

= (40 Nm^{-1} / 1 kg) object (n = 6) or a *K/M* = (200 Nm^{-1} / 5 kg) object (n = 6). Deviations in catch trial kinematics from post-learning trials were evaluated to estimate the impedance at the hand-object interface. Movement times for all conditions were also analyzed using a one-way repeated measures ANOVA with Tukey's 95% confidence intervals.

RESULTS

All subjects significantly improved their movement times with practice (Fig. 2A/B). Thus, subjects acquired the capacity to predictively control object dynamics. They did not simply slow down to avoid perturbations imposed by the object. Subjects also showed dramatic improvements in movement kinematics between initial exposure ("IE3") and post-adaptation ("PA3") trials (Fig. 2C/D).

All subjects exhibited substantial kinematic deviations when exposed to both the 1 kg (CT1) and 5 kg (CT5) catch trial objects, compared to 95% confidence intervals (CI) of post-adaptation (PA3) kinematics (Fig. 2E). Differences in total movement times between all conditions (Fig. 2B) were highly significant ($p \leq 0.001$), except that the 1kg catch trials (CT1) did not differ from the initial exposure (IE3) trials ($p = 0.207$).

DISCUSSION

Subjects in the present study adopted neither of the model-independent control strategies hypothesized. Increasing hand stiffness would increase resistance to larger perturbations. The 5 kg object generated larger interface forces relative to the learned 3 kg object, whereas the 1 kg object generated smaller interface forces. The large deviations exhibited, particularly in the CT1 trials, are inconsistent with high hand stiffness. Hand stiffnesses of the order of 1000N/m (within the known physiological range) would have been sufficient to suppress all but minimal perturbations to hand movements during the catch trials. Rather, these catch trial deviations (Fig. 2E) suggest a control strategy where subjects attempted to apply forces matched to those required for the 3 kg learned object (Fig. 2D). Thus, subjects exhibited behavior that was consistent with computing the force applied to the object based on a planned object movement (i.e. with the formation of an inverse model of object dynamics). These results have implications for motor learning and rehabilitation.

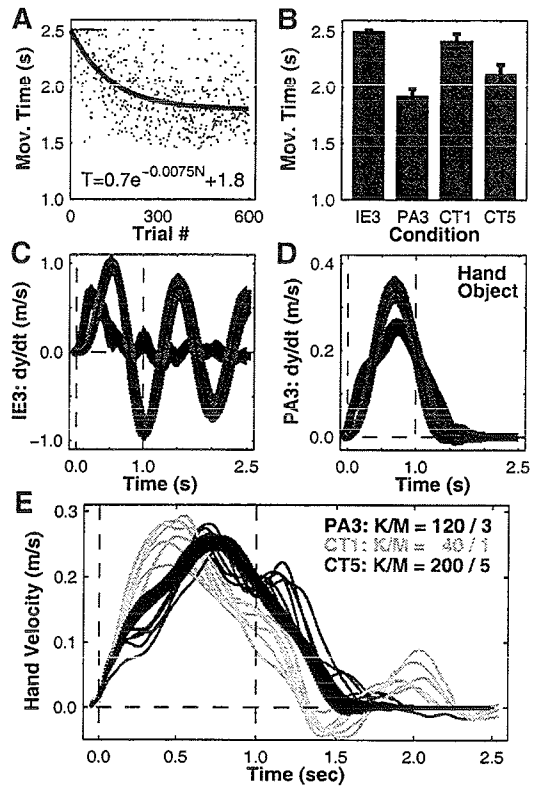

Fig. 2: Total movement times for (A) a typical subject and (B) all subjects and conditions. Velocity profiles for subject in A during initial exposure (IE3) trials (C) and post-adaptation (PA3) trials (D). Individual catch trial kinematics for subject in A for 1kg (CT1) and 5kg (CT5) objects vs. 95% CI for PA3 trials (E).

ACKNOWLEDGEMENTS

Partial funding was provided by NIH grants F32-HD08620-01 & T32-HD07418 and by NSF grant NSF-BES-9900684.

REFERENCES

Bock O (1990). *Behav. Brain Res.* **41**: 167-177.

Lackner JR and Dizio P (1994). *J. Neurophysiol.* **72**(1): 299-313.

Shadmehr R and Mussa-Ivaldi FA (1994). *J. Neurosci.* **14**(5): 3208-3224.

DYNAMIC SIMULATION OF JOINT CONTROL STRATEGIES DURING LANDING

Philip Requejo[1], Jill McNitt-Gray[1], Henryk Flashner[2]
[1]Biomechanics Research Laboratory, University of Southern California, Los Angeles, CA
[2]Department of Mechanical Engineering, University of Southern California, Los Angeles, CA

INTRODUCTION

Musculoskeletal injury, joint degenerative diseases, and bone remodeling have been strongly associated with loading experienced during multijoint movements involving impact. Experimental evidence indicates human subjects can modulate the external loading experienced during landing by as much as 8 times body weight (McNitt-Gray et al., 1993). Determination of the joint control strategies an individual uses to selectively distribute load within the musculoskeletal system during landing provides insight regarding the relationship between control laws at the subsystem and total body level. In this study, landing dynamics were simulated using three different joint control models (linear spring (S) (Farley et al., 1998, Arampatzis et al.,1999); spring and damper (SD), and a muscle (M) model based on mechanical properties of muscle (Selbie and Caldwell, 1996). Simulation results were then used to determine which representation of joint control best reflects experimental results.

METHODS

In this study, the human body was represented as a collection of planar 7 rigid segments interconnected by frictionless joints (Figure 1). The dynamics of the linked segment model was represented by a set of *N*-second-order differential equations of the form:

$$M(q)\ddot{q}=V(q,\dot{q})+G(q)+Tm+Fc$$

where $M(q)$ is the inertia matrix; $V(q,\dot{q})$ the vector describing the centrifugal and Coriolis effects; $G(q)$ defines the gravitational effects; $q,\dot{q},\ddot{q}$ are vectors of generalized coordinates. Tm are the net joint moments representing the torque contributions of the muscles. Fc is the ground reaction force. A mechanical simulation software (ADAMS, Mechanical Dynamics, Ann Arbor, MI) was interface with a Matlab/Simulink (Mathworks, Natick, MA) mathematical programming software to simulate the landing by integrating the set of ordinary differential equations. The length of each segment was scaled to each subject's anthropometric measures. The percent mass and radius of gyration were scaled according to the parameters reported by deLeva (1996). Initial conditions in the simulation were obtained from experimental data. The ground reaction force (Fc) was modeled by a non-linear visco-elastic/Coulomb(dry) friction element combination attached to the foot/surface interface (Gerritsen et al., 1995). The torque actuators (Tm) were implemented using the following models: 1) Rotational spring (S), 2) rotational spring and damper (SD), and 3) a joint torque generator incorporating physiological characteristics of human muscles (M): torque/velocity relation, a torque/angle relation, and an activation parameter (Selbie and Caldwell, 1996). The initial spring stiffness values were taken from Farley et al. (1998) and Arampatzis et al. (1999). An optimization algorithm (Design Synthesis, Provo, UT) was used to search for the combination of spring/damper constants or activation onset times that minimized the difference

between model simulated and experimental TBCM.

Experimental data were collected from drop landings performed by male and female divers (n=5) during a training session. During the performance of each landing, kinetic information regarding reaction forces were recorded using a force plate (600 Hz, Kistler, 0.4 x 0.6m force plate). Sagittal plane kinematics were recorded simultaneously using digital video camera (200Hz, NAC C^2S). Each coordinate of the body landmarks (deLeva, 1996) were digitized (Motus, Peak Performance, Inc.) and filtered using a fifth-order Spline (Woltring, 1986).

RESULTS AND DISCUSSION

During landing the M model calculated TBCM trajectory that mostly resembles that of the experimental data (Figure 2). The linear nature of center of mass trajectory determined using the S and SD model suggests that lower extremity joint control during landing involves non-linear coefficients that may incorporate kinematics and/or kinetic variables. The next step in model development is to explore the non linear nature of S and SD models as well as identification of subject specific coefficients of the M model that will capture experimental kinematics at the segment and joint level. Development of a dynamic model to simulate joint control behavior during landing will further our understanding of load distribution during multijoint tasks involving impact.

REFERENCES

McNitt-Gray, J. (1993). *J. Biomech.* **26**(9), 1037-46

deLeva (1996). *J. Biomech.***29**(9),1223-30

Gerritsen, K. et al. (1995), *J. Biomech.*, **28**(6),661-668

Selbie, W.S. and Caldwell G.(1996). *J. Biomech.*,**29**,1137-1146

Woltring (1986), *Adv. Eng. Soft.*,**8**(2), 104-107.

Farley et al. (1998) *J. Appl. Physiol.* **85**(3):1044-1055

Arampatzis et al.(1999). *J. Biomech.* **32**(12),1349-1353

ACKNOWLEDGEMENTS

This research is partially funded by the ISB Student Disscrtation Award and US Olympic Committee.

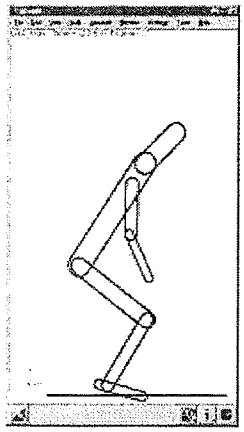

Figure 1: Multisegment Model.

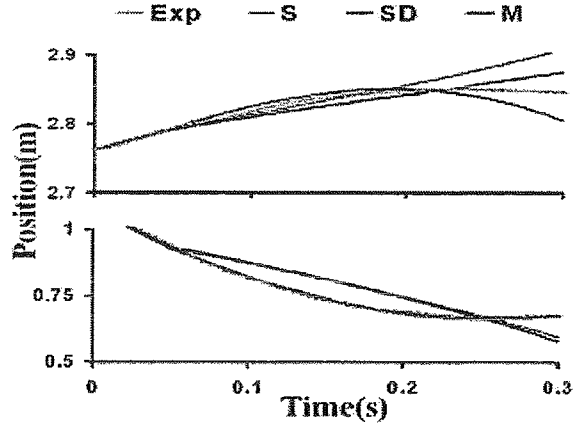

Figure 2: Simulated (S,SD,M) and Experimental (Exp) TBCM of a landing trial.

AUTOMATIC POSTURAL RESPONSES MIRROR SUPPORT SURFACE ACCELERATION

Lena H. Ting and Jane M. Macpherson

Neurological Sciences Institute, Oregon Health Sciences University, Portland, OR, USA
Email: tingl@ohsu.edu

INTRODUCTION

Automatic postural responses are rapid, centrally programmed muscular responses that stabilize the body during support surface perturbations. The initial EMG bursts are directionally specific responses and are thought to act in a feedforward or predictive manner to anticipate an impending destabilization of the body. Initial EMG burst amplitude is thought to be related to stimulus velocity. Finally, once triggered, it is believed that the initial burst cannot be modified for a fixed period of time by a subsequent stimulus.

This study investigated whether automatic postural responses could be rapidly altered to match changing perturbation direction. A series of compound ramps, in which the platform translation *reversed* direction 15-130 ms after movement onset was used. Typically, EMG responses occur at a latency of 40-60 ms. Resulting ground reaction forces occur at a further delay of ~50 ms, and therefore do not take effect until ~100 ms after perturbation onset. Therefore, the reversals in perturbation direction usually occurred before the force generated by the initial EMG response could develop. Thus, forces generated from the initial response are potentially destabilizing because they act after the platform has reversed direction. We investigated 1) whether the initial EMG burst is immutable, 2) which perturbation parameters could account for EMG scaling, and 3) whether the initial response was destabilizing when the platform reversed direction.

METHODS

Cats standing quietly were subjected to horizontal perturbations of the support surface, along an axis eliciting maximal automatic postural responses in flexors and extensors in the left hindlimb. Perturbations consisted of a randomized series of compound ramps with a driving function of 15-100 ms ramps immediately followed by a 370 ms ramp in the opposite direction. This elicited, for example, extensor and flexor responses in rapid succession.

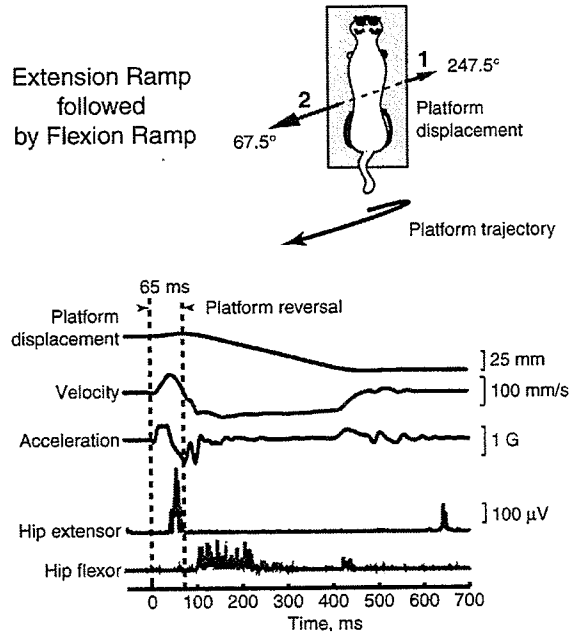

Figure 1 Example: platform displacement reverses direction 65 ms after movement onset. A brief extensor burst followed by a flexor burst is expected. The extensor response occurs at 40 ms latency, and is shut off by the time the platform reverses. The flexor response occurs at 55 ms after negative acceleration onset.

RESULTS AND DISCUSSION

Initial EMG bursts were always present even with the shortest reversal times, and they increased in duration and magnitude with increasing initial ramp duration. In fact, bursts in response to both the first and second ramps

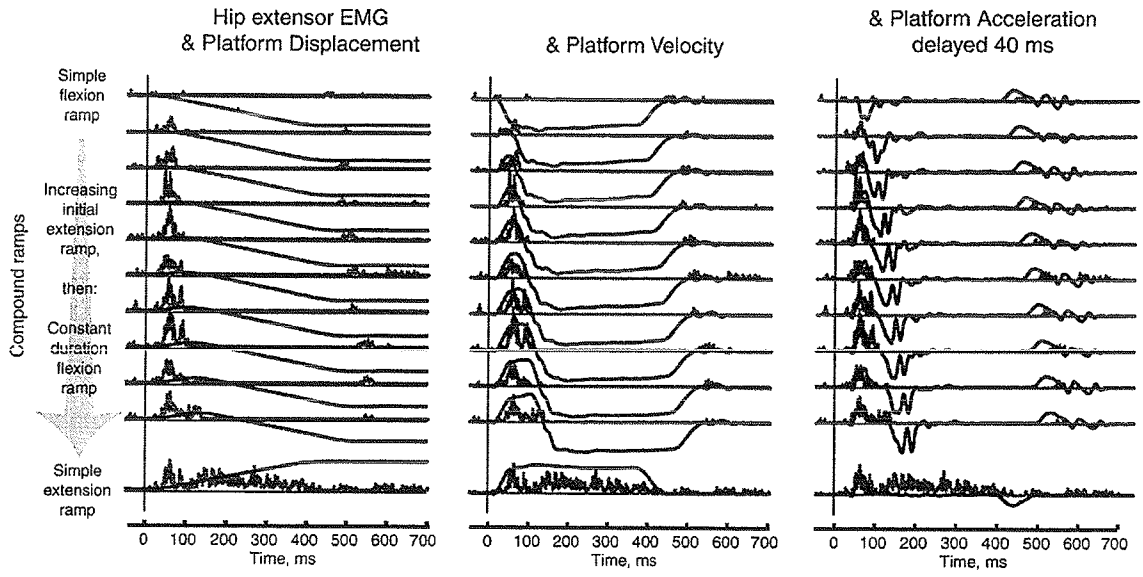

Figure 2 The extensor EMG burst was correlated to positive platform acceleration, at a delay of 40 ms. Platform displacement and velocity occur too late to be viable triggers of the response.

were correlated to the temporal features of platform acceleration at a fixed delay, characteristic to each muscle. Extensor EMG bursts were correlated to positive acceleration, and flexor bursts to negative acceleration. The integrated EMG of the initial bursts was linearly related to the initial platform impulse. Termination of initial EMG bursts was more correlated to zero crossings in acceleration than to velocity. However, acceleration and velocity were similar across all ramps because of limitations in the control of the hydraulic platform actuator.

Due to inertia, the center of mass (COM) initially moved in a direction opposite to the first ramp. It then reversed direction following platform reversal. The reversal in direction was due to both the passive response to the second ramp, in addition to the active response to the first ramp. The COM velocity following platform reversal increased as the initial ramp duration increased. Thus forces generated by the initial response do indeed accelerate the COM in the direction of the second ramp, thus further destabilizing it.

SUMMARY

The onset, offset, magnitude, and ongoing modulation of the initial postural response appears to mirror platform acceleration at a fixed latency. There was no evidence that the timing of the secondary response was affected by the first, antagonistic response. The nervous system may therefore use an acceleration signal to trigger, scale, and modulate automatic postural responses. This would allow stabilization of the body against unpredictable as well as continuous perturbations. Previous observations on the immutability of the initial burst may be due to stereotyped platform control systems with limited initial acceleration profiles. We speculate that cutaneous receptors, muscle spindles, and/or Golgi tendon organs could contribute to sensing the acceleration signal.

ACKNOWLEDGEMENTS

Supported by NIH NS29025. LHT is an O'Donnell Foundation Fellow of the Life Sciences Research Foundation.

Gaze Stabilization During Locomotion Requires Full Body Coordination

Mulavara, AP[1], Miller, CA[1], Houser, J[1], Richards, JT[1] and Bloomberg, JJ[2]

[1] Neuroscience Laboratories, Wyle Laboratories, Houston, TX, USA
[2] Neuroscience Laboratories, NASA, Johnson Space Center, Houston, TX, USA
E-mail: amulavar@ems.jsc.nasa.gov

INTRODUCTION

Maintaining gaze stabilization during locomotion places substantial demands on multiple sensorimotor subsystems for precise coordination. Gaze stabilization during locomotion requires eye-head-trunk coordination (Bloomberg, et al., 1997) as well as the regulation of energy flow or shock-wave transmission through the body at high impact phases with the support surface (McDonald, et al., 1997). Allowing these excessive transmissions of energy to reach the head may compromise gaze stability. Impairments in these mechanisms may lead to the oscillopsia and decreased dynamic visual acuity seen in crewmembers returning from short and long duration spaceflight, as well as in patients with vestibular disorders (Hillman, et al., 1999). Thus, we hypothesize that stabilized gaze during locomotion results from full-body coordination of the eye-head-trunk system combined with the lower limb apparatus. The goal of this study was to determine how multiple, interdependent full- body sensorimotor subsystems aiding gaze stabilization during locomotion are functionally coordinated, and how they adaptively respond to spaceflight.

METHODS

Data were collected from six crewmembers who lived on the Mir Space Station for 3 to 6 months (mean ±1S.E, age 42.8 ±2.03 yrs, weight 80.48 ±1.70 kg, and height 1.73 ±0.013m). Data were collected 10 days prior to launch and on one, 3 to 6 and 7 to 9 days postflight. Body segment motions were measured using a six-camera motion measurement system (Motion Analysis Corp., Santa Rosa, CA) sampled at 60 Hz. Head and trunk segments were targeted with three markers for 3D analysis, while the right lower limb was targeted with two markers each affixed to the thigh, shank and foot segments for sagittal plane analysis. The shock transmitted to the head and shank was measured using triaxial accelerometers (Entran, Fairfield, NJ) and sampled at 1 kHz.

During each test session, the subjects performed two walking trials on a motorized treadmill (Quinton Series 90 Q55), each 20 sec in duration, at 1.79 m/sec while fixating their gaze on a centrally located earth-fixed target positioned 2m away from the eyes. Marker data were processed to derive 3-D position information relative to a coordinate frame coincident with the surface of the treadmill. The marker trajectories and accelerometer data were filtered using a zero-phase, 4th order, Butterworth filter with cut-off frequency at 5 Hz and 15 Hz, respectively. Foot-switches were used to determine heel-strike and toe- off.

Head re trunk angular motion was calculated. The power in the head re trunk motion in the flexion-extension plane was summed in the frequency range of 1.5-2.5 Hz reflecting the contributions of reflexive head stabilization mechanisms (Keshner, et al., 1995). The lower limb response to heel-

strike was characterized by the total angular displacement of knee and ankle angles within the epoch from heel-strike to the first peak of knee flexion. The shock transmission characteristics of the body were assessed in the time and frequency domains (Lafortune, et al., 1996).

RESULTS AND DISCUSSION

The motion of the head re trunk during locomotion was significantly reduced ($p<0.05$) one day postflight in the flexion-extension plane compared to pre-flight (Figure 1). The knee and ankle total angular displacements were significantly increased ($p<0.05$) one day postflight indicating increased lower limb flexion subsequent to the heel-strike event (Figure 2). Evaluation of the shock wave transmission showed that the mean shock experienced by the shank and the head showed a significant decrease ($p<0.05$) of 40% and 20%, respectively, one day postflight compared to preflight levels.

We infer from these data that the subjects modulated their reflexive head stabilization mechanisms during locomotion after spaceflight to reduce the degrees of freedom to compensate for gaze instability. The increase in lower limb flexion may be an active gaze stablizing response designed to reduce the axial stiffness of the lower limb complex. This decreases the shock-wave to the head in response to the reduced dynamic visual acuity and oscillopsia experienced by returning crewmembers. Therefore, during normal terrestrial locomotion, dynamic modulation of head movement control coupled with the lower limb joint configuration may contribute to maintaining gaze stability. In this manner, we observed an emergent full-body coordination pattern produced to compensate for postflight gaze instability.

REFERENCES

Bloomberg, et al. (1997). *J Vestib Res.* **7**(2-3):161-77

McDonald, et al. (1997). *J Vestib Res.* **7**(2-3):239-50

Hillman, et al. (1999) *J Vestib Res.* **9**(1):49-57

Keshner, et al. (1995) *J Neurophysiol.* **73**(6):2302-12

Lafortune, et al. (1996) *J Biomech.* **29**(12):1531-7

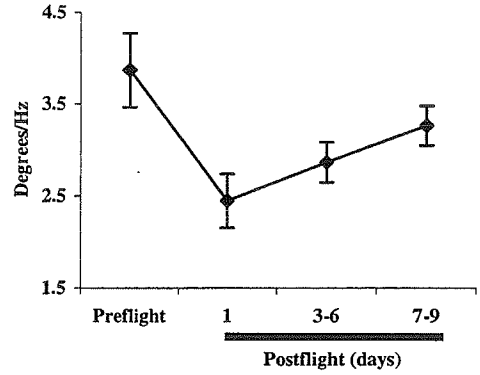

Figure 1: Comparison of the mean area (± 1 SE) in 1.5-2.5Hz for head re trunk flexion-extension movements.

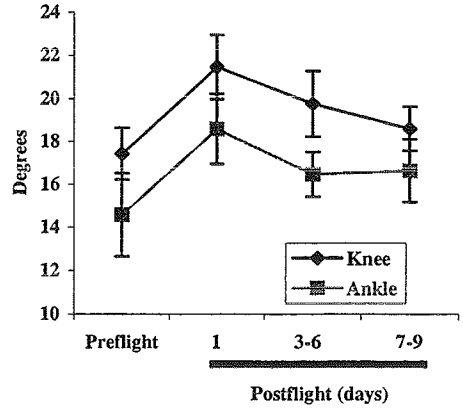

Figure 2: Comparison of the mean total angular displacement (± 1 SE) of the knee and ankle joints in the sagittal plane.

PREFLEXIVE AND REFLEXIVE COMPONENTS OF STABILITY: COCKROACH AS A MODEL MUSCULO-SKELETAL SYSTEM.

Kenneth Meijer, Thomas M. Libby and Robert J. Full
Department of Integrative Biology, University of California at Berkeley, Berkeley, CA, USA.
E-mail: kenneth@socrates.berkeley.edu

INTRODUCTION

During locomotion, animals deal with external perturbations effortlessly. Their ability to maintain stable locomotion results from reflexive actions of the nervous system and the intrinsic mechanical properties of the muscle-skeletal system (preflexes). It has been hypothesized that preflexes act as a first line of defense when dealing with rapid external perturbations (Brown and Loeb, 2000). Due to the complexity of most musculo-skeletal systems, an understanding of the relative contributions to control remains elusive. Cockroaches are ideal subjects to answer such questions, because their musculo-skeletal system and sensory system are well-defined (Full and Ahn, 1995; Wong and Pearson, 1976). This study aimed to determine the presence of preflexes and reflexes in perturbed cockroach legs.

METHODS

The perturbation experiments were performed on the hind-limbs of 10 cockroaches (*Blaberus discoidalis*), using a Single Leg Impedance Measurement device (SLIM). The thorax of the cockroach was rigidly attached to a tether. The left metathoracic limb was attached with a steel rod to the lever arm of a muscle lever system (300B-LR, Aurora Scientific). The animal was positioned in the natural standing posture. Perturbation experiments consisted of sinusoidal oscillations of leg position (amplitude = 1 mm; frequency = 2-25 Hz) roughly in the horizontal plane (Fig. 1). Recording electrodes were implanted into the coxal extensor muscles (177c, 179, and 177d) of the animals while they were immobilized. Force and EMGs responses to the perturbations were recorded.

Digital video was taken from below the animal at 125Hz (Kodak EktaPro, HG imager 2000). The videos were digitized and analyzed (Peak Performance Technologies) to obtain coxa-femoral and femoral-tibial angle changes over the course of the oscillations. Force and displacement data was fitted to a spring - damper model.

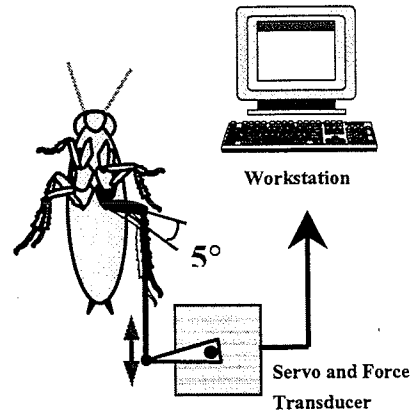

Figure 1. Schematic of our SLIM setup

RESULTS AND DISCUSSION

The positional perturbations of the leg resulted in small, 5-degree angular changes in both the coxa-femoral and femoral-tibial joints. Single legs of cockroaches with relaxed muscles responded to the positional perturbations with a relatively large force (Fig. 2). Forces ranged from 2.8 to 10 mN which is large compared to the average horizontal forces during running on level terrain (4.9 ± 0.7 mN; Full et al., 1991).

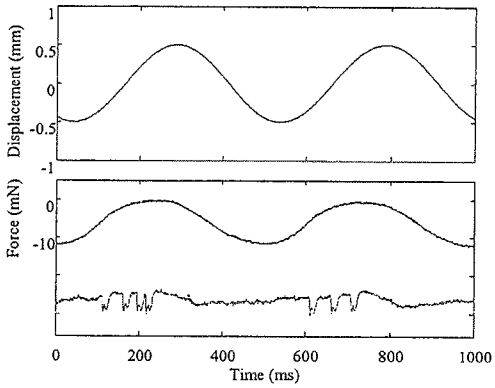

Figure 2. Leg displacement (top); Force and EMG of muscle 177d in response to leg oscillations (bottom)

The mechanical impedance, which was defined as the maximal change in force divided by the maximal change in position, was independent of the frequency at which the perturbation was applied. This suggests that the ability of the cockroach to deal with perturbations is rate-independent. Fitting of the spring-damper model to the data indicated that leg stiffness was independent of frequency, whereas the damping coefficient declined with increasing frequency.

EMG activity in response to the perturbation was found in muscle #177d (Fig. 2), but not in muscles #179 and #177c. Based on this pattern and the amplitude of the EMG signal, the EMG was identified as reflex activity from the slow motor axon in muscle 177d. The reflex activity measured in our experiments probably stems from sensory activity of specialized organs, called hairplates, which are located in the coxa-femoral joint (Wong and Pearson 1976). EMGs had a time delay with respect to the onset of joint flexion. The time delay decreased with increasing frequency and reached a constant value of about 12 ms for frequencies beyond 10 Hz, suggesting that this is the fastest response time possible by the reflex system. The average number of action potentials per perturbation cycle declined from 5 pulses at 2 Hz to less than 1 pulse for frequencies higher than 10 Hz. This suggests that the reflex system contributed less at the higher perturbation rates.

CONCLUSIONS

Our data support the hypothesis that cockroaches use both preflexes and reflexes to deal with external perturbations. The contribution of the reflexive component declines at higher speeds as indicated by changes in EMG signal. The decline is probably related to limitations in the response time of the reflex system. As speed and stride frequency increase, stride period decreases and reduces the time a reflex can produce an effective response. Since the mechanical impedance stays constant with increasing frequency, this means that the contribution of the preflexes becomes more important at the higher perturbation rates.

The behavior of the insect leg is consistent with the hypothesis that intrinsic mechanical properties act as zero order feedback signals, which can respond almost instantly to rapid perturbations (Brown & Loeb 2000). Preflexes can greatly simplify control during rapid gross rhythmic activity.

REFERENCES

Brown, IE and Loeb, GE (2000). *Biomechanics and Neural Control of Movement. Springer Verlag, New York* pp:148-163.

Full, RJ., Blickhan, R and Ting, LH (1991) *J. Exp. Biol.* 158: 369-390

Full, RJ and Ahn, A. 1995 *J. Exp. Biol.* 198:1285-1298

Wong, RKS and Pearson, KG 1976. *J Exp. Biol.* 64: 233-249

ACKNOWLEDGEMENTS

Supported by ONR MURI contract N00014-98-0747 and DARPA contract N00014-98-1-0669 to RJF.

MUSCLE PREACTIVATION AND LEG STIFFNESS IN MEN AND WOMEN DURING HOPPING

G.D. Heise[1], M. Bohne[1], and E. Bressel[2]

School of Kines. and Phys. Educ., University of Northern Colorado, Greeley, CO 80639
Department of HPER, Utah State University, Logan, UT 84322
E-mail: gheise@hhs.unco.edu

INTRODUCTION

When hopping and running, the leg(s) in contact with the ground can be modeled as a simple linear spring (see Fig 1). The stiffness of the leg spring (k_{leg}) is defined as the ratio of maximum force during foot contact to ΔL.

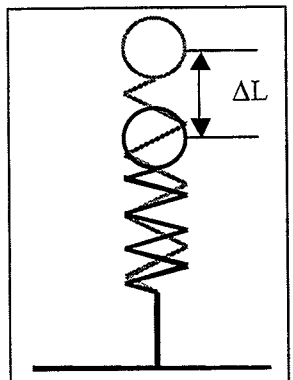

Fig 1: Leg spring model for hopping.

When hopping, k_{leg} increases as surface stiffness decreases (Farley et al., 1998). Adjustments to ankle stiffness were found to be the greatest contributor to changes in k_{leg}, whereas the timing of muscle onset did not change. Hortobagyi and DeVita (2000), however, found significant relationships between muscle preactivition times and leg stiffness when subjects stepped downward. They also reported differences between young and old subjects.

Motor control researchers have argued that joint stiffness is increased prior to ground contact when landing from a jump and is accomplished by preactivation of leg musculature (e.g., Santello & McDonagh, 1998). The lack of agreement over the role of muscle preactivation in leg stiffness was the primary motivation for this study. We hypothesized that differences in preactivation times of leg musculature would accompany differences in leg stiffness, which were identified previously between men and women (Heise et al., 1997).

METHODS

Ten healthy women and ten healthy men volunteered as subjects. Each participant attended one test session which included a 10-min warm-up walk at 1.57 m/s followed by hopping on a force platform at a preferred frequency while EMG data and vertical ground reaction force data were recorded. Surface EMG electrodes were positioned over the bellies of muscles rectus femoris (RF), vastus lateralis (VL), and gastrocnemius (GAST) after appropriate skin preparation. During hopping, vertical ground reaction force data and the EMG signals were sampled at 1000 Hz for 5 s. Data from all channels were then stored in digital format on a microcomputer.

Hopping frequency and k_{leg} were determined from force platform data (Farley et al., 1991). EMG data were full-wave rectified and muscle onset was identified using an interactive, computer-graphics program that plotted the rectified signal of each channel. Preactivation time for each muscle was calculated as the difference between muscle onset time,

determined manually, and the time when vertical GRF reached body weight. The mean of three hopping cycles for each subject was used for statisical analysis. A two factor ANOVA was used to detect differences between genders and between muscles.

RESULTS AND DISCUSSION

Preferred hopping frequency was the same between women and men (2.2 Hz). As reported by Heise et al. (1997), leg stiffness was significantly different between women and men (see Table 1). Mean values were similar to those previously reported (Chelly & Denis, 2001; Farley et al., 1991).

	WOMEN	MEN
k_{leg} (kN/m)	18.9 ± 0.6	24.6 ± 2.4 *

Table 1: Leg stiffness between women and men (mean ± SE; * $p < .05$).

The sequence of muscle onset is in agreement with previous findings (Farley et al., 1998; Hortobaghi & DeVita, 2000). GAST activity was initiated prior to the knee extensors (see Fig 2).

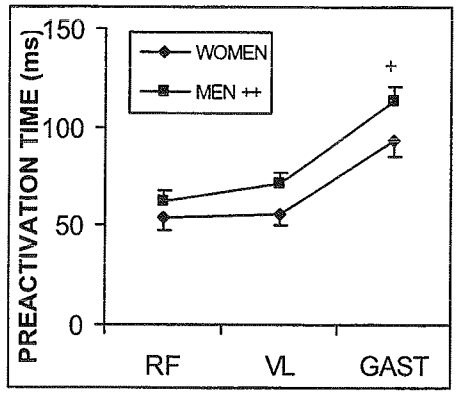

Fig 2: Mean preactivation times for all muscles. (error bars show SE; $^{+}$ GAST onset is earlier than RF and VL, $^{++}$ times for men are earlier than women, $p < .05$).

Men activated muscles significantly earlier than women (see Fig 2), which may partly explain why men exhibited higher leg stiffness. We also observed an increase in the amplitude of activity after onset in all subjects. Although this was not formally measured in the present study, it agrees with the measurements of Santello and McDonagh (1998). For men, this observation, coupled with their earlier preactivation time, may lead to greater tension in muscle and therefore, increased joint stiffness. A more complete analysis which includes joint stiffnesses and EMG amplitudes is required to better address this conjecture.

In summary, the differences in leg stiffness between men and women were accompanied by differences in muscle preactivation times.

REFERENCES

Chelly & Denis. *Med Sci Sport Exerc*, 33, 326-333, 2001.

Farley, C. T., et al. *J of App Physiol*, 71, 2127-2132, 1991.

Farley, C. T., et al. *J of App Physiol*, 85, 1044-1055, 1998.

Heise, G.D., et al. *ASB Proceedings*, Clemson, SC, pp. 284-285, 1997.

Hortobagyi, T. & DeVita, P. *J Electromyo Kines*, 10, 117-126, 2000.

McMahon, T.A. & Cheng, G.C. *J of Biomech*, 23(Supp), 65-78, 1990.

Santello, M. & McDonagh, M. *Exper Physiol*, 83, 857-874, 1998.

ACKNOWLEDGEMENTS

Funding provided by the Faculty Research and Publications Board of UNC.

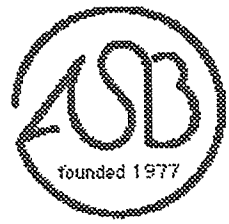

- PARALLEL SESSION -

Muscle

Friday, August 10, 2001
1100 to 1230

INTRAMUSCULAR PRESSURE IS A GOOD PREDICTOR OF ISOMETRIC STRESS AT LONG LENGTHS IN RABBIT TIBIALIS ANTERIOR MUSCLE

J. Davis[1], K. Kaufman[2] and R. L.Lieber[1]
[1]University of California and V.A. Medical Centers, San Diego, CA
[2]Mayo Clinic, Rochester, MN
E-mail: rlieber@ucsd.edu

Introduction

Electromyography (EMG) and joint kinematics are the most widely-used methods to assess muscle function during gait. However, the ability of EMG to provide an accurate prediction of relative muscle force is restricted to active conditions that are close to isometric, which may limit its practical use in gait analysis. Due to the redundancy in the musculoskeletal system, moment calculations combined with anatomical models yield estimates of muscle tension but the solutions are indeterminate. Although there are direct methods for measuring muscle force *in vivo* (Komi *et al.*, 1996) they are highly invasive and not applicable to use in children. Based on encouraging preliminary measurements of intramuscular pressure (IMP) to predict muscle force (Baumann *et al.*, 1979, Sutherland *et al.*, 1989), IMP may prove a useful adjunct in the assessment of active and passive muscle force during gait. The purpose of this study was to quantify the relationship between IMP and muscle stress during well-defined isometric muscle contractions of the rabbit tibialis anterior (TA).

Methods

The experimental model was the TA of the New Zealand White rabbit (mass=2.5 $\pm$0.5 kg, n = 12). The knee was fixed in a custom jig with 3.2 mm Steinman pins placed in the proximal tibia and distal femur. The TA was exposed and the distal tendon attached to a servomotor (Cambridge Model 300B, Aurora Scientific Inc.). A cuff electrode was placed around the peroneal nerve for muscle activation (Pulsar 6Bp Stimulator FHC Inc.). A 400 μm fiber optic pressure sensor (Luna Innovations Inc.) was inserted via an 18-gauge angiocatheter at a 10° angle in line with the long axis of the fibers. Optimal length (L_O) and maximum tetanic tension (P_O) were defined with tension measured at 5, 10, 20, 40, 60, 80, and 100 Hz. The length-tension curve was created using 40 Hz isometric contractions with 2 minutes of rest between each contraction to minimize the effects of fatigue. Measurements began at L_O–50% and progressed to L_O+50%, changing the length-tension in 5% L_O increments after each contraction. Length, tension, pressure, and temperature were recorded simultaneously using a data acquisition board in the LabView environment (National Instruments). Tension was converted to stress by dividing force by the muscle's calculated physiological cross-sectional area.

Results

Qualitatively, the length-tension curve for isometric contractions (Fig. 1) was mimicked by the length-pressure curve (Fig. 2) for both active and passive contractions. To quantify the correlation between stress and pressure, each data set was broken into groups for the ascending and descending limbs of the length-tension curve. Linear regression was performed individually for each animal for each portion of the length-tension curve and for active and passive conditions. Pressure-stress coefficients of determination ranged from .139-.963 (mean=.69$\pm$.23) for active contractions and

from .045-.982 (mean=.70±.32) for the passive condition (Table 1). Correlations were higher for the descending limb of the length-tension curve compared to the ascending limb.

Discussion

This study quantified the relationship between IMP and muscle stress during isometric muscle contractions. Our goal was to investigate the relationship for both active and passive conditions over a range of lengths. The positive correlation between IMP and muscle stress was strong for lengths on the descending limb of the length tension curve for both active and passive muscle contraction. For the ascending limb, however, a weaker relationship was observed that may be in part due to sensor movement near slack lengths (L_O–50% to L_O–35%). These data are encouraging under the conditions of static contractions. Further experiments are required to determine similar correlations during dynamic contractions.

References

Baumann *et al.* (1979). *Clin. Orthop. Rel. Res.* **145**:292-299.

Sutherland *et al.*, (1989). *Orthop. Trans.* **34**:319.

Komi *et al.* (1996). *Eur. J Appl. Physiol.* **72**:278- 280.

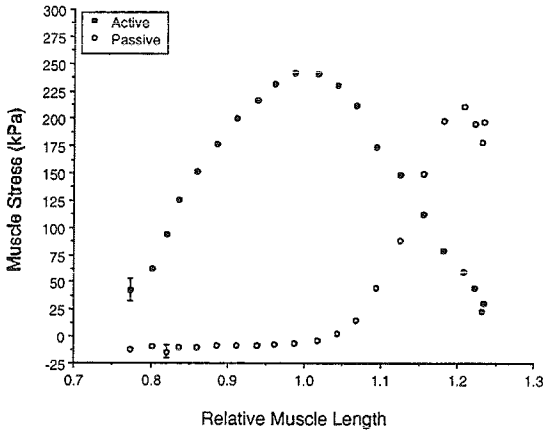

FIGURE 1: Relationship between isometric muscle stress and muscle length, relative to optimal length. The average SEM is shown as a single error bar for each graph for clarity of presentation.

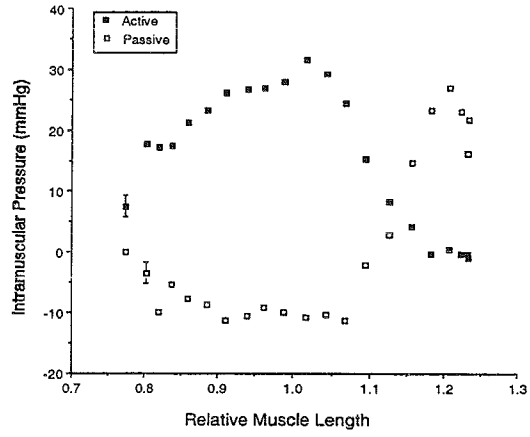

FIGURE 2: Relationship between intramuscular pressure and muscle length, relative to optimal length. The average SEM is shown as a single error bar for each graph for clarity of presentation.

	Active Pressure Coefficients of Determination	Passive Pressure Coefficients of Determination
Ascending Limb	.60 ± .25	.53 ± .38
Descending Limb	.77 ± .16	.86 ± .11

Table 1: Average active and passive pressure coefficients of determination split by limb on the length-tension curve.

CROSSBRIDGE MUSCLE MODEL PARAMETERS OF DIFFERENT FIBER TYPES

David C. Lin[1] and T. Richard Nichols[2]

[1]Department of Biological Systems Engineering, Washington State Univ., Pullman, WA, USA
[2]Department of Physiology, Emory Univ. School of Medicine, Atlanta, GA, USA
Email: davidlin@wsu.edu

INTRODUCTION

Skeletal muscle has a range of contractile properties which are dependent upon the types of myosin isoforms making up the muscle. Specifically, mechanical properties, such as maximal shortening velocity (V_{max}), are strongly correlated with myosin heavy chain (MHC) content. Mathematical models of muscle force generation account for these variations by having different sets of parameters. For instance, the Hill model would modify the hyperbolic force-velocity constants across fiber types. However, if muscle model parameters could be set according to the known biophysical measurements from the different MHC types, the model parameters could be determined without empirical curve fitting of mechanical data.

Crossbridge muscle models tie biophysical processes to macroscopic force predictions. One such model is the Distribution-Moment (DM) model (Zahalak, 1981), which is a computationally simplified model of the two-state Huxley model. The DM model parameters represent the biophysical processes of muscle contraction, namely the attachment and detachment rates of crossbridges. The aim of this study is to estimate DM model parameters for single muscle fibers with two distinct MHC types. The results will address two questions: how do the two sets of parameters differ? and are the differences consistent with biophysical measurements? The answers will validate the setting of crossbridge model parameters by the biophysical measurements from specific MHC types.

METHODS

Single muscle fibers were chemically skinned and dissected free from cat soleus and caudofemoralis (CF) muscles. Cat soleus fibers only express slow type I MHC, while CF fibers only express fast type IIx MHC (Talmadge *et al.*, 1996). Fibers were attached between a force transducer and motor, set at a sarcomere length of 2.5 μm, and maximally activated in a Ca^{++} solution at room temperature. One of two types of perturbations was then applied: a staircase length change to measure force-length (F-L) characteristics; or a linear change in force (i.e. a force ramp) to measure the force-velocity (F-V) relationship. The force ramp was a compact method to acquire F-V data (Iwamoto *et al.*, 1990). Both types of perturbations were applied in lengthening and in shortening. 25 CF fibers and 24 soleus fibers were used in this study.

The DM model was simulated for a force ramp perturbation. Five model parameters were identified: the crossbridge attachment rate (f_1); and the detachment rates (g_o for negative crossbridge displacements, g_1 for positive displacements within the crossbridge "reach" (h), and f_o' and f_1' for positive displacements beyond h). Parameter estimation was performed by the simplex method to minimize differences between the simulated F-V curves and experimental soleus and CF fiber F-V data.

RESULTS AND DISCUSSION

The force ramps produced hyperbolic F-V curves in both shortening and lengthening (figures 1 and 2). It should be noted that the force ramp F-V curves differ from a typical isotonic curve in that they had an offset in velocity (due to elasticity) and a larger estimate of V_{max}. However, this did not affect the parameter estimation since the force ramp was used in the simulations. The DM model fit the experimental data well (figure 2), which was not surprising since five parameters were free to vary. The parameter estimates are listed in Table 1. The parameters from CF fibers are larger than those from the soleus fiber, which is to be expected from faster crossbridge kinetics of the type IIx isoform.

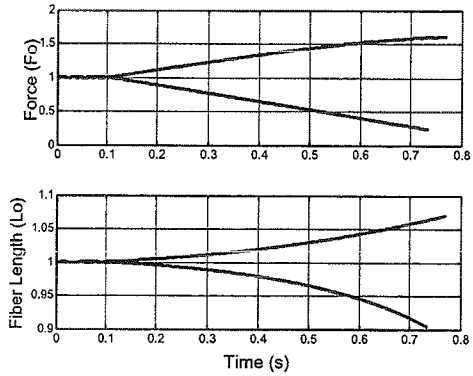

Figure 1. Shortening and lengthening force ramps and the length changes in a CF fiber.

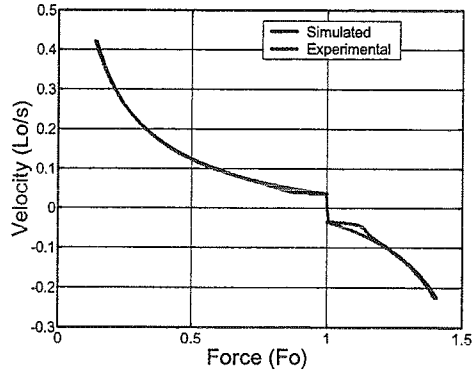

Figure 2. Average experimental and simulated F-V curves of soleus fibers.

Table 1. Parameters of the two fiber types.

Fiber	f_1	g_0	g_1	f_0	f_1
CF	84	680	37	37	68
SOL	52	330	1.9	40	22

In the literature, measurements of crossbridge kinetics in slow versus fast myosin types show that rate constants approximately differ by: (1) g_o: 3-6 times (2) f_1: 10 times and (3) g_1: 6-20 times (Potma et al., 1994; Millar and Hoshmer, 1992). The variations in values from Table 1 are in the range of literature values except for the variation of f_1. Little or no information exists in the literature on the lengthening rate constants. However, Table 1 suggests differences in the lengthening F-V are not due to the variation of a single rate constant, but of several rate constants.

SUMMARY

A crossbridge model was used to determine whether the variation of model parameters for different fiber types was consistent with biophysical data. There was some correspondence with the literature, and the parameter variations suggest values for other rate constants.

REFERENCES

Iwamoto, H., Sugaya, R., and Sugi, H. (1990). *J. Physiol. (Lond.)*. **422**, 185-202.

Millar, N.C. and Homsher E. (1992). *Am. J. Physiol.*, **262**, C1239-C1245.

Potma, E.J., van Graas, I.A., Stienen, G.J. (1994). *Biophys. J.*, **67**, 2404-2410.

Talmadge, R.J., Grossman, E.J., and Roy, R.R. (1996). *J. Exp. Zool.*, **275**, 413-420.

Zahalak, G.I. (1981). *Math. Biosci.*, **55**, 89-114.

ACKNOWLEDGMENTS

This work was supported by NIH grants HD32571-03 and F32 NS10688-01

Effects of pH on the length-dependent twitch potentiation in skeletal muscle

Dilson E. Rassier and Walter Herzog

Human Performance Laboratory, University of Calgary, Calgary (AB), Canada
Email: walter@kin.ucalgary.ca

INTRODUCTION

Staircase potentiation is the increase in twitch force production during low-frequency repetitive stimulation. There is a length dependence of twitch potentiation, such that force enhancement is greater at short than at long muscle lengths (Rassier and MacIntosh, 2000). When the muscle is elongated, there is an increased Ca^{2+} sensitivity of the myofilaments (Martyn and Gordon, 1988), indicating that length dependence of potentiation may be associated with length dependence of Ca^{2+} sensitivity (Rassier and MacIntosh, 2000). Changes in the charge potential of myofilaments, induced by a decrease in pH, are known to abolish the length dependence of Ca^{2+} sensitivity (Martyn and Gordon, 1988). This study was aimed at testing the hypothesis that a decrease in pH, and the concomitant loss of length dependence of Ca^{2+} sensitivity, depresses the length dependence of staircase potentiation.

METHODS

A small fiber bundle with approximately 10 to 30 fibers (10-14 mm long) was dissected from the extensor digitorum longus (EDL) of mice. The fiber bundle was transferred to an experimental chamber with continuous superfusion of Tyrode solution (NaCl, 121 mM; KCl, 5.0 mM; NaH_2PO_4, 0.4 mM; $MgCl_2$, 0.5 mM; $CaCl_2$, 1.8 mM; $NaHCO_3$, 24 mM; Dextrose, 5.5 mM), which was bubbled continuously with 95% O_2 and 5% CO_2 (pH = 7.4, 25°C). The two tendons of the fiber bundle were attached to a force transducer and to a motor arm, respectively, suspending the fiber bundle horizontally. Changes in pH were obtained by bubbling the solution with 70% O_2 and 30% CO_2 (pH = 6.6), or by changing the original Tyrode solution to: NaCl, 136.5 mM; KCl, 5.0 mM; NaH_2PO_4, 0.4 mM; $MgCl_2$, 0.5 mM; $CaCl_2$, 1.8 mM; $NaHCO_3$, 11.9 mM; Dextrose, 5.5 mM (pH = 7.8 without bubbling)(Westerblad et al., 1997).

Optimal length (L_o) was defined as the length at which maximal isometric force was obtained in response to a doublet stimulation (5 ms delay). The fiber bundle was tested for a range from L_o to L_o + 1.2 mm (0.3 mm steps). One twitch contraction was elicited at each of the 5 lengths (random order), followed by a 10 Hz stimulation train for 10 s. Then, twitch contractions at each of the 5 lengths were elicited again. The degree of twitch potentiation was calculated as the force difference between twitch contractions recorded after and before the 10 s, 10 Hz stimulation trains. The whole stimulation procedure was done at the three pH levels; 6.6, 7.4 and 7.8.

RESULTS AND DISCUSSION

During the 10 s of 10 Hz stimulation trains, potentiation was observed at L_o in all pH conditions investigated. However, potentiation was smallest at a pH of 6.6.

Figure 1 shows twitch contractions recorded before and after the 10 s, 10 Hz stimulation train, at L_o and L_o + 1.2 mm, at a pH of 7.4 and 6.6.

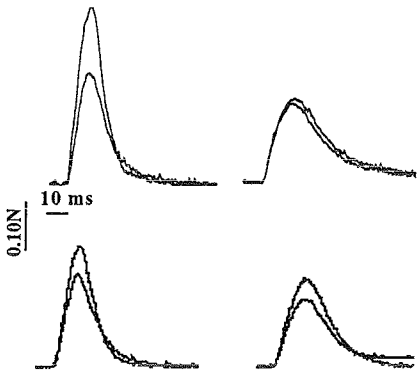

Figure 1: Twitch contractions recorded before and after 10 s of 10 Hz stimulation at pH levels of 7.4 (top panel) and 6.6 (lower panel), at L_o (left) and L_o + 1.2 mm (right).

There is an increase in active force after 10s, 10 Hz stimulation trains at both pH levels shown. At a pH level of 7.4, potentiation decreases with increasing fiber bundle length, but at a pH of 6.6, potentiation is virtually independent of fiber bundle length. Contractions at a pH of 7.8 (not shown) produced results similar to those observed at a pH of 7.4.

Figure 2 depicts mean values for the level of potentiation at the three pH conditions investigated. At a pH of 7.4 and 7.8, the degree of potentiation after 10 Hz stimulation showed a linear decrease with increasing fiber bundle lengths ($r^2 = 0.95$ and $r^2 = 0.99$, respectively). At a pH of 6.6, the length dependence of potentiation was abolished, and the slope of the length-potentiation relationship was not different from zero ($r^2 = 0.05$).

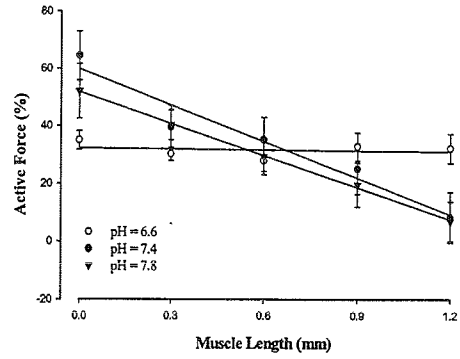

Figure 2: Relationship between potentiation and muscle length at different pH conditions.

In conclusion, it appears that length dependence of staircase potentiation is directly associated with the length dependence of Ca^{2+} sensitivity. This relationship is likely controlled, at least partially, by changes in charge potentials on the myofilaments.

REFERENCES

Martyn, D.A., Gordon, A.M. (1988). *J. Muscle Res. Cell Motil.* **9**, 428-445.

Rassier, D.E., MacIntosh, B.R. (2000). *Can. J. Physiol. Pharmacol.* **78**, 350-357.

Westerblad, H. et al. (1997). *J. Physiol.* **500.1**, 193-204.

MECHANICAL PROPERTIES OF THE RAT SOLEUS APONEUROSIS DURING VARIABLE RECRUITMENT *IN SITU*

Ryan J. Monti[1*], Roland R. Roy[2], and V. Reggie Edgerton[1,2]

[1] Department of Physiological Science, University of California, Los Angeles, CA, USA
[2] Brain Research Institute, University of California, Los Angeles, CA, USA
email: rmonti@oeb.harvard.edu

INTRODUCTION

During *in vivo* movements, the force output of skeletal muscle is regulated by the recruitment of varying numbers of motor units. Thus, the number and spatial distribution of active muscle fibers within a muscle varies throughout a movement as the functional demands placed on the muscle changes. In contrast, most *in situ* studies of the mechanical properties of the muscle-tendon unit vary muscle length or stimulation pattern to alter force. Thus, these studies describe the behavior of the muscle by varying the force output of a constant number of muscle fibers. In addition, when using length to vary muscle force it is not possible to separate the effects of each of these factors on the observed properties of the system.

In this experiment, we used ventral root stimulation to vary the force output of the rat soleus muscle, allowing force and length to be varied independently. Under these conditions we measured the stiffness of the distal aponeurosis at recruitment levels ranging from 10-100% and at five different muscle lengths.

METHODS

Small (<100 μm diameter) tungsten particles were implanted immediately deep to the distal aponeurosis of the rat soleus. These particles were visualized using an x-ray video microscope (Figure 1).

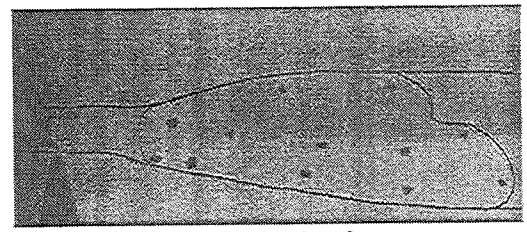

Figure 1. A captured video frame showing the appearance of the implanted tungsten particles in the rat soleus. The approximate outline of the muscle, apneurosis, and tendon are overlayed on the image.

The ventral roots contributing to the innervation of the soleus were isolated and split into three rootlets. All possible combinations of ventral roots were stimulated to provide seven different repeatable recruitment levels. The muscle was attached to an ergometer via a metal wire passed through the calcaneus. Maximal isometric tetanic contractions were elicited

* Present address for RJM:
Concord Field Station, Harvard University, Bedford, MA, USA

for each recruitment level, and muscle-tendon-unit length was varied from 2 mm above to 2 mm below L_o. Strain in the aponeurosis and tendon were measured as the change in spacing of the implanted particles during a contraction at each recruitment level. Strain was defined as the change in spacing of the particles during a contraction relative to the passive muscle at 2 mm below optimum length.

RESULTS AND DISCUSSION

Force-strain relationships were constructed using the seven tetanic contraction conditions at each length (Figure 2). The relationship is linear across all recruitment levels used. In addition, there is no effect of muscle-tendon unit length on the strain observed at each recruitment level. These results indicate that under *in vivo*-like conditions, the stiffness of the connective tissue in series with muscle fibers in the rat soleus is functionally constant. The presence of a linear force-strain relationship contrasts with reports for other muscles indicating that the tendon and aponeurosis act exclusively in the non-linear region of their force-strain relationship at loads typically encountered *in vivo* (Lieber *et al.*, 1991; Scott and Loeb, 1995). This difference may be a result of the inherent differences in the musculotendinous system studied or the *in vivo*-like recruitment methods used in the present study to load the aponeurosis. In either case, these results emphasize the importance of understanding of the *in vivo* mechanical properties of the muscle-tendon unit before interpreting its function.

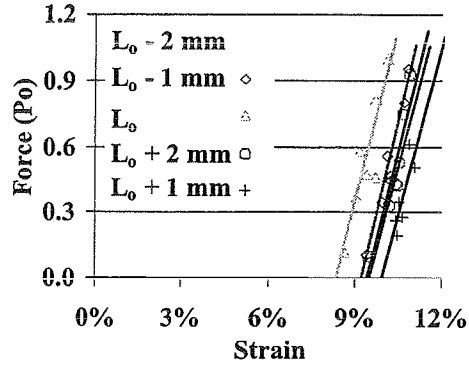

Figure 2. Force-strain relationships for one set of markers in the distal aponeurosis of the rat soleus at seven recruitment levels across five muscle lengths. The relationship is linear across all recruitment levels used, and there is no effect of muscle length on this relationship.

REFERENCES

Lieber, R. L., Leonard, M. E., Brown, C. G. and Trestik, C. L. (1991). *American Journal of Physiology,* **261**, C86-C92.

Scott, S. H. and Loeb, G. E. (1995). *Journal of Morphology,* **224**, 73-86.

ACKNOWLEDGMENTS

We thank Jim Weiss and David Mih of NASA's Jet Propulsion Laboratory for providing access to the x-ray video system.

SUBMAXIMAL STIMULATION AND HISTORY-DEPENDENT PROPERTIES EXPLAIN HOW SIMILAR MUSCLES CAN FUNCTION DIFFERENTLY

Anna N. Ahn

Dept. of Integrative Biology, Univ. of California, Berkeley, CA USA
Present address: Concord Field Station, Harvard University, Bedford, MA USA
E-mail: aahn@oeb.harvard.edu

INTRODUCTION

Even when experiencing identical strain and stimulation, two hindlimb muscles of the cockroach, *Blaberus discoidalis*, function differently under dynamic, *in situ* conditions (Fig. 1). Muscles 178 and 179 are two of six coxa-femur extensors that are innervated by the same, single excitatory motor neuron, extend a single degree-of-freedom joint, and have similar twitch kinetics and similar force-length and force-velocity properties when maximally stimulated (Ahn and Full, in prep). The muscles do not operate as antagonists negating each other's functions, but rather generate force at different phases of the contraction cycle (Fig. 1).

In vivo neural activation and muscle strain patterns in animals often differ from those conditions imposed during traditional *in vitro* studies of maximally stimulated muscle. In the present study, I test the hypotheses that extensor 178 force is greater under *in vivo* stimulation conditions than force generated by extensor 179; and secondly, that the two muscles exhibit different history-dependent properties, such as force enhancement due to passive stretch (Mutungi and Ranatunga, 1999). These infrequently examined properties may contribute to the differing mechanical functions of muscles 178 and 179 when strained and stimulated identically (Fig. 1).

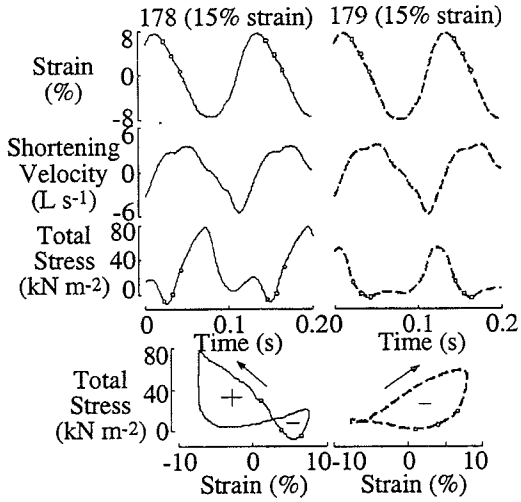

Fig. 1. Strain, shortening velocity, and force when muscles 178 and 179 operated under identical strain and stimulation conditions. The shaded area represents the shortening phase of the oscillatory cycle. The yellow squares represent spikes of stimulation. The arrows indicate the directions of the loops.

METHODS

A servo motor (Cambridge Technologies) was used to measure muscle force while controlling muscle length. The muscle was stimulated (Grass stimulator) through the

motor neuron using a suction electrode. Isometric contractions were elicited with trains of current pulses that served as the stimulation pattern. The *in vivo* stimulation pattern during preferred speed consists of a burst of 3 stimuli at 100 Hz (3s; Full et al., 1998).

RESULTS AND DISCUSSION

In submaximally stimulated muscle, the force at resting length was 82% and 72% of the maximum, normalized force in muscles 178 and 179, respectively (Fig. 2). As muscle length decreased, the difference in force generation between the muscles increased. For example, at -10% strain, muscle 178 generated twice the force generated by muscle 179 (Fig. 2).

Differences between the two muscles in their submaximal force-length relationships (Fig. 2) and in force enhancement after a passive stretch (shown for muscle 178 in Fig. 3) accounted for as much as 85% of the difference in peak force generated between the two muscles during oscillatory contractions. Using *in vivo* conditions and examining the history-dependent properties of these muscles provide clues to how the muscles function differently under identical cyclical conditions. In the insect leg system, simple neural control can result in functional diversity in seemingly synergistic muscles due to differences in contractile properties under *in vivo* conditions.

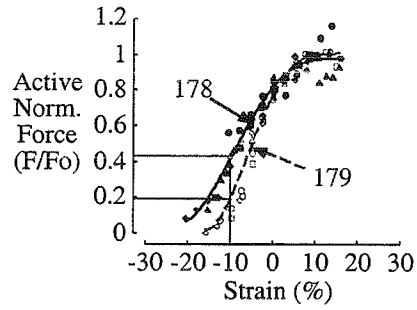

Fig. 2. Force-length relationship using the stimulation pattern during running (3s) comparing muscles 178 and 179.

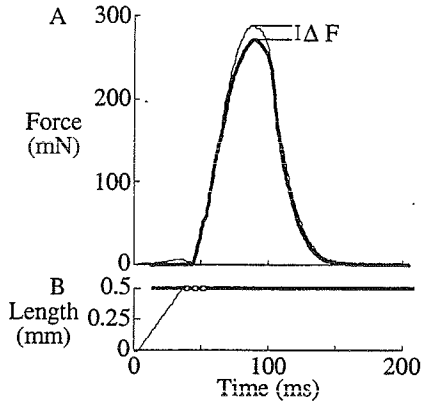

Fig. 3. Force enhancement in muscle 178. The thick and think lines are the forces generated by 178 during an isometric contraction vs. when stretched just prior to an isometric contraction, respectively. Force enhancement (ΔF) for this trial is 6%.

REFERENCES

Ahn, A. N. and Full, R.J. (in prep).

Full, R. J., et al. (1998). *J. exp. Biol.* **201**, 997-1012.

Mutungi, G. and Ranatunga, K. W. (1999). *J. Physiol.* **518P**, 88P-89P.

INFLUENCE OF MYOSIN ISOFORMS ON FORCE-VELOCITY PROPERTIES OF INTACT SINGLE FIBERS AND POWER PRODUCTION DURING JUMPING

Gordon Lutz, Shannon Bremner, Sarah Shappard-Palmer, Dustin Robinson, Shashank Sirsi and Richard Lieber

University of California San Diego and Veterans Medical Research Foundation, 3350 La Jolla Village Dr., San Diego, CA 92161
Email: glutz@ucsd.edu

INTRODUCTION

Intact frog single muscle fibers are favored for analysis of contractile kinetics but the definition of myosin heavy chain (MHC) and myosin light chain (MLC) isoforms in frog muscle has been lacking. We recently showed that the four major fiber types in *Rana pipiens* (type 1, type 2, type 3 and tonic) contain four unique MHC isoforms (for review see Lutz and Lieber, 2000). We have also identified the MLC isoforms in these fiber types (Lutz et al., unpublished).

The purpose of this study was to use intact single fibers from *Rana pipiens* to determine the influence of MHC and MLC isoforms on force-velocity and power-velocity properties and on mechanical power production during jumping.

METHODS

All experiments were performed on intact single fibers from the anterior tibialis muscle of adult *Rana pipiens* (n =13 fibers). All fibers contained type 1, type 2 or both type 1 and type 2 MHCs.

Mechanical recordings

A mechanical recording system was developed to measure simultaneously the length transients of ~1 mm segments along the full length of intact single fibers during contractions. Force-velocity (F-V) curves were generated using a series of step-ramp contractions. Cross-sectional area (CSA) of each segment was determined from diameters in two orthogonal views. Segment F-V data were averaged to provide fiber F-V data. All data are reported for fiber averages unless otherwise stated.

Some fibers (n = 8) were also driven through the length change and stimulus conditions that occur in extensor muscle fibers during maximal jumps (Lutz and Rome, 1994) and the resulting force and power production were measured.

MHC and MLC isoforms

After the mechanical experiments, fibers were freeze-dried and cut into the same segments from which mechanical data were obtained. MHC and MLC isoform content were measured in each segment using SDS-PAGE. MHC values are expressed as percentage of type 1 MHC (%MHC1) and MLC data as the molar ratio of MLC3/MLC1.

RESULTS AND DISCUSSION

F-V curves were measured in individual segments along the length of fibers and related to MHC and MLC isoform content (n = 66 segments from 13 fibers). Segments made up about 84% of the fiber length.

Fiber maximal shortening velocity (V_{max}) increased with %MHC1 ($p < 0.01$) but was not correlated with MLC3/MLC1 ($p = 0.13$). Velocity at half maximal isometric tension (V_{P50}) also increased with %MHC1 ($p < 0.0001$) but not MLC3/MLC1 ($p=0.07$). Among fibers with nearly all type 1 MHC (i.e., %MHC1>85%; $n = 6$) MLC3/MLC1 ratio did not influence V_{max} or V_{P50}. Maximal specific tension (P_o) and maximal mechanical power ($power_{max}$) both increased significantly with %MHC1 ($p<0.01$).

Mechanical power during contractions that simulate maximal jumps increased markedly with %MHC1. Type 1 fibers generated almost 2-fold greater power than type 2 fibers under these in vivo conditions.

Significant variability in V_{max} , P_o and $power_{max}$ was observed between segments of individual fibers. Variability in V_{max} between segments much larger than could be explained by differences in %MHC1.

SUMMARY

A significant positive correlation was found between %MHC1 (the fastest frog MHC) and V_{max}, V_{P50}, P_o, $power_{max}$ and power during jumping. Unexpectedly, no significant correlation was found between MLC3/MLC1 ratio and V_{max} or V_{P50}. These data suggest that the frog myosin heavy chain, and not the light chain influences F-V properties and mechanical power production in fast twitch fibers.

REFERENCES

Lutz, G.J. and R. L. Lieber. (2000) *Microscopy Research and Technique*. 50: 443-457.
Lutz, G. J. and L. C. Rome. (1994) *Science*. 263, 370-372.

ACKNOWLEDGEMENTS

Supported by NIH grants AR40050, AR45631 and AR46469 and a grant from the Department of Veterans Affairs.

- PARALLEL SESSION -

Orthopaedic Biomechanics

Friday, August 10, 2001
1100 to 1230

FAILURE MECHANISMS OF CONSTRAINED LINERS AND BI-POLAR THA DESIGN

[2] Mark E. Nadzadi, [1] Anneliese D. Heiner, [1,2] John J. Callaghan, and [1,2] Thomas D. Brown

Depts. of [1]Orthopaedic Surgery and [2]Biomedical Engineering, University of Iowa, Iowa City, IA
E-mail: tom-brown@uiowa.edu

INTRODUCTION

Dislocation incidence in total hip arthroplasty is typically between 2 and 11% in primary cases, and roughly double that for revision cases. Dislocation resistance of a construct can be characterized in terms of its range of motion (ROM) and peak resisting moment (PRM). For recurrent dislocations, replacement of the primary acetabular liner with a constrained liner (Figure 1), or complete exchange to a bi-polar system, is often performed as a last resort. These specialized designs are intended to increase PRM or ROM, respectively. Unfortunetly, bone quality is often poor in these patients, creating concern about the bone-prosthesis interface strength. Hence, the failure strength at the liner-shell and at the femoral head-liner interfaces in these specialty devices needs to be optimized, rather than maximized. The failure mechanics of several current variants of these devices are here reported, using a laboratory testing apparatus to create a reproducible impingement-subluxation-dislocation event.

METHODS

An MTS Bionx 858 (MTS Systems Corp., Eden Prairie, MN) was used with TestWare SX software, collecting data at 100Hz. A digital video camera recorded the failure event. The testing fixture (Figure 2) mounted the femoral component on the MTS actuator, with linear bearings providing free medial-lateral motion. The cups were potted in PMMA such that the cradle's rotation axis aligned with the cup center of the liner, and the cradle was attached to a load cell.

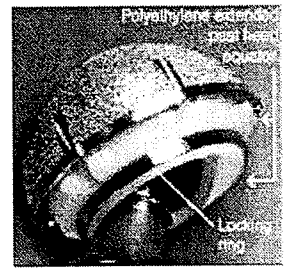

Figure 1: Typical constrained liner. Note extra liner height and locking ring.

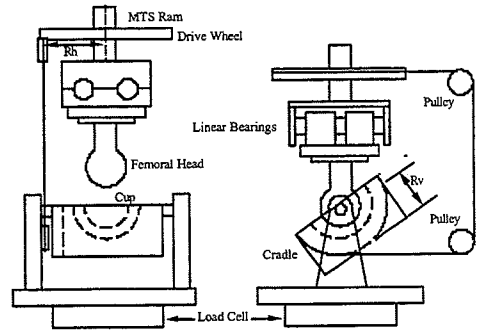

Figure 2: Testing fixture (L) left view prior to start; (R) front view during test.

The femoral component was axially loaded to 200N, and rotation of the cradle was imposed under angular control of the actuator. This imposed planar rotation resulted in an impingement and then failure of the implant, at either the liner-shell interface or at the head-liner interface. The load cell recordings and angular displacement of the drive wheel were converted into the resisting moment about the cup center and angular displacement of the cup. The spatial mean shear stress between the PMMA and liner was calculated from PRM.

Five different implants* were tested to failure. Four key outcome measures were

recorded: the cradle angle at impingement (CA-IMP), the peak resisting moment (PRM), the cradle angle at peak resistance (CA-PRM), and the cradle angle at device failure (CA-FAIL). For the four constrained liner series, each outcome measure was analyzed using one-way ANOVA and Duncan's multiple range tests, significant difference being at a=0.05.

RESULTS AND DISCUSSION

Both 28mm head series (E-28 and UR-28) generated readily visible deformation of the liner at the impingement site, and failed via "squeeze-out" at the head-liner interface, with a frank dislocation. The egress of the head created no visible deformation of the liner. The 32mm series (E-32 and UR-32) failed at the liner-shell interface, via rupture of the locking mechanism. The 32mm systems exhibited liner deformation patterns similar to the 28mm, although not as pronounced in magnitude. For both sizes, the PRM was around 20 times that of both the bi-polar (Bi) system and conventioanl (CONV) unconstrained liners. However, all four constrained liner configurations impinged around 20 degrees earlier than did the bi-polar system. The bi-polar system provided slightly more impingement-free motion than the traditional liner.

With poor bone quality, it is of salient importance to not damage the bone-prosthesis interface. Interfacial shear strength between bone and prosthesis is typically between 5 and 17 MPa, considering varying degrees of bone quality and amount of ingrowth due to porosity and other design variants (Engh, 1985). In this series, all calculated values of required average shear at the instant of device failure at the bone interface were below 0.5 MPa. This lends support to using constrained liners for recurrent dislocation patients, even those with poor bone quality, due to the corresponding fixation interface stresses being an order of magnitude below fixation interface strength. A key question that remains to be answered by clinical experience is which design approach results in a lower dislocation incidence: one with large impingement-free ROM but low PRM, or one with a high PRM at the tradeoff of reduced impingement-free ROM?

*__Series E:__ Endurance Stem, 28 & 32mm Articul/eze Head, S-ROM Constrained Liner, S-ROM ZTT 54mm Shell; DePuy (n=3) __Series UR:__ UNI-ROM Stem, 28 & 32mm S-ROM Head, S-ROM Constrained Liner, S-ROM ZTT 52mm Shell; DePuy (n=8) __Series Bi:__ Endurance Stem, Self-Centering 39/28/1 Head, Duraloc 100 54mm Shell; DePuy (n=12)

REFERENCES

Engh, C.A., Bobyn, J.D. (1985). *Biological Fixation in Total Hip Arthroplasty.* Thorofare, NJ, SLACK.

Scifert, C.F. et al. (1999). *Computer Methods in Biomechanics and Biomedical Engineering*, **2**, 139-147.

ACKNOWLEDGEMENT

Financial support provided by DePuy, Inc.

Table 1: Series mean ± standard deviation for each outcome measure, as well as point-of-reference data (Scifert, 1999) for a conventional (CONV) liner (Duraloc).

Series	CA-IMP (°)	NSD
UR-32	42.7 ± 0.3	
UR-28	43.4 ± 0.5	
E-28	45.6 ± 0.3	
E-32	47.2 ± 0.3	
CONV	60	
BI	65.7 ± 0.4	

Series	CA-PRM (°)	NSD
CONV	62	
UR-32	62.2 ± 0.5	
E-28	65.4 ± 0.4	A
UR-28	66.0 ± 0.9	A B
E-32	66.6 ± 0.6	B
BI	70.2 ± 0.6	

Series	PRM (N-m)	NSD
CONV	1.7	
BI	1.9 ± 0.1	
E-28	31.7 ± 0.6	
UR-28	35.9 ± 0.8	
UR-32	40.8 ± 0.7	
E-32	41.9 ± 0.5	

Series	CA-FAIL (°)	NSD
UR-32	62.7 ± 0.5	
E-32	67.1 ± 0.6	
CONV	70	
E-28	70.8 ± 0.8	C
UR-28	71.7 ± 0.8	C
BI	76.6 ± 0.7	

Interface Shear (MPa)	
BI	0.02
CONV	0.02
E-28	0.33
UR-28	0.41
E-32	0.43
UR-32	0.47

INFLUENCE OF ACETABULAR LOCKING MECHANISM ON MICROMOTION

Ryan Collins[1] Joan Bechtold[2] Craig Bourgeault[2]
[1] Department of Biomedical Engineering, University of Minnesota, Minneapolis, MN
[2] Orthopaedic Biomechanics Laboratory, Hennepin County Medical Center, Minneapolis, MN
Email: rcollins@rushu.rush.edu

INTRODUCTION

The production of wear debris from the polyethylene liner of total hip arthroplasty has been well documented. The majority of research has focused on debris from the primary articulating surface between the polyethylene liner and the femoral head classified as Mode-1 wear. However, it has been noted that the movement of the backside articulating surface between the polyethylene liner and the metal shell (Mode-4 wear) also contributes particulate debris (Guttman et al., (1994), Manley et al., (1994)).

The purpose of this study was to measure the backside micromotion associated with different numbers of locking splines in the acetabular component of a total hip arthroplasty. Our hypothesis was that a greater number of splines would reduce the motion measured between the polyethylene liner and the metal acetabular shell.

METHODS

The locking mechanism investigated was the Smith & Nephew Richards, Inc. (Memphis, TN) MicroStable® Reflection acetabular system. The passive mechanism is an interference fit of matching scalloped rims, or dove-tailed splines, between the rim of the titanium metal shell and the polyethylene liner. The number of dove-tail splines on the metal shell was varied among three groups (Fig. 1) tested that contained either the normal configuration with 0% splines removed (Group A), 30% of the splines removed (Group B), or 50% of the splines removed (Group C). A total of nine standard Reflection polyethylene liners were used to test each of the three groups (three liners per metal shell).

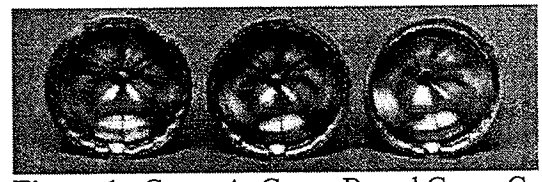

Figure 1: Group A, Group B, and Group C.

The acetabular cups were subjected to 8 million testing cycles using an EnduraTEC (Eden Prarie, MN) servo pneumatic testing machine. An axial load of 200-3000 N was delivered in phase with a ±2.5 N-m torsional load at 10 Hz. The components were tested in a 37°C water bath (Fig. 2).

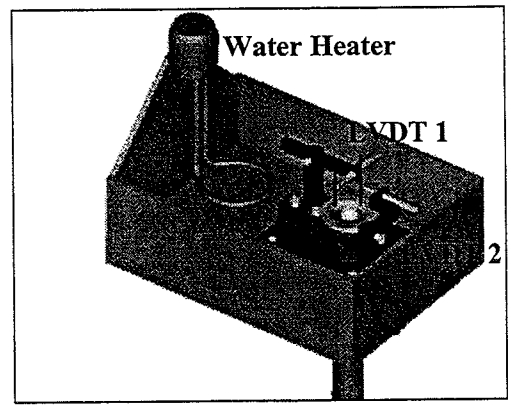

Figure 2: Schematic of LVDT placement.

The movement between the polyethylene liner and metal shell was measured using two linear variable differential transducers (LVDTs), located 90° from each other. Holes were drilled in the polyethlene liner

and stainless steel pins were placed perpendicular to the liner at a constant radius from the center. The liners were gold coated before testing to observe the wear by visual and scanning electron microscopy (SEM) analysis.

One-way analysis of variance was performed to compare the motion between the three groups and a Student-Newman Keuls method for pairwise multiple comparison procedure ($p<0.05$) was performed at every 500,000 cycles.

RESULTS

The only significant difference in the measured motion between Group A and Group C was at 3 million cycles. There were multiple significant differences seen in the displacements between Group B vs. Group A and Group B vs. Group C from 4.5 million to 6 million cycles.

There was no visual evidence of burnishing, scratching, abrasions, or pitting on the backside surface of the polyethylene liners. When viewed with SEM, all of the liners showed some pitting and marking of the polyethylene surface but no areas of burnishing or polishing that would be evidence of gross wear.

DISCUSSION

In the first million cycles, we observed random increases and decreases in the motion measured by LVDT 1 and LVDT 2 (Fig. 3). This period was noted by Manley et al. (1994) as the "running in period" in which the polyethylene liner displays creep deformation. This was observed in all the groups in the first million cycles. After the running in period ended, there were little changes in the overall measured motion in the next 7 million cycles. However, the amount of motion measured in Group B, Liner #2 could be considered an outlier as its motion decreased by 3-4 microns over the final 7 million cycles. This large decreasing trend is responsible for the significant differences in measured motion observed between Group B vs. Group A and Group B vs. Group C.

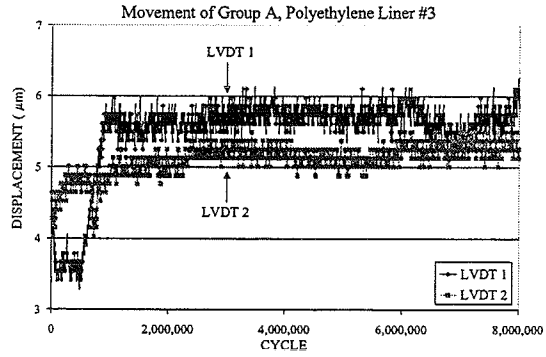

Figure 3: Example of typical motion data.

SUMMARY

This study showed that the current MicroStable® acetabular locking mechanism (Group A) creates a stable acetabular locking system. Furthermore, since the largest motion measured between the polyethylene liner and the metal shell was less than 8 microns for all the groups tested, it could be possible to use fewer locking splines.

REFERENCES

Fehring T.K., et al. (1999). *Clin Orthop*, 367: 306-314.

Guttmann D., et al. (1994). *40th ORS*, 178.

Manley M.T., Serekian P. (1994). *Clin Orthop*, 298: 137-146.

EVALUATION OF SYNTHETIC COMPOSITE FEMUR BONES FOR USE IN HIP PROSTHESES STUDIES: A PHOTOELASTIC STUDY

Randal P. Morris, Michael J. Grecula, William L. Buford, Jr., Rita M. Patterson

Department of Orthopaedic Surgery and Rehabilitation, The University of Texas Medical Branch, Galveston, TX
E-mail: rmorris@utmb.edu Web: www.utmb.edu/ortho/

INTRODUCTION

Recent studies in biomechanics have seen the increasing use of synthetic composite bones as an alternative to human cadaver specimens. Composite bones are a desirable alternative to cadaver specimens which can be difficult to obtain and maintain, have great inter-specimen variability, and are usually expensive. Pacific Research Labs, Inc. (Vashon, WA) released their second generation composite femur to the market over a decade ago, and its mechanical properties have been well documented in validation studies (Cristofolini, 1996) as well as comparison studies in hip arthroplasty (Otani, 1993), implant stability (Harman, 1995), and strain measurement (Grecula, 2000). The composite femurs are constructed of a glass fiber reinforced epoxy (cortical area) surrounding a core of polyurethane foam (trabecular area). The tensile and flexural strengths and moduli are consistent with human bone, and their geometry has been reported to be agreeable as well. The composite femurs have been found to fall within the range of cadaver specimens in axial and torsional loading tests, though some variability in deformation response and reduced stiffness values have been reported.

Early in the year 2000, Pacific Research Labs, Inc. introduced a third generation composite femur. The new designs are constructed of a combination of short glass fibers and epoxy resin, and offer a more anatomical cortical wall thickness and surface geometry, with uniform, repeatable properties throughout the length of the bone. Also new with this design is a medullary canal throughout the length of the bone. To the authors' knowledge, there has yet to be any comparative results reported using the third generation composites.

As part of a current photoelastic study to measure femoral surface strain differences after total hip arthroplasty, these new composites are to be included, as well as the second generation femurs and human cadaver specimens. As an inclusive subset of the broader study, the authors propose a comparison of the three femur types using traditional biomechanical analysis and photoelastic strain measurement (Figure 1).

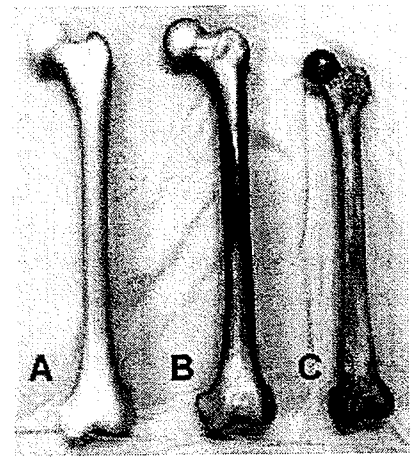

Figure 1. Second generation composite femur (A), third generation composite femur (B), and embalmed human femur (C).

MATERIALS AND METHODS

Four second generation composites, four third generation composites, and two embalmed cadaver femurs will be tested and compared under the same protocol. An MTS 858 Mini Bionix testing machine will provide an offset axial load to the head of the femurs, including an abductor load. The specimens will be loaded to approximate body weight and the resulting load deformation response will be analyzed to determine whole bone stiffness. The specimens will then be coated with a photoelastic coating, consistent with the techniques used in a previous study (Grecula, 2000). The photoelastic coating method can be applied to virtually any surface and is repeatable under varying load conditions. Full-field interpretation with a reflection polariscope allows the researcher to determine principal strain magnitudes and directions on the surface of the specimen. The protocol will employ a surface strain measurement technique that the authors have validated (Grecula, 2000) using digital imaging and computer analysis. Digital images of the bones (Figure 2) will be analyzed with computer methods to quantify differences in surface strain areas and principal strain distributions.

DISCUSSION

The previous study (Grecula, 2000) found that the second-generation composites were not significantly different in strain area measurements. The inter-specimen variability was not significant and the reproducibility of the composites and the photoelastic application were confirmed. Due to the differences in the newer composites to their predecessors, certain performance qualities can be expected. The use of the shorter glass fibers in epoxy may reflect improved stiffness values, more comparable to human bone. The presence of the medullary canal is expected to improve the deformation response and the overall strain distribution. If met, these qualities will be promising for the future use of these composites when evaluating the biomechanical differences between the many hip prostheses designs available.

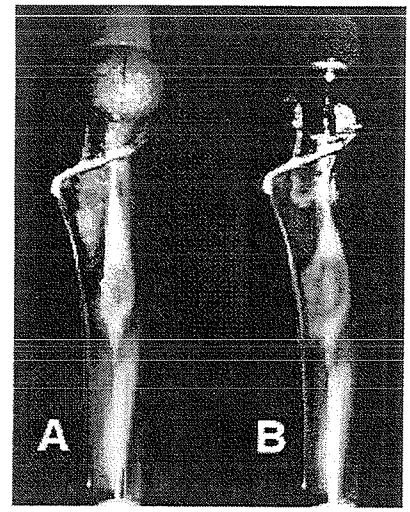

Figure 2. Photoelastic coated composite femurs (second generation) loaded to 2000N, illustrating the normal strain distribution (A) and the strain distribution after implanting a cementless prosthesis (B).

REFERENCES

Cristofolini, L., et al., (1996). *Journal of Biomechanics*, **29**, 525-35.

Otani, T., et al. (1993). *Journal of Arthroplasty*, **8(1)**, 67-74.

Harman, M. K., et al. (1995). *Medical Engineering and Physics*, **17(3)**, 163-171.

Grecula, M. J., et al. (2000). *IEEE Transactions on Biomedical Engineering*, **17(7)**, 926-933.

ACKNOWLEDGEMENTS

This work is supported by Zimmer, Inc.

THE INFLUENCE OF DONOR FACTORS ON THE MECHANICAL PROPERTIES OF PRE-SHAPED BONE-PATELLAR TENDON-BONE ALLOGRAFTS

John R Bianchi, PhD, Matthew Summitt, BS, Gina Scurti BS,
Kevin Carter, Rebecca Marshall BS, James E Keesling Jr, MS

Engineering Research Department, Regeneration Technologies, Inc., Alachua, FL
E-mail: jbianchi@rtitechnology.com

INTRODUCTION

In 1963, Jones popularized an open reconstruction technique using the patellar tendon (Jones, 1963). Since then, ligament reconstruction has seen significant advances. The bone-patellar tendon-bone (BTB) graft has become the most commonly implanted graft for several reasons - ease of graft fixation using interference screws, accessibility of the patellar tendon for autograft recovery, and strength of the patellar tendon (Clancy, 1982; Kurosaka, 1987; Noyes, 1984).

Regeneration Technologies, Inc. has recently introduced a patellar tendon allograft that is pre-shaped to precise dimensions. This graft contains cylindrical bone plugs and pre-drilled suture holes that were designed to maximize biomechanical properties by optimizing the bone block geometry and its contact in the tunnel. The success of anterior cruciate ligament (ACL) reconstruction can hinge on many factors including the biomechanical properties of the graft. It is commonly reported in the literature that for most activities, the reconstructed (ACL) must withstand at least a 454N load (Noyes, 1984). The purpose of this study was to determine the effects of donor age and method of preservation on pre-shaped allograft BTB strength.

METHODS

All pre-shaped BTBs consisted of 2 pre-sized bone plugs, one from the proximal tibia and the other from the patella. Each bone block was 10mm in diameter, 25–30 mm in length, and contained 2 drill holes to accommodate #5 braided suture. Each specimen was allowed to thaw to room temperature and then hydrated in saline prior to testing.

In this study, a total of 142 pre-shaped frozen allograft BTBs from 54 different donors 18-96 years of age, were tested. Table 1 shows the distribution of age and gender for the samples tested. In addition, a similar set of 21 rehydrated, freeze-dried, pre-shaped patellar tendons from 11 different donors, 24-62 years of age, were also tested.

Table 1: Age range and characteristics of the pre-shaped BTBs tested in this study.

Age Range	Total BTBs	Males	Females
<35 years	22	5	3
36-50	27	8	1
51-65	21	6	2
66-75	23	5	4
76-85	39	11	4
86+	10	4	1
Freeze-dried	21	9	2

Specimens were tested on an MTS Bionix 858 serohydraulic mechanical test apparatus using a custom collet system. The collet assembly was chosen to reproduce a clinically applicable "interference" fit. Each specimen was tested with a load cell calibrated to ± 2500N. Initially a pre-conditioning cycle was run between 10 and 250N in load control at a rate of 0.5 Hz for 5

cycles. The BTB was then tested to failure in displacement control at a rate of 50 mm/min. For each test, the maximum load and mode of failure was recorded. Stiffness of the allograft was calculated from the linear portion (between 10 and 250N) of the load displacement curve.

The types of failure were defined to be: (a) failure of the patellar bone by visual evidence of a cracked bone block, (b) failure of the tibial bone by visual evidence of a cracked bone block, (c) failure of the tendon (either tearing off the bone block or rupture between the bone blocks), or (e) slippage from the collet. The data was analyzed within each age interval by ANOVA and Newman-Keuls multiple comparison test. A significant difference was defined by $p<0.05$.

RESULTS AND DISCUSSION

Donors younger than 35 years were found to carry significantly higher load and have significantly higher stiffness than all the other age groups. No significant difference in stiffness was observed among the rest of the age groups. BTBs from donors 36-50 and 51-65 years had insignificant difference in load. BTBs from the three age groups older than 65 were identified to be similar but carried significantly less load than the younger age groups.

With the exception of one age group, most failures occurred in the tendon. In the 76-85 year old age group however, the failures were equally distributed between the patellar bone block, tibial bone block, and the tendon. Tendon failure appeared to initiate at the attachment of the bone block, the tendon was never observed to rupture between the bone blocks. There was no significant effect of freeze-drying and/or rehydration on the strength or stiffness.

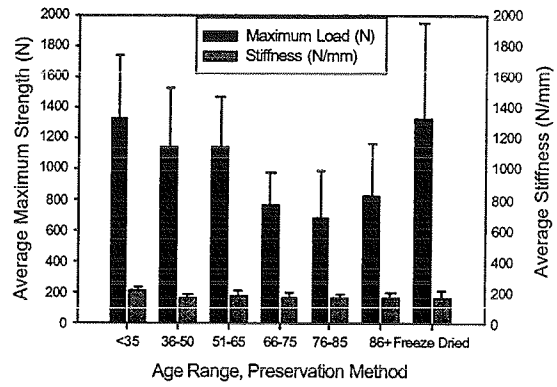

Figure 1: Average maximum strength (N) and Average Stiffness (N/mm) of the pre-shaped BTBs as a function of age and preservation method.

SUMMARY

The data indicates that freeze-drying and rehydration do not significantly reduce the tensile load of the BTB. Pre-shaped BTBs from donors younger than 35 years were found to carry significantly higher load than all other age groups, and BTBs in the age groups older than 65 carried significantly lower loads than the younger age groups. However, the 95% confidence interval for pre-shaped BTBs across all age ranges falls above the clinically recommended strength (450N) of ACL reconstruction materials.

REFERENCES

Jones K.G. (1963). *JBJS Am,* **45**, 925-932.

Clancy WG, et al. (1982). *JBJS Am,* **64**,352-359.

Kurosaka M, et al. (1987). *Am J Sports Med,* **15**, 225-229.

Noyes FR, et al. (1984). *JBJS Am,* **66**, 344-352.

CROSS-JOINT ARTICULATED EXTERNAL FIXATION OF THE KNEE: A MOTION RESISTANCE ANALYSIS

Mark B. Sommers[1], Kevin M. Kahn[2], J.L. Marsh[3], Michael Bottlang[1]

[1]Biomechanics Laboratory, Legacy Research & Technology Center, Portland, OR, USA
[2] Oregon Health Sciences University, Portland, OR, USA
[3]University of Iowa, Hospitals and Clinics, Iowa City, IA, USA
E-mail: mbottlan@lhs.org

INTRODUCTION

Severe injuries to the knee can be treated by rigid spanning external fixation. However, prolonged joint immobilization may produce degenerative effects on articular cartilage and connective tissue and is likely to contribute to post-traumatic osteoarthritis. Articulated fixation could maintain joint stability while allowing early controlled range of motion (ROM).

While it is commonly accepted, that the complex kinematics of active knee motion cannot be constrained to rotation around a fixed hinge, recent studies suggest that passive knee motion can be resolved into two distinct hinge rotations - predominant knee flexion, and axial rotation around the tibia [Hollister et al. (1993), Churchill et al. (1998), Iwaki et al. (2000)]. Thus, a hinged knee fixator may be applicable to replicate near-physiologic knee flexion in the unloaded knee over a limited ROM.

This biomedical cadaveric study investigates the applicability of articulated external knee fixation by determining the effects of constraining passive knee motion to a single flexion-extension axis. We specifically determined the attainable ROM for distinct fixator hinge positions.

METHODS

Nine fresh-frozen cadaveric leg specimens were sectioned 13 centimeters proximal and distal to the knee joint line. Specimens were dissected free of skin, subcutaneous, and muscle tissues, retaining only ligaments and the capsule. Each specimen was mounted on a rigid custom-built frame connected to a material test system (Instron 8874) in a way as to constrain knee motion about a fixed flexion-extension axis (Figure 1). Joint alignment was performed under lateral fluoroscopic guidance to ensure placement of the flexion extension (FE) axis to coincide with the centers of circles, fitted to the posterior femoral condyles, as described by Hollister et al. (1993). Knee flexion was induced by the linear actuator, acting on a wire rope, which was attached to a pulley. A unilateral load cell was used to measure the resulting flexion moment (M_F).

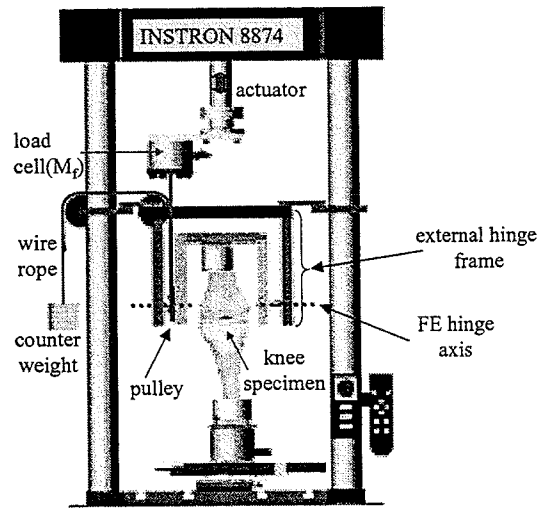

Figure 1: Experimental setup

Knee flexion and extension was induced at a constant angular velocity of 9°/s, starting at 60°, first toward extension and subsequently toward flexion. After application of "on-axis" knee motion, the fixed hinge was applied in 16 distinct orientational and translational off-axis positions (i.e., 5° and 10° varus, valgus, internal and external rotation; 5 mm and 10 mm anterior, posterior, proximal and distal translation). The range of motion, attainable within a moment envelope of ± 1 Nm was extracted from the moment versus knee flexion data. Statistical analysis was performed using a two-tailed, paired Student t-test.

RESULTS

The experimental setup was able to sensitively trace the motion resistance of the knee and to assess the effects of distinct knee kinematics constraints (Figure 2). The average ROM for unconstrained knees, for the 1 Nm moment envelope, was 121.7 ± 16.7°.

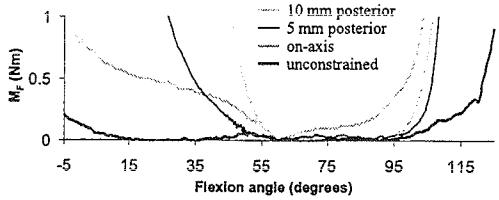

Figure 2: Flexion moment M_F corresponding to specific knee constraints.

Constraining the knee to rotation around an on-axis aligned hinge significantly reduced the average ROM by 30 % to 78.9 ± 32.6° (Figure 3). The 5 mm posterior translated position was the only axis alignment to demonstrate a larger average ROM (85.8 ± 17.2 °) than the on-axis hinge. However, this difference was not statistically significant and the resulting ROM was shifted toward terminal flexion. All other hinge alignments demonstrated a decreased average ROM as compared to the on-axis position. However, the ROM decrease for 10 mm posterior translation, 5°internal rotation, and 5°varus was not statistically significant. Off-axis rotations of 10° and translations of 10 mm decreased average ROM by up to 53% and 78%, respectively as compared to the on-axis aligned hinge.

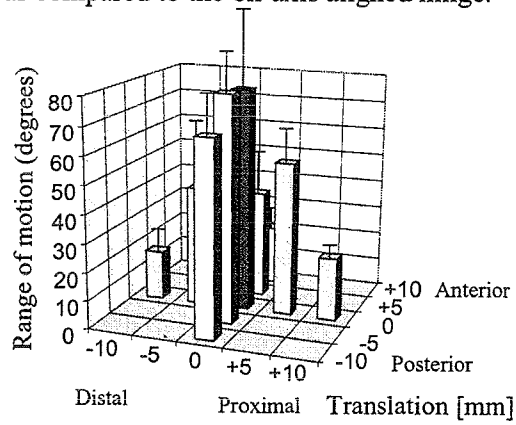

Figure 3: Axis translations - average ROM obtained within 1Nm moment envelope.

CONCLUSION

Confining the knee to rotation around a fixed hinge decreased the obtainable ROM within a given rotational moment envelope and increased motion resistance. Proper alignment of the hinge axis proved to be of critical importance to minimize "stiffening" of joint motion and to maximize the attainable ROM. Since knee mobility toward extension is of premier clinical relevance, hinge application along the FE axis reported by Hollister et al yielded the most favorable result.

REFERENCES

Hollister, A.M. et al. (1993). *Clin. Orthop.*, **290,** 259-268.

Churchill, D.L. et al. (1998). *Clin. Orthop.*, **356,** 111-118.

Iwaki, H. et al. (2000), *J Bone and Joint Surg.*, **82-B,** 1189-1195.

THREE DIMENSIONAL KINEMATICS AND KINETICS OF MENISCAL BEARING AND POSTERIOR CRUCIATE SUBSTITUTING TOTAL KNEE REPLACEMENTS

J. Hartford[1], T. Brindle[2], B. Segbarth[1], J. McCrory[2], J. Dobner[1] and R. Shapiro[2]
[1]Division of Orthopaedic Surgery, University of Kentucky, Lexington, KY, USA
[2]Biodynamics Laboratory, University of Kentucky, Lexington, KY 40506
E-mail: rshap01@pop.uky.edu Web: http://www.coe.uky.edu/biodynamics/

Introduction

Aberrant knee kinematics produced by total knee replacements may be a source for poor clinical performance and early prosthetic failure. Interest has developed in mobile bearing knee replacements due to the theoretical advantage of decreased polyethylene wear suggesting an increased life of the components. The purpose of this study is to compare the biomechanical data during gait and stair climbing for the meniscal bearing and posterior cruciate ligament (PCL) substituting total knee replacements in an aged matched group of patients and control subjects.

Materials and Methods

Ten subjects with a unilateral posterior cruciate substituting (IBII) total knee replacement (64 years), ten with a unilateral meniscal bearing (LCS) total knee replacement (PCL retaining) (70years), and ten aged-matched, healthy control subjects (69 years) were evaluated. Standard analytical techniques utilizing three dimensional motion analysis techniques synchronized with two Kistler force platforms were employed to collect biomechanical data. The patients were evaluated during ambulation along a twenty-one foot walkway and during ascending and descending a four-step stairway. All patients were a minimum of six months out from the operation and had a score of greater than 80 on the Knee Society rating system. All the subjects were male.

Results

Walking- Kinematics
Mean kinematic gait parameters of the hip, knee, and ankle were all within one standard deviation of the control group demonstrating the ability of both the meniscal bearing and the posterior stabilized total knee replacements to reproduce the gait kinematics of age-matched normal knees.

Walking -Kinetics:
Knee Flexion Moment: As shown in Figure 1 there was a decreased flexion (> 1 STD) moment during the initial landing phase for both IBII and LCS knee replacements as compared to the controls.

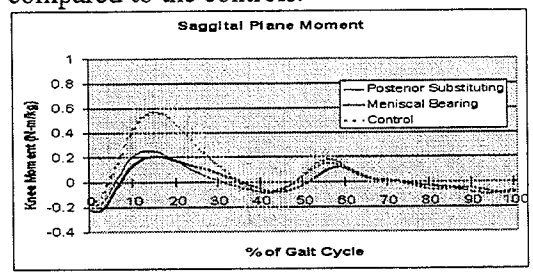

Figure 1. Saggital plane knee moments during walking normalized to body mass (control ±1 sd, + flexion, 0-60% stance).

Stair Ascent - Kinetics:
Knee Valgus Moment: An increased knee valgus moment (> 1 STD) was observed in the IBII knee compared to controls during weight acceptance. A decreased moment was observed in the LCS group.

Stair Descent -Kinematics
Knee flexion angle: Both LCS and IBII

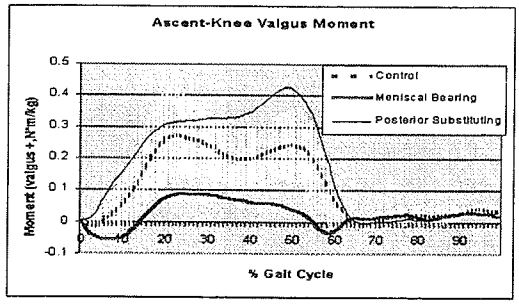

Figure 2. Frontal plane knee moments during stair ascent normalized to body mass (control ±1 sd).

knee replacements demonstrated a decreased flexion angle during swing phase of the stair descent as compared to the control group. LCS knees demonstrated earlier knee flexion compared to the IBII knees

Stair Descent - Kinetics

Knee Valgus Moment: IBII knees demonstrated a greater(>1SD) valgus moment compared to LCS knees during the weight acceptance phase of stair descent.

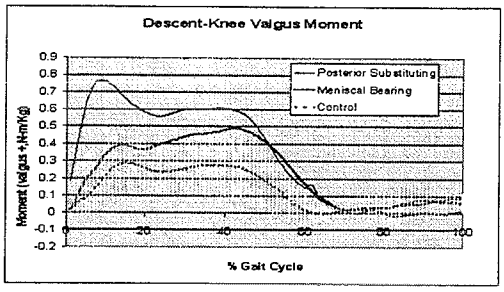

Figure 3. Frontal plane knee moments during stair descent normalized to body mass (control ±1 sd, 0%=initial contact).

Anterior-Posterior Knee Forces: Both LCS and IBII knee prostheses demonstrated anterior shear forces of the femur over the tibia during the weight acceptance phase of stair descent (> 1 STD) compared to the age-matched control group.

Knee Internal/External Moment: IBII knee replacements demonstrated a greater internal rotary moment throughout the stance phase of stair descent (> 1 STD). The LCS knee replacements demonstrated a similar rotatory moment pattern to the controls.

DISCUSSION

Kinematic data during ambulation demonstrated both knee designs employed accurately reproduced the kinematics observed in the normal knee while walking on level surfaces.

Kinematics during stair descent showed less knee flexion resulting in decreased toe clearance. The kinetics of the posterior cruciate substituting knee replacements during stair ascent and descent demonstrated a greater valgus moment during weight acceptance, which may compensate for a varus thrust. This suggests a decreased stability of the posterior cruciate substituting knee in the frontal plane during both stair ascent and descent over meniscal bearing total knee replacements and controls.

Anterior shear of the femur over the tibia also suggested decreased stability in the saggital plane of both meniscal bearing and posterior cruciate substituting knee replacements during stair descent compared to the age-matched controls.

Summary

Overall, both prostheses replicated normal kinematics during walking with diminished knee flexion observed during stair descent. An increased valgus moment associated with varus thrust was observed in the IBII group suggesting a possible compensation in this group. This pattern, however, was not observed during walking. Of concern may be the effect of increased moments at the knee as well as shear forces on the wear properties of the IBII knee.

- PARALLEL SESSION -

Symposium

Tendon

Saturday, August 11, 2001
0900 to 1030

BIOMECHANICS OF TENDON GLIDING

K. N. An, M. E. Zobitz, L. Berglund, C.F. Zhao, S. Uchiyama,
J. H. Coert, Y.L. Sun, T. Momose, P. C. Amadio
Biomechanics Laboratory, Department of Orthopedics
Mayo Clinic/Mayo Foundation, Rochester, MN 55905
E-mail: an.kai-nan@mayo.edu

INTRODUCTION: When tendon excursion occurs through a pulley, drag and friction are encountered at the interface. It has been hypothesized that the repetitive exposure to such friction and attrition could be detrimental. A system has been developed which enables us to measure the friction or drag resistance when tendon excursion takes place through pulley or bony tunnel. This presentation will report the biomechanics of tendon gliding and the factors affecting the gliding resistance.

METHODS: A tendon sliding through the pulley is analogous to a belt wrapped around a fixed mechanical pulley (Fig. 1). Assume that the total arc of contact between the belt and pulley is θ, $(\alpha + \beta)$, and the tensions in the belt on each side of the pulley are F_2 and F_1. If the impending motion of the cable is from F_1 to F_2, then F_2 is greater than F_1,

$$F_2 = F_1 e^{\mu\theta} \quad (1)$$

the frictional force

$$f = F_2 - F_1 = F_1 (e^{\mu\theta} - 1) \quad (2)$$

$$\text{Ln } F_2/F_1 = \mu\theta \quad (3)$$

where μ is a frictional coefficient.

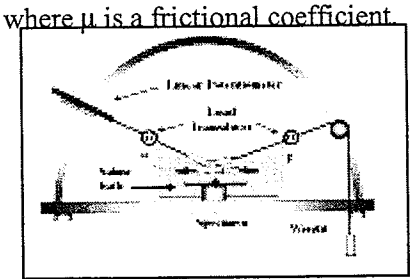

Figure 1 Device for measuring gliding resistance measurement between the tendon and pulley system.

The measurement system developed has been verified by comparing with that of theoretical derivation using the ideal Dacron and rod model.

FRICTION COEFFICIENT BETWEEN TENDON AND PULLEY: Nine normal index digits from nine fresh-frozen cadavers were used. Each specimen was prepared preserving the A2 fibrous pulley bony insertion but eliminating all bony contact with the FDP tendon. The specimen was mounted on the testing device. Continual irrigation with saline solution was performed to keep the specimen moist. The frictional coefficient, μ, of the specimen was obtained based on equation (3). The friction coefficients has been found to be 0.027±0.014 for flexion (R^2=0.85) and 0.075±0.017 (R^2=0.95) for extension. The relationship of tendon-pulley friction and angle was almost identical to the theoretical model. This measured frictional coefficient of the A2 tendon-pulley surfaces was somewhat greater than that of cartilage in a diarthrodial joint.

EFFECT OF HYALURONIDASE TREATMENT: To better understand the precise lubrication mechanisms at the tendon-pulley interface, the hypothesis that hyaluronidase-sensitive lubrication exists between the tendon and the pulley was evaluated. Fresh-frozen digits from 21 donors were used. The specimens were randomly divided into two groups. In group 1 the first test was performed immediately after dissection. Then, the surface of the FDP tendon was washed thoroughly using

saline solution and retested. After the second test the tendon was again taken out of the pulley and treated with 400U/ml hyaluronidase at room temperature for two hours, after which, the third test was performed. In group 2 the test sequence was the normal tendon, followed by the hyaluronidase treated tendon, and then the tendon washed with saline. In both groups, the resistance increased only after the hyaluronidase treatment.

EXTRASYNOVIAL AND INTRASYNOVIAL TENDON:
Extrasynovial tendon had comonly been used as tendon graft for reconstruction of intrasynovial tendon. Gliding ability of the flexor digitorum profundus tendon (FDP) and the palmaris longus (PL) tendon through the A2 pulley was compared. Fourteen digits and the ipsilateral palmaris longus tendons from fourteen donors were used. The gliding resistance of the PL was significantly greater than that of the FDP. Gliding resistance of the FDP tendon changed less with increasing tendon tension than did that of the PL tendon. The PL tendon is an extrasynovial tendon and thus does not have a synovial membrane. Instead, it has a paratenon of loose connective tissue.

SURFACE MODIFICATION BY HA:
Further investigation was performed to improve the gliding surface using hyaluronic acid (HA). Chemically binding of hyaluronic acid (HA) to extrasynovial tendon was considered. In this study, canine peroneus longus (PL) tendons were immersed into one of three different solutions (saline, 1% HA, 1% chemically modified HA) for 2 hours. The gliding resistance of treated PL tendons was measured at 1, 5, 10, 20, 50, and 100 cycles in a saline bath. After treatment with unmodified HA and chemically modified HA, the gliding resistance of the PL tendons decreased significantly compared to the saline treated tendons ($p<0.05$), and this effect of the two HA treatments persisted through 10 cycles. (Fig. 2). For cycles 20-100, the gliding resistance of PL tendons treated with chemically modified HA remained significantly lower than that of tendons treated either with saline or unmodified HA.

Figure 2 Gliding resistance of peroneus longus tendon with paratenon after

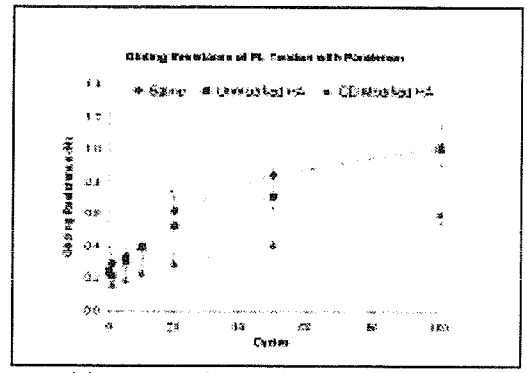

repetitive excursion. After treatment with unmodified HA or chemically modified HA, the gliding resistance decreased significantly compared to the saline treated tendons.

SUMMARY: The knowledge of tendon gliding biomechanics would provide better understanding of the potential etiology and the development of treatment modalities of tendon disorders associated with repetitive loading. Techniques and material used for tendon repair will all affect the gliding resistance and thus the outcome of tendon surgery. Improving of tendon gliding surface using chemical treatment or genetic therapy is the potential consideration for future investigation.

ACKNOWLEDGEMENT: This study is funded by NIH grant AR44391.

PREDICTING EXPOSURE OF FINGER FLEXOR MUSCLES AND TENDONS TO DYNAMIC LOADS DURING FINGER TAPPING

Dennerlein JT, Zhou Y, and Becker TE

Department of Environmental Health, Harvard School of Public Health, Boston,MA, USA
e-mail: jax@hsph.harvard.edu, http://www.hsph.harvard.edu/ergonomics

INTRODUCTION:

Exposure to different key switch designs within a computer keyboard has been associated with different levels of Carpal Tunnel Syndrome symptoms (Rempel et al., 1999). However, knowledge of the associated forces within the tendons that traverse the carpal tunnel remains limited. Biomechanical models predicting exposure often assume quasi-static equilibrium and neglect the dynamics of the finger mass (Buchner, 1988). Our goal was to use a lumped parameter dynamic model of the finger, predicting effective values for tendon forces during finger tapping to evaluate different motor control conditions.

METHODS

Ten healthy people (5 f, 5 m, 25-36 yrs) participated in the study, which was approved by the IRB Committee. Participants tapped repeatedly on a flat plate with their right index finger while the fingertip contact force and movement were measured simultaneously. A single-camera motion analysis system tracked the vertical position an infrared LED glued to the fingernail (Resolution = 0.040 mm). A strain gauge based force sensor mounted beneath the flat plate measured the fingertip force (rms noise = 3mN).

The finger was modeled as a linear second order mass-dashpot system (Hajian et al., 1997). The parameters for the dynamic model were only calculated for the first 40 ms of fingertip contact and therefore the effective muscle force was assumed to be proportion to time after the initiation of the fingertip contact with an initial level of force. Simple least squares regression techniques estimated the parameters for the model for each tap.

Four different tapping conditions tested the model robustness across motor control conditions. First, the hand and finger during the tapping task were relaxed with all five digits extended and in a natural orientation. Second, subjects curled digits three, four and five under the palm and squeezed with a moderate to high amount of effort creating a co-contraction. Third, subjects repeated the relax condition, but with an increased downward velocity of the fingertip prior to impact. Fourth, the co-contraction task was also repeated with an increased fingertip velocity. Subjects were instructed to minimize the contact time with the force sensor. Data were collected on a PC at 10kHz for thirty taps. Parameters were averaged across taps and each subject and then averaged across the subjects within each condition.

RESULTS and DISCUSSION

Most of the dynamic activity occured within the first 10 milliseconds with the inertia (acceleration) and damping (velocity) forces quickly approaching zero (Fig. 1). The effective muscle force contributes most of the force thereafter. The mass and damper parameters varied little over the four conditions tested and are consistent with Hajian et al. (1997). The effective muscle force, however, did vary considerably over the four conditions (Table 1). The rate of change in force increased significantly during the co-contraction of other hand muscles through the making of a partial fist. The initial muscle force increased with the speed of the tap down-stroke suggesting extra muscle effort was used to accelerate the finger during the faster taps.

The model had relatively small errors with root mean square errors (RMSE) of 0.3 N and the variance of the measured force accounted for (VAF) averaged 93%. A large portion of the error occured during the impact phase of the force trajectory. The inertia force diminished before the impact force began to decrease. This error was attributed to by the energy absorption of the interphalangeal (IP) joints increasing the duration of the impact. Measuring the IP joint angles during a keystroke would educe such a mechanism.

The results suggest that the lumped parameter model can be used to examine differences of effective muscle loads between motor control scenarios. The limitations of the model require future work investigating the specific IP kinematics during the impact phase of the key strike.

ACKNOWLEDGEMENTS: Whitaker Bioengineering Foundation

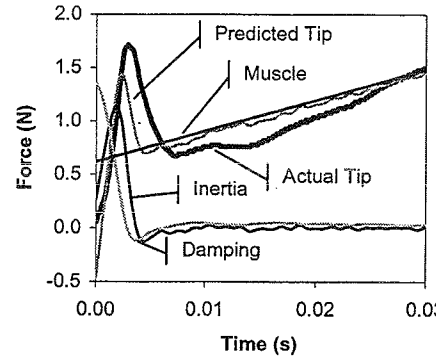

Fig. 1: Tip and model predicted force trajectories for a typical tap

REFERENCES:

Buchner et al. *J. Biomh* 1988; **21**(6): 459-68.

Hajian et al. *J Biomh-Eng* 1997; 119(1):109-14.

Rempel et al. *JOEM* 1999; 41(2): 111-9.

Table 1 Lumped parameter model estimates -- mean values and (standard deviation).

Parameter	Relaxed	Relaxed fast	Fist	Fist fast
Mass (g)	6.0 (0.6)	5.2 (0.4)	5.5 (0.7)	5.2 (0.6)
Damper (N/m/s)	1.9 (0.1)	2.3 (0.2)	2.0 (0.2)	2.4 (0.3)
Initial Force (N)	0.9 (0.2)	1.6 (0.3)	0.9 (0.3)	1.5 (0.3)
Force Rate (N/s)	-0.9 (6.3)	-10.8 (8.2)	34.7 (13.9)	47.9 (20.7)
RMSE (N)	0.3 (0.1)	0.4 (0.1)	0.2 (0.1)	0.4 (0.1)
VAF (%)	91 (1)	92 (2)	94 (1)	93 (2)

ACUTE AND CHRONIC TENDON OVERUSE IN A RABBIT MODEL

J.M. Archambault[1], W. Herzog[1], D.A. Hart[2]
[1]Human Performance Laboratory, University of Calgary, Calgary AB, CANADA
[2]McCaig Center for Joint Injuries and Arthritis Research, University of Calgary
E-mail: jarchamb@kin.ucalgary.ca

INTRODUCTION

Our research in the past few years has focussed on understanding how tendon overuse injuries develop. For this purpose, we modified the rabbit Achilles tendon overuse model originally presented by Rais (1961). Our modifications allowed us to control and measure the loading inputs to the tendon, load the tendon for one or multiple bouts, and evaluate the biological response of the tendon to this loading. We report here our findings of changes in the tendon following one day or 11 weeks of repetitive loading.

METHODS

The experimental model has been described in depth previously (Archambault et al. 1998), but will be reviewed here in brief. The rabbit was placed supine in a sling with the left leg placed in the loading apparatus (Figure 1). The foot was attached to a footplate interfaced with a stepping motor via a strain-gauge instrumented torque cell. The right leg served as the contralateral control, not subjected to the loading protocol. For the loading protocol, the motor moved the ankle joint through a range of 55° at 1.25 Hz. Surface electrodes (acute protocol) or a tibial nerve cuff (chronic protocol) were used to stimulate the triceps surae muscles for 132 ms, 50 Hz at 3-4 times motor threshold. Stimulation was superimposed to the motion of the ankle joint so that the muscles were active during both the eccentric and concentric phases of loading about full ankle dorsiflexion.

For the chronic protocol, loading was done with 4 adult female NZW rabbits for 2 hours, 3 days per week for 11 weeks. For the acute protocol, loading was done for 6 hours, then the animals were sacrificed at 12, 24 and 48 hours post-loading.

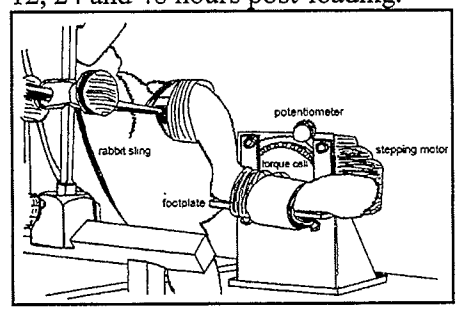

Figure 1. Apparatus used to load the rabbit Achilles tendon.

For each session of loading, the damage index was calculated based on a model of tendon fatigue behaviour (Schechtman & Bader 1997). A damage index is the ratio of the number of cycles done in a session to the number of cycles needed for failure at a given load. Force on the tendon during the loading procotol was calculated from the moments measured at the ankle joint. A maximal tensile load value of 1010 N for the rabbit Achilles tendon was used in the calculations (Nakagawa et al., 1996).

For the chronic protocol, tendons were evaluated for histological changes, water content and DNA content. For the acute protocol, tendons were evaluated for the expression and production of collagenase (MMP-1) and stomelysin (MMP-3).

RESULTS

As a result of the chronic loading, no changes were observed in the experimental and contralateral tendons at dissection or under the microscope. Matrix organization and cellularity were similar in all sections of the tendons (Figure 2). Water content and DNA content in the tissues did not change in response to the loading protocol. The average damage index for a 2 hour session of loading was 0.002, with peak moments of 30-40% of the isometric maximum.

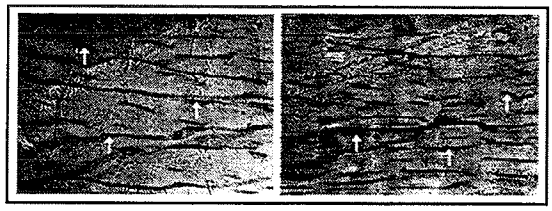

Figure 2. Micrograph of Achilles tendon of a contralateral (left photo) and experimental (right photo) leg.

The 6 hour acute loading protocol resulted in an average damage index of 0.005 (n=3 rabbits). Peak tendon forces were similar to those obtained during the chronic protocol. At sacrifice, no visible changes were observed in the tendons. The loading bout did not induce the expression or production of MMP-1 or MMP-3 in the Achilles tendon or paratenon at 12, 24, or 48 hours post-loading (Figure 3).

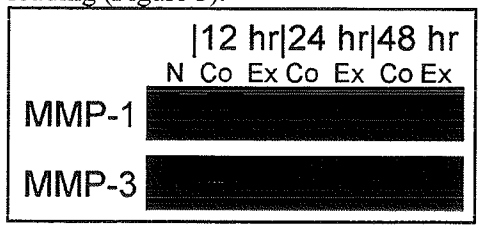

Figure 3. Gene expression of collagenase and stromelysin in **N**ormal, **C**ontralateral and **E**xperimental tendons.

DISCUSSION

With the chosen loading parameters, acute and chronic repetitive loading did not induce an overuse injury in the Achilles tendon of mature rabbits. This is in contrast to the report of an injury response in the Achilles tendon of immature rabbits with chronic loading by Backman and co-workers (1990). Rais (1961) had also reported that a 6 hour loading session produced inflammatory changes in the tendon. Both these studies used a movement frequency that we felt was unphysiological and used immature animals. These two factors may be responsible for the observed differences in injury response.

Our results suggest that the Achilles tendon of healthy adult rabbits is not easily injured during normal activity. It is possible that the muscles cannot produce enough force to cause substantial damage to the tendon, as indicated by our calculation of the damage index. This would suggest that repetitve loading within the range of normal activity is not sufficient to damage a tendon, nor induce enzymes such as collagenase or stromelysin that could result in matrix degradation.

We now hypothesize that tendon overuse injuries occur as a result of a combination of factors, not only repeated mechanical loading. *In vitro* data with rabbit tendon cells has shown that the application of a mechanical stimulus in combination with an inflammatory cytokine (IL-1β) resulted in greater production of stromelysin than if either stimulus is presented alone (Archambault et al., *submitted*). Future experiments will test this combined etiology hypothesis *in vivo*.

REFERENCES

Archambault et al., J Muscul Res, 2:283, 1998
Backman et al., J Orthop Res, 8:541, 1990
Nakagawa et al., Eur J Appl Physiol, 73:7, 1996
Rais, Acta Chir Scandinav Suppl, 268:1, 1961
Schechtman & Bader, J. Biomech, 30:829, 1997

BIOCHEMICAL AND BIOMECHANICAL EVALUATION OF THE FLEXOR TENDON REPAIR SITE

M. Boyer[1], R.Gelberman[1], P. Manske[1], M. Silva[1], J. Watson[1], S. Cai[1], D. Amiel[2], F. Harwood[2]
[1]Dept. Orthopaedic Surgery, Barnes-Jewish Hospital, Washington University School of Medicine, St. Louis, Missouri, USA
[2]Department of Orthopedics, University of California at San Diego, San Diego, CA
E-mail: boyerm@msnotes.wustl.edu

INTRODUCTION

Our research has focused on the healing of lacerated flexor tendons. Recent research has sought to quantify the temporal accumulation of VEGF at the repair site during the intrinsic angiogenic process that accompanies early healing, and evaluate if a rehabilitation protocol accelerates the maturation of repaired intrasynovial flexor tendons.

METHODS

Twenty-four flexor digitorum profundus tendons from 12 adult dogs were transected and repaired. The animals received either low-force or high-force rehabilitation. Animals were sacrificed 10, 21 or 42 days after surgery, and a 10 mm segment of tendon surrounding the repair site was harvested. These segments were evaluation for collagen content and cross-links.

To evaluate the time course of the VEGF mRNA accumulation during the early stages of flexor tendon healing, flexor digitorum profundus tendons were transected and repaired. Animals were sacrificed at 4, 7, 10 and 17 days after surgery. VEGF expression was evaluated by in-situ hybridization with a radiolabeled antisense riboprobe.

RESULTS AND DISCUSSION

In the first study, biochemical analysis revealed that the total collagen content was significantly reduced at each time point ($p<0.05$) and that the reducible crosslink ratio of DHLNL/HLNL was significantly increased at each time point after surgery. The flexor tendon site is still immature at six weeks post-operatively from the standpoint of collagen content and crosslink maturity. Since we have previously observed increases in biomechanical strength of the repair site between three and six weeks, factors other than increased collagen synthesis or altered repair-site collagen maturity must be involved. There was no difference in collagen content or cross-link values between low and high-force rehabilitation groups at any time point ($p>0.05$). The higher level of force used during the rehabilitation protocol did not accelerate the maturation of the repaired tendons, in contrast with prevailing clinical concepts.

In the angiogenesis study, selective accumulation of VEGF mRNA occurred at the intrasynovial flexor tendon repair sites as early as 4 days post-operatively, with peak levels achieved at 7 and 10 days post-operatively. Local VEGF mRNA expression at the repair site temporally preceded and was spatially distinct from the vascular ingrowth itself, which occurs maximally at day 17. This is the first report on the time course of VEGF mRNA accumulation during the early stages following intrasynovial flexor tendon repair and rehabilitation. These data support the concept that cells within the flexor tendon repair site are involved in angiogenesis, not only the synthesis of extracellular matrix.

UPREGULATION OF STRESS-ACTIVATED PROTEIN KINASES (SAPKs) IN RESPONSE TO CYCLIC STRAIN OF TENDON CELLS: A potential cellular mechanism for repetitive stress injuries in tendons

Steven P. Arnoczky
Laboratory for Comparative Orthopaedic Research, Michigan State University,
East Lansing, Michigan 48824
E-mail: arnoczky@cvm.msu.edu Web: www.cvm.msu.edu/LCOR

INTRODUCTION

The strain-induced signaling of cells through mechanotransduction pathways has been shown to play a significant role in maintaining the normal homeostasis of connective tissues. While cyclic loading has been shown to be beneficial to tendon health, repetitive tissue strain has also been implicated in the etiology of repetitive stress (overuse) injuries of tendons. Although the precise mechanism(s) by which repetitive strain initiates tissue injury is still unknown, it is likely that this is a cell-mediated event.

Previous studies in our laboratory have demonstrated that cells respond to physical stress by an up-regulation of stress-activated protein kinases (SAPKs) such as c-Jun N-terminal kinase (JNK). This appears to be mediated through a calcium dependent mechanotransduction pathway. SAPKs are a family of signal transduction proteins that are activated under a diverse set of environmental cellular stresses. The prolonged activation of JNK and its subsequent phosphorylation of various transcription factors have been implicated in the initiation of the apoptosis cascade in some cell lines. Induction of apoptosis and subsequent localized cell death may be an initiating factor in the pathogenesis of overuse injuries. Our lab has investigated the effects of cyclic strain as well as other environmental factors (i.e. heat, osmotic stress, etc) which have been implicated in the etiology of repetitive stress injuries on the upregulation of JNK in both tendon cells in monolayer as well as tendon cells *in situ*.

METHODS

Canine patellar tendon fibroblasts (TFbs) as well as rat tail tendons (RTTs) from adult Sprague-Dawley rats were used to evaluate the effect of cyclic strain as well as environmental conditions on the *in vitro* upregulation of SAPKs. The TFbs were cyclically strained in monolayer using a Flexercell® strain unit while the RTTs were cyclically strained using a custom designed computer driven cyclic strain device. The TFbs and the RTTs were cyclically loaded for 2hrs and phosphorylated JNK (p-JNK) expression was evaluated on a Western blot using a polyclonal antibody to p-JNK. The effect of strain amplitude as well as strain frequency on p-JNK was also examined. In addition, the effect of environmental stresses (hyperthermia [44°C], osmotic stress, and hypoxia), alone and in combination, on p-JNK expression were also evaluated.

RESULTS AND DISCUSSION

Cyclic strain resulted in an immediate up-regulation of p-JNK at 15 minutes. This activity peaked at 30 minutes and returned to near resting levels at 120 minutes. While the reason for this decrease in p-JNK expression is not clear it could due to an intracellular phosphatase system that is activated to regulate p-JNK expression.

The magnitude of cyclic strain was found to have a dose-dependent effect on the activation of phosphorylated JNK in both monolayer TFbs and tendon cells *in situ* (RTTs). However, the activation of p-JNK

was not affected by the frequency of the cyclic strain in either system.

Environmental stresses such as hyperthermia and hyperosmolality each result in an upregulation of p-JNK. When combined with cyclic strain both hyperthermia and hyperosmolality result in a persistent increase in p-JNK expression when compared to cyclic strain under normal environmental conditions. Thus, it appears that the upregulation of p-JNK expression can be cumulative. It is possible that under certain environmental stresses (which have been implicated in the pathogenesis of overuse injury) p-JNK expression could be prolonged enough to initiate localized cell death. This "intrinsic" stimulus may contribute to the pathogenesis of repetitive stress injuries in tendons.

The effect of hypoxia, alone and in conjunction with cyclic strain, as well as the effect of various combinations of environmental alterations on the expression of p-JNK is currently being evaluated.

SUMMARY

Cyclic straining of tendon cells in monolayer or *in situ* result in an upregulation of SAPKs. This occurs in a dose-dependent manner, which is amplitude regulated and not frequency regulated. Environmental stresses (hyperthermia, osmotic stress) have also been shown to upregulate p-JNK expression. We propose a cellular mechanism by which cyclic strain and local environmental conditions could produce and intrinsic stimulus, which may contribute to the pathogenesis of repetitive stress injuries.

BIOARTIFICIAL TENDONS: DYNAMIC 3D TENOCYTE CULTURE AS A MODEL FOR TENDON DEVELOPMENT, TENDON INJURY, TISSUE ENGINEERING & EVALUATION OF RESPONSE TO DRUGS AND GROWTH FACTORS

A.J. Banes[1,2,3,4], M. Lotano[1], J. Bruno[3]
[1]Department of Orthopaedics, [2]Biomedical Engineering, [3]Curriculum in Applied and Materials Sciences, University of North Carolina, Chapel Hill, NC.
[4]Flexcell International Corp., McKeesport, PA.
E-mail: ajbvault@med.unc.edu

INTRODUCTION

The biology of non-weight-bearing connective tissues has been under-studied due to the lack of a satisfactory *in vitro* model. An experimental system has been developed that permits 3D culture and load application to linear or circular cell-populated matrices. In this system, uniaxial or equibiaxial strain can be applied to the construct by means of a pressure-operated Flexercell™ Strain Unit and Tissue Train™ culture plates.

METHODS

Internal tendon fibroblasts were isolated from the tensile load-bearing matrix of human or chicken flexor digitorum profundus tendons (Banes et al., 1988; Banes et al., 1995). Cells were cultured in DMEM-H with 10% fetal calf serum (FCS), insulin, transferrin and selenium, 0.1 mM ascorbate-2-phosphate, 20 mM HEPES, pH 7.2, with penicillin and streptomycin.

Passage 3 cells were trypsinized and mixed at a concentration of 10^3-10^4 cells/µl in base-neutralized Vitrogen™, containing 10% FCS in DMEM. For each construct, 200 µl of the cell-matrix mixture was dispensed into the 25 x 3 x 3 mm trough present in the 6 wells of a flexible bottom, Tissue Train™ culture plate (Figure 1). A trough in the membrane was formed by placing the Tissue Train™ culture plate atop a loading jig with conduits allowing vacuum to deform the rubber membrane into a trough of the jig's dimensions, beneath each culture well. Flexible but inelastic nylon anchors were bonded at north and south poles of each well with free anchors to which the cells and matrix bonded. Once the cell-populated matrix had gelled, the vacuum was released and the linear 3D cell-matrix construct was left connected to the polar attachments.

Uniaxial force application was achieved by placing an arctangle loading post (rectangle with curved short ends) beneath each well and applying vacuum regulated for frequency, amplitude and duration by a Flexercell™ Strain Unit.

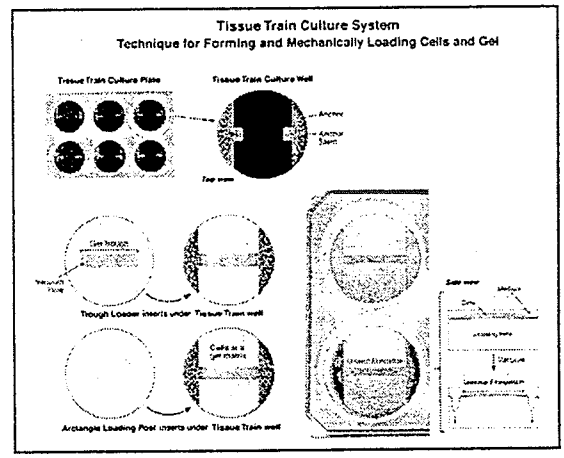

Figure 1: Tissue Train culture system

RESULTS

Tendon cells in a linear collagen gel attached to matrix-bonded anchor ends to form a 3D construct (Bioartificial tendon or BAT). These BATs were cultured for up to 30 days. The BATs initially assumed an hourglass shape, but then the cells reorganized the matrix within 2-3 days, leading to a radial contraction of the construct (Figure 2). This contraction process was inhibited by cytochalasin D, suggesting that the actin cytoskeleton is a necessary component to this event.

H&E stained control cultures showed that cells had elongated and spread evenly throughout the matrix but were densely packed on the surface of the BAT, similar to an epitenon (Figure 3). BATs subjected to 1% uniaxial elongation at 1 Hz for 8hours per day for up to 30 days, had the same overall architecture as controls but more elongated cells and collagen matrix separation.

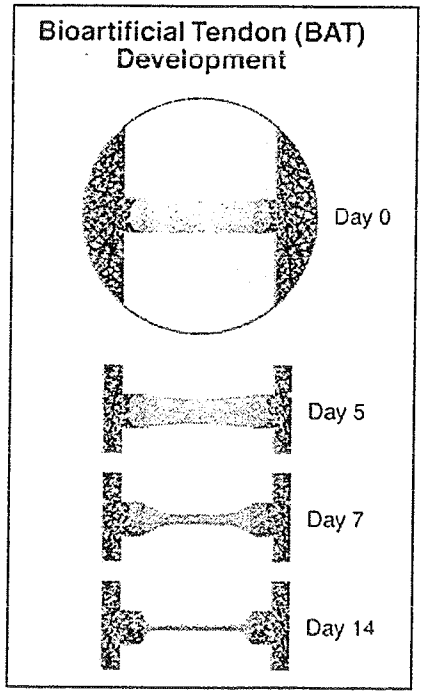

Figure 2: Bioartificial tendon reorganization

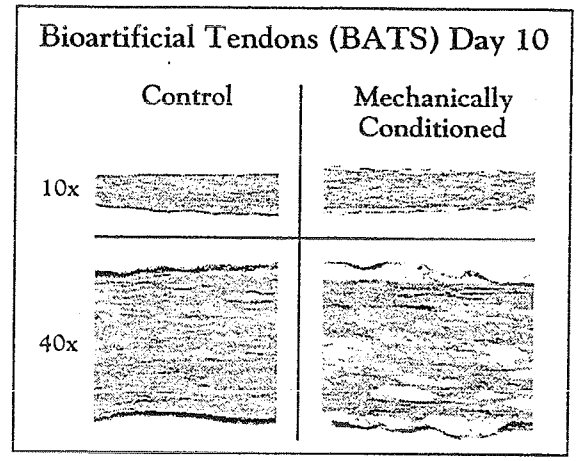

Figure 3: Bioartificial tendon after 10 days of culture, with and without mechanical conditioning.

DISCUSSION

The 3D tenocyte-populated linear BAT matrix is a unique model to study tendon cell interactions and responses to mechanical load. BATs can be maintained for up to 1 month with a tendon-like architecture and viable cells. Once biochemical, biomechanical and functional validation studies are performed, this model could be used to study tendon overuse injuries and response to growth factors and pharmaceuticals.

ACKNOWLEDGEMENTS

AR38121, Hunt Foundation

REFERENCES

Banes et al., *J. Orthop. Res.*, 6:83, 1988
Banes et al., *J. Biomech.*, 28: 1505, 1995

- PARALLEL SESSION -

Rehabilitation

Saturday, August 11, 2001
0900 to 1030

THE RELATIONSHIP BETWEEN BIOMECHANICAL FACTORS AND ULCER DEVELOPMENT IN THE DIABETIC FOOT

William R. Ledoux [1,2], Jane B. Shofer [3], Edward J. Boyko [4], Bruce J. Sangeorzan [1,2]

[1] RR&D Center for Excellence in Limb Loss Prevention and Prosthetic Engineering, VA Puget Sound, Seattle, WA, USA
[2] Department of Orthopaedics, University of Washington, Seattle, WA, USA
[3] Department of Medicine, University of Washington, Seattle, WA, USA
[4] Epidemiologic Research and Information Center, Seattle, WA, USA
Email: wrledoux@u.washington.edu Web: rehabctr.vamc.washington.edu

INTRODUCTION

One of the complications of diabetes mellitus (DM) is the formation of neuropathic foot ulcers with the possibility of infection and subsequent amputation. It has been shown that the alignment of the bones of the foot can affect the plantar pressure beneath the foot (Morag and Cavanagh 1999). High plantar pressure has been implicated retrospectively and prospectively in the ulceration process on a limited number of subjects (Boulton *et al.* 1983; Veves *et al.* 1992). Previous research has demonstrated retrospectively that there is a direct relationship between the position of the rearfoot and the location of metatarsal ulcers (Bevans 1992). Although these studies have demonstrated the relationship between various biomechanical factors and ulceration, there has not been a large scale prospective analysis. The purpose of this research was to further explore, in a prospective manner, the relationship between foot structure and ulcer development.

METHODS

The Seattle Diabetic Foot Study (SDFS) has been collecting data on the diabetic Veteran population since 1990 (Boyko *et al.* 1999). The subjects had no active ulcers at the time of enrollment and had their foot type determined subjectively as neutrally aligned, pes cavus (high arch) or pes planus (low arch). They were followed over a period of time and the location of the first (if any) ulcer was noted. Additionally, many biomechanical measurements were obtained when the subjects were first enrolled. The data included: 1) ankle, subtalar and first metatarsophalangeal joint mobility, 2) presence of foot deformity (muscle atrophy, bony prominences, as well as toe and metatarsal head deformities) and 3) various radiographic measurements.

For the analysis, each foot was considered separately. A chi-square test was used to test for an association between foot type and ulceration. The association between biomechanical measures and ulcer outcome was tested using a logistic regression of ulcer outcome on individual biomechanical measures. Models were adjusted for height, weight, duration of DM and DM treatment. A robust covariance estimator was used to adjust for non-independent observations.

RESULTS

There were 2097 feet that met the inclusion and exclusion criteria. No significant difference was found between foot type and the outcome of ulceration (see Table 1). There were, however, several significant differences between the various biomechanical factors and ulceration (see Table 2). Feet with ulcers had significantly higher amounts of calcaneal inversion (22.6°, S.D. 1.7° vs. 17.7°, S.D. 0.6°, $p = 0.0087$) at the subtalar joint and less hallux plantar flexion (28.6, S.D. 1.1 vs. 32.3, S.D. 0.3, $p = 0.0023$). Additionally, feet that developed ulcers also had significantly higher percentages of intrinsic muscle atrophy (71.8% vs. 58.9%, $p = 0.0086$), bony prominences (72.3% vs. 59.2%, $p = 0.0059$), hammer and/or claw toes (79.4 % vs. 68.4%, $p = 0.011$), and prominent metatarsal heads (73.0% vs. 61.8%, $p = 0.013$). Finally, none of the measured X-ray parameters were significantly different between the ulcerative and nonulcerative groups. Neither the potential confounding variables nor the robust covariance estimator resulted in a change in significance.

Table 1: The percent of each foot type that developed an ulcer.

	neutrally aligned	pes cavus	pes planus rigid	pes planus flex
% with ulcer	5.5	8.1	6.4	5.7

There was no significant differences with either a Chi-square test ($p = 0.2$) or a logistic regression on ulcer outcome adjusting for height, weight, DM duration and DM treatment ($p = 0.5$).

Table 2: The relationship between biomechanical variables and ulcer development.

	ulcer absent (n=1920)	ulcer present (n=127)	p (logistic regression)	p, adjusted [a] (robust) [b]
joint mobility (°), (n)				
dorsiflexion	8.0 ± 0.2 (1262)	7.9 ± 0.5 (105)	0.8	1.0
calcaneal ever.	15.4 ± 0.6 (181)	17.1 ± 1.9 (19)	0.4	0.5
calcaneous inv.	17.7 ± 0.6 (181)	22.6 ± 1.7 (19)	0.0087	0.0077, (0.0033)
hallux dorsi.	40.2 ± 0.3 (1354)	38.9 ± 1.3 (110)	0.3	0.3
hallux plan.	32.3 ± 0.3 (1350)	28.6 ± 1.1 (110)	0.0023	0.0041 (0.0013)
deformity, %, (n)				
int. mus. atrophy	58.9 (1347)	71.8 (110)	0.0086	0.017 (0.014)
bony prominences	59.2 (1344)	72.3 (112)	0.0059	0.0066 (0.0056)
hallux valgus	31.6 (1912)	30.4 (125)	0.8	1.0
hallux limitus	30.1 (1908)	31.7 (126)	0.7	0.8
hammer/claw toes	68.4 (1914)	79.4 (126)	0.011	0.031 (0.030)
prom. met. head	61.8 (1913)	73.0 (126)	0.013	0.024 (0.021)
plantar callus	55.0 (1919)	53.5 (127)	0.8	0.6
X-ray measures (n)				
met head lgth (mm)	4.18 ± 0.06 (782)	4.14 ± 0.18 (71)	0.8	0.7
IM angle (°)	9.5 ± 0.1 (786)	9.0 ± 0.3 (71)	0.11	0.15
HV angle (°)	14.4 ± 0.2 (779)	13.7 ± 0.8 (71)	0.4	0.4
PP 5th met angle (°)	11.4 ± 0.2 (781)	10.6 ± 0.8 (71)	0.3	0.3
lateral TC angle (°)	46.1 ± 0.3 (786)	45.6 ± 1.2 (71)	0.6	0.4
lateral TM angle (°)	-1.1 ± 0.4 (785)	-1.8 ± 1.4 (71)	0.5	0.6

[a] adjusted for height, weight, duration of DM and DM treatment
[b] estimated using robust variance estimator to correct for nonindependent cases

DISCUSSION

A prospective analysis of the effect of several biomechanical variables on ulcer development in diabetic subjects was conducted. Significant differences were seen in some joint mobility measurements and in the percentage of feet with certain deformities. For the most part, these data are indicative of an increase in plantar pressure, which would explain the higher incidence of plantar ulcers. When compared to feet that did not ulcerate, feet that developed ulcers had more calcaneal inversion and decreased hallux plantar flexion. While the relationship to calcaneal inversion is not intuitive, the reduced hallux range of motion could increase plantar pressure. Additionally, the feet that ulcerated had increased percentages of intrinsic muscle atrophy, bony prominences, hammer/claw toes and prominent metatarsal heads - all deformities that could be linked to increased plantar pressure. This study provides additional information on the relationship between foot structure and ulcer development.

ACKNOWLEDGEMENT

This work was funded by The Seattle Epidemiologic Research and Information Center.

REFERENCES

Bevans, J. S. (1992). *The Foot* **2**: 166-172.

Boulton, A. J., C. A. Hardisty, et al. (1983). *Diabetes Care* **6**(1): 26-33.

Boyko, E. J., J. H. Ahroni, et al. (1999). *Diabetes Care* **22**(7): 1036-42.

Morag, E. and P. R. Cavanagh (1999). *Journal of Biomechanics* **32**(4): 359-70.

Veves, A., H. J. Murray, et al. (1992). *Diabetologia* **35**(7): 660-3.

OFF-LOADING IN FOUR DEVICES USED IN THE TREATMENT OF PLANTAR ULCERATION.

Robert van Deursen[1], Benn Beuker[2], Patricia Price[3], Erik Manning[2], Sjef van Baal[2], and Keith Harding[3]

[1]Research Centre for Clinical Kinaesiology and [3]Wound Healing Research Unit, University of Wales College of Medicine, Cardiff, UK
[2]Diabetic Foot Unit, Twenteborg Hospital, Almelo, the Netherlands
E-mail: vandeursenr@cardiff.ac.uk

INTRODUCTION

Plantar off-loading is an important intervention for treating diabetic foot ulcers. Total contact casts can off-load the foot 31% by means of the cast wall (Shaw et al., 1997). Below ankle devices can use load transfer to other plantar areas (Bus and Cavanagh, 2000). Optimizing these mechanisms should improve the effectiveness of treatment. We compared four devices used in the Netherlands and the UK for treatment of diabetic foot ulcers to study the off-loading mechanism used in each device and the magnitude of the effects.

METHODS

Included in the comparison were a custom molded insole shoe (CMI shoe), a soft-cast shoe with custom molded rigid cast sole (MABAL shoe; Hissink et al., 2000), a bivalved total contact cast (BTCC) and a prefabricated pneumatic walking brace (PPWB). A Lohman Shoecast sole was worn under the MABAL shoe and BTCC. A control shoe with a rigid flat insole made of EVA was also used.
Sixteen healthy subjects (aged 37.0 ± 10.4) walked at their preferred speed wearing the different devices or control shoe on the right and the control shoe on the left. In shoe pressures were measured using a Pedar system for at least 8 steps. Walking speed was measured using opto-electric sensors and a timer. Gait analysis was performed using a Vicon 512 system and two Kistler force plates during a second visit. Gait velocity was again measured as before.
Using the mask proposed by Cavanagh et al. (1988), peak pressure of the MTP1 area (MTP1 PP), medial midfoot impulse and total plantar impulse (PI) were determined using NovelWin software. The integral of the vertical ground reaction force (GRFTI) measured with the force platform was calculated using Matlab software. Cadence and step length were calculated using Vicon Clinical Manager. PI and GRFTI data were not directly compared because forces recorded with the two methods tend not to match sufficiently (Shaw et al. 1997; Kalpen and Seitz, 1994). An ANOVA including a contrast with the control shoe was used. GRFTI was tested for differences between devices. PI was subsequently tested to compare the four devices with the control shoe to determine the reduction of plantar load by the four devices.

RESULTS

MTP1 peak pressure was significantly reduced compared to the control shoe for all devices ($p<0.01$) but most of all for

the BTCC (Table 1). Load on the medial midfoot area was increased significantly for all devices ($p<0.01$) but most of all for the BTCC.

Table 1: Mean (and std) of MTP1 peak pressure and medial midfoot impulse.

Device	MTP1 PP (kPa)	Med midfoot impulse (N.s)
Control shoe	303.5 ± 61.1	1.1 ± 1.6
Molded insole	241.5 ± 62.4	12.0 ± 6.7
MABAL shoe	156.9 ± 42.7	11.9 ± 6.8
BTCC	104.0 ± 36.7	15.6 ± 13.6
PPBW	110.0 ± 25.1	4.6 ± 3.5

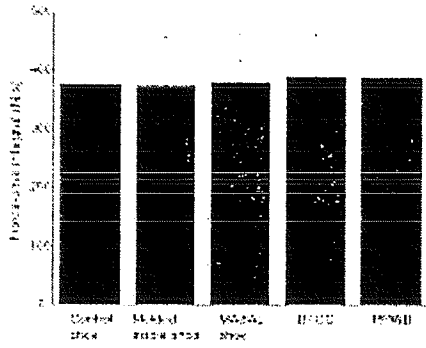

Figure 1: Ground reaction force time integral (N.s) for each device.

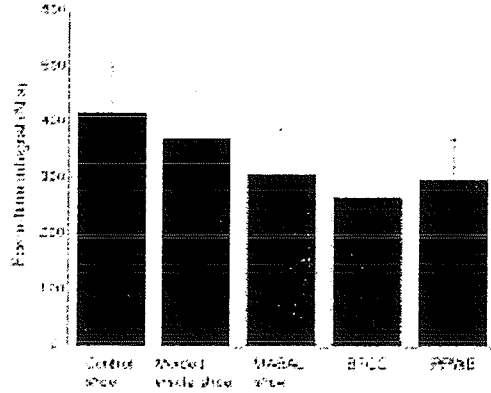

Figure 2: Plantar impulse (N.s) for each device.

There were no significant differences between devices for GRFTI ($p=0.129$) but there were significant differences for PI ($p<0.01$). Compared to the control shoe, PI was reduced by 11% in the CMI shoe, 26% in the MABAL shoe, 35% in the BTCC, and 28% in the PPWB. Walking speed did not differ between tests ($p=0.25$). There was a small but significant difference between devices in walking speed ($p<0.01$) and cadence ($p<0.01$) but not in step length ($p=0.58$).

DISCUSSION

Load transfer to the medial midfoot seemed to occur in the CMI shoe and MABAL shoe but most in the BTCC. Substantial foot off-loading occurred in the BTCC and PPWB but also in the MABAL shoe. Apparently, supporting the arch of the foot otherwise not in contact with the shoe/pressure insole can effectively off-load the plantar surface. Combining foot off-loading and load transfer to the medial midfoot and foot arch in the BTCC resulted in slightly more off-loading than achieved in the TCC studied by Shaw et al. (1997).

REFERENCES

Cavanagh, P.R. et al. (1987). *Foot and Ankle*, 7, 262-76.

Bus, S.A., Cavanagh, P.R. (2000). *Proceedings of ASB 2000*, 237-8.

Hissink, R.J. et al. (2000) *Foot and Ankle*, **4**, 320-3.

Kalpen, A., Seitz, P. (1994). *Gait & Posture*, **2**:236-7.

Shaw, J.E. et al. (1997). *Foot and Ankle International*, **18**:809-17.

Table 2: Mean and standard deviations of the gait parameters of each device.

	Control shoe	CMI shoe	MABAL shoe	BTCC	PPWB
Gait velocity (m/s)	1.46 ± 0.04	1.46 ± 0.04	1.41 ± 0.04	1.30 ± 0.04	1.35 ± 0.04
Step length (m)	0.76 ± 0.02	0.76 ± 0.02	0.72 ± 0.04	0.73 ± 0.02	0.75 ± 0.02
Cadence (steps/min)	140.9 ± 1.9	142.6 ± 2.6	138.8 ± 2.1	132.0 ± 1.7	132.8 ± 2.4

THE USE OF A LOWER BODY PRESSURE CHAMBER AS A REHABILITATION AND TRAINING MODALITY: A BIOMECHANICAL ANALYSIS

Eli R. Groppo, Andrew T. Mahar†, Rachel C. VanderLinden, Adnan Cutuk, Robert K. Eastlack, Amy Langemack, Greg C. Steinbach, Robert A. Pedowitz, Alan R. Hargens
Department of Orthopaedics, University of California – San Diego, San Diego, CA, USA
†Orthopaedic Biomechanics Research Center, Children's Hospital, San Diego, CA, USA
Email: egroppo@ucsd.edu

INTRODUCTION

Unweighted exercise using lower body positive pressure (LBPP) has previously been proposed as a rehabilitation modality (Whalen and Hargens) because it allows injured and postoperative patients the ability to ambulate with decreased lower extremity loading. Additionally, exercising within lower body negative pressure (LBNP) increases weightbearing (Hargens et al. 1991) and has been successfully tested to prevent deconditioning during simulated microgravity (Watenpaugh et al. 2000). The possibility of increasing exercise loads in excess of one bodyweight suggests that LBNP exercise may be a modality for improving athletic performance. Differential pressure is generated using a chamber with an airtight neoprene waist seal. A bi-directional air pump is then used to either increase (LBPP) or decrease (LBNP) the chamber pressure with respect to ambient pressure.

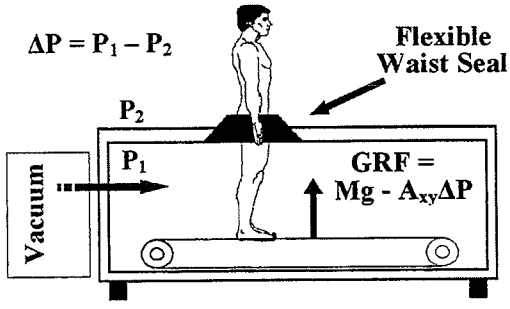

Figure 1. Schematic diagram of pressure chamber. Positive chamber pressures reduce GRF while negative chamber pressures increase GRF.

A standard treadmill inside the chamber allows the patient or athlete to exercise under both differential pressure conditions. The purpose of this study was to evaluate the effects of lower body positive and negative pressure on muscle activity, gait mechanics and cardiovascular load.

METHODS

Two protocols were used in this study to evaluate LBPP and LBNP separately. Both protocols were approved by the UCSD Institutional Review Board. In the first study, nine patients (4 female, 5 male) with an age range of 28-73 volunteered to undergo LBPP testing one week after unilateral arthroscopic meniscectomy. In random order, each subject walked (0.9 m/s) for two minutes under three different LBPP conditions (100%, 60%, and 20% of bodyweight (BW)). In the second study, six normal subjects (3 female, 3 male) with an age range of 22 to 34 ran (2.5 m/s) for three minutes under three different ramped LBNP conditions (100%, 110%, and 120% BW). For both studies, force sensitive shoe inserts (Electronic Quantification Inc., Pennsylvania, USA) were used to measure the vertical component of ground reaction force (GRF). Electrogoniometers (Biometrics Ltd., Gwent, UK) were placed about both knee joints to measure dynamic knee angle and range of motion (ROM). Surface electromyography (EMG) was collected bilaterally from the vastus medialis obliquous (VMO) and biceps femoris (BF)

of LBPP patients and from the left VMO, BF, tibialis anterior (TA), and medial gastrocnemius (MG) of LBNP subjects, using silver-silver chloride electrodes (Noraxon, Ltd., Phoenix, USA). All data were sampled at 1 kHz. EMG data were full-wave rectified and all data were linear enveloped using a 50-point moving average. EMG data were normalized to the peak activity at 100% BW. All data were broken into gait cycles (7-12 cycles per subject per condition), time normalized from 0 to 100% of a gait cycle (as determined by heel strike to heel strike) and averaged. Heart rate (HR) was measured using a Polar Heart Watch (Kempele, Finland) in LBPP patients. HR and oxygen consumption (VO_2) were measured in LBNP subjects using a COSMED K4b^2 pulmonary function analysis system (Rome, Italy). Cardiovascular data were sampled at 1 Hz and the mean HR and VO_2 during the final 10 seconds of each condition were compared. LBPP patients rated perceived pain and exertion using a ten point visual analog scale. Data were analyzed using a one-way repeated measures ANOVA, with Bonferroni *post-hoc* comparisons. Significance was set at $p < 0.05$.

RESULTS

Variable	100% BW	60% BW	20% BW
Normal VMO (norm)	1.0 (0)	0.66 (.08)	0.48 (.09)*
Postop VMO (norm)	1.0 (0)	0.75 (.08)	0.61 (.09)*
Normal BF (norm)	1.0 (0)	0.84 (.06)	0.76 (.13)
Postop BF (norm)	1.0 (0)	0.92 (.06)	0.88 (.09)
Normal GRF (N)	872 (37)	517 (47)*	203 (34)*
Postop GRF (N)	919 (49)	532 (48)*	177 (31)*
Normal ROM (deg.)	58.6 (2.5)	57.3 (2.4)	46.9 (1.9)*
Postop ROM (deg.)	49.1 (3.6)	45.7 (4.2)	36.8 (3.5)*
Heart Rate (bpm)	95 (6)	86 (6)*	81 (5)*

Table 1. Mean results from nine LBPP patients (±SEM). * Indicates significantly different from 100% BW condition.

Variable	100% BW	110% BW	120% BW
Peak VMO (norm)	1.0 (0)	1.04 (.06)	1.01 (.08)
Peak BF (norm)	1.0 (0)	0.92 (.03)	1.08 (.06)
Peak TA (norm)	1.0 (0)	1.09 (.09)	1.03 (.08)
Peak MG (norm)	1.0 (0)	1.01 (.02)	0.95 (.04)
Peak GRF (N)	1582 (90)	1648 (114)	1705 (130)
Knee ROM (deg.)	25.6 (1.4)	25.3 (1.4)	25.9 (1.4)
Heart Rate (bpm)	144 (7)	154 (7)*	160 (7)*
VO2 (ml/min)	2326 (163)	2464 (217)	2554 (204)

Table 2. Results from six LBNP subjects.

Results from LBPP patients and LBNP subjects are summarized in tables 1 and 2 respectively. Perceived exertion decreased significantly with LBPP. VO_2 and GRF both increased with LBNP although the results did not reach significance ($p = 0.11$ and $p = 0.07$ respectively).

DISCUSSION/SUMMARY

LBPP reduced GRF, which is necessary to protect healing tissue after injury or surgery, while maintaining relatively normal gait mechanics, muscle activation, and patient comfort. This indicates that LBPP may reduce rehabilitation times. LBNP induced a significant cardiovascular response without altering gait mechanics or muscle activation patterns. This may be an alternative to running uphill or carrying extra weight, both of which may alter gait mechanics and/or increase the risk of injury.

REFERENCES

Hargens, A.R. et al. (1991). *Aviation, Space, and Environmental Medicine*, **62**, 934-937.

Watenpaugh, D.E. et al (2000) *J. Applied Physiology*, **89**, 218-227.

Whalen, R.T. and Hargens, A.R. (1992) *U.S. Patent 5,133,339.*

ACKNOWLEDGEMENTS

Supported in part by Bristol-Myers OREF Center of Excellence and UCSD Chancellor's Associates grants.

THE EFFECT OF ADDED PROSTHETIC MASS ON PHYSIOLOGIC RESPONSES AND STRIDE TIME DURING MULTIPLE SPEEDS OF WALKING IN PERSONS WITH UNILATERAL TRANSTIBIAL AMPUTATION

Suh-Jen Lin, David H. Nielsen, Miao-Ju Hsu, and John Yack

Graduate Program in Physical Therapy & Rehabilitation Science,
University of Iowa, Iowa City, IA E-mail: suhlin@uiowa.edu

INTRODUCTION

Increased energy cost and decreased gait efficiency of walking has been a concern for persons with lower extremity amputation. In walking, there appears to be a particular combination of stride length, stride time and speed at which energy expenditure per unit distance is minimized (Zarrugh, M.Y.1974). Studies on transtibial prosthesis mass revealed controversial findings. It was suggested that there was no need to further decrease the prosthesis mass; on the contrary, heavier prosthesis may result in better gait symmetry (Lehmann, J.F.1998; Selles, R.W.1999). However, matching prosthesis moment of inertia to 100% of the intact leg resulted in increased energy cost and decreased gait symmetry (Mattes, S.J. 2000).

Both mass and mass distribution affect moment of inertia. The critical level of added mass has not been fully examined in multiple speeds of walking. Thus, the purpose of this study was to examine the effect of added prosthetic mass on several physiologic responses as well as stride time while walking at multiple speeds in persons with transtibial amputation.

METHODS

Eight male subjects (age: 36 ± 15 years (mean ± S.D); height 1.75 ± 0.06m; weight: 81.71 ± 9.64 kg; prosthesis mass: 1.68 ± 0.27kg) with unilateral traumatic transtibial amputation wearing the same type of prosthesis participated in this study. Subjects were considered in the high to very high activity level according to the Day activity scale 33.3 ± 6.8 (Day, H. 1981).

Mass of stump was simulated with an appropriately sized water bag. Three levels of added masses were 60%, 80% and 100% of estimated intact shank and foot mass (Winter, D. 1990). The average amounts of added mass for the three levels of mass were 0.3 ± 0.26kg, 1.31 ± 0.34 kg and 2.31 ± 0.45kg respectively. The center of gravity (CG) of each prosthesis was measured using a force plate. The mean CG of baseline prostheses was 55% of shank length from knee. Pliable lead strips were used as the material for the added mass and taped to the CG of each prosthesis. Subjects had at least three hours acclimation to each added mass condition.

For each added mass condition (randomly assigned), a multiple speed treadmill walking test was performed. The test involved four minutes of resting data collection, followed by five incremental speeds (2.0, 2.5, 3.0, 3.5, 4.0 mph) of four minute continuous walking stages, followed by an appropriate cool down period. A metabolic cart (Medgraphics MN), interfaced with a telemetry ECG system, was used for data collection of oxygen

consumption and heart rate. An instrumented treadmill (Gaitway, Kistler Ins. NY) was used for collection of stride time. Relative exercise intensity was defined as the percentage of age predicted maximal heart rate (% APMHR). Gait efficiency was defined as the oxygen consumption per distance traveled (ml/kg/m).

RESULTS AND DISCUSSION

Two-way (mass x speed) repeated measures analysis of variance was used for data analysis on oxygen consumption, gait efficiency, % APMHR and stride time. There was no effect of interaction. There was no significant difference in oxygen consumption and gait efficiency for the three mass levels across the five speeds studied.

Surprisingly, added mass up to 100% of prosthetic mass did not significantly increase energy cost. One possible reason might be that the proximal loading in current study results in less change in the moment of inertia compared to previous studies (Mattes, S.J. 2000). Furthermore, the mean 100% added mass value in current study was about 2.8% of body mass. Our subjects were considered high to highly active, which might explain their ability to adjust to this load without extra burden on the cardiovascular system.

There was significant difference in %APMHR ($p = 0.013$) and stride time ($p=0.0126$) for the three mass levels. Follow up t tests showed the %APMHR was increased between 100% mass and 60% mass ($p=0.0045$), and between 100% mass and 80% mass ($p=0.0327$). Because there was no significant increase in energy cost, the significantly increased heart rate responses might be due to a neural component.

Follow up t tests showed that significant increases in stride time occurred between the 60% and 100% ($p=0.0098$), and the 60% and 80% ($p=0.0008$) mass condition. The change of stride time with added mass reflected the immediate adaptation of gait to the change of moment of inertia of lower extremity. However, this change in moment of inertia does not reflect in any changes of the metabolic demand.

SUMMARY

The results showed adding mass at the center of gravity of prosthesis, up to 100% mass of intact limb, did not increase energy cost across five speeds of walking. Further study on the complete temporal-spatial parameters of gait might give us insight as to the impact of proximally added mass on gait symmetry. Stride time did change with the added mass. The relationship between stride time and its preferred resonant period needs further study in order to understand energy minimization in person with transtibial amputation.

REFERENCES

Day, H. (1981). *Prosth Ortho Intl* **5**, 23-28.

Lehmann, J.F. et al (1998) *Arch phys Med Rehab* **79** (2), 162-168.

Mattes, S.J. et al (2000) *Arch Phys Med Rehab* **81** (5), 561-568.

Selles, R.W. et al (1999) *Arch phys Med Rehab* **80** (12), 1593-1599.

Winter, D. (1990) *New York, John Wiley & Sons.*

Zarrugh, M.Y. et al (1974) *Eur J Appl Phys Occup Phys* **33**, 293-306.

ACKNOWLEDGEMENTS

This work was supported in part by Ottobuck Inc.

Abnormal Muscular Coordination in the Lower Extremity of Cerebral Palsy Subjects

Darryl G. Thelen, Scott A. Riewald*, Scott L. Delp
Biomechanical Engineering Division; Stanford University, Stanford, CA
*Sensory Motor Performance Program, Rehabilitation Institute of Chicago, Chicago, IL
Email: dthelen@stanford.edu, http://www.stanford.edu/group/nmbl/

INTRODUCTION

Subjects with cerebral palsy frequently walk with excessive adduction and internal rotation of the hip during stance (Sutherland et al. 1978), when extension of the limb is required. This pattern resembles the "extension synergy" commonly observed in patients with hemiplegia following stroke (Sawner et al. 1992). The extension synergy is thought to arise from primitive neural control that couples the motions of knee extension to hip extension, adduction, and internal rotation. While these combined motions are often observed in subjects with cerebral palsy, it is not known if neural coupling between these degrees of freedom contributes to the observed motions. The purpose of this study was to determine if maximum isometric exertions of the hip or knee extensors produced the other components of the extension synergy in subjects with cerebral palsy.

METHODS

Nine subjects with spastic cerebral palsy and six neurologically intact control subjects participated in this study. Subjects performed maximum isometric lower-extremity exertions while seated in a chair that provided support for the pelvis and restrained the upper body (Figure 1). A cast was placed around the ankle and was fixed to a six degree of freedom load cell. The load cell measurements were used along with measured limb geometry to determine the three-dimensional moments about the hip and flexion-extension moments about the knee. Bipolar surface electrodes were used to monitor the activities of eight muscles: gluteus maximus, gluteus medius, adductor magnus, rectus femoris, vastus lateralis, vastus medialis, semitendinosus and biceps femoris long head.

Subjects were asked to generate either a maximum hip extension moment or a maximum knee extension moment. They were free to use whatever strategy they desired to maximize this primary moment, which was displayed to them during a 4 second trial. The maximum primary moment, averaged over a moving 300 ms window, was determined in post-hoc analysis. The associated moments about the other degrees of freedom and muscle activities over this same 300 ms window were used to characterize the coordination strategy adopted by the subject. To facilitate comparisons between subjects, the moments for each subject were normalized to the maximum moment they could generate for each degree of freedom. The EMG activity of each muscle was normalized to the maximum EMG recorded over all trials for each subject. A repeated measures ANOVA was used to test for significant differences between the control and CP subjects in the normalized moments and EMG.

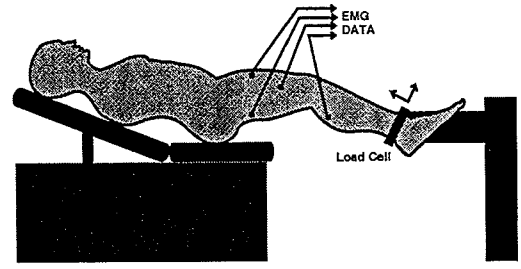

Figure 1. Experimental setup.

RESULTS

Maximum Hip Extension Exertion

When generating a maximum hip extension moment, control subjects simultaneously generated a knee flexion moment (Figure 2, upper chart). In contrast, CP subjects generated a knee extension moment ($p<0.005$) and a significantly larger hip internal rotation moment than controls ($p<0.05$). Significantly larger EMG activities in the rectus femoris and vasti muscles of CP subjects (Figure 2, lower chart) likely contributed to the knee extension moment generated by the CP subjects during a maximum hip extension.

Maximum Knee Extension Exertion

When generating a maximum knee extension moment, control subjects simultaneously generated a hip flexion moment. CP subjects demonstrated an opposite strategy by generating a hip extension moment during this task ($p<0.005$). On average, control subjects developed a hip abduction moment while CP subjects did not ($p<0.05$). EMG activities in the semitendinosus and biceps femoris muscles were significantly larger ($p<0.005$) in the CP subjects during maximum knee extension exertions, while EMG activity in the rectus femoris muscle was significantly smaller in the CP subjects ($p<0.05$). Given that the hamstrings generate a hip extension moment and the rectus femoris generates a hip flexion moment, these activation differences likely contributed to the tendency of the CP subjects to generate a hip extension moment.

DISCUSSION

Control subjects decoupled extension of the hip and knee in these isometric tasks. However, subjects with CP produced hip extension moments during maximum knee extension exertions and knee extension moments during maximum hip extension exertions. The subjects with CP also produced other components of the extension synergy, including internal rotation of the hip during hip extension, and a tendency to adduct the hip during knee extension. These results suggest that abnormal neural control, consistent with the extension synergy (Sawner et al. 1992), may contribute to stereotypical movement abnormalities in cerebral palsy.

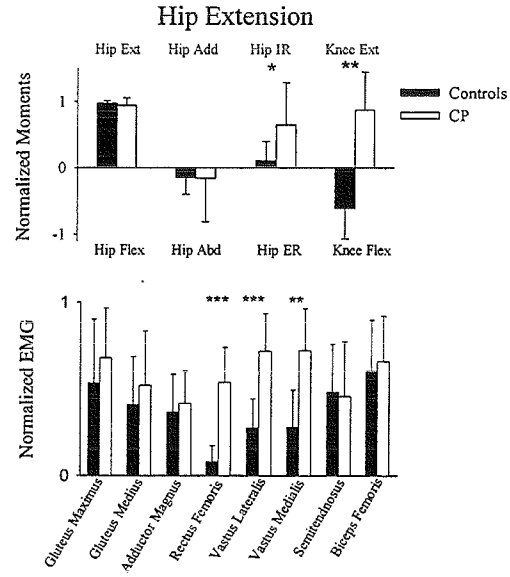

Figure 2. Associated moments and muscle activities during maximum hip extension exertions. Significant group differences are denoted: ***$p<0.005$; **$p<0.005$; *$p<0.05$. Hip and knee moments are abbreviated as extension (Ext), flexion (Flex), adduction (Add), abduction (Abd), internal rotation (IR), external rotation (ER).

REFERENCES

Sawner, K.A., LaVigne, J.M. (1992). *Brunnstrom's Movement Therapy in Hemiplegia.* 2nd Ed. Lippincott Williams & Wilkins.

Sutherland, D.H. et al. (1978). *Orthopedic Clinics of North America.* **9**, 143-154.

ACKNOWLEDGEMENTS

NIH R01 HD33929 and the Whitaker Foundation

ASSESSMENT AND PREDICTION OF SURGICAL REDUCTION OF TREMOR IN MS

Duane Morrow[1], Joseph Matsumoto[2], Ann Rabatin[1], and Kenton Kaufman[1]

[1]Motion Analysis Laboratory, Mayo Clinic/Mayo Foundation, Rochester, MN, USA
[2]Department of Neurology, Mayo Clinic/ Mayo Foundation, Rochester, MN, USA
E-mail: morrow.duane@mayo.edu

INTRODUCTION

Thalamotomy and Deep Brain Stimulation (DBS) are two procedures used to alleviate cerebellar tremor in patients with multiple sclerosis (MS). Traditional methods of evaluating the severity of MS rely heavily on the use of subjective clinical rating scales. However, tremor-related disability may be very difficult to assess as patients are often so disabled that they can perform few activities of daily living. General quality of life scales often are weighted heavily towards ambulation and are not sensitive to tremor. Other tremor-specific rating scales may also be misleading as they are subjective in nature. Accurate and reliable quantification of tremor is needed to evaluate disease progression and treatment efficacy. While accelerometry is still widely used to record tremulous signals, much work has centered on the use of electromagnetic (EM) sensors to characterize tremor. Studies in this and other laboratories have already shown their reliability [Morrow, 1999]. Additionally, recordings from EM systems have been used to discern between normal subjects and different pathological tremors, including MS Spyers-Ashby, 1999]. Our study proposes that Quantitative Movement Analysis (QMA) may be used to accurately quantify improvement in tremor. Further, our preliminary study indicates that QMA may be used to predict the potential for surgical tremor reduction.

METHODS

Nine patients (mean age = 44) diagnosed with either clinically definite or laboratory-supported definite MS were used in this study. Three received DBS and six underwent thalamotomies. Each patient was evaluated using: 1) a tremor-related disability scale (Disability scale, range 0-75, best to worst), 2) the Expanded Disability Status Scale (EDSS, range 0-10, best to worst), 3) the timed box and blocks test (BB), and 4) QMA. Patients were evaluated before surgery and at three months post surgery.

To assess the QMA score, a three-dimensional electromagnetic tracking device (Flock of Birds, Ascension Technologies, Burlington, VT, USA) was attached to the subject's dominant hand. Subjects were seated at a table with four target markers (the Left, Right, and Far targets were on the tabletop, while the Near target was elevated to chin-height). Position data was recorded for ten trials each at 144 Hz as the subject reached from the Left to the Right (LR) and from the Far to the Near (FN) targets. These reaches were selected to represent activities of daily living. Velocity data was calculated and a 512-point Fast Fourier Transformation (FFT) was calculated for each of the three orthogonal directions (zero padding used as needed). Power spectral densities (PSDs) were calculated from the FFTs. Mean spectra were calculated by averaging the PSDs for each of the ten trials for each direction of reach. The vector summation of the area under the modal tremor frequency

for the three orthogonal directions was taken as the power of the tremor for that reach. the QMA was defined as the log transform of the summation of the tremor power for the LR and FN reaches.

All measures were compared with pairwise correlations. Measures were also correlated with the calculated post-surgical changes. Statistical significance set at $p<0.05$ for all comparisons.

RESULTS

Results for the patients are in Table 1. Pairwise correlation (see Table 2) reveal strong correlations in pre-surgical EDSS and Disability scores. The pre-surgical QMA scores also correlated strongly with the post-surgical changes in both the QMA and BB scores. The improvement in BB scores correlated well with the change in QMA scores, though not significantly ($p=0.08$). Interestingly, the change in Disability had a strong negative correlation with the change in EDSS scores.

DISCUSSION:

Important to note is that no correlation exists between the functional task scores (QMA, BB) and the qualitative disability scales (EDSS and Disability). This indicates that these more global scales may not be able to accurately assess results of tremor-reducing treatments. Also of significance, however, is the strong correlation between functional post-surgical improvement scores as measured by the change in BB and QMA scores with a patients pre-surgical QMA evaluation. As the pre-surgical QMA scores rose above 4, the better the improvement with surgery. This suggests that a threshold may exist below which invasive surgery to reduce cerebellar tremor is not warranted.

Table 2: Correlations of tremor measures

Measure 1	Measure 2	Correlation
Pre Disability	Pre EDSS	0.9021
Pre QMA	BB Change	0.8138
Pre QMA	QMA Change	0.7024
Disability Change	EDSS Change	-0.7506
QMA Reduction	BB Change	0.6117*

*$p=0.08$. All other correlations $p<0.05$.

REFERENCES

Morrow, D. et al. (1999). *23rd Meeting of the ASB 1999.*

Spyers-Ashby, J. et al (1999). *Med Eng Phys*, **21**, 713-723.

Table 1: Pre- and Post-Surgical QMA, BB, EDSS, and Disability Scores

Subject	QMA Pre	QMA Post	BB Pre	BB Post	EDSS Pre	EDSS Post	Disability Pre	Disability Post
1	3.58	3.49	18	13	7.5	7.5	58	54
2	4.99	3.25	0	17	9	9	69	62
3	3.98	3.63	0	2	8.5	8.5	70	68
4	5.14	3.71	0	31	6.5	6.5	46	40
5	4.96	4.90	0	24	7.5	7.5	64	66
6	2.75	3.04	0	0.3	6.5	6.5	38	38
7	4.23	4.01	21	17	7.5	7.5	58	53
8	4.48	3.54	0	15	9	9	68	64
9	4.95	4.40	9	29	4.5	5	39	26

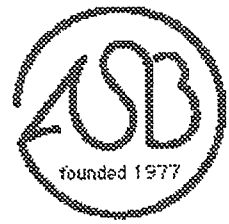

- POSTER PRESENTATIONS -

Friday, August 10, 2001
1530 to 1830

CENTER OF MASS STATE AT STEP CONTACT INFLUENCES THE ABILITY TO RESTORE BALANCE WITH A BACKWARD STEP

Michael Pavol and Yi-Chung Pai

Dept. of Physical Therapy, University of Illinois at Chicago, Chicago, IL
E-mail: mpavol@uic.edu

INTRODUCTION

Large postural perturbations require a stepping response to restore standing balance. The factors determining the success or failure of such stepping responses are not well characterized, however. For a backward loss of balance, body configuration at step contact appears to play an important role (Hsiao & Robinovitch, 2001). We used the concept of the feasible stability region (FSR) (Pai & Patton, 1997) to map how the ability to restore static posture with a backward step is influenced by the state of the body center of mass (COM) at step contact.

METHODS

Mappings employed a six-link sagittal-plane model of the body (Figure 1), controlled by active torques at ankle, knee, and hip of the posterior, recovery limb. The recovery foot was fixed. The contralateral, non-stepping limb moved passively, its foot constrained to slide along the ground. The coefficient of friction at the sliding foot was a sigmoid function of velocity. Active joint torques were generated by extensor-flexor pairs

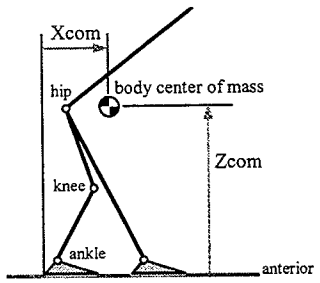

Figure 1: The six-link model used.

possessing first-order activation dynamics and angle- and velocity-dependent torque capacities for each muscle. A shared control signal specified the mutually exclusive inputs to opposing muscles. Angle-dependent passive torques limited the joint ranges of motion. Inertial and strength parameters were for an average young man.

To map the FSR, the initial velocity of the COM and either its initial horizontal displacement from the recovery heel (x_{com}) or its initial height (z_{com}) were specified. Optimizations then identified, for the other component of COM initial position, the minimum and maximum initial positions from which the COM could be brought to rest in 2 seconds. The FSR was mapped for initial horizontal velocities (vx_{com}) of 0, -15 and -30% body height (bh) per second and initial vertical velocities (vz_{com}) of 0, -30, and -60% bh/s. The most negative of these velocities were seen at step contact in falls from a slip during a sit-to-stand (Pai, 1999).

Optimization was by simulated annealing. "Control" variables were the initial joint angles, velocities, and muscle activations and the timing and amplitudes of the muscle control signals. Control signals comprised 5 periods of constant amplitude connected by 4 linear transition periods. Initial angles and velocities were restricted to physiological ranges. Costs were placed on a final COM position outside the recovery foot or below 40% bh and on a final COM velocity or acceleration not near-zero. Penalty functions enforced constraints on the vertical ground

reaction force, static friction force, center of pressure, and minimum knee and hip height.

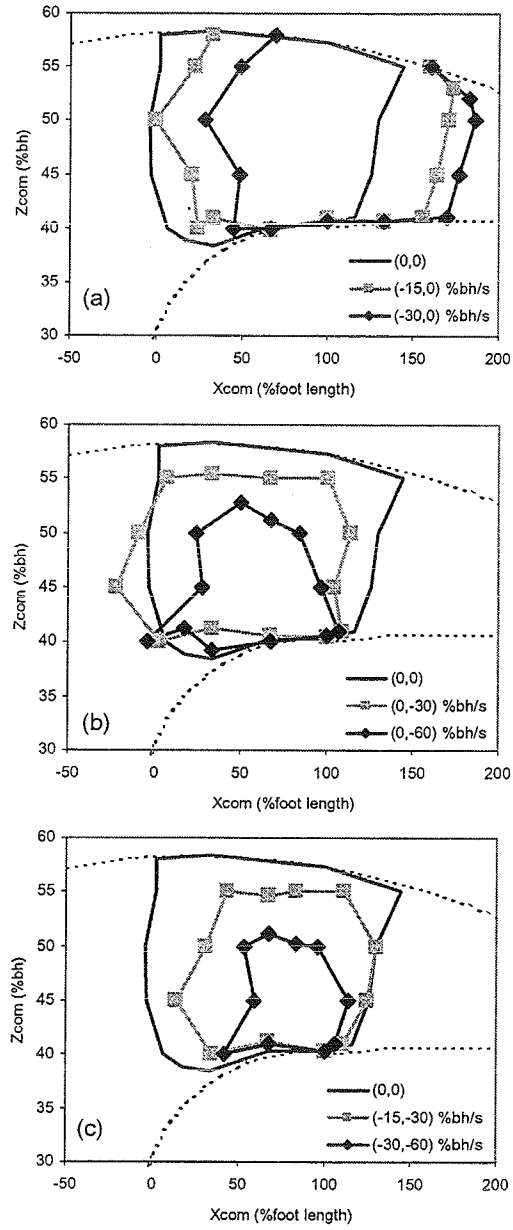

Figure 2: FSR's for indicated (vx_{com},vz_{com}). Static posture can be restored only for initial COM positions within the FSR. Influences of (a) backward, (b) downward, and (c) combined initial velocities are shown. Dotted lines indicate anatomical constraints.

RESULTS AND DISCUSSION

A complex nonlinear relationship was found between the COM state at step contact and the ability to restore static posture (Figure 2). With no initial velocity, the COM essentially had to be above the recovery foot for stability. Larger initial backward vx_{com} shifted the FSR progressively forward, but did not restrict the range of feasible z_{com}. Larger initial downward vz_{com} progressively lowered the FSR upper boundary. Low z_{com} remained feasible because vz_{com} could be attained through head-arms-torso flexion without an irreversible hip descent. The side boundaries of the FSR also contracted for large downward vz_{com}. When the COM possessed both backward and downward initial velocity, vz_{com} appeared to determine the shape of the FSR, while vx_{com} determined its anterior-posterior location.

The results show that, in general, the faster the COM is moving backward, the farther the recovery foot should be placed behind the COM. However, in the absence of downward COM motion, there appears to always be a wide range of foot placements that allows restoration of static posture. Downward COM motion will decrease the range of feasible foot placements for restoring static posture and, for some COM heights, can make it impossible to recover through a step of any length.

REFERENCES

Hsiao, E.T., Robinovitch, S.N. (2001) *J Gerontol Med Sci*, **56A**, M42-M47.
Pai, Y.-C. (1999) *J Biomech*, **32**, 1377-1382.
Pai, Y.-C., Patton, J. (1997) *J Biomech*, **30**, 347-354.

ACKNOWLEDGEMENTS

Funded by NIH #1-R01-AG16727-01

ELASTIC, YIELD, AND ULTIMATE PROPERTIES OF EMU CORTICAL BONE

Karen L. Reed[1], Thomas D. Brown[2,1]
[1]Department of Biomedical Engineering
[2]Department of Orthopaedic Surgery
University of Iowa, Iowa City, IA
Email: karen-reed@uiowa.edu

INTRODUCTION

Femoral head osteonecrosis remains an important unsolved problem in hip surgery, largely because reliable techniques are lacking to prevent mechanical collapse of the structurally compromised osseous lattice. Various animal models have been used, including dogs, rabbits, pigs, sheep, and horses. While each of these species has exhibited distinct early histological attributes of the condition, none has shown good concordance with the late collapse propensity in humans. We recently hypothesized this lack of collapse was due to biomechanical factors, since all of these model species are quadrupeds which can load-protect the affected limb. The emu *(Dromaius novaehollandiae)*, a large, flightless, bipedal bird, appears to overcome that key difficulty (Conzemius, 2000). Fully exploiting the utility of this new bipedal model for osteonecrosis (and other musculoskeletal research) will depend on rigorous understanding of the comparative biomechanics of emu versus human hips. One key aspect of this is the intrinsic mechanical properties of the bone itself. Since no data are available on the mechanical properties of emu bone, laboratory studies were undertaken to collect that information.

METHODS

39 rectangular beam specimens of cortical bone from the femurs of adult emus, oriented parallel to the bone's long axis (Figure 1), were taken from 5 separate donors. Specimens were milled to a nominal length, width, and depth of 56.6 mm, 7.4 mm, and 1.6 mm respectively. Individual exact dimensions were then documented by micrometer. During both the milling and subsequent testing processes, all samples were kept copiously irrigated with 0.9% saline. Specimens were intentionally left long to allow for overhang on the support span during testing.

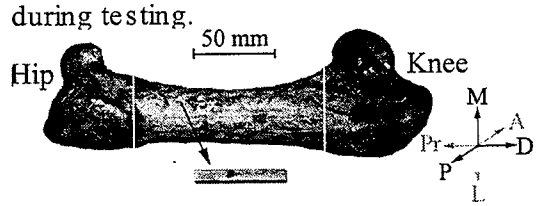

Figure 1: Specimen harvest region, within which samples were indexed according to circumferential (A,P,M,L) and longitudinal (Pr, D) site.

Modulus of elasticity and yield strength were characterized via a four-point bending test. Data collection was performed using an MTS Bionix 858 test machine (MTS Corp., Eden Prairie, MN). The fixture used had a support span of 25.4 mm and a loading span of 8.45 mm. All tests were performed as recommended by ASTM D790. The crosshead speed was adjusted to impose a longitudinal strain rate of 0.0005 s^{-1} at the specimen surface. Elastic modulus (E) was computed from: $E=(1/I)*(5/12)*(P/y)*c^3$, where P/y is the slope of the visually apparently linear portion of the load-deflection curve, I is the area moment of inertia, and c is the loading span distance. In all specimens P/y was nearly linear, with $R^2 > 0.99$. Yield stress was defined as that stress at which the stress-strain curve intersected a line having the same slope as the elastic modulus, but offset by 0.2% strain.

To determine whether strain rate significantly affected testing outcomes, eight specimens

were tested at three separate strain rates (0.000167 sec^{-1}, 0.00033 sec^{-1}, and 0.0005 sec^{-1}). The slow and medium loads were performed in the elastic region only, with a maximum force of 35 N (ε<0.15%). Each specimen was then tested to failure using the fastest strain rate.

RESULTS AND DISCUSSION

The stress-strain curves (Figure 2) generated by the four-point bending tests can be divided into two portions – a linear elastic, and a non-linear plastic section. At low strains (up to typically ε=0.6%) emu cortical bone exhibited elastic behavior. At higher strains the bone experienced plastic deformation and yield. Elastic modulus and yield stress and strain data are summarized in Table 1. At α=0.05, there was no significant dependence of elastic modulus or failure stress on donor femur (p=0.0928 for E and p=0.1246 for σ_y, both determined using MANOVA). Additionally, there was no significant dependence of E or σ_y on specimen harvest site. Also using MANOVA, anterior versus posterior E was found to have p=0.945, and σ_y had p=0.485. Medial versus lateral E had p=0.264, and σ_y had p=0.459.

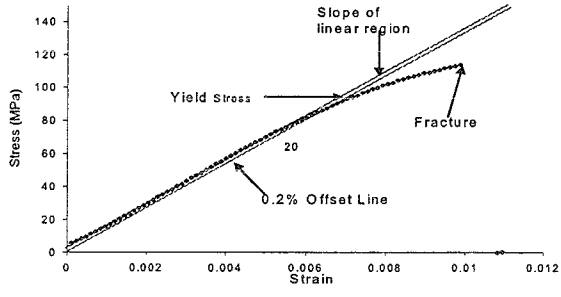

Figure 2: Typical stress-strain curve, terminating in brittle fracture for a trial

Roughly half of the bones experienced a brittle failure (i.e. snapped in half), while the other half lost all internal strength, but did not abruptly separate into two distinct fragments. There was no significant difference in E or σ_y between specimens which fractured into two distinct fragments versus those which did not (p=0.655 for E, p=0.274 for σ_y). Although the stress-strain curves for emu cortical bone were generically similar to those of human cortical bone, emu E, σ_y, and σ_{ult} were below mammalian levels. They fell in the range of other avian species (E=13.2 GPa for geese (McAlister, 1983), 16.95 GPa for turkeys (Ricos, 1996), 13.62 GPa for ostriches, and 13.43 GPa for "domestic fowl" (Yamada, 1970)) despite emu adaptation for bipedal terrestrial gait rather than flight.

Table 1: Elastic modulus E (GPa), yield y and ultimate ult strength σ (MPa), and yield and ultimate strain ε (%), as a function of harvest site, donor, and loading rate. Parenthesized values are standard deviations.

Variable, N	E	σ_y	σ_{ult}	ε_y	ε_{ult}
Anterior, 18	12.53 (3.09)	111.81 (26.79)	148.46 (23.49)	0.73 (0.18)	1.41 (0.46)
Posterior, 13	12.27 (5.01)	104.11 (32.59)	142.35 (44.63)	0.71 (0.12)	1.32 (0.16)
Medial, 14	11.22 (3.81)	104.86 (29.63)	136.12 (30.46)	0.78 (0.16)	1.31 (0.31)
Lateral, 17	13.23 (3.78)	112.54 (28.81)	153.81 (34.53)	0.72 (0.22)	1.35 (0.41)
Proximal, 16	13.03 (4.10)	120.84 (20.74)	158.77 (31.05)	0.74 (0.19)	1.34 (0.40)
Distal, 23	13.06 (3.92)	108.28 (28.94)	139.53 (31.26)	0.73 (0.17)	1.26 (0.34)
Bird #1,10	11.33 (4.83)	115.29 (33.63)	139.92 (35.78)	0.87 (0.22)	1.31 (0.35)
Bird #2, 11	12.66 (3.83)	111.96 (28.94)	153.63 (37.14)	0.70 (0.20)	1.35 (0.34)
Bird #3, 10	12.95 (2.92)	101.11 (21.70)	140.45 (25.74)	0.67 (0.08)	1.42 (0.42)
Birds #4 and #5, 8	15.86 (2.99)	126.54 (29.87)	154.6 (29.84)	0.68 (0.08)	1.03 (0.20)
Slow Load,8	13.05 (2.51)	N/A	N/A	N/A	N/A
Medium Load, 8	14.14 (2.57)	N/A	N/A	N/A	N/A
Fast Load, 8	15.86 (2.99)	126.54 (29.87)	154.6 (29.84)	0.68 (0.08)	1.03 (0.20)
Whole Series, 39	13.05 (3.94)	113.11 (29.15)	146.93 (32.20)	0.73 (0.18)	1.29 (0.36)

ACKNOWLEDGEMENTS

NSF Graduate Research Fellowship, NIH Grant #AR46601

REFERENCES

Conzemius et al. *ORS Proceedings* (2000) p. 206

McAlister et al. *J. Biomech*, (1983) **3**, 577-589

Ricos, V. et al. *J. Biomech,* (1996) **2**, 261-267

Yamada; *Strength of Biological Materials*, Williams & Wilkins Company, Baltimore 1970

ENERGY-BASED FRACTURE SEVERITY ASSESSMENTS IN CORTICAL BONE

Christina L. Beardsley[1], J. Lawrence Marsh[2], Thomas D. Brown[2,1]

Departments of [1]Biomedical Engineering and [2]Orthopaedic Surgery
University of Iowa, Iowa City, IA
Email: christina-beardsley@uiowa.edu Web: poppy.obrl.uiowa.edu

INTRODUCTION

At present, clinical fracture comminution severity assessments must rely on subjective visual judgements that are wrought with poor inter-observer reproducibility. It is our contention that actual *quantification* of comminution severity is possible, based on two key concepts: first, that the area of fracture surface created is proportional to the energy absorbed in crack propagation, and second, that computed tomography (CT) provides the capability for measuring fracture surface area. To explore these concepts, we conducted variable energy impactions of bovine cortical bone segments. Imaging the resulting fragments with a clinical CT protocol, we hypothesized that the fragment sets from impactions at higher energy levels would have a higher total interfragmentary area, and that the proportionality between fracture energy and liberated surface would be similar between groups.

PROCEDURES

Fresh frozen tibiae, harvested from skeletally mature cows, were cut into approximately 70 mm-long segments. These pieces were then milled to produce two parallel faces. Prior to impaction, CT data were collected of the bone segments using a standard orthopaedic protocol. Tare surface area of the parallel faces and endosteal and periosteal surfaces was computed for each intact specimen using digital image analysis. Drop tower testing was then conducted at two distinct energy levels (0.423 J/g (n=7) and 0.702 J/g (n=6)). Specimen fragments were gathered from a collection chamber in the drop tower. They were then suspended in a specially prepared resin, which mimicked the approximate CT Hounsfield density of soft tissue. Helical CT data were collected of these preparations, again using a standard orthopaedic protocol, and they were reconstructed at 1-mm intervals. Surface area measurements were extracted slice by slice for each fragment, using a custom-written digital image analysis algorithm (Figure 1). These values were summed for each fragment and then the original surface area of the intact specimen was subtracted. The fragment size (including new and original surface) distributions were plotted for each of the two groups (Figure 2). Also, the number of square millimeters liberated per input Joule (i.e., energy -to-surface conversion factor) was calculated for each specimen. *De novo* surface area was compared using a one-tailed, homoscedastic Student's t-test to test the hypothesis that the liberated surface area was greater in the specimens subjected to higher energy impacts. A two-tailed, homoscedastic Student's t-test was used to test for differences in surface production per unit energy absorption.

RESULTS AND DISCUSSION

The surface generated (Table I) in the specimens which absorbed greater energy was statistically significantly higher ($p=0.011$) than the *de novo* area in the lower energy group. Furthermore, as expected from engineering fracture mechanics, the energy-to-surface conversion factor was

indistinguishable (p=0.917) between the two groups.

The fragment size distribution plots (Figure 1) show that with higher energy impacts, the majority of surface area is comprised of fragments that each contribute less than 10% of the total specimen surface area. Conversely, over 60% of the surface area in the lower energy group is contributed by large fragments (fragments that singly constitute over 30% of the total specimen surface area). The fragment size distributions for the two groups of fragment sets follow the principles of comminution that have been observed in other materials. That is, higher energy absorption produces a greater number of small fragments.

Just as the delivered energy per specimen differed by about a factor of two, the liberated surface area of the higher energy group was also about twice that of the lower group. To the extent that the fracture event follows the theoretical ideal of directly converting impact energy into fragment free surface area, one would expect that the "conversion coefficient" would be independent of energy absorption. In that vein, it was noteworthy that the number of square millimeters produced per absorbed Joule from the present specimen groups was statistically indistinguishable.

This study demonstrates that, using CT-based measures of interfragmentary surface area, it is possible to objectively quantify cortical bone comminution severity. Extending this paradigm to the clinical realm holds the attraction of improved assessment of treatment efficacy, since injury severity could be better accounted for when comparing outcomes.

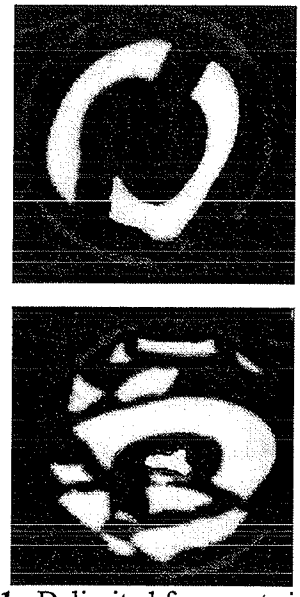

Figure 1. Delimited fragments in typical CT slices from low (top) and high groups.

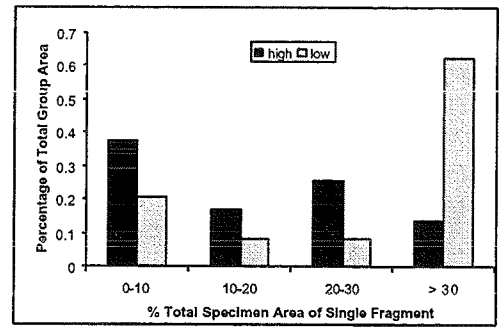

Figure 2. Fragment size distribution plot.

ACKNOWLEDGEMENTS

Ms. Christine Bertsch assisted in testing. Mr. William Lack assisted in specimen preparation. Financial support provided by EBI, Inc. and NIH grant #AR46601.

Table I. Liberated surface area and energy-to-surface conversion in shattered tibial segments.

Energy Input (J/g)	Liberated Surface Area (mm^2)	Energy-to-Surface Conversion (mm^2 per J)
0.423 ± 0.009	7672 ± 6700	194.8 ± 171.2
0.702 ± 0.026	17981 ± 7272	202.9 ± 70.8

Upper Extremity Kinematics and Reaction Forces Associated with a Novel Osteoporosis Intervention Program

Man-Ying Wang, George Salem, and Yi-Ju Tsai, Cliff Fornwalt, and Christopher Powers

Musculoskeletal Biomechanics Research Laboratory, University of Southern California, Department of Biokinesiology & Physical Therapy, Los Angeles, CA
Email: mwang@usc.edu Web: www.usc.edu/go/mbrl

INTRODUCTION

Age-related osteoporosis increases the risk of fracture, disability, and physical dependence. The estimated lifetime risk of distal forearm fractures in white women and men are 16% and 2.5%, respectively. Although human research studies have assessed the relations between exercise and bone mass in the distal radius (Simkin, 1987), none have characterized the relations between osteogenesis and mechanical loading factors. Animal studies suggest that mechanical loading characteristics that are 1) dynamic, 2) of a high magnitude, 3) of a high loading rate, and 4) exhibit an unusual strain distribution, are optimal for osteogenesis (Chilibeck, 1995). In an effort to bridge the gap between these animal and human studies, we developed an upper-extremity dynamic-impact loading model. This paper reports the upper extremity kinematics and reaction forces associated with this novel osteoporosis intervention program.

METHODS

These data were collected as part of a subgroup analysis of an upper-extremity osteoporosis intervention trial. Five healthy adults (25-29 yrs) performed the dynamic impact loading exercise (DILE) with their right arm at a distance of 40cm between the carpal surface and the wall (Fig.1). Reflective markers were applied to bony landmarks of the upper extremity and the participants performed three loading trials each. Three-dimensional coordinates of the exercise arm were recorded from a six-camera (60 frames/sec) motion analysis system (Vicon 370, Oxford Metrics, Oxford, UK). Reaction forces, including peak loads and loading rates, were collected from a force platform secured to the wall (AMTI, Watertown, MA) at 1200Hz. Data processing software, (Polygon and BodyBuilder; Oxford Metrics, Oxford, UK), was used to calculate the joint kinematics of the wrist and elbow (i.e., peak joint angle and joint angle change) during the loading phase of the exercise. Peak reaction forces and loading rates were calculated using Peak Fit (SPSS Inc., Chicago, IL, USA). Intraclass correlation coefficients (ICCs) of the sagittal-plane peak joint angles, joint angle changes, and perpendicular reaction forces were generated to assess the within-day and between-day reliability of the DILE.

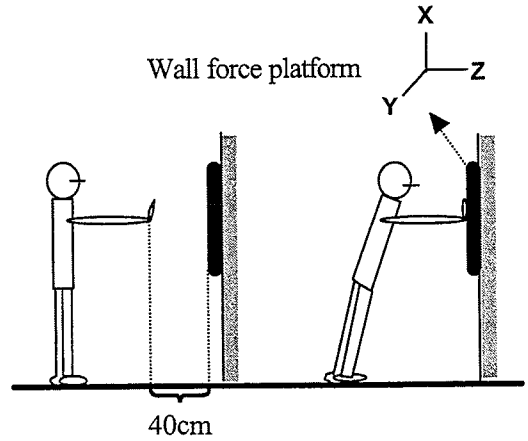

Figure 1: Dynamic impact loading exercise

RESULTS AND DISCUSSION

Within-day and between-day ICCs were excellent (.86-.97) for peak loads and loading rates perpendicular to the wall. Within-day and between-day ICCs were also high (.77-.99) for peak joint angles and joint angle changes at the elbow and wrist. These results suggest that the DILE is reproducible. Figures 2 and 3 illustrate the perpendicular reaction forces and joint kinematics during the loading phase of the exercise.

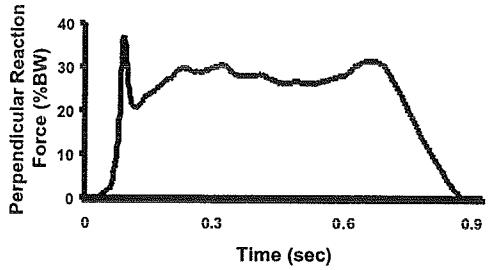

Figure2: Perpendicular reaction force (Z) of a representative subject.

Characteristically, the perpendicular reaction forces increased and then dropped dramatically within 0.1 second, resulting in an early peak load and high loading rate. The drop in force was accompanied by increased wrist and elbow flexion (Table 1), suggesting that the loading energy was absorbed during the upper-extremity joint excursions and potential eccentric muscle actions. Peak vertical shear force (X) and peak horizontal shear force (Y) were 15.4% and 14.6% of the perpendicular peak load (Z), respectively (Table 2).

SUMMARY

The DILE produces reliable joint kinematics and reaction forces in the upper extremity. It is easy to perform, and requires no equipment, supervision, or participant travel; thus, this type of exercise program may prompt longer-term adherence. This study is an important step in the development of a biomechanics-based osteoporosis intervention program, seeking to: 1) quantify musculoskeletal loading during exercise, 2) examine the relations between mechanical loading events and bone adaptation, and 3) assess the applicability of the DILE. Further studies should examine the efficacy of this novel osteoporosis intervention program and quantify glenohumeral excursions during the activity (a kinematic model of the gleno-humeral joint is currently being developed).

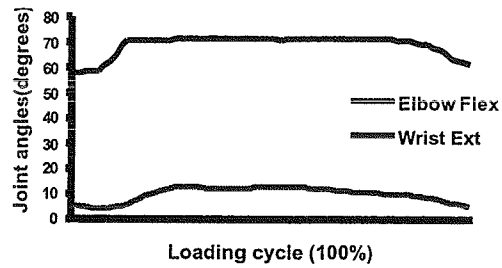

Figure 3: Elbow and wrist joint kinematics of a representative subject during the loading event.

Table 1: Joint kinematics of the elbow and wrist during loading phase of DILE.

	Elbow	Wrist
Peak angle	17.5±8.1	70.0±4.3
Angle change	13.0±4.8	18.0±4.2

REFERENCES

Simkin, A. et al. (1987). *Calcif Tissue Int,* **40**, 59-63.

Chilibeck, P.D. et al. (1995). *Sports Med,* **19**, 103-122.

Table 2: Three dimensional reaction forces during the loading phase of DILE.

	Peak Load (Z)	Peak Load (X)	Peak Load (Y)		Loading Rate (Z)
BW	39.6±12.7%	6.1±3.5%	5.7±1.5%	N/sec	4258.1±2232.9

THE RELATIONSHIP BETWEEN THE FRACTURE TOLERANCE OF FEMORAL CORTEX AND BONE DENSITY BY QCT

Ann E. Mallory, [1,2] Edward Ebramzadeh [1] and Lawrence Dorr [3]

[1]The J Vernon Luck Center for Orthopaedic Research, Los Angeles Orthopaedic Hospital, Los Angeles, CA, USA
[2] Biodynamics Engineering, Inc., Pacific Palisades, CA, USA
[3]The Dorr Arthritis Institute of Centinela Hospital, Inglewood, CA, USA
E-mail: annm@biodynamics-eng.com

INTRODUCTION

Femoral fracture risk is of great clinical significance because of the frequency and high morbidity of hip fractures. Identification of patients with increased fracture risk requires an understanding of the relationship between fracture tolerance and bone density. This relationship, however, is confounded by variation in bone geometry among patients, which affects the material and structural properties of whole bones.

The effects of bone density on the mechanical properties of femoral cortical bone have been isolated by performing strength testing on specimens machined to regular dimensions (Dickenson, et al. 1981; Lotz, et al. 1991; Wall, et al. 1979). These prior studies have used invasive methods to measure bone density. In the current study of femoral cortex breaking properties, non-invasive quantitative computed tomography (QCT) was used to measure bone density, allowing results to be compared to density measures taken *in vivo*.

METHODS

Rectangular specimens with nominal dimensions of 2 mm x 2 mm x 40 mm were harvested from each quadrant of the distal shaft of 10 fresh-frozen cadaveric femora. Where the cortex was thinner than 2 mm, smaller specimens were obtained.

Bone density was measured for each specimen using a Stratec XCT 3000 Research QCT scanner (Stratec, Pforzheim, Germany). Analysis was performed at the mid-point, with the cortical threshold set at 690 mg/cm^3.

Three-point bending tests on the femoral specimens were performed on an MTS materials testing machine (858 Mini Bionix, MTS Systems Corporation, Eden Prairie, MN), using a gauge length of 30 mm. Specimens were loaded to failure at a strain rate of 0.1 second^{-1} in order to simulate the typical strain rate in an osteoporotic fracture.

Force was measured with a 25-pound load cell (Futek, Irvine, CA). Deflection was measured from high-speed video at 2000 frames per second and by an extensometer mounted to the bending jig with a measuring prong suspended below the specimen. Force-deflection data was used to calculate elastic modulus (E), strength (S_{ULT}), and strain energy per unit volume (SE_V). Correlation analysis was performed using SAS statistical software (SAS, Cary, NC).

RESULTS AND DISCUSSION

Mean bone density of the specimens was 1163 mg/cm^3 (σ^2=78), with a range of 913 to 1274 mg/cm^3. Table 1 contains a summary of the mechanical properties determined in

three-point bending, along with the correlation of these properties to bone density. Scatterplots showing the relationship between bone density by QCT (D_{QCT}) and the mechanical properties are shown in Figure 1.

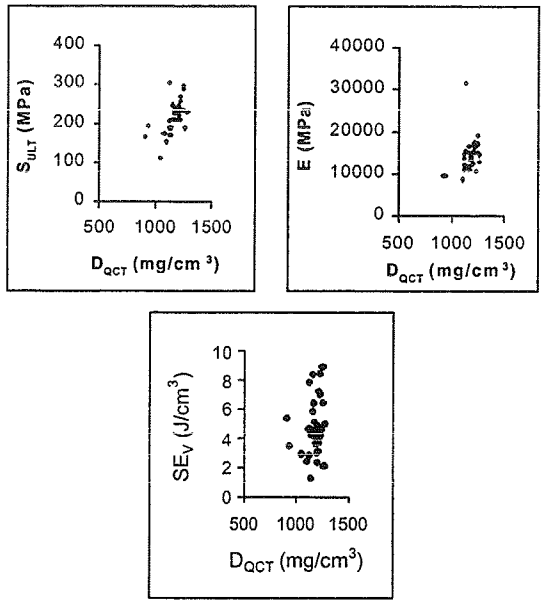

Figure 1: Scatterplots of mechanical properties versus bone density by QCT.

Correlation between femoral cortical strength and bone density by QCT was stronger in the current study than in a prior study of tibiae that employed computed tomography (CT) to measure density. (Snyder and Schneider 1991). Although density measures are not directly comparable, the relatively strong correlation of strength and density identified in this study, along with the wide range of mechanical properties, suggests that the specimens may have been more widely distributed in density than in prior studies.

The moderate correlation between specimen strength and density-related parameters in this study and in prior studies indicates that half or more of the variation in the material strength of cortical bone is explained by variation in density. Additional bone quality factors, not reflected in density measurements, may have substantial effects on the material strength of cortical bone. For the whole bone, these effects are added to the variation in structural strength related to bone geometry.

A specimen's toughness, reflected in its SE_V, describes its ductility and its strength. Bone density's moderately strong correlation with strength and its very weak correlation with SE_V, suggest that reduced bone ductility is not associated with reduced bone density but is more likely related to other age-related changes.

REFERENCES

Dickenson, R.P. et al. (1981). *J Bone Jt Surg* **63-B**, 233-238.

Lotz, J. C. et al. (1991). *J Biomech* **24**, 317-29.

Snyder, S.M., Schneider, E. (1991). *Journal of Orthopaedic Research* **9**, 422-431.

Wall, J.C. et al. (1979). *Calcified Tissue International* **27**, 105-108.

Table 1: Summary of mechanical properties and correlation to bone density.

	Mean (σ^2)	Range	Spearman Correlation Coefficient with Bone Density by QCT
E (MPa)	14,399 (4001)	8739-31,708	0.643 ($p<0.0001$)
S_{ULT} (MPa)	217 (41.1)	114-305	0.506 ($p=0.0027$)
SE_V (J/cm^3)	4.76 (1.92)	1.29-8.93	0.186 ($p=0.292$)

RELATIVE CONTRIBUTIONS OF MATERIAL CHARACTERISTICS TO FAILURE PROPERTIES OF CORTICAL BONE IN STRAIN-MODE-SPECIFIC LOADING: IMPLICATIONS FOR FRAGILITY IN OSTEOPOROSIS & AGING

J.G. Skedros[1], K.J. Hunt[1], M.T. Dayton[1], R.D. Bloebaum[1], K.N. Bachus[2]

[1]Bone and Joint Research Laboratories, Veterans Affairs Medical Center, Salt Lake City, Utah
[2]Orthopedic Bioengineering Research Laboratory, University of Utah, Salt Lake City, Utah
Email: jskedros@utahboneandjoint.com

INTRODUCTION

Recent studies of mechanical properties of cortical bone in osteoporotic and aged skeletons reveal significant reductions in toughness or energy absorption -- a hallmark of post-yield behavior (McCalden et al., 1993). Variations in mineral content (% ash), porosity, or secondary osteon population density (OPD), however, can not explain a large percentage of the variance in these mechanical test data. Additional material characteristics may also be important, including osteon cross-sectional area, osteon shape, and fractional area of secondary bone (FASB) (cement line interfaces). The artiodactyl (deer) calcaneus is an ideal model for investigating the relative contributions of various material characteristics because it has remarkable regional (i.e., within the same cross-section) variability in material organization. Recent studies have shown significant regional differences in %ash, OPD, FASB, porosity, osteon cross-sectional area, and osteon shape (Skedros et al., 1994a,b, 1997). These differences are greatest between cortices that experience primarily compression (cranial) or tension (caudal) loads.

In this study we examined the influence of multiple *material* characteristics on the pre- and post-yield behaviors of cortical bone of deer calcanei in the context of habitual in vivo "strain-mode-specific" loading (e.g., *compression testing* bone from a habitually *compressed* region). Evaluating mechanical influences of such histologic variables in the context of a habitual loading mode is important since: 1) in vivo studies have shown that long bones of all animals studied receive directionally consistent bending during typical daily gait-related activities (Biewener, 1993), and 2) cortical bone is substantially stronger and stiffer, has different fatigue behavior, and likely has greater toughness in compression than in tension.

METHODS

One calcaneus was obtained from each of 19 skeletally mature mule deer. Using a coring bit, one 3.0mm diameter, 5.0mm-height cylindrical specimen was removed from each cranial cortex of eight randomly selected bones. From the remaining calcanei, one specimen of each caudal cortex was milled into a dumbbell shape for tension testing (Riggs et al., 1993) with a gauge length of 10mm.

Compression tested cylindrical specimens were loaded to failure along the long axis of the bone (long axis of the cylinder) at a strain rate of $0.003sec^{-1}$. (Testing machine: Model 1125, Instron Corp., Canton, MA; 5kN-load cell)

Tension tested dumbbell-shaped specimens were aligned in grips, and an extensometer (MTS 632.13F-20, MTS Corp., Minneapolis, MN) was used for measuring displacement.

Elastic (to yield), plastic, and total (elastic + plastic; to ultimate stress) energy

absorption were calculated for both tension and compression loading. Fragments from near the fracture sites were examined for: 1) %ash at 550°C, 2) porosity, 3) OPD, 4) FASB, 5) osteon cross-sectional area, and 6) osteon cross-sectional shape.

RESULTS (Multivariate Analyses)

Elastic energy absorbed (to yield stress). Compression-specific loading showed that the greatest percentage of variance (43%; where total explained = 46%) was attributable to osteon area ($r = 0.817$, $p=0.02$) and OPD ($r = -0.807$, $p=0.02$). In tension-specific loading, all variables explained only 27% of variance.

Plastic energy absorbed (Total – Elastic). Compression-specific loading showed that the greatest percentage of variance (71%; where total explained = 72%) was attributable to OPD ($r = 0.834$, $p=0.02$), %ash (N.S. = non-significant, $p > 0.1$), and osteon shape (N.S.). Tension-specific loading showed that the greatest percentage of variance (72%; where total explained = 84%) was attributable to OPD (N.S.), osteon area (N.S.), and osteon shape (N.S.).

Total energy absorbed (to ultimate stress). Compression-specific loading showed that the greatest percentage of variance (40%; where total explained = 54%) was attributable to porosity ($r = 0.691$, $p = 0.085$) and %ash (N.S.). Tension-specific loading showed that the greatest percentage of variance (79%; where total explained = 81%) was attributable to OPD (N.S.), osteon area (N.S.), osteon shape (N.S.), and %ash (N.S.).

DISCUSSION

Only in compression-specific loading were significant correlations shown with the microstructural characteristics (osteon area and OPD). The conspicuous lack of statistical significance and inconsistent associations with the material characteristics and mechanical properties suggest that: 1) there is insufficient statistical power to demonstrate an effect, or 2) there are additional characteristics that more strongly, and consistently, explain the variance in these data. We favor the latter explanation. For example, predominant collagen fiber orientation has been shown to be preeminent in explaining the variance in energy absorption in strain-mode-specific loading of cortical bone from horse third metacarpals (Skedros et al., 2000). Microscopic mineral heterogeneity and the percentage of intermolecular collagen cross-links should also be targeted for investigation. There are data suggesting that such differential tissue organization might be expected, and beneficial in a biomechanical context, since notable disparities in microdamage accumulation can occur in "compression" vs. "tension" cortices during physiologic loading (Reilly et al., 1997, 1999). The skeletal fragility seen in osteoporosis and aging may be strongly influenced by microdamage accumulation in poor quality bone, since impaired homeostatic remodeling processes do not maintain tissue with normal material properties.

REFERENCES

Biewener, A.A. (1993). *Calcif. Tissue Int.*, **53(Suppl. 1)**:S68-S74.

McCalden, R.W., et al. (1993). *J. Bone Joint Surg.*, **75-A**:1193-1205.

Reilly, G.C., et al. (1997). *J. Orthop. Res.*, **15**:862-868.

Reilly, G.C., and Currey, J.D. (1999). *J. Experimental Biol.*, **202**:543-552.

Riggs, C.M., et al. (1993). *Anatomy and Embryol.*, **187**: 239-248.

Skedros, J.G., et al. (1994a,b, 1996, 1997). *The Anat. Record*, **239**:396-404, 405-413; **246**:47-63; **249**:297-316.

Skedros, J.G. et al. (2000). *Trans. 24th Am. Soc. Biomech.*, 173-174.

BIOMEDICAL AND FLUID FLOW CHARACTERIZATION OF MICRONEEDLE-BASED DRUG DELIVERY DEVICES

Ishaq Haider[1], Ronald J. Pettis[1], Norman Davison[2], Richard Clarke[1] and Jeffrey D. Zahn[3]

[1] BD Technologies, Research Triangle Park, NC [2] BD Visitech, Sarasota, FL
[3]Berkeley Sensor & Actuator Center, UC Berkeley, CA
E-mail: ihaider@bd.com

INTRODUCTION

The expanded development of biotechnology and genome-derived drugs has necessitated concomitant development of advanced drug delivery methods. Microdermal Delivery Devices (MDDs), utilize microscopic cannula (microneedles) to establish a biological interface for drug delivery while avoiding the psychological and physical discomfort often associated with traditional needles and syringes (Figure 1). However, efficient usage of such devices

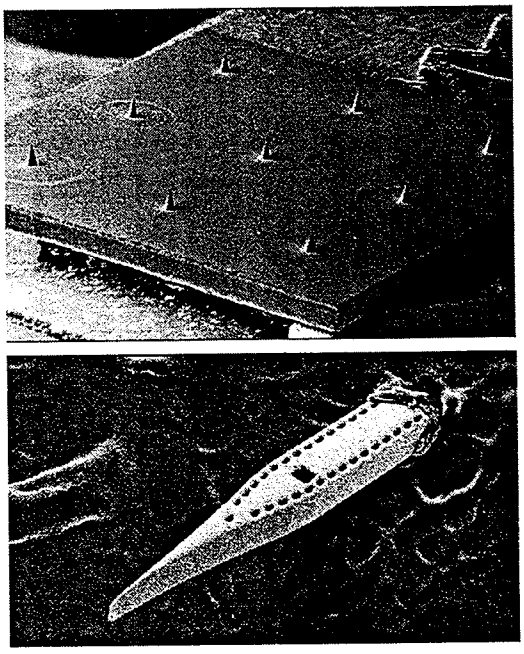

Figure 1: Photomicrographs of silicon microneedle drug delivery systems.

requires an understanding of the biomechanical forces involved in the skin penetration, and fluid flow properties of these systems. Since most biotech drugs are large macromolecules with complex folding structures, transport through MDDs could result in shear-induced protein denaturation resulting in drug inactivation or potency loss.

METHODS

MDDs were prepared using various materials and methods, including: micromachining, proprietary silicon etching techniques, and silicon vapor deposition micromolding. Internal lumen diameters ranged from 20-80 micron and external diameters were up to 200 micron. Various MDD designs incorporated from 1-10 individual microneedles, arranged in a variety of array configurations and inter-needle spacings. Standard gauge stainless steel needles (25-31 G) were used for comparative purposes. Relative penetration forces were examined using model polymer membranes and harvested swine skin. Forces were measured at a constant penetration rate and a 90° insertion angle, using an Instron automated force transduction system. Fluid flow through MDDs was controlled using a Harvard syringe pump, and pressure data was gathered with an instrumented pressure transduction system. Investigated variables included MDD lumen diameter, fluid flow rate, fluid viscosity, and outlet back-pressure to simulate a biological system. Shear stress was calculated based on volumetric flow parameters. The model protein drugs insulin and β-galactosidase were collected after

passage through MDDs. Physical stability was measured via liquid chromatographic methods, and functional activity was assessed via enzymatic assays.

RESULTS AND DISCUSSION

A strong correlation exists between penetration force, needle size and penetration depth (Figure 2). A reduction in needle diameter and length was shown to lower the penetration force requirements. Increased inter-needle spacing also reduces penetration forces.

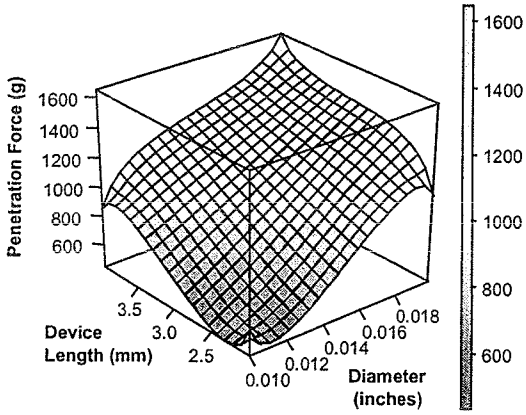

Figure 2: Penetration force response as a function of microneedle size and length at a constant 1.5 mm inter-needle spacing.

Fluid flow through MDDs was determined to be Newtonian and laminar. Experimental data correlates well with flow parameters calculated using the Hagen-Poiseuille Equation:

$$Q = \pi(P_O - P_L)\, R^4/8\mu L$$

where Q is the volumetric flow rate, μ is the fluid viscosity, P_O is the pressure at needle entrance, P_L is the pressure at needle exit, R is the inner radius and L is the fluid path-length. Since the pressure drop is inversely proportional to the 4th power of the radius, the pressure requirements for fluid delivery through MDDs was significantly increased relative to standard gauge needle cannula ($\geq$ 31G diameter), even though the path length is significantly reduced. To reduce the pressure drop required, additional micro-needle channels were incorporated in the exit flow path, thus increasing the effective cross-sectional area (Figure 3). Unlike insertion force, flow performance was independent of inter-needle spacing.

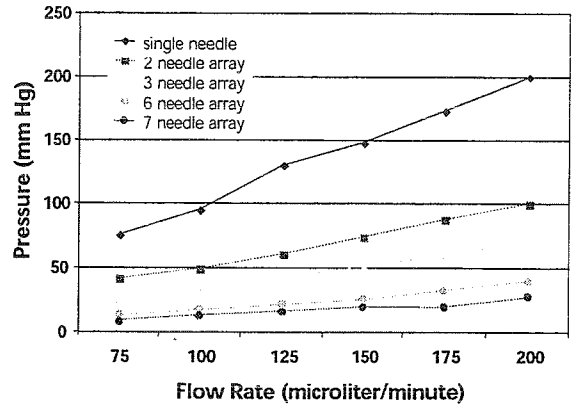

Figure 3: Pressure-flow rate relationships for MDDs containing from 1-7 individual microneedles of 75 μm internal diameter.

Calculated mass average shear values through MDDs was below the predicted threshold for producing protein degradation (Charm and Wong). Physical and functional assays of model proteins showed absolute recovery after passage through MDDs.

SUMMARY

Our findings demonstrate that MDDs have excellent potential as drug delivery systems, providing both reduced sensation for patients and effective delivery of biotech therapeutic compounds.

REFERENCES

Charm and Wong. (1970). *Biotechnol. and Bioengin.*, **12**, 1103-1109.

ENERGETICS OF LOW SPEED RUNNING

Alan Hreljac, Daryl Parker, Roberto Quintana, Estelle Abdala, Kyle Patterson, and Mitell Sison

Kinesiology and Health Science Department
California State University, Sacramento
E-Mail: ahreljac@hhs4.hhs.csus.edu

INTRODUCTION

The metabolic cost ($\dot{V}O_2$) of walking a given distance is minimized at a speed of approximately 1.25 m· s $^{-1}$ while the metabolic cost of running a unit distance is essentially independent of speed (Cavagna et al., 1976; Hreljac, 1993; Margari a et al., 1963). As a result, energy -speed curves for running are generally depicted as being linear with a slope of close to zero. Energetic cost -speed curves for running are generally determined by having subjects run at a variety of speeds greater tha n a subject's preferred transition speed (PTS) while monitoring $\dot{V}O_2$. A curve (line) is then fit to the data before extrapolating the curve to lower speeds. The intersection of the energy -speed curve for walking (curvilinear) and running (line ar) is considered to be the energetically optimal transition speed (EOTS), occurring at a speed of about 2.3 m· s $^{-1}$ (Hreljac, 1993). The PTS occurs at a significantly lower speed than the EOTS (Brisswalter et al., 1996; Hreljac, 1993; Minetti et al., 1994) . Since the energetic cost per unit distance approaches infinity as running speed approaches zero, it is logical to assume that the energy -speed relationship at low running speeds (below the PTS) would be non -linear. The purpose of this study was to determine whether energy -speed data during running conform better to a curvilinear (quadratic) or a linear model, and to determine the effect of model choice on the calculation of EOTS.

METHODS

Twelve young, healthy subjects (6 males, 6 females) were accommod ated to treadmill locomotion prior to determination of their walk -run, and run -walk transition speeds. Each transition speed was found three times in random order, then averaged to give an overall PTS, as described in earlier studies (Brisswalter et al., 1996; Hreljac, 1993, 1995). On a day following this procedure , $\dot{V}O_2$ data were collected as subjects ran at speeds of 60, 75, 90, 100, and 120% of the PTS, and walked at 70, 80, 90, 100, and 110% of the PTS. Exercise $\dot{V}O_2$ for each of the randomly ordered conditions was found by subtracting standing $\dot{V}O_2$ values from gross $\dot{V}O_2$. All $\dot{V}O_2$ data were then normalized to body mass and speed. Energy -speed curves were fit (all subjects combined) to the normalized data points for both walking and running with speed (in units of %PTS) along the abscissa and $\dot{V}O_2$ (units of ml· kg $^{-1}$· km $^{-1}$) along the ordinate . Both linear and quadratic models were tested for each gait using a least squares regression method.

RESULTS AND DISCUSSION

At the PTS (1.99 ± 0.12 m· s $^{-1}$), the energetic cost was significantly greater during running ($\dot{V}O_2$ = 155.1 ± 14.0 ml· kg $^{-1}$· km $^{-1}$) than walking ($\dot{V}O_2$ = 132.7 ± 18.9 ml· kg $^{-1}$· km $^{-1}$). A quadratic model fit the data better than a linear model for

both walking ($r^2 = 1.00$) and running ($r^2 = 0.94$) conditions. Minimum values of $\dot{V}O_2$ for the fitted curves occurred at 61.6% of PTS, and 96.2% of the PTS during walking and runnin g, respectively. The curves intersected (EOTS) at a speed of 110% of the PTS. The regression plots of the energy -speed relationships for each condition are illustrated in Figure 1.

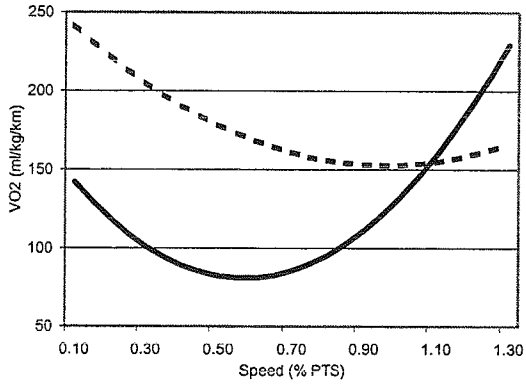

Figure 1: Relationship between $\dot{V}O_2$ per unit distance and speed (as a % of PTS) for walking (—) and running (- - -).

In this study, the speed of the minimum $\dot{V}O_2$ during walking (1.23 m· s^{-1}) was close to speeds previously reported (Cavagna et al., 1976; Hreljac, 1993; Margaria et al., 1963), while the minimum $\dot{V}O_2$ during running occurred at a speed near the PTS. The regression equation relating the $\dot{V}O_2$ to walking speed could be fit almost perfectly ($r^2 = 1.00$) to a quadratic model (Fig. 1). A curvilinear (quadratic) model ($r^2 = 0.94$) was found to represent the energy -speed data for running better than a linear model ($r^2 = 0.29$) at the low speeds tested. This relationship would likely be found only when very low running speeds are tested. The minimum $\dot{V}O_2$ of the best fitting curve during running occurred at a speed of 1.92 m· s^{-1} (96.2% of PTS) which is lower than speeds that have generally been tested by other researchers who have examined the relationship between $\dot{V}O_2$ and running speed.

The EOTS calculated in this study was not affected by running model choice, and was in agreement with prior studies (2.20 vs. 2.24 m· s^{-1}). The linear model calculated for running exhibited a negative slope, and was a poor fit. In previous studies (Hreljac, 1993; Minetti et al., 1994), running curves (lines) were depicted with slight positive or zero slopes.

SUMMARY

Combining evidence from previous studies with the results of the present study, it appears that the true energy - speed curve for runnin g is linear (and relatively constant) for most mid -range speeds, but increases in a curvilinear fashion when running speeds are at the extreme low and high ranges. The EOTS was not affected by the choice of regression model used during running, which help s to validate previously reported results.

REFERENCES

Brisswalter, J., Mottet, D. (1996). *Can. J. Appl. Physiol.*, **21**, 471-480.

Cavagna, G.A et al. (1976). *J. Physiol., London* **262**, 639-657.

Hreljac, A. (1993). *Med. Sci. Sports Exerc.*, **25**, 1158-1162.

Hre ljac, A. (1995). *J. Biomech.*, **28**, 669-677.

Margaria, R. et al. (1963). *J. Appl. Physiol.*, **18**, 367-370.

Mercier, J., et al. (1994). *Eur. J. Appl. Physiol.*, **69**, 525-529.

Minetti, A.E, et al. (1994). *Acta Physiol. Scand.*, **150**, 315-323.

EXTERNAL LATERAL STABILIZATION REDUCES METABOLIC COST OF WALKING

David W. Shipman [1], J. Maxwell Donelan [1], Rodger Kram [2], and Arthur D. Kuo [3]

[1] Dept. of Integrative Biology, University of California, Berkeley;
[2] Dept. of Kinesiology and Applied Physiology, University of Colorado, Boulder;
[3] Dept. of Mechanical Engineering & Applied Mechanics, University of Michigan, Ann Arbor
Email contact: david.shipman@alum.mit.edu

INTRODUCTION

Human walking appears to be laterally unstable (Kuo & Bauby, 1998). This requires active control involving muscle actions and thus, a metabolic cost. Our purpose was to quantify how much metabolic energy is associated with maintaining balance during walking. We hypothesized that providing external lateral stabilization would reduce the metabolic cost of walking.

We designed an apparatus to add external lateral stabilization for subjects walking on a treadmill. At zero step width, stabilization reduced metabolic cost by an average of 6%. We also found that stabilization reduced the preferred step width by an average of 41%.

METHODS

Ten healthy adults (6 male, 4 female) participated in the study after providing informed consent. Prior to the experimental trials, subjects practiced the experimental protocol. Subjects walked on a treadmill set to 1.25 m/s, both with and without external stabilization. We measured the subject's preferred step frequency and step widths. During the experimental trials, we enforced step frequency using a metronome set to the previously determined preferred step frequency. We had the subjects follow lines marked on the treadmill belt to enforce various step widths, including zero step width and the subject's stabilized and unstabilized preferred widths.

The external lateral stabilizer consisted of cords attached to the subject's waist pulling elastically in both lateral directions (fig. 1). Subjects wore a padded waist belt similar to that used with hip-supported backpacks. We attached lightweight nylon cord with adjustable straps to the sides of the belt extending laterally approximately 8 m. These ended in sections of elastic tubing approximately 0.5 m in length, anchored to the side walls. The apparatus exhibited an effective spring constant of 1700 N/m and an effective damping constant of 14 N-s/m. The relatively long side cords insured that any non-lateral forces exerted by the apparatus were negligible. Because the side cords prevent normal arm swinging, we had the subjects keep their arms crossed during all trials whether externally stabilized or not.

We measured net ground reaction forces and moments along 3 geometric axes as subjects walked on a force treadmill (Kram, et al., 1998). In-line force transducers on the

Figure 1: Lateral Stabilization Apparatus (Color movie clips may be found at http://socrates.berkeley.edu/~hbbiomxl/mdonelan)

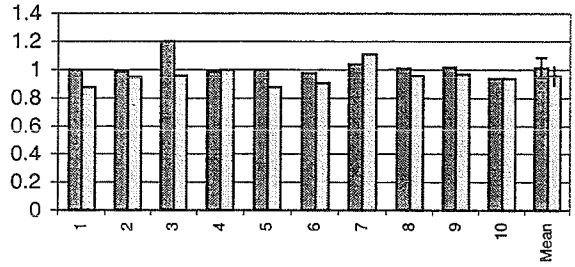

Figure 2: Metabolic cost decreased by a average of 6% with external lateral stabilization (light gray) compared to unstabilized (dark gray). Normalized costs are shown as fraction of unstabilized preferred-step-width metabolic power. Means and SDs are also shown.

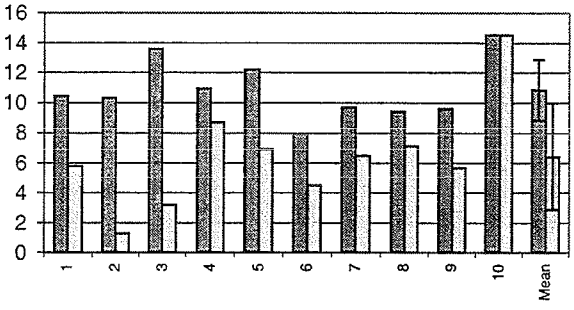

Figure 3: Preferred step width (cm) decreased by an average of 41% with external lateral stabilization (light gray) compared to unstabilized (dark gray).

stabilizer cords captured the lateral forces. Data were sampled at a rate of 100 Hz during the middle 5 minutes of each trial. We calculated actual step width from the force and moment data.

We determined metabolic cost by analyzing the gas content of expired breaths. Resting (standing) trials lasted 8 min, and walking trials lasted 7 min. We averaged steady-state O_2 and CO_2 flow rates from minutes 4 through 6. We calculated metabolic power (Watts) for each trial using standard metabolic equations (Brockway, 1997). We subtracted the metabolic power for standing from all walking values. We then normalized these net values relative to unstabilized walking at preferred width.

RESULTS AND DISCUSSION

At zero step width, average metabolic cost decreased by 6% (paired t-test: $p = 0.036$; fig. 2). We may infer that this reduction reflects the metabolic cost of zero step width stabilization. Active lateral stabilization may have a similar metabolic cost at normal step widths, because lateral instability does not vary greatly with step width (Kuo,1999).

Subjects selected a 41% smaller step width on average compared to walking without external stabilization (paired t-test: $p = 0.0016$; fig. 3). Wider step widths involve somewhat higher energy losses due to stance limb transition costs (Kuo, et al., 1999; Donelan, et al., 1999). It may be that subjects are trading off the stabilization cost of narrow walking against the higher stance limb transition costs of wide walking when they choose preferred step width. Another possible explanation for the smaller step widths may be that our subjects chose to walk with a gait that involves less lateral movement of the pelvis to avoid doing work against the stabilizer.

Because the external stabilizer allows walkers to maintain balance with less energy expenditure while maintaining a fairly normal gait, similar devices could be considered in clinical therapy situations involving patients having difficulty balancing, such as the elderly or those with inner ear disorders.

REFERENCES

Brockway JM (1987) Hum Nutri: Clin Nutri 41C: 463-471
Donelan JM, Kuo AD & Kram R (1999) ASB Conf. Proc.
Kram R, Griffin TM, Donelan JM & Chang YH (1998) J Appl Physiol 85: 764-769
Kuo AD & Bauby CE (1998) Proc. '98 NACOB Conf.
Kuo AD (1999) Int. J. Robotics Res. 18: 917-930
Kuo AD, Donelan JM & Kram R (1999) ASB Conf. Proc.

ACKNOWLEDGEMENTS

This research was supported in part by an NSERC fellowship to J. M. Donelan, NIH grant AR4468801 to R. Kram, and NIH grant DC0231201A1 to A.D. Kuo.

PER-STEP ENERGETIC COST OF CHANGING GAIT

Jim R. Usherwood and John E.A. Bertram

Department of Food, Nutrition and Exercise Sciences, Florida State University, Tallahassee, FL
E-mail: jbertram@garnet.acns.fsu.edu

INTRODUCTION

A change in gait is often termed 'transition'. For humans, the transition between walking (where potential and kinetic energies of the center of mass vary out of phase) and running (where PE and KE vary in phase) is distinct. The causes and implications of the walk-run and run-walk transition are not well understood. The determinant of the transition velocity cannot be related simply to energetics: preferred transition speeds are well below those that would minimize cost of transport (in terms of energy per distance), and hysteresis in the transition speed between walk-run and run-walk conditions further adds to the puzzle. Other potential factors in determining the transition speed include the undesirability of 'taking off' due to centrifugal effects at high walking velocities (Li et al., 1996), and the avoidance of some maximum stresses (Farley and Talylor, 1991) or joint angular velocities (Hreljac, 1995). However, the causal mechanism for determining preferred gait transition speeds remains enigmatic.

A further factor, which has received relatively little attention, but may have a considerable bearing on the naturally preferred gait transition speed, is the energetic cost of transition itself. This study is designed to determine the metabolic cost of gait transition.

METHODS

The power consumptions of 3 healthy, male, human subjects locomoting on a treadmill (Desmo Pro, Woodway, Waukesha, WI) were derived from oxygen consumption measurements (TrueMax 2400, Parvo Medics, Salt Lake City, UT).

Protocol

Day 1: Determination of the intersection of walking and running cost curves. Subjects were asked either to walk or run at a range of speeds for 7 minutes, with rests of 1-10 minutes between each trial to minimize fatigue. Steady-state oxygen consumption was achieved within 3-5 minutes, so the mean $\dot{V}O_2$ over the last 2 minutes of each trial was used to determine energetic requirements. Speeds were selected to bracket the intersection of the walking and running cost curves. The metabolic power of quiet standing was measured and removed from all locomotion values.

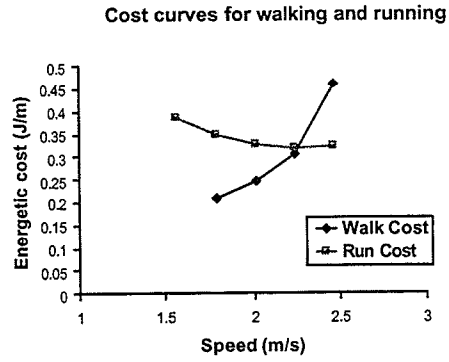

Figure 1: Typical intersecting cost curves for walking and running.

Day 2: Determination of the relative cost of transition. The three subjects were asked to locomote at their respective cross-over speeds, using a range of 'transition intervals' *TI*: transition (alternately between walking and running, and running and walking) occurred every *TI* steps. The power required for steady walking or running (equivalent to an infinite value of *TI*) at the cross-over speed was measured before and after the transition tests, and variations in power requirements between both locomotory styles and time of testing were small (CoV<0.05%).

RESULTS

Locomotion at the energetic cross-over speed requires more power with a decreasing interval between gait transitions. This can be described in terms of the relative cost of a transition step compared with a steady walking or running, non-transition step *Ct*/*Cn*.

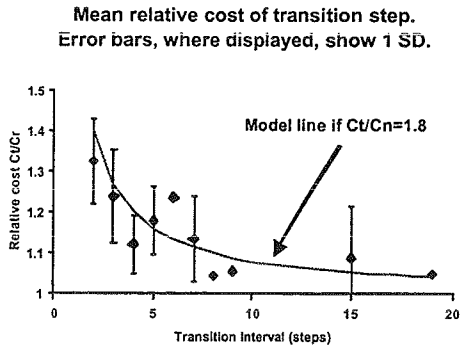

Figure 2: Mean results showing the relative power (compared with steady locomotion with no transitions) for a range of transition intervals at the personal cross-over speeds. The model line shows the relationship if *Ct*/*Cn*=1.8.

The relative cost of a transition step is approximately constant between transition intervals, but is more variable between subjects. Overall, *Ct*/*Cn* = 1.77 (SD=0.58): a transition step costs (in terms of energy, cost of transport, or power) around 1.8 times that of a 'normal' step.

DISCUSSION

These results show that there is some cost to gait transition. How this cost is divided between the walk-run transition as opposed to the run-walk transition is impossible to determine from these experiments, and the metabolic cost of a single step is unlikely to be directly measurable, at least in the near future. The cause of the cost may be related directly to the shifts in phase of KE and PE, or with forces associated with changing oscillations in other parts of the body (e.g. arms, guts etc.). Clearly these two effects are not independent, but it may be helpful to consider them separately, and relate them to force traces of transition steps.

While the direct costs of infrequent transition are relatively small, transition costs may be important at lower transition intervals associated with submaximal or challenged locomotion (such as struggling marathon runners or soldiers) or as an aspect of maneuverability. Also, a cost to transition, and the expected duration of locomotion at a given speed, may help to account for the phenomenon of hysteresis in preferred transition speed between walk-run and run-walk.

REFERENCES

Li, Y. et al. (1996). *Folia primatologica*, **66**, 137-159.

Hreljac, A. (1995). *J. Biomechanics*, **28**, 669-677.

Farley, C.T., Taylor, C.R. (1991). *Science*, **253**, 306-308.

ENERGETICS INCLINED RUNNING: GENERATING FORCE ECONOMICALLY VS. WORKING EFFICIENTLY

Peter G. Weyand [1,2], Octavio Gonzalez[1], David Wu[1], Thomas J. Roberts[1] and C. Richard Taylor[1]

[1]Concord Field Station, Museum of Comparative Zoology, Harvard University, Bedford, Mass. 01730
[2]United States Army Research Institute for Environmental Medicine, 42 Kansas Street, Natick, MA 01760

INTRODUCTION

We tested the hypothesis that the energetic cost of running increases with the inclination of the running surface due to the increased amount shortening muscles must do as animals run up progressively steeper inclines. The contractile and metabolic properties of skeletal muscle suggest that increases in relative muscle shortening velocities (V/Vmax) should correspond to discrete increases in efficiency and the metabolic cost force production (Hill, 1950). On this basis, we predicted that the net efficiency with which work was performed against gravity would likely vary on different inclines and for large vs. small animals, but would be invariant at any given estimated relative shortening velocities of the muscles active (i.e. V/Vmax). We also predicted that the metabolic cost of muscular force production during running (i.e., the cost coefficient, Kram & Taylor, 1990) would vary on different inclines and in large vs. small animals, but would also be invariant at any given relative shortening velocity.

METHODS

We measured the metabolic cost, and the efficiency of work done against gravity in six avian and mammalian species (size range: 0.1 to 150 kg) running at a range of constant speeds on inclines of 0°, 3°, 6°, 9°, and 12°. Metabolic rates were determined from steady-state rates of oxygen uptake. The average shortening velocities of the active muscles (V) was estimated from the animalís vertical velocity, while the Vmax of the active muscle fibers was estimated from the inverse period of foot-ground contact (1/tc). Net efficiency was determined from the ratio of the mechanical work rate against gravity to the net metabolic rate (metabolic rate during running ñ metabolic rate at zero speed) of the runner. The metabolic cost of muscular force production during running (J/N), or the cost coefficient, (C) was determined from the ratio of metabolic rate to the inverse time of foot-ground contact (1/tc, Kram & Taylor, 1990).

RESULTS AND DISCUSSION

On any given incline and at any given speed, smaller animals had greater mass-specific metabolic rates and lower net efficiencies than larger animals. For all animals, net efficiency with which work was performed against gravity, and the energetic cost of applying ground force (C), did not change across speed on a any given incline, but increased progressively with treadmill inclination. However, these increases were less pronounced in small than in large animals. Average muscle shortening velocities (V/Vmax) also increased progressively with treadmill inclination; with these increases also being less pronounced in small than in large animals. For all animals, inclinations, and running speeds, we found that neither net efficiencies nor the energetic cost of applying ground force (C) varied at any given estimated V/Vmax of the active muscles.

SUMMARY

We conclude that: 1) both mechanical efficiency and energetic cost of force production increase progressively with increases in relative shortening velocities of the active muscles in running animals, and 2) the relationship between relative shortening velocity and both mechanical efficiency and the energetic cost of muscular production in vivo is similar to that for isolated muscle.

REFERENCES

1. Hill, A.V. (1950). The dimensions of animals and their muscular dynamics. *Sci. Prog., Lond.* 38, 209-230.

2. Kram, R., & Taylor, C.R. (1990). Energetics of running: a new perspective. *Nature, Lond.* 346, 265-267.

PERSON-TO-PERSON VARIATION IN GAIT PARAMETERS CORRELATES WITH PERSON-TO-PERSON VARIATION IN METABOLIC COST

John E.A. Bertram[1], Andy Ruina[2], Anindya Chatterjee[3]

[1] Nutrition, Food & Exercise Sciences, Florida State University, Tallahassee, FL, USA
[2] Theoretical and Applied Mechanics, Cornell University, Ithaca, NY, USA
[3] Mechanical Engineering, Indian Institute of Science, Bangalore, INDIA
E-mail: jbertram@garnet.acns.fsu.edu Web: www.tam.cornell.edu/~ruina/hplab

INTRODUCTION

A common qualitative explanation for various features of gait is that animals tend to minimize energy usage. But different people walk in different ways. Could it be that these individual differences in coordination patterns are correlated with individual differences in individual energy use patterns?

A person constrained to walk at a given speed v on a treadmill chooses a particular step frequency f and step length $d = v/f$. Testing over a range of speeds generates a speed-frequency (v-f) relationship. Since $v = f\,d$ and since the "normal" v-f relationship reflects the most economical manner of walking, why shouldn't the variables v, f and d be interchangeable resulting in a single relationship that minimizes cost for a variety of situations? However, we previously found that subjects walking under different constraint circumstances – a range of fixed metronome beats or a range of spaced markers – produce v-f relations distinct from the standard constrained v relation (Bertram and Ruina).

The data in this paper show 1) that constrained optimization of metabolic cost per unit distance reasonably predicts three distinct frequency-velocity (f-v) curves for an individual, and 2) that the differences between individuals in their metabolic costs correlate with differences in their f-v curves.

Reviewing Bertram and Ruina, multiple speed-frequency relations are predicted if gait variables are chosen to optimize an underlying objective function, say metabolic cost of transport. In Fig. 1 schematic contours of constant metabolic cost are shown as a function of f and v. Each contour has a lower cost than the one outside it.

A line perpendicular to the v axis indicates a set speed (i.e. a subject on a treadmill). At this v, minimum cost occurs if the subject picks the frequency and step length combination where the constant v line grazes a cost contour (point A). The v-f relationship for constrained speeds is the locus of such points, one for each constrained v..

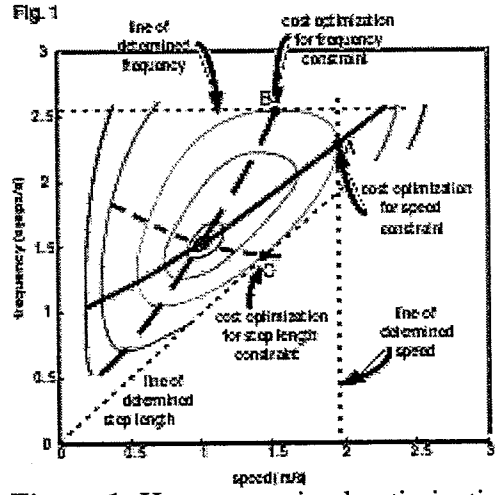

Figure 1: How constrained optimization predicts gait variable selection.

Optimization for a constant f will be determined in like manner (point B), except that a horizontal line will indicate the constraint. With a bowl shaped cost function, it is only at the global minimum that the constrained v and f curves cross.

Because $d=v/v$ constant step length is a line emanating from the origin. Cost is minimized for constant d walking where this line is tangent to a constant cost contour (point C).

Three different *v-f* curves are thus predicted, one for each kind of constrained task.

TESTING THE HYPOTHESIS

To test this prediction we measure both oxygen consumption and preferred constrained *v-f* curves for several individuals.

Part 1. Measurement of the cost surface. Subjects walked on a treadmill at eight speeds and step frequencies. Some combinations of low frequency and high speed were not possible; so a total of 49 O_2 consumption measurements were made. Oxygen data were taken using a metabolic testing system (TrueMax 2400, Parvo Medics, Salt Lake City, UT).

Measurements were taken on three different days with *v* and *f* mixed so that effort varied. Oxygen consumption was taken as the average over the last two minutes of a six-minute collection. Subjects rested for one minute before beginning a new *v-f* combination.

Part 2. Measurement of walking behavior We constrained, one at a time, speed, step frequency, or step length and measured the freely chosen values for the other two variables. Subjects were told simply to walk in a comfortable manner under the imposed conditions. Twelve subjects were tested.

ANALYSIS

Fig. 2

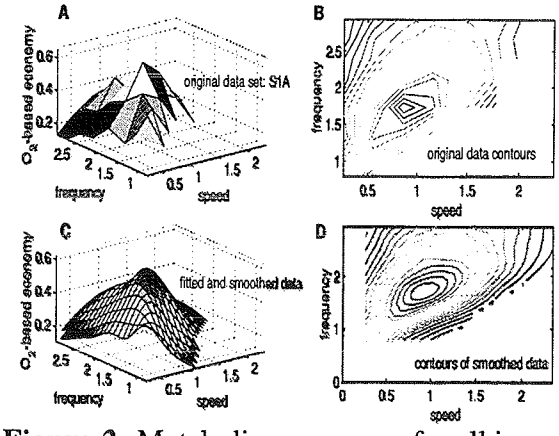

Figure 2: Metabolic economy of walking and the cost contours generated from it. A and B: Raw measures, C and D: smoothed data.

The 49 raw data points provide a rough characterization of the cost surface which we plot reciprocally as economy(Fig. 2A) and which generates the rough contours (2B). Note, both cost and reciprocal cost have the same contours.

We use a smoothing and interpolating algorithm that compromises between smoothness and passing through the data points to get plot (2C) which has the smooth contours of (2D).

RESULTS

Fig. 3

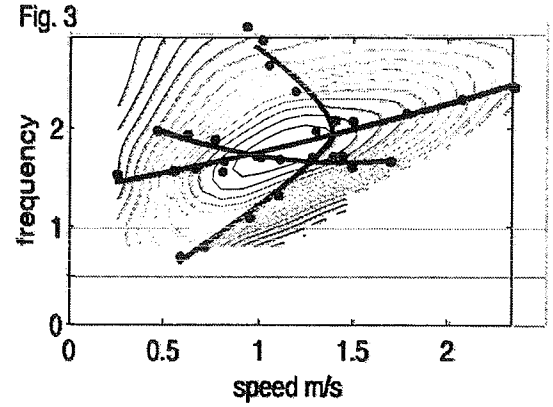

Figure 3: a plot of *v-f* curves overlayed on the cost contours for one of the subjects. The red plot is constrained speed (treadmill), blue is constrained frequency (metronome) and green is constrained step length (tape markers).

The predictions from the contours, based on constrained optimization, agree reasonably with the actual behavior of the subjects.

Differences between the contours and the behavior suggest that other factors also contribute to the choice of walking behavior. For example the data generally suggest that the underlying objective function punishes slowness as well as metabolic cost. Nonetheless, the idea of a task as a constrained optimization of something close to metabolic cost of transport correctly predicts trends that distinguish tasks and that distinguish the individuals from each other.

REFERENCES

Bertram, JEA, Ruina, A,. *J. of Theor. Biology* (in press).

MECHANICAL AND METABOLIC COST AS A FUNCTION OF STEP LENGTH IN HUMAN WALKING

J. Maxwell Donelan[1], Rodger Kram[2], and Arthur D. Kuo[3]
[1] Dept. of Integrative Biology, University of California, Berkeley;
[2] Dept. of Kinesiology and Applied Physiology, University of Colorado, Boulder;
[3] Dept. of Mechanical Engineering & Applied Mechanics, University of Michigan, Ann Arbor
Email: mdonelan@uclink4.berkeley.edu Web: http://socrates.berkeley.edu/~hbbiomxl/mdonelan/

INTRODUCTION

In the inverted pendulum model of walking, the center of mass moves along an arc dictated by the stance limb (Cavagna et al., 1977). While the single support phase can be nearly conservative (Mochon & McMahon, 1980), the transition from one stance limb to the next requires mechanical work to redirect the center of mass velocity from one pendular arc to the next (*stance limb transition cost*).

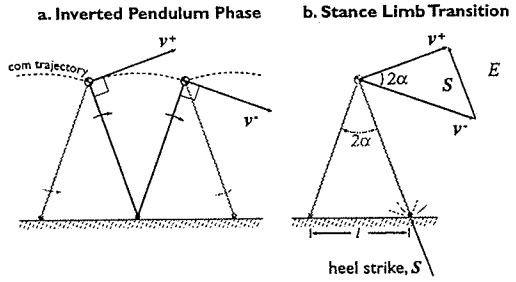

Figure 1. A simple model of bipedal walking consisting of a point mass, supported by two massless rigid legs. (a.) The direction of the center of mass velocity is perpendicular to the stance limb during inverted pendulum-like phases. (b.) Each transition to a new stance limb requires redirection of the center of mass velocity, from v^- to v^+, accomplished by an impulsive heel strike ground reaction force, S, acting along the leading limb. S also causes an instantaneous reduction in the magnitude of the center of mass velocity requiring negative work by the leading limb; $|v^+| < |v^-|$ with $E \propto |S|^2$ (shaded area). The magnitude of E depends on the angle between the legs, 2α, and the walking velocity, v. α is a nearly linear function of step length, l, and v is the product of l and step frequency, f.

Stance limb transition costs depend strongly on step length as illustrated by analysis of a simple bipedal model (Figure 1; Kuo, 2001). At each stance limb transition, the leading leg performs negative work to redirect the center of mass velocity. To maintain a steady walking speed, positive work is needed to replace the energy lost. The model predicts a stance limb transition cost dependent upon on step length, l, and step frequency, f:

$$E \propto f^2 l^3, \qquad (1)$$

where E is normalized for body weight and distance traveled to yield a dimensionless mechanical cost of transport.

We explored this theoretical stance limb transition cost by measuring the mechanical and metabolic costs of walking faster by increasing only step length while keeping step frequency fixed (*length modulation*). Based on our model's predictions (Eq. 1), and assuming constant muscular efficiency, we hypothesized that both mechanical and metabolic costs of transport will increase with the third power of step length:

$$E = Cl^3 + D, \qquad (2)$$

where C and D are empirical parameters to be identified from data.

METHODS

Ten healthy subjects (5 male, 5 female; mass 68.9 ± 12.2 kg; leg length 0.93 ± 0.05 m; mean ± S.D.) provided informed consent.

We used the external mechanical work performed by the individual limbs to estimate mechanical costs. We measured the individual limb ground reaction forces as subjects walked across two ground-mounted force platforms. The external mechanical power generated by each limb is the dot product of that limb's ground reaction force with the center of mass velocity. Center of mass velocity is calculated from the time integral of the center of mass acceleration, subject to appropriate boundary conditions. Center of mass acceleration is calculated from the resultant ground reaction force. The positive work performed by each limb is the time integral of the individual limb external mechanical power restricted to the domain over which power is positive. Total positive external mechanical work is the sum of the

positive external mechanical work generated by each limb (Donelan et al., 2001). We determined the dimensionless mechanical cost of transport, by dividing the work per step by body weight and step length. We averaged mechanical costs over three complete steps for each subject for each trial. Subjects walked at 6 speeds (0.75-2.0 m/s). At each speed, we enforced step frequency to be the frequency each subject preferred at 1.25m/s.

To estimate metabolic cost, we measured metabolic rates of subjects as they walked on a treadmill. We averaged steady-state O_2 and CO_2 flow rates from minutes 3-6 of the 7 minute trials. We calculated metabolic power (W) for each trial using standard metabolic equations (Brockway, 1997). We subtracted the metabolic power for standing from all walking values and then normalized these net values for body weight and walking velocity to yield a dimensionless metabolic cost of transport. Subjects walked at 4 speeds (1.25-1.90 m/s) using the same fixed step frequency as in the mechanics trials.

RESULTS AND DISCUSSION

In support of our hypotheses, mechanical and metabolic cost of transport increased with the third power of step length (Figure 2). Nonlinear regression yielded the coefficients $C_{mech} = 0.012l^{-3} \pm 0.001$ (95% confidence interval) and $D_{mech} = 0.033 \pm 0.004$ for the mechanical cost. For metabolic cost the coefficients were $C_{met} = 0.060l^{-3} \pm 0.007$ and $D_{met} = 0.120 \pm 0.028$. Metabolic cost increased in direct proportion to stance limb transition cost as a result of their same cubic dependence on step length.

Our length modulation results suggest that stance limb transition costs are an important biomechanical determinant of the metabolic cost of walking. But if this were the only cost to walking, then taking very short steps very quickly would minimize metabolic cost. Humans increase their step length and step frequency in almost equal proportion as they walk faster suggesting a substantial cost to swinging the limbs. In normal walking, there is likely a tradeoff between stance limb transition costs and the cost of swinging the limbs (Kuo, 2001).

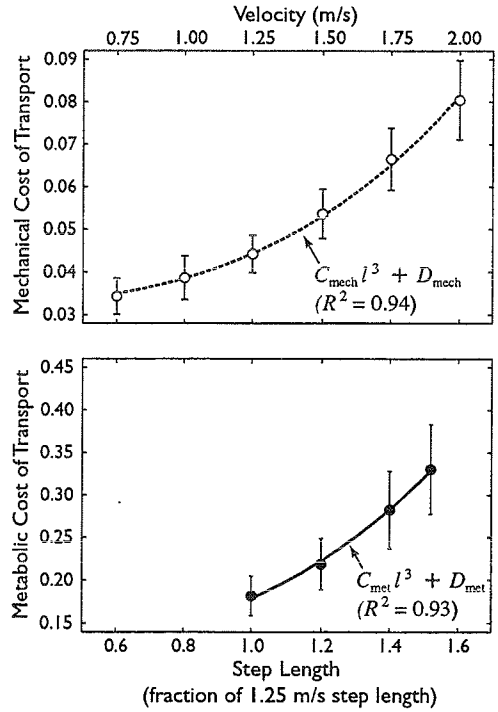

Figure 2. Mechanical and metabolic dimensionless cost of transport required for length modulated walking. Error bars are S.D.

SUMMARY

Theoretically, stance limb transitions require mechanical work, and thus metabolic energy, to redirect the center of mass velocity. These costs increase with step length. We explored stance limb transition costs by measuring the mechanical and metabolic costs of step length modulated walking. Our results suggest that stance limb transitions costs are an important biomechanical determinant of the metabolic cost of walking.

REFERENCES

Brockway, JM (1987) *Hum. Nutri. Clin. Nutri.* **41C**, 463.
Cavagna et al (1977) *Am. J. Physiol.*, **233**, R243.
Donelan et al (2001) *J. Biomech.* conditionally accepted.
Kuo, AD (2001) *J. Biomech. Engin.*, in press.
Mochon, S and TA McMahon (1980) *J. Biomech* **13**, 49.

ACKNOWLEDGEMENTS

Supported by an NSERC fellowship to JMD, NIH AR4468801 to RK, and NIH DC0231201A1 to ADK.

MECHANICAL POWER DOES NOT REFLECT METABOLIC COST OF WALKING WITH LEG LOADS

Todd D. Royer [1] and Philip E. Martin [2]

[1] Dept of Health and Exercise Sciences, University of Delaware, Newark, Delaware
[2] Exercise and Sport Research Institute, Arizona State University, Tempe, Arizona
Email: royer@udel.edu

INTRODUCTION

Metabolic energy cost (Ecost) of walking is sensitive to lower-extremity inertial properties. Manipulating leg inertia by adding loads to the legs simultaneously alters leg mass (m_{leg}) and moment of inertia about the hip (I_{hip}) making it difficult to assess independent effects of m_{leg} and I_{hip}. Previously we showed that Ecost increased similarly when m_{leg} and I_{hip} were increased independently by 5% relative to a nominal baseline condition, (Royer & Martin, 2000). Furthermore, emg analyses of select lower-extremity musculature indicated no significant trends that explained this observed changes in Ecost.

Various expressions of mechanical work and/or power have been used in an attempt to explain differences in submaximal Ecost of walking and running between adults (Martin et al., 1993) and within adults when running with leg loads (Martin 1985, Myers & Steudel, 1985). The purpose of this study was to determine whether lower-extremity mechanical power explains Ecost changes due to inertial manipulation. Relative changes in lower-extremity mechanical power was expected to parallel changes in Ecost due to inertial changes.

METHODS

Fourteen males and females (M_{age} = 27.8 ± 4.2 yrs; M_{height} = 170.2 ± 6.9 cm; M_{mass} = 69.4 ± 11.7 kg) were videotaped while walking on a treadmill at 1.5 m/s. Lower extremity position data and body segment parameter equations (de Leva, 1996) were used to estimate limb inertial characteristics. Three load conditions were modeled, in which m_{leg} or I_{hip} were each independently increased 5% from baseline (Figure 1).

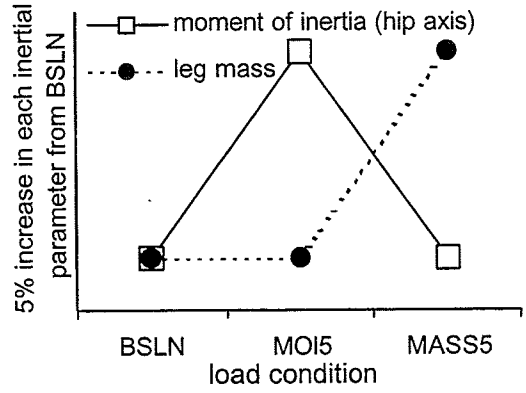

Figure 1: Moment of inertia (I_{hip}) and leg mass were independently increased 5% from BSLN for MOI5 and MASS5, respectively.

Loads were affixed to the proximal and distal aspects of the shank to achieve the desired changes in limb inertia (Table 1). A fourth condition with no load (NL) on the legs (all load in waist pouch) was included for normalization purposes.

Table 1: Mean loads (kg) added to the proximal shank, distal shank, and torso.

Condition	Proximal	Distal	Torso
NL	0	0	5.64
BSLN	1.33	.68	1.61
MOI5	0.81	1.20	1.61
MASS5	2.82	0	0

Rate of Ecost was estimated from oxygen consumption values collected during the final 2-min of 6-min walking trials and normalized to total subject mass. Lower-

extremity mechanical power was computed from 60 Hz video data using a segmental energy model:

$$E_{ij} = m_i g h_{ij} + \tfrac{1}{2} m_i v_{ij}^2 + \tfrac{1}{2} I_i \dot{\omega}_{ij}^2$$

where *i* represents the thigh, shank, or foot segment at time *j*. Mechanical work was computed with the following equation:

$$W = \sum^{j} \left| \sum^{i} \Delta E_{ij} \right|$$

Average mechanical power (P) was computed by dividing the work by stride time and normalizing to total subject mass. Percent changes in P and Ecost for the three load conditions were expressed relative to the NL condition. A two-factor, measure (P and Ecost) by condition (BSLN, MOI5, and MASS5) within-subjects ANOVA was used to test for a significant interaction.

RESULTS AND DISCUSSION

Power and Ecost results are provided in Table 2. The purpose of this project was to analyze relative changes, not absolute values, in mechanical and metabolic power across load conditions, which was reasonable given the between condition manipulations of limb inertia.

Table 2: Lower extremity mechanical power and whole body Ecost data.

Condition	Power	Ecost
NL	0.61 (0.05)	4.75 (0.38)
BSLN	0.72 (0.06)	4.88 (0.35)
MOI5	0.75 (0.06)	5.00 (0.44)
MASS5	0.73 (0.06)	5.04 (0.48)

note: values are the mean (sd) in Watts/kg

Percent changes from the NL condition (Figure 2) indicate a significant measure by condition interaction [$F(2,26) = 3.47$, $p=.046$]. The relative changes for MOI5 and MASS5 were not different for Ecost [$F(1,13) = 0.76$, $p=.4$] but were significantly different for power [$F(1,13) = 7.46$, $p=.017$]. As the shank rotated about the knee during the swing phase, the distally positioned shank center of mass (CM_{shank}) for MOI5 yielded greater changes in CM_{shank} height and linear velocity compared to the proximal CM_{shank} position for MASS5. This explains the greater change in mechanical work (and power) for MOI5 despite the larger total shank mass associated with MASS5.

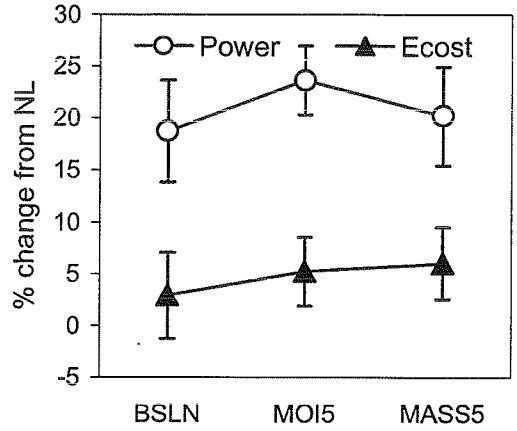

Figure 2: Relative changes in mechanical power were different than changes in Ecost.

SUMMARY

The hypothesis that relative changes in lower-extremity power reflect comparable relative changes in metabolic energy cost was not supported. Mechanical power was greater for MOI5 compared to MASS5; conversely, metabolic Ecost was not different between these two load conditions.

REFERENCES

de Leva, P. (1996). *J Biomech*, **29**, 1223-30.
Martin, PE. (1985). *MSSE*, **17**, 427-433.
Martin, PE et al. (1993) *MSSE*, **25**, 508-515.
Myers, MJ & Steudel, K. (1985) *J Exp Biol*, **116**, 363-373.
Royer, TD & Martin, PE. (1999) *MSSE*, **32**, S72.

ACKNOWLEDGEMENTS

Support from the ASB Graduate Student Grant-In-Aid Program and the ASU Conley Memorial Scholarship is acknowledged.

THE EFFECT OF MOTION DYNAMICS IN CALCULATION OF EXTERNAL JOINT MOMENTS DURING LIGHT INDUSTRIAL HAND MOTIONS

CR Dickerson, DB Chaffin, K Kim, BJ Martin, N Womack

Center for Ergonomics, University of Michigan, Ann Arbor, MI, USA
E-mail: cdickers@umich.edu

INTRODUCTION

Detailed studies have investigated the dynamic effects of locomotion, as well as many fast-paced sports motions, on physiological loading. This study examines the significance of considering the dynamics of simulated industrial handwork when calculating external joint moments, for a demographically diverse population, and for an individual with a lumbar spinal cord injury.

METHODS

Twenty healthy subjects (10 male, 10 female Age 18-80, 43.6 +/- 16.0 years), and one individual with a spinal cord injury (Age 28) participated in the study. Detailed anthropometric dimensions were obtained. Strength testing was performed implementing a previously used protocol (Chaffin, 1975). Subjects performed a sequence of seated tasks that required the lifting and placing of a light hand weight (20% of maximum lifting strength with the arm abducted 90 degrees) on to specified targets located at 0, 45, and 90 degrees clockwise from the anterior sagittal plane, and which varied vertically, as shown in Figure 1. This included over 500 studied motions.

Motion of the upper extremity was sampled at 25 Hz using a combination optical/electromagnetic recording system (MacReflex™, Flock of Birds™). Regression algorithms were applied to locate the relevant joint centers.

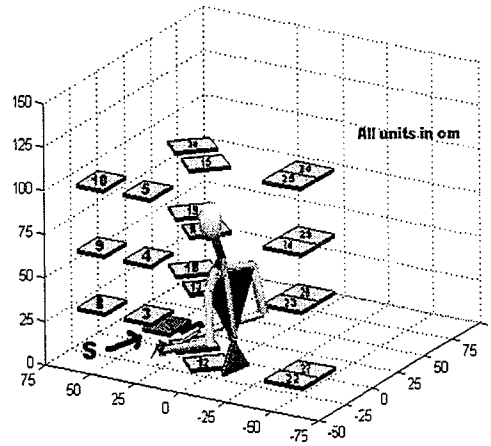

Figure 1. 3-D locations of task terminal targets. All tasks begin at point S.

Both inverse dynamic and quasi-static algorithms were designed to compute external shoulder joint torques using a top-down 3-D model. Kane's Method (Kane, 1983) was employed to obtain angular velocities and accelerations of segments. Figure 2 shows the local coordinate systems created. Segment inertial properties were calculated using scaling techniques in Chaffin (1993).

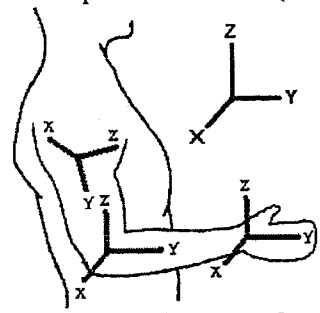

Figure 2. Local (light) Arm Coordinate Systems, Global System Frame (dark).

External moments were calculated for each task using both paradigms.

Comparisons were made between the methods for trapezoidal integration of the vector norm of the moment, as well as the peak external moment prediction.

RESULTS AND DISCUSSION

A representative task performed by both populations is shown in Figure 3. While the curves share the same general form, the static paradigm fails to capture peaks visible in the dynamic calculation. This is more pronounced for the unique subject, suggesting the dynamics differ.

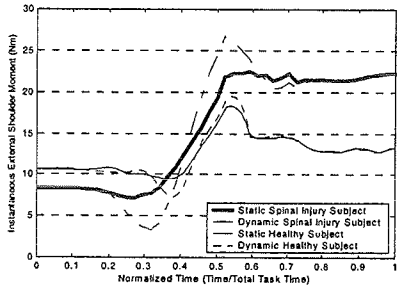

Figure 3. Typical Shoulder External Moment about local upper arm x-axis for two populations, by both methods.

While there are visible differences in each task (up to 22% of the mean moment for healthy, nearly 43% for spinal injured), comparison of the total moment for the exertion shows close linear similarity (Figure 4).

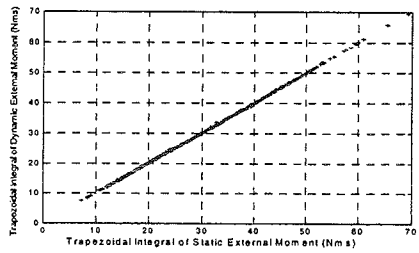

Figure 4. The integrated trapezoidal moment norm derived by two methods, (individual trials (+) [$R^2 > 0.9$].

For the relatively light load reaching motions studied in this experiment, the overall dynamic external shoulder moment was statistically significantly higher than that derived by the static method, ($p < 0.01$). However, as a percentage of the average of the two moments, this difference had a value of 0.70 +/- 0.52 %. To study the overall physical cost of certain types of normal work motions performed at industrial reaching speeds, static analysis may suffice, but peak external moments cannot be characterized well with static measures. Biomechanical analysis of the importance of these peaks continues.

SUMMARY

Careful examination of the nature of a task should precede the selection of an appropriate biomechanical analysis technique selection. Both identification of peak moments and analysis of high-speed motions require dynamic models, but static models can also provide a simple method to obtain important biomechanical information for analysis of the cumulative effects of many work tasks. Special attention should be paid to the impact of the dynamics of higher speed activities (i.e. the spinal injury subject) on moment calculations.

REFERENCES

Chaffin (1975). *AIHA J.* 35:505-510.

Chaffin, Anderson, Martin (1999). *Occupational Biomechanic, (3rd).* Wiley.

Kane, Likins, Levinson (1983). *Spacecraft Dynamics.* McGraw-Hill.

ACKNOWLEDGEMENTS

The Automotive Research Center and the partners of the HUMOSIM consortium (GM, Ford, Daimler-Chrysler, TRW International Truck, TACOM, Johnson Controls, EAI) provided funding for this experiment.

INFLUENCE OF DYNAMIC FACTORS ON ERRORS IN CALCULATING CUMULATIVE LOW BACK LOADS DURING LIFTING

Keown, K.J.[1], Andrews, D.M.[2], and Callaghan, J.P.[1]

[1] Department of Human Biology and Nutritional Sciences
University of Guelph, Guelph, Ontario, CANADA. Email:jcallagh@uoguelph.ca
[2] Department of Kinesiology, University of Windsor, Windsor, Ontario, CANADA

INTRODUCTION

Cumulative low back loads such as spine compression and shear forces have been linked to the reporting of low back pain (Norman 1998, Kumar, 1990). Estimating cumulative loading presents the difficulty of documenting the variation of spinal loads over time. In order to reduce data collection and processing time when working with video records of dynamic tasks, estimates of cumulative loading from discrete static data points have been used (Norman et al., 1998; Kumar, 1990). However, McGill & Norman (1985) reported peak L4/L5 moments from a static model of 19% lower than the dynamic model while the quasi-dynamic model findings were 25% greater than the dynamic model. Lindbeck (1991) also reported that static analyses underestimate the peak moment calculated during a dynamic lift by 23 to 100% depending on the type of lifting task. A quasi-static approach rendered data that agreed well with the dynamic model findings, with errors of less than 3%. The purpose of this study was to determine the error in cumulative spinal loads from a static or quasi-static modeling approach compared to a full dynamic model during sagittal plane lifting.

METHODS

Three males (age 23 ± 1 yr, height 1.81 ± 0.035 m, mass 88.3 ± 16.29 kg) performed each of three sagittal plane lifts, 5 times: from the floor to a table 73 cm above the ground; from a shelf height of 138.3 cm to a table 73 cm above the ground; and from the floor over a barrier of 55.3 cm to the floor. Lifts were performed at speeds of 0.2, 0.4, and 0.8 m/s with loads of 2.3, 8.8, and 15.9 kg for a total of 135 lifts. A jig equipped with a force transducer was used to measure the hand forces during lifting. The subjects performed each of the lifts five times. One lift per subject for each of the 27 lifting conditions was chosen for analysis. A complete lift cycle consisted of starting from upright relaxed standing, picking the load up, placing it on the appropriate surface, and returning to upright standing (Figure 1).

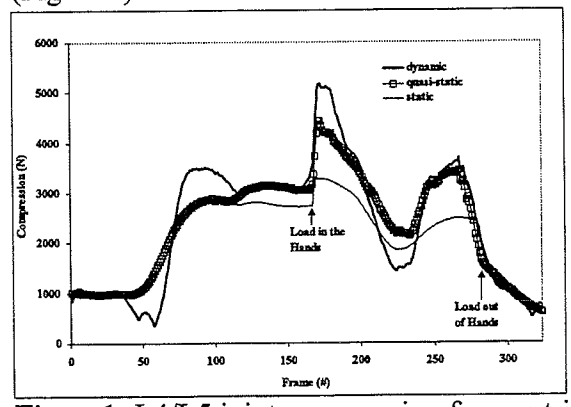

Figure1: L4/L5 joint compression for one trial, lift from floor to table, 8.8kg, medium speed, calculated by the three models.

Reflective markers at the wrist, elbow, shoulder, C7/T1, ear canal, and L4/L5 were auto-digitized using a PEAK Performance system at a rate of 60 Hz. Each trial was then run through a biomechanical model to yield

compression, joint shear, and reaction shear forces (N), and moment (N.m) at L4/L5 using a static, quasi-static, or dynamic link segment approach. Bone on bone forces were calculated for each frame using a single muscle equivalent approach with a 6 cm moment arm and 5.3 /angle of pull. Cumulative values were calculated by rectangular integration of each variable. A four way repeated measures ANOVA (dependent variables = task X approach X speed X mass, $\alpha = 0.05$) was used to compare the cumulative spine loading for the various tasks. Ryan-Einot-Gabrial-Welsch Multiple Range posttests were used to compare significant findings.

RESULTS AND DISCUSSION

Cumulative compression values were significantly different between each of the three modeling techniques across task, speed, and mass ($p<0.01$)(Figure 2). For reaction shear, joint shear and moment the static approach was significantly different ($p<0.01$) from each of the other two models while the dynamic and quasi-static models were not significantly different (Figure 1).

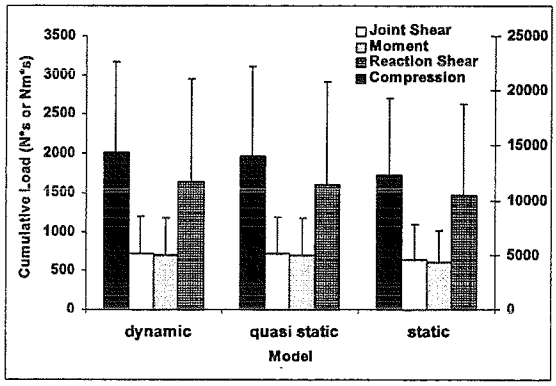

Figure 2: Cumulative moment and force (+1sd) calculated using each of the three modeling approaches. Compression is plotted against the secondary y-axis.

The relative differences between the static and dynamic approaches (Table 1) are smaller than those previously reported in the literature for peak loading (Lindbeck, 1991). The lower error for cumulative loading, compared with previously reported peak errors, can be attributed to the static and quasi-static models over predicting forces and moments when the accelerations are beneficial to the lifting action. These areas tend to offset the under prediction of joint loads at instances like the initiation of lifting, when the inertial forces contribute largely to the joint forces and moment (Figure 1).

Table 1: Relative error (%) between the models for each of cumulative compression, joint shear, reaction shear, and moment (Dyn = dynamic; QS = quasi static; Stat = static).

	Dyn-QS	Dyn-Stat	QS-Stat
Comp.	-2.3	-14.0	-12.0
J. Shear	-1.3	-10.9	-9.7
R. Shear	-1.5	-9.9	-8.6
Moment	-0.5	-13.9	-13.5

SUMMARY

Although there were statistically significant differences between the cumulative loading values determined from each of the models the relative differences were extremely small for quasi-static compared with dynamic and were in the range of 10% when a static model was used. These initial findings support the use of static models to estimate cumulative low back loading during sagittal plane lifting tasks of varying speeds and loads. Further study of more complex tasks involving asymmetrical postures is necessary.

REFERENCES

Kumar (1990) *Spine,* **15:**1311-1316.
Lindbeck (1991) *Ergonomics,* **34:**421-433.
McGill et al. (1985) *J. Biomech,* **18:**877-885.
Norman et al. (1998) *Clin Biomech,* **13:**561-573.

KINEMATIC ANALYSIS OF TRUNK MOTIONS DURING FREESTYLE LIFTS

Wayne J. Albert[1] and Joan M. Stevenson[2]

[1] Faculty of Kinesiology, University of New Brunswick, Fredericton, NB, CANADA
[2] School of Physical & Health Education, Queen's University, Kingston, ON, CANADA
E-mail: walbert@unb.ca

INTRODUCTION

In recent years trunk angular motion characteristics have been used for the quantification and classification of various low back disorders with some success (Marras et al., 1995). It was felt by the authors of this paper that the trunk motion characteristics could be used to gain a better understating of lifting technique. An earlier communication presented the use of a classical cluster analysis performed on a series of trunk motion profiles in order to group individuals with similar motions during their lift (Albert et al., 2000). The uniqueness of this methodology was that it identified individuals based on eleven separate curves rather than one or two discrete variables.

This paper presents the trunk motion characteristics that separated the industrial population of manual material handlers into separate lifting technique groups.

METHODS

The freestyle lifting techniques of 108 male experienced manual material handlers performing sagittal lifts of a moderate load (15kg) were tracked using the FASTRAK™ motion system. In order to define back motion, electromagnetic sensors were placed on the L1 and T1 vertebrae and on the L5/S1 intervertebral space. A sensor on the wrist tracked the box and defined arm motion. Data collection and subsequent computations produced eleven kinematic curves of interest that explained the motion of the upper body and were chosen to describe the technique of the experienced lifter. All motion curves were normalized to 50 points from the start to the end of the lift and were then averaged, at each time point, over the five trials within each subject. Datasets for those variables were grouped according to their descriptive purpose and the component curves were strung end to end within a single row representing a subject for purposes of cluster analysis. A separate cluster analysis was performed on each dataset of merged curves pertaining to posture profiles (sacrum height, trunk angle, wrist-to-sacrum distance), trunk flexion profiles (T1, L1 and L5/S1 flexion velocity), and trunk segment bend profiles (thoracic and lumbo-sacral bend, and their corresponding velocities).

The clustering exercise resulting in the subjects being divided into three groupings based on their division in each analysis. The 29 subjects who were consistently assigned to group 1 were considered the 'Squat Posture Group' as their average trunk flexion was 48 degrees at the start of the lift. The 33 subjects who were consistently assigned to group 2 were named the 'Squat Posture Group' since their corresponding trunk flexion was 91 degrees. The remaining 42 individuals were not consistent in their grouping. The following discussion focuses on trunk motions of the first two groupings only. Discussion of the third group will be presented in a future communication.

RESULTS and DISCUSSION

Trunk Flexion. The trunk flexion / extension velocities determined at T1, L1 and L5/S1 were all larger for 'Stoop Posture' Group. This group may have relied on the trunk momentum to overcome the inertia of the box to begin the lift. Starting from a flexed position, the trunk began to extend rapidly for the first 40% of the lift. This rapid extension served to lift the box, as there was only a slight increase in sacrum height during this period. The extension of the sacral (pelvic) segment led the motion of the trunk. The lumbar and thoracic segments lagged slightly behind, and then extended almost simultaneously. It is thought that initiation of motion by posterior pelvis rotation delays lumbar extension thereby shortening the moment arm of the external load resulting in less erector spinae stress (Farfan, 1978).

The 'Squat Posture' Group flexed their trunk slightly at the start of the lift indicated by the pronounced T1, L1 and L5/S1 flexion velocity during the first 20% of the lift. This may be the result of the sequence of movements used to lift the box from a squat position. Scholz et al. (1995) have indicated that a coordinated pattern whereby knee extension leads trunk extension exists in lifts initiated in squat and freestyle lifting postures.

Using the vertical motion of the sacrum as a proxy for knee flexion allowed for an evaluation of knee-trunk coordination. From the squatting position, the knees and pelvis extended well in advance of the trunk. Within the first 20% of the lift the knees have extended 0.20 m with little to no movement in the trunk angle. This would cause the trunk to flex forward under the weight of the box and in reaction to the body's upward momentum.

Thoracic and Lumbar Bend. The bend angles and their corresponding velocities also reflected the lower trunk activity in the 'Squat Posture' Group. There was only a slight thoracic bend throughout the entire lift and while the lumbar segment began in slight kyphosis it maintained a lordotic posture for most of the lift. As a result, the velocities of the thoracic and lumbar bend were slower and peak velocity occurred later in the lift. Lumbar kyphosis has been thought to be advantageous in reducing stress at the apophyseal joints, reducing compressive stress and providing compressive strength to the spine (Adams and Hutton, 1985). The 'Stoop Posture' Group displayed a larger range of motion in both the thoracic and lumbar regions. The lumbar bend was in kyphosis for the first half of the lift before attaining a lordotic posture. The velocities of 'Stoop Posture' Group bend angles were higher than 'Squat Posture' Group reflective of the quicker trunk motion used to lift the box.

CONCLUSIONS

Although it has been suggested that a single correct lifting technique does not exist, the results of the clustering approach reveal that there is consistency with respect to the trunk motions selected. It is also interesting to note that the different trunk motions and corresponding velocities, which defined the lift technique, resulted in similar box trajectories. Peak lumbosacral compression values were found to be within safe limits (according to NIOSH) irrespective of lift technique.

REFERENCES

Marras et al. (1995) Spine, 20(23): 2531-2546.
Albert et al. (2000) Canadian Soc. of Biomechanics Conference Proceedings, Montreal
Farfan (1978). Orth. Clin. In North Am. 6:135-144
Scholz et al. (1995). Phys. Therapy, 75(2) :133-144
Adams and Hutton (1985) J. Bone & Joint Surg. 67B:625-629

HEALTHY ADULTS CAN LEARN TO REDUCE HAND IMPACT FORCE IN A FORWARD FALL. A 3-MONTH INTERVENTION STUDY IN YOUNG MALES.

G.N. McCabe[1], K.M. DeGoede[2], and J.A. Ashton-Miller[1]

[1] Biomechanics Research Laboratory, University of Michigan, Ann Arbor, MI USA
[2] Elizabethtown College, Elizabethtown, PA USA.
E-mail: jaam@umich.edu

INTRODUCTION

Minimizing injury during a fall arrest entails substantial challenges. A common fall arrest strategy is to use the upper extremities to protect the head and trunk from impact (O'Neill et al., 1994; Hsiao, 1998). The biomechanics of forward fall arrests using fully extended arms have been studied by Robinovitch and co-workers (1998). The arrest of falls from a standing posture has been studied by Dietz (1981), van den Kroonenberg et al. (1995), and Hsiao (1998). The biomechanics of an active, martial arts-style, fall arrest have been described by Sabick (1999). Finally, a recent study by DeGoede (2000) showed that hand impact forces during a forward fall from an initial shoulder height of 1m can be volitionally reduced by up to 29%.

The purpose of this study was first to confirm the hypothesis that young males can be taught, in less than 10 minutes, to successfully reduce peak hand impact forces while arresting a standardized forward fall. Then, if the first hypothesis was supported, to test the second hypothesis that, without intervening practice, these subjects could retain the ability to land with reduced impact force at 3 and 12 week's follow-up.

METHODS

Ten healthy young males participated in this study (mean ± SD age: 23 ± 3 years, body weight: 72 ± 9 kg, and height: 1.743 ± 0.037 m). Subjects were only included if they did not have any previous falls training (e.g. no karate, gymnastics, etc.). The institutional review board approved all test procedures and each subject gave their written informed consent.

Each fall was initiated from a shoulder height of 1 m above padded AMTI force plates on which each hand landed. Body segment kinematics were measured at 300 Hz using an Optotrak system. At the baseline visit each subject performed five falls without instruction (termed "*natural* falls"), followed by a 10 minute instructional period (intervention) designed to teach them the skill of arresting the forward fall with reduced impact force (termed "*reduced-impact* falls"). They were taught to try to "catch" the ground (by reducing the hand-ground relative velocity as much as possible prior to impact). They were shown several types of demonstrations so that they could visualize what they had to attempt to do. To be rated as "successful", a trial not only had to result in a reduced peak hand force, but the subject's torso had to pass through an imaginary 15 cm-ground clearance threshold with a downward velocity < 0.5 m/s. Following the teaching intervention, subjects performed five 'reduced-impact' fall arrests, each time being given verbal feedback on the preceding trial's peak impact force and torso speed at the 15 cm threshold. At the 3 and 12-week follow-up, subjects performed five additional 'reduced-impact' falls without

further practice, instruction or knowledge of results.

The first null hypothesis was tested using a two-sided, paired t-test comparing the average of the 'natural' falls to the average of the 'reduced-impact' falls during the baseline test session. The second null hypothesis was tested, using a two-sided paired t-test, comparing the average of the baseline 'reduced-impact' falls to the initial 'reduced-impact' fall at three and twelve weeks. In all cases $p<0.05$ was considered significant.

RESULTS AND DISCUSSION

During the baseline visit, subjects volitionally reduced their average hand impact force by 11% ($p=0.017$) over initial values. At 3 and 12 weeks follow-up, the subjects had successfully remembered how to maintain the reduction in hand impact force. Their initial hand impact forces, during the 3 and twelve week follow ups, were not significantly different from the average baseline 'reduced impact' arrests, with reductions from the average natural falls of 9% ($p=0.725$) and 8% ($p=0.383$).

Across all subjects in the first trial block the average force reduction of 11% is significantly less than the 29% achieved by similar subjects in DeGoede (2000). This discrepancy can be explained by the introduction of the 15 cm-ground clearance criterion in this experiment. This new criterion had the subject attempting to reduce their torso speed to less than 0.5 m/s at the threshold. This caused a diminution of the reduction in peak impact force because the subjects had less time and distance during the post-impact "ride-down" and were not allowed to use the torso itself to arrest any downward momentum.

To our knowledge this may be the first prospective study to demonstrate that fall-related impact forces can be volitionally reduced, in this case by a 10-minute intervention and maintained over a 12-week follow-up period. We acknowledge the limitation of a missing untrained control group, and this is currently being addressed. The most common fall direction at any age is forwards (O'Neill, 1994). The present findings suggest that interventions aimed at training people to fall forward safely may have promise.

SUMMARY

1. Healthy young males could learn in less than 10 minutes how to reduce hand impact forces in a forward fall.
2. They could also retain this skill for a period of up to twelve weeks, without the need for intervening practice sessions.

REFERENCES

DeGoede, K. M. (2000). PhD Thesis. Mechanical Engineering. Ann Arbor, University of Michigan.

Dietz, V., J. Noth, et al. (1981). J Physiol **311**: 113-25.

Hsiao, E. T., S. N. Robinovitch (1998). J Biomech **31**(1): 1-9.

O'Neill, T. W., J. Varlow, et al. (1994). Ann Rheum Dis **53**(11): 773-5.

Robinovitch, S. N., J. Chiu (1998). J Orthop Res **16**(3): 309-13.

Sabick, M. B., J. G. Hay, et al. (1999). J Biomech **32**(9): 993-8.

van den Kroonenberg, A. J., W. C. Hayes, et al. (1995). J Biomech **29**(6): 807-811.

ACKNOWLEDGEMENTS

PHS grants AG 10542 and AG 08808.

FOOT ELEVATION AND WHOLE BODY MEDIAL-LATERAL SWAY IN ELDERLY PATIENTS WITH BALANCE DISORDERS

Michael E. Hahn [1], Li-Shan Chou [1], Kenton R. Kaufman [2] and Robert H. Brey [3]

[1] Department of Exercise and Movement Science, University of Oregon, Eugene, OR
[2] Department of Orthopedic Surgery and [3] Department of Otorhinolaryngology
Mayo Foundation, Rochester, MN
E-mail: chou@oregon.uoregon.edu

INTRODUCTION

Falling to the side has been found to be an important risk factor for hip fracture (Greenspan et al., 1998). Additionally, imbalance and tripping over obstacles have been confirmed as two of the most common causes of falls in the elderly (Tinetti et al., 1989). An increased understanding of the factors influencing falls in the elderly should help reduce the risk of falls, thereby limiting the number of debilitating injuries suffered later in life.

Imbalance of the whole body during obstacle crossing may cause inappropriate movement of the lower extremities or misplacement of the swing foot, which can consequently lead to a foot-obstacle contact and result in a fall. Anterior-posterior and vertical displacements of the whole body center of mass (COM) were shown to increase in young adults while negotiating obstacles of increasing height (Chou et al., 2001). However, no significant increases in medial-lateral (M-L) displacement (sway) and peak velocity were noted, possibly indicating a successful control strategy used to maintain M-L balance during obstacle crossing. This suggests that differences in M-L motion of the COM while negotiating obstacles might serve as an effective indicator to distinguish individuals at risk for sideways falling from healthy individuals. Therefore, the purposes of this study were to determine if elderly patients with balance disorders display greater M-L sway and peak M-L velocity of the COM as compared to healthy elderly while negotiating obstacles and whether increases in M-L sway and peak velocity are influenced by foot elevation during obstacle crossing.

METHODS

Eleven subjects, including five healthy elderly adults (mean age, 70.4 years) and six elderly patients with imbalance (mean age, 75.7 years), were recruited for this study. Whole body kinematic data were collected from each subject using a six-camera ExpertVision™ system (Motion Analysis Corp., Santa Rosa, CA) during unobstructed level walking and when stepping over an obstacle of height corresponding to 2.5%, 5%, 10%, or 15% of the subject's height. All trials were conducted at a comfortable self-selected walking speed while barefoot. The order of obstacle height was randomly selected.

A 13-link biomechanical model of the body was used to compute the kinematics of the whole body's COM. The 3-D trajectory of the whole body's COM was computed from the weighted sum of the segmental COMs. Linear velocities of the whole body's COM were computed using the GCVSPL algorithm (Woltring, 1986). Correlation analyses were performed between foot elevation (vertical position when toe crosses

obstacle, relative to ground) and M-L sway of the COM, and between foot elevation and peak M-L velocity of the COM. A two-way ANOVA with repeated measures of obstacle height was used to test for group differences for these variables.

RESULTS AND DISCUSSION

Group differences were identified in both M-L sway and peak M-L velocity ($p=0.025$ & $p=0.02$, respectively) across all obstacle heights. Patients with imbalance demonstrated greater sway and peak velocity while crossing obstacles of all heights, indicating higher risk for M-L instability. M-L displacement (sway) and peak M-L velocity of the COM did not show significant increase for either group when obstacle height increased.

Significant group mean differences ($p=0.04$) in toe-obstacle clearance of the leading limb (normals=12.9cm, patients=16.0cm) were found. Mean toe-obstacle clearances of the trailing limb were also greater in the patient group (normals=15.0cm, patients=16.7cm), but not significantly. Toe-obstacle clearances of both limbs did not differ significantly across obstacle heights. Increased toe-obstacle clearance as exhibited by the patient group may indicate a risk-avoidant strategy in which the patient attempts to ensure obstacle clearance by increasing foot elevation.

With increased foot elevation of the leading limb, M-L sway and peak M-L velocity of the COM also increased for both groups combined (see Figure). Although these correlations were not significant, the trends of increasing M-L sway ($p=0.065$) and peak M-L velocity ($p=0.12$) with foot elevation indicate a potential for significance, with increased sample size.

SUMMARY

The finding that COM M-L sway and peak velocity were significantly greater in the patients with imbalance than the healthy group provides insight into identification of dynamic instability. Results from this study indicate a trend of M-L sway and peak velocity increasing as the foot is progressively elevated to cross obstacles. As more elderly gait is analyzed using this protocol, a distinction between healthy elderly subjects and those at risk for falling may become more evident.

REFERENCES

Chou, L-S et al. (2001) *Gait & Posture* **13**: 17-26.

Greenspan, SL et al. (1998) *Am J Med* **104**:539-45.

Tinetti, ME et al. (1989) *N Engl J Med* **302**: 1055-1059.

Woltring, HJ (1986) *Adv Eng Software* **8**: 104-113.

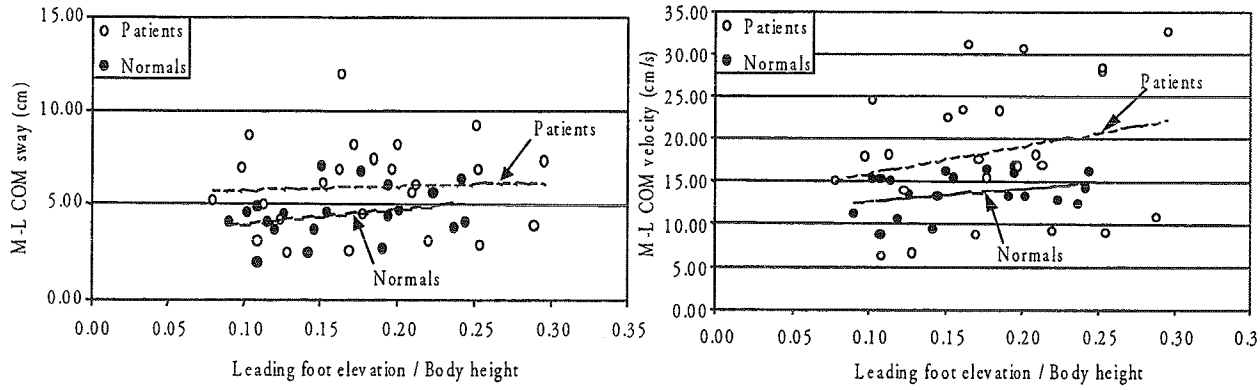

Figure. M-L COM sway and peak velocity as functions of leading foot elevation.

MAXIMUM RECOVERABLE ANGLE OF LEAN DOES NOT DIFFER BETWEEN OLDER MEN AND WOMEN

Tammy M. Owings [1], Michael J. Pavol [2], and Mark D. Grabiner [1]

[1] Department of Biomedical Engineering, Cleveland Clinic Foundation, Cleveland, OH
[2] Department of Physical Therapy, University of Illinois at Chicago, Chicago, IL
Email: owings@bme.ri.ccf.org

INTRODUCTION

Falls cause significant injury and death in older adults. Epidemiological studies indicate that older women fall with greater frequency than older men. We have experimentally confirmed than women are more likely than men to fall following a trip (Pavol et al. 1999).

A study of single-step recovery from a forward lean revealed that older women have a decreased ability to successfully recover compared to older men (Wojcik et al. 1999). The present study sought to determine if our previously reported gender-specific difference in fall frequency is related to gender-specific differences in the ability to recover from a forward lean with a single step.

METHODS

Fifty older women (mean age: 70 ± 5 years) and 29 older men (mean age: 73 ± 4 years) participated in this study. Subjects were identical to those of Pavol et al. (1999). They were screened for the presence of exclusion factors, tested for femoral neck bone mineral density of at least 0.65 g/cm^2, and gave written informed consent.

During all trials, subjects were secured in a safety harness attached to a ceiling-mounted track by a pair of dynamic ropes. A calibrated load cell measured the force exerted on the ropes. Subjects were released without warning from a statically unstable forward lean by deactivation of an electromagnetic support system. Prior to release, subjects maintained a rigid body, flexing only at the ankles, and kept the heels of their shoes in contact with the floor. The instructions were to, upon release, take one step to recover, keep the arms folded across the chest, and maintain floor contact with the non-stepping foot.

During testing, the angle of lean was determined manually via a goniometer as the angle between vertical and the axis between the lateral malleolus and the greater trochanter (referenced to the angle measured during quiet stance). The first angle of lean tested was 5 degrees. Once a successful recovery occurred, the angle of lean was increased by 5 degrees. Trials continued until repeated attempts failed to produce a successful recovery. Failed recoveries resulted if multiple recovery steps were taken, the subjects' arms became unfolded, or their body was completely supported by the dynamic ropes.

A six-camera motion analysis system (Santa Rosa, CA) operating at 60 Hz recorded the position, at the time of the release, of 14 hemispherical passive markers placed over select anatomical landmarks. Post-processing determined the angle of lean as the included angle in the sagittal plane between vertical and the axis from the ankle

joint to the body center of mass. Rope-assisted recoveries, in which the peak post-release force applied to the load cells exceeded 20% body weight, were also identified and excluded during post-processing.

RESULTS

An independent t-test revealed that the difference between the maximum angle of lean between the men (16.07 ± 4.22 degrees, n=18) and the women (15.16 ± 3.36 degrees, n=33) was not significant (p=0.40). The maximum recoverable angle of lean determined for 51 subjects ranged from 8.7 to 22.0 degrees for the women and 8.2 to 24.6 degrees for the men (Figure 1). The remaining 28 subjects had either load cell data that could not be analyzed or were rope-assisted at their furthest angle of lean.

DISCUSSION

Although it had been previously determined that these women fell four times as frequently as these men (Pavol et al. 1999), the difference in their maximum, recoverable angle of lean was not significant. This contradicts a previous study (Wojcik et al. 1999) that showed older women had a maximum angle of lean that was significantly smaller than the older men (16.2 ± 4.5 and 24.0 ± 4.0 degrees for women and men, respectively; p=0.01). While the results for the women in both leaning studies were similar, the men of the previous study leaned 50% farther than the men of the present study (Figure 1). Because this discrepancy was not seen across genders, the differences may not be related to methodology. At this time, the cause for this discrepancy is unknown.

In conclusion, the maximum recoverable angle of lean does not differ between older men and women. Thus, an association between the gender-specific difference in fall frequency and the ability to recover from a forward lean is questionable.

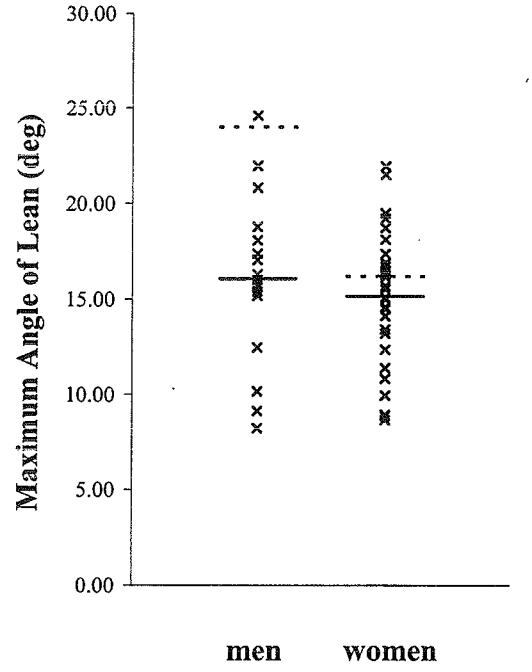

Figure 1: Maximum, recoverable angle of lean for older men (n=18) and women (n=33). The solid line is the mean for each group. The dotted line is the mean data from Wojcik et al. 1999.

REFERENCES

Pavol, M.J. et al. (1999). *J. Gerontol: Med. Sci.*, **54A**, M103-M108.

Wojcik, L.A. et al. (1999). *J. Gerontol: Med. Sci.*, **54A**, M44-M50.

ACKNOWLEDGMENTS

Funding by NIH-R01AG10557 (MDG).

BIOMECHANICS OF RECOVERY FROM A BACKWARDS FALL

Masao Tomioka, Tammy M. Owings, David Lord, Mark D. Grabiner

Department of Biomedical Engineering, The Cleveland Clinic Foundation
grabiner@bme.ri.ccf.org

INTRODUCTION

The direction of a fall is as important a risk factor for hip fracture as bone mineral density and body mass index. In particular, falls to the side and to the rear have a high probability of exposing the greater trochanter to impact.

Backward falls are not uncommon during everyday activities (Hsiao and Robinovitch, 1998). However, to date, there are no reports of experimental approaches studying the biomechanics of backwards falls initiated by a trip. The purposes of the present study were to characterize the movement strategies used to recover from a backwards trip and to determine biomechanical variables that distinguish between those subjects who recover and those who fall following the trip.

METHODS

Eighteen healthy young adults participated. Subjects wore a safety harness that prevented falls to the floor but did not impede the falling motions (Pavol et al., 1999).

Trips were induced by a metal obstacle (height = 20.5 cm) while the subjects walked backwards. Segmental kinematics were recorded using a six-camera motion capture system operating at 120 Hz.

Each trip outcome was classified as a successful recovery or a fall and the recovery strategy was classified as an elevating or a lowering strategy (Pavol et al, in press).

The dependent variables of the initial analysis included walking speed, the elapsed time from the trip to recovery foot placement on the floor, the horizontal distance between the COM and recovery foot placement on the floor, the vertical distance the COM moved during the recovery effort, and the angular distance the trunk deviated from vertical during the recovery. Distance and speed were normalized to body height (BH).

RESULTS AND DISCUSSION

The lowering strategy was the dominant stepping response to the backward trip (16 of 18). Within the lowering strategy, two

further categories were identified based on the foot-obstacle interaction. The impact with the obstacle was either followed by the entire foot being lowered to the floor (full contact, n=8) or followed by ankle plantarflexion that lowered the forefoot to the floor while the hindfoot maintained contact with the obstacle (partial contact, n=8).

Collectively, for the 16 subjects who implemented a lowering strategy, those who fell were not walking faster at the time of the trip (72±7 % BH•sec^{-1}) than those who recovered (67±12 % BH•sec^{-1}). However, subjects who recovered placed the recovery foot 9±8 % BH posterior to the COM whereas subjects who fell placed the recovery foot 11±12% BH anterior to the COM (p=0.004). The between-group differences for the other variables were not significant. Nevertheless, the subjects who recovered had a qualitatively smaller trunk excursion from vertical during the recovery compared to the subjects who fell (6±6 vs. 13±10 degrees, respectively, power = .27).

Further analysis was conducted on the subjects categorized as partial contact who fell (n=4) and recovered (n=4). This group of subjects was similar in overall statistics to the larger group, i.e., walking speed and the distance between the body COM and the recovery foot placement. However, the COM of the subjects who recovered rose to a larger vertical height during the recovery step (65±3 %BH) compared to those who fell (60±8 %BH). Notably, the subjects who recovered had a qualitatively smaller trunk excursion from vertical during the recovery compared to the subjects who fell (8±5 vs. 17±11 degrees, respectively, power = .17).

SUMMARY

Similar to recovery from an anteriorly-directed trip, recovery from a backward-directed trip is reliant on arresting the body rotation induced by the trip. Placement of the recovery step relative to the body COM, and the subsequent influence of the resulting ground reaction, appears to be a crucial recovery variable. Given the restrictions on the step length in the backwards direction, a given recovery step length would tend to be more effective in retarding body rotation if the trunk is maintained more vertically. The relationship between neuromotor control of the trunk musculature and the influence of the moment generated by the ground reaction is presently of interest.

REFERENCES

Hsiao ET., Robinovitch SN (1998) *J Biomechanics*; **31**: 1-9

Pavol MJ, et al. (1999) *J Gerontology:Med Sci*, **54A**:M103-M108

Pavol MJ et al (in press) *J Gerontology: Med Sci*

QUIET-STANCE BEHAVIOR CAN PREDICT THE DYNAMIC POSTURAL CONTROL RESPONSE

E.T. Hsiao-Wecksler[1], K. Katadare[1], J. McKillop[1], W. Liu[1,2], L.A. Lipsitz[3], and J.J. Collins[1]

[1]Center of BioDynamics, Dept of Biomedical Engineering, Boston University, Boston, MA, USA
[2] Dept of Physical Therapy Education, Univ of Kansas Medical Center, Kansas City, KS, USA
[3] Hebrew Rehabilitation Center for Aged, Harvard Medical School, Boston, MA, USA
Email: ethw@bu.edu, Web: http://cbd.bu.edu/abl/

INTRODUCTION

Fluctuations in the center of pressure (COP) during quiet-standing can be represented as a correlated stochastic process (Collins and Deluca, 1993). For many stochastic systems, the fluctuation-dissipation theorem (FDT) can be applied. This theorem compares the correlations in the fluctuations of a system and its relaxation to equilibrium following a perturbation. More specifically, it provides a relationship between the output of a quasistatic system, and the system's dynamic response to a perturbation. Recently, Lauk et al. (1998) applied the FDT to show that in young adults COP fluctuations during quiet stance could be used to predict the dynamic response of the postural control system to a weak perturbation. Young individuals, however, rarely have postural control problems. Therefore in this study, we examined whether this method could be extended to elderly individuals, including those with a history of falling.

METHODS

Seventeen healthy, community-dwelling elderly adults (7 with a history of falling, 10 without; age: 68-86 yrs; weight: 51-81 kg, height: 1.5-1.7 m) and ten young adults (age: 21-30 yrs; weight: 51-89 kg, height: 1.6–1.8 m) were included in this study.

Twenty randomly-presented trials were conducted on each subject: 10 quiet-standing trials and 10 perturbed trials, all 30 s in duration. To generate a weak impulse perturbation (a backward tug), the subject was tethered to a suspended 11 kg weight that was released after a random delay of 10-20 s. After the weight fell, the tether slackened and allowed the subject to readjust to an upright posture. The subject stood with both feet on a forceplate, arms crossed at the chest, and eyes open. Anterior-posterior (AP) COP data (Fig.1) were determined from the forceplate recordings.

For the quiet-standing trials, the derivative of the correlation function, dC(t)/dt, was calculated from the average of all 10 trials. This was accomplished by first determining the autocorrelation of COP fluctuations of each trial, and then calculating its derivative. The time of the maximal amplitude was used as the trigger point. Each trial was normalized to unity at the trigger point. Results from all trials for a given subject were then averaged.

For the perturbed trials, the response function R(t) was calculated from the average of the COP measurements for all 10 trials. The time of the maximal sway amplitude following the perturbation was used as the trigger point (Fig.1b). Each trial was then normalized to unity at the trigger point.

Applying the FDT, the two functions were fit to a linear regression with errors in both variables, $R(t) = a + b \cdot (dC(t)/dt)$, for each subject, for the first 4 s (or 480 data points). The goodness of fit was evaluated by a χ^2

test with $\nu = 478$, that is, $\chi^2 = 478$ represents a moderately good fit, and the fit improves as χ^2 decreases.

RESULTS AND DISCUSSION

For all young, eight elderly non-fallers, and all elderly fallers, results from the χ^2 test indicate that the two curves are significantly well matched (χ^2 values between 45 and 431), which imply that the two curves can be linearly predicted from one another. Two of ten elderly non-fallers had χ^2 greater than 652. Thus, in the majority of cases, we can predict the behavior of R(t) from dC(t)/dt.

All subjects exhibited the expected curve shape (Fig. 2), i.e., both curves decay from 1.0 and then fluctuate around an equilibrium state. The curves can be visually evaluated over three conditions: the rate of decay, the magnitude of the equilibrium state, and the time at which equilibrium was attained. χ^2 decreases as the similarities between the two curves increase.

These results suggest that it may be possible to predict an individual's postural control behavior during a weak disruption to balance from quiet-standing COP data. This implies that the postural control system may use the same control mechanisms under quiet-standing and perturbed conditions.

Clinically, these findings suggest that elderly individuals, especially those with compromised postural stability, may not need to be perturbed to have their postural control capacity characterized. Consequently, testing procedures may be safer since subjects would not be put at risk to falls during tests that involve perturbations. Additionally, this would eliminate the need for complicated perturbation devices since only quiet-standing data would be necessary.

REFERENCES

Collin, J.J., Deluca, C.J. (1993). *Exp Brain Res* **95**, 308-318.

Lauk, M. et al. (1998) *Phys Rev Letters* **80**, 413-416.

ACKNOWLEDGEMENTS

This study was funded by grants from the NIH, NIDRR, and NSF.

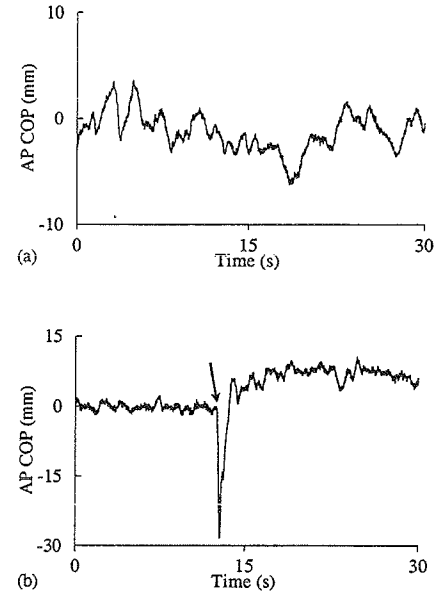

Fig.1. (a) Typical 30 s AP COP times series for quiet-stance trial. (b) Typical AP COP time series for perturbed trial; arrow indicates application of perturbation.

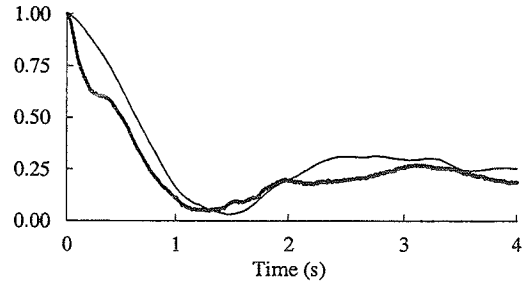

Fig.2. Response function R(t) (bold) and derivative of correlation function dC(t)/dt (thin) for a subject; $\chi^2 = 59$.

MOTOR CONTROL CHANGES IN AMBULATORY ELDERLY

K. Katdare[1], M. Slavin[2], C. Laughton[1], L. Nolan[1], J. Bean[3], C. Kerrigan[4], L. Lipsitz[3], and J. Collins[1]

[1]Center for BioDynamics, Dept. of Biomedical Engineering, Boston University, Boston, MA, USA
[2]Center for Rehab Effectiveness, Sargent College of Health at Boston University, Boston, MA, USA
[3] Hebrew Rehabilitation Center for Aged, Harvard Medical School, Boston, MA, USA
[4]Harvard Medical School Department of Physical Medicine and Rehabilitation, Spaulding Rehabilitation Hospital, Boston, MA, USA
E-mail: laughton@bu.edu Web: http://cbd.bu.edu/abl

INTRODUCTION

The goal of this study was to gain an understanding of how age-related functional changes in motor control affect both muscle activity and quantitative measures of balance. Previous work has established that traditional summary statistics were not sensitive enough to detect age-related differences in the 'quasi-static' dynamics of the postural control system (Collins et al., 1995). In contrast, stabilogram diffusion analysis (SDA) has detected age-related increases in short-term scaling exponents indicative of an open-loop postural control mechanism that drifts towards instability (Collins et al., 1995). Furthermore, significant age-related increases in short-term effective diffusion coefficients were found in elderly individuals identified as at risk for falling compared to young healthy.

A possible mechanism behind these changes is a postural control strategy in which muscle activity is increased. An increase in muscle activity is likely to lead to increased short-term fluctuations across the lower limb joints resulting in decreased stability. Therefore, the aim of this investigation was to assess the relationship between lower-limb muscle activity and postural sway as assessed by SDA in both elderly and young individuals.

METHODS

Data were collected from thirty subjects classified into one of three groups: (1) elderly individuals at risk of falling (Er) (range=69-92yrs, N=10), (2) elderly healthy (Eh) (range=68-82yrs, N=10), and (3) young healthy (Yh) (range=24-32yrs, N=10). Individuals with gait or postural disorders were excluded from the study. Prior to testing, all subjects gave informed consent. Individuals with specific impairments that could affect balance were deemed ineligible. Subjects were categorized as fallers if they experienced two or more unexplained falls during normal activities over the last 12 months.

The Neuromuscular System 3-8 EMG Biofeedback unit (NeuroDyne Medical Corporation, MA) was used to collect EMG data bilaterally from the Tibialis Anterior (TA), Soleus (SO), Vastus Lateralis (VL), and Biceps Femoris (BF). COP data were sampled by a Kistler 9287 multi-component force platform. Both EMG and COP data were sampled at a rate of 1500Hz.

For the normalization process, three baseline trials (minimum muscle activity in a seated position) and three isometric maximal voluntary contractions (MVC) were collected from each muscle. Ten quiet-standing trials of 30s were collected from each subject. The EMG data were bandpass filtered between 25-550Hz using an inverse chebyshev filter and processed with a moving 40ms running window RMS. To reduce noise in the signal, the mean baseline EMG for each muscle was subtracted from its respective EMG signal during the quiet-standing trials. A muscle was considered to be "on" when the activity level reached 3X the standard deviation of the baseline trial data. The % of the 30s trial that a particular muscle was on was determined (%-on). The

% of the trial in which co-contractions of the TA and SO (TA-SO) and the VL and BF (VL-BF) were present was also determined. Muscle activity was normalized (nEMG) to the maximum MVC activity level from the three MVC trials. These parameters were obtained for the right and left sides then averaged. COP trajectories were analyzed as one-dimensional and two-dimensional random walks according to SDA as described by Collins and DeLuca (1993).

For each dependent measure, separate ANOVAs followed by post-hoc t-tests were used to examine group differences ($p<0.05$). Bivariate regression analysis was performed to determine relationships between nEMG activities and short-term (*Dys*) and long-term (*Dyl*) effective diffusion coefficients in the anterior-posterior (AP) direction.

RESULTS

Significant increases in short-term diffusion coefficients as well as the AP and radial scaling exponents were found in both elderly groups compared to the young healthy subjects. No significant differences were found in any of the SDA parameters between the Eh and Er groups.

Er and Eh groups demonstrated increased %-on, co-contraction, and nEMG compared to the Yh group (Table 1). No significant differences were found between the Er and Eh groups in any of the muscle activity parameters.

Regression analysis determined that moderate relationships existed between *Dys* and nBF, and between *Dyl* and nTA (Table 2).

Table 2. Relationship between nEMG and SDA (R^2).

	Dys	*Dyl*
nTA	0.11	0.36
nSO	0.21	0.01
nVL	0.06	0.15
nBF	0.37	0.08

DISCUSSION

Specific SDA measures are significantly higher for the elderly groups compared to young in agreement with previous reports (Collins et al., 1995). Initial results also demonstrate increased overall muscle activity in the elderly (Er & Eh) compared to the young group (Yh). There appears to be a positive relationship between both short-term and long-term diffusion coefficients and muscle activity.

These data represent the initial phase of an ongoing study that will test 200 subjects. Additional subjects are likely to strengthen the findings and elucidate the subtle differences in motor control between young healthy, elderly healthy, and elderly individuals who have been identified as at risk for falling. The question remains whether elderly subjects demonstrating significantly increased muscle activity will exhibit improved stability after participating in a training program designed to decrease muscle activity.

REFERENCES

Collins J.J. et al.(1995) *Exp Brain Res,* **104**, 480-492.

Collins J.J. and DeLuca C.J.(1993) *Exp Brain Res*, **95**, 308-318.

ACKNOWLEDGEMENTS

Funded by NIA Grant # PO1 AGO4390.

Table 1: Muscle activity during quiet stance trials.

	%-on				Co-contraction (%)		nEMG			
	TA	SO	VL	BF	TA-SO	VL-BF	nTA	nSO	nVL	nBF
Er	46.9*	89.1	63.2*	48.5	44.5*	32.1*	0.035	0.168*	0.081*	0.061
Eh	39.5*	88.1	54.1*	43.1	34.8*	26.2*	0.030*	0.125	0.066*	0.038
Yh	10.0	82.3	2.7	40.6	7.1	1.0	0.014	0.100	0.013	0.029

*significantly different from Yh group ($p<0.05$)

CAN TRAJECTORIES OF INDIVIDUAL BONY LANDMARKS INDICATE MEDIAL-LATERAL INSTABILITY DURING OBSTACLE CROSSING?

Michael E. Hahn [1], Li-Shan Chou [1], Kenton R. Kaufman [2] and Robert H. Brey [3]

[1] Department of Exercise and Movement Science, University of Oregon, Eugene, OR
[2] Department of Orthopedic Surgery and [3] Department of Otorhinolaryngology
Mayo Foundation, Rochester, MN
E-mail: chou@oregon.uoregon.edu

INTRODUCTION

As the elderly population continues to grow, the need for indicators of dynamic instability during locomotion also increases. Such indicators may enhance early identification of at-risk individuals, thereby reducing the risk of traumatic falls. Greenspan et al. (1998) found that falls to the side are a major risk factor for hip fracture. Additionally, Tinetti et al. (1989) showed imbalance and tripping over obstacles to be two of the most common causes of falls in the elderly. Therefore, medial-lateral (M-L) body sway during obstacle crossing may be used to distinguish individuals at risk for sideways falling from healthy individuals.

The whole body center of mass (COM) is commonly calculated in research laboratories to assess stability during locomotion. However, this calculation can be time-intensive and possibly not realistic for all clinical laboratories. If a more direct motion measurement could be made that would effectively distinguish dynamic instability to the same extent as COM, a more expedient assessment would be available to the clinician.

Therefore, the purpose of this study was to determine whether displacement of selected bony landmarks, while negotiating obstacles, could indicate an individual's M-L instability to the same extent as whole body COM.

METHODS

Eleven subjects, including five healthy elderly adults (mean age, 70.4 years) and six elderly patients with imbalance (mean age, 75.7 years), were recruited for this study. A six-camera ExpertVision™ system (Motion Analysis Corp., Santa Rosa, CA) was used to capture and reconstruct the three-dimensional coordinates of surface markers. A 13-link biomechanical human model was used to compute the coordinates of the whole body's COM. Subjects were assessed in conditions of unobstructed level walking and when stepping over an obstacle of height corresponding to 2.5%, 5%, 10%, or 15% of the subject's body height (BH). All trials were conducted at a comfortable self-selected walking speed while barefoot. The order of obstacle height was randomly selected. The bony landmarks selected for comparison were the forehead (HD), right acromion (SHLD), and right anterior superior iliac spine (ASIS). A two-way ANOVA was used to test for group differences in the M-L displacement of these landmarks and COM.

RESULTS AND DISCUSSION

There were significant group differences in ASIS ($p=0.022$) and COM sway ($p=0.025$), across all obstacle heights. Group differences in HD and SHLD sway were not significant. However, sway values for all measures were greater in elderly patients

than in healthy elderly. These results possibly reflect a decreased ability to control segment motion during obstacle crossing in elderly patients.

For all sway measurements, the greatest mean difference between groups was at the lowest obstacle condition (2.5% BH). Elderly patients showed 24.5% greater sway for the HD, 56.5% for the SHLD, 61.5% for the ASIS and 80.8% for the COM during the lowest obstacle condition than healthy elderly.

Although COM sway showed the greatest relative difference between group means in the 2.5% and 5% BH conditions, relative differences in ASIS sway were greater in the 10% and 15% BH conditions (see Figure). This may indicate a more rigid whole-body sway at lower obstacles and more lateral trunk flexion at the greater obstacle heights. These group differences in either ASIS or COM sway possibly result from a decrease in proprioceptive awareness of segment position or neglect of segmental control in a focused effort to clear the obstacle. Due to a pre-existing sense of instability, elderly patients increase foot elevation despite the subsequent increase of M-L pelvic and trunk motion.

SUMMARY

These results indicate a distinction between M-L sway for healthy elderly and elderly patients with imbalance. Because both sway measurements of the ASIS and COM demonstrated significant differences between groups, measuring displacement of landmarks on the pelvis or lower trunk may be adequate for indicating M-L instability during obstacle crossing.

REFERENCES

Chou, L-S et al. (2001) *Gait & Posture* **13**: 17-26.

Greenspan, SL et al. (1998) *Am J Med* **104**:539-45.

Tinetti, ME et al. (1989) *N Engl J Med* **302**: 1055-1059.

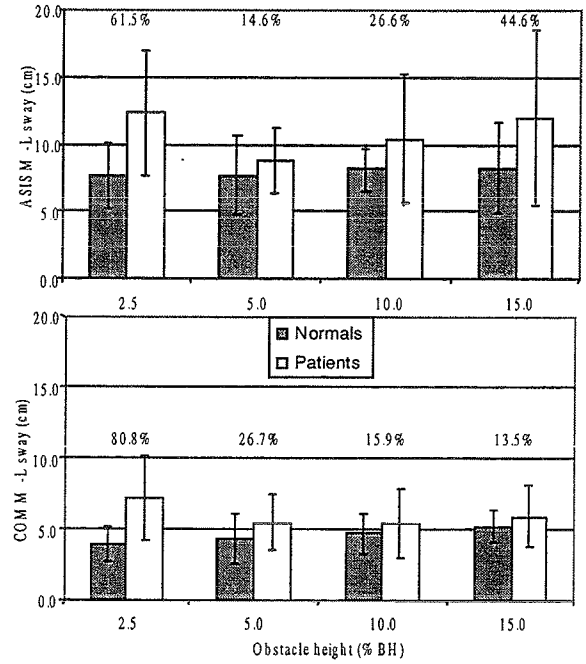

Figure. Comparison of M-L sway magnitudes for the ASIS and COM. Inset values indicate the relative difference between groups for each obstacle height ({Pt-N}/N*100).

AN ANATOMICAL VOXEL-BASED FE CONTACT ANALYSIS FORMULATION

Nicole M. Grosland Douglas R. Pedersen Thomas D. Brown

Department of Orthopaedic Surgery, University of Iowa, Iowa City, IA
E-mail: nicole-grosland@uiowa.edu, Web: poppy.orbl.uiowa.edu

INTRODUCTION

The manual labor required to generate three-dimensional meshes of geometrically complex bone morphologies almost always limits finite element (FE) analyses to a single representative specimen. Such models are based on 'average' bone geometry and material definitions, thereby compromising correspondence with patient-specific clinical outcomes. Voxel-based models are ideally suited to accommodate a large range of geometric and density-distribution variations. The premise of voxel-based meshing is the transformation of CT image data directly into elements for FE models, using eight-noded hexahedral elements.

Analysis of intra-articular contact is a particularly important class of orthopaedic finite element problems. Imprecise surface definitions, however, plague the tractability of voxel-based meshes for contact modeling purposes. Consequently, we have developed a technique to smooth the "stair-step" geometric irregularities inherent in voxel-based models, near plausible contact regions. Initially, we have focused our modeling efforts on the articulation of the hip, as well as spherical and cylindrical articulations. A substantial attraction of working initially with such geometries (sphere and cylinder) has been the availability of a corresponding gold standard (the Hertz elastic contact solution) for model validation. In principle, voxel-based pre-processing is an attractive approach for patient-specific studies of a broad class of aberrant articular joint contact conditions, such as deformities or imprecisely reduced intra-articular fractures. Such models, for example, may aid patient-specific surgical planning of optimal fragment reduction.

METHODS

The FE model formulation initiates with CT image source data (Visible Human, male) in the form of a voxel array, where the modulation of voxel grayscales reflects the density of the object imaged (Figure 1a).

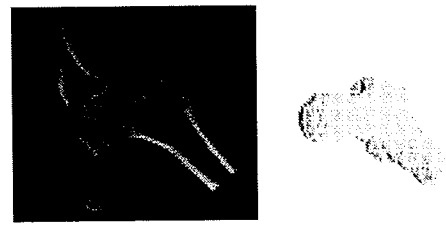

a b

Figure 1: Coronal image of the proximal left femur, (b) FE model (element size: 3x3x3 mm^3).

Given an operator-specified threshold for background exclusion, a specific set of object-composing voxels is readily identified whose grayscale values exceed the threshold (Figure 1b). Stair-step boundary artifact is clearly evident. A threshold-driven, custom-written variant of the marching cubes algorithm is used to interpolate a continuous three-dimensional surface (discretized into triangular facets of arbitrary refinement) that best delimits the physical object. The operator is prompted to identify the region of interest for contact stress analysis, normally the articular surface. The voxel-based grid structure enables nodes to be positioned at the

intersection of the triangulated surface and the pre-established grid, thus generating a smoothed surface with nodes coinciding with the underlying voxel vertices. A numerical relaxation routine is invoked to disperse nodes between the newly formed surface and the underlying voxel vertices, such that element distortion occurs over multiple elements, rather than being concentrated solely at the surface. Having thus attenuated the geometric distortions imposed by smoothing, the remaining voxel vertices are converted directly into nodes of a corresponding cubically connected array of hexahedral continuum elements.

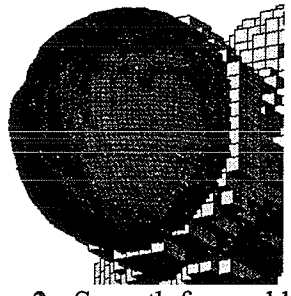

Figure 2: Smooth femoral head

An additional use of the triangulated surface is the direct conversion to a rigid-body FE model (e.g., pelvis). Once the model is geometrically established (Figure 3), the continuum element material property distributions are specified, the loading and boundary conditions of interest assigned, and the contact solution executed (ABAQUS, version 5.8).

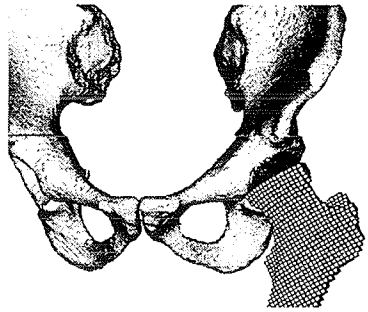

Figure 3: Complete anatomical FE model

RESULTS AND DISCUSSION

Compared to corresponding Hertzian contact formulations, the voxel-based contact solutions each (spherical and cylindrical) had errors of less than 2%. Furthermore, as the conformity of the contacting surfaces increased (flat plate to congruent), peak stress levels decreased. Enroute to establishing appropriate spatial resolution to address local articular incongruities, while maintaining computational compatibility, the use of MPCs or multiple point constraints, has been investigated. Such constraints enable multiple voxels (i.e., 3x3x3) to define a single element on a regional basis, thereby enabling multiple elements to abut a single element. This method reduces the number of elements overall, while retaining regions of high refinement juxta-articularly. Figure 4 illustrates a resultant von Mises stress contour pattern in response to a 2000N vertical load acting downward through the pelvis.

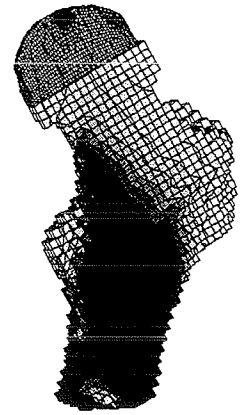

Figure 4: Von Mises stress contour in response to a 2000N vertical load through the pelvis

ACKNOWLEDGEMENTS

Financial support provided by NIH AR46601. Special thanks to Dr. Vincent Magnotta and the Iowa Mental Health Clinical Research Center's (MH-CRC) image processing laboratory.

LOCALLY ORTHOTROPIC FEMUR REMODELING

Thomas J. Impelluso
Department of Mechanical Engineering, San Diego State University
5500 Campanile Drive, San Diego, CA 92182
E–mail: impellus@kahuna.sdsu.edu

INTRODUCTION: Bone has long been known to adapt its structure to its loading conditions. This adaptation occurs on a micro–structural level: density is redistributed, principal material directions are realigned and, as a result, the anisotropic material parameters change. Such remodeling has been described several ways. Jacobs, et. al. [2] put forth a model which is based upon modern continuum damage mechanics; they showed how this model predicts regions of density distribution, and regions of principal material directions of stiffness. Bagge [1] utilized an optimization scheme to model principal material directions for a three dimensional case. This paper extends this work by supplying a finite element mesh of the femur in which each element has local principal material directions of orthotropy.

Principal material directions are vertical in the shaft of the femur; however; there is a local and continuous change of both material properties and, most significant for this paper, principal material directions with distance toward the femoral head. These issues pose great difficulty for commercial finite element (FE) codes. In such codes it is nearly impossible to create a mesh in which each element has its own unique principal material directions and properties. Certainly one can create regions of elements with the same unique properties (i.e.: sections of constant orthotropic directions), but to create a total locally orthotropic mesh is nearly impossible. This paper presents a FE code that can produce such a mesh, and also manifests the potential to model growth and remodeling.

METHODS: The 2D FE algorithm is:

1) run a plane stress orthotropic analysis in which each element has randomly oriented principal material directions, initially.
2) compute principal stress directions for compressive load on the femoral head;
3) reorient principal material directions to be parallel to the principal stresses;
4) compute the effective strains for each element and repeat from (1) until principal material directions no longer change.

The four orthotropic material constants used in the analysis are found in the table below.

Property	*Value used*
E_{11}	17.0 GPa
E_{22}	11.0 GPa
G_{12}	3.3 GPa
ν_{12}	0.41

For an orthotropic material that has only one symmetry plane coincident with the coordinate plane 1–2, the stress–strain relations must be generalized as:

$$\begin{bmatrix}\sigma_{11}\\ \sigma_{22}\\ \sigma_{12}\end{bmatrix}=\begin{bmatrix}Q_{11} & Q_{12} & Q_{13}\\ Q_{21} & Q_{22} & Q_{23}\\ Q_{31} & Q_{32} & Q_{33}\end{bmatrix}\begin{bmatrix}e_{11}\\ e_{22}\\ e_{12}\end{bmatrix} \quad \text{Eq. 1}$$

In Eq. 1, the Q's depend upon the material constants in the table, and on the angle of principal material directions. Following Tsai and Pagano [3], this relationship can be written in compact form. It is not presented here; it can be found in the literature.

RESULTS AND DISCUSSION: This method presents a 2D mesh of the femur in which each element manifests local orthotropy. Presented in Figure 1 is the well known Wolff stress trajectories for the femur. In Figure 2 is a micrograph of the femoral head. Figure 3 presents the principal material directions for the FE code after six iterations. Initially, the principal material directions were completely random. In Figure 3 they have reoriented themselves; this can be shown to minimize strain energy.

A comparison of the figures shows how the bony microstructure is concentrated along the lines of principal mechanical stress according to the principal of functional adaptation. The algorithm developed in this paper predicts this structure–function relationship as a consequence of growth and remodeling under normal loading conditions.

REFERENCES

Bagge, M. (2000). A Model of Bone Adaptation as an Optimization Process. J. of Biomechanics, 33, 1349–1357

Jacobs, C.R., et. Adaptive Bone Remodeling Incorporating Simultaneous density and anisotropy considerations. J. of Biomechanics, 30, 1996, 603–613

Tsai, S. W., and Pagano, N. J., (1968). Invariant Properties of Composite Materials. Composite Materials Workshop. Technomic Publication Company, Westport Connecticut.

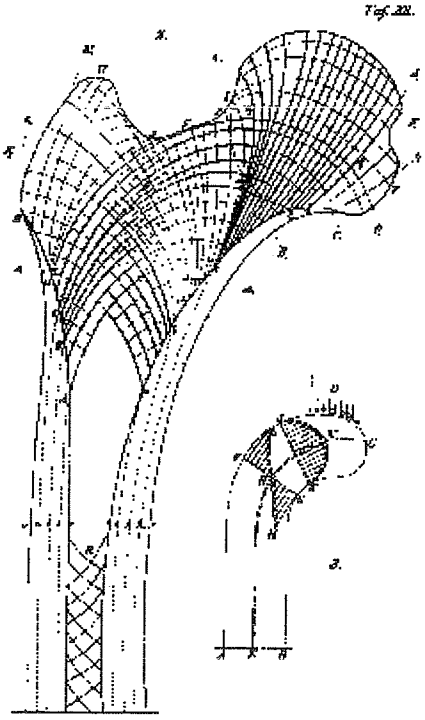

Figure 1. Micrograph of femoral head showing cancellous bone microstructure.

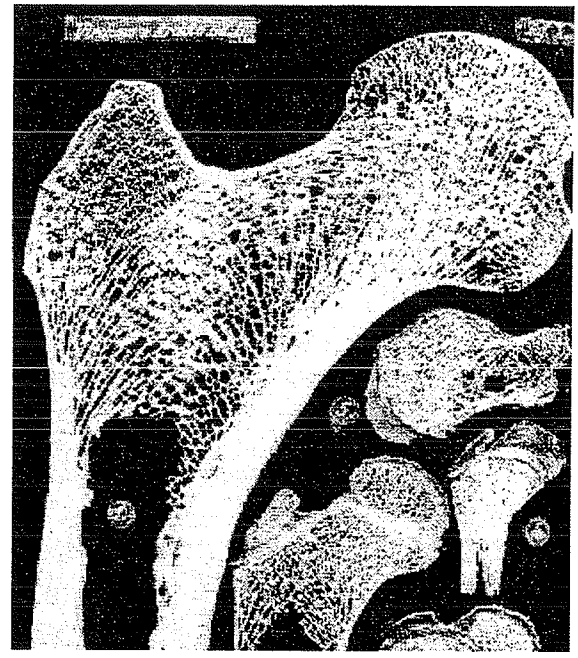

Figure 2. Wolff stress trajectories.

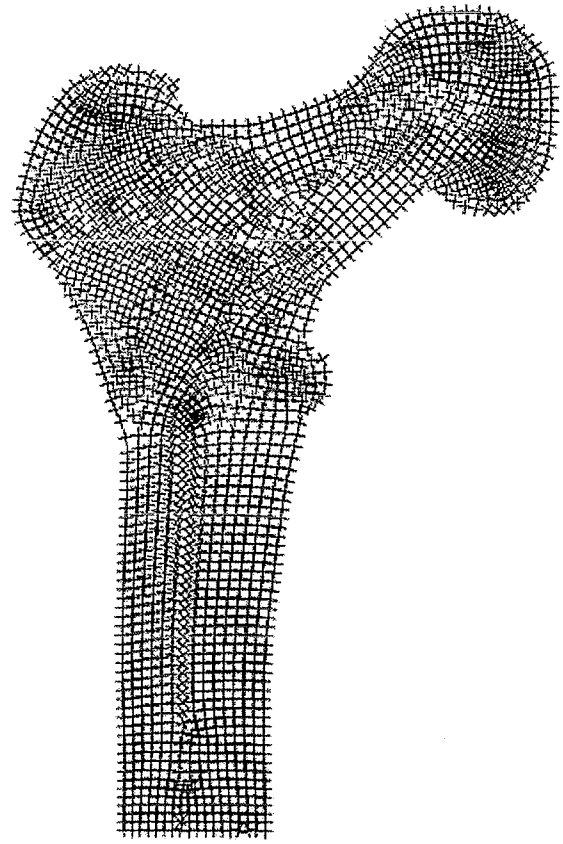

Figure 3. Principal material directions after 6 iterations; element edges not drawn; lines indicate local principal material directions.

WHEELCHAIR PROPULSION ANALYSIS USING QUATERNIONS

Konstantinos Vrongistinos[1], Yong Tai Wang[2], Dan Marghitu[3], Young Hwang[4], David Pascoe[3].

[1] Biomechanics Laboratory, California State University, Northridge, CA, USA
[2] Biomechanics Laboratory, Georgia State University, Atlanta, GA, USA
[3] Auburn University, Auburn, AL, USA
[4] California State University, San Bernardino, CA, USA
E-mail: kv61497@csun.edu Web: http://www.csun.edu/~kv61497

INTRODUCTION

Mathematics requires three markers to define a local coordinate system to calculate rotations in three dimensions (3D), as three coordinates are necessary to specify the orientation of a rigid body with respect to a fixed set of space axes. However, it is not uncommon in wheelchair literature to find papers (Veeger, et al., 1991) that used only two markers to define segment rotation in three dimensions and subsequently use the results to calculate joint forces. But two markers cannot define a rotation matrix. If someone does not use rotation matrices, results are confined to report segmental projection angles and not directional cosines.

The local coordinate system that allows a complete description of a vector in space has been documented before (Cole, et al., 1993). Yet its usefulness is emphasized in terms of reporting meaningful results in terms of anatomical positions. But there is more to the story. Lack of rotation matrices creates dual error. First, the inertia tensor is calculated in respect to a different axis (not the axis that the rotation is taking place), and second, instead of finding the real angular velocities researchers are using the rate of change of the projection angles. This is acceptable in pure kinematics analysis but not in kinetics analysis. It is also acceptable to use the linear velocity over the radius ratio in two dimensions to calculate the angular velocity without error. However, it is erroneous to calculate angular velocities in 3D by dividing the linear velocities with the radius of the curvature, because there is no definition for the inverse of a vector.
It is common to represent a transformation parametrically with Euler or Bryant-Cardan angles, although other representations such as helical axis, Euler parameters (normalized quaternions) can also be used. Euler angles suffer from gimbal locks, and more than one parameterizations can represent one rotation. However, transformation matrices are necessary for the inverse dynamics problem to calculate either the change in the Inertia Tensor (equation 1) or the local angular velocity (equation 2).

$$\vec{M}_p = \frac{d(I\vec{\omega}_G)}{dt} - \vec{M}_d - (\vec{r}_d \times \vec{R}_d) - (\vec{r}_p \times \vec{R}_p) \quad (1)$$

$$\vec{M}_p = I^S\vec{\alpha} + (\vec{\omega} \times I^S \bullet \vec{\omega}) - \vec{M}_d - (\vec{r}_d \times \vec{R}_d) - (\vec{r}_p \times \vec{R}_p) \quad (2)$$

where M means moment, r is the moment arm, R the reaction forces, d means distal, p means proximal, ω_G is the global angular velocity, ù is the local angular velocity, I is the Inertia Tensor (IT), I^S the local IT, and á the angular acceleration.

The purpose of this paper was to define a unique parameterization for each segment from frame to frame using quaternions (Q3). A secondary purpose was to compare the quaternion method with a method that uses projection angles (two-markers M2) for inverse dynamic analysis.

METHODS AND ALGORITHMS

Quaternions are equivalent to a rotation matrix without the drawback of gimbal locks. Euler-parameters or normalized quaternions represent the eigenvector (u) that is derived from the unit eigenvalue (see Figure 1.) of a transformation matrix. Contrary to Euler angles Euler-parameters have only two parameterizations for segmental rotations. This uncertainty hindered researchers to use quaternion as an alternative to Euler angles.

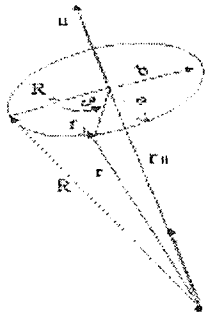

Figure 1: Unit eigenvector (u) that identifies the rotation defined by the unit eiganvalue of the rotation-matrix. Another eigenvector (-u) results in an equivalent rotation

However, if someone hypothesizes that movements from frame to frame happen in the possible shortest arc then the answer is given by a trick used in animations (Watt, & Watt, 1992). To find the shortest arc during rotations between two quaternion pairs *p* and *q*, the magnitude of their difference is calculated as *(p-q)⊗(p-q)*, and later compared with the magnitude of the difference when the second quaternion is negated, as *(p-(-q))⊗(p-(-q))*. The smaller number belongs to the shortest path and thus a transformation from frame to frame is defined uniquely.

Three markers were used for each segment to define a transformation matrix and derive the Euler parameters (see figure 2).

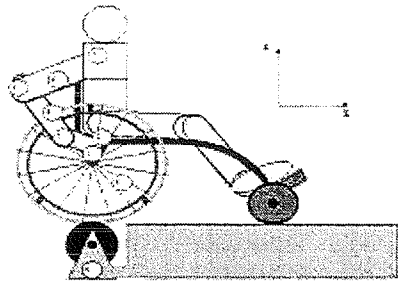

Figure 2: Marker placement is such a way as to have a triplet of markers in each segment to define a local coordinate system

Data were collected from a participant propelling a wheelchair on a roller for 36 s, with a Watsmart system at 200 Hz.

The forces and moments calculated with Q3 were compared with the values of M2. The results are reported as percent differences:

$$P_{error} = \frac{Q3_{variable} - M2_{variable}}{Q3_{variable}} \quad (3)$$

RESULTS

The theory dictates that three points should be used to describe angular movements of segments, so three points per segment should be used for accurate kinematic and kinetic analysis. The differences lie on the moments of course. In practice the error in moments range from 2.3% to 18.36% (see Table 1).

Table 1: Mean calculated differences to Q3 method in 3D for three segments

Error %	X	Y	Z
Hand	3.8	9.1	2.6
Forearm	11.5	18.36	15.76
Humerus	2.3	7.7	5.8

DISCUSSION

Segmental transformations from frame to frame can be unique by using the shortest quaternion arc. This can have a significant implication in human motor control as computations of state variables are notably reduced. Small segmental inertias may minimize the error using M2, but three markers give more accurate and more meaningful results.

REFERENCES

Cole, et al. (1993). Application of the joint coordinate system to 3-D joint attitude and movement representation: a standardization proposal. *Journal of Biomechanical Engineering*, **105**,136-144.

Veeger, H.E.J., van der Woude, L.H.V., & Rozendal, R.H. (1991). Load on the upper extremity in manual wheelchair propulsion. *Journal of Electromyography and Kinesiology*, **4**, 270-280.

Watt, A., & Watt, M. (1992). *Advanced animation and rendering techniques*. New York, New York: ACM Addison-Wesley

VERIFICATION OF MUSCLE-TENDON PATHS FOR INTERACTIVE, 3-DIMENSIONAL COMPUTER SIMULATION OF THE EXTREMITIES

William L. Buford, Jr., Munir Shah, Clark R. Andersen, Karin S. Elder, Rita M Patterson, Steven F. Viegas

Department of Orthopaedics and Rehabilitation, University of Texas Medical Branch, Galveston, TX, USA
E-mail: william.buford@utmb.edu

INTRODUCTION:

Simulation of musculoskeletal kinematics as a tool for the study of functional anatomy, a predictive research tool, and for computer assisted prosthesis design or surgery is a rapidly growing area in biomechanics research and development. Realism has been increasing at a rapid rate as imaging resolution, 3_D structural development and kinematic modeling capabilities improve. However, the accuracy of such modeling efforts should not be taken for granted and researchers in the field must continuously concentrate upon experimental verification of the component models in their simulations. This report concentrates upon verification of muscle-tendon path models developed for a 3-D simulation of the extremities through the comparison of muscle moment arms generated by the simulation with those measured in fresh cadaver experimentation.

METHODS:

Using the simulation described in [1], hypotheses are tested for several proposed muscle-tendon-joint models by interactively rotating a given joint through its range-of-motion, and observing/recording the calculated moment arms of the muscles crossing that joint. This study undertook experimental verification of the normal moment arm for the extensor pollicis longus (EPL) to the thumb (at the CMC joint), and the moment arms following release of the EPL from its distal radius pulley (Lister's tubercle). Moment arms are derived from tendon excursion – angular motion data as the derivative of excursion with respect to angle.

SIMULATION PREDICTIONS:

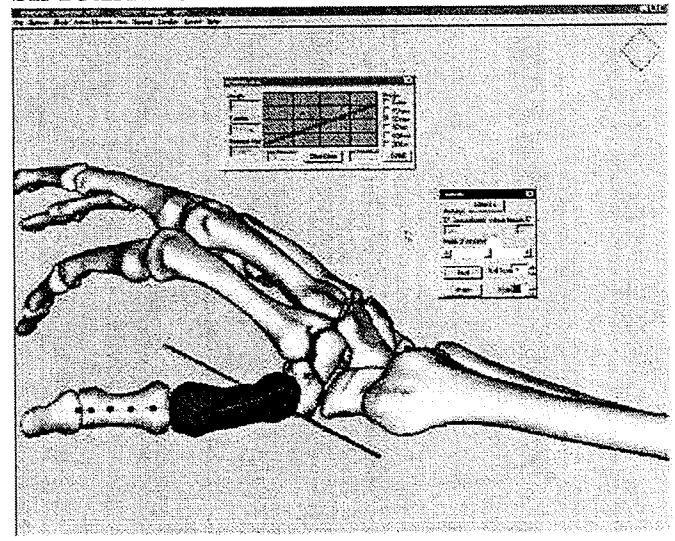

The figure above is a captured image from the upper extremity simulation depicting the path of the normal EPL muscle/tendon unit when modeled as a B-spline curve through a few anatomical control points (highlighted as blue spheres). The tendon exits the forearm at Lister's Tubercle on the dorsal surface of the distal radius and courses directly to a soft tissue pulley structure at the distal end of the first metacarpal (this

bowstringing action forms the dorsal part of the "snuffbox." – the extensor pollicic brevis forms the more volar part).

The following figure is the same for the path of the EPL released from the pulley structure of Lister's tubercle. The simulation predicts a significantly reduced moment arm for the released EPL throughout the abduction-adduction range-of-motion. In both, the moment arm is minimum at full abduction and increases as the tendon bowstrings during adduction. The moment arm is calculated anddisplayed (see the upper center graph) in real-time as the joint is rotated using the mouse controlled slider (in the box to the right above the radius and ulna).

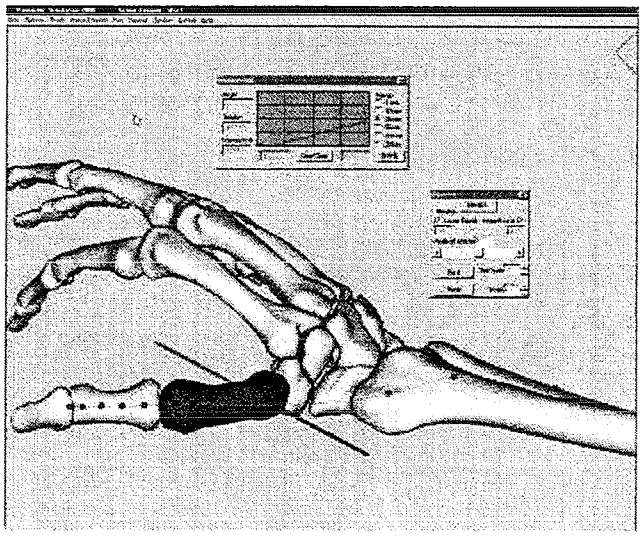

EXPERIMENTAL RESULTS:

The moment arms determined in a single fresh cadaver experiment for the normal and released EPL are depicted in the folowing figure (EPL Average Moment Arms). Note that the moment arm decreased nearly 50% following release from the pulley point(at Lister's tubercle).

CONCLUSIONS:

The simulation predicted a reduction in moment arm for the released EPL to 25%,

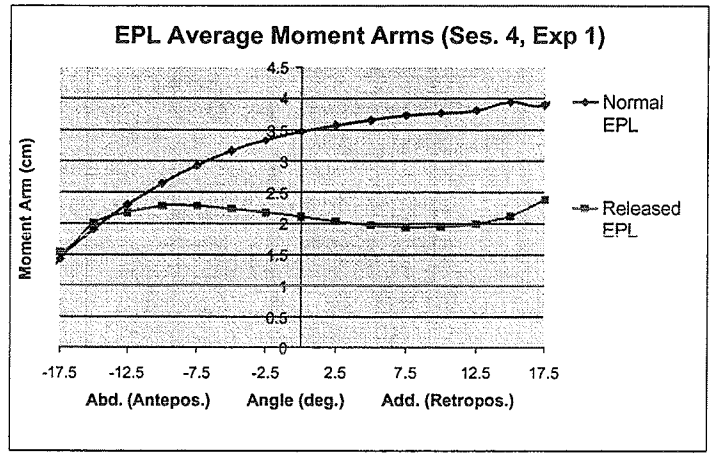

50%, and 75% of the normal EPL at full adduction, mid-range and full abduction respectively. Experimental results confirm the bowstringing (increasing moment arm with adduction) seen in the simulation prediction. However the experimentally released EPL does not exhibit bowstringing. The experimental moment arms exhibited less bowstringing in adduction motion than that of the simulation. The extension moment arms agreed in magnitude and had similar bowstringing, suggesting that another soft tissue constraint should be considered in the B-spline model for abduction-adduction at the CMC joint. Future work includes continued experimental validation and investigation of varied blending functions for improved muscle/tendon B-spline paths.

REFERENCE: [1] Buford, W. L., Jr., Andersen, C. R., Elder, K. W, Pickard, J.M., and Patterson, R.M., **Proceedings**, VII[th] International Symposium on Computer Simulation in Biomechanics, Aug 5-7, 1999.
ACKNOWLEDGEMENTS: Supported by the Texas Advanced Technology Program (Grant Number: 004952-0111-1999), and a research grant from Sulzer Orthopaedics, Inc., Austin, TX.

THE EFFECT ON STRAIN RELIEF OF FIXATION METHODS OF LONG STEMS IN REVISION TKA: A PARAMETRIC FINITE ELEMENT ANALYSIS

J.S. Nyman,[1] S.J. Hazelwood,[1] and J.J. Rodrigo[2]

[1]Orthopaedic Research Laboratories, University of California Davis, Sacramento, CA 95817
[2]Department of Orthopaedic Surgery, University of California Davis Medical Center, Sacramento, CA 95817
e-mail: jsnyman@ucdavis.edu

INTRODUCTION

Two general mechanisms that degrade bone stock prior to aseptic loosening of arthroplasties include debris-induced osteolysis and disuse osteoporosis, commonly called stress shielding. Bone loss necessitates the use of long stems to stabilize the prosthesis when revising a failure of a primary joint arthroplasty. Clinical follow-up studies have advocated securing tibial components in revision TKA with, without, or with partial bone cement. (Barrack et al., 1999) Because of the abundant mitigating factors that may influence results in clinical studies (e.g. gender, age, activity level, implant design), the lack of consensus on a fixation technique is understandable. Insensitive to patient factors, finite element models of the tibia and tibiae with implants were developed to assess the effect of stem diameter, presence of cement, and crosslocking screws on relieving the functional strain incurred by intact bone in the metaphyseal region.

METHODS

The geometry of a tibia, created from a digitized, frontal x-ray of an amputated left leg, was meshed with 4 node, quadrilateral, plane strain elements. The mesh was designed to accommodate a stem with a length of 160 mm and the implant features depicted in figure 1. Below the tibial tray, 5 models of different constructs (table 1) and the intact tibia had an identical mesh consisting of 3737 nodes and 3559 elements with a size no greater than 2 mm by 2 mm. Linearly elastic, isotropic material behavior was assumed. Heterogeneous distributions of Young's modulus and Poisson's ratio were given to elements of trabecular bone. (Lewis et al., 1998) Values of E for the diaphyseal and metaphyseal region of cortical bone were 15,000 MPa and 5,000 MPa, respectively ($\nu = 0.3$ for both). The stem and the screws, located 25 and 50 mm from tip of the stem, were made of titanium. Component material values from Lewis et al. were used. To account for the out-of-plane contribution to stiffness, the 2D elements were assigned a thickness value based on the relative physical size of the modeled region. Fifty-five percent and 45 % of a downward resultant force of 2000 N (approximately 3x body weight) was distributed over the medial and lateral condyles, respectively, with the distal end constrained. After ABAQUS 5.8 (HKS, Pawtucket, RI) solved the FE models, minimum principal strains within regions of interest were recorded (as % of intact strain).

RESULTS AND DISCUSSION

As shown in figure 2, all fixation methods cause a reduction in strain on the trabecular bone below the tibial tray, indicating stress shielding in this region. This is concurrent with observations of bone mineral loss in the metaphyseal region after TKA (Levitz et al., 1995). Apparently, the use of a large stem without cement (i.e. press-fit) in lieu of a fully cemented small stem may have a slightly greater reduction in strain (% of intact strain difference is 4.7 and 2.9 on the medial and

Table 1. Re-assignment of material properties to elements allowed 5 constructs with these variables to be modeled with the same mesh.

Model name	Stem diameter (mm)	Presence of Cement
Full cement	12	tray & stem
Cementless	16	none
Partial small	12	tray only
Partial large	16	tray only
Crosslock	12	tray only

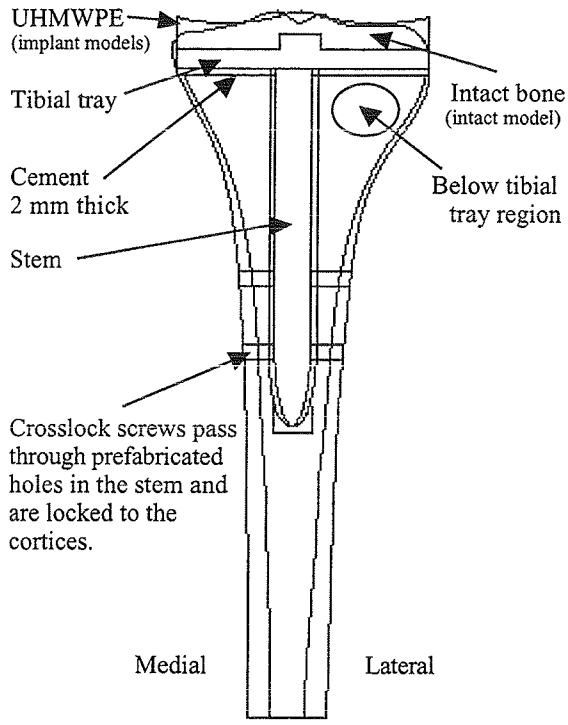

Figure 1. Super-imposed features for the finite element models of constructs and the intact tibia dictated mesh design.

lateral sides, respectively). A cemented tibial tray with a large stem (partial large) may slightly decrease the strain loss observed in the cementless, press-fit implant. A cemented tray with a small stem (partial small) has the least reduction in strain. Having the advantage of a small stem, the crosslocking procedure has been found clinically to provide functional stability of the implant. (Rodrigo et al., 2001) Unfortunately, the present work found that the screws, when assumed to be in intimate contact with the stem, might worsen the occurrence of stress shielding (lower by 5.3 % of intact strain compared to cementless).

SUMMARY

Because fully cemented stems are difficult to remove, other means of securing a stem to weak bone at revision have been developed. Such methods as pressing a large stem into the intermedullary canal may lead to bone loss and pain at stem tip. In the present work, canal filling stems were found to cause

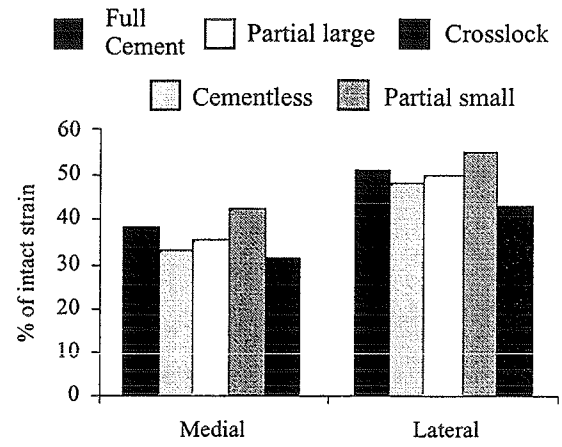

Figure 2. The average % of intact strain below tibial tray shows a reduction in strain for each fixation method.

slightly more stress shielding than fully cemented small stems. Securing a stem with crosslocking screws circumvents the poor contact pressure associated with small stems, which may cause inadequate initial fixation. With regards to long-term effects of stress shielding, the crosslocking procedure does not appear to retain the benefits of a small stem. However, if the screws allowed the stem to subside (by passing through oblong holes, for example) while restraining it from rotation, the strain distribution may be similar to the fixation procedure of a cemented tray with a small stem.

Limitations of this model include: (1) plane strain assumptions, (2) isotropic material behavior, (3) no muscle forces, and (4) intimate bond at interfaces. A 3D solid element model with contact elements at the interfaces may be necessary to account for tibial and implant complexity.

REFERENCES

Barrack, R. L. et al. (1999). *Clin Orthop*, **367**, 216- 225.

Levitz, C. L. et al. (1995) *Clin Orthop*, **321**, 68-72.

Lewis, G. et al. (1998) *BioMed Mater Eng*, **8**, 11-23

Rodrigo, J.J. et al. (2001) *Clin Orthop*, In press.

NUMERICAL INVESTIGATION OF NUTRIENT TRANSPORT IN INTERVERTEBRAL DISCS

Éric Sélard [1], Jill P.G. Urban [2] and A. Shirazi-Adl [1]

[1] Department of Mechanical Engineering, Ecole Polytechnique, Montréal, CANADA
[2] Physiology Laboratory, Oxford University, Oxford, ENGLAND
E-mail: abshir@meca.polymtl.ca

INTRODUCTION

The intervertebral disc consists of an extra-cellular matrix that is synthesized and maintained by its own cells. It is also the largest avascular structure in the body (cells can be as far as 8 mm from the nearest blood vessels) and an inadequate nutrition could be one of the causes of disc degeneration. The nutrients, essential for the cell viability, are transported to the disc from the blood vessels. It has been found that diffusion is the main mechanism of transport into the disc for small solutes (e.g., oxygen and glucose) as compared with that by the fluid transport and convection generated during motion and loading (Holm et al,1981; Katz et al, 1986; Urban et al, 1982).

In the current computational model, the effect of tissue thickness, cell density, exchange area, diffusivity and consumption rate on oxygen and glucose concentrations are investigated using nonlinear consumption-concentration relationships derived from published experimental measurements.

METHODS

The Poisson's differential equation governing the nonlinear steady state diffusion was used in two different finite element models to compute solute concentration and flux. A 2D periodic pore model with isotropic material constants for which an analytical study has already been reported (Stairmand et al, 1991) was first developed and employed to evaluate the effect of changes in exchange area, cell density and thickness on results. Nutrients were supplied through the exchange areas while the remaining boundaries were taken to be adiabatic (no flux). Subsequently, a second more realistic axisymmetric model of an intervertebral disc with annulus and nucleus regions having distinct diffusivities and nutrient incorporation rates was developed and used. Nutrients (oxygen and glucose) were supplied both through the annulus boundary and the end plate adjacent to the nucleus (Fig. 1). The effect of variations in exchange area, diffusivity and consumption rate on predictions was studied.

RESULTS AND DISCUSSION

The predictions are in general agreement with results of previous models (Stairmand et al, 1991; Maroudas et al, 1975) and experimental studies (Holm et al, 1981). The present models demonstrate the marked influence of exchange area (Figs. 2 and 3), tissue thickness and cell density on nutrient concentrations in the disc. The changes in exchange area could simulate the state of an end-plate from a normal to a diseased condition. The nutrient concentration is low at the disc center away from the supply

source and may reach a level threatening the cell viability if nutrient supply is impeded. Moreover, the diffusivity and consumption rate are found to have significant effects on nutrient concentrations. Diffusivity could change, for example, as the matrix is squashed while the consumption rate is altered following cell death or stimulation by growth factors.

Future work will incorporate the likely effect of the mechanical environment and the interaction between various nutrients on the human intervertebral disc nutrition.

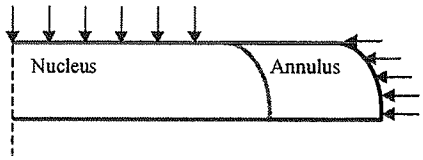

Figure 1: A schematic representation of the axisymmetric intervertebral disc model. Changes in the porosity are considered only for the input nutrition on top of the nucleus.

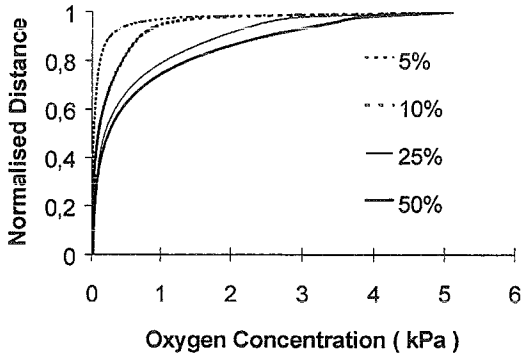

Figure 2: Oxygen concentration along the intervertebral disc axis for different porosity values on top of the nucleus.

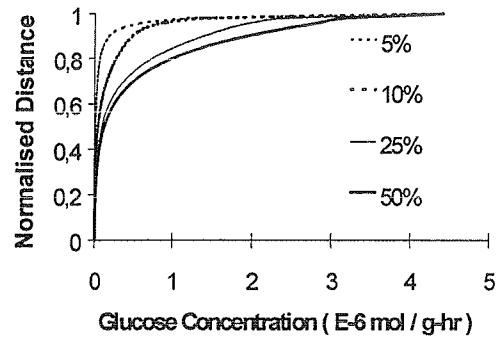

Figure 3: Glucose concentration along the intervertebral disc axis for different porosity values on top of the nucleus.

REFERENCES

Stairmand, JW. et al. (1990). *Spine*, **16**, 444-449

Maroudas, A. et al. (1975). *J Anat*, **120**, 113-130

Holm, S. et al. (1981). *Connect. Tissue Res*, **8**, 101-119

ACKNOWLEDGEMENTS

This work is supported by grants from NSERC-Canada and FCAR-Québec.

Hydraulic Model of the Systemic Resistance

Leiterman D.[1], Pražák J.[2], Musil J.[2], Poušek L.[3], Konvičková S.[1]

e-mail: leiterma@fsid.cvut.cz

[1] Czech Technical University in Prague, Faculty of Mechanical Engineering, Technicka 4, 166 07 Prague 6 - Dejvice
[2] Institute of Thermomechanics, Academy of Sciences of the Czech Republic, Dolejskova 5, 182 00 Prague 8
[3] Czech Technical University in Prague, Centrum of Biomedical Engineering Zikova 4, 166 36 Prague 6

INTRODUCTION

The mechanisms producing stroke volume, heart rate and adequate mean pressure in the cardiovascular system (CVS) enable corresponding perfusion through the systemic organs according to the load. Thus the cardiovascular resistances, representing the pulmonary and systemic resistances situated in series with the right and left cardiac ventricles, represent among others, the dependent variables ensuring the body tissue oxygen demands at changing load levels. The main problem is situated into the systemic circuit because the systemic resistance value is approximately six-times higher than pulmonary one.

METHODS

The laboratory modeling of the CVS may give us important information about the properties of this complex system in a human body. It means, it would be useful to characterize some features of the main parts of the whole blood circuit, not only the heart. CVS is controlled by lots of regulatory mechanisms at different levels. The CVS's behavior, as a whole, can be described by Frank-Starling's (FS) curve, i.e. the dependence of cardiac output on heart frequency only, the changes of other magnitudes being included into this function implicitly. The more realistic model of the CVS could be obtained if some greater particular regulations are included in this study. The aim of model was not the description of behavior in human body, but rather the description of common flow regulatory mechanism. In this paper we focused our attention to the suggestion of the resistance of the systemic circuit (mechanical study) and its influence on the support process of the failing heart by the rotary pump.

RESULTS

Generally, all kinds of hydrodynamic resistance are connected with a drop of pressure in the hydrodynamic circuit concerned. In out preliminary mechanical studies in the mock-line circuit the systemic resistance was modeled by the hydrostatic pressure of the column of liquid placed behind the pulsating ventricle. This model of resistance comprised the constant pressure only, which corresponds to the resistance being (not very physiologically) a reciprocal function of flow.

The first study of the supported failing heart on the mock-line was performed with the unchangeable systemic resistance adjusted on 130 MPa.s.m^{-3} , i.e. statistic physiological value at 70 beats/min. The task was solved as the hydrodynamic problem and it allowed us to describe basic properties of the support process. Though

it was performed successfully, the depicted FS's curve of this proposed mock-line had the negative slop only, which does not correspond to the biological reality, but makes possible study of some hemodynamical questions.

The throttle valve connected to the mock-line corrected the shape of FS's curve, but the required resistance values were adjusted with low level of accuracy. The usual valve was used, but the problem with the precision setting is awaited with all throttle valves. The valve with smaller diameter shifted the applied values into the range with lower sensitivity. The more realistic shape of FS's curve was obtained, though the ratio of the cross-sectional area of aorta and all capillaries was not kept.

The next model of systemic resistance was suggested in accordance with the two preconditions. The first one was the ratio of aorta's and capillaries' cross-sectional area, i.e. the capillary's one being twice larger than the aorta's one, which fact would be enough for our study. The second presumption was the laminar flow through the capillaries, which can't be reached with any kind of throttle valve. The next proposed model consisted of the thin tubes connected in parallel. The change of its resistance value was achieved by the breaking of the flow in particular pipes. The resistance model was proposed in accordance with the Weisbach's formula, the resistance value depending on the width and length of tubes and on their amount. The length is determinated by the equation

$$l_C(d_C) = \frac{\pi \cdot n_C \cdot R_{70} \cdot d_C^4}{128 \cdot \nu \cdot \rho}$$

l_C – tube length, n_C – amount, R_{70} - systemic resistance, d_C – tube diameter, ν - kinematic viscosity, ρ - density.

The liquid used in this experiment is distilled water.

RESULTS AND DISCUSSION

The finite suggestion suitable to the presumptions consists of 338 elastic tubes with the diameter of 2 mm and the length of 3.83 m; the value of 130 MPa.s.m^{-3} being reached on 75 tubes were opened. This model does not exactly correspond to the physiological conditions, but it enabled to contribute to the study of pulsating wave's transport in elastic tubes and to find out the fundamental influence of the changeable systemic resistance value during the support process of the failing heart.

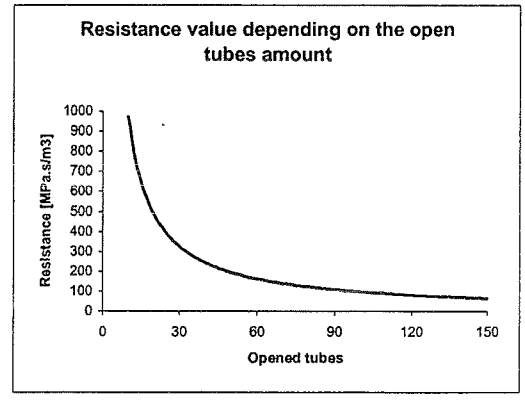

REFFERENCES

[1] PRAŽÁK J., MUSIL J., LEITERMANN D.: *Model of Insufficient Heart Supported by Rotary Pump (Mechanical Study).* Biomechanics of Man 2000, 8th Conference of the Czech Society of Biomechanics with International Participation, Olomouc, Czech Republic, 2000, pp. 165-168.

[2] PŘEVOROVSKÁ S., MUSIL J., MARŠÍK F., ADAMEC J.: *Heart Rate and Resistance Changes in Cardiovascular System.* CTU Workshop '97, 1997, Biomedical Engineering 1075-1076.

ACKNOWLEDGEMENTS

This project is supported by grand no.: PP2/52U.

A REALISTIC HUMAN ELBOW MODEL FOR DYNAMIC SIMULATION

N. Lan and T. Murakata

Alfred E. Mann Institute for Biomedical Engineering
Dept. of Biomedical Engineering, University of Southern California
Los Angeles, CA 90089

INTRODUCTION

The objective of this study is to construct realistic biomechanical models of neuromuscular system for studying sensorimotor control and for development of control system for functional electrical stimulation (FES). In this paper, an elbow model with flextion/extension and supination/pronation degrees of freedom is described. Muscles are defined so that their moment arms match those of experimental measurements (Murray et al. 2000). The graphic model is converted into a Simulink block for general use of dynamic simulation in Matlab.

METHODS

The elbow model is constructed in SIMM (Musculographics, Inc. USA), as shown in Figure 1. It consists of the scapula bone (ground), the glenohumeral joint, the humerus segment, the elbow joint, the radius and ulna bones of the forearm. The model has five degrees of freedom (DOFs), i.e, three rotations at the glenohumeral joint, flexion/extension at the elbow plus supination /pronation of the forearm. Forearm muscles in this model are biceps brachii, triceps brachii, brachialis, brachioradialis, pronator teres and supinator, etc. Muscle origin and insertion are defined initially based on anatomical landmarks. Muscle insertion points are fine tuned to match the moment arm data obtained from cadaver measurements [1,2]. The segmental lengths, mass center of segments, and inertial properties are listed in Table 1 [3,4]. Wrapping objects are defined in this model to prevent muscle line going into bone surface, in particularly, at the extreme of range of motion (ROM). The shape and size of the wrapping objects are carefully selected to fit the bony structure, and to match the moment arm data measured in experiments. There are totally 9 wrapping objects defined in this model, two for the glenohumeral joint, two for humerus bone, two for the radius bone, and three for the elbow joint.

TABLE 1

	Length (cm)	Mass (kg)	Mass center (cm)	Inertias (kg-cm^2)	
				I_t	I_l
Humerus	30.0	1.79	13.08	132.08	16.69
Ulna	24.1	0.545	10.36	28.17	3.48
Radius	22.6	0.545	9.72	28.17	3.48

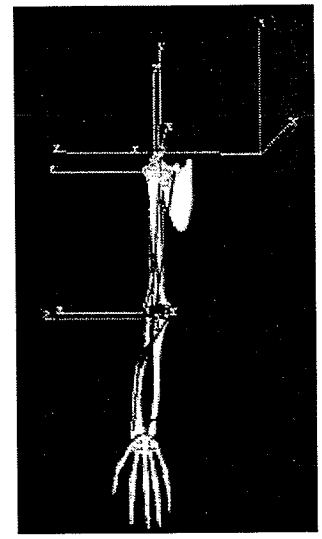

Figure 1, the configuration of the elbow model. The hand is shown for cosmetics.

The Dynamics Pipeline of SIMM allows us to convert the elbow model into a dynamic model. We are able to further convert the dynamic model into a Simulink block in Matlab [5], so that the elbow block can be connected with virtual muscles^{TM} [6] for dynamic simulation. Matlab/Simulink is a

convenient environment to integrate the blocks of model components to construct a larger system, such as an FES control system.

RESULTS AND DISCUSSION

Muscle moment arms from the model are matched to experimentally measured moment arms from cadaver [2]. Figure 2 shows the fitting of moment arms of two head of biceps and three heads of triceps to experimental data. The results indicate that if the peak value of the experimental data is matched, the rest of the model moment arm values match to experimental data very well. Note for biceps, the wrap object takes effect at about 30°. An exception for triceps is that below 70°, the data tends to be flat, while the model moment arm is larger. This may be attributed to the fact that one wrapping object may not be able to replicate the musculotendon path of the triceps faithfully.

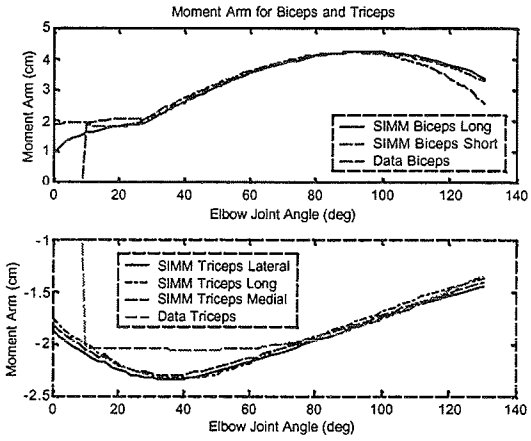

Figure 2, model moment arms fitted to cadaver measurements.

Results also show that wrapping objects are effective in matching the moment arms of other muscles, e.g. brachialis, brachioradialis, and pronator teres, etc. For the brachioradialis, a via point is introduced to achieve a more realistic muscle path. For those muscles that have little data on moment arms, their moment arm is defined according to their anatomical landmarks.

Figure 3 shows the Simulink block of the elbow model. It accepts muscle forces as input, and computes outputs of joint motions and musculotendon lengths, the latter can be used to drive the virtual muscle^{TM} blocks. The block contains equations of motion of the elbow model, and can be integrated with Matlab engines.

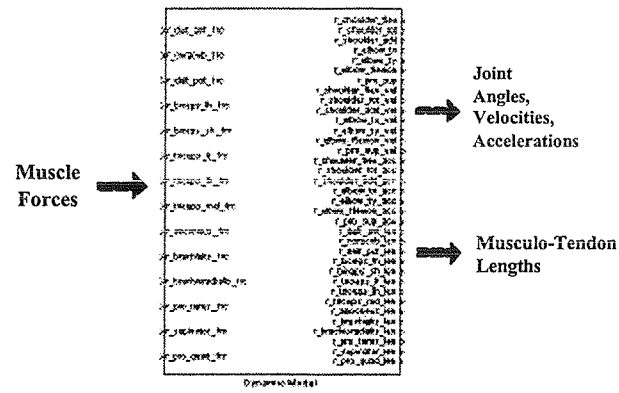

Figure 3, the Simulink block of the elbow model.

SUMMARY

A realistic human elbow model is constructed using SIMM. The elbow model is for general purpose, and can be integrated with other components, such as muscles, sensors, regulator and controllers, to perform dynamic simulation of movement control.

REFERENCES

1. Murray, WM, Buchanan, TS, and Delp, SL (2000), *J. Biomechanics*, 33(8): 943-952..
2. Murray, WM, (1997), PH.D. Thesis, Northwestern University.
3. Veeger, H.E.J., Yu, B., An, K-N and Rozendal, R.H. (1997), J. Biomechanics, vol. 30(6):647-652.
4. Seireg, A. and Arvikar, R. (1989), **Biomechanical Analysis of the Musculoskeletal Structure for Medicine and Sports**, Hemisphere Publishing.
5. Davoodi, R and Loeb, GE (2001), submitted to 6th Ann. Conf. IFESS.
6. Cheng, EJ, Brown, IE, and Loeb, GE, (2000), J Neurosci Methods, vol. 101, no. 2, pp. 117-130.

ACKNOWLEDGEMENTS: this work is supported by Alfred E. Mann Institute for Biomedical Engineering. The authors also thank Drs. Brown, Davoodi and Loeb for useful discussion.

AN INHOMOGENEOUS, ANISOTROPIC SPRING MODEL OF ARTICULAR CARTILAGE

Thomas Koehler, Andras Z. Szeri, and Thomas S. Buchanan

Center for Biomedical Engineering Research, Department of Mechanical Engineering, University of Delaware, Newark, DE, USA 19716 E-mail: tck@udel.edu

INTRODUCTION

Articular cartilage is a multiphasic material primarily composed of a fluid phase and a solid phase. Mow and co-workers have shown that mixture theory can be successfully applied to modeling the types of solid-fluid interactions that occur in articular cartilage (e.g., Mow et al., 1980). However, though models such as the biphasic theory have provided many insights into the deformation behavior of the cartilage, they can only with difficulty represent a mixture that is both inhomogeneous and anisotropic, such as cartilage, in which anisotropy changes during loading. The purpose of this study was to model the solid phase of cartilage with a network of springs. In addition, sensitivity analyses on the parameters of the model were performed and subsequently tuned so that the spring network model deformed in the same manner as the solid phase of cartilage samples did in experiments.

METHODS

In this study, the solid phase of cartilage is modeled with a 2D network of massless springs of various orientations (Figure 1). For this initial treatment, the springs are linear. Each spring within the model can be thought of as a long bar of length 'L', with uniform cross-sectional area 'A', an elasticity modulus 'E' and subjected to an axial load 'F'. The deformation behavior of such a bar is modeled with the following equation:

$$F = (AE/L)\,\Delta L_T$$

where ΔL_T is the change in length of the bar. The quantity AE/L is analogous to the spring constant 'k' in the equation of a spring. In our model, 'A' is set equal to unity and the 'spring stiffness parameter' input is 'E'. Spring stiffness parameters may be varied according to location and orientation within the network. The spring stiffness parameters of the model are tuned to reproduce the results from experiments on cartilage. A nonlinear optimization routine is used to determine, upon the application of a load, the equilibrium configuration of the nodal points where the springs connect. Equilibrium is reached when the summation of the forces on the nodal points is judged to be sufficiently close to zero.

Sensitivity analyses were performed on the spring stiffness parameters in the following loading configurations: (1) confined compression, (2) unconfined compression, and (3) indentation with a plane-ended indenter. Using the patterns observed from the sensitivity analyses, we reproduced the results from cartilage experiments conducted under the assumption of linear elasticity and isotropy. The experimental results reproduced from these experiments were the elasticity modulus, the bulk modulus and the Poisson's ratio.

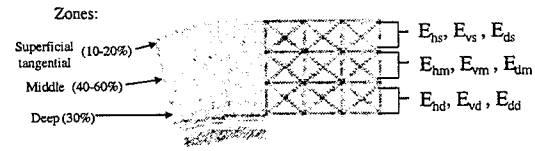

Figure 1: 2D network of massless nonuniform springs with horizontal (h), vertical (v) and diagonal (d) orientations, as well as superficial tangential (s), middle (m), and deep (d) zones.

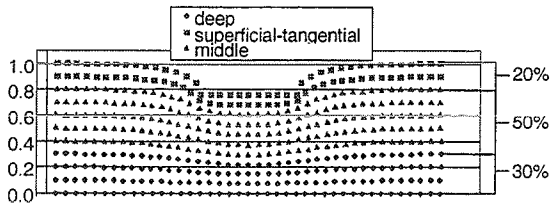

Figure 2 A 41x11 node mesh deformed by a plane-ended indenter.

RESULTS AND DISCUSSION

A sample model of an experiment for indentation with a plane-ended indenter tip is shown in Figure 2. A 0.080 MN load was applied through the indenter to a 41x11 node mesh (37 nodes in the horizontal direction and 10 nodes in the vertical direction). The radius of the indenter was .5 mm and the original thickness of the cartilage layer was 1 mm. In addition, the 41x11 node mesh was assumed to be of unit depth with a surface area of 4.0 mm^2. Figure 3 shows an example of a sensitivity analysis for a 19x13 node mesh performed with different horizontal, diagonal, and vertical spring stiffness parameters (E_h, E_d and E_v) for an unconfined compression loading configuration. In this test, stiffness did not vary with cartilage depth. The patterns observed from a series of analyses such as these were used to reproduce the results of selected experiments.

Columns 1 through 4 of Table 1 show the results of confined and unconfined compression tests that were performed on a series of excised cartilage samples. The experimental material properties measured that were relevant to modeling the solid phase of the

Table 1: Solid phase properties of cartilage from experiments conducted in Jurvelin et al. (1997) on the bovine humeral-head.

ν	H_A	E	h	E_h/E_d	E_d/E_v
0.174 ±0.106	0.754 ±0.198	0.677 ±0.223	0.95 ±0.33	3.00	1.45

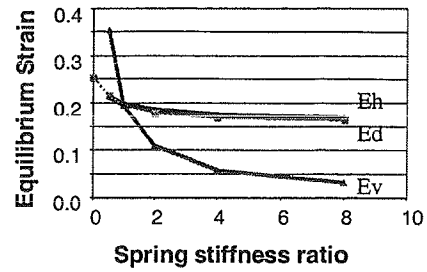

Figure 3: 19x13 unconfined compression: equilibrium strain vs. spring stiffness ratio.

matrix were the elastic modulus 'E', bulk modulus 'H_A', Poisson's ratio 'ν' and the thickness 'h'. For models that ignored depth dependence, these quantities were reproduced with three parameters: E_h, E_d and E_v. The relationships between these parameters (shown in columns 5 and 6) are all that is necessary to reproduce the experimental results.

This study showed that for a linear spring model, three parameters are sufficient for modeling the solid phase of cartilage if it is assumed to be linearly elastic and homogeneous. Cartilage inhomogeneity can be readily modeled to characterize tissue properties by varying the depth and directional dependent parameters as more cartilage experimental data is extracted. Our future plans are to couple this Lagrangean solid phase of the model with an Eulerian fluid phase of the model as is done in Peskin's Immersed Boundary Method (e.g., Peskin, 1997). This approach will, we believe, yield new types of cartilage models that characterize its unique constitutive properties.

REFERENCES

Jurvelin et al. (1997). *J. Biomech.* 30, 235-241.

Mow et al. (1980). *J. Biomech. Eng.* 102, 73-84.

Peskin. (1997). *J. Comp. Physics.* 25: 220-252.

A DIRECT METHOD FOR STUDYING THE INTERACTION BETWEEN MUSCLE VOLUME, LIMB INERTIAL PROPERTIES AND LOWER LIMB MOVEMENT PERFORMANCE

Alan Barr and David Hawkins

Human Performance Laboratory, University of California, Davis, CA, USA
E-mail: dahawkins@ucdavis.edu

INTRODUCTION

Skeletal muscles generate the active forces to move and stabilize the limbs. They are highly adaptable, experiencing large volumetric changes throughout life. Skeletal muscle hypertrophies during maturation and in response to strength training and other increased loading stimuli. Skeletal muscle atrophies in response to reduced loading stimuli (e.g. disuse, space flight) and various neuromuscular diseases. Changes in muscle volume affect the muscle's force producing capability, the muscle's line-of-action as well as the line-of-action of peripheral muscles, and the inertial properties of the limb segments containing the muscle. Further, these changes directly affect limb dynamics in a complex, non-linear manner. Current state-of-the-art musculoskeletal modeling strategies model muscle architecture and limb inertial properties as independent quantities. This limits a researcher's ability to study the affects that muscle-tendon morphologic changes have on limb dynamics. The objective of this project was to develop a method for studying the complex interactions between muscle volume, limb inertial properties and lower extremity dynamics.

METHODS

The methodology developed to achieve the stated objective integrated digital data representing lower limb tissue morphology, computational techniques to simulate muscle volume changes within digital tissue data, computational techniques to calculate limb mass, center of mass location, and moments of inertia based on digital tissue data, and musculoskeletal modeling and movement simulation software. The lower limb digital anatomy data used in this study were obtained from a prior study involving the National Library of Medicine's Visual Human Male (VHM) (Barr and Hawkins, 2000). Muscle volume changes were simulated within this data set using algorithms previously developed in our laboratory (Hawkins and Barr, in press). Numerical methods were developed to calculate limb mass, moments of inertia, and center of mass locations. These methods were validated by applying them to common geometric shapes with known inertial quantities.

The above methods allow muscle volume changes to be simulated and new limb inertial properties determined. This approach provides a method for creating a consistent set of data (muscle volume and limb inertial properties) that can be utilized in Software for Interactive Musculoskeletal Modeling (SIMM, Motion Analysis Corporation) to study a variety of musculoskeletal modeling and movement performance issues. The utility of this approach was demonstrated by using it to investigate two specific issues (1) the interactions between muscle volume, limb inertial properties, and movement dynamics, and (2) the implications of using simple

regression equations to estimate limb inertial properties in movement simulations. Two lower limb movements were simulated using SIMM, (1) maximally flexing the hip while standing and maintaining a straight leg and (2) maximally flexing the knee while standing and maintaining a neutral hip angle. The movements were purposely chosen to be one joint, unidirectional movements involving maximal effort. This eliminated the need for complex neural control strategies. Limb inertial parameters were defined in these simulations using simple regression models or the methods described above.

RESULTS AND DISCUSSION

There were no errors associated with the numerical method calculations of mass, center of mass and moments of inertia when applied to bodies with known parameters. This provided confidence that the numerical methods could be applied to other bodies. Altering muscle volumes in the VHM model had a greater affect on the shank with respect to increasing the moment of inertia and a greater affect on the thigh with respect to altering the center of mass location. Increasing the mass of triceps surae by 40% increased shank mass by 14.3%. Increasing the mass of the quadriceps by 40% increased thigh mass by 9.6%. Increasing the mass of the quadriceps muscles by 40% had the effect of moving the center of mass location distally by 0.4% of the limb length. Increasing the mass of the triceps surae muscles by 40% had the affect of moving the shank center of mass location proximally by 1.1% of segment length.

The above results contributed to an increase in the moment of inertia of the thigh from 2.4% at 10% hypertrophy up to 8.9% at 40% hypertrophy and the shank from 2.9% at 10% hypertrophy up to 12.1% at 40% hypertrophy. Results show that simple regression equation estimates of segment mass, center of mass and moment of inertia may be in error by 15-35%. However, the nature of these errors tends to offset each other in the equations of motion, allowing simple regression estimates to provide reasonable dynamic responses for the movements simulated. Vmax for both the hip and knee increased similarly as the limbs were hypertrophied. Hip flexion Vmax for the morphed quadriceps conditions shows a steady increase up to 5.3% above the original for a 40% increase in quadriceps muscle volume. Knee flexion Vmax for the morphed shank conditions increased steadily to 5.1% above the original.

SUMMARY

A method for studying the complex interactions between muscle volume, limb inertial properties and lower extremity dynamics was developed. While this method demonstrated there were errors in simple regression equation estimates of limb mass, center of mass location and moments of inertia, the errors in each of the quantities tended to offset each allowing the regression equations to provide reasonable estimates of limb dynamics for simple movements.

REFERENCES

Barr A., Hawkins D., 2000. *Journal of Applied Biomechanics*, 16:301-308.

Hawkins, D. and Barr, A. (In press). *Computer Methods in Biomechanics and Biomedical Engineering.*

ACKNOWLEDGEMENTS

The authors are grateful to the J.C. Downing Foundation for financially supporting this project and the NLM Visual Human Project for the images of the lower extremity.

RISK FACTORS FOR OVERUSE INJURIES IN CHILDREN: A MODELING & MOVEMENT SIMULATION APPROACH

Matt Fry and David Hawkins

Human Performance Laboratory, University of California, Davis, CA, USA
Email: mtfry@ucdavis.edu

INTRODUCTION

Many children participate in organized sports programs involving year-round repetitive training that can lead to overuse musculoskeletal injuries. Developmental factors have been suggested to contribute to these injuries such as tissue strength imbalances and tissue growth rate differences, (Tipton 1978, Woo 1990, Edwards 1995). However no scientific studies have been conducted to test these ideas and there has been little work done to determine cause-effect relationships between growth and development, injury and movement performance (Tipton 1978).

The objective of this research was to develop an approach to investigate the interactions between growth and the loads imposed on specific tissues during jumping. This approach was then used to test the hypotheses that growth-spurt induced muscle strength and limb inertial property changes increase the stresses in tendons and apophyses. Tissues of the lower extremity are common sites of overuse injuries in children and jumping is a common movement associated with many children's activities. Thus, a musculoskeletal model of the lower extremity and simulated jumping movements were considered in this study.

METHODS

The lower extremity bone model provided with Software for Interactive Musculoskeletal Modeling (SIMM, Motion Analysis Corporation) was modified to represent the anatomy of a 12-13 year old child. This was achieved by scaling the nodal bone mesh of the femur and tibia. Nodes near the growth plates were longitudinally translated to represent an average growth spurt (Figure 1). Muscle-tendon insertions and slack lengths were scaled accordingly. Data from Jensen (1987, 1988), and Seger (2000), were used to estimate segmental mass, center of mass, moments of inertia, and length for the foot, shank, thigh and head-arms-torso(HAT) segments of the model pre- and post-growth spurt.

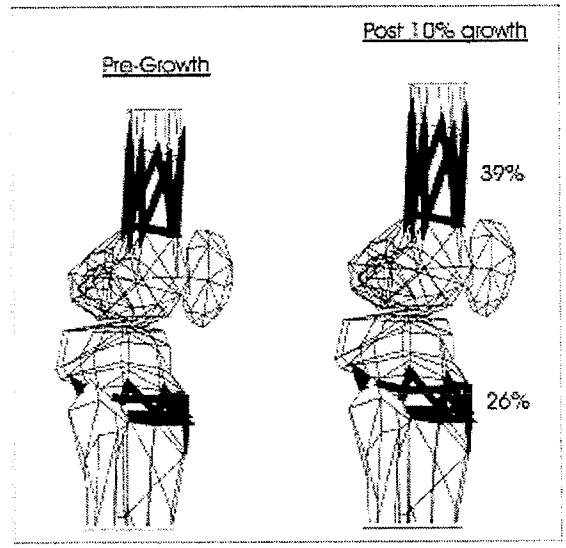

Figure 1. Illustration of growth model. 10% leg growth has been partitioned such that 39% occurs in the distal femoral epiphysis and 26% in the proximal tibial epiphysis (Martin, 1998).

Sample kinetic, kinematic, and muscle activation data were collected on an individual performing a maximum effort vertical jump (Figure 2). These data are being used to define the movement profile of a jumping child in SIMM.

Once the movement parameters are defined, then the jumping movement is simulated using SIMM for both the pre- and post-growth spurt anthropometry and strength characteristics. Joint moments and tissue loading curves will be compared between the pre- and post-growth spurt simulations to test the stated hypotheses.

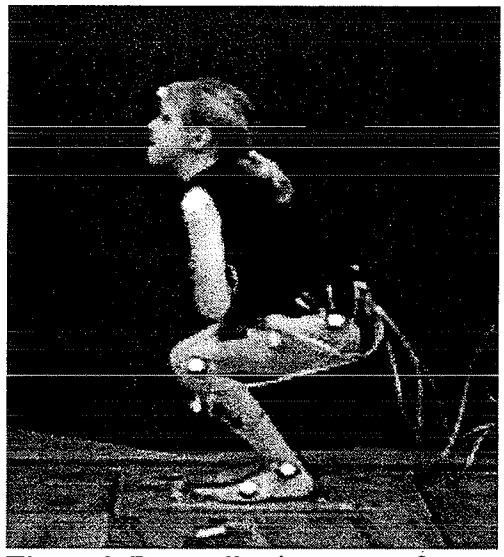

Figure 2. Data collection setup of an adolescent subject performing a maximum effort vertical jump.

RESULTS & DISCUSSION

The growth modeling approach has been developed, and the vertical jump simulations are currently underway. Forward dynamic analyses are being run in SIMM, with joint moments and tissue loads output and compared between the pre- and post-growth spurt input conditions.

It is anticipated that these growth/movement simulations will result in an increase in tendon and apophysis loading following the growth spurt. Higher loads are expected to result from shifts in limb inertial properties that require greater muscular effort to produce the same jump height performance.

The advantage of this approach is that it allows the decomposition of the interactions between tissue loading factors. For example, tendon preload changes, as a result of asynchronous bone-tendon growth, may be modeled independently of muscle strength changes or limb inertial properties, to test the affects such changes have on tissue loads and movement dynamics.

This study provides the foundation to thoroughly and accurately simulate the biomechanical behavior of an active adolescent. This approach is valuable for identifying factors that do and do not contribute to adolescent injury, thereby facilitating a decreased cost of study of this phenomenon in-vivo. In the future, this approach may be altered to investigate other growth or atrophy related phenomena.

REFERENCES

Tipton, CM. (1978). *J of Bone and Joint Surgery.* 60(A): 230-234.

Woo SLY. (1990). *J of Orthopaedic Research.* 8:713-721.

Edwards PH. (1995). *J Am Acad Orthop Surg.* 3:63-69.

Jensen, RK. (1988). *Medicine and Science in Sports and Exercise.* 20(6):594-604.

Jensen, RK. (1987). *Human Biology.* 59(1):173-189.

Seger, JY. (2000). *Eur J Appl Physiol.* 81:54-61.

Martin RB. (1998). *Skeletal Tissue Mechanics.* Springer-Verlag, New York. p. 59.

MATHEMATICAL MODEL FOR EVALUATING THE VARIABILITY OF THE SUPERIMPOSED TWITCH FORCE IN VOLUNTARY CONTRACTIONS

Rachid Ait-Haddou and Walter Herzog

The Human Performance Laboratory, University of Calgary, Calgary, Alberta, CANADA
E-mail: walter@kin.ucalgary.ca

INTRODUCTION

The superimposed twitch technique (Merton, 1954) is a commonly used approach to determine the active state of a muscle (e.g., Belanger and McComas, 1981). In this technique, an artificial, electrical stimulation (twitch or doublet) is superimposed on the voluntary contracted muscle. This superimposed twitch will produce a force beyond the voluntary force if not all motors units are recruited at high frequencies. Clinically, the superimposed twitch has been used frequently to assess muscle inhibition during maximal voluntary contractions in patients with musculoskeletal problems such as ligament loss (Hurley et al, 1994), swelling of the joint (Fahrer et al, 1988) or pain (Suter et al, 1998). One of the limitations of the superimposed twitch technique has been its variability (Suter et al., 1996). Even under precisely controlled laboratory conditions, the superimposed twitch force may vary by 50% for repeat measurements. This variability does not appear to be associated with measurement problems, but with an intrinsic inability to reproduce tests reliably. We have speculated that the variability in the superimposed twitch technique is associated with the stochastic nature of the firing of the twitch application relative to the stimulation pulses of the ongoing voluntary contraction of the motor units. The purpose of this study was to test whether the random firing of the motor units and the stochastic nature of the superimposed twitch can explain this observed variability.

METHODS

We developed a mathematical model of the neuro-motor control system to simulate the effects of a superimposed, artificial, electrical twitch on voluntary contractions. To accommodate experimental observations, the force of the superimposed twitch was assumed to be greater if it fell within 10ms of the pulse of the voluntary stimulation train (Burke et al, 1975) than if it fell outside the 10ms window. The superimposed twitch force was assumed to be inversely related to the motor unit firing frequency. In the first simulation, the number of motor units was assumed to be large to allow for a continuous probability distribution of the firing frequency range. In the second simulation, we considered a discrete case, in which the number of motor units was assumed to be small (between 100 and 300 motor units).

RESULTS

In the continuous and discrete simulations, we quantified the variability of the enhanced force following a superimposed twitch for three different levels of excitation: (1) a uniform distribution of the firing frequencies within the range of 20Hz-50Hz; (Figure 1) (2) a great number of motor units firing at high frequencies; and (3) a great number of motor units firing at low frequencies (Figure 2). In all cases, we found a low variability of

the enhanced force compared to the observed experimental variability. However, the discrete case produced more variability in the superimposed twitch force than the continuous case.

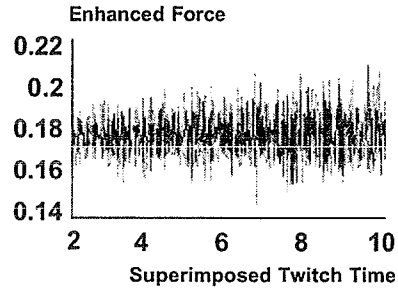

Figure 1. Variability of the enhanced force for a discrete uniform distribution of the firing frequencies.

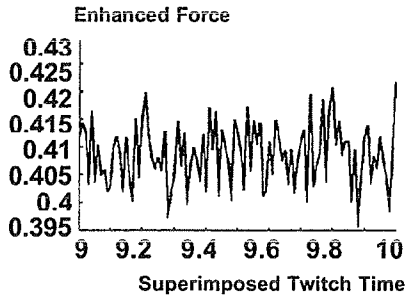

Figure 2. Variability of the enhanced force for a discrete low frequency distribution of motor unit firing rates.

CONCLUSIONS

The low variability of the enhanced force following a superimposed twitch is in disagreement with experimental observations. There could be two reasons for this discrepancy: first, our model is not correct, or second, our model is inherently correct, but it does not contain the factor that causes the great experimental variability. Most of our model assumptions regarding the number of motor units, their firing rates, and the local force enhancements as a function of timing, are based on experimental evidence, and therefore should be reasonable. However, two features of motor unit firing were not incorporated into the model: inter-pulse variation and synchronization across motor units. Realistically, only the latter of the two features can influence our results. Therefore, synchronization of motor units during voluntary contraction might have to be included into the model to obtain the great variability observed experimentally.

REFERENCES

Suter. E, et al. (1996). *Muscle and Nerve,* 19, 1046-1048.

Merton, P. J. (1954). *J. Physio*, 123, 553-564.

Belanger A. P., A. J. McComas. (1981). *J. Appl. Physio,* 51, 1131-1135.

Suter. E, et al. (1998). *J. Appl. Biomech*,14, 360-373.

Hurley. M. V. et al . (1994). *Clin. Sci*, 86, 305-310.

Fahrer. H. et al. (1988). *J. Bone. Joint. Surg*, 70-B, 635-638.

Burke. R. E. and Edgerton. V. R. (1975). *Ex. Sport. Sci. Rev*. 3-31.

ACKNOWLEDGEMENTS

NSERC of CANADA

A CONTRIBUTION TO THE OPTIMUM DESIGN OF ORTHOPEDIC ITEMS

Miloslav Vilimek, Miroslav Sochor

Department of Mechanics, Faculty of Mechanical Engineering, Czech Technical University in Prague, Prague, Czech Republic

E-mail: vilimek@fsk211d.fsid.cvut.c

INTRODUCTION

Ongoing remodeling takes place in bone consisting of cortical and trabecular parts. This remodeling procedure results from the stress on the bone due to its loads and all the force influences. If these boundary conditions are changed the bone remodels to obtain an optimum stress distribution (Wolff's Law). When a bone part is substituted by a replacement, the bone may remodel resulting in bone resorption at the interface with the replacement. This procedure results in loosening of the replacement, and subsequent gradually increasing movements cause higher resorption, which may result in rejection of the replacement. Knowledge of bone loading may enable us to optimize the load of the replacement+bone system and, consequently, to optimize the shape and structure of the replacement. The optimum replacement shape would be a shape that will introduce to the neighboring bone the same stress as the original bone did.
As similar types of human movement when walking result in similar types of lower limb loading, the problem can be generalized and an optimization procedure for the replacement+bone system can be projected.

MATERIALS AND METHODS

The biomechanical model that was developed of the lower limb (Fig.1) was designed as a four-hinge 3D-mechanism which included seventeen specified most important muscles, not only in their flexion-extension state of movement but comprising also a knowledge of their complete spatial configuration. The model requires space input data. Every limb segment (or section) has a local coordinate system, and all parameters measured were related to it.

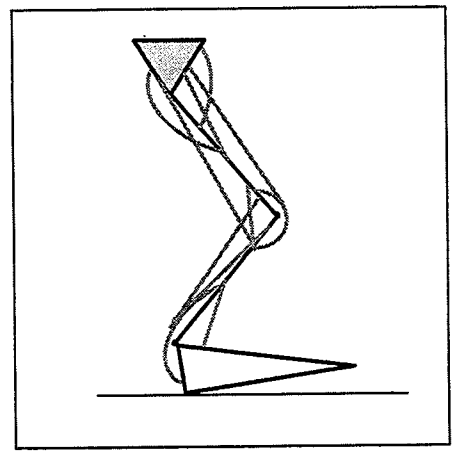

Figure 1.: Lower limb mechanism

At the beginning of this project the necessary input data was obtained through experiments. As a first step, the ground reactions forces (GRF) between the human lower limb and the force plate had to be measured, respectively, their time dependences during locomotion. The reactions measured were decomposed into three perpendicular directions: one vertical and two horizontal (divided into the sagital plane and the right-left direction). Since it was necessary to calculate the kinematic parameters (path, velocity, acceleration) with segments of the human lower limb, synchronized with the measurement of

ground reaction forces, the human gait was also simultaneously recorded by videocameras with a recording frequency of 25 frames per sec, or 50 halfframes per sec for faster movement. Clappers were used to synchronize the GRF and kinematic parameter measurements. This helped us to calculate the force and stress distribution in the whole leg.
The last data to be obtained experimentally were those of the forces exerted in the muscles. As it is very difficult to measure muscular forces, it was necessary to find new parameters that would simplify the task and serve for the assessment of muscular forces.
The paramenters consist of muscular electrical activity (EMG) and the velocity of the shortening of the muscle length. The idea that EMG should relate in some way to muscular force is appealing. After all, an increase in the firing rates of motor units is known to increase muscular force and the integrated form of EMG, and the recruitment of an increasing number of motor units increases the muscular force and also the corresponding IEMG (integrated electromyogram). The force-velocity relation applied to a muscle and the corresponding velocity of its shortening were measured in accordance with Hill's equation. The assessment of the force distribution among the muscles participating in a specific joint movement was based on the principle of minimum virtual work.
The calculation of the moments of inertia of the human lower limb segments was based either on the measured anthropometric data or literature data.

RESULTS AND DISCUSSION

From the experiments we were able to determine the inertial, gravitational, muscular and ground reaction forces and the kinematic parameters of human movement. From these results and from the model, the forces and moments in human limb joints were calculated, and these served as the input data for the FEM stress analysis of the human bones.
A better knowledge of the force exertion in the human lower limb joints can contribute to the process of optimizing the design of bone and joint replacements. Optimum design of replacements can better distribute the stress between the implanted replacement and the bone.

SUMMARY

An optimization procedure of bone replacements and orthopedic items is presented. A biomechanical model of the lower limb was applied. This model assessed the contact forces and moments in the lower limb joints during human movement. The data obtained was used as input data for an FEM stress analysis, yielding a force relation in the lower limb bones which contributes to an optimized design of orthopedic items and joint replacements.

REFERENCES

Nigg, B. M., Herzog, W. (1999): 'Biomechanics of the musculo-skeletal system', (J.Wiley and Sons, New York)
Pandy M., Anderson F. (1999): 'Mathematical modeling, numerical optimization, and computer simulation of human locomotion', Proc. EMBEC'99 European Medical and Biological Engineering Conference, Vienna, Austria, 1999, pp. 238-239.

ANOWLEDGEMENTS:

This project has been supported by the interdisciplinary project: No.: CEZ J04/98:210000012 "Laboratory of Biomechanics of Man" and project GACR No: 106/00/0017
We offer our special thanks to Dr. Ing. H.A.C. Jacob, PhD., Head of Biomechanics Unit of the Balgrist Orthopedics clinic, Zurich.

BLUNT TRAUMA FROM NONPERFORATING IMPACT OF FABRIC ARMOR

Martin N. Raftenberg [1], CDR Marlene DeMaio [2], CDR Steven A. Parks [2],
Walter Blethen [3], Thomas Carlson [3], and James K. Mackiewicz [4]

[1] U.S. Army Research Laboratory, Aberdeen Proving Ground, MD, USA
[2] Armed Forces Institute of Pathology, Washington, DC, USA
[3] U.S. Army Aberdeen Test Center, Aberdeen Proving Ground, MD, USA
[4] U.S. Army Natick Research, Development, and Engineering Center, Natick, MA, USA
E-mail: mnr@arl.army.mil

INTRODUCTION

Three tests were performed in which a 9-mm parabellum bullet (lead core plus copper jacket) was fired at 425-450 m/s into a vest of multiple plain-weaved plies of Kevlar KM2. The vest was placed over human thoracic tissue. The aim point was the center of the sternum. The tissue was instrumented with four accelerometers implanted on the posterior sternum, carina of the trachea, ligamentum arteriosum, and spinous process of the T7 vertebra. The purposes were to assess the partitioning of motion and deformation throughout the thorax and to provide benchmarking data for finite element modeling.

METHODS

The tests were approved by three institutional review boards. Endevco accelerometers were attached with sutures. The accelerometer models are identified in Table 1. Table 2 presents their characteristics.

The Wayne State Thorax Model, WSTM (Wang, 1995), a finite element mesh plus material properties, was run on the LS-DYNA finite element wavecode (Livermore Software Tech. Corp., 1999). The mesh is anatomically detailed, consisting of 41 parts, 15671 nodes, 4333 8-node solid elements, 11075 shell elements, and 45 beam elements. A typical element edge length is 10 mm. All thoracic materials were modeled as isotropic. Heart and lung tissue were represented as nonlinear, with stiffness increasing with increasing strain. All other tissues were modeled as linearly elastic with moduli based on quasi-static data. For heart and lung tissue, quasi-static stresses were multiplied by 10 to account for rate hardening.

Table 1: Peak acceleration measurements/Endevco accelerometer model.

Test/ v(m/s)	Stern.	Trach.	Heart	Spine
524 425.5	1190g 7264B	5g 7265A	N.D.	58g 7265A
637 445.6	2350g 7270A	N.D.	11g 7264B	N.D.
678 448.1	5900g 7270A	N.D.	24g 7270A	N.D.

Table 2: Endevco accelerometer characteristics (Endevco Corp., 1999)

Model	Mass (gm)	Frequency Range (kHz)	Amplitude Range (g's)
7264B	1	0 to 3.0	± 500
7265A	5	0 to 0.8	± 100
7270A	1.5	0 to 50	± 20000

A mesh for the fabric vest, consisting of 4235 nodes and 2053 solid elements, was added to the WSTM. The typical element in-plane dimension was 10 mm. There was one element through the thickness. The fabric was modeled with isotropic linear elasticity. Young's modulus was 74.0 GPa, the uncrimped stiffness measured for plain-weaved 850-denier KM2 (Johnson et al., 1999). Poisson's ratio was 0.2, and density was 1440 kg/m^3. The vest thickness was set to 3.625 mm to produce the desired areal density of 5.22 kg/m^2. The bullet was modeled by a single solid element with properties of lead and the correct mass and cross-sectional area.

RESULTS AND DISCUSSION

Measurements of peak accelerations are presented in Table 1. The values at the trachea, heart, and spine were two to three orders of magnitude smaller than at the sternum. Autopsies revealed intact sutures.

Figure 1 compares the LS-DYNA sternal acceleration results to the peak measurements. The correct order of magnitude was achieved.

At the three other locations, the calculations substantially overpredicted the measured peak accelerations (Table 3). Possible computational sources for this discrepancy include anatomy and material property representations, neglect of blood and air, meshing, and performance of the contact algorithm. Possible experimental sources include time response and frequency response of the instrumentation, the inertial contribution and possible slippage of the accelerometers.

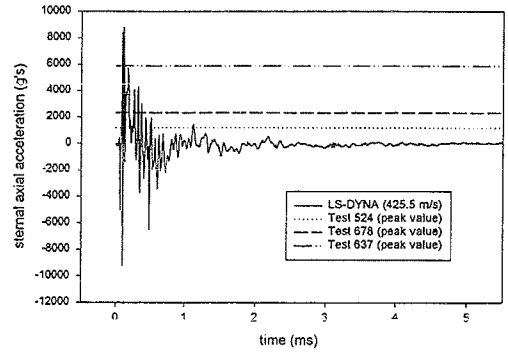

Figure 1: Sternal axial acceleration vs. time from calculation, peak value from experiments.

Table 3: Peak accelerations in computations (g's).

Sternum	Trachea	Heart	Spine
8801	583	199	667

SUMMARY

In three tests a fabric vest protecting human thoracic tissue was impacted by a 9-mm bullet at 425-450 m/s. Accelerations were measured at the sternum, trachea, heart, and spine. Experiments were simulated with finite elements. Reasonable agreement with experiment was achieved for peak sternal acceleration, but accelerations at the other locations were overpredicted.

REFERENCES

Endevco Corp. (1999). *Endevco Instrumentation Catalogue*, San Juan Capistrano, CA.

Johnson, G.R., Beissel, S.R., Cunniff, P.M. (1999). *18th International Symp. Ballistics*, San Antonio, TX, 962-969.

Livermore Software Technology Corp. (1999). *LS-DYNA Keyword User's Manual*, Version 950, Livermore, CA.

Wang, H.-C.K. (1995). Ph.D. Thesis, Wayne State University, Detroit.

MUSCULAR CONTROL OF STANCE PHASE KNEE EXTENSION DURING NORMAL WALKING: A STEP TOWARD IDENTIFYING THE CAUSES OF CROUCH GAIT

F. Clay Anderson[1], Allison S. Arnold[1], Marcus G. Pandy[2], and Scott L. Delp[1]

[1]Biomechanical Engineering Division, Stanford University, Stanford, CA, USA
[2]Department of Kinesiology, The University of Texas at Austin, Austin, TX, USA
E-mail: fca@stanford.edu

INTRODUCTION

Crouch gait, characterized by excessive flexion of the knee during stance, is one of the most common abnormalities among children with cerebral palsy. In some cases, tight hamstrings and/or psoas muscles are presumed to contribute, and surgical lengthening of these muscles is performed (Bleck, 1987). In other cases, weak knee extensors, hip extensors, or plantarflexors are thought to be factors, and strengthening exercises or orthoses are prescribed (Gage, 1991). Unfortunately, treatment is not always successful, in part, because the mechanisms that control knee extension are not well understood, even during normal walking. The mechanisms are complex because motions of the knee are influenced not only by muscles that cross the knee, but also by muscles that span other joints (Zajac and Gordon, 1989). As a step toward rigorously evaluating the hypothesized causes of crouch gait, this study characterized the angular accelerations of the knee during normal gait induced by muscles that are common targets of treatment of cerebral palsy.

METHODS

The accelerations of the knee joint induced by gluteus maximus, vasti, hamstrings, soleus, gastrocnemius, and iliopsoas during stance were computed based on the dynamic optimization solution for normal gait solved by Anderson and Pandy (*in review*). The body was modeled as a 10-segment, 23-degree-of-freedom articulated linkage actuated by 54 muscles. The back joint and hips were modeled as ball-and-socket joints. The knees, subtalar, and metatarsal phalangeal joints were modeled as hinges. The force generating properties and path geometries of the muscles were based on data reported by Delp et al. (1990). The interaction between each foot and the ground was modeled using five stiff spring-damper units distributed under the sole of the foot. The performance criterion for the dynamic optimization problem was to minimize the metabolic energy consumed per unit distance traveled by the center of mass. The muscle excitation patterns, limb kinematics, and ground reaction forces predicted by the solution were similar to experimental data obtained from five subjects (Anderson and Pandy, *in review*).

The contributions of individual muscles to the acceleration of the knee joint were computed using the equations of motion for the model (Zajac and Gordon, 1989):

$$\ddot{\bar{q}} = \bar{I}(\bar{q})^{-1} \cdot \{\bar{C}(\bar{q}, \dot{\bar{q}}^2) + \bar{G}(\bar{q}) + \bar{R}(\bar{q}) \cdot \bar{f}_m + \bar{S}(\bar{q}) \cdot \bar{f}_s\}, \quad (1)$$

where $\bar{q}$ is the vector of generalized coordinates, $\bar{I}(\bar{q})^{-1}$ is the inverse of the system mass matrix, $\bar{C}(\bar{q}, \dot{\bar{q}}^2)$ is the vector of force terms arising from angular velocities, $\bar{G}(\bar{q})$ is the vector of gravitational forces, $\bar{f}_m$ is the vector of applied muscle forces, $\bar{R}(\bar{q})$ is the muscle moment arm matrix, $\bar{f}_s$ is the vector of ground spring forces, and $\bar{S}(\bar{q})$ is a matrix of measure numbers for $\bar{f}_s$ (Kane and Levinson, 1985). Each muscle induced acceleration was calculated by setting all force terms in Eq. (1) to zero except for the muscle force in question, $\bar{f}_{m_i}$, and the corresponding portion of the ground reaction force caused by muscle i, $\bar{f}_s^{m_i}$:

$$\ddot{\bar{q}} = \bar{I}(\bar{q})^{-1} \cdot \{\bar{R}(\bar{q}) \cdot \bar{f}_{m_i} + \bar{S}(\bar{q}) \cdot \bar{f}_s^{m_i}\}. \quad (2)$$

$\bar{f}_s^{m_i}$ was computed by assuming rigid contact of the foot springs with the ground. To quantify the potential of a muscle to accelerate the knee, the induced acceleration *per unit force* was computed by setting

$\bar{f}_{m_i} = 1$, computing the corresponding $\bar{f}_s^{m_i}$, and substituting these quantities in Eq. (2).

RESULTS AND DISCUSSION

In early stance, both vasti and gluteus maximus produced substantial knee extension accelerations (Fig. 1A). In fact, per unit force, gluteus maximus had greater potential to extend the knee than vasti (Fig. 1B). These results support the hypotheses that weak knee or hip extensors could contribute to crouch gait.

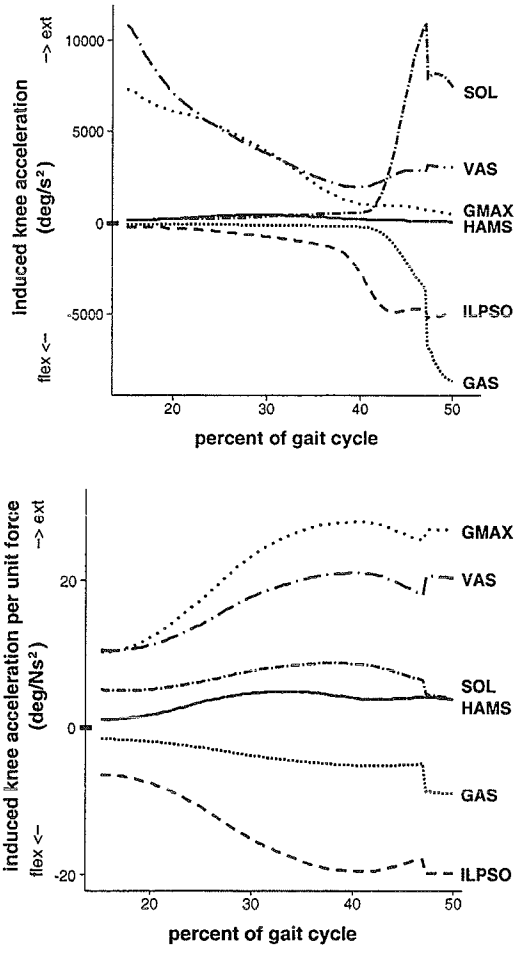

Figure 1. Angular accelerations of the knee (A) and angular accelerations per unit force (B) induced by vasti (VAS), gluteus maximus (GMAX), hamstrings (HAMS), soleus (SOL), gastrocnemius (GAS), and iliopsoas (ILPSO) during the single support phase of normal gait as computed from the dynamic optimization solution of Anderson and Pandy (*in review*).

In late stance, soleus generated large knee extension accelerations, and gastrocnemius generated large knee flexion accelerations (Fig. 1A). This suggests that decreased strength of the soleus or excessive force in gastrocnemius may contribute to reduced extension of the knee in some subjects with crouch gait. Tight iliopsoas muscles could also contribute since our analysis suggests that these muscles have the potential to flex the knee throughout stance (Fig. 1B).

Hamstrings had little effect on knee motion during stance (Fig. 1A), in part, because the forces generated by hamstrings were small. However, examination of the muscle-induced accelerations per unit force revealed that the hamstrings had the potential to *extend* the knee throughout the stance phase (Fig. 1B). This result suggests that tight or spastic hamstrings— a reputed cause of crouch gait— may *not* be the direct source of excessive knee flexion in some patients.

The non-intuitive findings, that gluteus maximus has perhaps greater potential to extend the knee than vasti and that hamstrings may actually extend the knee during gait, emphasize the need to quantify the contribution of muscles to joint motion when attempting to identify the underlying causes of movement pathologies.

REFERENCES

Anderson FC, Pandy MG (in review). *J. Biomechanical Engineering.*

Bleck EE (1987). *Orthopaedic Management in Cerebral Palsy.* Mac Keith Press, London.

Delp SL et al. (1990). *IEEE Transactions on Biomedical Engineering*, **37**, 757-767.

Gage (1991). *Gait Analysis in Cerebral Palsy.* Mac Keith Press, London.

Kane TR, Levinson DA (1985). *Dynamics: Theory and Application.* McGraw-Hill, New York.

Zajac FE, Gordon ME (1989). *Exercise and Sport Science Reviews*, **17**, 187-230.

ACKNOWLEDGMENTS

NIH, The Whitaker Foundation, NASA Grant NAG5-2.

A SOFTWARE TOOL FOR FASTER DEVELOPMENT OF COMPLEX MUSCULOSKELETAL MODELS IN SIMULINK™

Rahman Davoodi and Gerald E. Loeb
Dept. of Biomedical Engineering and A.E. Mann Institute for Biomedical Engineering
University of Southern California, Los Angeles, CA 90089 USA
Email: davoodi@usc.edu, Website: http://ami.usc.edu

INTRODUCTION

Computer models of musculoskeletal systems are useful in the study of various aspects of movement and control in humans and animals. Unfortunately, developing such models is usually a challenging task by itself.

SIMM™ (Musculographics Inc., USA) is the only commercial software for developing anatomically realistic musculoskeletal models (Delp and Loan 2000). The user generates a set of input files describing bone surfaces, articulations, and muscle-tendon parameters, and uses SIMM to assemble these graphically into an anatomically realistic model (Fig. 1). With the help of SD/Fast (Symbolic Dynamic Inc., USA) SIMM generates a set of files in the programming language "C" containing the equations of motion for the musculoskeletal model. This process requires the user to understand the structure of the SIMM-generated C-programs and to write additional programs for any other components required by the system under study (e.g. sensors, controllers). SIMM also has substantial limitations on its ability to incorporate run-time changes of muscle excitation, external forces, prescribed motion, and initial conditions, which handicap its use to study control algorithms. For example, the muscles can only be excited in an open-loop manner while many applications involve closed-loop control of muscles.

Our main objective is to build reusable I/O blocks for different components of the neuromusculoskeletal systems. We have chosen to do this in Simulink (Mathworks Inc., USA), an attractive, easy to use, and popular software package for simulation of complex systems. One particularly relevant source of such component blocks is the Virtual Muscle™ package developed by Cheng et al. (2000), which generates Simulink blocks representing the force-generating properties of realistic muscle models with user-specifiable parameters.

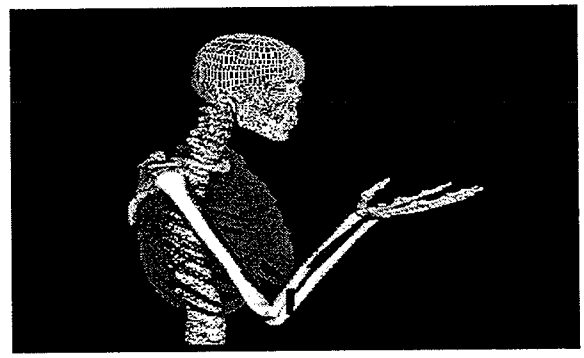

Figure 1. Example arm model with 5 segments, 10 DOF, and 12 muscles in SIMM window.

MUSCULOSKELETAL MODELING IN SIMULINK (MMS)

MMS is a set of Matlab scripts and C-files that are added to the normal model-building process in SIMM to generate Simulink models, and to add additional functionality without the user having to write any C-code

at all. MMS generates compiled C-code that calls the SIMM code and files as required. This compiled C-code is wrapped in a Simulink S-function, which permits it to be connected to other Simulink blocks and called during simulations. Within Simulink, the MMS output appears graphically as a large block with intuitively labeled input and output connectors for all of its state variables (Fig. 2). MMS also provides three major enhancements to the capabilities of SIMM to allow simulations of closed-loop sensorimotor control systems.

1. It allows the use of any non-SIMM model of muscle force production such as Virtual Muscle (Cheng et al. 2000).
2. It allows the user to change the initial configuration of the musculoskeletal model in each simulation run without recompilation. This includes restricting DOFs in the model, as long as the basic topology is preserved.
3. It allows the interactive configuration and run-time modification of the external forces, external torques, and prescribed motions. The prescribed motions can be modified in run-time, including locking/unlocking the joints.

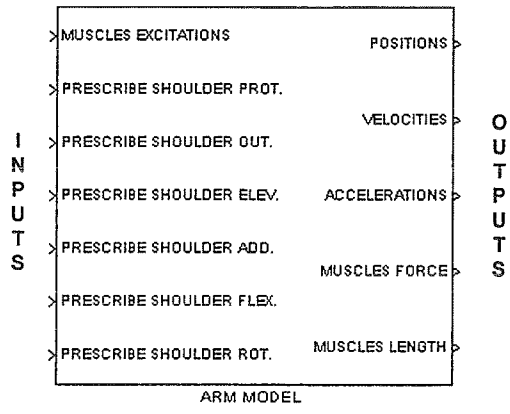

Figure 2. Generic representation of the MMS-generated Simulink block for the example arm model. Shoulder motion is prescribed by the user and the rest of the DOF are controlled by the muscles.

Once the Simulink block is generated, the user only needs to connect the inputs (e.g. muscle excitations) and outputs (e.g. joint angles) of the block to appropriate sources and destinations and run the simulation. More advanced applications can take advantage of the utilities, toolboxes and easy programming environment in Matlab and Simulink for design and optimization of controllers.

SUMMARY

SIMM is currently the most popular software for graphic and dynamic simulation of movement in musculoskeletal systems. Building dynamic models with SIMM requires substantial C programming, thereby limiting its use. We have developed MMS software to convert the SIMM musculoskeletal and kinetics models to Simulink blocks. In addition, MMS removes some runtime constraints so that the resulting blocks can be used in simulations of closed-loop sensorimotor control systems. Researchers, clinicians and educators in the fields of motor control and biomechanics are among the potential users who may benefit from using MMS. SIMM licensees can obtain a free copy of MMS by contacting the authors.

REFERENCES

Delp, S. L., Loan, J. P. (2000). *Computing in Science & Engineering*, **2**, 46-55.
Cheng, E. J. et al. (2000). *J. Neuroscience Methods*, **101**, 117-130.

ACKNOWLEDGMENTS

We would like to thank Drs. Ning Lan and Ian Brown for helpful discussions. Funded by the A.E. Mann Institute for Biomedical Engineering.

Neuromuscular Variability During Locomotion is Affected by Footwear

Max J. Kurz[1] and Nicholas Stergiou[2]
[1]Nonlinear Dynamics Laboratory, University of Colorado at Denver, Denver, CO
[2] HPER Biomechanics Laboratory, University of Nebraska at Omaha, Omaha, NE
E-mail: mjkurz@ouray.cudenver.edu Web: www.unocoe.unomaha.edu/hper/hper.htm

INTRODUCTION

It has been suggested that variability within the neuromuscular system may be an indicator of human health (Dingwell et al., 1999). Furthermore, few studies have attempted to quantify changes in the organization of the neuromuscular system as shoe hardness is discretely changed (Bates and Stergiou, 1996; Hamill et al., 1992). The goal of this investigation was to examine variability in locomotive patterns while wearing footwear and shoes of different hardness. Based on previous research (Lake and Lafortune, 1999), we hypothesized that an increased perception of the sensory information by the foot during the stance period would result in more variability in the locomotive pattern. We speculated that an increase in variability was related to neuromuscular strategies to avoid injury.

METHODS

Eight male heel-to-toe runners ran on a treadmill at a self-selected pace for the following randomly selected conditions: barefoot, hard shoe and soft shoe. The two shoes were tested using an Impact Testing System (Exeter Research Inc.) in accordance with ASTM recommended procedures. The two shoes were classified as hard (15g) and soft (10g) based upon the impact testing results. Ten consecutive footfalls were analyzed for each condition. Right side, sagittal kinematic data was collected with a 180 Hz camera. Positional coordinates were smoothed using a Butterworth Low-pass Filter with a selective cut-off algorithm (Jackson, 1979). The cut-off frequency values used were 13-16 Hz. The angles of the thigh, shank and foot with respect to the right horizontal were determined from the positional coordinates. An absolute approach was used to calculate joint angles ($\theta_{Knee} = \theta_{Thigh} - \theta_{Shank}$; $\theta_{Ankle} = \theta_{Shank} - \theta_{Foot}$).

Mean ensemble curves for the stance period were created for the knee and ankle of each subject-condition. A least squared method was utilized to fit polynomials to the respective standard deviation curves. We suggested that the standard deviation about the mean ensemble curve for each condition represented the spanning set for all possible neuromuscular solutions. The spanning set can be visualized as the edges of the plane that define the subspace for all neuromuscular solutions. A greater distance between the endpoints of the two vectors, that define the spanning set, would indicate more variability within the neuromuscular system. Since P_n is isomorphic to R^{n+1}, we utilized the coefficients from the respective polynomials to define vectors of the spanning set. The magnitude of the spanning set was determined by calculating the norm of the difference between the two vectors. One-way repeated measures ANOVA's (with Tukey as post-hoc) were performed to determine significant differences between the spanning sets of each respective condition.

Table 1. Mean and standard deviations for the magnitude of the respective spanning sets. The spanning set represented the variability in the neuromuscular system. Larger spanning set magnitudes indicated an increase in variability. Significant differences ($p<0.01$) are indicated by a superscript.

Joint	Soft Shoe	Hard Shoe	Barefoot
Ankle	2.49 ± 0.9^{Barefoot}	2.86 ± 1.0^{Barefoot}	7.24 ± 3.5
Knee	4.98 ± 2.0^{Barefoot}	4.57 ± 1.7^{Barefoot}	9.05 ± 4.9

RESULTS AND DISCUSSION

The results of this investigation indicated that significant differences ($p<0.01$) in variability existed for the knee and ankle joints. Significant differences for both joints were found between the barefoot and hard shoe, and barefoot and soft shoe (Table 1). An increased amount of variability was found during the barefoot condition where more sensory information was available. In the absence of a shoe, an increased amount of variability may be necessary to provide a mechanism to prevent injuries that can occur with increased impact forces.

No statistical differences ($p>0.01$) were found in the variability between the two shoe conditions (Table 1). Lake and Lafortune (1998) determined that individuals were not able to perceive differences in impact between small incremental changes in material densities. This study may have experienced similar results, where changes in shoe hardness may have not been sufficient to promote an increase in variability, and resulted in no differences between the two shoe conditions.

CONCLUSIONS

The goal of this investigation was to define changes in variability during locomotion as shoe hardness and footwear were modified. Our analysis technique utilized the polynomials from the standard deviation curves to define a spanning set that described the variability in locomotive patterns. The vectors that were analyzed were from continuous polynomials. Therefore, this analysis technique does not look at discrete points; rather evaluates variability in the entire period. This analysis technique can provide a new insight on the measurement of variability. Our results suggest that the neuromuscular system's perception of impact may be an important factor that influences variability in locomotion.

REFERENCES

Bates, B.T., Stergiou, N. (1996). *J. Human Mov. Studies,* **31**, 189-210.

Dingwell, J.B. et al. (1999). *Gait and Posture*, **10(1)**, 21-9.

Hamill, J. et al. (1992). *Med. Sci. Sports Exc.,* **24(7)**, 807-813.

Jackson, K.M. (1979). *IEEE Trans. Biomed. Eng.,* **26**, 515-521.

Lake, M.J., Lafortune, M.A. (1998). *Med. Sci. Sports Exc.,* **30(1)**,136-143.

The Spanning Set Defines Variability in Locomotive Patterns

Max J. Kurz[1] and Nicholas Stergiou[2]
[1]Nonlinear Dynamics Laboratory, University of Colorado at Denver, Denver, CO
[2] HPER Biomechanics Laboratory, University of Nebraska at Omaha, Omaha, NE
E-mail: mjkurz@ouray.cudenver.edu Web: www.unocoe.unomaha.edu/hper/hper.html

INTRODUCTION

Evaluation of the standard deviation of a mean ensemble curve has been used to describe the amount of variability in locomotive patterns (Dingwell et al., 1999; Hamill et al., 1999; Winter, 1983). However, few investigations that have utilized such an approach have found statistical differences in variability present during locomotion. In the present study, we suggested that the standard deviations about the mean ensemble curve represented the spanning set for all possible neuromuscular solutions. The greater distance between the two vectors that define the spanning set, the more variability within the locomotive pattern. Thus, our purpose was to present an alternative method for defining variability in locomotive patterns, and to compare this method to traditional measures of variability.

METHODS

A healthy subject ran on a treadmill at a self-selected pace while barefoot and with footwear. Ten consecutive footfalls were analyzed for each condition. Right side, sagittal kinematic data was collected with a 180 Hz camera. Positional coordinates were smoothed using a Butterworth Low-pass Filter with a selective cut-off algorithm (Jackson, 1979). The cut-off frequency values used were 13-16 Hz. Angles of the thigh, and shank were calculated with respect to the right horizontal. An absolute approach was used to calculate the knee joint angle ($\theta_{Knee} = \theta_{Thigh} - \theta_{Shank}$). Mean ensemble curves for the stance period were created for the knee joint for each condition. Measures of variability during the stance period were calculated using the Coefficients of Variation (CV) (Winter, 1983) and the Mean Deviation (MD)(Hamill et al., 1999).

$$CV = \sqrt{1/N \sum_{i=1}^{N} s^2_i} \Big/ 1/N \sum_{i=1}^{N} |X_i|$$

$$MD = \left(\sum_{i=1}^{N} | S_i | \right) / N$$

Where N = number of samples (100), Xi= average angle at the *i*th point, and S_i= standard deviation about X_i. The spanning set was defined by initially utilizing a least squared method to fit seventh order polynomials to the respective standard deviation curves. Coordinate mapping was used ($\mathbf{f} \rightarrow [\mathbf{f}]_B$) to introduce a familiar coordinate system that could be utilized to describe the properties of the polynomials in R^n. Since P_n is isomorphic to R^{n+1}, the coefficients from the respective polynomials were used to map a vector space that could be used to define vectors in the spanning set. Coordinate mapping was possible because the spanning set formed a basis (linearly independent set). Since $[\mathbf{f}]_B$ was a basis, the coordinate mapping resulted in a 1:1 relationship, and accurately described the properties of the polynomials.

Table 1. Measures of variability used to describe knee joint during stance.

Measure	Footwear	Barefoot
CV (%)	4.37	6.42
MD (deg)	2.35	2.85
Magnitude of the Spanning Set	7.26	20.0

The magnitude of the spanning set was determined by calculating the norm of the difference between the two vectors of the spanning set.

RESULTS AND DISCUSSION

Graphically, differences in the variability between the two conditions were evident during the stance period (Figure 1). While CV and MD revealed larger values for the barefoot condition, these differences were small (Table 1). It is possible, that previous investigations that have used such traditional measures, were not able to show significance due to such small differences (Dingwell et al, 1999; Hamill et al., 1999). The magnitude of the spanning set showed larger differences in variability between the two conditions (Table 1). It seems that compared with the other measurements, the magnitude of the spanning set was a more sensitive measure of variability. Furthermore, the magnitude of the spanning set coincides better with the graphic observation that the barefoot condition was more variable (Figure 1).

CONCLUSIONS

The usage of the spanning set is a novel method of quantifying variability in locomotive patterns. Based on our data, this approach may be able to provide a sensitive measure of differences in variability during locomotive patterns. Future investigations may want to utilize this method to quantify variability in locomotive patterns.

REFERENCES

Dingwill et al. (1999). *Gait and Posture*, **10**:21-29.

Hamill et al. (1999). *Clin. Biomech.*, **14**: 297-308.

Jackson (1979). *IEEE Trans. Biomed. Eng.*, **26**, 515-521.

Winter (1983). *J. Motor Behav.*, **15(4)**:302-330

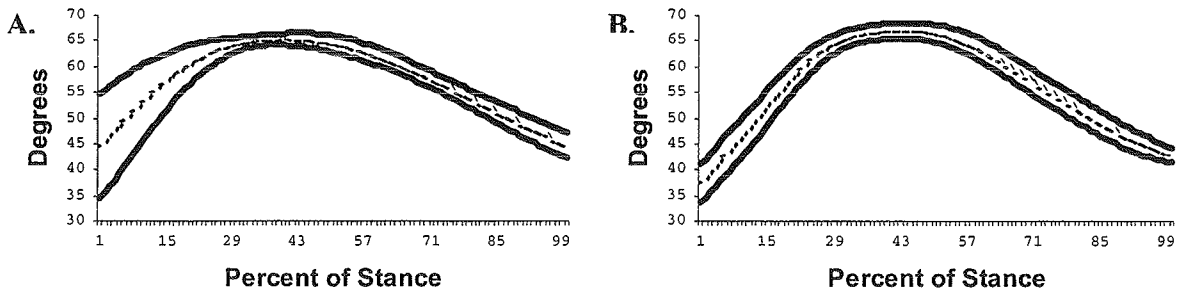

Figure 1. Mean ensemble curves (dashed line) and standard deviations (bold line) for the knee joint from the respective conditions: A.) Barefoot, B.) Footwear.

JOINT MOMENT NORMALIZATION: A COMPARISON OF TWO TECHNIQUES

Kirsten Moisio [1], Debra Hurwitz [2], Susan Shott [3], and D.Rick Sumner [1, 2]

[1] Department of Anatomy, Rush Presbyterian St. Luke's Medical Center, Chicago
[2] Department of Orthopedic Surgery, Rush Presbyterian St. Luke's Medical Center, Chicago
[3] Department of Obstetrics and Gynecology, Rush Presbyterian St. Luke's Medical Center, Chicago
E-mail: kmoisio@rushu.rush.edu Web: www.ortho.rush.edu/gait/index.html

INTRODUCTION

Joint moments obtained from gait analysis are commonly used to characterize normal and pathologic gait. However, it is well known that factors such as height and weight influence these joint moments. As a result, various joint moment normalization techniques have been devised to help account for these anthropometric differences. Two of the more common methods include normalizing the joint moment by body weight times height (BWHT) [1] or by body mass (BM) [2]. The purpose of the present study was to determine in a cross-sectional study which joint normalization method (body weight times height or body mass alone) most reduced the effects of height and weight on hip, knee, and ankle joint moments in a group of normal subjects.

METHODS

A group of 158 normal subjects (74 females, 84 males) were retrospectively collected from the gait laboratory database. Subjects were included if they had no previous history of musculoskeletal involvement and had a right and left side walking trial between 0.9-1.4 m/s. Average age, weight, and height were 33.9 ± 13.6 yrs, 73.3 ±15.0 kgs, and 1.73 ± 0.09m respectively.

Gait analysis was performed using an optoelectronic system with a passive marker system (CFTC) and a multi-component force plate (Bertec). Inverse dynamics were used to calculate the three dimensional local external moments (all moments reported from this point forward are external joint moments). Out of the possible18 joint moments, the 10 most clinically relevant moments were chosen which included hip flexion, extension, abduction, adduction, internal rotation, external rotation; knee flexion, extension, adduction; ankle dorsiflexion. The average speed for representative walking trials was 1.18 ± 0.1 m/s.

Stepwise multiple regression procedures were used on three different data sets. These data sets included the raw joint moments, joint moments normalized by BWHT, and joint moments normalized by BM. The analyses determined which independent variables (height or weight or speed) were most highly correlated with dependent variables (joint moments). The criteria for entering a variable was p=0.05 and for eliminating a variable after having been entered p=0.01. A 0.05 significance level was used for all statistical analyses. For the analyses, the most effective normalization would have the lowest r^2 value.

RESULTS AND DISCUSSION

Both normalization methods significantly reduced the variance in the moments ascribed to height and weight. However, the

efficiency of the normalization methods was not equivalent for each moment examined.

As expected, the raw data analysis demonstrated that weight and height had a significant impact on explaining the variance in the ten joint moments. Weight entered the equation for 9 out of 10 moments before speed and had a range of adj r^2=0.16-0.82. Weight had its largest effects on the hip adduction moment (adj r^2=0.60), knee extension moment (adj r^2=0.47), and the ankle dorsiflexion moment (adj r^2=0.82). Height entered the equation for 6 out of 10 moments, but was always the second or third variable (after weight and/or speed), with a change in the adj r^2 of 0.01 to 0.07. The largest effect was for the knee flexion moment.

For the moments normalized by BWHT, weight entered the equation for 4 moments, always after speed, with a change in the adj r^2 of 0.02 to 0.06. But out of these, only the hip extension moment accounted for >5% of the variance. Height only entered the equation for one moment, hip adduction, but was the first variable in with an adj r^2=0.13.

For the moments normalized by BM, weight entered the equation for only one moment, hip extension, with a change in the adj r^2=0.02. Height accounted for some degree of variance in 4 moments. In two cases, height was the first variable entered and had the largest effect on the ankle dorsiflexion moment (adj r^2=0.22).

SUMMARY

The two joint normalization techniques investigated in this study were both successful in reducing the effects of height and weight on joint moments. However, their effectiveness varied with the joint and moment being evaluated. Therefore some caution should be used when interpreting joint moments that have been normalized since height and weight may still be contributing to the variance in the data.

REFERENCES

Andriacchi T.P., Strickland A.B. (1985). *Biomechanics of Normal and Pathological Human Articulating Joints.* Martinus Nijhoff Publishers.

Winter D.A. (1991). The Biomechanics and *Motor Control of Human Gait: Normal, Elderly, and Pathological.* University of Waterloo Press.

ACKNOWLEDGEMENTS

Whitaker Foundation
NIH Grant 1RO1 AR 46225-01A1

ECCENTRIC MUSCLE ACTIVITY FUNCTIONS AS A BRAKE AND AN ACCELERATOR DURING NORMAL WALKING

R. R. Neptune[1,2], S.A. Kautz[1,3] and F.E. Zajac[1,3,4]

[1] Rehabilitation R & D Center, VA Palo Alto HCS, Palo Alto, CA
[2] Department of Mechanical Engineering, University of Texas, Austin, TX
[3] Departments of Functional Restoration and [4] Mechanical Engineering, Stanford University, Stanford, CA
Email: rneptune@mail.utexas.edu

INTRODUCTION

Interpretations of the functional role of eccentric muscle activity during walking are often limited to the joint(s) spanned by the muscle (e.g., eccentric knee extensor muscle activity brakes knee flexion during early stance), even though dynamic multi-link coupling allows the eccentric muscle to potentially accelerate unspanned joints. While eccentric knee extensor activity does result in a force that decelerates knee flexion, that force also results in joint reaction forces throughout the body that can either accelerate (increase the energy of) or decelerate (decrease the energy of) individual segments through energy transfer mechanisms. Thus, eccentric muscle activity may result in positive power flow to multiple body segments while decelerating others. For example, during early stance, the eccentric knee extensor activity is thought to simply provide shock absorption and limb "stability" (support) by controlling knee flexion (e.g. Perry, 1992). However, this eccentric activity may contribute significantly to forward progression by causing a forward directed hip joint reaction force that accelerates the trunk forward. Therefore, the objective of this study was to determine how eccentric muscle activity contributes to the functional tasks of support and forward progression during the stance phase of normal walking. We hypothesized that eccentric muscle activity functions beyond simply acting to absorb shock and support the limb, but also contributes directly to vertical support and forward progression of the trunk.

METHODS

A sagittal plane forward dynamics simulation of normal walking was generated. The musculoskeletal model and simulation were developed using SIMM/Dynamics Pipeline (MusculoGraphics, Inc.) and consisted of rigid segments representing the trunk, right and left legs, with each leg consisting of a thigh, shank, and foot. The trunk was allowed to translate and rotate in the sagittal plane, while the hip, knee and ankle joints were modeled as frictionless revolutes. The model's dynamical equations-of-motion were derived using SD/FAST (Symbolic Dynamics, Inc.). The contact between the foot and the ground was modeled with discrete visco-elastic elements located on the bottom of the foot.

The model was driven by fifteen individual Hill-type musculotendon actuators for each leg that were combined into ten muscle groups, with muscles within each group receiving the same excitation signal. The individual muscle excitation patterns were modeled as block patterns defined by onset, duration and magnitude, except for the soleus (SOL) and gastrocnemius (GAS) which were modeled with three magnitude levels to allow for the characteristic increasing excitation pattern (e.g. Perry, 1992). An optimization framework was used to systematically vary the muscle controls to produce a simulation that replicated experimental data. Constraints were enforced on the muscle controls to ensure timing was similar to that observed in experimental data (e.g. Perry, 1992).

A muscle's contribution to support and forward progression was determined by quantifying its contributions to the acceleration of the trunk segment in the vertical and horizontal directions, respectively (Kepple et al., 1997). This analysis was combined with a segment power analysis to identify the biomechanical mechanisms individual muscles use to accelerate the trunk. Eccentric muscle activity was defined to occur when the muscle was active while the musculotendon unit was lengthening.

RESULTS

Eccentric muscle activity occurred throughout the stance phase (0 - 60% gait cycle). Rectus femoris (RF) and vasti (VAS) were eccentric (Fig 1A: RF

musculotendon power (solid line) is negative) during early stance (0 - 15% gait cycle), which acted to decelerate the leg and transfer energy from the leg segments (dashed line is negative) to the trunk (dotted line is positive) to provide both support and forward progression (Fig 1B: both lines are positive).

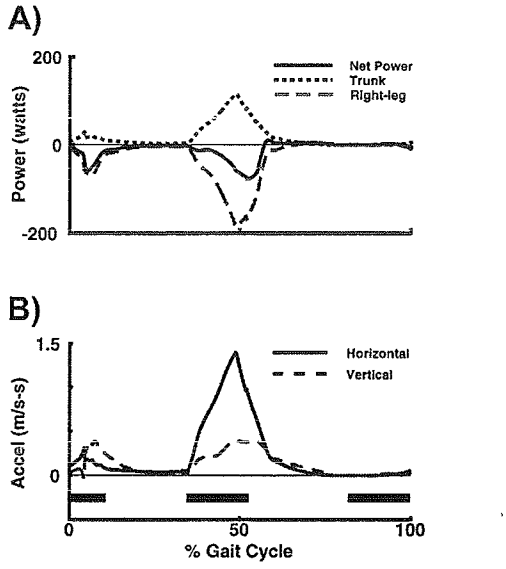

Figure 1: Right-leg A) mechanical power distribution to the leg and trunk and B) trunk induced accelerations in the horizontal (positive = forward) and vertical (positive = upwards) directions produced by RF during the gait cycle. The *net power* produced by RF is the sum of the power flow to or from the leg segments (*Right-leg*), trunk segments (*Trunk*), and contralateral leg segments (small and not shown). Positive (negative) net power produced by the muscle indicates power generation (absorption). Thick horizontal lines indicate muscle excitation timing.

During single-leg stance (10 - 50% gait cycle), SOL and GAS undergo mostly eccentric activity, which accelerated the trunk vertically to provide support. This eccentric activity during early single-leg stance also decelerated the trunk in the horizontal direction to impede forward progression. Then during late single-leg stance and pre-swing (40 – 60% gait cycle), a second burst of RF activity was eccentric (Fig. 1A: 40 – 60%, solid line is negative) and acted to transfer energy from the leg to the trunk. This transfer of energy acted to accelerate the trunk horizontally and vertically to provide forward progression and support, respectively (Fig. 1B: solid and dashed lines are positive).

DISCUSSION

Although significant mechanical energy was dissipated by the eccentric activity, it proved to be an effective mechanism to provide support and forward progression. The eccentric activity reduced the energy of the leg beyond the amount dissipated by transferring additional energy from the leg segments to the trunk through the hip intersegmental joint force. For example, during early stance, the hip intersegmental joint force produced by eccentric RF and VAS activity is directed forward and upwards (Fig 2A) which acts to accelerate the trunk's center-of-mass in the vertical and horizontal directions, respectively. Similarly, the hip intersegmental joint force produced by eccentric RF activity in late stance acts primarily to accelerate the trunk horizontally to provide forward progression (Fig 2B). In addition, eccentric activity plays an important role in storing tendon elastic energy during the lengthening phase that can be released later in the gait cycle to contribute to the task requirements (i.e., energy stored in the GAS (SOL) tendon during stance was later released during pre-swing to accelerate the leg into swing (trunk forward)).

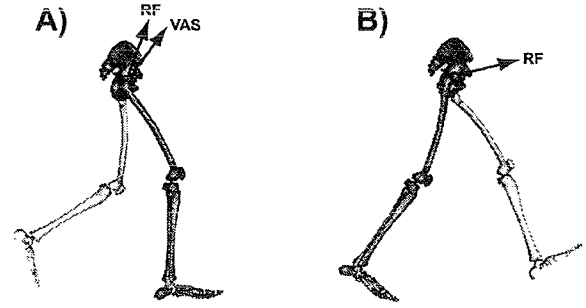

Figure 2: Hip joint intersegmental forces produced by A) VAS and RF at 10% and B) RF at 45% gait cycle.

REFERENCES

Kepple et al, *Gait Posture* **6**:1-8, 1997.

Perry, J. *Gait analysis: normal and pathological function.* Thorofare, NJ, Slack Inc, 1992.

ACKNOWLEDGEMENTS

This work was supported by NIH grant NS17662 and the Rehabilitation R&D Service of the Department of Veterans Affairs (VA).

THE EFFECT OF SPEED ON PERFORMER VARIABILITY DURING LOCOMOTION

Tracy A. Dierks[1], Nick Stergiou[1], Ugo H. Buzzi[1], Scott M. Keenan[1], and Jack Heidel[2]
[1]HPER Biomechanics Lab, University of Nebraska at Omaha, Omaha, NE, USA
[2]Dept. of Mathematics, University of Nebraska at Omaha, Omaha, NE, USA
Email: nstergio@unomaha.edu Web: www.unocoe.unomaha.edu/hper.htm

INTRODUCTION

Slower speeds have shown to lead to increased variability during walking (Winter, 1983). That was also found to be true with neuropathic patients (Dingwell et al., 2000). However, Dynamical Systems Theory (DST) predicts that the least amount of variability (a highly stable state) will be present at a self-selected pace. When the system is perturbed, then variability increases. Based on DST, variability in locomotion can then be modeled as a parabola. This model has also been supported by energy expenditure data. Furthermore, the examination of variability has been traditionally conducted using standard deviations across multiple strides. However, such an approach implies that locomotion is a sequence of independent strides. Tools for analyzing nonlinear time series have been shown to provide a more detailed analysis and can possibly reveal information about underlying control mechanisms (Dingwell et al., 2000; Stergiou et al., 2000). The purpose of this study was to investigate the effect of speed on variability during two different modes of locomotion, walking and running. We examined biomechanical parameters using tools of mathematical chaos.

PROCEDURES

Twenty subjects (range: 19-35 yr) attended 5 test sessions on 5 different days. On the first day, the subjects walked on a treadmill to establish a comfortable self-selected pace. This pace was used as the baseline speed for subsequent testing. Following this procedure, the subjects were required to walk for 5 minutes at 5 different speeds: baseline, 10% and 20% faster, and 10% and 20% slower. The same procedure was used for running. The subjects completed one walking and one running condition each day. The order of presentation of the conditions was randomized. A quartz shear piezoelectric accelerometer (PCB Piezotronics) was attached to subjects' distal anteromedial aspect of the right tibia with a tight elastic wrap. The time series from the accelerometer data sampled (180 Hz) were analyzed using the Chaos Data Analyzer software (Sprott, 1992). The Lyapunov Exponents (LE) and the Correlation Dimensions (COD) were calculated. LE is a measure of the stability of a dynamical system and its dependence on initial conditions. COD describes the geometric dimension of a dynamical system. All calculations were performed using five embedded dimensions. The embedded dimension, a description of the number of dimensions needed to unfold the structure of a given dynamical system, was calculated from a Global False Nearest Neighbor (GFNN) analysis (Abarbanel, 1996). Mean group values for LE and COD were analyzed statistically using one-way repeated measures ANOVAs ($p<0.05$).

RESULTS AND DISCUSSION

The average baseline speeds were 1.35 $m \bullet s^{-1}$ and 2.45 $m \bullet s^{-1}$ for walking and running, respectively. All LyE results were positive (Table 1), which may indicate that the

system is behaving chaotically. However, a time series consisting of random or noisy data can also produce positive LE. Thus, to assist in our evaluations we processed time series from periodic data (sine wave), from randomly generated data, and from known chaotic data (Lorenz attractor). When these data are compared with our LyE results, we can see that our results are more chaotic than noisy. It is also evident that both LyE and COD significantly decreased with increases in running speed. This may indicate a change in variability, which can be interpreted as an increase in periodicity and less control with larger speeds. No significant differences were observed for LyE during walking. The COD values were significant and actually, the 20% slower speed had the larger COD value. This result partially supports previous findings that indicated increased variability with slower speeds. Random data also have high COD in comparison with chaotic or periodic. Thus, it is possible that this increased variability is the result of higher noise within the system.

SUMMARY

The time series collected from a tibia located accelerometer were analyzed with tools of mathematical chaos. Our results did not confirm the DST parabolic model of variability for both walking and running, since the self-selected speed did not have the smaller value for either LyE or COD. In fact, the results revealed a linear relationship between variability and speed during running. The methods used in this study can assist in understanding the control mechanisms in complicated nonlinear systems such as the human.

REFERENCES

Abarbanel, H.D.I. (1996). *Analysis of Observed Chaotic Data*, Springer-Verlag.

Dingwell, J.B. et al. (2000). *J. Biomech.*, 33, 1269-1277.

Sprott, J., Rowlands, G. (1992). *Chaos Data Analyzer*. American Institute of Physics.

Stergiou, N. et al. (2000). *Proceedings of the ASB'00*, 75-76.

Winter, D.A. (1983). *J. Motor Behavior*, 15, 302-330.

ACKNOWLEDGMENTS

Supported by the University Committee on Research of the University of Nebraska at Omaha.

Table 1: Chaotic parameters evaluated for both modes of locomotion (group means). Significant means ($p < 0.05$) are identified with superscripts.

	20%Slower	10%Slower	Self-Selected	10%Faster	20%Faster
WALK - LyE	0.164	0.158	1.161	0.167	0.156
WALK – COD	$4.121^{10\%S,\ 20\%F}$	$3.769^{10\%F}$	3.935	4.065	3.899
RUN - LyE	$0.154^{20\%F,\ 10\%F,\ SS}$	0.135	0.128	0.125	0.114
RUN - COD	$3.548^{20\%F,\ 10\%F,\ SS}$	$3.339^{20\%F}$	3.245	3.239	3.139
	PERIODIC	**CHAOTIC**		**RANDOM**	
LyE	-0.001 ± 0.032	0.100 ± 0.035		0.469 ± 0.037	
COD	1.167 ± 0.334	1.941 ± 0.110		4.723 ± 0.723	

THE EFFECT OF ACL RECONSTRUCTION ON LOCOMOTOR VARIABILITY

Ugo H. Buzzi [1], Nick Stergiou[1], Giannis Giakas[2], Tracy A. Dierks[1], and Anastasios D. Georgoulis[3]
[1] HPER Biomechanics Lab, University of Nebraska at Omaha, Omaha, NE, USA
[2]SATRU, Dept. of Geriatric Medicine, University of Manchester, UK
[3]Dept. of Orthopaedic Surgery, Univ. of Ioannina Medical School, Ioannina, Greece
Email: nstergio@unomaha.edu Web: www.unocoe.unomaha.edu/hper.htm

INTRODUCTION

Anterior cruciate ligament (ACL) ruptures are among the most common and debilitating injuries in sports and usually require surgical intervention (Timoney et al, 1993). There is much debate concerning biomechanical changes associated with ACL reconstruction. Due to the uncertainty present when traditional biomechanical parameters are evaluated, it may be necessary to seek alternate approaches to identify the effects of ACL reconstruction on gait. ACL rupture and reconstruction may cause changes in neuromuscular variability. This variability has been described as a "healthy" flexibility within the neuromuscular system (Pool, 1989). Severe injury can possibly result in a loss of this flexibility that may not be regained despite surgical treatment. The purpose of this study was to examine differences in variability during locomotion following ACL reconstruction. We used tools of mathematical chaos to examine variability.

PROCEDURES

Ten subjects who had undergone ACL reconstruction using an autogenous patellar tendon graft and who were fully rehabilitated (months post-surgery = 40.55$\pm$ 49.56), and ten healthy controls participated in the study. Kinematic data from 30 continuous footfalls were collected at 60 Hz from both legs of the experimental group and the left leg of the control group, while the subjects walked and ran on a treadmill at their self-selected pace. The time series from the unfiltered relative angles of the knee and ankle joints were analyzed using the Chaos Data Analyzer software (Sprott, 1992).

Lyapunov Exponents (LyE) and Correlation Dimensions (COD) were calculated for both legs-groups. LyE is a measure of the stability of an attractor and its dependence on initial conditions. COD describes the geometric dimension of an attractor in the state space. All calculations were performed using 5 embedded dimensions. The embedded dimension, a description of the number of dimensions needed to unfold a given attractor, was calculated from a Global False Nearest Neighbor (GFNN) analysis (Abarbanel, 1996).

The angular data was also surrogated using a phase randomization technique (Dingwell et al., 2000). Surrogation removes the deterministic structure from the original data set, generating a random equivalent with the same mean, variance, and power spectra as the original. The surrogate data set is then analyzed in a similar manner to the original. If significant differences are found between the two data sets, then the original is not a randomly derived data set. Mean group values were calculated for LyE and COD for both legs-groups of the original and surrogate data sets for running and walking and were analyzed statistically using independent and correlated t-tests ($p < 0.05$).

RESULTS AND DISCUSSION

No significant differences were found for either LyE or COD for running. In walking, the results identified significant differences in the ankle LyE and the knee COD between the ACL reconstructed leg and the control. Knee and ankle LyE of the non-injured leg were found to be significantly smaller than the control. Furthermore, the control LyE for both joints were larger than the experimental group for both legs. This may indicate that variability differences exist between the two groups during walking. These differences may be the result of the rupture and the subsequent reconstruction. The knee COD for the ACL reconstructed leg was also found to be greater than the non-injured leg during walking. All LyE were found to be positive, suggesting the existence of chaotic dynamics within the data. Significant differences in LyE between the original and surrogate data sets for all variables analyzed confirmed that the original data sets were not randomly derived and had deterministic origin. This result indicates that the neuromuscular variability may be chaotic in nature. As it has been indicated (Pool, 1989), such chaotic behavior may allow the nervous system to adapt to changing conditions, while generating effective movement patterns.

SUMMARY

Variability in locomotion of surgically treated and control subjects was found to be clearly distinguishable from random noise. This may indicate that the lower extremity exhibits chaotic behavior during both walking and running. ACL reconstruction seems to preserve control strategies employed by the nervous system to generate effective locomotor movement patterns. However, variability differences do exist during walking between healthy controls and individuals with surgically reconstructed knees.

REFERENCES

Abarbanel HDI, (1996). *Analysis of Observed Chaotic Data*, Springer-Verlag.

Dingwell, J.B. et al. (2000). *J Biomech.*, 33, 1269-1277.

Pool, R. (1989). *Science*, **243**, 604-607.

Sprott, J., Rowlands, G. (1992). *Chaos Data Analyzer*. American Institute of Physics.

Timoney et al. (1993). Am. J Sports Med., **21**, 887-889.

Table 1: Group means of Original and Surrogate data during walking and running.

	WALK			RUN		
	LyE	**S-LyE**	**COD**	**LyE**	**S-LyE**	**COD**
ACL Leg-Knee	0.086	0.260*	2.731*†	0.093	0.268*	2.079
Healthy Leg-Knee	0.084*	0.266*	2.425	0.097	0.267*	2.046
Control Knee	0.107	0.260*	2.360	0.108	0.256*	2.076
ACL Leg- Ankle	0.140*	0.313*	3.343	0.151	0.285*	2.863
Healthy Leg-Ankle	0.140*	0.324*	3.254	0.148	0.285*	2.974
Control Ankle	0.173	0.325*	3.496	0.147	0.279*	3.090

*Sig. different to the control; †Sig. different to the healthy leg; *Sig. different to original data set

ANISOTROPIC COMPRESSIVE AND SHEAR PROPERTIES OF HEEL PADS IN WALKING AND RUNNING HUMANS

Kai-Jung Chi
Biology Department, Duke University, Durham, NC, USA
E-mail: kc12@duke.edu

INTRODUCTION

Heel pads are believed to bear weight, to cushion impact, to stabilize feet, and to return elastic energy. However, to perform these multiple roles, the pad has to be compliant and stiff, damped and resilient. These conflicting demands present a paradox for heel pad design. To date, only compressive properties of the stabilized heel pads have been examined (in vivo pendulum tests: Kinoshita et al., 1993; Cavanagh et al., 1984; in vitro tests: Bennett and Ker, 1990; Aerts et al., 1995). It is unclear how the pads behave mechanically in barefoot walking and running humans. In this study, I used synchronous kinetic and kinematic data to characterize the mechanical behavior of heel pads in moving subjects. I hypothesized that: (1) Heel pads are subject to **both** compressive and shear loading during impact, and the resultant pad stiffness depends on the shear component. (2) Heel pads show **anisotropic** properties to achieve multiple mechanical roles in locomotion.

METHODS

During walking and running, a significant impact is generated because the momentum of the foot changes after heel strike. It is well accepted that the characteristics of this impact are solely determined by the foot inertia and the mechanical properties of the heel pad (Whittle, 2000). In this study, I treated impact as a natural and non-invasive perturbation event during which I can examine the mechanical response of heel pads in moving humans.

Heel pads of three healthy adults were examined in the Vertebrate Movement Lab of Duke University. Each subject walked or ran at various speeds on the trackway, within which a force plate (9281C, Kistler) was mounted to record the ground reaction forces at 3000Hz in three orthogonal directions. The foot was filmed at 1000 frames/sec using a high-speed video camera. Kinetic and kinematic data were collected simultaneously using a motion measurement system Motus 2000 (Peak Performance Technologies, Inc). Displacement of a skin-mounted marker overlying the heel bone was digitized using Motus, and was used to describe the deformation of the pad. When the pad deforms, the impact energy [E_I] put into the pad is either stored as strain energy [E_S] or dissipated as heat [E_D]. E_D can be calculated mathematically as $E_D=E_I-E_S$, and normalized as percentage of impact energy [$E_{D\%}$]. E_S is calculated as the area under the load-deformation curve. E_I, which is also the kinetic energy of the foot prior to impact, can be calculated as $E_I = 1/2 m_{eff} v_0^2$, where m_{eff} is effective foot mass and v_0 is impact velocity. When the mass decelerates, the change of momentum imparts an impulse to the ground. So m_{eff} can be estimated from the impulse-momentum equation, $\int_0^t F dt = m_{eff}(v_0 - v_t)$. Forces and displacement of vertical and horizontal directions were treated separately as compressive and shear.

RESULTS AND DISCUSSION

Among 41 steps analyzed, v_0 ranged 0.7-1.8 m/s, m_{eff} ranged 4-6 Kg (cf. 3.6 Kg estimated by Ker *et al.*, 1989), and impact energy ranged 0.2-3.2 J. Load-deformation curves of the pad under impact loading were J-shaped, i.e. pad stiffness increased with deformation.

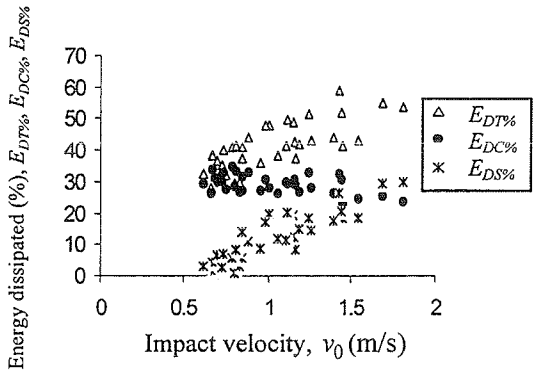

Figure1: *Relationship between energy dissipation in compression* [$E_{DC\%}$], *shear* [$E_{DS\%}$], *and total* [$E_{DT\%}$] *versus impact velocity* [v_0].

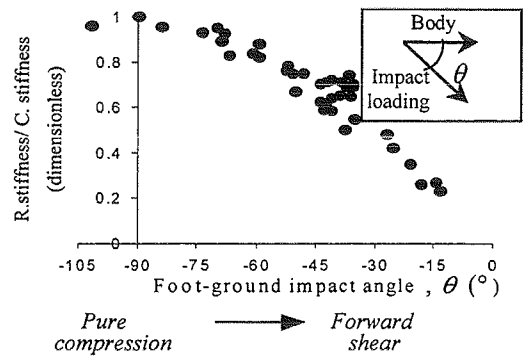

Figure 2: *Resultant stiffness-compressive stiffness ratio versus foot-ground impact angle* θ (°). *When* $\theta = 90$, *the loading is in pure compression;* $\theta < 90$: *forward shear;* $\theta > 90$, *rearward shear.*

Energy dissipation. The relationship between energy dissipated ($E_{DC\%}$, $E_{DS\%}$, $E_{DT\%}$) and impact velocity [v_0] is shown in Fig.1. $E_{DC\%}$ slightly decreases with v_0, which is consistent with previous studies (Ker, 1996); while $E_{DS\%}$ increases with v_0. The net effect is an increase of total energy dissipated [$E_{DT\%}$] with v_0. The mechanical consequences of this anisotropy are that when humans run faster, the pad becomes more resilient in compression to help lift the foot (Ker, 1996), but more damped in shear to cushion braking and prevent the foot from rebounding backward.

Stiffness. Resultant stiffness of the pad, normalized as a fraction of its compressive stiffness, is plotted against the impact angle as shown in *Fig.* 2. The results suggest that when the pad is subject to more shear, the pad as a whole becomes more compliant. The data for initial shear stiffness also exhibit anisotropy. The shear stiffness is greater when shear is rearward (35.59 $N/°$) as compared to forward (6.68 $N/°$). Mechanical consequences of this anisotropy are that the pad is more compliant to cushion braking in the forward direction. Greater stiffness of the pad in a rearward direction conversely restricts foot motion at heel strike and potentially stabilizes the foot.

SUMMARY

Mechanical properties of heel pads were examined in walking and running humans. The results suggest that at each step the heel pads are subject to both compression and shear. When the shear force is greater, the pad as a whole becomes more compliant. The results also suggest that the heel pad has anisotropic properties—it is compliant and damped in forward shear, stiff in rearward shear, and resilient in compression. Such anisotropic properties allow heel pads to perform multiple mechanical functions.

REFERENCES

Aerts, P. et al. (1995). *J. Biomech.***28,** 1299-1308.

Bennett, MB, Ker, RF (1990). *J. Anat.***171,** 131-8.

Ker, RF (1996). *J. Exp. Biol.* **199,** 1501-1508.

Kinoshita, H et al. (1993). *Int. J. Sports Med.* **14,** 312-319.

Pain, MTG, Challis, JH. (2001). *J. Biomech.***34,** 327-333.

Whittle, MW (1999). *Gait and Posture* **10,** 264-275.

ACKNOWLODGEMENT

I thank Dr. D. Schmitt and colleagues in the Vertebrate Movement Laboratory of Duke University for their support to this project. Part of this study was funded by the Society of Integrative and Comparative Biology grant-in-aid of research (2000).

COM PARAMETERS IN CHILDREN WALKING AT DIFFERENT VELOCITIES

C.A. Hughes[1], K.R. Kaufman[1], R.-J. Cherng[2], W.J. Shaughnessy[1]
[1]Motion Analysis Laboratory, Mayo Clinic/Foundation, Rochester, MN
[2]Dept. of Physical Therapy, National Cheng Kung University, Tainan, Taiwan 701, R.O.C.
E-mail: kaufman.kenton@mayo.edu

INTRODUCTION

In order to interpret and explain pathological gait in children, we must first understand what changes, especially in center of mass (COM), take place when we modify our velocity. Therefore, the purpose of this study was to determine if the differences in COM and temporal distance parameters could be attributed to walking faster or slower.

METHODS

Nine healthy normal children (7 females and 2 males) were recruited for this study. The subject population had a mean age of 10 years ±2 (range 8 to 14 years). Their mean height was 144 cm (±14) and their mean weight was 36 kg (±12.6). The protocol involved level walking at three velocity conditions. 1) Natural self-selected, 2) fast, and 3) slow. Initially, each subject walked at his or her self-selected pace. Thereafter, it was randomized as to what grouping, fast or slow trials, would follow. A set of 27 reflective markers was placed on body landmarks of the subject. An eight-camera RealTime system (Motion Analysis Corp.) was used to collect 3-D marker trajectories at 60 Hz during gait. Kinetics were calculated from three force plates, two Kistler (type 9281 B, Kistler Instrumente AG, Winterthur, Switzerland) and one Bertec (type 4060A, Bertec Corp, Worthington, OH). EVa software (Motion Analysis Corp.) was used to track the trials and create virtual marker trajectories which were used to define joint centers. A customized MATLAB program calculated the whole body COM based on a 13-link biomechanical model of the human body. Subsequently, the following COM parameters were calculated: Displacement of the whole body's COM in three orthogonal directions (COM A/P, COM M/L, COM Vert), and maximum velocities (anterior-posterior (A/P), medial-lateral (M/L), upward and downward). Finally, OT4 (Motion Analysis Corp.) was used to calculate the following temporal distance parameters: Velocity, stride length, right and left step length, right and left single support time, step width and cadence. Three trials were analyzed and averaged for each condition. A one-way repeated-measures ANOVA was used for statistical analysis and all pairs were compared using a Tukey-Kramer Honestly Significant Difference (HSD).

RESULTS AND DISCUSSION

There was a significant difference ($p<0.05$) between the fast and slow walking velocities when analyzing the displacement of the whole body COM in the three orthogonal directions (table 1). There was a significant difference between all conditions for the maximum A/P velocity, but no significant differences between any of the conditions for the maximum M/L velocity. When analyzing the maximum upward velocity, there was a significant difference between all conditions while maximum downward velocity was significantly different between all conditions with the exception of normal and slow walking velocities. When analyzing the temporal distance parameters, there was a significant difference ($p<0.05$) shown in velocity between all conditions (table 2). Stride length and right and left step lengths exhibited significant differences between only fast and slow walking conditions. The percentage of right leg single support time showed a significant

difference between all conditions except the normal and slow walking conditions, while the percentage of the left leg single support time showed a significant difference between only the fast and slow walking conditions. The step width showed no significant difference among any of the conditions; however, the cadence showed a significant difference between all conditions. Comparisons of COM and temporal distance parameters revealed a strong correlation (p=0.0000) between the COM A/P and stride length as well as between the COM maximum A/P velocity and velocity parameter for all conditions.

SUMMARY

The results indicate distinct differences in the COM and temporal distance parameters as the study subjects altered their walking velocities. The most remarkable differences were noted in the COM maximum A/P and maximum upward velocities along with velocity and cadence temporal distance parameters. No significance was noted between any of the conditions for the COM maximum M/L velocity or step width parameter. These results, which establish a foundation of normal gait parameters, are valuable guidelines when working with children who have gait abnormalities or other related gait pathologies.

REFERENCES

Chou, L.S. et al. (1999). *Gait & Posture*, **9**, 124.

ACKNOWLEDGEMENTS

The Mayo Foundation supported this study. The assistance of Diana Hansen, Ann Walker, Brian Kotajarvi, Denny Padgett and Duane Morrow is greatly appreciated.

Table 1: COM Parameters

Parameter		Fast Mean (SD)	Norm Mean (SD)	Slow Mean (SD)
COM A/P (m)	*	1.38 (0.16)	1.21 (0.15)	1.12 (0.14)
COM M/L (m)	*	0.03 (0.01)	0.03 (0.01)	0.04 (0.01)
COM Vert (m)	*	0.04 (0.01)	0.03 (0.01)	0.03 (0.01)
Max A/P (m/sec)	*†‡	1.74 (0.12)	1.38 (0.13)	1.10 (0.14)
Max M/L (m/sec)		0.12 (0.03)	0.11 (0.03)	0.13 (0.02)
Max Up (m/sec)	*†‡	0.30 (0.03)	0.21 (0.04)	0.17 (0.02)
Max Down (m/sec)	* ‡	0.29 (0.04)	0.21 (0.05)	0.16 (0.04)

Table 2: Temporal Distance Parameters

Parameter		Fast Mean (SD)	Norm Mean (SD)	Slow Mean (SD)
Velocity (m/s)	*†‡	1.57 (0.10)	1.22 (0.11)	0.99 (0.13)
Stride (m)	*	1.38 (0.15)	1.22 (0.15)	1.14 (0.14)
R_Step (m)	*	0.70 (0.07)	0.61 (0.08)	0.57 (0.08)
L_Step (m)	*	0.68 (0.08)	0.61 (0.07)	0.57 (0.06)
R_Single Support Time (%)	* ‡	40.65 (1.32)	39.20 (1.29)	38.38 (0.83)
L_Single Support Time (%)	*	40.72 (1.65)	39.19 (1.23)	38.04 (1.18)
Step Width (m)		0.10 (0.03)	0.09 (0.02)	0.09 (0.02)
Cadence (steps/min)	*†‡	136.39 (10.89)	120.96 (8.29)	104.49 (12.08)

$p<0.05$ * = clinical significance between fast and slow, † = clinical significance between norm and slow, ‡ = clinical significance between fast and norm

PERIPHERAL SENSORY FEEDBACK AFFECTS LOCOMOTOR 'COMPLEXITY'

Jonathan B. Dingwell[1] , Peter R. Cavanagh[2], and Joseph P. Cusumano[3]

[1]Sensory Motor Performance Program, Rehabilitation Institute of Chicago, Chicago, IL
[2]Center for Locomotion Studies, Penn State University, University Park, PA
[3]Department of Engineering Science and Mechanics, Penn State University, University Park, PA
Email: j-dingwell@northwestern.edu Web: http://manip.smpp.northwestern.edu/dingwell/

INTRODUCTION

It has been argued that peripheral sensory feedback is "essential" for maintaining stable bipedal locomotion (Winter 1983). However, completely passive walking machines that exhibit stable locomotion (McGeer 1993) call this assumption into question. Patients with diabetic neuropathy provide a unique model for studying the role of peripheral feedback in locomotor control.

Nonlinear and chaotic behavior of analytical models of locomotor systems (Collins and Stewart 1993; Goswami et al. 1998) demonstrate that linear analyses can not fully characterize locomotor complexity. The present study used methods from nonlinear time series analysis to provide a mathematically rigorous means of quantifying the structural complexity of locomotor kinematics.

METHODS

Fourteen diabetic patients with significant peripheral neuropathy (NP) and 12 appropriately matched controls (CO) participated. Upper-body 3D accelerations and sagittal plane hip, knee, and ankle angles were recorded at 66.7 Hz for 10 min during overground walking (Dingwell et al. 2000).

Multi-dimensional state spaces were reconstructed from each time series and its time-delayed copies (Takens 1981; Sauer et al. 1991). An embedding dimension of $d_E = 5$ was used (Dingwell and Cusumano 2000).

Locomotor complexity was defined from the correlation sum, $C(r,N)$, which quantifies how *geometric* correlations between points in state space scale with the distance (r) between those points (Kantz and Schreiber 1995; Dingwell and Cusumano 2000). "Self-similarity" in chaotic systems produces linear variations of $\log[C(r,N)]$ with $\log[r]$. Because real-world systems often exhibit more complex structure, Local Scaling Exponents (LSE) were quantified from the local derivatives of $\log[C(r,N)]$ vs. $\log[r]$ (Fig. 1). As length scales (r) varied from very large to very small (Fig. 1: A → D), the observable dimensionality of the system varied from a dimensionless point (LSE = 0) to a 1D limit cycle (LSE ≈ 1) to more complex structures (Fig. 1C). At the smallest length scales, only high dimensional noise (LSE ≈ d_E = 5) was observed (Kantz and Schreiber 1995).

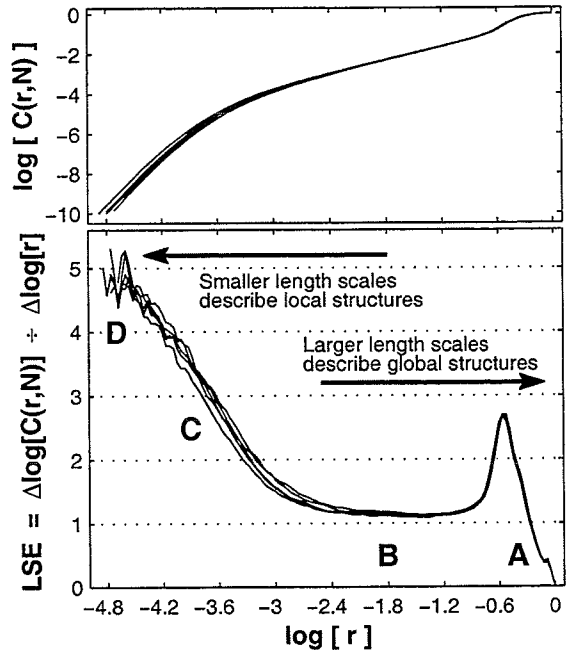

Fig. 1: Example of "Local Scaling Exponents" (LSE) defined as the local slopes of correlation integrals (top) computed from knee data of a typical subject.

It is believed that basic locomotor patterns are generated by spinal cord mechanisms. Sensory feedback acts mainly to modulate these patterns. Thus, it was hypothesized

that peripheral neuropathy would alter the apparent dimensionality of locomotor patterns on smaller length scales (Fig. 1C), but not at larger length scales (Fig. 1A & B).

LSEs curves were constructed for all subjects for all 6 time series. These curves were sub-sampled at evenly spaced intervals of $\Delta\log[r] = 0.6$ for statistical comparison. A repeated measures ANOVA tested for between-group differences using a Bonferroni correction for multiple comparisons.

RESULTS

NP patients exhibited greater LSEs than CO subjects at intermediate length scales *above* the noise floor, but *below* the range dominated by the global limit cycle dynamics (Fig. 2). Increased LSEs imply greater structural complexity of locomotor dynamics in NP patients. Similar increases occur when natural stride-to-stride fluctuations are replaced by correlated random noise (Dingwell and Cusumano 2000). This loss of deterministic structure implies a degradation of fine motor coordination in the control of NP gait.

A previously described multiple regression analysis procedure (Dingwell et al. 2000) demonstrated that differences in LSEs at the knee were significantly predicted by differences in sensory status, even after accounting for differences in strength, flexibility and walking speed. Differences in LSEs for the other kinematic variables were found to be related to a combination of intrinsic differences and differences in walking speed.

DISCUSSION

Peripheral sensory feedback does appear to play a role in reducing the complexity of locomotor kinematics. However, the present results indicate that even severe sensory loss produces only small increases in local dimensionality and only at those length scales where it was anticipated that sensory feedback would play the greatest role. The present results support the notion that sensory feedback plays a role in fine-tuning locomotor patterns, but not in generating the global features of those patterns. Although it is still not clear how NP patients learn to compensate for their sensory loss, these results confirm the visual observation that peripheral sensory feedback is not "essential" for maintaining stable bipedal locomotion.

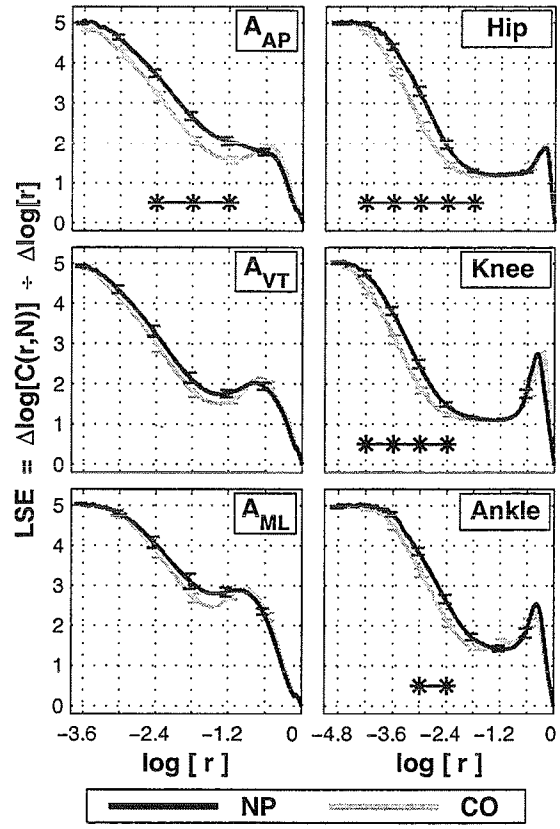

Fig. 2: Mean (± SE) local scaling exponents (LSE). Stars (*) indicate statistically significant differences between NP and CO groups.

REFERENCES

Collins JJ and Stewart IN (1993). *J. Nonlin. Sci.* **3**: 349-392.

Dingwell JB and Cusumano JP (2000). *Chaos* **10**(4): 848-863.

Dingwell JB et al. (2000). *J. Biomech.* **33**(10): 1269-1277.

Goswami A et al. (1998). *Intl. J. Robotics Res.* **17**(12): 1282-1301.

Kantz H and Schreiber T (1995). *Chaos* **5**(1): 143-154.

McGeer T (1993). *J. Theor. Biol.* **163**(3): 277-314.

Sauer T et al. (1991). *J. Stat. Phys.* **65**(3/4): 579-616.

Takens F (1981). *Dynamical Systems and Turbulence*. Springer-Verlag. **898**, pp. 366-381.

Winter DA (1983). *J. Mot. Behav.* **15**(4): 302-330.

ASSESSMENT OF ELECTROMAGNETIC MOTION TRACKING FOR QUANTITATIVE MEASUREMENT OF RELATIVE FOOT/SHANK MOTION

Peter M. Quesada, PhD[1], Patricia A. Brock, Meng[1], & Gregory S. Rash, EdD[2]
[1]Dept. of Mech. Engin., Univ. of Louisville; [2]Div. of Phys. Ther., Univ. of Louisville
E-mail: pmques01@gwise.louisville.edu

INTRODUCTION

Electromagnetic motion tracking systems measure absolute position and orientation of individual sensors with respect to a magnetic field source. Relative angular motion between two body segments can then be computed from their absolute orientations. Two advantages of electromagnetic tracking, with respect to optoelectronic tracking are: (i) line of sight to sensors is not needed, and (ii) only a single sensor is needed to quantify segment orientation.

This study sought to evaluate feasibility of obtaining clinically relevant, mid-foot/shank relative motion, during stance phase, via electromagnetic tracking. It was conceived that reliable, electromagnetic, foot/shank motion data could be used to detect individual responses to orthotic intervention. It was noted that relative motions between the actual foot (rather than the shoe) and shank would be needed to properly assess response to orthotic intervention.

METHODOLOGY

Foot and shank motions were measured, for 10 healthy young volunteers, with an electromagnetic motion tracking system. Sensors were placed on each right foot dorsum and anterior tibial surface. A standard work shoe was then donned with the tongue folded forward over the toe region, so as not to contact the foot sensor. Laces were secured at the top and bottom eyelets. In this manner, the shoe was reasonably well secured, while the foot sensor was isolated from contacting the shoe. Subjects were permitted time to acclimate to the experimental environment.

A static alignment trial was performed with foot and shank in a neutral standing position such that their local coordinate systems (LCSs) were approximately parallel to each other, and to the global coordinate system (GCS). For this position rotation matrices that aligned the LCSs were determined. These rotation matrices were then applied for each sampling interval. Five trials were collected for each of two conditions. In one condition no orthotic insoles were used. In the other, orthotic insoles, which have been marketed as being able to modify ankle kinematics, were inserted in the shoes. These insoles were liquid gel-filled, with the gel being a thick viscoelastic silicone type.

For each sampling interval, the shank LCS was rotated into the foot LCS using an Euler angle sequence (sagittal axis – frontal axis – transverse axis) to obtain relative foot/shank motions. For each trial these motions were plotted versus percentage of stance phase.

RESULTS

Relative sagittal and frontal foot/shank angular motions for the no insole and gel-filled insole conditions are shown, in figures 1 and 2, for two individual subjects. All subject trials, as well as the ones shown, demonstrated noticeable consistency within each condition. For the subject in Figure 1, it was noted that sagittal plane motions were similar for both conditions, while use of the

gel-filled insole appeared to shift frontal plane motion toward a more neutral posture during stance. The subject represented in figure 2, however, showed no discernable frontal plane effects with the insole, but demonstrated a tendency toward greater dorsiflexion throughout stance, that was more pronounced during early stance.

Discussion

Successful optoelectronic measurement of three-dimensional relative foot/shank motion has been previously reported; however, the need for line of sight necessitated a barefoot condition (Kidder et al. 1996). Moreover, the need for line of sight to several foot and tibial markers restricted measurement to be primarily below knee level.

Results of the present study have demonstrated that electromagnetic motion tracking can be successfully applied to relative foot/shank motion measurement for a shod condition. In this manner, an individual's kinematic response to an orthosis can be evaluated clinically in much the same manner as individual plantar pressure response to an orthosis can be assessed with shoe based plantar pressure measurement systems.

Electromagnetic tracking could enable clinicians to assess relative foot/shank motion effects of orthotic interventions, while shoes are worn, when such effects may be too subtle to be discerned via optoelectronic tracking of markers outside of the shoe.

REFERENCE

Kidder, S.M. et al. (1996). *IEEE Trans on Rehab Engin.*, **4**, 25-32.

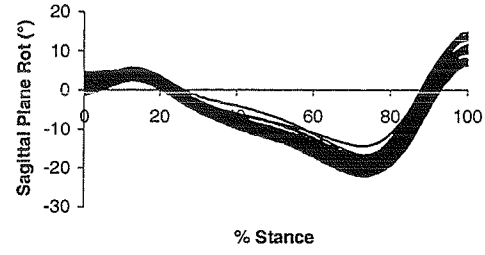

(a)

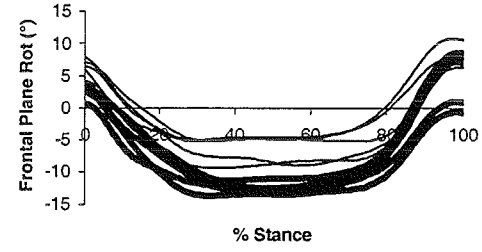

(b)

Figure 1: Relative foot/shank motions in (a) sagittal and (b) frontal planes for subject 1 with (thin lines) and without (thick lines) gel-filled insole.

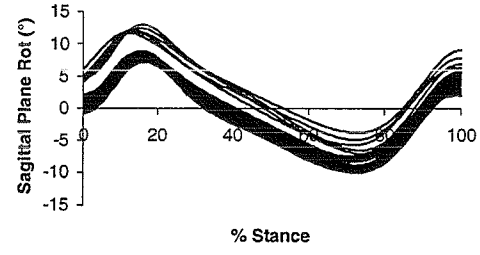

(a)

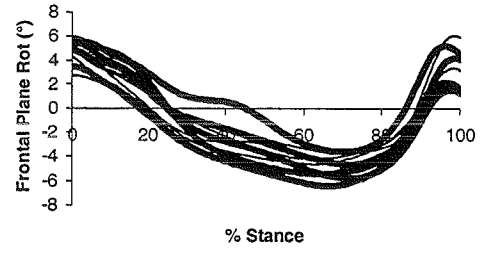

(b)

Figure 2: Relative foot/shank motions in (a) sagittal and (b) frontal planes for subject 3 with (thin lines) and without (thick lines) gel-filled insole.

STRIDE LENGTH EFFECTS ON GROUND REACTION FORCES DURING RUNNING

J.A. Mercer[1], D. Black[1], D. Branks[1], A. Hreljac[2]

[1]Department of Kinesiology, University of Nevada, Las Vegas
[2]Department of Kinesiology, California State University, Sacramento
E-mail: jmercer@nevada.edu Web: www.unlv.edu/faculty/jmercer

INTRODUCTION

Ground reaction force (GRF) impact magnitudes are affected by running velocity (Hamill et al., 1983; Munro et al., 1987) with increases in velocity accomplished by changes in stride length (SL) and frequency. Since simulation studies have reported that impact magnitudes during running are related to lower extremity geometry at impact (Gerritsen et al., 1995), it seems reasonable to suspect that SL is related to lower extremity geometry at impact. Although there is a wealth of documentation regarding GRF during running, there is very little research on the effect of SL changes on GRF. Therefore, the purpose of this study was to investigate SL effects on the impact magnitude and running velocity relationship. Additionally, the relationship between direction of line of application of resultant GRF and velocity was investigated.

METHODS

Subjects were 10 physically active college students (age: 25 ±4 yr; ht: 175 ±7.3 cm; mass: 76.1 ±12 kg). After giving informed consent and self-directed warm-up, subjects practiced running across a force plate flush with the floor in the middle of a 20 m runway. Running velocity was calculated by placing timing light sensors on both sides of the force plate. GRF data were recorded (1000 Hz) for each subject at a range of velocities during three conditions: preferred SL (PSL), SL set to 2.5 m (SL2.5), and SL set to 3.0 m (SL3.0). During SL2.5 and SL3.0 conditions, markers were placed on the floor 2.5m and 3.0m apart, respectively, and subjects targeted the markers. Subjects were instructed to complete 15-20 trials at a variety of running velocities per condition. The exact number of trials was dependent on the subject's ability complete an even distribution of velocities. Condition order was counterbalanced.

Resultant GRF (Fr) was calculated from vertical and anterior posterior force data, normalized to body weight (BW) and impact peak (IP) identified and recorded. The angle (θ_{IP}) between IP and the horizontal was calculated and recorded. The relationship between IP and running velocity was quantified by generating a scatterplot of IP vs. running velocity data for each subject-condition combination. The data were then fit with a linear model. Calculated slopes ($BW/m \cdot s^{-1}$) were used for subsequent analysis. An ensemble plot for all subjects was generated by averaging slopes and y-intercepts across subjects. The θ_{IP} vs. running velocity relationship was quantified using identical procedures.

Slopes for IP vs. running velocity and θ_{IP} vs. running velocity were analyzed using repeated measures ANOVA (SPSS version 10.1). Simple effect contrasts were used to compare PSL to SL2.5 and SL3.0. Correlations were calculated between IP and velocity and θ_{IP} and velocity relationship for all subject data per condition.

RESULTS AND DISCUSSION

Running velocity averaged 3.6 ±0.4 $m \cdot s^{-1}$, 3.6 ±0.4 $m \cdot s^{-1}$, and 3.9 ±0.5 $m \cdot s^{-1}$ for PSL, SL2.5, and SL3.0 conditions, respectively. The relationship between IP and velocity was different between conditions (Figure 1, $p<0.05$), with IP vs. velocity slope during PSL greater than SL3.0 ($p<0.05$) but not different that SL2.5 ($p>0.05$). The slope of the θ_{IP} vs. running velocity relationship was greater positive during PSL than both SL2.5 and SL3.0 (Figure 2, $p<0.05$).

Significant correlations ($p<0.05$) existed between IP and velocity during PSL ($r=0.53$) and SL3.0 ($r=0.31$), but not at SL2.5 ($r=0.13$). θ_{IP} vs. velocity correlations were significant ($p<0.05$) during PSL ($r=0.31$), SL2.5 ($r=-0.35$) and SL3.0 ($r=-0.31$).

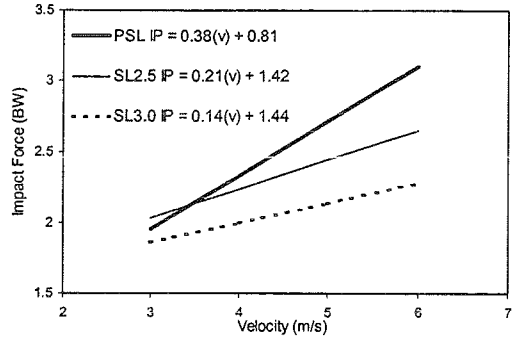

Figure 1: IP vs. velocity relationship

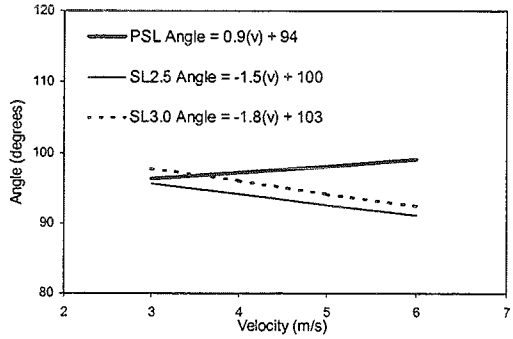

Figure 2: θ_{IP} vs. velocity relationship

Resultant GRF impact magnitude increased 0.38 BW on average for each 1 $m \cdot s^{-1}$ increase in velocity when SL was freely chosen at the different velocities. This relationship is similar to that reported by Munro et al. (1987) who reported that vertical GRF impact peak (F1) increased 1.6 BW across 2 $m \cdot s^{-1}$, or 0.35 $BW/m \cdot s^{-1}$. Further inspection of their data indicates that F1 increased on average 0.38 $BW/m \cdot s^{-1}$. In the present study, during SL2.5, impact forces increased by only 0.21 $BW/m \cdot s^{-1}$, and during SL3.0, impact forces increased by only 0.14 $BW/m \cdot s^{-1}$ (Fig. 1). This suggests that the relationship between IP and velocity during PSL was affected in part by changes in SL. However, given that IP increased, to a lesser extent, with velocity during SL2.5 and SL3.0 compared to PSL, other factors besides SL account for changes in IP.

The θ_{IP} and velocity relationship was affected SL changes. When SL was allowed to freely vary, θ_{IP} increased by 0.9 $°/m \cdot s^{-1}$, but when SL was 2.5 and 3.0 m, the line of application changed –1.5 and –1.8 $°/m \cdot s^{-1}$ (Fig. 2) relative to the horizontal. Although magnitude of change of θ_{IP} across velocities was small, this is important since impact attenuation may be related to θ_{IP} relative to the knee joint (Derrick et al., 1998).

SUMMARY

The relationship between IP and running velocity as well as the relationship between θ_{IP} and running velocity is partly explained by changes in SL.

REFERENCES

Derrick et al. (1998). *Med. Sci. Sp. Ex.*, 30(1), 128-135.
Gerritsen et al. (1995). *J. Biomech.*, 28,661-668.
Hamill et al. (1983).*Hum.Movt. Sci.*,2,47-56.
Munro et al. (1987). *J.Biomech.*,20,147-155.

THE EFFECT OF INTERSPECIMEN VARIATIONS IN MOMENT ARMS ON THE ENDPOINT FORCE PRODUCED BY FLEXOR POLLICIS LONGUS

Joseph Towles[1,2], Wendy Murray[1], Felix Zajac[1,2,3]

[1]Rehabilitaion R&D Center, VA Palo Alto Health Care System
[2]Departments of Mechanical Engineering and [3]Functional Restoration, Stanford University
Palo Alto, CA, USA; e-address: towles@stanford.edu

INTRODUCTION

Severe reductions of pinch force are observed after cervical spinal cord injury, and limit an individual's ability to perform important activities of daily living. In order to design and assess rehabilitative strategies that restore function (e.g., functional neuromuscular stimulation, tendon transfers), it is important to understand the endpoint force produced by specific muscles of the thumb. Muscle forces are transformed into endpoint forces via musculoskeletal geometry, including muscle moment arms and segment lengths. Because these parameters can depend on either joint angle or on anthropometric factors, it is critical to evaluate how musculoskeletal geometry influences the actions of thenar muscles.

The purpose of this study was to evaluate how the reported variability in published moment arm data of the flexor pollicis longus (FPL) at the three joints of the thumb (Smutz *et al.*, 1998) influenced estimates of the endpoint force FPL produced.

METHODS

A static, moment-driven, skeletal model of the thumb was developed using an approach previously applied to the index finger (Valero-Cuevas *et al.*, 1998). The thumb model was positioned in a lateral pinch posture. All the joints were neutrally abducted; the trapezio-metacarpal joint (proximal joint) was extended 30°, the metacarpo-phalangeal joint (middle joint) was flexed 30°, and the inter-phalangeal joint (distal joint) was in 0° of flexion (Fig. 1). The moments produced at the thumb's three joints by 10 N of muscle force were calculated by multiplying force by FPL's flexion moment arms. The joint moments were then transformed into an endpoint force vector via the Jacobian matrix.

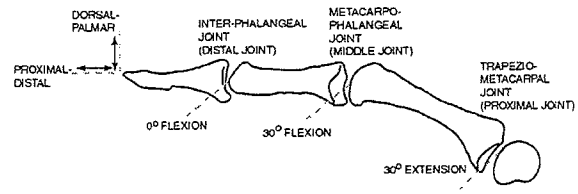

Figure 1: Static model of the right thumb in its plane of flexion-extension.

The nominal endpoint force vector of FPL was calculated using the moment arms of thenar muscles reported by Smutz *et al.* (1998), an average of data collected from seven specimens (Table 1). We also estimated the endpoint force vectors that resulted from altering the flexion moment arms by ±1 standard deviation (SD) about their means.

	Distal	Middle	Proximal
Mean (mm)	8.7	8.7	14.3
SD (mm)	1.2	1.2	4.0
V (%)	14%	14%	28%

Table 1: Moment arm data from Smutz *et al.* (1998); Coefficient of variation, $V = \frac{100 * SD}{mean}$.

RESULTS

The magnitude and orientation of the endpoint force at the thumb produced by FPL was highly dependent on the ratio of its flexion moment arms at the three joints of the thumb. The nominal endpoint force had a magnitude of 1.8 N and was rotated 127° relative to the distal phalanx (Fig. 2a). The average moment arms have a ratio of 1:1:1.6 (distal:middle:proximal). A concomitant 1-SD increase in all three moment arms altered the ratio (1:1:1.8), decreased the

endpoint force's magnitude (1.7 N) and decreased its angle (106°). A concomitant 1-SD decrease altered the ratio (1:1:1.4), increased the endpoint force's magnitude (2.1 N), and increased its angle (144°) (see Fig. 2b).

When moment arms of the three joints were varied in isolation, 1-SD changes in the moment arm at the proximal joint had the greatest effect on the endpoint force. When FPL's moment arm at the proximal joint was varied by ±1 SD, the magnitude of the force vector ranged from 1.5 N to 3.0 N and its orientation ranged from 73° to 152° (see Fig. 2c); at the middle joint, 1.4 N to 2.4 N and 108° to 138° (see Fig. 2d); and at the distal joint, 1.6 N to 2.0 N and 121° to 132° (see Fig. 2e). When we considered every combination of moment arm variation, the endpoint force's magnitude ranged from 1.3 N to 4.0 N and its orientation ranged from 43° to 155°.

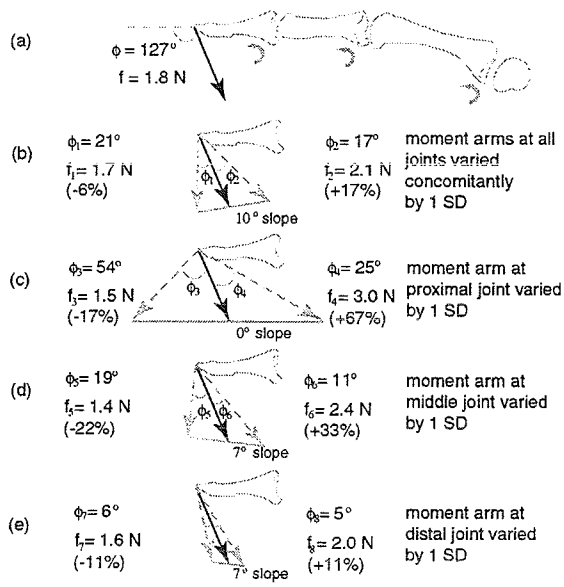

Figure 2: Effect of changing moment arms at three joints by ±1 SD. (a) depicts nominal force, (b) concomitant moment arm changes, (c) through (e) isolated moment arm changes.

DISCUSSION

This study illustrates that varying FPL's flexion moment arms by ±1 SD can substantially alter the magnitude and direction of its endpoint force vector.

The analysis indicates that if the moment arms of the three thumb joints vary independently from each other, FPL could have very different actions at the endpoint in different individuals. For instance, ±1-SD variations of the moment arm at the proximal joint result in endpoint forces with either sizable, proximal or sizable, distal components (see Fig. 2c). This means that in one individual, FPL could push an object away and out from the thumb (which is useful for securing an object with tip pinch) and in another person, pull in an object toward the thumb (which is useful for compressing the distal joint).

In contrast, if FPL's moment arms co-vary, the endpoint forces are much less divergent. The concomitant changes indicate that FPL's endpoint force is palmarly-directed in general (see Fig. 2b), and thus, would push an object down and away from the thumb (which is useful for securing an object with lateral pinch).

Surgical intervention after spinal cord injury sometimes increases FPL's moment arm at one thumb joint. The prevailing thought is that this will increase the magnitude of the endpoint force, thus improving grasping. However, this study suggests that increasing FPL's moment arm in isolation may decrease the magnitude of its endpoint force vector and re-direct it in an undesirable manner; thus, comprising grasping ability.

REFERENCES

Smutz, W. P. *et al.* (1998). *J. Biomech.*, **31**, *565-70.*

Valero-Cuevas, F. J. *et al.* (1998). *J. Biomech.*, **31**, *693-703.*

ACKNOWLEDGEMENTS

The authors thank Francisco Valero-Cuevas, PhD for helping to develop an earlier version of the thumb model. Also this work was supported by the VA Rehabilitation R&D Service (project number B898-3RA).

AMBULATORY GAIT ANALYSIS USING GYROSCOPES

K. Aminian[1], B. Najafi[1],C. Büla[2], P.-F. Leyvraz[3] and Ph. Robert[1]

[1]Swiss Federal Institute of Technology (EPFL), Metrology Laboratory, Lausanne, Switzerland
[2] Service of Geriatric Medicine, CHUV & CUTR Sylvana, Epalinges, Switzerland
[3]Hôpital Orthopédique de la Suisse Romande, Lausanne, Switzerland
E-mail: kamiar.aminian@epfl.ch

INTRODUCTION

Recently, technical progress has made possible to realize miniature kinematic sensors such as accelerometers and angular rate sensors (Sparks et al. 1998). These sensors can be battery powered and are promising tools for ambulatory gait monitoring and analysis. The possibility to detect simple parameters such as steps and cycle time from trunk or heel acceleration has already been demonstrated (Aminian et al, 1995). Gait analysis using gyroscope has proved to be an other alternative technique for gait analysis (Tong and Granat, 1999). Unlike the accelerometer, the gyroscope can be attached anywhere to a body segment since the angular rotation is still the same along the segment. However no clear correspondence has been established between gait events and the patterns of angular velocity. In this study we describe an ambulatory system for temporal parameters estimation using gyroscopes. The accuracy of the measurement was assessed using as criterion standard the information provided by footswitches. To show the effectiveness of the method in a wide range of walking performance, gait parameters were obtained from young and old subjects.

METHODS

Measurement were taken from a group of 9 young (21±2 years) and 11 elderly (79±8 years) subjects. Informed consent was obtained from all subjects. Each young subject performed four trials including at least 20 gait cycles. Three trials corresponded to walking on a treadmill at the preferred speed, under and over the preferred speed. The fourth trial was performed over ground at preferred speed. The elderly performed only two trials over ground at their preferred speed. A miniature gyroscope was attached on each shank. These sensors measure the velocity of angular rotation parallel to the mediolateral axis. Footswitches placed under the right foot (beneath the heel and beneath the big toe), have been used as criterion standard to validate the temporal parameters estimated by the gyroscopes. All signals were digitized at a sampling rate of 200 Hz by a portable data logger and stored on a memory card.

Gait phases were determined for each leg from the precise moments of heelstrike and toe-off. These events give rise to distinctive features on shank angular velocity signals in form of rather sharp negative peaks. A multi-resolution wavelet decomposition (Mallat, 1989) was used to enhance the toe-off and heel-strike event during walking. Temporal parameters of a gait cycle were computed from heelstrikes and toe-offs as percentage of gait cycle. In order to reach a good precision for the temporal parameters, at least 20 gait cycles have been considered for analysis. For each trial the value of temporal parameters was averaged over all cycles.

RESULTS AND DISCUSSION

Fig. 1 shows a good correspondence between gait events detected by footswitch and gyroscopes. An excellent agreement (r=0.99) is found. The difference between estimated stance (gyroscope) and actual value (footswitch) is not significant (N=58, p>0.80) with an RMS error of 0.023s (2.8%). No significant change is neither observed between estimated gait cycle and actual (N=58, p>0.97). The RMS error is 0.008s (0.5%). The 95% confidence interval for the difference between heelstrike detection by footswitch and gyroscope is [0.007s, 0.013s]. Gyroscope detects heelstrike 0.01 s (in average) later than footswitch. The 95% confidence interval for the difference between toe-off detection by footswitch and gyroscope is [-0.005s, 0.004s]. Therefore there is no significant difference in toe-off detection. As expected, the gyroscopes provide the same time for both left and right gait cycles, with RMS error less than 0.015s (r>0.99, 1.3%). In addition, results did not suggest any differences in validity of the system across age group. The proposed method reveals a promising monitoring tool for functional evaluation of gait improvement. It allows measuring gait temporal features (stance, swing, single and double support) during a long period of walking and supplying in this way the stride-to-stride variability of gait. It has many potential clinical applications such as outcome measure after total knee or hip replacement, prosthesis adjustment for amputees, gait disturbances analysis in neurological diseases, and fall risk estimation in elderly. The system is light (300 gr), portable, and low cost and involves no discomfort for the patient who can carry it for a long period of time.

SUMMARY

A new method using wavelet transform to detect toe-off and heelstrike from shank angular velocity is proposed. A high correlation with actual gait events detected with footswitch was found. No significant error is observed for toe-off detection, while a slight systematic delay (10ms in average) exists between heelstrike obtained from gyroscopes and footswitch. By considering a sampling period of 5ms (200Hz) this error is acceptable.

REFERENCES

D.R. Sparks, X. Huang, W. Higdon, J.D. Johnson, (1998). Microsystem Technologies 4, 139-142, Springer-Verlag

Aminian K, Robert P, Jequier E, Schutz Y (1995). *Med Sci Sports Exerc.*, 27:226-34.

K. Tong, MH. Granat, Med. Eng. Phys., 21, 1999, 87-94

S.G. Mallat, (1989). IEEE Trans., Pattern Anal.& Machine Intelligence, 11, 674-693

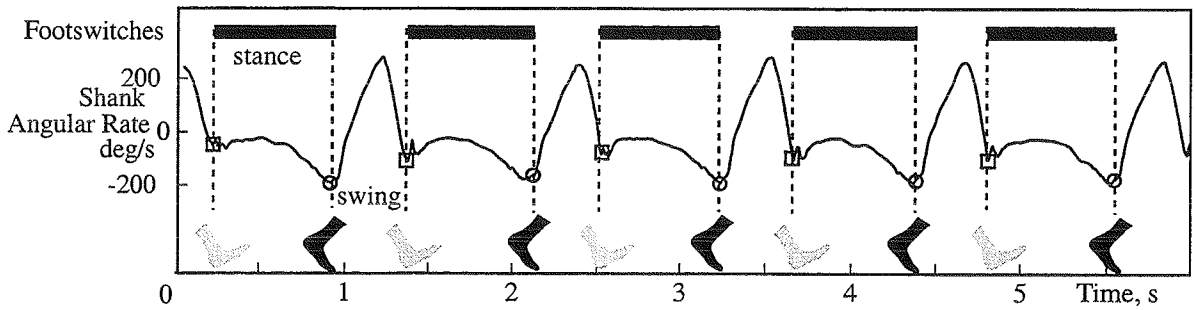

Figure 1- Correspondence between gait events detected by footswitches and gyroscopes. Negative peaks of angular rate corresponding to heelstrikes(□) and toe-off (○) are detected after wavelet transform.

SLOW ECCENTRIC CONTRACTIONS ARE NOT ALWAYS LESS STEADY THAN CONCENTRIC CONTRACTIONS FOR OLD ADULTS

Douglass Laidlaw, Sandra Hunter and Roger Enoka

Neural Control Of Movement Laboratory, University of Colorado, Boulder, CO, USA
Email: laidlaw@colorado.edu Web: www.colorado.edu/kines/Lab/NCM.html

INTRODUCTION

When old adults attempt to exert steady muscle forces during submaximal isometric and anisometric contractions, the force and acceleration fluctuations are greater compared with young adults, especially at low forces (Galganski *et al.*, 1993; Keen *et al.*, 1994; Laidlaw *et al.*, 2000). Moreover, old adults are less steady when performing eccentric contractions compared with the concentric contractions (Laidlaw *et al.*, 2000), and have particular difficulty with the transition from concentric to eccentric contractions. It has been shown previously in a hand muscle (Laidlaw *et al.*, 2000) that the differences in steadiness with age during isometric and during concentric-eccentric contractions are primarily due to an increased variability of motor unit discharge in old adults. However, it is not known whether the reduced steadiness of eccentric contractions is due to some unique property of eccentric contractions, or due to the change in motor command from the CNS during the transition from concentric to eccentric contractions. The purpose of this study was to determine if the reduced steadiness of eccentric contractions observed in old adults is due to a feature that is intrinsic to eccentric contractions, or if it depends on the details of the task.

METHODS

Twenty healthy subjects were assigned to one of two age groups, an old group (n=10; average 68.3 yrs; range 62-79 yrs) and a young group (n=10; average 22.9 yrs; range 19-26 yrs). All subjects were carefully screened for neuromuscular disorders. The tasks performed by the subjects involved the index finger of the left hand and were: (1) one-repetition maximum (1-RM) and (2) position-tracking trials.

The 1-RM task was performed with the index finger moving horizontally through its passive range of motion in the abduction-adduction plane (15-25 deg). The weight was attached to the index finger at the proximal interphalangeal joint to provide a load in the adduction direction. The load was raised and lowered during 2-s of abduction (concentric contraction) and 2-s of adduction (eccentric contraction), respectively. A triangular template was displayed on the monitor and each subject was given practice trials to become familiar with the timing and amplitude of the movement. The load applied in the adduction direction was increased in increments of 50-100 g until the load could no longer be raised through the complete range of motion.

The position-tracking trials were performed with loads of 2.5%, 10% and 35% of 1-RM. Three trials with each load were performed with the index finger moving through the range of motion. Index finger position and acceleration in the abduction-adduction plane were detected with a linear variable displacement transducer and a miniature piezoresistive accelerometer, respectively. For the position-tracking trials the subjects performed two different sequences: (1) concentric-eccentric, and (2) eccentric-concentric. The duration of each contraction was 10 s. The triangular template was inverted for the eccentric-concentric (lowering-raising) sequence. The subjects were encouraged to match the desired finger displacement template as closely as possible.

The steadiness of each contraction was quantified as the standard deviation of acceleration over the duration of the contraction, normalized to the load lifted. The average data from the three trials with each load was used for the analyses.

RESULTS AND DISCUSSION

The 1-RM strength was greater for the young (1.79 ± 0.13 kg) compared with the old (1.21 ± 0.10 kg) subjects.

The concentric and eccentric contractions during the position-tracking task were less steady for the old subjects compared with the young subjects, for both contraction sequences. For each comparison, the normalized acceleration was greater for the old subjects compared with the young subjects. The largest differences between age groups were observed during the trials with the lightest load. There were no differences between the young and old for comparisons of range of motion and average velocities during the concentric and eccentric contractions.

As previously reported, the normalized acceleration during the eccentric contractions was greater compared with the concentric contractions with the 2.5% load (Figure 1).

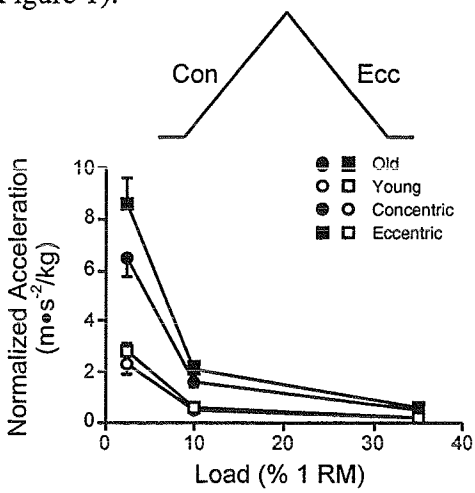

Figure 1. Normalized acceleration of the index finger for the young and old subjects performing the concentric-eccentric sequence during the position-tracking task. A schematic of the template is shown at the top.

In contrast, there were no differences in steadiness between the contraction types for the old subjects during the eccentric-concentric sequence trials (Figure 2). While the steadiness of the eccentric contractions was not different compared with the concentric-eccentric sequence, the normalized acceleration for the concentric contractions with the 2.5% load was significantly greater compared with those during the concentric-eccentric sequence.

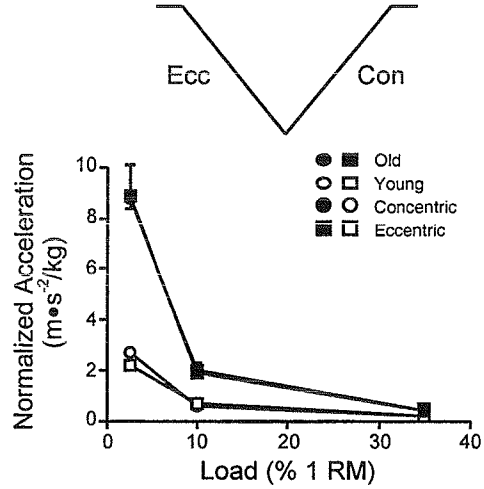

Figure 2. Normalized acceleration of the index finger for the young and old subjects performing the concentric-eccentric sequence during the position-tracking task.

These findings suggest that the increased variability of motor unit discharge underlying the reduced steadiness of eccentric contractions in old adults is preserved during the subsequent concentric contractions. This effect is greatest during low-force contractions when the discharge behavior of the most recently recruited motor unit has a relatively greater effect on the steadiness compared with a higher-force contraction.

SUMMARY

- The old subjects were less steady than young subjects when lifting and lowering light loads with the first dorsal interosseous muscle.
- The steadiness of concentric and eccentric contractions for the old subjects with the lightest load were similar for one task but different for another task.

REFERENCES

Galganski, M.E., Fuglevand, A.J., Enoka, R.M. *J. Neurophysiol.* 69: 2108-2115, 1993.

Keen, D.A., Yue, G., Enoka, R.M. *J. Applied Physiol.* 77: 2648-2658, 1994.

Laidlaw, D.H., Bilodeau, M., Enoka, R.M. *Muscle Nerve* 23: 600-612, 2000.

In vivo skeletal muscle tension measurement using Magnetic Resonance Elastography (MRE)

TR Jenkyn, PhD[1], RL Ehman, MD[2], KR Kaufman[1], PhD, K-N An[1], PhD

[1]Biomechanics Laboratory, Div. of Orthopedic Research, Mayo Clinic, Rochester, MN, USA
[2]Dept. of Diagnostic Radiology, Mayo Clinic, Rochester, MN, USA
Email: jenkyn.thomas@mayo.edu

INTRODUCTION

Indeterminacy is the primary obstacle for inverse kinematic modeling in musculo-skeletal biomechanics. Force transducers and EMG provide clues of muscle load sharing, but do not completely solve joint indeterminacy.

Magnetic Resonance Elastography (MRE) is a new technique for quantifying tissue stiffness in vivo (Muthupillai, 1995). Muscle stiffness has been shown to change with state of contraction (Dresner, 2001). MRE applies shear waves to muscle and images the wave propagation through the tissue. Imaged wavelength changes with muscle stiffness and is therefore directly related to muscle tension.

This study assesses MRE applicability to biomechanics by directly measuring isometric muscle tension.

METHODS

Subjects lay supine in a GE MRI scanner (aged 26-32, 3 female, 4 male) within an ankle loading apparatus. Moment was applied to the ankles in neutral position (8Nm, 16Nm plantar-flexing and 30Nm, 60Nm dorsi-flexing) which was isometrically opposed. A vibrator applied shear waves of frequency 150Hz (f) and amplitude 30μm. Tibialis anterior (TA) and triceps surae (TS) were imaged with a gradient-echo, cyclic motion sensitizing sequence (TR/TE of 100ms/min full, 256x64 acquisition matrix, 24cm FOV). To determine muscle tension, muscle tissue was modeled as fibers in a viscous medium. Tension (T) is therefore a function of wavelength (λ) as in Equation 1.

$$T = \frac{\lambda^2}{4\pi^2}\left(\zeta^2\omega^2 + \rho^2 A^2 \omega^4\right)^{\frac{1}{2}} \cos\left[\frac{1}{2}\arctan\left(\frac{\zeta}{\rho A \omega}\right)\right]$$

Equation 1: The λ– T relationship where ζ is viscosity, ρ is density, A is cross-sectional area, and ω=2π f (Graff, 1975).

Surface EMG was also collected from TA and TS (sampled at 1000Hz, bandpass 30-500Hz, gain 350) while repeating the experiments outside the MRI. EMG was integrated and normalized with maximum voluntary contraction (IEMG).

RESULTS AND DISCUSSION

MRE shear wavelength increased in TA as it opposed increasing plantar-flexing moment (Figure 1). Wavelength increased to a lesser extent with applied dorsi-flexing moment as TA acted as an antagonist.

TA tension and IEMG both increased with applied plantar-flexing moment (Figure 2). TS tension increased with applied dorsi-flexing moment. This agreed qualitatively with IEMG activity (Figure 2). MRE measurement of tension in multiple muscles simultaneously has been demonstrated. Since not all the ankle muscles were imaged, the internal joint moment due to muscle tensions did not match the externally applied ankle moment. Imaging all active muscles about the ankle and balancing internal muscle moment with

externally applied moment is currently underway.

MRE is sensitive to the muscle λ– T relation used. Currently, this relation is derived from wave motion of strings with tension in a viscous medium. This models the contracting muscle well but models relaxed muscle less well. Further derivation of the λ– T relation is on-going to address this.

MRE noninvasively quantifies tension in multiple muscles simultaneously. MRE can potentially overcome joint indeterminacy and yield tremendous insight into musculoskeletal biomechanics.

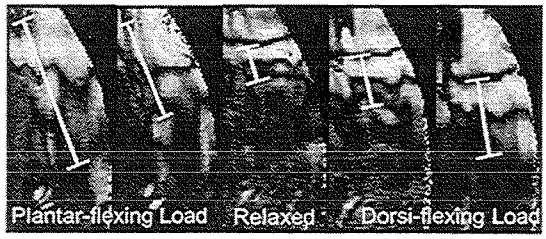

Figure 1: MRE imaged shear waves in TA for each applied ankle moment.

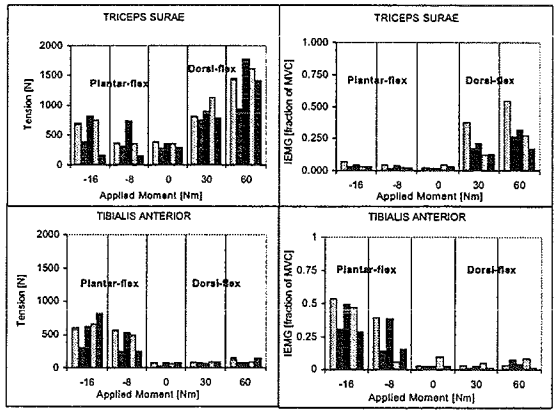

Figure 2 MRE tensions (left) and IEMG (right) in TA (top) and TS (bottom) for each applied moment.

ACKNOWLEDGEMENTS

Funded by NIH-NICHD.

REFERENCES

Dresner MA, et al. (2001) "MRE of Skeletal Muscle" *JMRI* **13**(2) pp269-76

Graff KF *Wave Motion in Elastic Solids*. Ohio State Univ Press:1975

Muthupillai R, et al. (1995) "MRE by direct visualization of acoustic strain waves" *Science* **269** pp1854-7

DEFICITS IN ISOMETRIC FORCE BUT NOT PEAK STRETCH FORCE DEPEND ON THE ACTIVATION LEVEL DURING STRETCHES OF SKELETAL MUSCLES

Mark Willems and William Stauber

Department of Physiology, West Virginia University, Morgantown, WV, USA
E-mail: mwillems@hsc.wvu.edu

INTRODUCTION

Skeletal muscles exposed to unaccustomed stretches during activation, immediately lose the ability to produce maximal isometric force which is related to the peak stretch force (McCully & Faulkner, 1986; Warren et al., 1993). In isolated muscle preparations, peak stretch force has been varied by fatigue, stretch velocity, stimulation frequency and the amount of lengthening (McCully & Faulkner, 1986; Warren et al., 1993). In intact rats, we examined deficits in isometric and peak stretch force of skeletal muscles during stretches with high and low stimulation frequencies. The hypothesis tested was that deficits in isometric and peak stretch force would be larger for stretches with high stimulation frequency than for stretches with low stimulation frequency.

PROCEDURES

Female Sprague Dawley rats [(n = 12, body mass: 276 ± 5 g (mean ± SE)] were positioned with flexed knee (1.57 rad) and the left foot pressing on an aluminum plate connected to a dynamometer (Cutlip et al., 1997). Plantar flexor muscles were activated via a cuff electrode around the tibial nerve (200 μs width pulse, 5.5 ± 0.3 V). Force was measured under the sole of the foot (Willems & Stauber, 1999). Twenty stretches [(i.e. dorsiflexion of the foot; range of motion 0.70-1.57 rad (i.e. 40°-90°); acceleration 52.3 rad·s^{-2} (i..e. 3000 °·s^{-2})] were imposed on isometric contractions at 1.57 rad (i.e. 90°) with high and low stimulation frequency (80 Hz and 20 Hz). Rest periods between contractions were 3 minutes. The highest forces during the isometric phase and the stretch phase (see Fig. 1 for phases) were measured.

RESULTS AND DISCUSSION

Force recordings of plantar flexor muscles during the 1st contraction are shown in Fig. 1. Force reached a peak at the end of the movement [i.e. at the end of the stretch (Fig. 1)] with 80 Hz activation.

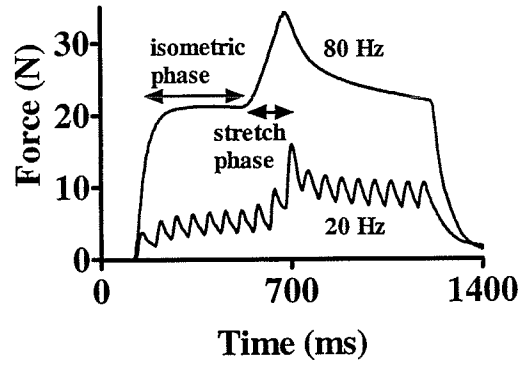

Figure 1: Examples of forces of rat plantar flexor muscles during the 1st stretch imposed on an isometric contraction with a stimulation frequency of 20 Hz and 80 Hz.

Peak stretch forces were larger for all stretches with a stimulation frequency of 80 Hz (1st stretch: 30.4 ± 2.1 N, 20th stretch: 19.6 ± 1.0 N) than for stretches with a stimulation frequency of 20 Hz (1st stretch: 16.5 ± 1.8 N, 20th stretch: 12.1 ± 1.5 N). The relative deficits in isometric force were substantially larger for stretches with a

stimulation frequency of 80 Hz than for stretches with a stimulation frequency of 20 Hz (Fig. 2A) (ANOVA, $P < 0.05$). In contrast, relative deficits in peak stretch force were not different for stretches with a stimulation frequency of 20 Hz and 80 Hz (Fig. 2B).

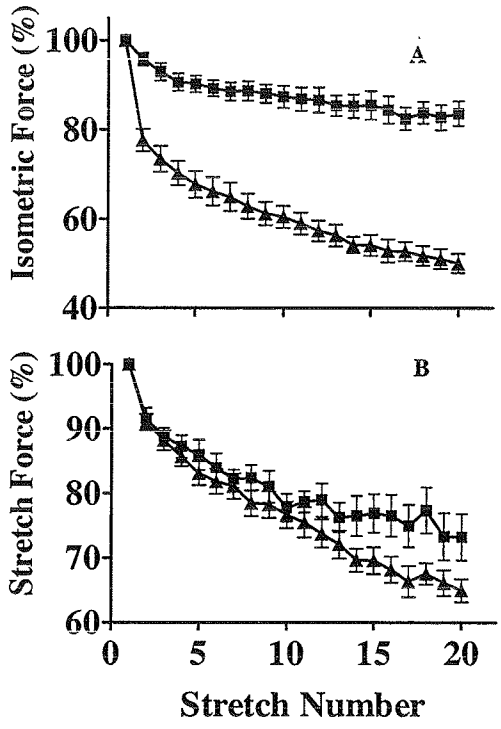

Figure 2: Relative deficits in isometric force (A) and peak stretch force (B) as a function of stretch number for 20Hz (■) and 80 Hz (▲) stretches. Forces were normalized with respect to the forces in the 1st contraction in each series of stretches.

Force deficits by stretches of activated skeletal muscles are caused by excitation-contraction coupling failure and alteration of force producing structures (Morgan & Allen, 1999). The discrepancy between the relative loss in isometric force and peak stretch force, most obvious for stretches with a stimulation frequency of 20 Hz suggests 1) that the contribution of mechanisms responsible for the loss in isometric force is different for the loss in peak stretch force or 2) additional mechanisms contribute to the loss in peak stretch force. During stretches of active skeletal muscles, it is thought that "active" cross-bridges produce larger forces than "active" cross-bridges during isometric contractions. Some cross-bridges could lose their ability to produce stretch force after stretches with high and low levels of nerve activation.

SUMMARY

Repeated stretches of rat plantar flexor muscles using a stimulation frequency of 20 Hz resulted in smaller relative deficits in isometric force but similar relative deficits in peak stretch force compared to stretches with a stimulation frequency of 80 Hz. Stretch-induced deficits in isometric force but not in peak stretch force seems to be related to the peak stretch force.

REFERENCES

Cutlip, R.G. et al. (1997). *Med. Biol. Eng. Comput.* **35**, 540-543.
McCully, K.K., Faulkner, J.A. (1986). *J. Appl. Physiol.* **61**, 293-299.
Morgan, D.L., Allen, D.G. (1999). *J. Appl. Physiol.* **87**, 2007-2015.
Warren, G.L. et al. (1993). *J. Physiol.* **464**, 457-475.
Willems, M.E.T., Stauber, W.T. (1999). *Exp. Physiol.* **84**, 379-389.

ACKNOWLEDGEMENTS

This work was supported by the National Institute of Occupational Safety and Health Centers for Disease Control (R01-0H-02918).

STRAIN RATE MODULATION OF SKELETAL MUSCLE MEMBRANE PERMEABILITY

Thomas J. Burkholder

Department of Health and Performance Sciences, Georgia Institute of Technology, Atlanta, GA, USA. e-mail: thomas.burkholder@hps.gatech.edu

INTRODUCTION

Force generation in skeletal muscle depends on the length, velocity, and biochemistry of the sarcomeres (Close, 1972). To generate maximum power, a muscle must shorten at its optimal velocity along the plateau of the length-tension relationship (Lutz & Rome, 1994).

Skeletal muscle architecture can adapt to meet functional demands (Herzog, *et al.*, 1991). Fiber length plays a critical role in determining the functional characteristics of whole muscle (Gans & Gaunt, 1991). Fiber length is also particularly responsive to mechanical signals (Williams & Goldspink, 1973). While passive stretch is a sufficient stimulus for muscle growth, structural optimization requires that this growth be modulated by the velocity of stretch.

The mechanical responsiveness of many cell types is influenced by the time dependent characteristics of stimulation. Endothelial cell response varies with the rate of change of shear stress (Frangos et al., 1996). FGF-2 release from smooth muscle is modulated by strain rate (Cheng, et al., 1997). Even firing of mechanoreceptors is influenced by stretch rate (Houk et al., 1981).

Several mechanisms for stretch induced growth have been proposed, including release of growth factors through transiently disrupted cell membrane. This disruption should depend on the transfer of strain energy to the membrane and cytoskeleton, which may be influenced by strain rate.

The goal of this project was to determine whether the membrane disruption of cultured myotubes subjected to stretch is modulated by stretch rate.

METHODS

C2C12 myoblasts (ATCC) were maintained at low density in DMEM supplemented with 10% fetal bovine serum (FBS, Hyclone), 100 IU/ml penicillin and 100 μg/ml streptomycin. Mechanical stimulation chambers were prepared by coating silastic membrane with 1 $\mu g/cm^2$ collagen (type I from rat tail) and 0.1 $\mu g/cm^2$ laminin from EHS tumor prior to application of 25% initial stretch. Myoblasts were seeded onto the stretched membranes at a density of 10^4 $cells/cm^2$ and allowed to proliferate to confluence. Confluent membranes were switched to differentiation media (DM) consisting of DMEM supplemented with 10% horse serum and antibiotics. Under these conditions, cells fuse into myotubes aligned with the direction of stretch in about 4 days.

Immediately prior to stimulation, cultures were rinsed once with DM and bathed in DM containing 1 mg/ml fluorescein conjugated dextran (FDx). Cultures were then subjected to 60 minutes of mechanical stimulation, consisting of 60 repetitions of 45 seconds of sinusoidal stretch interrupted by 15 second rest periods. Strain amplitude was ±5% or ±10% of rest length, and frequency varied between 0 and 2 Hz.

Following mechanical stimulation, aliquots of media were reserved, cultures were rinsed extensively to remove unincorporated label and lysed in detergent buffer. Protein content in cell lysates was quantitated by BCA assay (Pierce), and FDx content quantitated by fluorescence or absorbance. Fluorescence was normalized to protein content and media label concentration. Because of the variation between cultures, each preparation was normalized to identically treated, unstretched control cultures.

RESULTS AND DISCUSSION

FDx capture by cells has been used as a marker for cell membrane integrity because the 10 kD molecule is excluded by intact membranes. FDx capture by mechanically stimulated myotubes showed a clear dependence on strain rate (fig. 1).

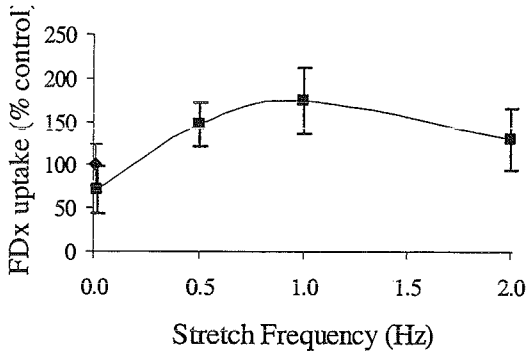

Figure 1: FDx uptake in cells stretched at various frequencies. Hashed band represents control ±SD

The influence of strain amplitude was less apparent, as 1 Hz stimulation at ±10% and ±5% yielded nearly identical FDx incorporation (175±38% and 170±26%, respectively).

To verify cell viability after the high frequency stimulation, 0.2% trypan blue was added to the incubation media after stretch. No difference in uptake was found.

This pattern of strain rate dependence is similar to that shown by stretch induced protein synthesis (Clark et al, 2001; fig 2), and suggests a common mechanism. FGF-2 induced activation of MAP kinase kinase in differentiated myotubes leads to activation of p70S6 kinase and enhanced protein translation. Thus, these results are supportive of the hypothesis that transient, stretch induced disruptions of the cell membrane permit the release of growth factors, which stimulate cell growth.

The stretch amplitudes used in this study were intended to be typical of common use. Larger strains (>15%) may be more representative of injurious strains, and hence a different mechanism.

SUMMARY

Uptake of a marker for membrane permeability shows distinct strain rate dependence in cultured myotubes, which is similar to the stretch induced increase in amino acid incorporation.

REFERENCES

Cheng,G.C. *et al.*, (1997). *Circ Res* **80**:28-36

Clark, C.B. *et al,* (2001). *Rev Sci Instr, in press*

Close, R.I. (1972). *Physiol Rev* **52**:129-197

Frangos, J.A. *et al.* (1996). *Biochem Biophys Res Commun* **224**:660-665

Gans, C., Gaunt, A.S. (1991). *J Biomech* **24S1**:53-65.

Herzog, W. *et al.* (1991). *Med Sci Sports Exerc* **23**:1289-1296.

Houk, J.C., *et al.* (1981). *J Neurophysiol* **46**:143-166

Lutz, G.J., Rome, L.C. (1994). *Science* **263**:370-372.

A MODEL OF HUMAN MUSCLE ENERGY EXPENDITURE

Brian R. Umberger, Karin G. M. Gerritsen, and Philip E. Martin

Exercise and Sport Research Institute, Arizona State University, Tempe, AZ USA
E-mail: brian.umberger@asu.edu

INTRODUCTION

Hill-type muscle models allow for a direct assessment of mechanical energetics during movement simulations (Zajac, 1989), but do not account for liberation of metabolic energy. The belief that minimizing metabolic cost is important in many human movements has led to the development of models of muscle heat production (eg: Schutte et al., 1993) for use in conjunction with the standard Hill-type model. Many of these models rely heavily on extrapolations from amphibian data and suffer uncertainties regarding temperature scaling. Also, most models have not been adequately evaluated to show that reasonable estimates of human muscle energy expenditure are predicted. Until recently (eg: González-Alonso et al., 2000) there have been few data on human muscle heat production in dynamic contractions to compare model results with.

Our purpose was to develop a model of human muscle energy expenditure that provides reasonable predictions of energy liberation over a range of activation levels. Model performance was evaluated at three distinct levels of complexity.

METHODS

The total rate of muscle energy liberation ($\dot{E}$), in Watts per kg of muscle ($W \cdot kg^{-1}$), was represented as the sum of activation ($\dot{h}_A$), maintenance ($\dot{h}_M$), and shortening-lengthening heat rates ($\dot{h}_{SL}$), and mechanical work rate ($\dot{w}$) (Woledge et al., 1985)

$$\dot{E} = \dot{h}_A + \dot{h}_M + \dot{h}_{SL} + \dot{w}. \quad (1)$$

The combined ($\dot{h}_A + \dot{h}_M$) term was predicted from muscle fiber type composition (Bolstad & Ersland, 1978). $\dot{h}_{SL}$ was calculated as the product of contractile element (CE) velocity and a coefficient. The coefficient for shortening was set such that total energy rate was five times the isometric energy rate at a velocity corresponding to maximal shortening velocity for slow twitch fibers (Barclay et al., 1993). The coefficient for lengthening was 6X the shortening coefficient. The $\dot{h}_{SL}$ and 40% of ($\dot{h}_A + \dot{h}_M$) were scaled by the force-length relation at lengths longer than optimal CE length (Homsher & Kean, 1978). Mechanical work rate was determined from CE force and velocity.

For submaximal activation, heat production was first scaled to account for the rapid rise and slow decay of heat production (Schutte et al., 1993). Separate nonlinear scaling factors were then applied to reflect the *relative* increase in ($\dot{h}_A + \dot{h}_M$) (Saugen & Vøllestad, 1995) and *relative* decrease in $\dot{h}_{SL}$ (Buschman et al., 1995) at submaximal activation. Finally, the total heat rate was scaled by a factor S to account for anaerobic (S=1.0) and aerobic (S=1.5) metabolic conditions (González-Alonso et al., 2000).

The model was evaluated by simulating isolated muscle testing (isovelocity contractions at speeds up to V_{max}), single joint motion (repetitive knee extension-flexion), and whole body locomotion. All simulations were performed using the musculoskeletal model of Gerritsen et al. (1998).

RESULTS AND DISCUSSION

Isovelocity Contractions. Results for shortening from the plateau of a maximal isometric contraction at various speeds (Figure 1) are consistent with data from mammals and other species (Barclay et al., 1993; Woledge et al., 1985).

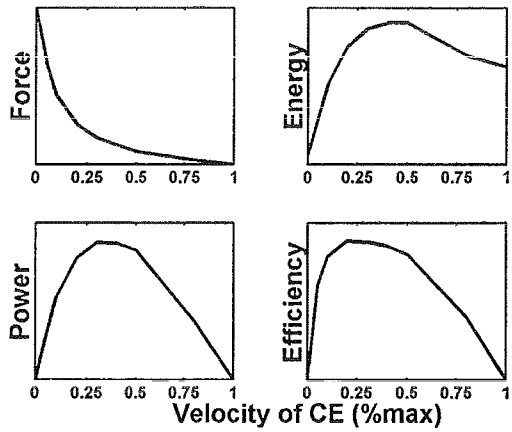

Figure 1: Dependence of force, energy rate, power, and efficiency on shortening rate. Energy rate, power, and efficiency peaked at 0.50, 0.35, and 0.25 V_{max}, respectively.

Results for lengthening are consistent with work by Constable et al. (1997) on mouse muscle. Work done on the muscle was ~2X the heat produced at most speeds.

Knee Extension/Flexion. In simulations of the experimental protocol used by González-Alonso et al. (2000), the model performed cyclic knee extensions/flexions at the same rate (1 Hz) and average power output (30.7 $W \cdot kg^{-1}$) as reported for their subjects. Under simulated anaerobic conditions (S=1.0) the quadriceps liberated energy at a rate of 56.4 $W \cdot kg^{-1}$ compared to 57.9 $W \cdot kg^{-1}$ for the subjects during the first several cycles of motion. For aerobic conditions (S=1.5) the quadriceps energy rate was 69.2 $W \cdot kg^{-1}$ compared to 73.0 $W \cdot kg^{-1}$ for the subjects.

Locomotion. Model energy predictions were evaluated using a 2D forward dynamics simulation of walking at 1.2 $m \cdot s^{-1}$. The optimization criterion was to minimize total energy expended per unit distance traveled. Assuming aerobic conditions, whole body energy rate (including non-involved tissues) was 5.5 $W \cdot kg^{-1}$ compared with 4.2 $W \cdot kg^{-1}$ for humans walking at the same speed (Waters & Mulroy, 1999).

SUMMARY

The present model is based almost entirely on mammalian muscle data, with preference given to human data wherever possible. Results are in qualitative and quantitative agreement with experimental observations under varying conditions. Future computer simulation work incorporating the present energy model should allow more insight into the energetics of human physical activity.

REFERENCES

Barclay, C.J. et al. (1993). *J. Physiol.*, **472**, 61-80.

Bolstad, G., Ersland, A. (1978). *Eur. J. Appl. Physiol.*, **38**, 171-179.

Buschman, H.P.J. et al. (1995). *Pflügers Arch.*, **430**, 160-167.

Constable, J.K. et al. (1997). *J. Physiol.*, **505**, 205-215.

Gerritsen, K.G.M. et al. (1998). *Motor Cont.*, **2**, 206-220.

González-Alonso, J. et al. (2000). *J. Physiol.*, **524**, 603-615.

Homsher, E., Kean, C.J. (1978). *Ann. Rev. Physiol.*, **40**, 93-131.

Saugen, E, Vøllestad, N.K. (1995). *J. Appl. Physiol.*, **79**, 2043-2049.

Schutte, L.M. et al. (1993). *IEEE Trans. Rehab. Eng.*, **1**, 109-125.

Waters, R.L., Mulroy, S. (1999). *Gait Posture*, **9**, 207-231.

Woledge, R.C. et al. (1985). *Energetic Aspects of Muscle Contraction*. Academic Press.

Zajac, F.E. (1989). *Crit. Rev. Biomed. Eng.*, **17**, 359-411.

IN VIVO STRAIN OF THE TRICEPS SURAE DURING AN ISOMETRIC CONTRACTION

A.Lai[1], S. Sinha[2], J. Hodgson[1], V.R. Edgerton[1].
Departments of [1]Physiological Science and [2]Radiological Science,
University of California Los Angeles, USA
E-mail: amlai@ucla.edu

INTRODUCTION

In both animals (Griffiths, 1991; Lieber et al., 1992; Proske and Morgan, 1984) and humans (Magnaris and Paul, 2000; Ito et al., 1998; Narici, 1999) considerable muscle fiber shortening occurs during isometric contractions while passive connective tissue components are compliant and stretch. These data demonstrate important interactions between the contractile (muscle fiber) and connective tissue elements (e.g., tendon and aponeurosis) during an isometric contraction. The dynamics of the interconnecting active and passive elements interaction and strain on a whole muscle level is still poorly understood, particularly during sub-maximal activations and normal recruitment of muscle. We hypothesize that this interaction results in a marked heterogeneity of tissue strain within the muscle-tendon unit. The purpose of this study is to identify the changes in strain magnitude and distribution within the triceps surae muscle complex of normal subjects during a voluntary submaximal isometric contraction and to identify the dynamic strain properties at specific anatomical sites.

MATERIALS AND METHODS

Six normal subjects were scanned on a 1.5T LX scanner (GE, Milwaukee), using a gated, phase contrast, velocity encoded (Drace and Pelc, 1994), fast segmented sequence, with 4 phase-encoding levels per segment. The subject's leg was placed in a fiberglass cast immobilizing the knee at full extension (0°), with both legs in the MRI coil. Calibrated strain gauges placed at appropriate points in the cast generated a signal proportional to force exerted which was digitized and recorded for subsequent analysis. The force signal was displayed on an LED display mounted on the scanner and visible by the subject. The subject exerted approximately 50% of maximal force repeatedly through the phase encoding cycles of the MR acquisition, timed to an audio cue generated from a computer and fed through headphones. Velocity was generally encoded only in S/I (superior/inferior) direction with VENC values of 10 cm/sec. Dynamic images were acquired in both the axial and sagittal planes during the muscle contraction. Acquisition matrix was 256x256, FOV 22 cm, TE: 5.3ms, TR: 11.3ms, flip angle 30°, slice thickness 10mm, Avg. 2, bandwidth 32 kHz and total acquisition time of about 1.5 min.

A set of high resolution axial images were initially acquired, volume rendered (using Vitrea, MN), and utilized to identify anatomical locations within the velocity encoded sagittal images (e.g., the soleus , lateral gastrocnemius medial gastrocnemius the aponeurosis and Achilles tendon). Cine PC sagittal images created at every 64 ms during the contraction, were then overlayed with a grid system of markers "tagging" the MR image pixels to represent a small volume of tissue. The motion of these markers was calculated throughout the sequence of cine images. Briefly, the optical density of a pixel of tissue in the MR sagittal images was proportional to its velocity (v). The distance (d) moved by the

pixel of interest is predicted by the expression d=t*v where (t) is the interval between cine images.

RESULTS AND DISCUSSION

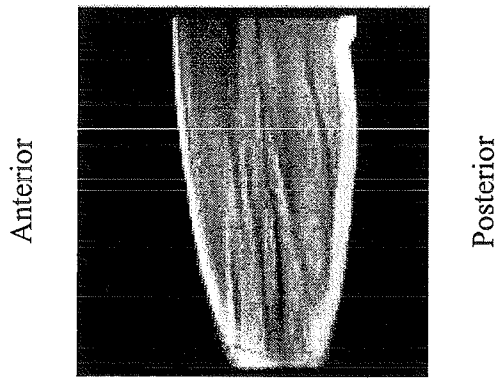

Figure 1: MR image of a sagittal section of the triceps surae showing the location of muscle and connective tissue

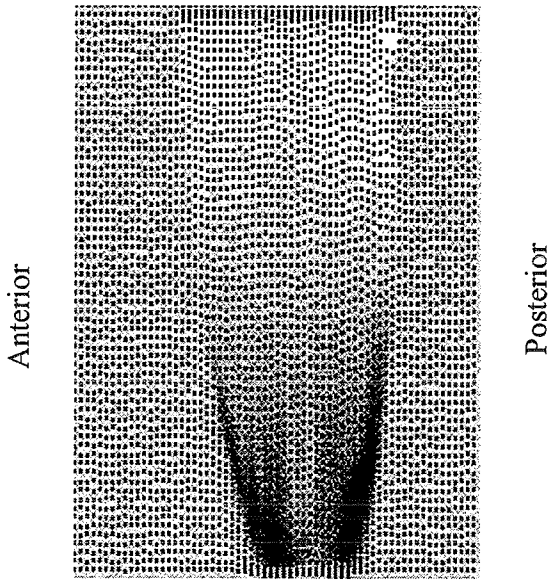

Figure 2: Example of deformation of grid system superimposed on Cine PC MR image showing tissue strain heterogeneity in triceps surae muscle complex.

The deformation of the grid system at various sites within the triceps surae complex demonstrates considerable heterogeneity of tissue strain (and shortening) both at different times during the isometric contraction and at different locations within the muscle-tendon unit. This is evident by the marked changes in marker location at various sites distributed throughout the entire triceps surae.

During a submaximal isometric contraction only a fraction of the muscle-tendon unit's population of muscle fibers are active. An uneven distribution of active and passive muscle fibers may contribute to uneven distribution of stress and, therefore, strain. The magnitude of the strain in any region of the muscle will also be a reflection of the density distribution of specific tissues within a region of the muscle and on the mechanical properties of those tissues, i.e. the modulus of elasticity. The amplitude and distribution of strains within a given region of a muscle and within and among motor pools depend not only on structure and distribution of the active and passive tissue components but also on the levels of motor unit recruitment.

REFERENCES

Drace, J.E. and N.J. Pelc, (1994). J Magn Reson Imaging, **4**(2), 157-63.

Griffiths, R.I., (1991). J Physiol (Lond) **436**, 219-36.

Ito, M., *et al.*, (1998). J Appl Physiol, **85**(4), 1230-5.

Lieber, RL, *et al.*, (1992). J Biomech, **25**(4), 421-8.

Proske, U. and D.L. Morgan, (1984). J Neurophysiol, **52**(3), 459-68.

Maganaris, C.N. and J.P. Paul, (2000). J Exp Biol, **203 Pt 4**, 751-6.

Narici, M., (1999). J Electromyogr Kinesiol, **9**(2), 97-103.

TOWARD THE ULTIMATE SKELETAL MUSCLE MODEL

Ian E. Brown and Gerald E. Loeb

Alfred E. Mann Institute for Biomedical Engineering, University of Southern California, Los Angeles, CA, 90089.
ianbrown@usc.edu; gloeb@usc.edu; http://ami.usc.edu

INTRODUCTION

Mathematical models of muscle are a useful tool for exploring theories of motor control as well as for guiding the clinical restoration of movement to paralyzed muscles through functional electrical stimulation. We have previously developed a model for these purposes that more accurate predicts muscle force over a wider range of operating conditions than any previous model (Brown et al., 1999; Brown and Loeb, 2000b; Cheng et al., 2000). However, our previous model had some limitations: most notably there was no obvious way to extract energy consumption nor was there any simple way to model other effects such as fatigue.

METHODS

The data upon which our model is based were collected primarily from the exclusively fast-twitch feline caudofemoralis muscle and published in Brown et al. (1999) and Brown and Loeb (2000b). Additional data for slow-twitch muscle and tendon properties were garnered from numerous previously published studies on feline soleus (cited in our prior papers). For each step in the modeling process, parameter estimation was accomplished using the Levenberg-Marquardt algorithm for non-linear least-squares curve-fitting.

THE MODEL

The basic form of the model (Figure 1) is the same as our previous version and that of many others. The tendon and aponeurosis are represented by a series elasticity (SE) and the passive properties of fascicles are represented by a parallel elasticity (PE). There are then one or more parallel and independently controlled contractile elements (CE) that represent sub-populations of motor units. In its simplest form, a model might consist of just one CE, representing all motor units in a given muscle. More realistically, particularly for muscles composed of multiple fiber types, multiple CEs will be used, each representing the force production of a sub-population of real motor units firing at a particular frequency.

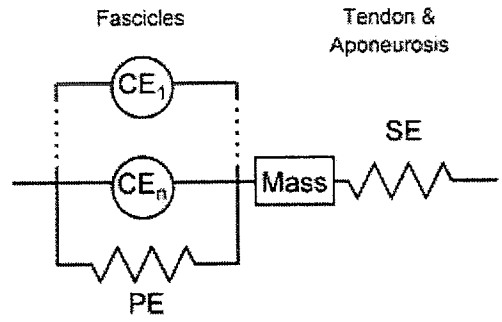

Figure 1: Schematic representation of the basic form of the model.

The SE and PE are represented simply as non-linear springs as described previously (Brown et al., 1999). In contrast, there has been a major re-working of the form of the CE as compared to our previous model. The summary equation for the CE is shown below, in which A represents the fraction of attached, force-producing cross-bridges relative to maximal activation when A=1; FL represents filament overlap that accounts for the isometric force-length relationship

and F_X represents the mean force per-cross-bridge (normalized so that F_X=1 under isometric conditions). Note that there is no force-velocity (FV) relationship explicitly stated here. The effects of velocity emerge through the effects of velocity on both A and F_X.

(1) $F_{CE}=A*FL*F_X$

The activation term A is calculated via two first order processes. The first process represents the calcium release/uptake dynamics. This process is presumed to be length and velocity independent. There is an indirect effect of activation in that the rate of calcium uptake is modeled to increase during a contraction for fast-twitch muscles (which is a proposed mechanism for sag during sustained contractions at subtetanic frequencies). The second process represents the rates of cross-bridge attachment and detachment. We assume that velocity affects these rates because length changes shift the cross-bridge angle. We assume that both attachment and detachment rates are also length dependent as a result of effects on filament lattice spacing in isovolumetric muscle fibers. We model the binding of calcium to troponin as if it were in a fast-equilibrium because it is a significantly faster process than either of the other two processes. We assume that calcium binding is cooperative. Similarly, we assume that there is cooperativity in cross-bridge attachment. These combined cooperative mechanisms are necessary to reproduce the steep force-frequency relationship that is known to exist and also to reproduce the prolonged duration of activation that occurs following high frequency stimulation.

The cross-bridge force term, F_X, is calculated by tracking mean cross-bridge distortion and assuming that F_X is linearly related to distortion. Cross-bridge distortion is calculated by accounting for changes in distortion that occur as a result of (i) movement; (ii) cross-bridge detachment at one angle and reattachment at another angle; (iii) changes in the number of attached cross-bridges.

RESULTS & DISCUSSION

This version of our model is able to replicate all features of our previous model. This includes the tetanic FL and FV relationships; the effects of stimulus frequency on FL; the effects of stimulus frequency and length on each of FV, sag and rise and fall times; the effects of stimulus frequency, length and velocity on yielding.

New features that this model now accounts for include the effects of velocity on fall time and the transient forms of shortening-induced force depression and stretch-induced force enhancement (Brown and Loeb, 2000a). Furthermore energy consumption can be calculated directly from the rate of cross-bridge detachment.

The new model is actually simpler and easier to understand because its basic elements are tied more closely to underlying physiological processes. This should also make it easier to add elements to the model to account for features such as fatigue, which occurs through changes in one or more of those processes.

REFERENCES

Brown, I.E., et al., G.E. (1999). *J. Muscle Res. Cell Motil.* **20**: 443-456.

Brown, I.E. & Loeb, G.E. (2000a). *J. Muscle Res. Cell Motil.* **21**: 21-31.

Brown, I.E. & Loeb, G.E. (2000b). *J. Muscle Res. Cell Motil.* **21**: 33-47.

Cheng, E., Brown, I.E. & Loeb, G.E. (2000) *J. Neurosci. Meth.* **101**, 117-130

THE INFLUENCE OF WRIST POSITION ON INDIVIDUAL FINGER FORCE PRODUCTION

Z. M. Li, M. Flaherty, T. Porco, J. Nethery
Department of Physical Therapy, Walsh University, North Canton, Ohio 44720
E-mail: zli@walsh.edu

INTRODUCTION

A number of factors play a role in finger force production. Wrist position has been shown to be one of the most important regulators for grip and pinch strength capabilities (Kang et al., 1996; LaStayo & Hartzel, 1999). Most of the previous studies have concentrated on the influence of wrist postural changes on force output of a single finger (e.g., pinch), or the total force output of multiple fingers (e.g., grip). Very few studies looked at how force production capability of individual fingers is influenced by wrist position (Hazelton et al., 1975). In addition, previous attempts to evaluate the effect of wrist position on grip strength have concentrated on a few limited static wrist positions (Hazelton et al., 1975; Pryce, 1980).

The purpose of this study was to determine the influence of wrist position on individual finger forces and force sharing among individual fingers during functional tasks when subjects sustain maximum grip of an instrumented handle while voluntarily moving the wrist joint continuously. It was hypothesized that varying wrist position would lead to changes in (1) individual finger forces and total force production, and (2) the pattern of force sharing among individual fingers.

METHODS

Nine male college students volunteered to participate in the study. The subjects had no known trauma or neuropathy in the hand or upper extremity. A custom-made instrumented clay handle functioned as a grasping object. Four piezoelectric sensors were used to register force production of individual fingers. A two-axis electrogoniometer was taped over the dorsal side of the wrist to monitor the wrist joint position in the directions of flexion/extension motion (FEM) and radial/ulnar deviation (RUD). The task was to grasp the handle as hard as possible with varying wrist positions while maintaining maximum voluntary contraction (MVC). The subject was encouraged to explore all unconstrained wrist positions in the directions of FEM and RUD. Four channels of force data and 2 channels of goniometer data were collected simultaneously. In order to obtain finger forces at identical positions for different subjects, interpolation procedures were performed for the data of each subject. Individual finger forces, total force, and force sharing at 18 representative positions were selected for statistical analyses.

RESULTS AND DISCUSSION

Individual finger forces and total force, averaged across the 9 subjects are represented using linear gray-scale maps (Figure 1). The darkness of each map (i.e., relative magnitude of force) was dependent on wrist position. Individual finger force and total force showed

similar force change patterns. The peak individual forces and peak total force occurred at wrist position 20 degrees of extension and 5 degrees of ulnar deviation. At this position, the index, middle, ring, and little fingers produced 37.0, 37.5, 27.0, and 13.4 N, respectively, with a total force of 114.9 N. As the wrist deviated farther and farther away from this position, the forces generated by individual fingers and total force became less and less. In general, force generated in extension territory was higher than force generated in flexion territory. Moreover, finger forces vary more with wrist flexion than extension.

Two-way ANOVA (FE × RUD) performed on selected 18 wrist positions showed that individual finger forces and total force production was dependent on FEM and RUD ($p < 0.001$). No significant interaction between FEM and RUD was found for individual finger force or total force ($p > 0.62$). The effects of FEM and RUD on force sharing of individual fingers were different on different fingers. Among the selected positions, for example, the index finger force sharing was significantly affected by RUD ($p < 0.001$), but not by FEM ($p = 0.47$). When the wrist deviated from (0, 0) to a radial position at (0, 15), the force sharing of the index finger showed an increase from 31.0% to 42.6%, an absolute increase of 11.6%.

The utilization of the current results may assist hand rehabilitation, functional assessment, injury prevention, and ergonomic design.

REFERENCES

Hazelton, F. T. et al. (1975) *J Biomech* **8**, 301-6

Kang, H. J. et al. (1996). *J Hand Surg* **21**, 963-8;

LaStayo, P. & Hartzel, J. (1999) *J Hand Ther* **12**, 212-8;

Pryce, J. C. (1980) *J Biomech* **13**, 505-11.

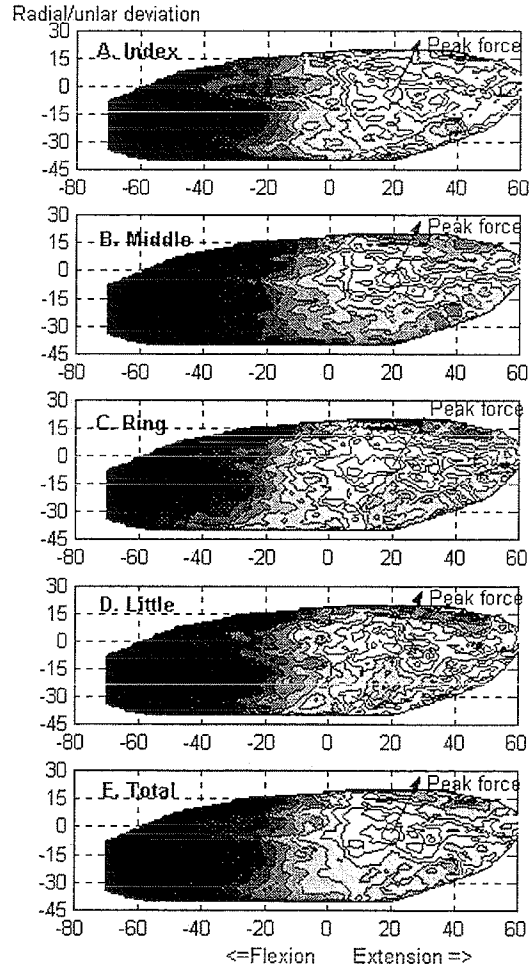

Figure 1. Gray map for individual finger forces and total force indicating the dependence of force on wrist position. The darkness in each graph is proportional to the magnitude of force. Peak individual forces and peak total force occurred at wrist position (20, -5).

Protective ankle muscle activation strategies during quick cutting movement in humans

TR Jenkyn[1] and AC Nicol[2]

[1]Biomechanics Laboratory, Div. of Orthopedic Research, Mayo Clinic, Rochester, MN, USA
[2]Bioengineering Unit, University of Strathclyde, Glasgow, UK
Email: jenkyn.thomas@mayo.edu

INTRODUCTION

Sprain of the lateral ligaments is the most common ankle injury in sports and activities of daily living (Liu, 1999). This often occurs during quick medially directed cutting turns causing rapid inversion and plantar-flexion of the foot. The greatest risk factor for sprain is history of previous sprain (Thacker, 1999), but occurrence seems unrelated to subtalar positioning at touchdown or joint laxity (Wright, 2000).

This study examines the ankle muscle activation patterns, which may protect against sprain during quick cutting movements.

METHOD

12 normal subjects (6 male, 6 female, aged 20-37) performed walking and turning tasks in a motion analysis laboratory. EMG was collected from 8 ankle muscles (Ag-AgCl electrodes, sampled at 1000Hz, bandpass 30-500Hz with gain 350). The leg was modeled as two segments (thigh and shank) and the foot as four segments (hindfoot, midfoot, lateral and medial forefoot). Kinematics of both the ankle and subtalar joints and the joints of the foot were measured.

Muscle and ligament positioning and wrapping on the bones of the leg and foot was reconstructed from CT and anatomical images (Visible Human Project, NIH) and with the kinematics, instantaneous muscle lengths, velocities, lines of action and lever arms were calculated throughout the tasks. Individual muscle tensions were calculated with an EMG-based Hill-type muscle model. Ligament loading was then calculated with an optimization routine, which minimized the maximum ligament load.

RESULTS AND DISCUSSION

The medial ground reaction force (GRF) component was larger in a cutting turn than in walking. A peak of 0.68xBW occurred in early stance (Fig. 1A). Inverting subtalar joint moment was also larger during turning (Fig. 1B). Peroneal tension was greater in early stance during turning (Fig. 2A). Combined dorsi-flexor tension was also increased in early stance with turning (Fig. 2B).

Lateral ankle ligaments are more vulnerable to injury during rapid medial cutting turns than during walking due to a greater medial GRF component. When turning is anticipated and controlled, ankle muscle activation stabilizes the joints and protects lateral ligaments from injury. Peroneal tension increases to oppose the greater inverting subtalar moment during a turn. Increased dorsi-flexor tension stiffens the joints through antagonism with the plantar-flexors and peroneals. Thereby, lateral ligament loading is not enough to cause injury.

Perhaps if the turn is not fully anticipated and these protective patterns are late or absent, the kinematics and GRF conspire to overload the lateral ligaments resulting in injury.

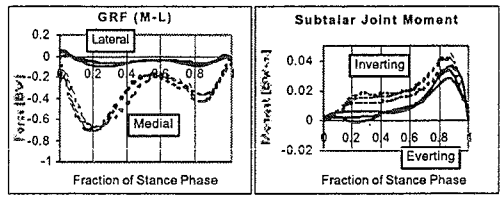

Figure 1: A) Medio-lateral GRF and **B)** subtalar joint moment during walking (solid) and turning (turning).

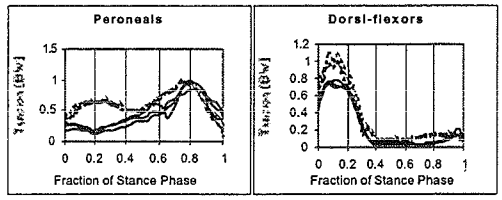

Figure 2: A) Combined tension in peroneals and **B)** dorsi-flexors during walking and turning.

ACKNOWLEDGEMENTS

Sponsored by the Overseas Research Scholarship.

REFERENCES

Liu SH et al. 1999 "Ankle sprain and other soft tissue injuries" *Curr Opin Rheumatol* **11(2)** 132-7

Thacker SB et al. 1999 "Prevention of ankle sprains in sports" *Am J Sports Med* **27(6)** 753-60

Wright IC et al. 2000 "The influence of foot positioning on ankle sprains" *J Biomech* **33(5)** 513-9

A METHOD FOR NON-INVASIVELY MEASURING THE HELICAL AXIS OF UPPER ARM MOTION

S. LaScalza[1], L.N. Gallo[1], J.E. Carpenter[2], R.E. Hughes[1,2]

[1] Department of Biomedical Engineering, University of Michigan, Ann Arbor, MI, USA
[2] Department of Orthopaedic Surgery, University of Michigan, Ann Arbor, MI USA
E-mail: slascalz@umich.edu

INTRODUCTION

Practical, non-invasive measurement of *in vivo* kinematics would be a valuable tool for the study of human shoulder disorders. Investigators have done this by computing Euler angles from electromagnetic tracking device measurements (McQuade and Smidt, 1998, Ludewig and Cook, 2000). Morrey and An (1990) have suggested that helical axis may be useful for the clinical assessment of shoulder pathology. A cuff has been developed in our laboratory to reduce the effects of soft-tissue motion on kinematic measurements during humeral motion. The purpose of this investigation was to evaluate the accuracy of the humeral cuff in determining the orientation and location of the helical axis of motion (HAM), as well as the magnitude of rotation about the HAM during complex three-dimensional motions.

METHODS

Design of the Humeral Cuff: The humeral cuff consists of two pieces of molded thermoplast that are placed on the medial and lateral skin surfaces from the epicondyles to the mid-shaft of the humerus (Figure 1). At the distal end, Velcro tabs located on the inside of the two thermoplast pieces mate with Velcro tabs previously attached to the epicondyles with adhesive. The cuff is secured by a belt which fastens about the humerus and a piece of theraband which is stretched between the distal cuff ends. Additionally, a polyvinyl chloride (PVC) platform provides an attachment site for an electromagnetic sensor.

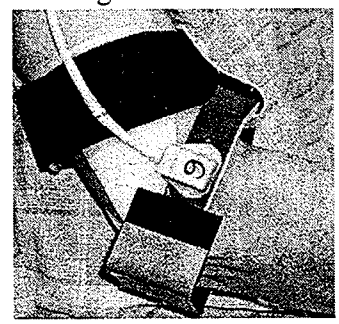

Figure 1. Design of the humeral cuff.

Experiment: Fresh frozen upper extremities from 5 cadavers were used. The humeral cuff was placed on the upper extremity and a sensor was mounted onto the cuff. An additional sensor was mounted onto a PVC platform and screwed directly to the humerus to provide a standard reference for bone motion. The arm was moved through two series of motion trials: 1) free trials in which the humerus was unrestrained by the fixture and 2) fixed trials in which the humerus was attached directly to the testing apparatus.

Initially, the scapula was rigidly fixed while the upper extremity was moved by the experimenter through specified motions including abduction, flexion, external rotation and a slow overhand throw ('free' motions). The humerus was then disarticulated from the scapula and rigidly fixed onto a PVC block, which was then rotated dynamically from 0°- 90° for motions of abduction, flexion and external rotation ('fixed' motions). At the beginning

of each fixed motion trial, two points along the axis of rotation of the testing fixture were digitized to provide a standard reference for the helical axis location and orientation.

Statistics: The data were filtered using a two-pass, fourth-order Butterworth filter with a cutoff of 5 Hz. The helical axis was then computed in 10° increments throughout the duration of the motion. The mean absolute error and standard error of measurement were calculated for the orientation, location and magnitude of rotation about the helical axis for all trials. For the free motion trials, the measurements from the humeral cuff were compared directly to the bone measurements. For the fixed motion trials, measurements from both the humeral cuff and the bone were calculated with respect to the known rotational axis of the testing fixture.

RESULTS AND DISCUSSION

During the free motion trials, the mean absolute orientation and location errors of the cuff compared to the bone were less than 5.5° and 2.1 cm, respectively, while the mean absolute rotation error was less than 3.9° (Table 1). The fixed motion trials showed mean absolute errors less than 3.1° and 0.7 cm for both the bone and the humeral cuff when compared to the known rotational axis of the testing fixture (Table 2). The mean absolute rotation error about the helical axis of motion was less than 2.9° for both the bone and the humeral cuff in the fixed motion trials.

Thus, the humeral cuff provides a viable, non-invasive method for determining the location and orientation of the helical axis of motion, as well as the magnitude of rotation about the HAM of the humerus during dynamic three-dimensional motions of the upper extremity.

REFERENCES

Ludewig, P.M. and Cook, T.M. (2000) *Physical Therapy*, **80(3)**, 276-291.

McQuade, K.J. and Smidt, G.L. (1998) *J Orthop Sports Phys Ther*, 27,125-133.

Morrey, B.F. and An, K-N. (1990) *Biomechanics of the Shoulder.* In the Shoulder (Eds. C.A. Rockwood and F.A. Matsen). W.B. Saunders. p. 222.

ACKNOWLEDGEMENTS

This research was supported by the Whitaker Foundation and the Clinical Research Partnership Fund grant from the University of Michigan.

Table 1. Mean absolute error (SEM) of the cuff compared to the bone during the free trials.

	HAM orientation error (deg)	HAM location error (cm)	Rotational error (deg)
Abduction	5.1 (0.5)	1.8 (0.2)	2.1 (0.5)
Flexion	5.4 (1.5)	2.0 (0.1)	1.7 (0.3)
Ext. Rotation	2.1 (0.5)	1.1 (0.2)	3.8 (1.5)
Throw	4.0 (1.0)	1.7 (0.5)	2.0 (0.3)

Table 2. Mean absolute error (SEM) of the humeral cuff and the bone compared with the known rotational axis of the test fixture during the fixed motion trials.

	HAM orientation error (deg)		HAM location error (cm)		Rotational error (deg)	
	Bone	Cuff	Bone	Cuff	Bone	Cuff
Abduction	1.1 (0.1)	2.0 (0.2)	0.2 (0.0)	0.6 (0.1)	2.6 (1.0)	1.5 (0.7)
Flexion	2.3 (0.6)	3.0 (0.3)	0.4 (0.2)	0.6 (0.1)	2.6 (1.0)	1.6 (0.7)
Ext. Rotation	1.0 (0.2)	0.7 (0.1)	0.3 (0.0)	0.1 (0.0)	2.8 (0.7)	1.5 (0.4)

COMPUTATIONAL QUANTIFICATION OF THE INFLUENCE OF THE Q-ANGLE ON THE PATELLOFEMORAL CONTACT PRESSURE DISTRIBUTION

John J. Elias, Andrew J. Cosgarea, Mehran Armand, and Edmund Y. Chao

Orthopaedic Biomechanics Laboratory, Johns Hopkins University, Baltimore, MD, USA
E-mail: jelias@jhmi.edu Web: www.biomech.jhu.edu

INTRODUCTION

Patellar maltracking is often attributed to an excessive Q-angle. The Q-angle is defined as the angle between a line from the patella center to the tibial tubercle and a second line from the patella center to the anterior superior iliac spine when the knee is fully extended. The lateral component of the resultant force applied by the quadriceps and patella tendon to the patella increases as the Q-angle increases. For patients with anterior knee pain due to maltracking, surgery may be performed to reduce the Q-angle.

Dynamic simulation of knee flexion is typically performed to characterize patella tracking. The relationship between patella tracking and the patellofemoral contact pressure distribution is not clear, however. A computational model has been developed to quantify the patellofemoral contact pressure distribution based on knee kinematics obtained through dynamic knee simulation. The model has been used to characterize the influence of the Q-angle on the pressure within the patellofemoral joint.

METHODS

Six cadaver knees were tested on a dynamic knee simulator to determine the influence of the Q-angle on patellofemoral kinematics (Mizuno et al., 2001). The Q-angle was increased and decreased by shifting the simulated quadriceps insertion point laterally and medially, respectively. The average Q-angles were $4° \pm 3°$, $11° \pm 5°$, and $20° \pm 4°$ for the decreased, normal and increased Q-angle cases, respectively.

A graphic model of the Visible Human Male knee (National Library of Medicine) was positioned to reproduce the alignment of a cadaver knee within the simulator and the local coordinate systems used to describe knee kinematics. The patella was shifted in the medial-lateral direction and rotated based on the average kinematic data. The rotated and shifted patella was aligned with a parallel surface within the trochlea at each angle of knee flexion (Fig. 1).

A surface midway between the patella and the femur was created to represent the potential area of cartilage contact between the two bones. A layer of compressive springs was modeled on the contact surface. Rows of tensile springs were modeled between the medial and lateral edges of the patella and the femur to represent the joint capsule. The joint capsule was assumed to be ten times stiffer than the cartilage.

A static analysis was performed at individual flexion angles to quantify the joint pressure distribution. With the femur fixed in place, a resultant force and moment were applied to the patella centroid. The resultant force and moment were calculated from the average experimental quadriceps load acting at the proximal patella and a calculated patella tendon load acting at the distal patella (Huberti et al., 1984). The

deformation of each spring in response to the applied load was quantified using the discrete element analysis technique. This technique minimizes the potential energy within the springs based on Castigliano's theorem. The deformation of each spring, which determines the contact pressure distribution, was quantified at 40° and 80° of flexion for all three Q-angles.

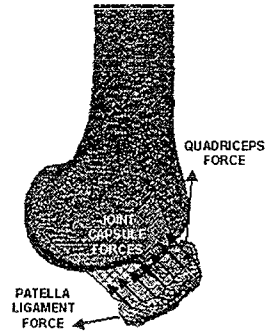

Figure 1: The model of the patellofemoral joint at 80° of flexion.

RESULTS AND DISCUSSION

Increasing the Q-angle from the normal value increased the average patellar lateral shift by more than 5 mm, increased the average medial tilt by approximately 4.5°, and increased the medial rotation by more than 3° throughout flexion. Decreasing the Q-angle had little influence on the average shift or rotation, but decreased the medial tilt by approximately 2.5° throughout flexion.

For the normal Q-angle, the contact pressure was concentrated at the distal patella at 40° of flexion. At 80° of flexion, the contact area was more proximal, with a predominately lateral pressure concentration. The peak pressure was approximately 0.6 MPa for both flexion angles.

At 40° of flexion, increasing the Q-angle decreased the contact area and approximately doubled the peak contact pressure on both the lateral and medial condyles. Decreasing the Q-angle increased the contact area and reduced the peak contact pressure by 0.1 MPa. At 80° of flexion, decreasing the Q-angle increased the medial contact pressure. Increasing the Q-angle shifted the lateral concentration in contact pressure proximally (Fig. 2). .

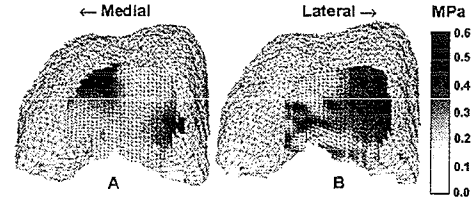

Figure 2: The contact pressure distribution superimposed over the femur surface at 80° of flexion for a decreased (A) and increased (B) Q-angle.

DISCUSSION

Varying the Q-angle altered the region of contact within the patellofemoral joint. In general, the lateral contact pressure increased as the Q-angle increased. Because the patella tilted in the opposite direction of the shift as the patella rode up each condyle, increasing and decreasing the Q-angle did not completely unload the medial and lateral cartilage, respectively. The patellofemoral model developed for this study is a valuable tool to improve the clinical relevance of the conclusions that can be drawn from knee simulation studies.

REFERENCES

Huberti H.H. et al. (1984). J Orthop Res **2**, 49-54.

Mizuno, Y. et al. (2001). *J Orthop Res.* (in press).

ACKNOWLEDGMENTS

Funding was provided by a research grant from the Whitaker Foundation.

THE CHANGES IN EMG AND STEADINESS WITH VARIATION IN MOVEMENT SPEED DIFFER FOR CONCENTRIC AND ECCENTRIC CONTRACTIONS

Evangelos A. Christou, Minoru Shinohara, and Roger M. Enoka

Department of Kinesiology and Applied Physiology, University of Colorado at Boulder
Email: echristo@colorado.edu Web: www.Colorado.EDU/kines/Lab/NCM.html

INTRODUCTION

The activation of muscle by the nervous system differs for concentric and eccentric contractions (Enoka & Fuglevand, 2001). These differences appear to involve both the descending command (Aagaard et al. 2000; Semmler et al. 2000) and movement-related sensory feedback (Burke et al. 1978; Schieber & Thach, 1985). Because the relative contribution of sensory feedback declines with movement speed, fast contractions are largely determined by the descending command. We asked the question, does the difference in muscle activation between concentric and eccentric contractions change with movement speed? The purpose of the study was to compare the changes in muscle activation and steadiness with variation in the speed of movement for concentric and eccentric contractions.

PROCEDURES

Ten healthy and active young individuals (30.4 ± 1.4 years, 6 males and 4 females) were recruited for this study. Each subject attended one testing session and performed the following tasks with the index finger of the left hand: (1) maximum load lifted in one repetition (1RM) and (2) position-tracking trials. The position-tracking trials were performed with a load equal to 15% of 1-RM within a 10° range of motion in the abduction-adduction plane. The weight was attached to the index finger at the proximal interphalangeal joint to provide a load in the adduction direction. Each subject raised (concentric contraction) and lowered (eccentric contraction) the load at six different velocities (1.7, 3.3, 6.7, 16.7, 33.3, and 66.7 °/s). Prior to movement, each subject supported the load with an isometric contraction; thus, each anisometric contraction was preceded by an isometric contraction. For the position-tracking task, each participant was instructed to match a line displayed on an oscilloscope by controlling movement speed of the index finger. To familiarize the participants with each velocity, several practice trials (< 10) were given prior to data collection. In addition to verbal feedback, subjects received visual feedback for the first few practice trials. To eliminate the effect of visual feedback during data collection trials, subjects were given visual feedback only after the trial was completed. Data were collected until the subjects matched the slope of the target line three times. A rest period of 10 seconds was given between data collection trials and 120 seconds between target velocities. The order of target velocities and contractions were assigned randomly for each subject.

Position of the index finger was detected with a linear variable displacement transducer. Steadiness of the movement in the horizontal plane (abduction-adduction plane) was measured by a piezoresistive accelerometer attached to the proximal interphalangeal joint of the index finger. The muscle activation (EMG) of the first dorsal interosseus, which is the only muscle that abducts the index finger, was measured

with 4 mm silver-silver chloride surface electrodes. For both contractions at each velocity, average rectified EMG (AEMG) and standard deviation (SD) of acceleration were computed from the middle one-third of the trial.

RESULTS AND DISCUSSION

The mean AEMG of the first dorsal interosseus was greater during concentric contractions ($p<0.05$). There was a contraction x velocity interaction ($p<0.05$) due to the increases in AEMG with velocity during the concentric but not the eccentric contractions (Figure 1).

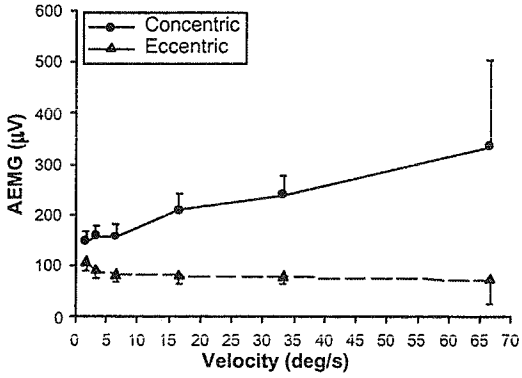

Figure 1. Average EMG increased with movement velocity for concentric but not eccentric contractions.

In contrast to the EMG findings, the standard deviation of acceleration was greater during eccentric contractions compared with concentric contractions ($p<0.05$). Furthermore, there was a contraction x velocity interaction ($p<0.05$) due to the greater increase in the SD of acceleration with movement velocity for the eccentric contractions compared with the concentric contractions (Figure 2).

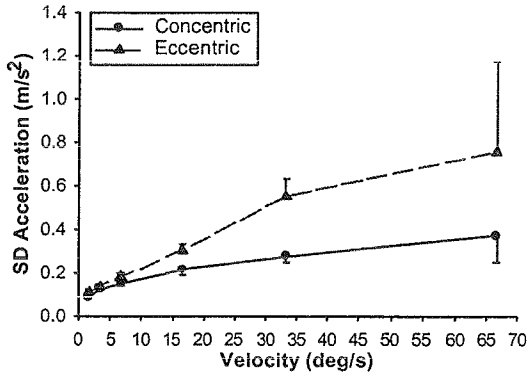

Figure 2. SD of acceleration increased more for eccentric than for concentric contractions with movement velocity.

Differences in muscle activation between concentric and eccentric contractions were augmented with increases in movement speed. This finding suggests that the descending control of muscle action, at least for fast movements, differs for concentric and eccentric contractions. Furthermore, this difference in activation of the muscle impairs the ability of the subjects to perform steady eccentric contractions.

SUMMARY

The results of this study indicate that increases in movement speed were accomplished with less AEMG and reduced steadiness for eccentric contractions compared with concentric contractions.

REFERENCES

Aagaard P, et al. *J Appl Physiol* 89:2249-2257, 2000.
Burke D, et al. *J Physiol* 277: 131-142, 1978.
Enoka RM, Fuglevand AJ. *Muscle Nerve* 24: 4-17, 2001.
Schieber MH, Thach WT. *J Neurophysiol* 54: 1228-1270, 1985.
Semmler JG, et al. *Soc Neurosci Abstr* 26: 463, 2000.
Supported by NIH AG09000

INDEPENDENT ANALYSIS OF LOAD MAGNITUDE AND LOADING RATE: VARIABLES IN OSTEOGENESIS

Jeremy J. Bauer and Christine M. Snow

Bone Research Laboratory, Oregon State University, Corvallis, OR, USA
E-mail: bauerje@ucs.orst.edu

INTRODUCTION

Quantifying the force magnitude and rate of force application is central to defining a dose response of bone to mechanical loading via exercise. We have shown that drop landings from 24" increase hip bone mass in young children and concluded that both high magnitude loads and fast loading rates contributed to this outcome (Fuchs et. al, 2001). However, we do not know the independent effect of each variable on the bone response, and thus cannot determine their relative importance. In animal models, researchers have studied the independent effects of strain magnitude and strain rate on bone. However, no attempt has been made to evaluate the independent contributions of the analogous variables, load magnitude and loading rate, to a bone response in humans. Load magnitude and loading rate measured at the ground can be considered the noninvasive analogous variables for strain magnitude and strain rate used in animal models. In a recent study we have shown that up to 81% of the ground reaction force from drop landing is transmitted to the hip (Bauer et. al, 2001 in press).

Load magnitude and loading rate can be easily quantified by analyzing ground reaction force (GRF) traces. To study the independent effects of load magnitude and loading rate on osteogenesis in humans, each variable would have to be held constant while manipulating the other. We expect that varying drop height should result in different maximum load magnitude while holding loading rate constant. In addition, changing landing style should result in different loading rates between heights while providing similar maximum load magnitude. In this pilot study our aim was to determine whether we could separate load magnitude and loading rate in drop landings by varying drop height and landing kinematics.

METHODS

Seven prepubescent children (males=4, females=3, age 6.4 ± 1.0 years) dropped off 12" and 24" boxes onto a force plate (1000 Hz, filtered at 125 Hz using 2nd order two pass Butterworth filter). Each subject dropped 5 times from each box height for each of three landing styles: normal/no instruction (norm), internal knee angle > 90 degrees (hard), internal knee angle < 90 degrees (soft). To insure that each subject would achieve a knee angle < 90 degrees upon landing he/she was asked to squat down with an internal knee angle < 90 degrees. While in the squat position a small light placed on a tripod was positioned at the level of the head of the subject. Each subject was asked to land so that the light was at eye level. Similarly, for the hard condition the light was positioned at eye level when standing upright. Each subject was asked to keep his/her eyes above the light. The order of landing styles and height was chosen randomly for each subject before testing.

Load magnitude was defined as the maximum GRF in each trial. Loading rate

was calculated by differentiating the filtered force data. The maximum value of the time derivative of the force trace was treated as the maximum loading rate for each trial. Maximum loading rate always occurred in the positive slope of one of the two impact peaks (Figure 1).

ANOVA was used to compare means for each subject across all conditions. LSD was used post-hoc to determine where the differences in the data occurred. SPSS 9.0 was used to calculate all statistics.

RESULTS AND DISCUSSION

There were several conditions where load magnitude was different while loading rate was the same (Table 1). Load magnitude for 24norm and 24hard was greater than all 12" conditions ($p<0.05$). In addition, 24soft was greater than 12soft ($p<0.05$), while magnitude for all 12" heights was similar. By contrast, we observed few differences in loading rate between landing conditions. For loading rate, the only significant difference was that 24norm and 24hard were greater than 12soft ($p<0.05$). We expected differences in loading rate between the hard and soft landing conditions. However, the small number of subjects limited our statistical power and high standard deviations reduced our ability to observe significant differences between landing conditions.

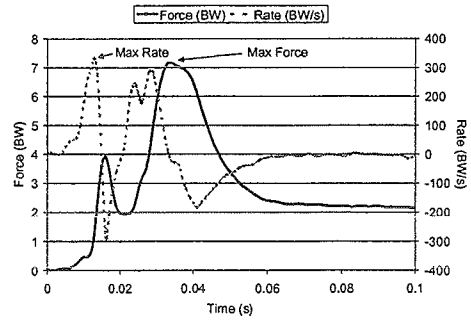

Figure 1. Plot of force and rate (24norm).

SUMMARY

In this small sample of children, we have shown that we can independently study load magnitude but not loading rate. If we can learn to separate loading rate in future studies, then it would be possible to study the independent osteogenic effect of these variables in humans.

REFERENCES

Bauer, J.J., Fuchs, R.K., Smith, G.A., Snow, C.M. (2001 in press). *J. Appl. Biomech.*

Fuchs, R.K., Bauer, J.J., Snow, C.M. (2001). *J. Bone and Miner. Res.*, **16,** 148-156.

Table 1. Average. maximum force and loading rate for drop landings from a 12" box landing hard, normal and soft and from a 24" box landing hard normal and soft. (mean ± standard deviation, n=7 subjects for each condition).

Variables	12norm	12hard	12soft	24norm	24hard	24soft
Force (BW)	6.3 ± 2.3	6.1 ± 1.5	5.4 ± 1.7	9.0 ± 2.5	9.3 ± 2.5	7.5 ± 2.3
Rate (BW/s)	324 ± 204	263 ± 123	192 ± 86	410 ± 208	429 ± 224	342 ± 155

EFFECTS OF PERCEIVED VOLUNTARY CONTRACTION EFFORT, MUSCLE AND GENDER ON QUADRICEPS FEMORIS MEDIAN FREQUENCY

Danny M. Pincivero[1], Robert M. Campy[2], Yuliya Salfetnikov[1], Ashley Bright[1], Alan J. Coelho[2]

[1] Human Performance and Fatigue Laboratory, Department of Physical Therapy, Eastern Washington University, Cheney, WA, USA
[2] Department of Physical Education, Health and Recreation, Eastern Washington University, Cheney, WA, USA
E-mail: dpincivero@mail.ewu.edu

INTRODUCTION

The quadriceps femoris (QF) is a unique group of 4 anatomically distinct muscles that share a common nerve and function. Previous studies have demonstrated different electromyographic (EMG) patterns between the superficial portions of the QF during constant force contractions (Alkner et al, 2000; Pincivero and Coelho, 2000; Pincivero et al, 2001). Few investigations, however, have addressed the EMG signal of these muscles under constant effort contractions. The purpose of this study was to examine the effects of perceived voluntary contraction effort on inter-muscle and inter-gender EMG median frequency (f_{med}) differences.

METHODS

Fifteen healthy male (mean age = 24.6 $\pm$ 4.1 years, mean height = 178 $\pm$ 9.8 cm, mean mass = 77.8 $\pm$ 11.2 kg) and 15 healthy female (mean age = 24.3 $\pm$ 5.2 years, mean height = 167 $\pm$ 6.9 cm, mean mass = 60.5 $\pm$ 6.2 kg) volunteers participated. Subjects performed an active warm-up involving 5 min of sub-maximal cycling, followed by 3-4 sub-maximal and maximal effort isometric QF contractions. For the isometric contractions, subjects sat in an upright position and were stabilized with thigh, pelvic and torso straps on the Biodex System II isokinetic dynamometer. Subjects then performed 5 isometric maximal voluntary contractions (MVC) with their knee AT 60 deg flexion. The MVCs were performed for 5 sec, with 2 min rest in between each contraction. Immediately following each MVC, the perceptual range was anchored by having the subject assign a rating of "10" to their feelings during the contraction, by observing a 10-point scale. Following a 2 min period of rest, subjects were instructed to sit quietly and to assign a rating of "0" to the feelings in their QF muscle. Sub-maximal isometric contractions were then separately performed at the following perceived effort levels on the 10-point scale: 1, 2, 3, 4, 5, 6, 7, 8 and 9, in a random order. Subjects were instructed to maintain the contraction at each perceived effort level for 5 sec.

Surface EMG for the vastus medialis (VM), vastus lateralis (VL), and rectus femoris (RF) muscles was recorded with pre-amplified bi-polar circular electrodes (Ag/AgCl) that were placed on pre-determined areas of each muscle with a fixed inter-electrode distance (center to center) of 2 cm. The reference electrode was placed over the medial shaft of the tibia. EMG activity was collected at 1000 Hertz (CMRR=87 dB at 60 Hertz, input impedance >25 Mohms at dc) with a gain of 10K. Median frequency of the 3 muscles was assessed through a power spectral analysis performed over 11 consecutive, 512

msec epochs overlapping each other by half their length (256 msec) during the middle 3 sec of each contraction. The f_{med} for each of the 11 epochs was then determined for each muscle, followed by calculation of the mean and normalized coefficient of variation ([standard deviation/mean] x 100%) for each contraction.

RESULTS AND DISCUSSION

The results demonstrated that the mean VL f_{med} was significantly greater than the other 2 muscles, and RF f_{med} was significantly greater than the VM (Figure 1).

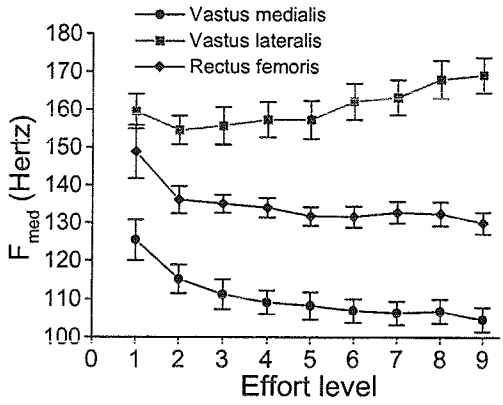

Figure 1: Median frequency for VM, VL and RF muscles across perceived voluntary contraction levels 1 to 9.

The VL demonstrated a significant increase in mean f_{med} across the contraction efforts, as compared to the VM and RF that displayed a significant decrease. Males displayed significantly higher VM f_{med} values than the females, as well as experiencing a greater increase across the contraction efforts for the VL than the females (Figure 2). Median frequency variability was shown to be significantly highest for the VM, as compared to the VL and RF.

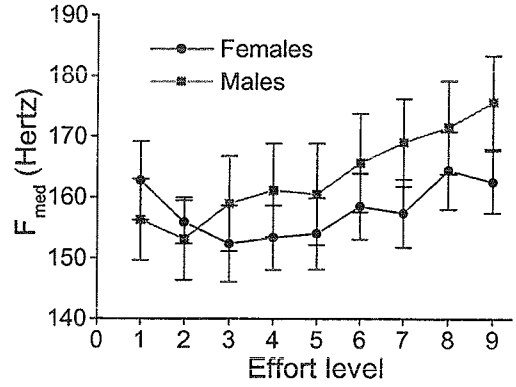

Figure 2: Median frequency for the VL in males and females across perceived voluntary contraction levels 1 to 9.

SUMMARY

The findings of the present study appear to corroborate our previous investigation (Pincivero et al, 2001) regarding contraction effort and gender effects on the VL muscle. The current findings also suggest that sensitivity of the EMG f_{med} to an increase in contraction intensity is muscle specific, as shown by the lack of an effort effect on the VM and RF muscles. Such findings may be reflective of differential muscle fiber type proportions that may exist between the superficial QF muscles.

REFERENCES

Alkner, B.A., et al. (2000). *Med Sci Sports Exerc*, **32**, 459-463.

Pincivero, D.M., Coelho, A.J. (2000). *Muscle Nerve*, **23**, 393-398.

Pincivero, D.M., et al. (2001). *J Appl Physiol*, **90**, 804-810.

ACKOWLEDGEMENTS

Office of Grants and Research Development, Eastern Washington University.

SCAPULAR KINEMATICS DURING ACTIVE AND PASSIVE ARM ELEVATION

David Ebaugh[1], Andrew Karduna[1], and Phillip McClure[2]

[1] Rehabilitation Sciences, MCP Hahnemann University, Philadelphia, PA
[2] Physical Therapy, Beaver College, Glenside, PA
email: debaugh@drexel.edu

INTRODUCTION

Due to large rotational and translational motions, the scapula plays an important role in the normal kinematics of the shoulder complex (Kibler, 1998). The production and control of these motions are primarily regulated by active muscle contraction (Bagg and Forrest, 1986; Bagg and Forrest, 1988; Pink and Perry, 1996). Understanding the mechanisms behind this regulation would further our understanding of the importance of active muscle contractions in scapular kinematics. The purpose of this study was to examine this controlling mechanism by comparing the three-dimensional (3D) scapular and clavicular kinematics during active and passive arm elevation.

MATERIALS AND METHODS

Kinematics

The Polhemus 3Space Fastrak (Colchester, VT) was used to collect 3D scapular and clavicular kinematics. A thoracic receiver was placed over T3 using double sided tape, a humeral receiver was placed at the level of the deltoid tuberosity using an elastic strap, and a scapular receiver was fixed to a scapular tracker device that was attached to the scapular spine and acromion process using Velcro strips. The scapular tracker device has been shown to be accurate in measuring scapular kinematics (Karduna, 1998). The arbitrary axes defined by the Polhemus were converted to appropriate anatomical axes using digitized bony landmarks.

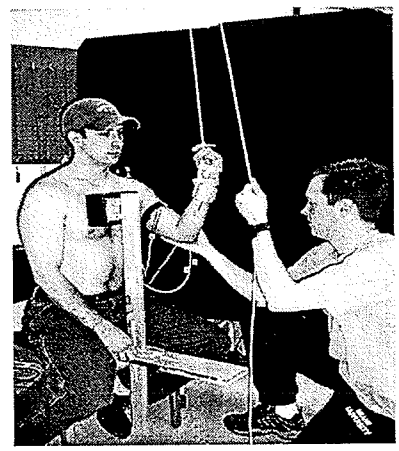

Figure 1 Passive Elevation System

Electromyography

Surface electrodes were used to collect electromyographic (EMG) activity from the upper and lower trapezius, lower serratus anterior, anterior deltoid, and infraspinatus muscles. Raw EMG data was band pass filtered (10 – 750 Hz) and collected at 1200 Hz (Instech Laboratories, Exton, PA.). EMG data from the active and passive trials were normalized to a maximum voluntary contraction for each muscle.

Protocol

Thirteen healthy subjects performed three trials of active elevation in the scapular plane. Their wrist was then placed in a splint, which was attached to a rope that ran

over an overhead pulley system (figure 1). The other end of the rope was used to passively elevate their arm (three times) in the scapular plane.

ANALYSIS

Averaged active/passive kinematic differences for scapular posterior tilt, upward rotation, external rotation, and clavicular retraction and elevation were evaluated at the following positions of arm elevation: 35°, 55°, 70°, 85°, 100°, 115°, and 135°. Paired t-tests were used for statistical comparisons. At the afore mentioned positions, normalized EMG data was processed using a RMS filter.

RESULTS

Significant differences were found for scapular upward rotation, clavicular retraction, and clavicular elevation. See figure 2 for upward rotation example. During active motion there was a greater amount of scapular upward rotation, clavicular retraction, and clavicular elevation. No differences were found for scapular external rotation or posterior tilt.

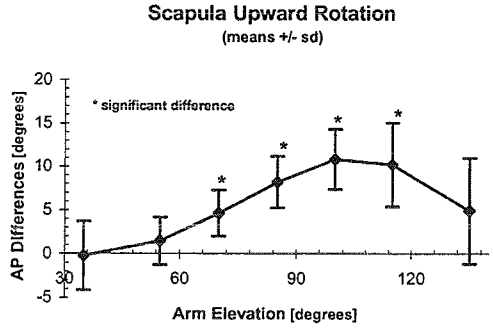

Figure 2 Means and standard deviations for active/passive differences for scapular upward rotation. *Significant difference

EMG activity for all muscles at each position of elevation was lower during passive elevation, ranging from 1-12% of a MVIC. This demonstrates that our method was indeed passive.

DISCUSSION

Active elevation resulted in greater scapular motion, particularly within the range of 70°-115° of elevation. These findings are consistent with a similar study by McQuade and Smidt (1998). Muscle control of scapular position may be most important in this range. Beyond 115°, active and passive motion became similar which seems to suggest a passive mechanism controlling scapular position such as capsular tension or passive muscle tension. The active/passive kinematic differences reported in this study maybe altered in patients with shoulder pathology who demonstrate impaired muscle performance and/or abnormal tightness of the capsule and surrounding muscles. This type of information would provide clinicians with an understanding of some of the underlying biomechanical impairments associated with shoulder pathologies which in turn could be used in the clinical decision making process for the selection of appropriate treatments.

REFERENCES

Bagg, S., Forrest, W. (1986). *American Journal of Physical Medicine,* **65**, 111-124.
Bagg, S., and Forrest, W. (1988). *American Journal of Physical Medicine and Rehabilitation,* **67**, 238-245.
Kibler, W. (1998). *American Journal Of Sports Medicine,* **26**, 325-337.
Karduna, A., et al. (1998). *North American Congress of Biomechanics*, 575-576.
McQuade, K. et al. (1998). *Journal of Orthopedics and Sports Physical Therapy,* **28**, 74-80.
Pink, M.M., and Perry, J. (1996). *Biomechanics.* In *Operative techniques in Upper Extremity Sports Injuries.* St.Louis, Mosby.

THE RELATIONSHIPS AMONG GROUND REACTION FORCES, JOINT ANGLES, AND ANTHROPOMETRIC MEASURES DURING FRONT AND LATERAL STEP-UPS

Kristen Jagger, Christine Ensch, Mark Tillman

Biomechanics Laboratory, University of Florida, Gainesville, FL, USA
Email: kjagger@ufl.edu

INTRODUCTION

In rehabilitation settings, functional tasks have become a standard treatment option and it is thought that the use of exercises that mimic activities of daily living will accelerate an individual's return to normal function. Common exercise regimens for lower extremity dysfunction involve the use of variable height steps to increase strength, balance, and proprioception. Exercises such as front and lateral step-ups are often used to achieve these goals, but there is little evidence to support the reasoning for the choice of step height (Cook et al.1992, Brask et al. 1984).

Although a patient's height or leg length may affect the mechanics of the stepping exercise, this is seldom taken into account when determining a step height for rehabilitation. Changes in the flexion angles of the lower extremity joints place varying amounts of tension and compression on the joint structures due to altered kinematics.

The purpose of this study was to determine the ground reaction forces and relative flexion angles at the hip, knee, and ankle in individuals of different height during both front and lateral step-ups. Three common step heights of 10.1 cm, 15.2 cm, and 20.3 cm (4, 6, 8 inches, respectively) were used.

METHODS

Ten male (1.75 ± 0.08 m, 74.7 ± 7.3 kg) and ten female (1.62 ± 0.06 m, 60.9 ±5.7 kg) subjects with no current history of lower extremity or low back pain/pathology participated in this study. Of the three different steps were used for testing, the first was the height of a Bertec™ force plate (10.1 cm). The other heights were achieved by adding appropriate wooden supports.

Reflective markers were placed on the participant's dominant extremity on the following bony landmarks: acromion, iliac crest, greater trochanter, lateral knee axis, lateral malleolus, lateral calcaneus, and distal head of the fifth metatarsal. The markers were used to define body segments and to compute flexion angles of the hip, knee, and ankle. Sagittal plane motion during front and lateral stepping maneuvers was videotaped with a 60-Hz camera aligned at the level of the knee. Video data were analyzed using the Peak Motus™ motion analysis system, while National Instruments Labview 6i™ was used to process ground reaction forces.

A repeated measures analysis of variance (ANOVA) was used to detect differences in joint flexion angles and GRFs among step heights and between directions, while a linear regression was performed to determine if individual anthropometric variables were predictive of the maximum angle of joint flexion.

RESULTS AND DISCUSSION

A significant difference in the magnitude of the anterior-posterior (AP) ground reaction

forces (GRFs) was found between front and lateral step-ups in this population ($p<0.001$). Larger anteriorly directed forces were found during the front step-up than during the lateral step-up ($p<0.001$). Medial-lateral and vertical force magnitudes, as well as moments about the x-, y-, and z-axes, were not found to be significantly different between front and lateral stepping directions, though the direction of applied force varied among subjects and between stepping directions. No statistical significance was found when comparing magnitudes of GRFs across the three step heights.

Regression results indicate that ankle, knee, and hip flexion angles increase significantly with each increase in step height ($p<0.001$). Stepping direction was also found to effect the joint angles significantly. Knee and hip flexion angles were greater during front step-ups than during lateral step-ups ($p<0.001$), while ankle dorsiflexion angles were greater during lateral step-ups than front step-ups ($p<0.001$).

Significant regression equations were discovered for maximum knee, hip, and ankle angles on all step heights. The best predictors for the maximum knee flexion angle during the front step-up are illustrated in Table 1 as an example.

TABLE 1: Regression for front step-up.

Step Height	Predictor	R^2	P
Knee – 4 in.	Total height	0.389	0.003
Knee – 6 in.	Trunk length	0.220	0.037
Knee – 8 in.	Total height	0.370	0.004

Finally, when maximum flexion angles were assessed among subjects for each step height, a significant difference was found. Those individuals with longer leg lengths had lower flexion angles at the knee, hip, and ankle than did those with shorter leg lengths for each step height. This finding is in agreement with comments made by Vergis and Gilquist (1998).

It is apparent from these data that step height, step direction, and an individual's leg length should be taken into account when prescribing stepping exercises in rehabilitation. Front step-ups should be avoided if minimal AP GRFs are recommended. Step height and direction should be based on the angle of joint flexion desired and the leg length of the individual. Medial-lateral and vertical GRFs are not significantly different among step heights and between directions; thus joint resultant forces become a function of the joint flexion angle and segment moment arms. These findings indicate that the amount of joint flexion should be carefully considered with respect to pathology.

SUMMARY

Results of this study indicate that rehabilitation stepping exercises should be tailored based on individual anthropometric data, desired lower extremity joint flexion, and the nature of pathology in order to provide a safer and more efficient return to daily function.

REFERENCES

Brask, B. et al. (1984). *Phys Ther*, **64**, 324-329.

Cook T.M. et al. (1992). *J Orthop Sports Phys Ther*, **16**, 108-113.

Vergis, A., Gillquist, J. (1998). *Am J Sports Med*, **26**, 841-846.

Muscle Activation Patterns during Combined Stepping and Cutting Activities

Houck, J. R.

Ithaca College-Rochester Campus, 300 E. River Road, Rochester, NY

INTRODUCTION

The loads experienced during cutting activities are theorized to challenge subjects with knee instability, and therefore, are useful to understand in order to determine rehabilitation strategies for subjects with ligament ruptures (Colby, 1998). Yet, requiring injured subjects to perform rapid cutting activities exposes them to further injury. Alternatively, a recent study (Houck, 1999) used a stepping and cutting activity to expose muscle adaptations used by subjects that are ACL deficient (Houck, 1999). The knee moments and powers suggested a changing role of knee muscles and ankle plantar flexors (Houck, 2000), however the muscle activations were not tested. The purpose of this study was to compare patterns of muscle activation of healthy subjects during stance of a straight step off a curb, a step combined with a 45 ° crossover cut and a step combined with a 45 ° sidestep cut.

METHODS

Eight subjects (22.5 ± 2 y.o.) participated in the study. The muscles tested included the medial/lateral gastrocnemius, medial/lateral hamstrings and lateral quadriceps. Silver –Silver chloride electrodes spaced 2 cm apart, pre-amplified at a gain of 35 (differential amplifier), were placed over each muscle. The signal was low passed filtered at 25 Hz and stored for processing at 1000 Hz via a 12 bit A/D converter. A 1-volt trigger was used to synchronize the EMG and force plate recordings. Stance was determined using a 10 N threshold for heel strike and toe off. The EMG signals were rectified and filtered using a 4th order Butterworth filter with a cut-off frequency of 15 Hz. The EMG data for each muscle was time normalized to percent stance at 1 % intervals. To obtain relative activation, the processed EMG signal was divided by the average EMG signal over stance for the step straight activity. Every 10 % of stance the signal was averaged for each activity to gain a representative value (Figure 1).

All the activities included stepping off a 21 cm high curb at an approach speed of 1.24 m/s. The curb was placed 50 % of the subjects stride length from the center of the force plate. Subjects were required to step and change direction 45° by crossing the contralateral leg over the stance leg (crossover cut) toward the new plane of progression or by moving the ispislateral leg toward the new plane of progression (sidestep cut). The control condition was stepping straight off the curb. Each subject completed 15 trials of each condition. The order of testing was randomized.

RESULTS AND DISUCSSION

The first peak vertical ground reaction force peak was equal between activities ($p > 0.05$) suggesting equal loading during initial stance among the activities. Unlike other EMG studies that suggest

higher quadriceps activation associated with cutting (Colby, 1998), the quadriceps activation was equal during early stance ($p = 0.39$). However, previous studies did not specifically control approach velocity or foot landing strategies, which may partially explain the discrepancy.

Significant differences were observed in the medial/lateral gastrocnemius (Figure1) and hamstring activation patterns. The medial gastrocnemius showed higher activation during late stance of the sidestep cut, which could induce tibiofemoral external rotation. While the lateral gastrocnemius showed higher activation during the crossover cut, which could induce tibiofemoral internal rotation.

The hamstrings showed significantly higher patterns of activation during mid stance (40 – 60 %), which is consistent with higher sagittal plane hip and knee moments observed during a stepping and crossover cutting activity in a separate study (Houck, 2000). Consistent with invoking tibiofemoral internal rotation only the medial hamstring showed higher activation during the crossover cut activity. Yet, both the knee flexors and ankle plantar flexors are two joint muscles, hence changes in activation may also reflect demands at other joints.

SUMMARY

The muscle activations of the plantar flexors and knee flexors are hypothesized to reflect their contribution to transverse and frontal plane control during the cutting activities. Programs to return athletes to cutting activities may need to consider the roles of the knee flexors and ankle plantar flexors.

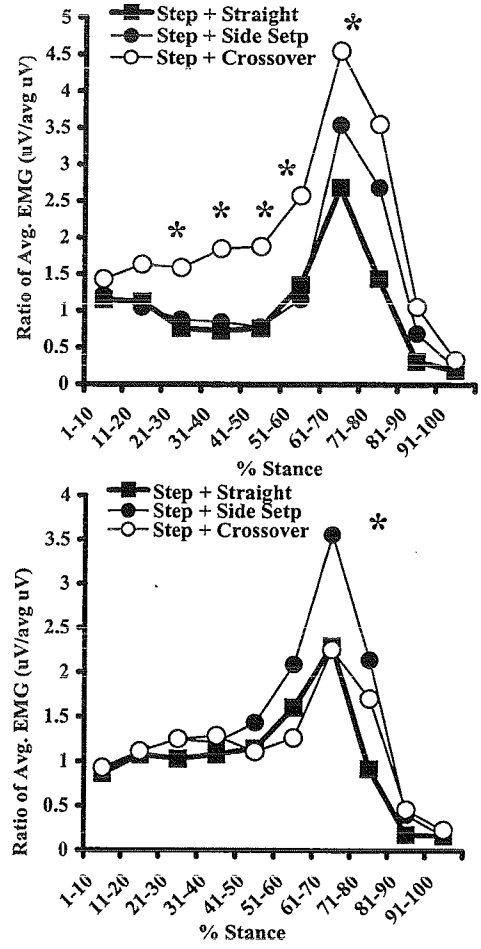

Figure 1. A. Lateral Gastrocnemius B. Medial Gastrocnemius (* indicates significance $p < 0.05$)

REFERENCES

Colby, S. et al. (2000) *Am. J. Sports Med.*, **28**, 234-240

Houck, J. R., Yack, H. J., *Proceedings CSB 2000*, 126.

Houck, J.R., Thesis, University of Iowa, 1999

ACKNOWLEDGEMENTS

Ithaca College Physical Therapy Students that worked on this project Spring of 2000.

MEASUREMENT OF TIBIOFEMORAL JOINT MOTION USING CINE-PHASE CONTRAST MRI

Peter Barrance [1], Glenn Williams [1], Frances T. Sheehan [2], Thomas S. Buchanan [1]

[1] Center for Biomedical Engineering Research, University of Delaware, Newark, DE, USA
[2] Department of Mechanical Engineering, The Catholic University of America, Washington, DC

E-mail: peteb@udel.edu

INTRODUCTION

In cine-phase contrast (cine-PC) magnetic resonance imaging, velocity-dependent pulse sequences are used, and velocity information is extracted from the phase relationship of the MR signal. The utility of the application of this imaging method for determination of patellofemoral joint kinematics has been demonstrated previously (Sheehan, et al., 1998). In this abstract, preliminary results on the application of the technique to the measurement of tibiofemoral joint motion are reported.

METHODS

Cine-PC data was acquired while subjects performed a repetitive knee flexion/extension exercise within an MRI scanner (GE Signa LX.) The subjects lay face up, the thigh was raised via a ramp to flex the hip, and knee extensions were performed against the weight of the shank only. The ramp was adjusted until the knee was fully extended as the toe just touched the highest point of the imager's bore. The MR signal receiving coils were secured vertically, adjacent to each side of the knee, using a custom-made jig.

In the study protocol, the subject is instructed to flex and extend the knee through the available range of motion, at a frequency of 35 cycles per minute. This occurs by voluntary synchronization with the beat of a metronome. The MRI system collects a sequence of 24 frames of data through the cycle on a user-specified sagittal image plane. An optical trigger, positioned under the heel of the subject, is used to synchronize the acquisition of data with the motion.

Each resulting data frame yields four separate images on the selected plane; one is the usual anatomical cross-section (magnitude image), and the others are encoded with velocity information in each of three orthogonal directions. The experiment requires the subject to perform the cyclic exercise over a scan time of approximately 5.5 minutes.

Rectangular regions within the femur and tibia, as displayed in the first magnitude image, were user-selected for motion tracking. An integration algorithm (Zhu, et al., 1996) was used to process the velocity information and thereby compute the trajectory for each of these regions through the motion cycle. Coordinate axes were constructed from the two edges of each region, and 3D transformation matrices were computed relative to the fixed coordinate frame of the scanner. The longitudinal axis of the femur was defined based on anatomical landmarks in one image of the cine-PC data at which the knee was in full extension.

In addition to the cine-PC data acquisition, cine-MRI data was collected on a transverse plane through the femoral condyles. The knee flexion axis was defined in the image of this

dataset for which the knee was fully extended.

An anatomical coordinate frame was defined in the femur based on the above axes. A transformation was calculated between the position of the tracked coordinate frame (from the cine-PC data) at full extension, and the anatomical frame. This transformation was then applied to the cine-PC coordinate frame at the other time points to calculate the position and orientation of the anatomical frame. The position and orientation of a coordinate frame aligned with the femoral frame at full knee extension yet fixed to the tibia was similarly calculated. The rotation matrix relating the tibial frame to the femoral frame was next calculated and decomposed using a 1-2-3 Euler angle sequence. The quantities computed represent flexion, varus/valgus, and axial rotations relative to the position at full extension.

RESULTS AND DISCUSSION

Four subjects (eight knees) were tested using the above methods. No knees had any history of injury or pathology. Figure 1 shows the resulting angles as averaged across the subjects, along with standard deviation margins.

The trajectories in flexion/extension are consistent across the subject knees (Fig. 1A.) Relatively little varus/valgus excursion is seen (Fig. 1B). The data show a significant coupled internal rotation with knee flexion (Fig. 1C), in accordance with the commonly observed 'screw home' phenomenon (Frankel and Nordin, 1980.)

SUMMARY

The data presented demonstrate the use of cine-PC MRI data to study tibiofemoral kinematics. Future studies will seek to assess the kinematic variations associated with pathological conditions.

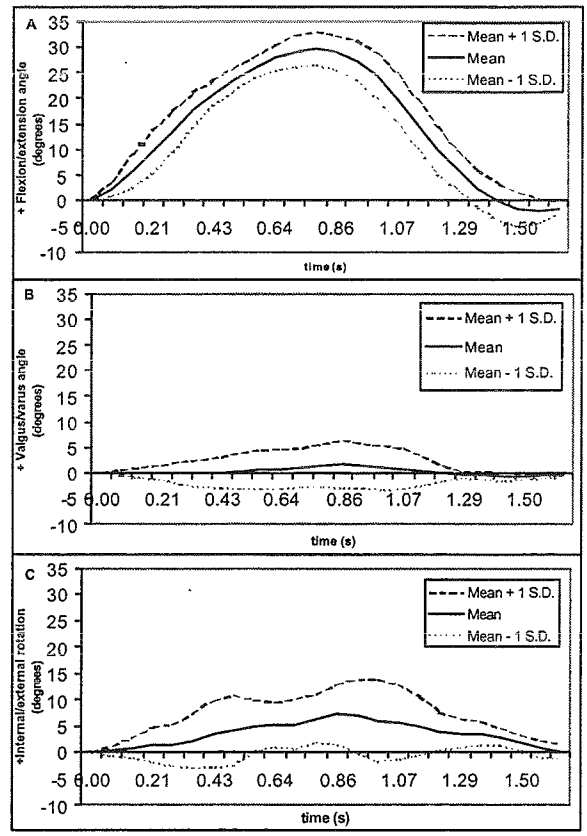

Figure 1: Mean plus/minus one standard deviation for joint angles measured in four subjects (eight knees)

REFERENCES

Frankel, V.H., and Nordin, M. (1980) *Basic Biomechanics of the Skeletal System.* Lea & Febiger

Sheehan, F. T., F. E. Zajac, and J. E. Drace (1998) *J Biomech.* **31,** 21-6.

Zhu, Y., M. Drangova, and N. J. Pelc (1996) *Magn Reson Med.* **35,** 471-80.

ACKNOWLEDGEMENTS

Supported by NIH Grant R01AR46386.

MAXIMUM HIP FLEXION POWER IN YOUNG ADULTS: EFFECTS OF INITIAL JOINT ANGLE AND ALLOWABLE RANGE OF MOTION

Cécile Smeesters, Neil M. Cole [1], and James A. Ashton-Miller

Biomechanics Research Laboratory, University of Michigan, Ann Arbor, MI, USA
[1] Bio Logic Engineering Inc., Dexter, MI, USA
E-mail: smeester@umich.edu Web: http://me.engin.umich.edu/brl/

INTRODUCTION

The ability to complete a compensatory step in time to arrest an on-going forward fall can require the hip flexor muscles to maximize hip flexion power (Schultz, 1997). Measurements of maximum hip flexor muscle power have been reported for hip velocities up to 210 °/sec (Cahalan, 1989), but higher peak velocities are required to arrest actual falls (Thelen, 1997). We are not aware of data on maximum hip flexor power capacity at these higher velocities. In addition, the effects of initial hip joint angle and the allowable range of hip joint motion on torque, velocity and power are unknown. Using a custom dynamometer, we tested the hypotheses that neither the initial hip joint flexion angle nor the allowable range of motion would influence the maximum instantaneous hip flexion power or torque at velocities over 210 °/sec.

METHODS

Maximum instantaneous hip flexion power was measured in 10 healthy young subjects (18 to 23 years old), with equal numbers of males and females, on a custom dynamometer. Because measurements of maximum muscle power are prone to gravitational and inertial artifacts (Winter, 1981; Sapega, 1982), the calculations of the net joint torque and power compensated for gravitational and inertial effects. Subjects were asked to attempt to maximize hip torque, velocity and power in seven distinct leg movements. Each movement was performed by the dominant leg with an extended knee. Subjects were instructed "to swing their leg as fast and as hard as they could", until their leg angular momentum was arrested by an external device. Hip flexion angle was referenced to the neutral posture (denoted as 0° flexion). Subjects performed up to three trials for each of the seven combinations of initial joint angle (ANG) and range of motion (ROM) (Table 1), presented in a randomized sequence. For each ANG*ROM combination, the trial with the highest maximum power was found. After the data were normalized to each individual's maximum value in the 0° - 90° test condition (Table 1), the hypotheses were tested using repeated measures analyses of covariance (covariates: height, mass, age, and physical activity). A $p<0.05$ value was considered significant.

RESULTS AND DISCUSSION

The combinations of ANG*ROM significantly affected the maximum hip flexor muscle power ($p < 0.0005$, Table 1). As initial joint angle increased from 0° to 60°, maximum power decreased ($p < 0.0005$). For 30° ROM movements this decrease was 35% . As the allowable range of motion was decreased from 90° to 15°, maximum power decreased by 19% ($p = 0.003$). This was principally due to the decrease in the maximum velocity attained.

The ANG*ROM combinations significantly

affected maximum angular velocity ($p < 0.0005$). For a 30° ROM, as initial joint angle increased from 0° to 60° maximum velocity decreased by 19 % ($p < 0.0005$); but as range of motion decreased from 90° to 15° maximum velocity decreased by 61 % ($p < 0.0005$). Maximum velocity ranged from 359 to 504 °/sec across all subjects.

The ANG*ROM combinations significantly affected maximum torque ($p = 0.001$, Table 1). The initial joint angle did not affect the maximum torque ($p = 0.588$), but the effect of the range of motion was significant ($p < 0.0005$). However, this latter result was mostly due to the 0 -15° test movement result, and to some extent to the 0 - 30° test movement result. Because preliminary results from subsequent blindfolded tests did not show this effect, we surmise that the original results were due to *a priori* knowledge of the next ROM to be tested and greater motivation at the small ROM angles.

The overall outcome values are consistent with trends reported by Cahalan (1989). In this study, the effect of gender on ANG and ROM effects was removed by the normalization procedure and repeated measures design. However, significant age and gender effects on the absolute values of torque, velocity and power have been found in a larger sample of young and old subjects using similar methods (Smeesters 2001).

Table 1: Average ± Standard Deviation Maximum Power, Velocity and Torque

ANG*ROM	Power	Velocity	Torque
0° to 90°	205±69 (Watts)	398±43 (°/sec)	46±11 (Nm)
0° to 90°	1.0	1.0	1.0
0° to 60°	0.99±.24	0.93±.09	0.99±.16
30° to 90°	0.78±.17	0.84±.05	0.90±.11
0° to 30°	0.92±.20	0.76±.06	1.07±.18
30° to 60°	0.73±.17	0.69±.06	0.99±.21
60° to 90°	0.60±.09	0.62±.06	0.90±.13
0° to 15°	0.81±.23	0.59±.07	1.20±.22

SUMMARY

(1) A greater *initial* hip flexion angle limited the maximum power attained, principally by limiting the maximum achieved velocity.
(2) Smaller ranges of motion also limited maximum power, again by limiting the maximum achievable velocity.
(3) Maximum torque was unaffected by initial joint angle and, quite probably, by range of motion.
(4) In order to maximize hip flexion power, initial flexion of the hip joint should be minimized and a sufficiently large range of motion allowed for the individual to reach their maximum angular velocity.

REFERENCES

Cahalan, T.D. et al. (1989). *Clin. Orthop.*, 246, 136-145.

Sapega, A.A. et al. (1982). *Med. Sci. Sports Exerc.*, 14(5), 368-375.

Schultz, A.B., Ashton-Miller, J.A., Alexander, N.B. (1997). *Muscle Nerve*, (Suppl 5), S60-64.

Smeesters, C., Cole N.M., Ashton-Miller, J.A. (2001) *17th International Association- of Gerontology Mtg*, Vancouver, Submitted.

Thelen D.G., Wojcik L.A., Schultz A.B. *et al.*, (1997) *J. Gerontol.: Med. Sci.* 52A: M8-13.

Winter, D.A., Wells, R.P., Orr, G.W. (1981). *Eur. J. Appl. Physiol.*, 46(4), 397-408.

ACKNOWLEDGEMENTS

We gratefully acknowledge the assistance of Tricia Bass and Elizabeth Lee, along with the support of PHS grants R42 AG13587, P01 AG10542 and P60 AG08808.

THE EFFECTS OF KNEE ANGLE ON QUADRICEPS FEMORIS ACTIVATION AND KNEE EXTENSOR TORQUE

Danny M. Pincivero[1], Robert M. Campy[2], Alan J. Coelho[2], Yuliya Salfetnikov[1]

[1] Human Performance and Fatigue Laboratory, Department of Physical Therapy, Eastern Washington University, Cheney, WA, USA
[2] Department of Physical Education, Health and Recreation, Eastern Washington University, Cheney, WA, USA
E-mail: dpincivero@mail.ewu.edu

INTRODUCTION

It has previously been demonstrated that the maximal voluntary contraction (MVC) torque for the quadriceps femoris (QF) muscle occurs within the mid-range (i.e., 45 – 90 deg flexion) of knee range of motion (Ng, et al, 1994; Suter and Herzog, 1997; Welsch et al, 1998). Decreases in voluntary torque generation at the extremes of the functional joint range of motion (0 – 90 deg flexion) may be attributed to mechanical and/or muscle activation factors. The purpose of this study was to examine the effects of knee joint angle on QF activation and knee extensor torque.

METHODS

Fifteen healthy male and 15 healthy female volunteers participated (mean age = 24.2 $\pm$ 4.2 years, mean height = 171.8 $\pm$ 8.0 cm, mean weight = 69.8 $\pm$ 2.5 kg). Subjects performed an active warm-up involving 5 min of sub-maximal cycling, followed by 3-4 sub-maximal and maximal effort isometric QF contractions. For the isometric contractions, subjects sat in an upright position and were stabilized with thigh, pelvic and torso straps on the Biodex System II isokinetic dynamometer. Subjects then performed a series of isometric maximal voluntary contractions (MVC) with their knee in the following positions: 0, 10, 30, 50, 70, and 90 deg flexion. Each subject performed 3 MVCs (5 sec each) at each angle, in a random order, with 2 min rest in between each contraction.

Peak torque (PT) was recorded and averaged for the 3 MVCs at each knee angle. Muscle activation was assessed via surface EMG for the vastus medialis (VM), vastus lateralis (VL), and rectus femoris (RF) muscles. Pre-amplified bi-polar circular electrodes (Ag/AgCl) were placed on pre-determined areas of each muscle with a fixed inter-electrode distance (center to center) of 2 cm. The reference electrode was placed over the medial shaft of the tibia. EMG activity was collected at 1000 Hertz (CMRR=87 dB at 60 Hertz, input impedance >25 Mohms at dc) with a gain range of 1K to 5K. The raw EMG signal was bandpass filtered (20-500 Hertz), full-wave rectified and integrated over the middle 3 sec of each contraction. A 2-way ANOVA (knee angle by gender) with repeated measures was performed on isometric PT. A 1-way ANOVA with repeated measures (knee angle factor) was performed for isometric EMG activity for each muscle, separately.

RESULTS AND DISCUSSION

The results demonstrated a significant angle ($F_{5,140} = 270.85$, $p<0.05$), gender ($F_{1,28} = 29.35$, $p<0.05$), and angle by gender interaction ($F_{5,140} = 19.81$, $p<0.05$) for QF PT. It was observed that peak isometric QF

torque was attained at a 70 degree angle, and that males experienced a significantly greater increase in torque from angles 30 to 70, than females (Figure 1).

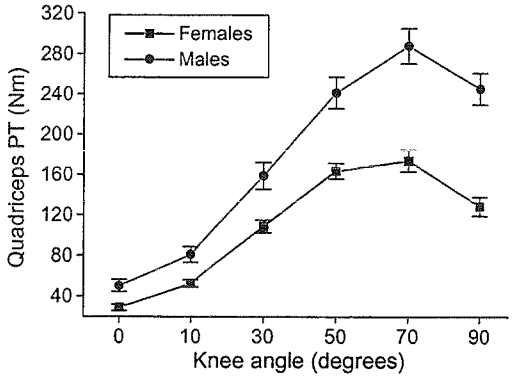

Figure 1: Isometric QF PT at knee angles 0, 10, 30, 50, 70, and 90 degrees flexion in males (n=15) and females (n=15).

These findings appear to be similar to those of Ng et al (1994) and Welsch et al (1998) who found that isometric quadriceps PT was highest at 60 degrees flexion. Although this specific knee angle was not investigated in the present study, Welsch et al (1998) also demonstrated minimal differences in isometric torque between 60 and 78 degrees flexion. The present findings, however, are in contrast to those of Suter and Herzog (1997) who observed peak isometric QF torque to occur at 90 degrees flexion, as opposed to 60 degrees.

The results showed a statistically significant increase in VM EMG from knee angles 0 to 50 degrees ($F_{5,145} = 13.87$, $p<0.05$), and no significant differences between angles 50 to 90. There were no significant differences in VL EMG between the different knee angles. Rectus femoris EMG activity was found to significantly increase from knee angles 0 to 10 ($F_{5,145} = 4.78$, $p<0.05$), while angles 10 to 90 were not significantly different.

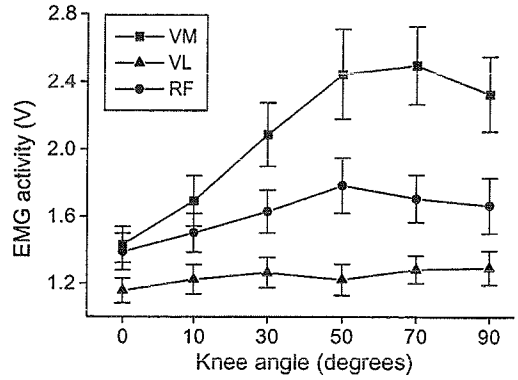

Figure 2: Isometric EMG activity of the VM, VL and RF muscles at knee angles 0, 10, 30, 50, 70, and 90 degrees flexion in males (n=15) and females (n=15).

This pattern of activation of the VL muscle is similar to the findings of Suter and Herzog (1997) in which the same muscle demonstrated no significant EMG differences across knee angles 15, 30, 45 and 60 degrees. However, the EMG signal was found to be significantly highest at a knee angle of 90 degrees (Suter and Herzog, 1997).

SUMMARY

The major finding of the present study demonstrates that peak QF isometric torque occurred at 70 degrees flexion in both males and females. It was also observed that the EMG signal of the VM muscle only, followed a similar trend as the PT values. Vastus lateralis and RF muscle EMG appeared to be less sensitive to changes in knee joint angle.

REFERENCES

Ng, A.V., et al. (1994). *J Appl Physiol*, **76**, 2561-2569.

Suter, E., Herzog, W. (1997). *J Electromyogr Kinesiol*, **7**, 123-130.

Welsch, M.A., et al. (1998). *Arch Phys Med Rehabil*, **79**, 971-978.

The Relationship Between Knee Joint Angle, Stretch-Shorten Cycle Performance, and Jump Distance In Ski Jumping.

[1]Seth Paradis, [2]Jeff McBride, [2]Carl Foster,[2]Tom Kirnozeck,
[1]Scott Lephart and [1]Freddie Fu
[1](University of Pittsburgh, Pittsburgh, PA, USA)
[2](University of Wisconsin-La Crosse, La Crosse, WI, USA)
Email:sethparadis@hotmai.com

INTRODUCTION: Ski jumping is a very complex skill involving several phases such as the inrun, take-off, flight and preparation for landing. The take-off requires an extension of the hip and knee joints to produce a negative aerodynamic effect (Antonio and Renato, 1987; Hubbard, et al., 1989; Komi and Virmavirta, 1996; Tveit and Pederson, 1981). It is known that a stretch-shorten cycle is used in most athletic events (Bosco et al., 1982;Wilson et al., 1991); however, there is a lack of literature concerning the possible use of a stretch-shorten cycle during ski jumping.

The purpose of this study was to investigate the relationship between the change in knee joint angle, representing the stretch-shorten cycle and the jump distance of elite ski jumpers. It is hypothesized that the stretch-shorten cycle would occur and result in a longer jump distance.

METHODS: Forty-eight competitors were filmed at 120 Hz during the first round of the Westby Continental Cup in Westby, Wisconsin on February 12, 2000. The subjects consisted of national and international elite jumpers on a (K108) jump.

The take-off was examined as a two-dimensional motion of the subjects at take-off. The jumper's body and equipment were modeled as four sections: the upper body, thigh, lower leg, and ski. This allowed hip (1), knee (2), and ankle (3) angular displacement to be measured. The change of the knee angle was used to determine the existence of a stretch-shorten cycle during the take-off motion. A Regression Analysis test was used to analyze the data with at an $\alpha = .05$.

Joint locations were estimated during digitization in accordance with the noninvasive video data collection style used by (Arndt et al., 1995). Joint centers were estimated by locating anatomical landmarks on the jumpers

RESULTS: The average knee angle displacement was calculated by examining 44 subjects' knee angles 8 m previous to the end of the take-off table. The average distance jumped was 99.03 ± 11.6 m. During the apparent stretch-shorten cycle movement, the average knee flexion was -.11521 ± .0681 (rad) and the average knee extension was .1546 ± .0838 (rad). Average knee angle flexion was represented as a negative angular change due to the decrease of the knee angle at the onset of the SSC movement. The average flexion/extension ratio was 0.85 ± 0.5. The knee-joint extension velocity averaged 9.2 radians • s^{-1}.

DISCUSSION: The purpose of the take-off is: (1) to give the jumper-ski system a maximum velocity, (2) to produce a favorable body position at the jump's edge, and (3) to provide an initial turning moment for the forward rotation of the body over the skis immediately after take-off (Campbell, 1980). This experiment adds another

purpose to the take-off: to perform a stretch-shorten cycle.

The data show the existence of a stretch-shorten cycle (SSC) movement 0.08 s before the edge of the ski jump lasting approximately 66 ms. An elite ski jumper must utilize the SSC movement to increase their jump distance. It is important to recall the information in Figure 2. The data demonstrate there were a significant (α= .05) quadratic relation between flexion of the knee joint and the jump distance. This demonstrates a relationship between optimal knee joint flexion and maximum jump distance. This suggests that when a jumper resists against and doesn't utilize the centrifugal force entering the take-off table to flex the knee joint, they may not be harnessing the full potential of the stretch-shorten cycle movement. Also, the jump distance may be hindered if the athlete flexes the knees too much. It is possible the proper knee joint flexion angle may create a build-up of elastic energy resulting in a more explosive knee extension velocity. This is all dependent on the jumper's ability to produce a quality take-off motion followed by a stable flight phase. Therefore, the stretch-shorten cycle may be an important factor in determining the length of the jump. It is important to remember that several aspects must work together to produce a long jump distance.

Not only does the SSC movement exist, but there also may be an ideal amount of knee flexion to utilize the elastic energy in the SSC movement to produce a successful jump distance. This study concluded that when an elite jumper utilized a proper stretch-shorten movement, in combination with proper form on the take-off table and in the air, they would produce a longer jump distance.

REFERENCES:

Antonio, P., & Renato, R. (1987). Evaluation of biomechanical motor patterns in ski jumpers during simulations of take-off. International Series on Biomechanics, Biomechanics X-B, 679-684.

Arndt, A., Bruggeman, G., Virmavirta, M., & Komi, P. (1995). Techniques used by Olympic ski jumpers in the transition from take-off to early flight. *Journal of Applied Biomechanics*, **11**, 224-237.

Bosco, C., Tarkka, I., & Komi, P. V. (1982). Effects of elastic energy and myoelectric potentiation of triceps surna during stretch-shorten cycle exercise. *International Journal of Sports Medicine*,.**3**, 137-140.

Campbell, K. R. (1980). Biomechanical analysis of take-off technique in ski jumping. *Journal of the United States Ski Coaches Association*, *3*, 35-41.

Hubbard, M., Hibbard, R. L., Yeadon, M. R., & Komor, A. (1989). A multisegment dynamic model of ski jumping. *International Journal of Sport Biomechanics*, **5**, 258-274.

Komi, P. V., & Virmavirta, M. (1996). Ski jumping take-off performance: Determining factors and methodological advances. First International Congress on Skiing and Science, St. Chrisoph a. Arlberg, 3-26.

Tveit, P., & Pederson, P. O. (1981). Forces in the take-off of ski jumping. In Morecki, A., Fidelus, K., Kedzior, K., & Wit, A. (Eds.), Biomechanics VII-B, (pp. 478-482). Baltimore: University Park Press.

Wilson, G. J., Wood, G. A., & Elliott, B. C. (1991). The performance augmentation achieved from the use of the stretch-shorten cycle: The neuromuscular contribution. *The Australian Journal of Science and Medicine in Sport*, **23**, 97-101.

Effects of Arch Support on Changes in Arch Height and Center of Pressure Under Different Foot Positions While Loading

Shing-Jye Chen [1], John Mercer [2] and Krystyna Gielo-Perczak [3]

[1]Biomechanics and Sport Medicine Laboratory, University of Oregon, Eugene, OR, USA
[2] Department of Kinesiology, University of Nevada, Las Vegas, NV, USA
[3] Liberty Mutual Research Center for Safety & Health, Hopkinton, MA, U.S.A.
E-mail: sjchen@darkwing.uoregon.edu

INTRODUCTION

Shoe support and orthotic research, design and development have focused on an attempt to improving/ correcting the movement of the foot/ankle complex and to maintain rearfoot movement/position in a neutral position (Clement et al., 1981). The support is designed to "fit" the structure of the arch (Subotnick, 1999). It is not presently clear how the shoe-arch support affects performance of the foot-arch since the foot-arch naturally undergoes structural changes during locomotion. Other researchers have questioned the function of the shoe-arch (Nigg et al., 1999). This study tends to fill the gap in understanding the mechanics of the arch in barefoot (BF) and when it is impeded by an arch support (AS). The purpose of the study was to investigate the effect of shoe-arch support on medial longitudinal arch performance during loaded conditions.

METHODS

A total of ten injury-free volunteers (7 males and 3 females) participated in the study (24 ±4.7 yr; height, 180.0 ± 8.5 cm; weight: 80.5±11.7 kg) excluding abnormal foot types. The left foot of each subject was tested under a load of 712 N. The load was applied to the leg while the subject sat on a chair with the left foot positioned on the force plate (AMTI) and the thigh parallel with the ground. A total of twelve (2) mm square reflective markers were used with eight of the twelve markers placed on the medial longitudinal arch described by Phillips (1996). Eight markers (numbered t1 to t8) placed on the medial longitudinal arch then were sequentially lined up with the force plate's center marker during each of the differing foot positions. Each subject was tested under eight conditions, with each condition consisting of position the foot in a new position relative to the force vector of the applied load. This was accomplished by lining up one of the medial longitudinal markers with the center of the force plate. For each condition, a different marker was lined up with the force plate center for a total of eight foot positions. These measurements simulate the positions of the foot (i.e., plantar flexion to dorsiflexion) during midstance. Each arch height change was measured from the marker on the navicular to the floor when the foot was positioned. The upper trunk and left thigh were immobilized by strapping them to the chair to prevent movement. Force data were collected at 1000 Hz for 5 seconds concurrent with a kinematic recording (30 Hz) of the foot arch. The kinematic data were manually digitalized by using the HU-M-AN (Human Movement ANalysis) software version 2.0. Mean arch height change and center of pressure (COP) shift in the medial-lateral (x) direction repeated measures for each foot position were calculated and means were compared to determine statistical significance.

RESULTS AND DISCUSSION

Figure 1 reports the group mean of the arch

height changes in the barefoot and arch support conditions across the eight foot positions (BF, 35.43 ± 6.39 mm; AS, 41.92 ±5.76 mm). There was a significant increase in arch height in the arch supported condition higher than in the BF condition and a greater variability of AH in BF across the eight foot positions. Figure 2 shows the group means of the COPx (mm) [an indication of vertical ground reaction force (VGRF) in the medial lateral direction] changes in both barefoot (BF) and arch supported (AS) conditions. A greater variability of COPx shift in the BF than in the AS across the same eight foot positions was shown (BF: -1.9 ± 0.72 mm; AS: -2.1± 0.40 mm).

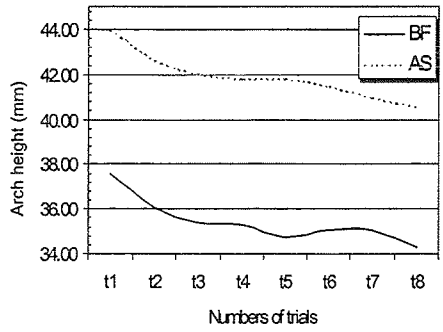

Figure 1. Arch height changes (mm)

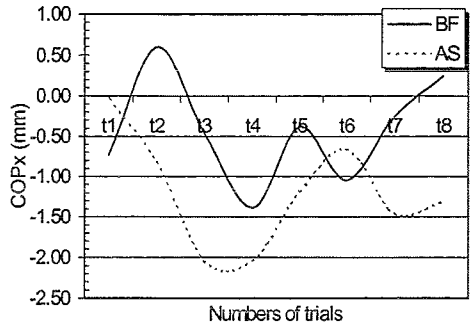

Figure 2. COPx (mm)

The arch height decreased as the foot was moved posteriorly relative to the line of application of the applied load. When the ankle was moved from a plantar flexed position to a dorsiflexed position, the arch height reduced. Since the result of the arch height change shows a greater variability in the BF condition than in the AS condition, the AH change reflects greater foot adaptability in the BF condition than in the AS condition.

When the barefoot was loaded with weight, and the ankle joint was moved from a plantar flexed position to a dorsiflexed position, the COP along the x axis of the force plate changed more than when the arch supported foot was placed in the same positions. This greater variability of the COPx shift in the BF condition suggests the barefoot had a greater dynamic for change of the arch's distribution of force than in the AS condition. On the other hand, the impedance by the arch support influenced the force distribution resulting in less change of the COPx shift over the trials and tended to shift the COP even more in the medial direction which has greater negative values.

SUMMARY

When the arch support was used, it impeded the arch from achieving its fullest potential. The VGRF was relocated to act on the arch as demonstrated by the shifts of the COP in the x direction. In order to attempt to achieve the barefoot's changes in AH & COP, the data suggests the supported arch had to compensate for the lack of the AH changes by relocating the COP corresponding to the VGRF.

REFERENCES

Clement, D. B. et al. (1981). Physician Sports Medicine, **9**, 47-58.

Subotnick, S. (1999). In S.I. Subotnick (2nd Ed.), Sports Medicine of the Lower Extremity (pp. 465-479).

Nigg, B. M. et al. (1999). Medicine & Science in Sports & Exercise, 31(7), 421-428.

Phillips, R. D. et al. (1996). J. American Podiatric medial Association, 86(10), 474 - 486.

WRIST AND ELBOW LOADING DURING SIDE AIR BAG DEPLOYMENT

Stefan M. Duma[1], Brian M. Boggess[2], and Jeff R. Crandall[2]
[1]Impact Biomechanics Laboratory, Virginia Tech, Blacksburg, Virginia
[2]Automobile Safety Laboratory, University of Virginia, Charlottesville, Virginia
Email: duma@vt.edu URL: www.ibl.vt.edu

INTRODUCTION

While automobile side air bags are designed to reduce primarily the risk of thoracic and head trauma in a side impact, their deployment may result in an increase risk upper extremity injury. These injuries may occur in normally positioned occupants whose upper extremity occupies the space needed for the side air bag. Experimental tests with human cadavers and side air bags have illustrated the risk of wrist fractures as the hand may become entrapped in a door mounted hand grip (Jaffredo,1998). Additional testing has elucidated the risk of chondral and osteochondral fractures in the elbow (Duma, 1998). In order to investigate these injury mechanisms and design side air bags that may reduce the risk of wrist and elbow injuries, the kinematics and kinetics of side air bag interaction with the upper extremity must be established. The purpose of this paper is the quantify the loads on the wrist and elbow during side air bag deployment.

METHODOLOGY

Data was collected from side air bag deployments onto a newly designed dummy upper extremity. The tests were conducted in a static environment using an automobile test buck. Computer simulations were used to identify the worst-case position for upper extremity loading (Figure 1). Three seat mounted, thoracic side air bags were used that varied only in their level of inflator output and were labeled A, B, and C with increasing aggressivity respectively. The air bags were prototypes intended for use in a luxury sedan, which contained flexible interior door surfaces with minimal padding.

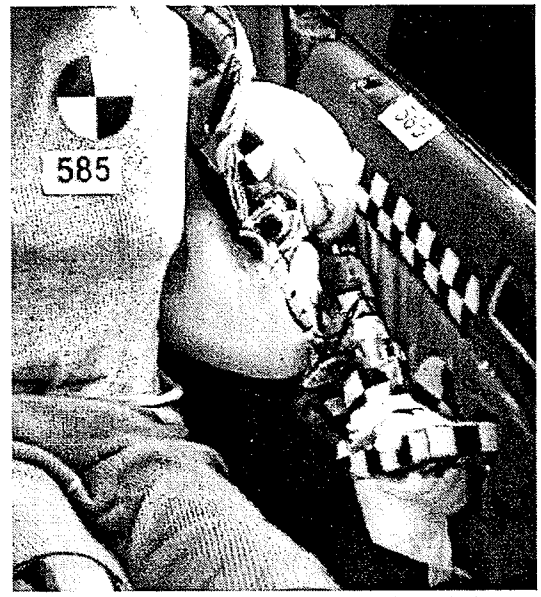

Figure 1. Oblique view of the side air bag loading the upper extremity 15 ms after deployment initiation.

The HIII 5th percentile female dummy was used with the corresponding instrumented 5th percentile upper extremity. Given that previous side air bag simulations illustrated the importance of forearm pronation to accurately model the handgrip interaction, the dummy upper extremity was designed to allow for forearm pronation (Duma, 2000). Instrumentation included a six-axis load cell in the humerus and the forearm. A two-axis load cell was added to the distal forearm to measure wrist bending moments. Internally mounted potentiometers measured forearm flexion and forearm pronation. Accelerometers and magnetohydrodynamic angular rate sensors on the forearm, humerus, and spine were used to track the upper extremity kinematics.

RESULTS

In all tests, the air bag deployed through the seat seam and drove the humerus and forearm forward, thereby forcing the hand into the handgrip. Although the handgrip interaction for each test was slightly different, the overall upper extremity interaction patterns were similar.

In contrast to previous experiments without a handgrip, the experiments with a handgrip resulted in a double peak in the forearm axial load from the inertial loading as well as contact with the handgrip (Figure 2).

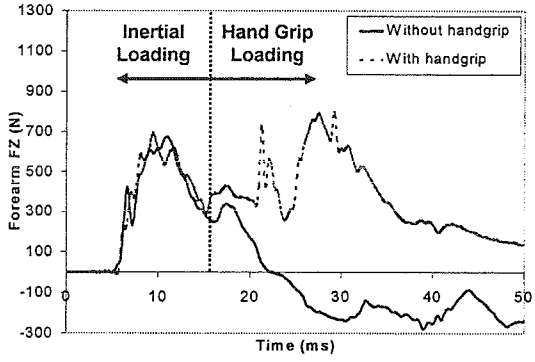

Figure 2. Forearm axial force for tests with and without a door mounted handgrip.

The forces at the wrist and elbow were calculated from the forearm load cell, accelerations, and masses (Table 1). The elbow axial force was the summation of the mid-shaft load cell axial force (FZ) and the forearm axial acceleration (AZ) multiplied by the 0.74 kg, or the approximate mass of the forearm portion between the elbow and center of the forearm load cell. The wrist resultant force was determined by inertially compensating the X, Y and Z axis forearm load cell recordings for the 0.47 kg portion of the forearm between the load cell and the wrist. Unlike the elbow axial load, all three of the inertially compensated wrist loads were included because the interaction of the wrist with the handgrip included significant off-axis loading. The elbow axial and wrist resultant forces are presented with positive polarities indicating an applied compressive load to the elbow or wrist respectively.

Table 1. Upper extremity loading summary.

Test	Air Bag	Humerus Resultant Bending Moment (Nm)	Elbow Axial Force (N)	Wrist Resultant Force (N)
1	A	38	925	1019
2	B	74	1660	1021
3	C	94	2439	1415

DISCUSSION

As expected, the upper extremity loads increased with the increasing air bag aggressivity. For all tests, the humerus resultant bending moments were well below the established dynamic injury tolerance of 128 Nm and did not indicate a risk of humerus fracture (Duma, 1999). For air bag C the peak elbow load was 2439 N and peak resultant wrist load was 1415 N. While the dynamic injury tolerances for these joints are not well defined, it is anticipated that these loads are sufficient to result in the elbow in wrist injuries observed in similar cadaveric testing. This test data will allow the designer to minimize the risk of upper extremity injury while keeping the beneficial aspects of the side air bag.

REFERENCES

Duma, S., Crandall, J., Hurwitz, S., Pilkey, W., (1998), Stapp International Car Crash Conference.

Duma, S., Schreiber, P., McMaster, et al., (1999), Journal of Anatomy.

Duma, S., Boggess, B., Sieveka, et al., (2000), American Society of Biomechanics Conference.

Jaffredo, A., Potier, P., Robin, S., et al. (1998), International Research Council on the Biomechanics of Impact.

ROTATIONAL DISLOCATION PROPENSITY OF AN UNCONSTRAINED TOTAL WRIST IMPLANT

[1]Nicole M. Grosland [3]Renee D. Rogge [1,2]Thomas D. Brown [1,2]Brian D. Adams

[1]Dept. of Orthopaedic Surgery, [2]Dept. of Biomedical Engineering,
University of Iowa, Iowa City, IA
[3]Dept. Biomedical Engineering, Macon University, Macon, GA
E-mail: nicole-grosland@uiowa.edu, Web: poppy.orbl.uiowa.edu

INTRODUCTION

Post-operative dislocation has emerged as a common complication of unconstrained total wrist arthroplasty. A favorable implant design consists of a convex carpal component residing in a radial concavity. The concavity of the articulating radial surface, although designed to provide immediate stability when the components are inserted under appropriate tension (Menon, 1998), is relatively shallow. As a result, stability of the implant relies heavily on soft tissue balance. Due to the complexity and nonlinearity of the articular contact, it is difficult to appreciate the relationship between soft tissue induced tension and stability. The present investigation sought to analyze the propensity for rotational dislocation of a dual-curvature-radius unconstrained total wrist implant under varying compressive loads. Both computational and experimental analyses were performed.

METHODS

A three-dimensional finite element non-linear contact analysis was performed. CAD (Pro E) models were imported into PATRAN (version 8.5), enabling the FE meshes to be generated of each component, Figure 1. Each metallic component was modeled as a rigid body. The carpal and radial components were represented by 4-noded quadrilateral elements (6,710) and 3-noded triangular elements (1,366), respectively. The polymeric component was modeled via 20,130 8-noded hexagonal elements (E = 634.92 MPa, $\nu = 0.45$). An additional 14,370 elements were defined internally by ABAQUS 5.8 for contact purposes.

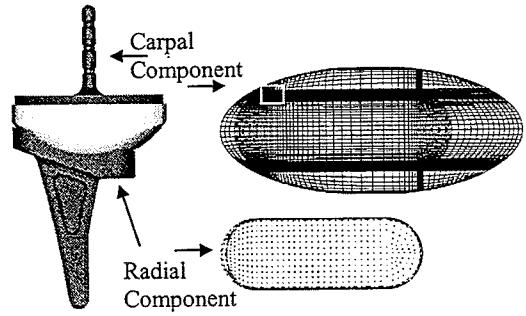

Figure 1: Dual-radius-of-curvature total wrist implant (a) CAD model in the neutral position, and (b) FE mesh of the articulating UHMWPE and radial surfaces. Note: Contact convergence required extremely high degrees of mesh refinement in regions of potential contact. The box highlights a region where the mesh density is ≈ 215 elements/mm^2.

Initiating in the 'neutral' position (Figure 1a), the radial component was free to translate in the radial-ulnar and volar-dorsal directions, while the carpal-poly complex was unconstrained along the vertical axis. A compressive load was maintained while the prescribed rotation (in increments of 0.1 degrees) was applied about a central axis parallel to the long stem of the carpal

component. The compressive load was varied between models from 10N to 110N, in 20N increments, to simulate various degrees of soft tissue tension. The poly-radial interface was assumed frictionless for modeling purposes.

Experimental validation was performed on a BIONIX 858 Test System (MTS). Initiating in the neutral position, the carpal component was rotated +45 degrees with respect to the radial component, after which it was swept back through the neutral position to an angle of –45 degrees, at a rate of 1 deg/sec. A x-y stage was used to provide the translational freedom to the radial component. Six replicate trials were performed for each of the six compressive loads (10N – 110N; 20N increments).

RESULTS

The computational and experimental resisting moments were in good agreement; Table 1. The results show an extreme sensitivity to rotational misalignment, even sub-degree rotations.

Table 1: Maximum Resisting Moments (Nmm): FE and Experimental.

LOAD	FE	Avg(+45)	Stdev	Avg(-45)	Stdev
10N	51.5	62.06	1.65	68.19	2.24
30N	149.4	139.56	1.61	159.13	1.84
50N	243.9	213.68	2.41	237.95	1.09
70N	334.6	308.70	8.33	342.07	7.52
90N	423.5	372.18	1.90	415.94	2.14
110N	509.5	447.81	1.35	501.83	3.73

Once neutral alignment was lost, there was a shift in the contact area, in terms of both position (Figure 2) and extent of engagement. This was further accompanied by an abrupt increase in peak contact stress.

DISCUSSION

Within the reasonably physiologic loading range explored, neither an identifiable efficacy threshold nor a point of diminishing return was observed in compressive load versus stability. Rather, a monotonic, almost linear relationship between axial load and resistance to rotational dislocation presented itself. The dislocation propensity associated with the rotational contact may be attributed to the high conformity of curvature between the convex UHMWPE surface and the concave radial surface. Enroute to achieving a convergent FE mesh, considerable effort went into obtaining an appropriate local zoning density. The shallow concavity of the radial component, coupled with its abrupt lip dictated the mesh of the UHMWPE component. Establishing a mesh, based on differing predicted regions of contact for differing geometries, can be awkward and computationally expensive for parametric design studies. Consequently, adaptive meshing procedures are very attractive for this class of problems.

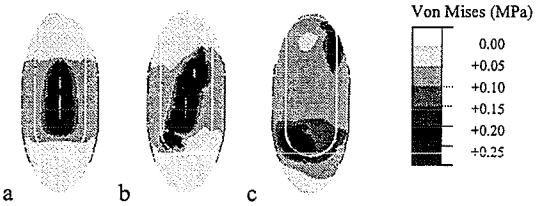

Figure 2: Von Mises (MPa) contour plots at (a) 0, (b) 0.3, and (c) 0.7 degrees rotation, for a 50N compressive load. The white oval delineates the perimeter of the articulating radial surface.

REFERENCES

Adams, B.D. (2000), *Seminars in Arthroplasty*, **11**(2), 72-81.

Menon, J., (1998) *J. Arthroplasty*, **13** (5), 515-523.

ACKNOWLEDGEMENTS

Financial support was provided by a NIH Grant AR-07075 and by Kinetikos Medical, Inc.

** Universal Total Wrist Implant, Kinetikos Medical, Inc., Size: Med., +2 poly.

THE EFFECT OF REMOVING BLOOD AND BONE OIL ON THE MECHANICAL STRENGTH OF CEMENT-BONE INTERAFACE

Shojiro Terashima[1], Takahiro Seki[2], Go Omori[2], Yoshio Koga[3], and Toshiaki Hara[4]
[1] Dept. of Mechanical & Control Eng., Niigata Institute of Technology, Niigata, JAPAN
[2] Dept. of Orthopaedic Surgery, Niigata University, Niigata,
[3] Dept. of Orthopaedic Surgery, Niigata Kobari Hospital, Niigata,
[4] Dept. of Mechanical & Control Eng., Niigata University, Niigata,
E-mail: george@mce.niit.ac.jp web: www.niit.ac.jp

Introduction:

Loosening is one of the major causes of late failures of total joint replacements. Almost all cases of loosening occur on the cement-bone interface. Therefore, loosening can be avoided by improving the mechanical strength of cement-bone interface.

We hypothesized that removal of blood and bone oil improves the mechanical strength of the cement-bone interface. In this study, using cancellous bone, we compared the mechanical shear strength of cement- bone interface with and without blood and bone oil.

Methods:

6 pairs of ox tibiae were used. Each proximal tibia was osteotomized 20mm below the medial plateau, and vertical holes (7.5 mm diameter) were drilled in the tibiae. Each cut surface was washed using palsatile lavage to clean out bone debris.

Two cases of experiment were carried out to investigate each influence of blood and bone oil. To examine the influence of remaining blood, one side of the 3 pairs of tibiae was soaked in a fresh human blood to simulate bleeding from the bone (*BLOOD+*), and the other side was left as it is (*BLOOD-*). Likewise, to learn the effect of removing bone oil, one side of the 3 pairs tibiae was cleaned using 1 percent aqueous surfactant used as food additive (*OIL-*), and the other side saline solution (*OIL+*).

Doughy cement (Simplex P) was injected into each hole using a caliber syringe under pressure. Then, 3 cross sections of 10 mm thickness were sliced off from the proximal tibiae, and each cylindrical cement buried in the bone plates was pushed-out by Instron mechanical test machine. The maximum load at failure was converted to an interface shear stress (ISS). 103 and 117 pieces of cylindrical cement were pushed to test the effect of blood removal, as the groups of *BLOOD+* and *BLOOD-*, respectively. Likewise, 139 and 121 pieces of cement were used to test the effect of oil removal using surfactant, as *OIL-* and *OIL+*.

Results:

The ISS (means ± 1 S.D.) of the result of with and without blood is shown in the Figure 1. The ISS of *BLOOD+* and *BLOOD-* were 2.3(1.1) MPa and 2.7(1.3) MPa, respectively, so the ISS of *BLOOD-* shows an increase of 18 percent as compared with *BLOOD+*. Figure 2 shows the results of *OIL+* and *OIL-*. The ISS of *OIL+* was 2.6(1.5) MPa, and *OIL-* was 3.8(1.9), so the ISS of *OIL-* shows an increase of 46 percent as compared with *OIL+*. Statistically significant differences were found in the ISS between *BLOOD+* and *BLOOD-* ($p<0.01$, Student's t-test), and *OIL+* and *OIL-* ($p<0.0001$, Welch's t-tset). Removal of blood

BIOMECHANICAL COMPARISON OF FIXATION STABILITY OF 4 TYPES OF ROTATOR CUFF REPAIR TECHNIQUES

Andrew Mahar[1], Charles Pettit[2], Robert Boswell[2] and Robert Pedowitz[2]

[1]Orthopedic Biomechanics Research Center, Children's Hospital – SD, San Diego, CA, USA
[2]Department of Orthopaedics, University of California – SD, San Diego, CA, USA
Email: amahar@chsd.org

INTRODUCTION

New techniques and devices are continually being developed for use in rotator cuff repairs. Previous biomechanical studies evaluating the efficacy of such developments have tested single load to failure and axial pullout tests. Neither of these testing scenarios simulates the typical post-surgery loads on the repair or direction of physiologic loading. Therefore, little biomechanical data exists that can be used with any level of clinical relevance. A better understanding of which devices or techniques are the most stable under cyclic, sub-maximal loads can help clinical decision making when considering type and location of tear, patient's age and activity level. A study was undertaken to compare a new bio-absorbable poly-L lactic acid screw to several common surgical devices when tested under physiologically representative loads and directions.

METHODS

Twenty, 12-week old bovine shoulders were divided equally between four repair groups (Table 1).

Table 1: Repair method for each group (n=5)	
Group 1	2 PLLA screws + toothed washers
Group 2	2 single armed suture anchors
Group 3	2 double armed suture anchors
Group 4	2 horizontal mattress sutures

The same surgeon performed each repair using standard repair techniques for the BIONX BioCuff screw placement (Bionx, Inc., Tampere, Finland) and Super QuickAnchor Plus sutures anchors (Mitek Surgical Products, Westwood, MA). Right and left shoulders were randomly assigned among groups. The shoulders were dissected leaving the infraspinatus tendon insertion intact while all other soft tissues were removed. The proximal humerus was sectioned and potted in two-part epoxy resin (Bondo-Marhyde, Atlanta, GA). A 2" wide by 1" long defect was artificially created and repaired under direct vision. Each shoulder was mounted in a custom designed fixation rig. The tendon was secured in a serrated clamping device that held approximately 1.5 inches of tendon with another 4 inches between the clamp and the tendon's insertion. The loading tests pulled on the tendon in a direction perpendicular to the insertion angle of screws/anchors. This was representative of the physiologic loading direction of the human rotator cuff. An MTS machine (Eden Prairie, MN) applied a cyclic load test between 10 and 180N over 5 seconds. This was repeated for a maximum of 2500 cycles at which point the test was stopped if failure had not been reached. Failure was indicated at 5mm and 10mm of axial displacement of the repaired tissue measured directly with digital calipers. Number of cycles to failure at 5mm and 10mm were averaged and compared

between treatment groups using a one-way ANOVA ($p<0.05$) and Tukey's post-*hoc* comparison when significant differences were found.

RESULTS AND DISCUSSION

The performance for each repair technique is shown in Table 2. Failures were noted to occur as tissue pullout through the screws or anchors, although instances of suture breakage in the single and double armed anchor groups were noted. There were no instances of screw or anchor breakage.

	5mm	5mm	10mm	10mm
	Mean	SE	Mean	SE
Group 1	**1111**	449.6	**2070.3**	430
Group 2	39	19.6	212.2	81.7
Group 3	40.2	17.6	800.8	234.6
Group 4	30.4	16.9	851.6	296.6

The shoulders repaired with two PLLA screws and toothed washers demonstrated a significantly greater number of cycles to failure at 5mm during sub-maximal cyclic loading ($p=0.008$). There were no differences between repair types for the simple sutures or mattress sutures. The PLLA screws also had a greater number of cycles to 10mm of failure during sub-maximal cyclic loading compared to the other repairs ($p=0.003$). There were no differences in number of cycles to failure at 5 and 10mm between repair types for the simple sutures or mattress sutures. The performance for Groups 2-4 was very similar to 5mm of failure. However, the number of cycles to 10mm of failure showed trends where greater surgical complexity of repair was indicative of a greater number of cycles to failure. There were no differences between Groups 2-4 in number of cycles to failure at 10mm due to high standard errors. These higher errors can be associated with small differences in the surgical repair. This is influential since clinical interpretation of a successful repair may not be sensitive enough to detect failure potential while biomechanical information indicates that even small surgical differences in the repair influence strength and durability.

In four out of five specimens repaired with PLLA screws, the maximum number of cycles (2500) was attained while no other repair reached this level. These data obtained for Groups 2-4 were similar to data reported previously for cycles to failure at 5 and 10mm for simple suture repairs.

SUMMARY

Poly-L lactic acid screws with toothed washers may provide more stable fixation than single armed suture anchors, double armed suture anchors or mattress sutures during the immediate post-operative period. Due to a possible greater stability provided by PLLA screws, a more aggressive rehabilitation protocol may be used.

REFERENCES

Barber, F.A., et al. (1993). *Arthroscopy,* **9(6)**, 647-652.

Barber, F.A., et al. (1997). *Arthroscopy,* **13(3)**, 340-345.

Burkhart, S.S., et al., (1997). *Arthroscopy,* **13(6)**, 720-724.

Goradia, V.K., et al., (2000), *Proceedings of the Arthroscopy Association of North America*, 106.

ACKNOWLEDGEMENTS

Support was provided by Bionx, Inc.

NANOINDENTATION OF POLYETHYLENE TIBIAL COMPONENTS

S. Woodard[1], L. Riester[2], A. Eberhardt[1]

[1]Department of Biomedical Engineering, University of Alabama at Birmingham, Birmingham, AL
[2]Oak Ridge National Laboratory, Oak Ridge, TN
E-mail: woodas04@eng.uab.edu

INTRODUCTION

Delamination is a common failure mechanism in ultra-high molecular weight polyethylene (UHMWPE) tibial inserts [Wright and Rimmnac, 1988]. Changes in polyethylene mechanical properties, such as subsurface embrittlement due to oxidation, may promote crack propagation. The assessment of through-thickness properties may, therefore, provide insight into delamination mechanisms. Using the small punch test [Kurtz et al., 1997], researchers have studied changes in subsurface mechanical properties in aged and unaged tibial components [Edidin et al., 1999; Ely et al., 2000]. In this present study, we used nanoindentation to measure stiffness and hardness profiles in cross sections of unused polyethylene tibial components. Nanoindentation has previously been used to characterize surface properties of UHMWPE [Schmidt et al., 2000].

MATERIALS AND METHODS

Preliminary work focused on specimen preparation and the establishment of optimal nanoindentation parameters. UHMWPE tibial inserts of unknown origin were used for this purpose. Samples were cut from the tibial plateau and the cross sections microtomed to eliminate surface roughness. Nanoindentation was first performed on specimens as microtomed. Other specimens were polished using a technique developed at Oak Ridge National Laboratory (ORNL) for this project (Table 1).

Table 1. Polishing protocol for UHMWPE specimens

Abrasive	SiC paper	Diamond	Diamond
Grain Size	800, 1200, 2400, 4000	3 micron	3 micron
Lubricant	Water	DP-LUB	DP-LUB
Speed (rpm)	150	150	150
Force (N)	20	30	25
Time (min)	1 for each grain size	10	5

Nanoindentation was performed at the ORNL High Temperatures Material Laboratory using a Nanoindenter II (MTS/Nano Instruments, Oak Ridge, TN). In the preliminary tests, the nanoindenter was operated using the continuous stiffness method [Oliver and Pharr, 1992] with a Berkovich indenter at a rate of 20 nm/s to a maximum depth of 400 nm. The load was held for 15 seconds while contact stiffness was measured, then the specimen was unloaded to 80% for measurement of thermal drift. Five indents were made at each location, from which average properties were determined. This was done every 200 μm across the entire cross-section.

The results of the preliminary work demonstrated that the ORNL polishing protocol adequately prepared the UHMWPE specimens for nanoindentation. Furthermore, nanoindentation using the Berkovich indenter in continuous stiffness mode provided repeatable indentation measures for UHMWPE.

Mechanical properties of samples cut from two unused UHMWPE tibial inserts were then measured using nanoindentation. The first was a machined isostatically molded

1900H component. The second was a direct compression molded 1900H component. Both had been sterilized with gamma irradiation (25-40 kGy, in argon) in December 1995 and February 1996, respectively. They had been subsequently packaged in an argon environment and remained sealed until they were removed for sectioning. Cross sections were microtomed and polished, and nanoindentation was performed using the Berkovich indenter in continuous stiffness mode, as described previously.

RESULTS

Profiles of stiffness, modulus, and hardness were obtained from the nanoindentation experiments. Figure 1 shows an example plot of stiffness versus depth through three cross sections of the machined isostatically molded 1900H component. The figure shows increases in stiffness from the surface to depths of 0.5 - 1 mm, followed by a decline in stiffness to approximately 3 mm below the surface. Here, samples 1 and 2 both show a trend of increasing stiffness with increased depth, while the third specimen stiffness remained low. Hardness and modulus profiles revealed similar trends.

DISCUSSION

The subsurface elevations in stiffness and hardness reported here are consistent with observations of subsurface peaks in oxidation levels at 1-2 mm beneath the surface [Sutula et al., 1995]. Further characterization of oxidation levels should be performed to validate this conjecture.

The results of the present study suggest that nanoindentation may provide an alternative to the small punch test [Kurtz et al., 1997] to examine the through-thickness characteristics of polyethylene components. The technique may be used in future studies to examine variations in mechanical properties associated with shelf-aging, accelerated aging and delamination wear.

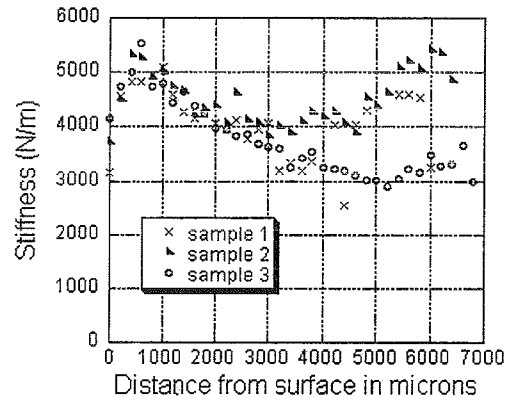

Figure 1. Stiffness vs. depth beneath the surface for machined isostatically molded 1900H component.

REFERENCES

Edidin et al., *Trans. 45th ORS,* 74, 2000.
Ely et al., *Trans. 46th ORS,* 558, 2000.
Kurtz et al., *Biomaterials,* **18**(24), 1659-1663, 1997.
Oliver and Pharr, *J Mat Res,* 7(6), 1564-1583, 1992.
Schmidt et al., *Proc Soc. Biomats.,* 1255, 2000.
Sutula et al., *Clinical Orrthpedics,* **319,** 28-40.
Wright and Rimnac, *JBJS,* **70**(9) 202-208, 1998.

ACKNOWLEDGEMENTS

The authors acknowledge the support of Biomet, Inc., and the technical assistance of Joel Higgins and Dave Schroeder.

ACL STRAIN DURING SIMULATED FREE-SPEED WALKING

Li-Qun Zhang [1-4], Jay M. Minorik [3], Fang Lin [1,2],
Jason L. Koh [3], Mohsen Makhsous [1,2], and Zhiqiang Bai [1,2]

[1]Sensory-Motor Performance Program, Rehabilitation Institute of Chicago
Departments of [2]Physical Medicine & Rehabilitation, [3]Orthopaedic Surgery, and
[4]Biomedical Engineering, Northwestern University Chicago, Illinois
Email: l-zhang@northwestern.edu

INTRODUCTION

The anterior cruciate ligament (ACL) is an important structure in controlling knee joint stability. ACL injuries disrupt the delicate balance of knee structures and may affect knee functional activities. ACL deficient subjects may reprogram their muscle activations and alter knee kinematics to compensate for the injury. Development of the compensatory mechanism is closely related to the role of ACL in stabilizing the knee. Although it seems clear that ACL is loaded in strenuous activities like inward cutting and running[2,3], it is not clear whether the ACL is loaded during moderate activities like walking and whether compensation is needed. Considering the essential importance of walking, it is important to evaluate ACL loading during locomotion and better understand the compensatory mechanisms. The purpose of this study was to evaluate the ACL strain during simulated walking using a cadaver model, with the knee placed at various axial rotation and anteroposterior translation positions.

METHODS

Fresh frozen knee specimens were used to evaluate ACL strain during walking. After exposing the ACL through a parapatellar incision on the specimens, a MicroStrain? DVRT transducer was sutured onto the anteromedial band of the ACL with appropriate initial positioning. The femoral intercondylar notch was enlarged to avoid potential impingement of the DVRT against the intercondylar notch[1]. After closing the cut, the knee specimen was mounted onto an experimental apparatus (Fig. 1). The femur was fixed rigidly to the frame. The tibia was fixed to an attachment mechanism, which was driven by a servomotor. The tibial attachment mechanism provided adjustment of tibial abduction, flexion, axial rotation, and three orthogonal translations of the tibia relative to the femur. A six-axis force sensor was used to measure the forces and moments exerted onto the tibia, and precision potentiometers were used to measure tibial rotations and translations. A position sensor was placed on the patella to measure patellar tracking. Ropes were sutured to individual muscles crossing the knee (vastus medialis oblique, vastus medialis longus, vastus intermedius, rectus femoris, vastus lateralis, gracilis, sartorius, semitendinosus, semimemberanosus, long and short heads of the biceps femoris, and IT band) through fiberglass mesh. Ropes and pulleys were used to load the muscles according to the muscle physiological cross sectional area. Only the ACL strain during simulated walking is analyzed here.

Average knee flexion pattern during free speed walking obtained from 30 normal subjects was used to control the servomotor and simulate walking on the cadaveric knee. About 13 "strides" were repeated in each 16 sec long trial. The test was repeated with the tibia placed at difference axial rotation (-7°, 0°, and 7° internal rotation) and anterior-

posterior translation (-10mm, neutral, and 10mm) positions.

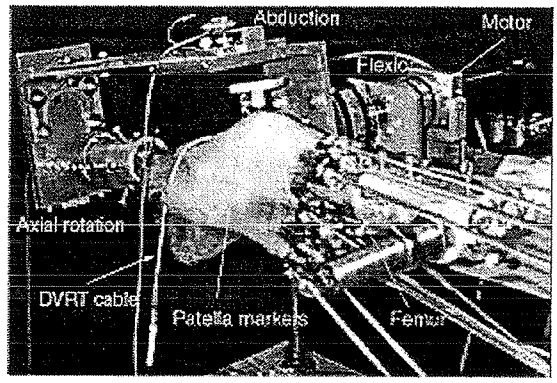

Figure 1: Experimental setup.

RESULTS AND DISCUSSION

The ACL strain varied systematically with knee position during the simulated "walking". The ACL was loaded considerably during "free-speed walking" and the largest strain was observed at full knee extension (Fig 2). Furthermore, the ACL strain increased markedly with tibial internal rotation and anterior translation (Fig. 2). On the other hand, tibial external rotation and posterior translation reduced the ACL strain substantially (fig. 2). Over a trial, the strain variation was usually larger during the first stride and became smaller and more repeatable afterwards.

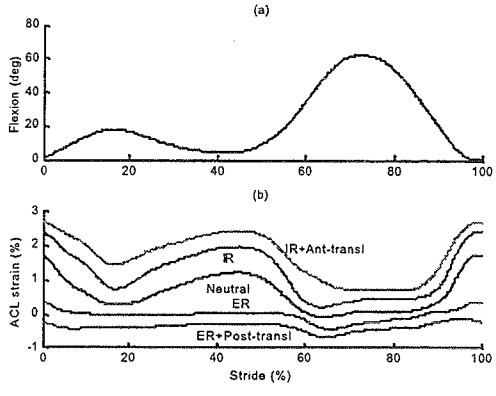

Figure 2: ACL strain during simulated "free-speed walking" using a cadaver model. (a) Knee flexion as a function of stride %; (b) ACL strain during simulated "free-speed walking", averaged over 48 strides. From top to bottom, the five curves represent the ACL strain with the tibia positioned at internal rotation (7°) plus anterior translation (10 mm), internal rotation (7°), neutral, external rotation (7°), and external rotation (7°) plus posterior translation (10 mm), respectively.

SUMMARY

The present study provided us a useful tool to evaluate ACL loading in well-controlled and systematically varied patterns. The cadaver setup also provided the flexibility of evaluating ACL strain under conditions that were difficult to implement in an in vivo setup (e.g., ACL strain at full knee extension). The results show that the ACL is loaded considerably during free-speed walking, indicating the need for compensation for ACL deficiency during locomotion. Since internal rotation of the tibia loads the ACL strongly[4], one compensatory mechanism adopted by ACL deficient subjects is to externally rotate the tibia relative to the femur to avoid loading a partially torn ACL and/or to avoid unstable knee positions[5]. Further work needs to be done to test a larger sample at systematically varied knee positions in 3-D space.

REFERENCES

1. Arms, S.W. et al. (1984). *Am J Sports Med,* **12**, 8-18.
2. Beynnon, B.D., Fleming, B.C. (1998). *J. Biomech.*, **31**, 519-525.
3. Beynnon, B.D. et al. (1995). *Am. J. Sports Med.*, **23**, 24-34.
4. Markolf, K.L. et al. (1995). *J. Orthop. Res.*, **13**, 930-935.
5. Zhang, L-Q. et al. (1998). *Gait & Posture,* **7**, 156.

HIERARCHICAL CLUSTER ANALYSIS OF AREA AND LENGTH OF FOOT AND ANKLE LIGAMENTS

Chimba Mkandawire[1], William Ledoux[1,2], Bruce Sangeorzan[1,2] and Randal Ching[1,2]

[1]Center of Excellence for Limb Loss Prevention and Prosthetic Engineering, Puget Sound VA, Seattle, WA, USA
[2]Department of Orthopaedics, University of Washington, Seattle, WA, USA
E-mail: bluntme@u.washington.edu Web: http://rehabctr.vamc.washington.edu/

INTRODUCTION

A computational model of the human foot and ankle has been developed by our research group (Ledoux 2000) to assist in treatment of diabetic foot ulcers. The model currently includes 51 ligaments, with each ligament modeled as a spring and dashpot in parallel. Materials testing has been conducted on ankle ligaments (Funk 2000, Siegler 1988) and little work has been done on foot ligaments. Thus, mechanical properties for the 51 modeled ligaments were extrapolated from Siegler's ankle ligament data (1988). We hypothesize that the mechanical properties of a representative sample of ligaments, based on similar area and length relationships, can be used to predict the properties of all ligaments in our computational model. The purpose of this research was to identify such groups for mechanical testing.

METHODS

Ligament geometry was obtained from the right foot of the female specimen of the NIH Visible Human Project (National Library of Medicine, Bethesda, MD). Digital image analysis software (NIH Image, National Institutes of Health, Bethesda, MD) was used to identify the three-dimensional cross-sectional area and length from the anatomical image set. Resolution in the plane of each microtome was 0.33 mm, with 0.33 mm slice thickness.

Thirty-nine of the 51 ligaments in our model were clearly identified with distinct origins and insertions. Morphology calculations were based on whether ligaments were normal or parallel to the imaging plane. For bifurcated or fasciculated ligaments, an average area and length was calculated.

Ligaments unparallel to the imaging plane. Five ligament sections were used to measure area and length: origin, insertion, and three evenly-spaced intermediaries. Overall length was determined from a cubic spline of five cross-sectional centroids using Igor Pro (WaveMetrics, Inc., Lake Oswego, OR). Area was averaged over five locations, corrected by the angle between the ligament axis and the imaging plane.

Ligaments parallel to the imaging plane. Over the entire thickness of the ligament, two insertion and two origin positions were identified every third slice, measured at one millimeter intervals. This produced a stacked series quadrilateral ends from which the areas and lengths were measured. Two additional midpoints were used for ligaments that followed a curved path.

A hierarchical cluster analysis was performed using SPSS 7.5 (SPSS Inc., Chicago, IL) to group ligaments based on their area and length.

RESULTS

Table 1 lists the ligaments (as labeled by Sarrafian 1993) examined with their

measured cross-sectional area, length and cluster grouping.

Table 1: Ligament Morphology & Grouping

Ligament	Area	Length	Cluster
IntMet4Met5	86.68	1.90	1
IntMet1Met2	54.71	2.22	2
IntCun2Cub	32.55	2.85	3
AntDorCun3Cub	7.52	1.18	4
PostTibTal	59.62	10.75	2
DorMet3Met4	37.07	6.99	3
AntTibTal	24.26	6.73	3
MedTalCal	14.91	4.74	4
PosDorCun3Cub	13.80	4.92	4
IntCubNav	14.01	5.05	4
DorTalNav	35.15	16.62	3
FirPlaCun1Met1	19.35	13.26	3
Cervical	21.47	15.50	3
LatCalNav	9.23	6.76	4
PosTalCal	14.96	11.55	5
AntTalFib	15.28	11.99	5
DorLatCalCub	10.28	9.54	4
TibNav	34.84	33.22	6
DorCubNav	13.10	12.54	5
DorCun3Nav	11.61	12.21	5
MedCun1Met1	25.86	27.65	6
InfCalNav	13.98	14.99	5
CalFib	7.60	8.24	4
MedCalCub	7.16	8.40	4
IntCun2Met2	9.76	12.72	5
DorCun1Met2	10.23	14.04	5
PlaCun1Nav	12.59	19.00	7
TibCalc	19.18	29.79	7
PosTalFib	13.50	21.44	7
DorCun2Nav	10.33	17.27	5
SupMedCalNav	16.82	29.16	7
DorCun2Met2	11.19	20.81	7
DorCubMet5	10.85	20.83	7
PlaCun3Nav	7.12	14.18	5
PlaCun2Nav	8.10	16.93	5
FirDorCun1Met1	12.86	30.06	7
LatTalCal	6.84	16.29	5
PlaCun3Met3	8.41	20.86	7
DorCun1Nav	6.46	27.80	7

Figure 1 shows the results of the cluster analysis, where the average area, length and stiffness data from Siegler (1988) is overlaid with the calculated cluster centers.

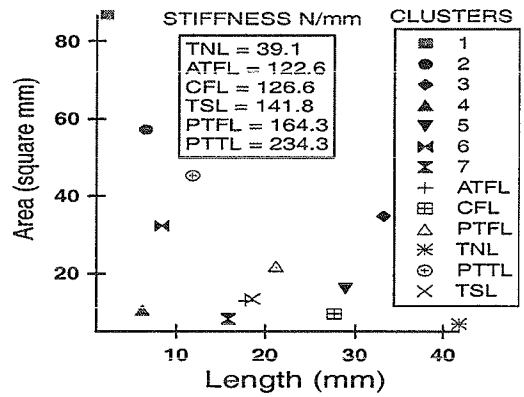

Figure 1: Cluster analysis centers (1-7) overlaid with Siegler stiffness data (1988).

DISCUSSION

Linear elastic theory predicts that ligament stiffness is proportional to area and inversely proportional to length. Figure 1 illustrates that Siegler's data (1988) follows an expected distribution. Namely, four tightly clustered ligaments with similar stiffness values, one long and thin ligament with a small stiffness, and one short ligament with a large area and large stiffness. In conclusion, the results of this study will enable us to reduce the overall number of biomechanical ligament tests.

REFERENCES

Funk J.R., Hall G.W. (2000). et al. *J Biomech Eng.* 122(1):15-22.

Ledoux, W., Camacho D., et al. (2000). The World Congress on Medical Physics and Biomedical Engineering, Chicago, USA.

Sarrafian, S. K. (1993). *Anatomy of the Foot and Ankle.* J.B. Lippincot Co.

Sasaki N., Odajima, S. (1996). *J Biomech.* **29**(5):655-8.

Siegler S., Block J., et al. (1988). *Foot & Ankle.* **8**(5):234-242.

ACKNOWLEDGMENTS

This work was funded by a VA Associated Health Pre-Doctoral Rehabilitation Research Fellowship.

ANGULAR ROTATIONS OF THE ACETABULAR FRAGMENT FOLLOWING THREE SURGICAL TECHNIQUES FOR CORRECTION OF CONGENITAL DEFORMITIES OF THE HIP

Andrew Mahar[1,2], Afshin Aminian[2], Walid Yassir[2], Dennis Wenger[2]

[1]Orthopedic Biomechanics Research Center, Children's Hospital – SD, San Diego, CA, USA
[2]Department of Orthopedic Surgery, Children's Hospital – SD, San Diego, CA, USA
Email: amahar@chsd.org

INTRODUCTION

Deformities of the hip joint in the adolescent and young adult are commonly treated with periacetabular osteotomies that allow for greater contact and congruency between the acetabulum and the femoral head. The primary goal of these surgeries is to move the acetabular fragment anteriorly and laterally to address the problem of hip subluxation and dislocation. Optimal coverage is designated as twenty degrees of anterior and twenty degrees of lateral rotation. Two dimensional radiographic data does not provide a clear description of the complex three-dimensional motion associated with the acetabular osteotomy fragment. The purpose of this study was to compare three types of surgical procedures for acetabular osteotomies to determine which provides the greatest range of motion (ROM) in flexion, abduction and external rotation.

METHODS

The osteotomies performed were the Bernese periacetabular osteotomy of Ganz and Carlioz' and Tonnis' modifications of Steel's triple innominate osteotomy. The Bernese osteotomy is recognized as posing significant technical challenge, while various modifications of the triple innominate osteotomy enjoy widespread use. These were undertaken as described in the literature. The Ganz osteotomy preserves the posterior acetabular column, while the Carlioz preserves the ligamentous attachments of the acetabular fragment to the posterior column (sacrospinous and sacrotuberous). Sectioning the sacrospinous ligament from the ischial spine converts the Carlioz osteotomy into the Tonnis osteotomy.

Six human cadavers were dissected from the lumbar spine through the mid-femur. Muscular tissue was removed from each specimen while keeping the hip joint capsule and ligamentous structures intact. External fixation devices were used to fix the femoral shafts to the pelvis. This was required for specimen stability during testing. The femurs were fixed in a rig that generated approximately eight degrees of anterior pelvic tilt to simulate quiet standing. Surgical procedures were randomized to right and left sides for each pelvis. Nine millimeter retro-reflective markers were placed on each anterior superior and posterior superior iliac spines as is typical when collecting gait data. Three markers were also attached to each fragment area to generate embedded coordinate systems. Static data prior to surgery were captured at 30Hz for 5 seconds using a three-camera Qualisys motion measurement system (Glastonbury, CT).

Each fragment was tested in maximal flexion, maximal abduction and maximal external rotation. Kinematic data were

smoothed with a five point moving average filter. Static orientations were subtracted from the dynamic motions to determine accurate ranges of motion. Peak rotations were calculated and averaged across treatments. Data were analyzed using a one-way ANOVA and followed by a Tukey's *post-hoc* evaluation when significant differences were found.

The Tonnis group was also analyzed to determine the effect of the sacrospinous ligament on restricting motion. Motion data for each test were collected at 30Hz for 20 seconds and a minimum of three cycles of range of motion (ROM) data were used for analysis.

RESULTS/DISCUSSION

The Ganz procedure produced significantly greater ($p<0.01$) flexion ROM ($58.2\pm26.6°$) than the Carlioz ($17.5\pm6.0°$) and the Tonnis ($41.2\pm14.7°$) techniques. The Tonnis technique was also significantly greater ($p<0.01$) than the Carlioz technique in flexion. The Ganz procedure produced significantly greater ($p<0.01$) abduction motion ($17.6\pm14.6°$) than either the Carlioz ($3.8\pm1.9°$) or Tonnis ($6.7\pm3.1°$) techniques which were statistically similar. The Ganz procedure produced statistically equivalent external rotation ($16.1\pm8.5°$) when compared to Carlioz ($10.4\pm5.3°$) and Tonnis ($17.3\pm9.4°$) procedures. However, the Tonnis technique was significantly greater than the Carlioz technique ($p<0.03$). It is important to note that while maximum angles were achieved during the imposed motions, these motions did not occur discretely. Coupled motions were seen in some cases but most frequently with the Carlioz technique (Figure 1). The insertion angle of the sacrospinous ligament restricted motion and generated large external rotations during tests of flexion and abduction.

Figure 1: Coupled motions during flexion test

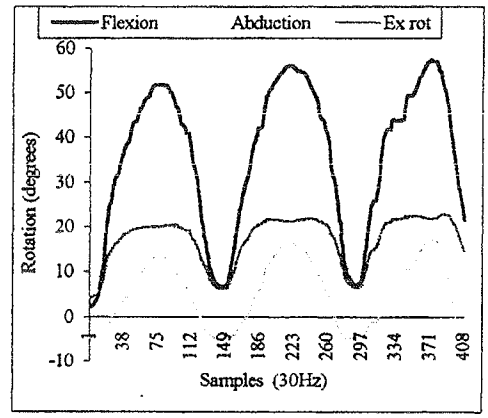

SUMMARY

The technical challenge of the Ganz procedure makes surgical alternatives attractive. If these alternatives do not achieve the desired '20/20' degrees of anterior and lateral coverage, then their usefulness is limited. These data show that although the Tonnis technique may not generate the same maximal angular range of motion that a Ganz procedure does, it satisfies the '20/20' criterion. Further study as to the instability due to the sectioned sacrospinous ligament is necessary.

REFERENCES

Ganz, R, et al. (1988) *Clinical Orthopedics,* **231**, 26-36.

Tonnis, D. (1981) *J Pediatric Orthop.*, 1:241-249.

ACKNOWLEDGEMENT

This research was financially supported by the Children's Hospital Orthopedic Research Foundation.

IMPACT CHARACTERISTICS OF COCONUT COIR

Sharon E. Sonenblum[1] and Joseph J. Crisco[1,2]
[1]Division of Engineering, Brown University, Providence, RI
[2]Department of Orthopaedics, Brown University, Providence RI
E-mail: Sharon_Sonenblum@Brown.edu

INTRODUCTION

The coconut is the fruit of the *Cocos nucifera*, a tropical plant of the *Arecaceae (Palmae)* family. While found predominantly in Sri Lanka and India, it is cultivated in over 85 countries. These palm trees can grow to heights of over 100 feet, requiring the nut to survive tremendous falls. Various sources suggest that the husk, composed of ligin and cellulose based coir fiber and coir pith serves as a defense mechanism to protect the nut during that fall. The aim of this study was to evaluate the energy absorption properties and compare them to manmade materials designed to absorb impact energy. Peak accelerations over multiple impacts and various drying times were compared.

METHODS

Eight intact coconuts were acquired, of which 6 were cut into thirds (approximately 4x4" sections), known as *transverse samples* and 2 were cut in half and will be referred to as *half samples*. The inner nut and meat were removed. The transverse samples were tested at various states of dryness (Day 0, 8, 25).

For the transverse samples, the test apparatus used was a twin wire drop frame utilizing a spherical impactor and a half-inch 56 Shore A rubber pad (MEP). The combined weight of the spherical impactor and flying arm was approximately 5.0 kg. For the half coconut samples, the MEP pad was replaced with a flat, metal anvil. A triaxial accelerometer located at the center of the spherical impactor provided acceleration data, sampled at a rate of 20 kHz. Data acquisition and analysis was performed with LabView 5.0 software. The impactor was dropped from a height of approximately 0.7 meters (to correspond to a velocity between 3.88 and 4.04 m/s) at intervals of 60 seconds. All transverse coir and Brock Foam (Brock USA, Boulder, CO) samples were kept at room temperature and secured to the MEP to ensure a repeatable impact location. Half samples were tested following the procedure described in EN 967 for the certification of Ice Hockey Helmets. Samples were attached to the spherical impactor and dropped onto the flat surface. This test procedure was also performed with a child's bicycle helmet constructed of expanded polystyrene. Peak acceleration values were acquired for each impact. The peak acceleration of the spherical impactor directly impacting the MEP was 250±0.5 g's.

Table 1: Specifications of transverse coir samples and the commercially available material.

	Thickness (cm)	Avg. Density (g/cm^3)
Brock	1.4	0.05
Coir Day 0	1.9 (1.1-2.5)	0.6
Coir Day 8	1.7 (0.6-3.2)	0.4
Coir Day 25	1.3 (0.6-1.9)	0.5

The significance of the effects of time and multiple impacts on the performance of the transverse samples were determined using a repeated measures ANOVA with a Bonferroni multiple comparison post-hoc test.

RESULTS

Day 0 transverse samples reduced the peak acceleration of the direct MEP impact by an average of 39% on their first impact. After multiple impacts and as the samples dried, impact performance decreased. The mean peak accelerations for the transverse samples increased after the first and second impacts, then tended to be constant after the third impact (Figure 1). The peak acceleration on the fifth impact was significantly ($P<0.01$) greater than that on the first impact by approximately 27% for Day 0 transverse samples. At Day 8 and Day 25, the average peak acceleration also increased significantly ($P<0.01$) by 55% and 42% over the first impact, respectively.

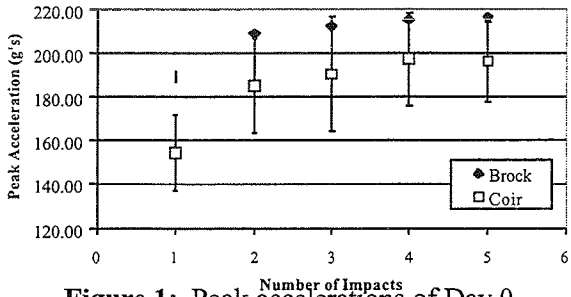

Figure 1: Peak accelerations of Day 0 transverse coir samples and Brock sample.

When considering the impact performance with time, the response differed for the first impact and the fifth impact (Figure 2). As the samples dried, there was no change in response of the transverse samples' first impacts. However, the performance on the fifth impact significantly ($P<0.01$) decreased by about 25% with time.

In the laboratory test, the half samples would have passed one aspect of the hockey helmet standard, as the peak acceleration was 178 ± 36 g for three impacts, which is below the 300 g threshold used to certify ice hockey helmets.

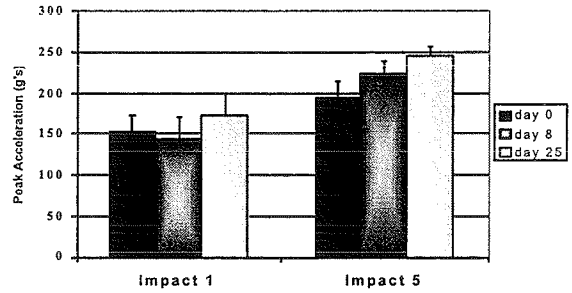

Figure 2: Peak accelerations of Day 0, 8, and 25 transverse coir samples for impacts one and five.

DISCUSSION

We have measured the impact response of coconut coir over a 25-day time span and multiple impacts. As the coir dries out, the shape and mass change significantly, which may contribute to the increasing acceleration with multiple impacts on the transverse samples.

While the aforementioned results demonstrate the energy absorption properties of coir, it is possible that coir evolved rather as a flotation device or as protection from animals and rotting prior to seedling growth (Gonzalez and Vista, 1914). Processing and weaving could certainly be formulated to improve performance, but even straight out of the supermarket coir compares favorably with modern man-made energy absorbing materials.

REFERENCES

European Standard, BS EN 967 : 1997

Gonzalez, B.M. and Vista, T.N, *Philippine Agriculturist and Forester*. (1914) **3**, 25 and (1915) **4**, 105.

ACKNOWLEDGEMENTS

Funding was provided in part by the Undergraduate Teaching and Research Assistanceship (UTRA) at Brown University, Providence, RI. The technical assistance of Dave Spenciner and James Paiva is acknowledged.

THE EFFECT OF PROLONGED STATIC AND CYCLIC STRETCHING ON ANKLE JOINT STIFFNESS IN HUMANS WITH SPASTICITY

Eadric Bressel [1] and Peter J. McNair [2]

[1] Biomechanics Laboratory, Utah State University, Logan UT, USA
[2] Neuromuscular Research Unit, Auckland University of Technology, Auckland, New Zealand
E-mail: ebressel@coe.usu.edu

INTRODUCTION

Spasticity is a broad neurological term that describes common features seen in patients with cerebral palsy and cerebral-vascular accidents. Patients with spasticity often exhibit exaggerated stretch reflexes, impaired walking ability, and increased resistance to passive joint movement. In regard to these impairments, the approaches to treatment often include drug therapy, which may have undesirable side effects, and prolonged static stretching, which has shown favorable results (Tremblay et al., 1990). Concerning stretching, researchers have shown that continuous passive motion (i.e., cyclic stretching) of the ankle joint is more effective than static stretching at reducing passive ankle joint stiffness in non-spastic people (McNair et al., in press). Cyclic stretching has been a widely accepted approach for rehabilitation of orthopedic problems, yet few studies have considered its application in neurological disorders. Therefore, the purpose of this study was to compare in a spastic population the short-term effect of prolonged static and cyclic calf stretching on passive ankle joint stiffness.

METHODS

Ten community dwelling individuals (9 male, 1 female) medically diagnosed with spasticity due to a cerebral-vascular accident were asked to volunteer for this investigation (M_{age} = 64.6 ± 8.8 yrs). The study design required participants to engage in one 30 min static stretch held at 80% of the participants' maximal passive dorsiflexion angle, and one 30 min cyclic stretch that consisted of continuous ankle joint motion between neutral (10° of plantar flexion) and 80% of the participants' maximal passive dorsiflexion angle. The angular velocity of the foot segment was 5°/s. Stretches were completed on separate days, randomly assigned, and performed on their spastic lower extremity using a KinCom® isokinetic dynamometer that was set-up according to Figure 1.

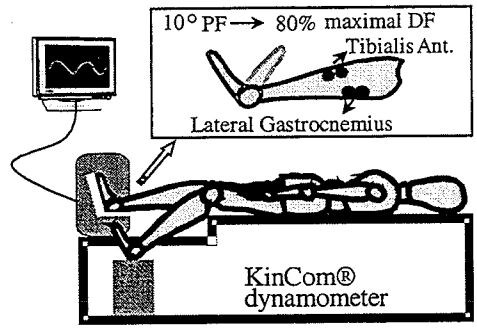

Figure 1: Experimental set-up for stretch treatments

The computerized dynamometer was programmed to manually move the foot according to the stretching protocols and to collect torque and angle measures simultaneously. Electromyographic (EMG) signals from muscles tibialis anterior and lateral gastrocnemius were recorded during each stretch to determine the contribution of

the stretch reflex to the stiffness measures. Raw EMG signals were analyzed with a root mean square value and normalized to reflect a percentage of maximal voluntary contraction. Ankle joint stiffness was calculated from the change in torque divided by the change in angular displacement during the movement of the foot segment into dorsiflexion (Figure 2). Stiffness values were quantified before and immediately after each condition.

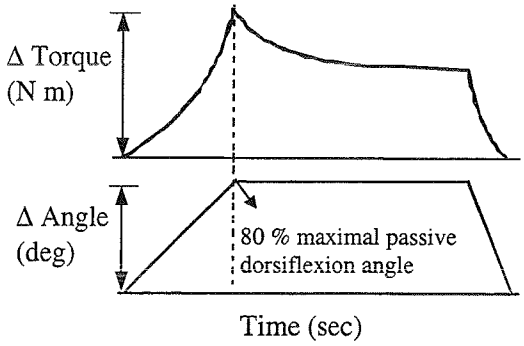

Figure 2: Schematic representation of the stiffness measure

Mean stiffness and EMG values between and within conditions were assessed with a multivariate test and follow-up univariate statistics with the probability of Type I error set at .05.

RESULTS AND DISCUSSION

Ankle joint stiffness values were significantly decreased after the static and cyclic stretches. No differences were observed between conditions (Table 1).

Table 1: Mean (± SD) stiffness values (N m/deg).

Condition	Pre	Post
Static	1.50(.42)	.98(.33)*
Cyclic	1.54(.61)	1.08(.44)*

*Significantly different from pre, $p < .05$

In part, these findings are consistent with Tremblay and co-workers (1990) and supports previous contentions that prolonged static stretching is effective at reducing symptoms of spasticity. The results of the present study further suggest that prolonged cyclic stretching may be equally effective at decreasing ankle joint stiffness.

The stiffness values reported in Table 1 display a greater magnitude than values reported for normals (Bressel & McNair., in press). This is consistent with the finding that passive properties of spastic muscle undergo a transformation over time that results in greater stiffness (Hufschmidt & Mauritz, 1985).

Our results showing no difference between conditions is not in agreement with previous work examining non-spastic participants (McNair et al., in press). The conflicting results may be related to the participants' capacity to relax during the prolonged stretches. Normalized EMG data of this study indicated that participants had more difficulty relaxing during the cyclic stretching condition as values were greater compared to the static condition.

In summary, these data indicate that ankle joint stiffness decreases after both prolonged static and cyclic stretches though neither technique appears to be superior at reducing stiffness in humans with spasticity.

REFERENCES

Bressel, E. & McNair, P.J. (in press). *Am J Sports Med.*

Hufschmidt, A. & Mauritz, K.H. (1985). *J Neurol Neurosurg Psychiat*, **48**, 676-685.

McNair, P.J. et al. (in press). *Med Sci Sports Exerc.*

Tremblay, F. et al. (1990). *Scand J Rehab Med*, **22**, 676-685.

THE STRENGTH-DEXTERITY TEST AS A MEASURE OF PINCH PERFORMANCE IN THE ABLE AND IMPAIRED HAND

F.J. Valero-Cuevas[1,2], N. Smaby[3], M. Venkadesan[1], J. Pretz[1], K. Ramakrishna[1], N. Wilson[1], J. Skaliotis[1] and M. Peterson[2]

[1]Neuromuscular Biomechanics Laboratory, Cornell University, Ithaca, New York, U.S.A.
[2]Department of Biomechanics, The Hospital for Special Surgery, New York, New York, U.S.A.
[3]Mechanical Engineering Department, Stanford University, Stanford, California, U.S.A.
E-mail fv24@cornell.edu Web: http://www.mae.cornell.edu/valero

INTRODUCTION

We currently lack quantitative and objective measures of key and opposition pinch to effectively diagnose pinch impairment and compare treatment outcomes. To address this need, we developed and tested a method to evaluate the dynamic interaction between pinch force magnitude (**strength**) and directional accuracy (**dexterity**) the fundamental building blocks of effective manipulation *(Murray et al., 1994; Valero-Cuevas et al., 1998)*. The strength-dexterity (S-D) test is based on the ability to use pinch to fully compress springs with different requirements of strength (i.e., force to fully compress) and dexterity (i.e., proportional to slenderness (free length/diameter); more slender springs require greater directional accuracy not to buckle). The propensity to buckle is *independent* of spring rate, hence strength requirement *(Samónov, 1980)*. This study evaluates the repeatability of the S-D test and compares S-D scores from able and impaired adults.

METHODS

Every possible combination of strength and dexterity is a point on the S-D plane defined by two orthogonal axes representing strength and dexterity. We approximated the S-D plane by 87 springs, each 25-mm long, with 14 strength (range: 1 to 92 N) and 8 dexterity (A through H, range: 0.28 to 2.33 m/m) levels (see Figure 1). All subjects

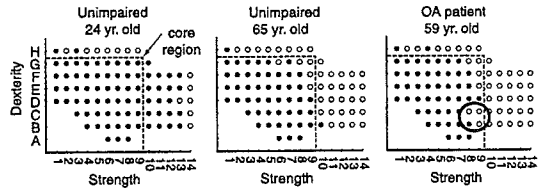

Figure 1. S-D tests in opposition pinch by representative females of each group. Fully compressed springs are shown as filled circles. The dashed line shows the core region young adults could achieve, the oval highlights the OA patient's deficit compared to the older adult.

read, understood and signed the consent form approved by University Committee on Human Subjects at Cornell University. We asked each subject to attempt to fully compress all springs using key (Figure 2) and opposition (pads of thumb against pads of index and middle finger) pinch in random order, providing a 5 s rest between spring presentations. The strength and dexterity scores are the summation of the strength and dexterity levels, respectively, of all springs the person could compress fully. Of the 29 participants, 17 were unimpaired adults under the age of 40 yrs. (**group A**, mean age 22– 5 yrs, range 18 - 39), 7 were unimpaired adults over the age of 40 yrs. (**group B**, mean age 54– 13 yrs, range 40 -78), and 5 were older adults with thumb osteoarthritis

Figure 2.
Compressing a spring with key pinch.

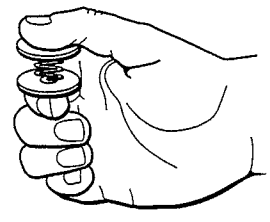

(**group OA**, mean age 65– 12 yrs, range 50 - 79). To test repeatability, we tested 14 group A subjects on two different days.

RESULTS

The test-retest analysis yielded a subject-wise repeatability ≥ 0.94 for all springs.

Every subject of group A could compress all springs in the core region shown in Figure 1.

In contrast, most of group B and all OA participants could not compress all springs in the core region. S-D scores for the core region are numerically lowest for the OA group and highest for group A (Table 1).

DISCUSSION

The essence of dexterous manipulation, particularly for lightweight objects, is the ability to simultaneously and dynamically modulate the magnitude and direction of force at the fingertips. In contrast to pinch meters (the most common test of pinch function) that measure maximal force against a stable object, the S-D test assesses the sensorimotor ability to dynamically produce well directed forces of submaximal magnitude. As such, it is a reproducible measure that is descriptive of the ability to manipulate lightweight objects essential to our activities of daily living.

The core S-D region found in this study describes the expected minimum pinch performance of unimpaired young adults.

We see two important trends in the B and OA groups, to be tested statistically when we sample more subjects. First, not all older adults achieved this minimum S-D score, suggesting that continuing this work may improve our ability to quantify the sensorimotor degeneration known to occur in old age *(Falconer et al., 1991)*, for which no simple clinical tests exist.

And second, because OA patients achieved consistently lower S-D scores than older adults, the S-D test can quantify the pinch impairment known to occur in OA, and help assess pinch impairment and compare treatment outcomes.

A limitation of this study is that a more precise S-D kit is needed. Note, for example, the discontinuity in the H row of the OA patient, which may be due to variable tolerances of commercial springs. Custom springs will be built to remove this possible experimental artifact.

With further work, the strength-dexterity test can become a simple, reliable clinical tool to quantify pinch impairment and to compare treatment outcomes.

	Key Pinch				Opposition pinch			
	dexterity score, m/m		force score, N		dexterity score, m/m		force score, N	
Group	Mean	SD	Mean	SD	Mean	SD	Mean	SD
A	37.3	0	716.4	0	37.33	0	716.4	0
B	35.8	1.7	658.5	61.1	36.06	2.1	665.71	53.5
OA	28.6	13.4	500.0	280.8	27.78	12.1	448.3	250.9

Table 1. Average S-D scores for core region

REFERENCES

Falconer, J., et al. (1991) *J Am Geriatr Soc* **39**, 695-699.

Murray, R. M., et al. (1994) *A mathematical introduction to robotic manipulation.* CRC Press.

Sam nov , C. (1980) ASME Paper 80DET69.

Valero-Cuevas, F. J., et al. (1998). *J Biomech* **31**, 693-703.

ACKNOWLEDGEMENTS

Dr. Yasmeen Moody for recruiting OA patients.

UPPER LIMBS MOVEMENTS BEFORE AND AFTER INTRATHECAL BACLOFEN PUMP IMPLANT

Federica Sibella[1], Manuela Galli[1], Francesco Motta[2], Marcello Crivellini[1]

Bioengineering Dept., Politecnico di Milano, Milano, Italy
Paediatric Orthop. Dept., "V.Buzzi" Hospital, Milano, Italy
e-mail: sibella@biomed.polimi.it

INTRODUCTION

Intrathecal baclofen implant (ITB) consists of a pump that is implanted subcutaneously in the abdominal wall with a catheter surgically placed into the subarachnoid space. By delivering the baclofen drug directly to the spinal cord, higher concentrations can be placed near the target with lower doses than the oral route. The drug dose is adjusted to provide maximal spasm relief while minimizing weakness. Main indication for intrathecal baclofen implant are non-walking cerebral palsy (CP) patients as some clinical works assessed[1]. It results very important to evaluate the outcome of this treatment using a test able to quantify the improvement in motor ability.
The aims of this pilot study are to develop a new protocol for analysing upper limb movements and to apply it to non-walking CP subjects before and after ITB treatment.

METHODS

9 non-walking subjects affected by CP (average age: 10 years, range 6-18 years) were analysed before ITB, 5 of them were analysed also after ITB. In order to analyse the movement using a 3D optoelectronic system, reflective passive markers were placed bilaterally on 7 bony landmarks (Figure 1): on the acromions, elbows, wrists, forehead, and on a control object (CO).
Each subject was asked to perform 3 different movements, starting from a fixed position (moving the CO forward to the self-selected maximum extension and back; moving the CO laterally to the self-selected maximum extension and back; taking the CO to the mouth and back). Each movement was performed twice for each limb to assess data consistency. These movements were chosen on the basis of daily activity usefulness.

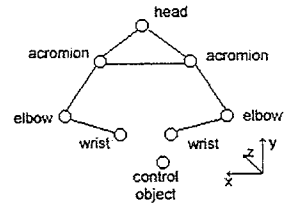

Figure 1: marker positioning

From kinematic data, the range of motion (ROM) of each marker was calculated for each movement in each direction (x, y and z), then the percentage difference between upper limbs analysis before and after ITB was extracted [%ΔROM=(ROM after ITB-ROM before ITB)*100/ ROM before ITB]. From these data, the area of the ellipsis that characterise the movement in each plane (xy = frontal plane, xz = horizontal plane and yz = sagittal plane) and the volume of the ellipsoid that contains the 3D movement, were calculated and the differences between each patient's situation before and after ITB were evaluated.

RESULTS AND DISCUSSION

The severity of the initial conditions was different from subject to subject, therefore they couldn't be analysed as a group. A preliminary subdivision could be made using the clinical evaluation data, which allowed us to discriminate between very severe and less severe initial conditions. On this basis, subjects 323 and 324 started from the worst initial conditions, while subjects 438, 471 and 474 started from better conditions as far as movement capability is concerned.
After ITB implant the ROMs of subjects 323 and 324 result increased in all 6 requested

tasks. In Table 1, %ΔROMs for all tasks are evidenced. The calculated ellipsis area (that takes into account the planarity of the movement and the 2D covered distance) improves for all the movements: in Figure 2, the ellipsis relative to the object motion is plotted for one subject taken as example.

Subject	Lateral movement (%ΔROMx)	Forward movement (%ΔROMz)	CO-to-mouth movement (%ΔROMy)
323right	1.62E+02	No motion before ITB	2.08E+02
324right	8.26E+01	No motion before ITB	5.90E+02

Table 1: %ΔROMs for subjects 323 and 324

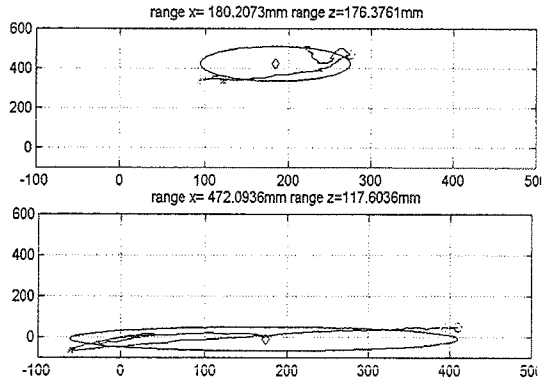

Figure 2: example of how the ellipsis area changes after ITB in a very severe impaired subject, lateral movement: range x increased and range z diminished. Above: before ITB; below: after ITB.

Subject	Lateral movement (%ΔROMx)	Forward movement (%ΔROMz)	CO-to-mouth movement (%ΔROMy)
438right	6.68E+01	4.31E+01	1.25E+01
438left	3.62E+01	3.41E+01	6.00E+00
471right	4.49E+00	1.68E+01	-3.27E+00
471left	-1.55E+01	-3.73E-01	4.63E+00
474right	-2.04E+01	-5.85E+00	-2.42E+01
474left	No motion before ITB	No motion before ITB	-2.53E+01

Table 2: %ΔROMs subjects 438, 471, 474

On the contrary, the three subjects that reveal a better initial condition behave apparently in a random way, only the first showing a visible improvement in the ROM (see Table 2, only object %ΔROM are reported).

An explanation for this contrast in the results can be given in terms of changes in the motor ability induced by ITB. In fact, in very severe impaired subjects a good improvement is visible due to ITB, instead less severe impaired patients seem to move in a more "random" way, sometimes improving and sometimes diminishing ROM in the different required tasks.
It happens in this last case, that ITB contributes to relax the subject's muscles overall, thus, applying the same power to obtain a movement that was already possible for the patient before the treatment, the subject is not able to coordinate him/herself and the movement results apparently "random" in respect to the previous situation. It could be very interesting to repeat upper limbs analysis after a few months, to evaluate if the effects of physical rehabilitation after ITB could lead to new movement coordination. On the other hand, very impaired subjects, who couldn't perform many tasks before the treatment, improve their motor ability leading to a situation similar to the one showed by the less impaired subjects before ITB.

SUMMARY

This pilot study analyses upper limbs movements in non-walking patients before and after intrathecal baclofen implant. The first results show a good improvement in terms of ROM and planarity of the movement in those subjects, who showed the worst initial conditions. Instead, the subjects who showed better initial conditions seem to move after the treatment in a less coordinate way. This result can be explained observing that these patients are not used to their more "relaxed" muscular conditions, thus they use the same force and power as before, but they cannot perfectly control their movements.

REFERENCES

Penn RD et al., Intrathecal baclofen for severe spasticity, *Lancet, 2:125-127, 1985*

AN ANKLE-FOOT ORTHOSIS POWERED BY ARTIFICIAL MUSCLES

Daniel P. Ferris[1], Joseph M. Czerniecki[3,4], and Blake Hannaford[1,2]

Departments of [1]Electrical Engineering, [2]Bioengineering, and [3]Rehabilitation Medicine, University of Washington, Seattle, WA; [4]VA Puget Sound Healthcare System, Seattle, WA
E-mail: dferris@u.washington.edu

INTRODUCTION

Increasing evidence suggests that locomotor training can greatly improve human walking ability after neurological injury (Barbeau et al. 1998). After stroke or spinal cord injury, treadmill stepping with manual assistance and partial body weight support facilitates re-learning how to walk. However, manual assistance is labor intensive and highly variable from therapist to therapist. A lightweight powered lower limb orthosis that can assist locomotor training would decrease labor requirements and provide more consistent therapy. In addition, a powered orthosis would also provide the means to design controlled motor learning studies on human locomotion. Thus, we designed a pneumatically powered, myoelectrically controlled ankle-foot orthosis as a tool for rehabilitation and studying human locomotor adaptation.

METHODS

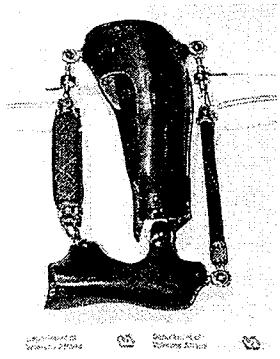

Figure 1: The orthosis has a carbon-fiber shell and a hinge joint at the ankle. Two identical artificial pneumatic muscles (McKibben muscles) are attached. The dorsiflexor is contracted and the plantarflexor is relaxed in the figure at right.

The artificial pneumatic muscles are lightweight and can produce high power outputs. They are made from latex tubing surrounded by a braided polyester shell. Inflating the tubing causes the shell to expand radially and shorten axially. A desktop PC used programs written in SIMULINK and implemented in dSPACE to regulate the pressure in the artificial pneumatic muscles proportional to the amplitude of low-pass filtered EMG. Force transducers mounted in series measured tension of the artificial muscles. Orthosis weight is 1.4 kg. We performed benchtop isometric tests on the muscles to compare artificial muscle mechanical properties with published data from human muscle. We also recorded kinematic and kinetic data on one healthy subject walking on a treadmill for thirty minutes with the orthosis.

RESULTS AND DISCUSSION

Mechanical properties of the artificial muscles were similar to the properties of human muscle. Single twitch tests with 5 ms pulse stimuli revealed a time to peak tension of 69 ms and a half relaxation time of 69 ms for the artificial muscles. Respective values for human triceps surae are 101 ms and 94 ms (Rice et al. 1988) and for human tibialis anterior are 99 ms and 87 ms (Connelly et al. 1999). During physiological activation, the artificial muscles had an electromechanical delay of 51 ms between EMG burst onset and initial rise in muscle tension. Electromechanical delay values for human soleus and gastrocnemius are 27 ms and 35 ms (Komi et al. 1987), respectively.

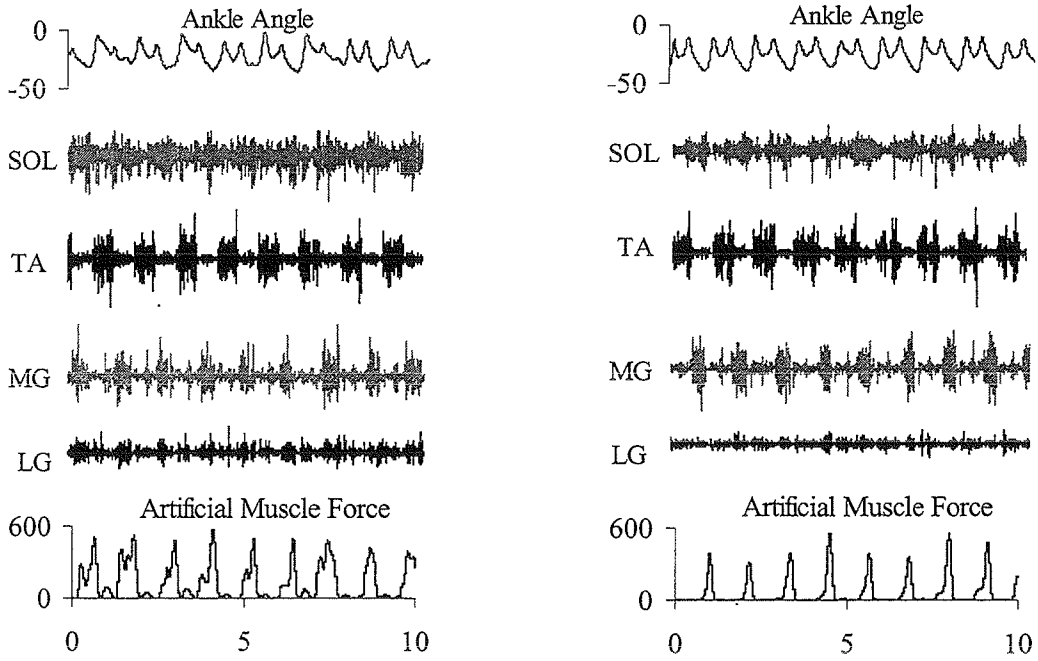

Figure 2: The left graphs show data during the first minute of walking on the treadmill (1.2 m/s) with the orthosis activated. The right graphs show data after thirty minutes of continuous walking. Only the plantarflexor artificial muscle is attached (moment arm = 11 cm). Soleus EMG amplitude decreased by 25% and lateral gastrocnemius EMG amplitude decreased by 41%. Tibialis anterior and medial gastrocnemius EMG amplitudes were unchanged. Mean artificial muscle force decreased by 48%. Notice the decrease in interstride variability in ankle kinematics and artificial muscle force with practice. Ankle angle is in degrees, EMG units are arbitrary but consistent across time, force is in Newtons, and the x-axis is Time in seconds.

SUMMARY

We have built a pneumatically powered ankle-foot orthosis that can be used to assist gait rehabilitation and study human locomotor adaptation. Preliminary data using proportional myoelectric control on a non-disabled subject indicate that the human nervous system selectively modifies muscle activation patterns to control the orthosis with practice. Kinematic or kinetic data (e.g. foot contact or hip angle) could also be used to control the orthosis when sufficient EMG signals are not present due to stroke or spinal cord injury. Future work will extend the concept to a hip-knee-ankle foot orthosis to provide assistance at other joints.

REFERENCES

Barbeau, H. et al. (1998). *Ann. N.Y. Acad. Sci.* **860**, 377-392.

Connolly, D.M. et al. (1999). *J. Appl. Physiol.* **87**, 843-852.

Komi, P.V. et al. (1987). *Int. J. Sports Med.* **8(suppl.)**, 3-8.

Rice, C.L. et al. (1988). *Eur. J. Appl. Physiol.* **58**, 165-170.

ACKNOWLEDGMENTS

Supported by NIH AR08602 and U.S. Dept. of Vet. Affairs Center Grant #A0806C. We appreciate the help of Glenn Klute, Jocelyn Berge, Eric Rohr, & the VA orthotists.

CHANGES IN HAND RIM WHEELCHAIR PROPULSION TECHNIQUE AND MECHANICAL EFFICIENCY AFTER A 3-WEEK PRACTICE PERIOD

S. de Groot[1], L.H.V. van der Woude[1], H.E.J. Veeger[1,2]

[1] The Institute of Fundamental and Clinical Human Movement Sciences (IFKB), Vrije Universiteit, Amsterdam, Netherlands
[2] Man-Machine Systems and Control Group, Delft University of Technology, Delft, Netherlands
E-mail: s.de.groot@fbw.vu.nl Web: www.ifkb.nl

INTRODUCTION

In rehabilitation, recently injured individuals have to learn a new motor task, e.g. propelling a wheelchair. According to Sparrow (1983), motor performance of novices is relatively inefficient even though they may perform at a rate optimal to their stage of learning. With practice, the movement pattern will be refined to approximate more closely that which is biomechanically and physiologically optimal within the constraints of the task. It is hypothesized that improved mechanical efficiency (ME) as a consequence of task proficiency is closely linked with improved propulsion technique. Therefore, the purpose of this experiment was to study changes in propulsion technique and gross ME during a 3-week wheelchair-practice period.

METHODS

Twenty able-bodied subjects were randomly divided over one experimental group (EXP, n = 10) and one control group (C, n = 10). EXP received a 3-week wheelchair-practice period (3·wk^{-1}, i.e. 9 trials) on a computer-controlled wheelchair ergometer, while C only participated in trial 1 and 9. Every trial comprised of two four-minute exercise blocks at two different levels of external power output (block 1: 0.15 W·kg^{-1} and block 2: 0.25 W·kg^{-1}) at a velocity of 1.11 m·s^{-1}, with two minutes of rest before each exercise block. Force application, bilateral symmetry, inter-cycle variability, timing and gross ME were determined on all 9 trials during the last minute of an exercise block.

RESULTS AND DISCUSSION

Gross ME increased over the trials in EXP compared to C (Table 1). This increase could theoretically *not* be due to a training effect because the exercise blocks were at a too low intensity and of a too short duration. Increased efficiency and thus task proficiency was only expressed in a limited

set of propulsion technique parameters. No significant differences between the groups over time were found for the effective force application (FEF) (Table 1), bilateral symmetry and inter-cycle variability. It may be suggested that these variables change more rapidly – i.e. in the first minutes - or on a much longer time span than 3 weeks. The push frequency (f) and the negative deflection in the power output curve at the start of the push phase (PnegS; Fig.1) diminished significantly while the work per cycle (Wcycle), push time (PT) and cycle time (CT) increased significantly over time in EXP in contrast to C (Table 1). This was also found in a previous training study (Woude et al., 1999). Changes in the timing variables (f, PT, CT and subsequently Wcycle) indicate a change in segment excursions and velocities, next to changes in muscle contraction characteristics. This may have led to the increase in gross ME.

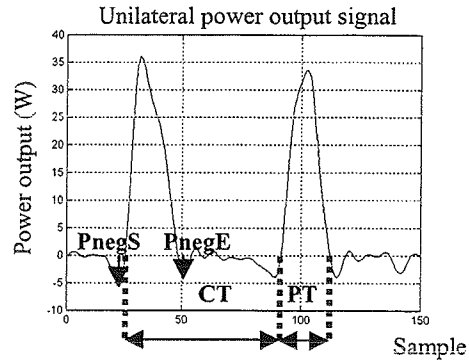

Figure 1. Definition of variables.

SUMMARY

A 3-week wheelchair-practice period had a favorable effect on timing parameters, work per push and gross ME, indicating a possible effect of the timing parameters on ME.

Although no changes in force application parameters, bilateral symmetry and inter-cycle variability occurred during the wheelchair-practice period, these variables may optimize in the initial minutes of practice or on a (much) longer time scale than 3 weeks.

REFERENCES

Sparrow, W.A. (1983). *J. Motor Behavior*, **15(3)**, 237-61.

Woude, L.H.V. van der, et al. (1999). *Med.Sc.Sp.Exerc.*, **31(2)**, 331-41

Table 1. Change over time of the measured variables (mean). * significant at $p < 0.05$

	Trial	PnegS (W) *	PnegE (W)	FEFmax (%)	f (pushes / min) *	PT (s) *	CT (s) *	Wcycle (J) *	ME (%) *
EXP	1	-5.64	-1.95	80.03	62.83	0.37	0.99	0.38	7.45
	9	-2.93	-1.26	83.93	46.35	0.45	1.40	0.54	8.11
C	1	-4.41	-2.56	80.84	63.52	0.35	1.00	0.39	7.37
	9	-4.01	-2.08	82.64	60.20	0.36	1.08	0.41	7.23

HUMAN PERFORMANCE-BASED PEDIATRIC WHEELCHAIR PRESCRIPTION

Jeremy Carrle and David Hawkins

Human Performance Laboratory, University of California, Davis, CA, USA
E-mail: dahawkins@ucdavis.edu

INTRODUCTION

Mobility impaired children between the ages of 2 and 5 need appropriately designed and sized wheelchairs. Configuration guidelines exist for adults but little work has been done to establish appropriate guidelines for children (Brubaker, 1986). It was hypothesized that the propelling capabilities of pediatric wheelchair users could be predicted and improved using biomechanical analysis and testing.

Wheelchair wheels were tested to determine the forces required to initiate movement of a pediatric wheelchair. A static mathematical model and experimental testing techniques were utilized to identify the required joint torques in the initial pre-movement phase of the push. Seat configuration guidelines were developed based on results from these analyses and validated with human subjects. User friendly software was developed to assist therapists and wheelchair dealers prescribe age and strength appropriate wheel configurations that maximize the user's capabilities.

METHODS

A 3-phase design was implemented to develop pediatric wheelchair prescription guidelines. The forces required to initiate movement of a pediatric wheelchair were experimentally measured and validated in phase 1. Static coefficients of rolling friction were determined for three front wheels and three rear wheels on short carpet, wood, and a 0.95 cm high door threshold (Al-Eiwasi, 1999). Combinations of surface materials and wheels were tested on a fully assembled chair to insure that the coefficients were valid.

A static model of a pediatric wheelchair and child was developed and used in phase 2 for the purposes of determining a child's ability to self-propel and to determine an optimal wheelchair configuration. The model uses child-chair specific data (wheel type, ground material, age, weight, body segment lengths, and maximum voluntary contraction (MVC) joint torques) to examine the effect of variations in model parameters (normal force (F_n), hand position (θ_h), torso angle (θ_t), and distances to the hub (t_x,t_z)) on the minimum required joint torques (Figure 1).

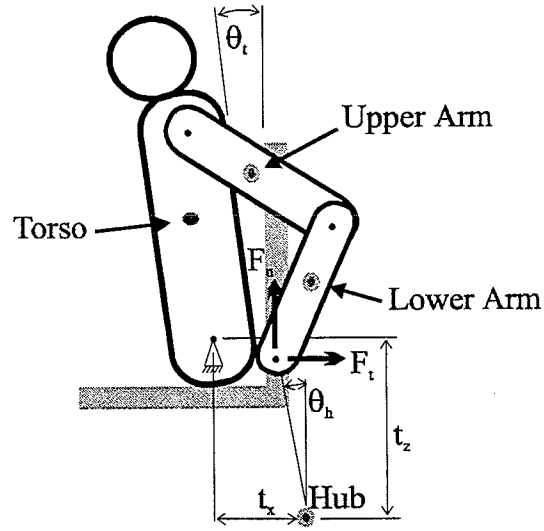

Figure 1. Model parameters.

Joint torques are calculated with static equations of equilibrium and normalized with respect to the subject's (MVC) torques. A cost function (the sum of the cubed normalized joint torques) is used to identify the model parameters that minimize the muscular effort required to initiate chair movement. The required torques of the optimal case are then specified and compared

to the child's MVC torque data to determine if the child is strong enough to self propel.

The model is being validated by comparing data collected with a simulated wheelchair and pediatric wheelchair users, ages 4 and 5, with model predictions. The simulated pediatric wheelchair was designed to measure values corresponding to each model parameter in addition to the tangential forces (F_t) exerted on the handrim (Hughes 1992). Force and video data, recorded for each static, simulated wheelchair push, are used to obtain actual parameters for comparison with those predicted by the model.

Phase 3 of the project involves the development of software to assist in pediatric wheelchair prescription. Software incorporates the model of pediatric wheelchair and child to determine if the child can successfully self-propel and if so prescribe an appropriate configuration.

RESULTS AND DISCUSSION

Coefficient of static rolling friction (μ_{sr}) data depended on wheel type, diameter and ground material (Table 1). For a given wheel type, resistance was less as wheel diameter increased. Larger diameter, pneumatic wheels had greater resistance to movement than small rubber or polyurethane wheels. Lowered air pressure in pneumatic wheels decreased the resistance to traversing a threshold.

Table 1. Coefficients of Static Rolling Friction (μ_{sr}). Note: Italics indicate an exponential best-fit equation.

Wheel Diameter And Type	Wood	Carpet	0.476 cm Threshold
7.9 cm Polyurethane	0.015	0.126	0.375
12.4 cm Rubber	0.015	0.108	0.384
15.2 cm Pneumatic	0.019	0.096	$0.569F_n^{0.904}$
32.9 cm Pneumatic	0.023	0.049	$0.573F_n^{0.823}$
39.4 cm Pneumatic	0.023	0.045	$0.512F_n^{0.830}$
52.4 cm Pneumatic	0.015	0.037	$0.397F_n^{0.873}$

Additionally, for the pneumatic-threshold case, resistance was non-linearly dependent on normal force. The μ_{sr} data allowed accurate prediction of the static friction associated with initiating chair movement.

Preliminary results from testing one child in two horizontal positions (wheel ±15.24 cm relative to the hip) indicated that MVC torque measurements at the shoulder and elbow were, on average, 18% (S.D. 12) greater than predicted values. Torque at either the elbow or shoulder was the limiting factor in all trials. The subject's actual measured forces and model-predicted forces both exceeded that required for self-propelling on wood, carpet, and an access ramp. The forces required to self-propel over a threshold were very similar to the child's MVC capabilities. Actual values indicated that the subject could self-propel in both configurations tested. The model predicted the child could not self-propel in the forward wheel configuration.

SUMMARY

A new approach is being developed to facilitate pediatric wheelchair prescription. This approach determines if a child can self-propel and if so prescribes the optimal seating configuration.

REFERENCES

Al-Eiwasi, K.W. (1999). *Applied Ergonomics.* 30(4): 235.

Brubaker, C.E. (1986). *J. of Rehabilitation Research and Development.* 23(4):19-26.

Hughes, C.W. (1992). *Archives of Physical Medicine and Rehabilitation.* 73:263-269.

ACHKNOWLEDGEMENTS

NSF support, Grant BES-9813634

PEAK SHOULDER KINETICS AND KINEMATICS IN DURING WHEELCHAIR PROPULSION

Margaret A. Finley[1], Kevin J. McQuade[1,2], and
Mary M Rodgers[1,2]

[1] University of Maryland, Baltimore, Department of Physical Therapy
[2] VA Maryland Health Care System, Research and Development Service,
Baltimore, MD
Email: mfinley@som.umaryland.edu Web: pt.umaryland.edu

INTRODUCTION

Thirty-two to 74% of wheelchair users (WCU) are reported to experience shoulder pain. Rapid application of propulsive forces (Robertson, 1996), loading of joints in extreme positions (Veeger, 1998), and fatigue (Rodgers, 1994) have all been implicated as potential mechanisms of upper extremity pathology. It has been shown that individuals who propel with more trunk flexion have greater shoulder joint excursion, and utilize trunk excursion to assist the upper extremities in generating propulsive forces and moments, especially when fatigued (Rodgers, 2000). Additionally, it has been suggested that these individuals may be more at risk for shoulder injury.

In previous work, the magnitude of the propulsive moment was not found to be different between trunk styles[3]. However, the shoulder joint angle when peak moments occurred was not assessed. The purpose of this study was to determine shoulder angle when peak propulsive moments occur in groups with differing propulsion styles and in the fatigued state. It was hypothesized that shoulder angle when peak moments occurred would be different with differing propulsion styles and with fatigue.

METHODS

Fourteen individuals (12 = M, 2 = F) who used a manual wheelchair for at least 50% of home and community mobility served as subjects. The subjects' diagnoses included spinal cord injury (T4-T9 = 3, T12-L1 = 7), spina bifida (2), cerebral palsy (1), other (1). Refer to Table 1 for further demographic information of the subjects.

Table 1: Subject characteristics

Age (yrs)	37.8 ± 9.8
Height (cm)	169.9 ± 13.7
Weight (kg)	81.6 ± 13.6
Years in WC	9.9 ± 4.9

Following medical screening, propulsion mechanics were measured at a standard velocity of 3 km/hr during a submaximal exercise test to exhaustion (defined as volitional inability to sustain the designated velocity). Load for the fatigue test corresponded to 60% of the maximal load achieved during the graded maximal exercise test on the wheelchair ergometer. The wheelchair ergometer was instrumented with a PY-6 six-component force/torque transducer (Bertec Corp, Worthington, OH) in the wheel hub to detect handrim forces (Fx, Fy, Fz) and moments (Mx, My, Mz). Orientation of the x-y-z transducer coordinates was tangential (forward+), radial (up+) and medial-lateral (out of the wheel+), respectively. Kinetic data were collected at 360 Hz. A potentiometer monitored the angular position of the wheel, transducer, and handrim assembly. Kinematic data were collected at 60Hz using video cameras and the data acquisition

system (Peak Performance Tech., Colorado Springs, CO). Joint kinetics were calculated using a 3-D, linked segment, inverse dynamics model.

Right upper extremity joint kinematics and kinetics were averaged over three cycles (contact to contact). The timing of peak handrim and joint forces and moments were normalized to total cycle time. Shoulder joint angles at the time corresponding to the peak handrim propulsive moment (Mz) and peak shoulder Mz were determined.

Subjects were classified by propulsion style. The flexion group (FG) had peak trunk flexion angles less than 90° during contact when fresh or fatigued (n = 9). All others were classified as non-flexors (NFG, n = 5). Repeated Measures Analysis of Variance ($p \leq 0.05$) was used to compare peak handrim Mz and shoulder flexion moments (Mz), and time of peak moments, at the fresh and fatigued states, within and between flexion groups.

RESULTS AND DISCUSSION

Handrim Mz (21.5 ± 8.8 Nm) was significantly smaller ($p \leq 0.05$) than shoulder Mz (60.3 ± 38.7 Nm). Differences in shoulder angles were found between groups (Figure 1). The NFG was in a position of greater shoulder extension when peak handrim and shoulder Mz occurred (Figure 1). No difference in timing of the peak torque was found between the handrim and shoulder. Fatigue did not change the magnitude or timing of handrim or shoulder Mz nor the shoulder angle at the time peak moment occurred. Application of peak moments in extreme positions has been suggested as a potential mechanism of injury. In the current study, both groups applied similar magnitudes of handrim and shoulder Mz, but they were applied in very different shoulder positions.

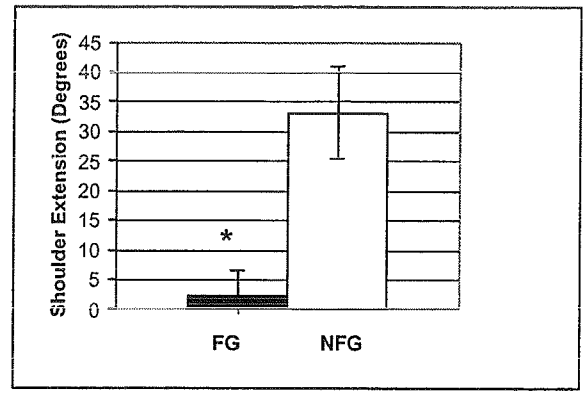

Figure 1: Shoulder angle ($\bar{x}$ ±SEM)at time of peak Mz are illustrated for the flexor group (FG) and non-flexor group (NFG). * ($p \leq 0.05$)

SUMMARY

People who propel a wheelchair in a more upright trunk posture have a more extended shoulder position when maximal handrim and shoulder Mz occur as compared to a trunk flexion style. Whether this difference predisposes one of the groups to potential injury requires further investigation. Fatigue does not appear to alter the magnitude, or timing of the peak handrim or shoulder Mz.

REFERENCES

1. Robertson, R.N. et al. (1996). *Arch Phys Med Rehabil*, 77; 856-64
2. Rodgers, M.M. et al. (1994). *Arch Phys Med Rehabil*, 75; 85-93
3. Rodgers, M.M. et al. (2000). *J Rehabil Res Dev,* 37, 283-295
4. Veeger, H.E.J., et al. (1998). *J Rehabil Res Dev*, 3; 305-13.

ACKNOWLEDGEMENTS

This project was supported by the Veterans Affairs Rehabilitation Research and Development Service Merit Review Grant #B2168RA and the Foundation for Physical Therapy.

A MODEL OF FEMORAL COMPRESSION AND SHEAR DURING STANDING FOR INDIVIDUALS WITH COMPLETE SPINAL CORD INJURY

Laura A. Frey Law and Richard K. Shields

Graduate Program in Physical Therapy & Rehabilitation Science,
University of Iowa, Iowa City, IA E-mail: richard-shields@uiowa.edu

INTRODUCTION

Osteoporosis is a serious medical complication following spinal cord injury (SCI). Bone mineral density (BMD) in the lower extremities can decrease by approximately one-third in the first six months after injury (Garland, D.E., et al., 1992; Roberts, D., et al., 1998). Correspondingly, for individuals with complete SCI, the rate of long-bone fracture is more than 20% greater than for the general population (Frisbie, J.H., 1997). Although several studies have investigated the effects of various forms of limb loading exercise on BMD in individuals with SCI, no studies included estimates of the bone loads generated. To determine a dose-response curve for exercise induced bone loading following complete SCI, the mechanical loads from an intervention must be assessed. The purpose of this study was to develop a mathematical model to predict compression and shear forces in the distal femur during passive and active standing exercise in individuals with SCI.

METHODS

Individuals with SCI are able to stand independently with the use of a standing frame. One example of such an apparatus provides kneepads for anterior support, a hip belt for posterior support, and optional upper extremity support. Standing may be performed either passively, relying on the kneepads to maintain knee position, or actively with the addition of electrical stimulation of the quadriceps muscle. Higher quadriceps muscle forces may be obtained with added resistance to knee extension (only with active condition) for increased levels of muscle training.

A quasi-static model, based on the standing frame described, was developed using a two-bar linkage representing the thigh segment and the shank segment of one lower limb. External forces included ground reaction forces, kneepad reaction force, and hip-belt reaction force. The weight of the head, arms and trunk were assumed to act downward at the hips (single force vector); the weights of the segment links were assumed to act at their respective centers of mass. No internal muscle forces were included for the passive model; however, a simplified quadriceps muscle force was included in the active model. The quadriceps force was modeled at the precise moment the kneepad normal reaction force was reduced to zero. Thus, the resultant quadriceps force across the patella (horizontal component) was assumed to be equal to the kneepad force at rest (passive condition) plus any added resistance to knee extension. The compression and shear forces in the distal femur were modeled at a distance of 85% of femur length from hip to knee for both the active and passive conditions. This location was chosen to approximate a common site of pathological lower limb fractures in individuals with SCI.

Matlab computer software (version 5.3) was utilized for all equations. The model was generalized such that body weight and height were inputted to the model. All limb lengths and center of mass values were based on anthropometric standards (Chaffin, D. and Andersen, G., 1998) and thus were a function of height. Model parameters, e.g. coefficients of friction and segment angles, were determined from experimental data resulting from a hand-held goniometer, a custom-instrumented kneepad force transducer, and a Kistler force plate. The sensitivities of the model parameters were evaluated by altering one parameter at a time over a range of expected values, leaving the remaining parameters constant. The model was most sensitive to alterations in the internal knee angle and the coefficient of friction between the foot and the ground (u_{gr}). Based on the experimental findings taken at five different standing positions, u_{gr} was set equal to 0.2 and the belt angle was set equal to 10°. Upper extremity support and frictional forces at the kneepad and hip belt were assumed to be negligible.

RESULTS AND DISCUSSION

The distal femur compression estimates for the passive condition were in the range ~40-75 percent body weight (%BW), varying with segment angles. The compression estimates for the active condition (no added resistance) were approximately two times larger than for the passive condition (range ~70-130%BW). The addition of 100 lbs of resistance behind the knee (extreme condition of 77% BW horizontally, using 130 lbs BW as model input) increased the femoral compression forces by three to four times the passive condition (range ~175-200%BW). The modeled shear forces at the distal femur were low for all conditions (range ~1 – 20%BW). Segment angles of the thigh and shank (with respect to horizontal) had a substantial influence on the compression, shear, and muscle force predictions of the model as seen in the range of values reported above.

This model provides a simple method for estimating loading dose for a standing exercise in persons with SCI. If movement is allowed, then the quasi-static nature of the preceding model may be in error. However, most movements would likely have relatively low displacements and velocities, as movement deceleration is a critical issue in individuals with complete SCI.

SUMMARY

Overall, this model provides potentially valuable information regarding the compression and shear in the distal femur during passive as well as active standing. Shear force predictions never exceeded 20%BW even when the compression force predictions peaked at ~200%BW, suggesting that this type of exercise is a reasonably safe option for individuals with SCI.

REFERENCES

Chaffin, D.Andersen, G. (1998). *Occupational Biomechanics*, third edn. Williams & Wilkins.

Frisbie, J. H. (1997). *Journal of Spinal Cord Medicine* **20,** 66-69.

Garland, D. E., et al. (1992). *Journal of Orthopaedic Research* **10,** 371-378.

Roberts, D., et al. (1998). *Journal of Clinical Endocrinology & Metabolism* **83,** 415-422.

ACKNOWLEDGEMENTS

This work was supported in part by NIH RO1HD39445 and the Carver Foundation.

HARNESS-SUPPORT COMPLIANCE IN TREADMILL TRAINING IN POST-STROKE HEMIPARESIS

G Chen[1,2], C Patten[1,3], CG Burgar[1,3], SA Kautz[1,3], FE Zajac[1,2,3]

1-Rehab R&D Center (153), VA Palo Alto HCS, Palo Alto, CA 94304
Depts. of 2-Mech. Eng. & 3-Func. Restoration, Stanford Univ., Stanford, CA 94305
E-mail: gchen@stanford.edu

INTRODUCTION

Harness-supported treadmill training, where individuals are partially supported by a harness while stepping is practiced on a motorized treadmill surface, has generated tremendous clinical excitement for its potential to enhance locomotion in individuals with spinal cord injury (SCI) and post-stroke hemiparesis (Dobkin, 1999; Hesse et al., 1995). The technique is believed to be effective because it provides task-specific training and makes the sensory inputs associated with walking more normal for individuals who cannot otherwise walk with proper gait kinematics. Body weight support (BWS) has been accomplished using a number of different methods (i.e., with a winched rope, springs, pneumatic lift, or counterbalancing weights) that permit different degrees of body motion. Compliant support systems permit modest trunk motion while maintaining a relatively stable support force. Stiffer systems exert a more variable force while constraining trunk motion more tightly. Differences in the BWS system used during treadmill walking has been shown to affect vertical ground reaction forces (GRFs) and center of mass movement in neurologically healthy and SCI subjects (Gordon, et al., 2000). In this study, we compared the effect of incremental adjustments in harness-support compliance on 3-D harness forces (vertical, anterior-posterior, and lateral) and vertical GRFs generated by four neurologically healthy subjects and one individual with post-stroke hemiparesis during treadmill walking.

METHODS

Vertical, ant-post, and lateral harness forces applied to the subject were quantified using a custom-made harness support frame instrumented with a 6-axis force/torque sensor (Chen et al., 2001). Vertical GRFs were estimated using insole pressure sensors. Harness-support compliance was set between 0 – 0.855 mm/N by connecting 0 – 3 springs (K = 35.1 N/cm) in series with the support cable. Body weight support was set between 0 - 55% of the subject's bodyweight. Treadmill speed was set between 0.45 – 1.79 m/s for neurologically healthy subjects and 100 - 140% of self-selected overground walking velocity (0.58 – 0.81 m/s) for the hemiparetic subject. Data was collected from 30-sec walking trials and averaged and normalized to a gait cycle beginning and ending with right heel strike.

RESULTS AND DISCUSSION

In neurologically healthy subjects, vertical harness support was highest during double limb support (when trunk height is lowest) and lowest during midstance (when trunk height is highest) (Fig.1). When harness-support compliance was increased from 0 to 3 springs, mean peak-to-peak fluctuation in vertical harness support decreased from 173.6 (±19.6) N to 36.0 (±10.7) N. Concurrently, vertical GRFs changed from a flat to a normal, double-peaked profile.

In the left-hemiparetic subject, vertical harness support was higher during stance of the paretic left limb, indicating greater

reliance on the harness (Fig. 2; from approximately 60 – 20% of gait cycle). When harness-support compliance was increased from 1 to 3 springs, the difference in vertical harness support between the two stance phases decreased, while cycle to cycle variability in ant-post harness forces and vertical GRFs of the paretic limb increased (Fig. 2). The small difference in treadmill velocity between the two trials (0.81 m/s vs. 0.70 m/s) is unlikely to cause the observed differences.

In both neurologically healthy and hemiparetic subjects, changes in harness support tension at low compliance levels accentuated fluctuations in ant-post harness forces but were of more consequence in the hemiparetic subject who generated much higher levels of ant-post harness force (compare Fig. 2 with 1).

SUMMARY

Neurologically healthy and hemiparetic subjects achieved different interactions with the harness. In neurologically healthy subjects, harness-support compliance affected fluctuation in vertical harness support, which altered vertical GRF profiles. In the hemiparetic subject, harness-support compliance affected vertical harness support on the paretic limb, gait cycle variability, and ant-post harness force fluctuation magnitude. Differences in gait mechanics due to harness-support compliance could influence afferent information important to treadmill training. Understanding how abnormal gait mechanics and harness forces interact may lead to improved training parameters for rehabilitation patients.

REFERENCES

Chen, G. et al. (2001). *6th Annual Gait and Clinical Movement Analysis Meeting,* (accepted).

Dobkin, B.H. (1999) *Neurorehabilitation and Neural Repair,* **13**, 157-65.

Gordon, K.E. et al. (2000). *2000 Society for Neuroscience Abstracts,* **26**:160.

Hesse, S. et al. (1995). *Stroke,* **26**, 976-81.

ACKNOWLEDGEMENTS

This work was supported by a Whitaker Foundation Predoctoral Fellowship, NIH grant NS17662, and the Rehabilitation R&D Service of the U. S. Department of Veterans Affairs (VA). We also thank Dr. Daniel Ferris for his assistance.

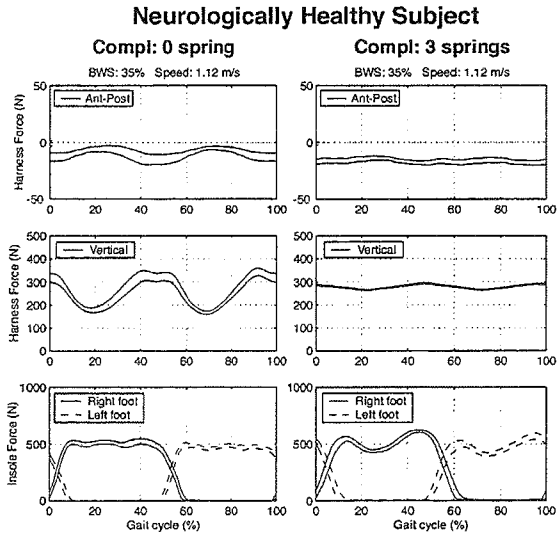

Fig. 1 Normalized trials of a neurologically healthy subject at a support compliance provided by 0 and 3 springs. Region between lines represent ±1SD of mean. Harness forces applied to the subject directed upward and forward are shown as positive.

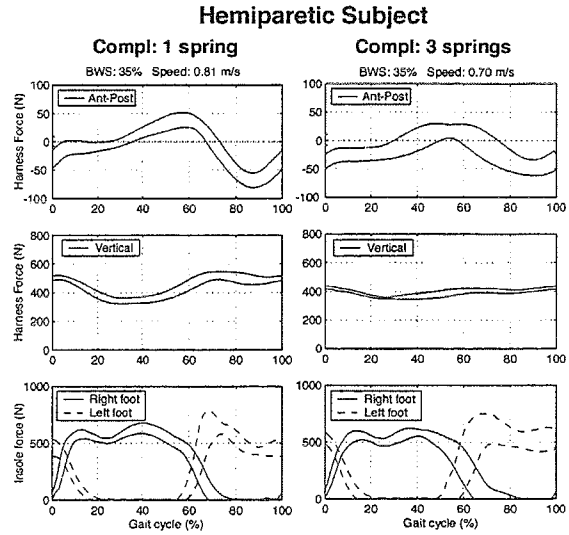

Fig. 2 Normalized trials of a left-hemiparetic subject at a support compliance provided by 1 and 3 springs.

OBJECTIVE DIFFERENTIATION BETWEEN THE ADULT DIABETIC FOOT AND THE NORMAL ADULT FOOT USING PASSIVE TORQUE vs RANGE-OF-MOTION MEASUREMENT OF THE FOOT/ANKLE COMPLEX

William L. Buford, Jr., T. Nakamura, Kevin M. Charron, Paul J. Hume, Steven D. Brown, Saul G. Trevino, Rita M. Patterson

Department of Orthopaedics and Rehabilitation, University of Texas Medical Branch, Galveston, TX, USA
E-mail: william.buford@utmb.edu

INTRODUCTION

The study has been performed on normal subjects and diabetics patients at the University of Texas Medical Branch (UTMB) and affiliated hospitals. In an earlier study, the inter- and intra-rater reliability of this device designed to measure the passive mechanical properties of the foot-ankle complex was ascertained [Hume, et al.]. On a regular basis the foot and ankle endure a tremendous amount of stress. In the injured or diseased foot, these forces can result in severe complications, such as the Charcot arthropathy in diabetic patients. In this example, the insensibility of the diabetic foot predisposes patients to exacerbate breakdown of the foot and ankle with irregular walking which would normally be prevented by pain.

The goal in the treatment of the diabetic foot and other pathology of the feet is to protect it from harmful forces and pressures and to allow for protective ambulating. With this in mind, the objective of this research is to provide a more in-depth understanding of the passive viscoelastic properties of the foot/ankle complex with the prospects of improving diagnosis and treatment. The hypothesis of this study is that the mechanical parameters derived from passive TROM curves will be significantly different between normal and diabetic adults.

METHODS

The TROM device is a tranducer system based on a prototype developed in our lab that is manually rotated through plantar and dorsiflexion. The device and method of application are described in [Hume, et al.]. The device is a single degree-of–freedom hinge connected to molded thermoplastic splints which iare strapped to the calf and foot. With the patient in a relaxed, sitting position in a recliner chair, the device is passively rotated at a slow rate (a metronome is used at 40 beats per minute) during a 50 second data acquisition period. A cantilever beam strain guage provides the torque signal and a precision single-turn potentiometer provides plantarflexion-dorsiflexion angle to a two-channel portable pc data acquisition system.

Parameters determined from the TROM curve are maximum ROM (ROM 1 in the figure [next page]), normal or functional ROM (ROM 2 in the figure), the hysteresis area proportional to the energy absorbed in the loading/unloading cycle, dorsiflexion stiffness (Slope1,Tangent a1), working ROM stiffness (Slope 2, Tangent a3), and plantarflexion stiffness (Slope 3, Tangent a2). All parameters are automatically calculated using a Basic language program as a macro in Microsoft Excel.

RESULTS AND DISCUSSION

The results are shown in Table. 1 with t-test statistics (Microsoft Excel). The study included 49 normal and 27 diabetic adult feet. For a probability level of 0.01 there was a significant difference between the AREA, and both dorsi- and plantar-flexion stiffnesses. Neither ROM nor the normal ROM stiffness (tan a3) differed between the normal and diabetic populations. This leaves a summarized conclusion that adult diabetic feet absorb more energy during cyclic motion (thus must dissipate more energy per cycle) and are stiffer in the terminal regions (where muscle-tendon-ligament properties prevail) than normal adult feet. Future work includes measurement of patients with other foot-ankle problems, correlation of these results with other parameters of clinical interest, and development of a three degree-of-freedom device in order to measure the passive properties for the foot in internal-external and inversion-eversion rotation as well as plantarflexion-dorsiflexion.

	Normal		Diabetic		t-stat.
	Avg.	S.D.	Avg.	S.D.	P
ROM 1	59.17	12.25	60.02	10.57	0.76
ROM 2	43.31	8.93	42.27	7.74	0.61
AREA	81.04	30.66	103.69	31.41	< 0.01
Slope 1	0.43	0.16	0.59	0.19	< 0.01
Slope 2	0.077	0.05	0.076	0.039	0.95
Slope 3	0.33	0.13	0.50	0.15	< 0.01

Table 1. Results for Normal and Diabetic subjects with t-statistics.

REFERENCES

Hume et al, "Analysis of TROM for the Passive Viscoelastic Properties of the Foot/Ankle Complex," Abstracts, 18th Annual Meeting, HSEMB, Univ. Hilton Hotel, Houston TX, 10-11 Feb, 2000, p124.

ACKNOWLEDGEMENT

This work was supported in part by the John Sealy Foundation.

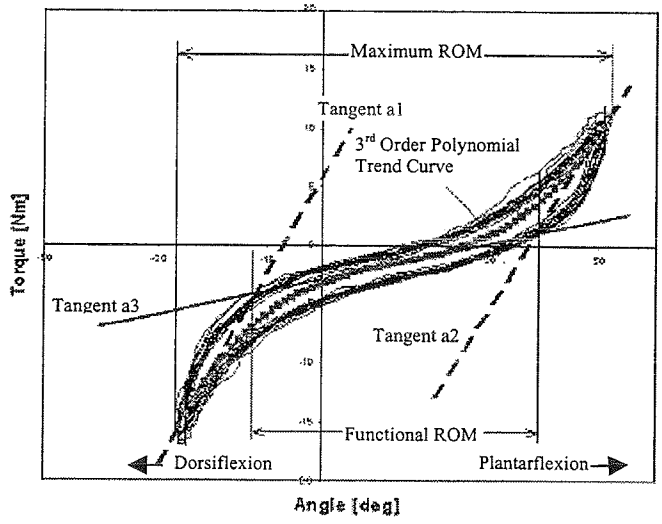

Figure. A typical TROM curve for a normal adult foot.

MECHANICAL ENERGY AND POWER FLOW OF THE UPPER EXTREMITY IN MANUAL WHEELCHAIR PROPULSION

Lan-Yuen Guo[1&2], Fong-Chin Su[1], Hong-Wen Wu[3]
[1]Institute of Biomedical Engineering, National Cheng Kung University, Tainan, Taiwan
[2]Department of Physical Therapy, Tzu Chi College of Technology, Hualian, Taiwan
[3]Department of Physical Therapy, China College of Medicine, Taichung, Taiwan
E-mail: yuen@tccn.edu.tw

INTRODUCTION

Complex movements, such as walking, often lead to the calculation of segmental kinematics from which mechanical energies are derived and be used as a tool for the evaluation of locomotion disorders (Olney et al., 1987). Body energy can also be purely calculated from kinematical and kinetic data by the power flow analysis approach. The characteristics of energy generation, absorption and transfer by muscles and energy transfer through the joints could be computed thereafter (Gordon et al., 1980; Winter 1994).

The mechanical efficiency of wheelchair propulsion is very low, only up to 10%. Most studies investigated the mechanical energy and power flow of human walking; the energetic model in analyzing wheelchair propulsion has not been available in the literature. Therefore, we studied the mechanical energy and power flow of upper extremity in manual wheelchair propulsion to understand inefficiency in energy expenditure.

METHOD

Twelve young normal male adults (mean age 23.5 years old) were studied. The ExpertVision^{TM} system (Motion Analysis Corp., Santa Rosa, CA) and an instrumented wheel system were used for three-dimensional kinematics and kinetic analysis of upper extremity in wheelchair propulsion

The total mechanical energy of an object is the sum of its potential and kinetic energies. The rate at which the mechanical energy level is changing was calculated to determine the mechanical power requirementsFor power flow analysis, the power calculated from the vector dot product of the force and the translational velocity, is called passive joint power (P_j). However, the active muscle power (P_m) was calculated from the vector dot product of the joint moment and the body rotational velocity. Power flow (P_f) of each segment were determined by adding the passive power flow at the proximal end and distal end, combined with the active (muscle) power at the proximal end and distal end, and weight power (P_w) (Gordon et al., 1980; Winter 1994). The energy cost per propulsion calculated from the rate of mechanical energy (E_m) and power flow (E_p) and their discrepancy (E_d) by Wwb method which allowing transfers of energy between adjacent segments of the same limb, but not between limbs and trunk. Wwb method was proved to be a reliable indication of energy cost during submaximal walking(Unnithan et al., 1999).

RESULTS AND DISCUSSION

The upper arm, forearm and hand had the different total mechanical energy pattern (Figure 1), the hand reached the peak value in propulsion phase earlier than the forearm and upper arm segments did. The dissimilarityin mechanical energy pattern mainly resulted from the difference in kinetic energy.The

upper arm, proximal part of upper extremity, move latest and act as a stabilizer during early propulsion phase.

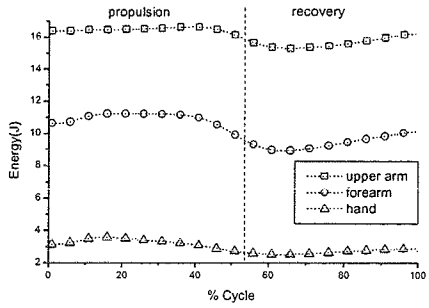

Figure 1: Mean mechanical energy.

The energy change could be further explained by the power flow analysis. Figure 2 showed the components of power flow of the upper arm during propulsion. During propulsion phase, the increased mechanical energy was mainly from both shoulder muscular power and passive shoulder joint power. The shoulder joint power is produced by the trunk flexor and shoulder muscular power is from the shoulder flexor. Both types of power are combined and transferred to forearm and hand to propel the wheel forward. From the terminal propulsion to middle recovery phase, the joint power flow is transferred upward to trunk from upper arm and forearm to conserve the energy of upper extremity in trunk for next propulsion phase. Mechanical power and power flow of forearm (Figure 3) have similar pattern with less discrepancy. In contrast, greater discrepancy found in upper arm may result from its larger power components but less movement. (Gordon et al., 1980).

The energy cost per propulsion calculated from the rate of mechanical energy (E_m) and power flow (E_p) and their discrepancy (E_d) was 9.4±2.4, 13.7±3.5 and 4.1±2.1 J, respectively. The E_p is significant larger than E_m or E_d (P<0.05). The discrepancy between these two power estimates indicates inefficiency in energy expenditure during wheelchair propulsion. Thus, the power supplied to segments is often greater than the mechanical requirements. And we could use it as an index to individualized guidelines for the configuration of handrim wheelchairs.

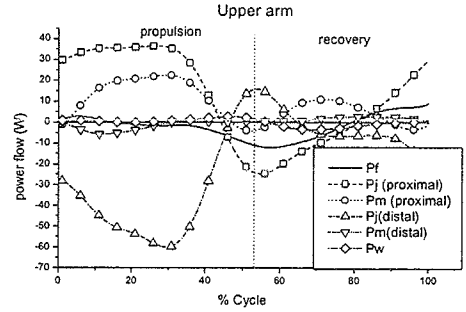

Figure 2: Components of mean power flow.

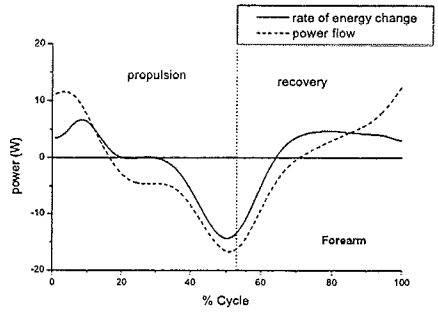

Figure 3: Power flow and mechanical power of forearm.

REFERENCES

Gordon, D. et al. (1980). *J. Biomech,* **13**, 845-854.

Olney, S. J. et al. (1987). *Phys Ther,* **67**, 1348-54.

Unnithan, V. B. et al. (1999). *Med. Sci. Sports Exerc,* **31**, 1703-1708.

Winter, D. A. (1994). *Biomechanics and motor control of human movement.* John Wiley & Sons.

ACKNOWLEDGEMENTS

Supported by grant NSC89-2614-E-242-001 and NHRI-EX90-9019EL.

CONTRALATERAL AND IPSILATERAL CANE USAGE BY PATIENTS WITH OSTEOARTHRITIC KNEE

Grace Chan[1], Andrew W. Smith[1], Chris Kirtley[2] and William W.N. Tsang[1]

[1] Department of Rehabilitation Sciences, The Hong Kong Polytechnic University, Hong Kong
[2] Department of Biomedical Engineering, Catholic University of America, Washington, DC
E-mail: channyg@hkstar.com Web: www.rs.polyu.edu.hk

INTRODUCTION

Knee osteoarthritis (OA) is frequently associated with pain and deformity. OA is the most prevalent rheumatic disease in the world (Badley & Tennant, 1993; March & Schwarz, 1994) and the knee is the most often-affected weight bearing joint. A walking cane is prescribed to reduce loading across the affected joint. The cane placement is important in order to minimize joint loading and slow the progression of the osteoarthritis. The efficacy of contralateral cane usage for relief at the hip joint is well established (Neumann, 1988). However, the contralateral use of a cane to unload the knee joint in patients with knee osteoarthritis may not necessarily have the same effect as at the hip. The aim of the study was to compare the knee joint unloading effect of ipsilateral and contralateral cane use of patients with osteoarthritic knee during walking.

METHODS

The gait of fourteen subjects with osteoarthritic knee was studied under three walking conditions. According to the six point Knee Pain Scale (Rejeski et al, 1995), half of the subjects were rated as score 3, having "discomforting pain" during most of their daily activities, while half fell into the "very severe" group (points 11-13) for the Lequesne Algofunctional Index (Lequesne et al, 1987). The Vicon Clinical Manager calculated the degree of knee deformity. Eight of the subjects were having knee varus (2°-10°) and the remaining six were with knee valgus (1°-10°).

The walking conditions were: (a) walking unaided, (b) walking with a cane held on the ipsilateral (same) side, and (c) walking with a cane held on the contralateral (opposite) side to the affected knee. The kinematics and ground reaction force data of each walking condition were measured by a VICON 370 motion analysis system and multiple AMTI force platforms respectively. These data were combined with the anthropometric measures to calculate the knee joint moments by the process of inverse dynamics. Values were then obtained for the sagittal and coronal plane knee moments, coronal plane hip moment, and temporal-spatial variables. The hip abduction moment was used as an internal control variable. Differences between the three walking conditions were identified using the repeated measures ANOVA.

RESULTS AND DISCUSSION

The reliability results showed acceptable (ICC: 0.416) to excellent reliability (ICC: 0.904) for the frontal plane knee moment, sagittal plane knee moment and frontal plane hip moment during ipsilateral and contralateral cane usage. Good reliability (ICC: 0.76) was also obtained in sagittal plane moment for unaided walking. Poor reliability was found in frontal plane knee moment (ICC: 0.046) and hip moment (ICC: 0.230) during unaided walking.

The data for mean peak knee and hip moments for both knee deformity conditions are summarized in Table 1. Contralateral cane use gave rise to the lowest knee valgus and knee flexion moments of force in both

knee deformity (varus/valgus) conditions. Figure 1 is an example of the mean knee valgus moment for the subgroup of subjects with knee varus deformity.

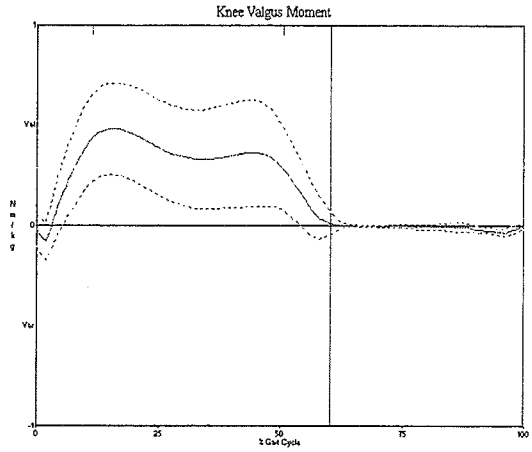

Figure 1: Frontal plane knee moment from subjects (n=8) with knee varus deformity. Mean (solid) ± s.d. (dotted) knee moment of force (Nm/kg)

Significant differences were found between with cane and without cane data in speed and cadence. Significant differences were also illustrated in the values of knee valgus (abduction) moment, hip abduction moment between ipsilateral and contralateral cane use. A significant difference was also obtained in knee flexion moment between contralateral cane use and unaided walking. Non-significant differences were obtained in stride length, hip abduction moment (contralateral versus unaided), knee valgus moment (contralateral versus unaided) and knee flexion moment (ipsilateral versus contralateral, ipsilateral versus unaided).

SUMMARY

From the results of this study, it can be seen that a cane may play a beneficial role in persons with knee osteoarthritis by placing it on the contralateral side of the affected extremity.

REFERENCES

Badley, E.M. & Tennant, A. (1993). *Ann. Rheumatic Dis.*, **52**, 6-13.

Lequesne, M. et al. (1987). *Scand. J. Rheumatology*, **65**, 85-89.

March, L. & Schwarz, J. (1994). *Osteoarthritis Cartilage*, **2 Supp 1**, 41

Neumann, D.A. (1998). *Phys. Ther.*, **78(5)**, 490-501.

Rejeski W.J. et al. (1995). *J. Rheumatology*, **22**, 1124-1129.

Table 1: Mean Peak Knee And Hip Moments For The Knee Varus And Valgus Conditions

Walking Conditions		Mean Moment of Force (± s.d.)	
		Varus Knee (Nm/kg)	Valgus Knee (Nm/kg)
Ipsilateral cane:	Frontal plane knee	0.67 (± 0.25)	0.92 (± 0.64)
	Sagittal plane knee	0.4 (± 0.23)	0.41 (± 0.27)
	Frontal plane hip	1.08 (± 0.26)	1.46 (± 0.72)
Contralateral cane:	Frontal plane knee	0.54 (± 1.09)	0.46 (± 0.18)
	Sagittal plane knee	0.34 (± 0.22)	0.28 (± 0.15)
	Frontal plane hip	0.88 (± 0.15)	0.91 (± 0.22)
Unaided:	Frontal plane knee	0.55 (± 0.15)	1.99 (± 3.44)
	Sagittal plane knee	0.45 (± 0.14)	0.32 (± 0.23)
	Frontal plane hip	0.90 (± 0.19)	1.06 (± 0.41)

QUADRICEPS FEMORIS MUSCLE FATIGUE AND PERCEIVED EXERTION IN ACL-RECONSTRUCTED INDIVIDUALS

Danny M. Pincivero[1], Esther Suter[2], Kimberly Clarke[1], Yuliya Salfetnikov[1]

[1] Human Performance and Fatigue Laboratory, Department of Physical Therapy, Eastern Washington University, Cheney, WA, USA
[2] Human Performance Laboratory, University of Calgary, Calgary, AB, CANADA
E-mail: dpincivero@mail.ewu.edu

INTRODUCTION

Injury to the anterior cruciate ligament (ACL) is a common and debilitating occurrence that yields residual strength deficits following surgical reconstruction (Rosenberg et al, 1992). A higher rating of perceived exertion was shown in individuals with a uni-lateral ACL-deficient knee during a sustained isometric quadriceps femoris (QF) contraction to failure while the rate of increase in EMG activity was not found to be significantly different between the superficial QF components (Tho et al, 1997). The purpose of this study was to examine muscle fatigue and perceived exertion in healthy individuals with a uni-lateral ACL-reconstructed knee.

METHODS

Subjects included 10 healthy volunteers (5 females, 5 males, mean age=29.1 $\pm$ 6.9 years, mean height=171.2 $\pm$ 10.2 cm, mean mass=68.5 $\pm$ 14.2) that had undergone a uni-lateral ACL reconstruction (central 1/3 patellar tendon augmentation). Subjects self-reported as functional, via the Cincinnati Knee Rating System (mean score = 8.8 out of 10, range = 7-10). Following a 5 min period of sub-maximal cycling, subjects were evaluated for 5 maximum voluntary isometric contractions (MVC), performed 2 min apart. Approximately 2 min following the establishment of the 5 MVCs, subjects then performed an isometric contraction equivalent to 80% of the 3 averaged highest MVCs, to the point of failure, during which time the subjects' ratings of perceived exertion was recorded. Perceived exertion was measured with the Borg category-ratio (CR-10) scale. Both legs of each subject were assessed in a random order.

Muscle activity was assessed, via EMG, for the vastus medialis (VM), vastus lateralis (VL), and rectus femoris (RF) muscles during all contractions. Pre-amplified bipolar circular surface electrodes (Ag/AgCl; 0.8 cm diameter) were placed on each muscle with a fixed interelectrode distance (center to center) of 2 cm. The raw EMG signals were full-wave rectified and integrated (IEMG) every 10% during the 80% MVC. Each IEMG value was expressed as a 1 sec avg and then normalised to a 1 sec avg of the activity during the 3 averaged MVCs.

RESULTS AND DISCUSSION

The results demonstrated no significant differences (t_9=1.47, p=0.18) for peak torque (PT) between the involved (mean PT=221.96 $\pm$ 90.43 N•m) and non-involved (mean PT=238.23 $\pm$ 79.81 N•m) limbs. The results also showed no significant differences (t_9=0.96, p=0.36) for 80% MVC endurance time between the involved (mean time=21.4 $\pm$ 5.7 sec) and non-involved (mean time=19.7 $\pm$ 6.5 sec) limbs.

The results demonstrated significant muscle ($F_{2,18}$=13.27, $p<0.05$) and time ($F_{9,81}$=15.83, $p<0.05$) main effects for normalized EMG activity. There was no significant limb main effect, nor any 2- or 3-way interactions. These results showed that during the 80% MVC, a significant increase in EMG activity occurred for all muscles in a parallel manner within the first part of the contraction (Figures 1 and 2).

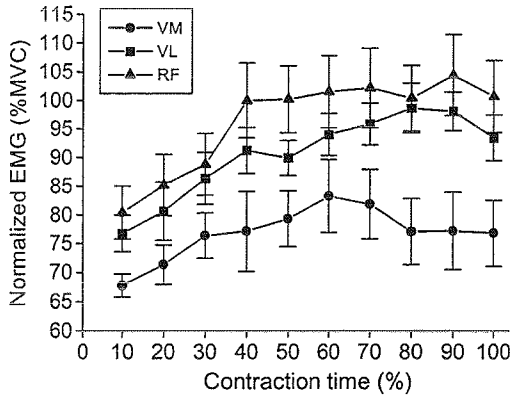

Figure 1: Normalized EMG activity of the VM, VL and RF muscles of the involved limb during a sustained 80% MVC.

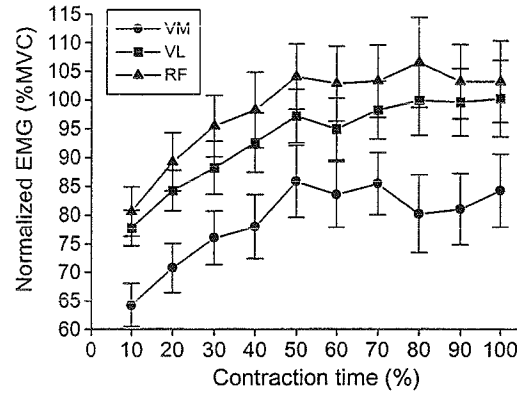

Figure 2: Normalized EMG activity of the VM, VL and RF muscles of the non-involved limb during a sustained 80% MVC.

These results also demonstrate that overall activation of the VM was significantly lower than the VL and RF muscles. Overall activation of the VL and RF muscles were not significantly different.

The perceived exertion response was found to increase significantly ($F_{2,18}$=35.06, $p<0.05$) during the 80% MVC in both involved and non-involved limbs (Figure 3). There were no significant differences between the limbs.

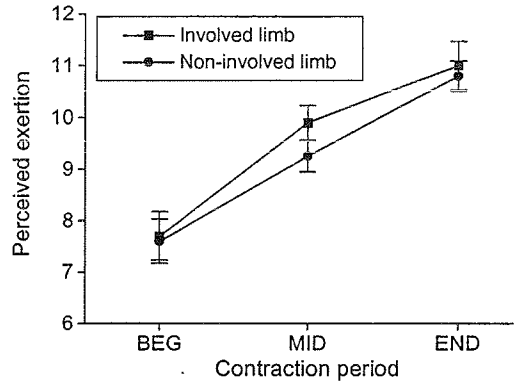

Figure 3: Perceived exertion responses at the beginning (BEG), middle (MID), and end (END) of the 80% MVC of the involved and non-involved limbs.

SUMMARY

These findings suggest that individuals with a uni-lateral ACL-reconstructed knee who self-report as highly functional demonstrate minimal bi-lateral QF strength, muscle activation and endurance, and perceived exertion deficits. The results also support previous findings of a parallel increase in QF muscle activation during fatigue (Pincivero and Gear, 2000; Tho et al, 1997) while the VM remains activated to a lower level than the VL and RF muscles (Pincivero and Gear, 2000).

REFERENCES

Pincivero, D.M., Gear, W.S. (2000). *Muscle Nerve*, **23**, 514-520.

Rosenberg et al. (1992). *Am J Sports Med.*, *20*, 519-526.

Tho et al. (1997). *Clin Orthop Rel Res*, **340**, 142-151.

ELECTROMYOGRAPHIC COMPARISON OF UPHILL WHEELCHAIR PROPULSION BETWEEN YOUNG MALES AND FEMALES

John W. Chow[1], Tim A. Millikan[2], Les G. Carlton[3], Woen-Sik Chae[3], and Eric D. Vidoni[3]

[1]Department of Exercise and Sport Sciences, University of Florida, Gainesville, FL 32611
[2]Divison of Rehabilitation Education, University of Illinois, Urbana, IL 61801
[3]Department of Kinesiology, University of Illinois, Urbana, IL 61801
E-mail: jchow@hhp.ufl.edu

INTRODUCTION

Wheelchair users may encounter a great variety of ramp slopes in everyday activities, necessitating the need to study the demands imposed on the body by various ramp angles. Very few studies have been conducted to examine muscle function during uphill wheelchair propulsion. Also, no attempt has been made to compare the electromyographic (EMG) characteristics of uphill stroking between males and females. To fill the void, the purpose of this study was to compare the EMG levels during wheelchair propulsion over ramps of different slopes exhibited by young males and females.

METHODS

Subjects. Nine male (age 21.1±3.8 yrs) and five female (21.4±3.3 yrs) wheelchair users of different functional levels with no history of persistent joint disorder or musculoskeletal trauma in their upper extremities served as the subjects.

Ramp. A wooden ramp [7.3 m (24') long and 1.1 m (3.5') wide] of adjustable slopes – 0° to 10° at intervals of 2° – was constructed (Figure 1). Because of the crank and pulley systems, the slope of the ramp can be adjusted in a very short time with minimum effort.

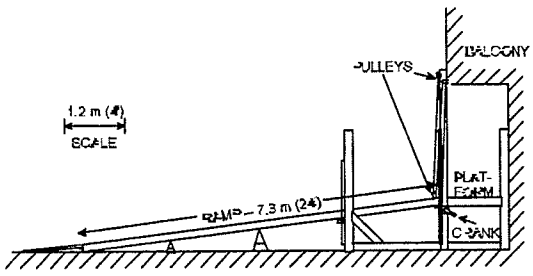

Figure 1. Side view of a wooden ramp.

Trials. Using his/her own wheelchair, each subject pushed up the ramp two times for each slope condition at a self-selected normal speed. The sagittal view (right-hand side) of the stroking movement was recorded by a S-VHS camcorder (60Hz).

EMG. Six pairs of surface electrodes with on-site preamplification circuitry (Liberty Technology MYO115) were attached to the right side of the body to monitor the extensor carpi radialis (EC), triceps brachii (TB), antero-middle (AMD) and postero-middle deltoids (PMD), pectoralis major (PM), and latissimus dorsi (LD). To obtain maximum EMG levels of the selected muscles/muscle groups, maximum effort isometric wrist flexion extension, elbow extension, shoulder flexion, extension, horizontal adduction, and elevation was performed before the experimental trials.

The EMG signals were stored in a small battery operated data logger (Tattletale Mode 8) attached to the chair and downloaded to a computer hard disk at the end of each trial. The sampling rate and duration were set at 1,000 Hz and 5s, respectively. In order to synchronize the EMG and corresponding video recordings, a large light-emitting diode (LED) was attached to the floor and was visible to the camera view. The LED became active automatically at the beginning of the 5-s EMG data recording period.

Data Reduction. The video recordings were used to identify the instants of initial contact, release, and second contact. For the purpose of this study a stroke cycle starts at the instant of hand contact (the beginning of the push phase) and ends at the instant immediately before the next hand contact. A stroke cycle

consists of two phases – *push* and *recovery phases*. The push phase starts at the instant of hand contact and ends at the instant the hand losses contact with the rim. The recovery phase is the period from the end of contact phase to the instant of initial contact.

The raw EMG signals were band pass filtered at a cutoff frequency range of 10 - 1,000 Hz and full-wave rectified. The processed signals were normalized to the maximum EMG levels observed during the isometric trials. One stroke cycle when the subject was in the mid-section of the ramp was selected from each trial for analysis. The average profile over two stroke cycles (one from each trial) was obtained. For each subject, the peak EMG value (expressed as % maximum) and the average EMG over the two phases of the stroke cycle, was determined for each muscle/muscle group.

Statistical Analysis. For each average/peak EMG measure, means and standard deviations were computed for the males and females for each slope condition. A one-way ANOVA was conducted to test for significant difference between the two genders for each EMG measure ($p < 0.05$).

RESULTS AND DISCUSSION

As expected, the EMG levels increased with increasing slope. In general, the TB, AMD, and PM were more active during the push phase while the PMD was more active during the recovery phase. Both EC and LD were equally active in both the push and recovery.

Significant differences in mean EMG activity between males and females were found in the LD during the push phase (Fig. 2) and PM during recovery phase (Fig. 3), as well the peak activity during the push phase in the AMD and LD (Fig. 5) and the recovery phase in the PM (Fig. 6). The female subjects in general had greater levels of muscle activation for each muscle group.

The results indicate that while there is little difference in the muscle activation pattern between men and women during uphill stroking, women in general use a greater

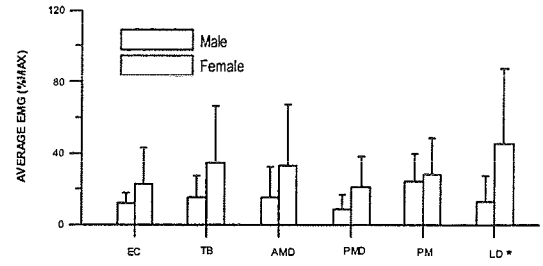

Figure 2. Average Muscle Activity during the Push Phase

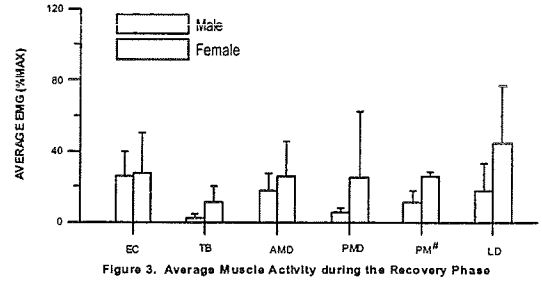

Figure 3. Average Muscle Activity during the Recovery Phase

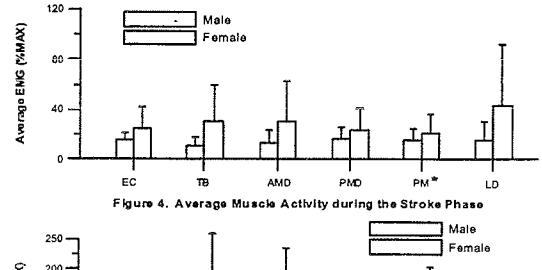

Figure 4. Average Muscle Activity during the Stroke Phase

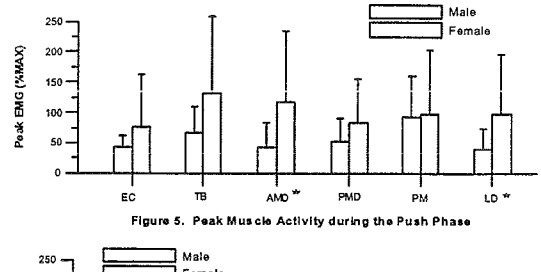

Figure 5. Peak Muscle Activity during the Push Phase

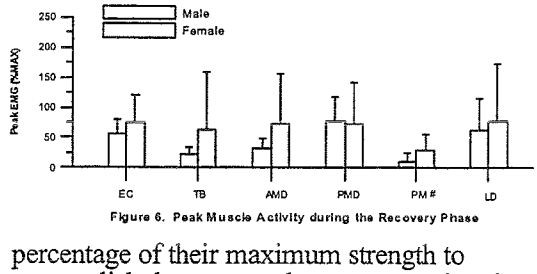

Figure 6. Peak Muscle Activity during the Recovery Phase

percentage of their maximum strength to accomplish the same task as compared to the male subjects.

ACKNOWLEDGMENT

Funded in part by the Mary Jane Neer Research Fund.

KINETICS OF THE LACHMAN TEST: INFLUENCES OF VARIATION IN FORCE APPLICATION

Wendy L. Hurley, Rhonda L. Boros, & John H. Challis

Biomechanics Laboratory, Department of Kinesiology, The Pennsylvania State University, University Park, Pennsylvania
Email: wlh127@psu.edu

INTRODUCTION

Tests of ligamentous stability are commonly included as part of the clinical examination of patients with knee injuries. Despite advances in technology and specialized diagnostic tests, stress testing to determine ligamentous stability remains the mainstay of knee injury evaluation, and the capability to skillfully perform a Lachman test is fundamental to accurate knee evaluation (Malone & Kegerreis, 1988). To date, it is not clear what are the consequences of variation of rate and magnitude of force application used to translate the tibia on the femur during the Lachman test (Noyes et al., 1974; Cooperman et al., 1990; Frank, 1986). However, the accuracy and reliability of the Lachman test vary according to the kinematics of the skill execution (Hurley et al., 2001).

It was the purpose of this study to examine the influence of force application on tibial displacement and strain in the anterior cruciate ligament (ACL) during the Lachman test.

METHODS

Videotape analysis of clinician grip configurations and upper extremity joint movement patterns was made for 22 certified athletic trainers during Lachman test performance to evaluate ACL integrity for 12 knee patients. Clinicians were instructed to perform the Lachman test in the manner consistent with their typical clinical practice. Presentation order of knee patients was randomized across participant clinicians. Videotaped Lachman test trials were coded by classifying clinician grip configurations according to thumb placement of the "tibia hand" as (the hand used by the clinician to displace the patient's tibia relative to the femur) for each trial of the Lachman test. Categories represent the predominant grip configuration during at least 80% of the Lachman trials across knee patients. This type of coding system has been reported to have high inter-experimenter reliability in classifying grip categories (Newell et al., 1989).

A model of the knee in the sagittal plane was developed to permit simulation of the performance of the Lachman test. The model permitted examination of the stress placed on the ACL during the Lachman test. The geometry of the distal femur was modeled based on cadaver data (Nuno & Ahmed, 2001), and the tibial plateau as a flat surface appropriately angled relative to the femur (Draganich et al., 1987). The ligaments were modeled as non-linear elastic elements with their properties, and locations based on cadaver data.

The femur was assumed fixed, the relative orientation of the lower leg to the femur could be adjusted to reflect test conditions. Motion of the lower leg was achieved by a force applied to the "posterior" surface of the shank, then the strain on the ACL measured. The inertial parameters of the shank and foot were determined by modeling subjects' lower leg as series of geometric solids. The muscles were assumed to not be active during the test, which reflects the instructions given to the subjects.

RESULTS

Clinician grip configuration was classified into two categories according to clinician thumb placement of their "tibia hand" in reference to the patient's knee: thumb on knee joint space (category A); thumb on or distal to tibial tuberosity (category B). Of the certified athletic trainers sampled, 84.2% demonstrated category B condition although clinicians under the category A condition achieved a greater mean number of accurate assessments than those under category B ($F=14.335$; $p=.001$).

Simulations of the loads on the lower leg produced ACL strains similar to those measured experimentally in vitro (Pioletti & Rakotomanana, 2000). The model was used to simulate the Lachman test, mimicking the two clinician groups with the force applied more proximally (2 cm from knee axis), and then more distally (8 cm). ACL strain was considerably greater under category A compared with category B (2.4% versus 0.4%). Similarly anterior translation of the tibia was greater under category A (1.8 mm vs. 0.35 mm). But irrespective of point of force application, ACL strain and tibial translation were relatively insensitive to the level of force application during the Lachman test.

DISCUSSION

Primary and secondary ligament restraints safeguard the knee against the effects of force application during the Lachman test. Grip configurations using more distal tibial hand placement appears to alter force application to the ACL. Ligamentous stability would therefore be masked during the Lachman test potentially hindering clinical evaluation accuracy.

The model is a parsimonious representation of a complex system that appears to capture the essential elements of the system that influence the variability in which a group of subjects chose to execute the Lachman test.

REFERENCES

Cooperman, J.M., et al. (1990). *Phys. Ther.*, **70**, 225-233.

Draganich, L.F., et al., (1987). *J.Orthop.Res.*, **5**, 539-547.

Frank, C. (1986) *Clin. Orthop.*, **213**, 163-166.

Hurley, W.L., et al. (2001). *NATA 2001 Educators Conference*, Fort Worth, TX.

Malone, T., Kegerreis, S.T. (1988) *Physical Therapy of the Knee.* Churchill Livingstone, New York.

Newell, K.M., et al. (1989). *Dev Psychobiol.*, **22**, 817-832.

Noyes, F.R., et al. (1974). *J Bone Joint Surg.*, **56**, 236-253.

Nuno, N., Ahmed, A.M. (2001) *J. Biom. Eng.*, **123**, 18-26.

Pioletti, D.P., Rakotomanana, L.R. (2000). *J.Biom.*, **33**, 1729-1732.

PROSTHETIC AND INTACT LEG STIFFNESS COMPARISON IN SUBJECTS WITH UNILATERAL BELOW KNEE AMPUTATION

Jin Jia and Gerald Smith

Biomechanics Lab, Oregon State University, Corvallis, Oregon
Email: Gerald.Smith@orst.edu

INTRODUCTION

The stance limb of humans and other animals behaves like a spring during running and hopping and can be described by a single linear mass-spring model. (McMahon and Cheng, 1990) During hopping, leg stiffness is mainly adjusted by modulating ankle stiffness (Farley and Morgenroth, 1999). For people with unilateral below knee (UBK) amputation, there is little or no ability to modulate the artificial ankle stiffness on the prosthetic limb under different conditions such as varying running speeds or hopping frequencies while the sound ankle on the intact limb can be adjusted in stiffness to match demands.

Based on these ideas, we hypothesized that leg stiffness of a prosthetic limb would be substantially different from a subject's intact limb across a range of hopping frequencies. We selected frequency as the independent variable because of its importance in adjusting leg stiffness during bouncing gaits such as hopping and running (Farley et al, 1996). A secondary focus of this study was to investigate how leg stiffness of a prosthetic limb and an intact limb are combined during double leg hopping.

METHODS

Two male UBK subjects participated in this initial investigation. The first subject (34 yrs; 104 kg; 1.93 m) was an active sport participant, while the second subject (33 yrs; 82 kg; 1.81m) was less active. Both subjects used the same socket attached to the Flex-Foot Re-Flex VSP model prosthetic. A vertical shock pylon is built into this device, creating a spring-damper system. The spring stiffness is adjusted to the person's body weight and activity level. In this case, the first subject used a number 9 pylon while the second subject used a number 6 pylon. Combined pylon-foot stiffness ranges between about 31 to 38 kN/m (Miller and Childress, 1997).

Vertical force data (1000 Hz sampling frequency) and sagittal plane kinematics (60 Hz) were collected during single and double legged hopping. For each condition, preferred hopping frequency (PHF) was initially used with the subject hopping comfortably for about 10 seconds. Four additional hopping frequencies (10% and 20% greater and less than the preferred frequency) were recorded. Five consecutive hops were analyzed. Leg stiffness of each hop was calculated using the ratio of peak force to the maximum displacement of the center of mass.

RESULTS AND DISCUSSION

Preferred hopping frequencies for single legged hopping on the prosthetic leg, intact leg and for double legged hopping were similar for subject 2 while subject 1 preferred higher frequencies on the prosthetic leg (see figure 1). Leg stiffness of both the prosthetic leg and the intact leg increased substantially as frequency increased. While prosthetic and intact leg stiffnesses were not identical, for subject 1 the prosthetic leg was generally stiffer than the intact leg while for subject 2 this pattern was reversed. These results suggest that humans can change leg stiffness without changing ankle stiffness.

With constant prosthetic ankle joint stiffness, knee and hip stiffness were adjusted to affect overall leg stiffness. This more complex strategy allowed prosthetic

leg hopping through a range of frequencies much like what is done with an intact leg and varying ankle stiffness. However, it was very difficult for either subject to hop on the prosthetic leg for more than 10 seconds due to balance and strength limitations.

The combined leg stiffness of double leg hopping was found to be similar to single leg hopping. From these two subjects, we did not get a clear trend about how the prosthetic and intact legs mixed to determine combined stiffness and frequency.

During hopping, leg stiffness is the ratio of peak force to maximum center of mass displacement. In previous measurements we have observed that for a normal leg, frequency and stiffness are increased by maintaining peak force nearly constant but decreasing vertical displacement. In this study, the subject with greater motion functionality of the prosthetic leg showed this same strategy for adjusting leg stiffness in all three leg conditions. But the second subject increased leg stiffness by both increasing peak force and decreasing center of mass vertical displacement in a similar proportion. This was probably a more demanding strategy but was required by the strength and motion limitations of the subject's prosthetic leg.

SUMMARY

This study provides useful information for clinicians and designers of prosthetics for UBK amputees. We found that subjects were able to increase leg stiffness to control hopping frequency for both intact and prosthetic legs. Depending on the level of an amputee's adaptation to the prosthetic, leg stiffness was adjusted by various amount of vertical displacement and ground reaction force changes.

REFERENCES

Farley, C.T. et al. (1996). *J. Biomech.*, **29**, 181-186.

Farley, C. T., Morgenroth, D. (1999). *J. Biomech.*, **32**, 267-273.

McMahon, T.A., Cheng, G.C. (1990). *J. Biomech.*, **32**, Suppl. 1:65-78.

Miller, L.A., Childress, D.S. (1997). *J. Rehab. Res. Dev.*, **34**, 52-57.

ACKNOWLEDGEMENTS

The authors thank Mr. Bill Roberts of Advanced Prosthetics of Salem, Oregon for his assistance with the project.

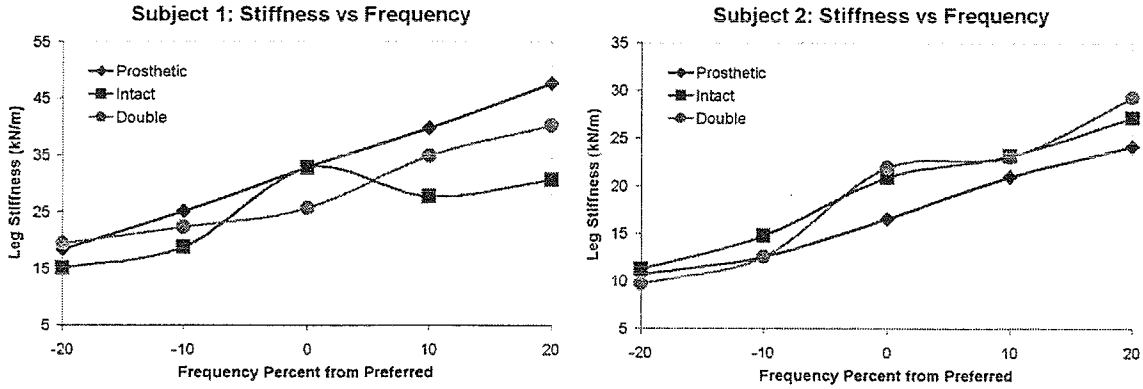

Figure 1. Comparison of leg stiffness across frequencies for subjects 1 and 2. Preferred hopping frequency for subject 1 was 2.3 Hz (intact leg), 2.7 Hz (prosthetic leg), and 2.3 Hz (double leg). For subject 2 preferred frequencies were 2.2 Hz, 2.1 Hz and 2.1 Hz, respectively. Data points are the mean of five consecutive hops for each frequency.

THE COMPARISON OF TWO DIFFERENT PROPULSIVE TECHNIQUES FOR MANUAL WHEELCHAIR PROPULSION

Hong-Wen Wu[1], Yi-Wen Chang[2], Fong-Chin Su[3], and Ka-Nan An[4]

[1]School of Physical therapy, China Medical College, Taichung, TAIWAN
[2]Department of Physical Therapy, Foo-Yin Institute of Technology, Kaohsiung, TAIWAN
[3]Institute of Biomedical Engineering, National Cheng Kung University, Tainan, TAIWAN.
[4]Orthopedic Biomechanics Laboratory, Mayo Clinic, Rochester, MN55905, USA.
E-mail: wuh@mail.cmc.edu.tw

INTRODUCTION

Repetitive strain injuries, such as rotator cuff tears and carpal tunnel syndrome, resulting from long-term or incorrect use of manual wheelchair, are the main complain of the patients with spinal cord injury, who are an important subgroup of those using wheelchair for their primary mobility (Bayley et al., 1987). The high pressure on the musculoskeletal system, in conjunction with abnormal distribution of stress, contributes to the high rate of injury problem. Understanding this incidence distribution to the underlying upper extremity biomechanics of wheelchair propulsion would allow the clinicians and wheelchair designers to adjust the factors that produce injuries. Based on the well developed instrumented wheel to measure the three-dimensional forces and moments on the handrim applied by the wheelchair user, a three-dimensional dynamic model for estimating the joint forces and moments in the upper extremity has been established (Wu et al., 1998 and 1999). Therefore, the purpose of this study was to compare the kinematic and kinetic parameters between two different propulsion techniques (pumping and pull-push), in order to better understand the effect of propulsive technique on the biomechanics of wheelchair propulsion.

METHODS

Twelve ambulatory physical therapists, who were familiar with wheelchair propulsion, propelled the wheelchair with two different techniques. Each subject was asked to propel the wheelchair at a self-selected comfortable speed on the level floor. Seventeen reflective markers were placed on left upper extremity and trunk of the subjects, and the wheel in order to define the orientations of trunk, upper arm, forearm, hand and wheelchair. The ExpertVision™ motion analysis system synchronized with the instrumented wheel were used to record three-dimensional positions of the reflective markers and handrim contact forces and moments. Euler angle was used to describe the angular movements of the joints in upper extremity. The intersegmental forces and moments of the shoulder, elbow, and wrist were computed with the inverse dynamic method. The mechanical efficiency, defined as the ratio of tangential force divided by the total handrim contact forces, was derived in this study. Besides, the maximum isometric voluntary strengths of the shoulder, elbow, and wrist joints were also collected. In order to facilitate the understanding of how net joint resultant loads may predispose wheelchair users to musculoskeletal problems, the wheelchair propulsion strength rating (WPSR), defined as the ratio between the maximum intersegmental moment generated during propulsion and

that generated during an isometric maximum strength test, was calculated in this study.

RESULTS AND DISCUSSION

The peak mechanical efficiency in push-pull (0.81) was significantly greater than that in pumping technique (0.67, $P<0.05$). However, there is no significant difference in mean mechanical efficiency (0.49 vs. 0.47). The comparison of joint range of motion (ROM) between these two propulsion techniques was listed in Table1. There were significant differences in ROM for all joints between pull-push and pumping techniques, except the ROM for the movement of trunk rotation. This would indicate that the ROMs needed for these two techniques during wheelchair propulsion were substantially different. The comparison of WPSR was shown in the Figure 1. The WPSR of shoulder extension and forearm supination in pumping technique are significantly greater than that in pull-push technique. In general, the pumping technique was found in wheelchair athletes to increase the race speed. It was implied that using pumping technique would increase the risk of injury since the joint loading was increased. However, it did not increase the mechanical efficiency of wheelchair propulsion. It would be suggested that the pumping technique was not suitable for the new wheelchair users.

REFERENCES

Bayley, J.C. et al. (1987), *J. Bone Jt. Surg (AM),* **69**, 676-678.

Wu, H.W. et al. (1998), *J. Biomed. Eng.* **120**, 533-535.

Wu, H.W. et al. (1999), *Biomedical Aspects of Manual Wheelchair Propulsion*, ISO Press, 134-137 & 152-155.

ACKNOWLEDGEMENTS

This study was funded by grant NSC89-2614-E-242-001, from the National Science Council, TAIWAN, and by grants HD07447 & HD33806, from the National Institutes of Health, USA.

Table 1: Comparison of the range of motion between pull-push and pumping techniques. (F: flexion; E: extension; abd: abduction; add: adduction; R: radial deviation; U: ulnar deviation; P: pronation; S: supination)

ROM (degree)		pull-push	pumping
trunk	F/E*	8.6±2.2	6.9± 1.5
	abd/add*	3.2±1.0	2.6±0.6
	rotation	7.5±2.4	6.5±1.8
shoulder	F/E*	52.7±6.6	34.0±5.6
	abd/add*	16.6±3.9	5.9±5.8
	rotation*	46.7±8.0	29.9±4.7
elbow	F/E*	43.1±5.8	35.2±8.5
	abd/add*	2.0±1.0	1.7±0.9
	rotation*	3.0±1.7	2.1±1.8
wrist	F/E*	46.8±8.2	29.2±7.2
	R/U*	29.9±9.3	20.3±7.2
forearm	P/S*	37.8±12.	25.6±13.

* pair-t test: $p<0.05$

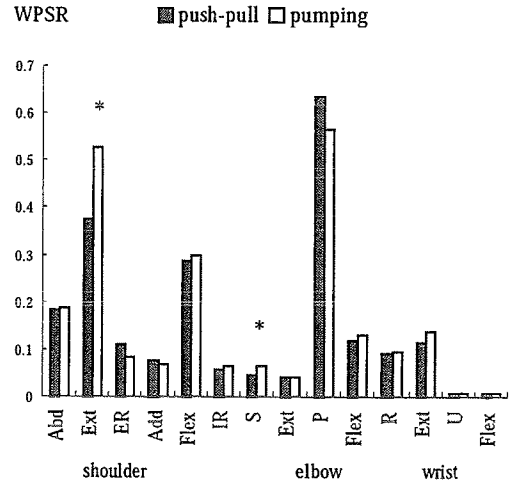

Figure 1: The WPSR during wheelchair propulsion. * pair-t test: $p<0.05$. (Abd: abduction; Ext: extension; ER: external rotation; Add: adduction; Flex: flexion; IR: internal rotation; S: supination; P: pronation: R: radial deviation; U: ulnar deviation).

BIOMECHANICAL DIFFERENCES BETWEEN NEUTRALLY ALIGNED, PES CAVUS AND PES PLANUS FEET IN DIABETIC PATIENTS

William R. Ledoux [1,2], Jane B. Shofer [3], Edward J. Boyko [4], Bruce J. Sangeorzan [1,2]

[1] RR&D Center for Excellence in Limb Loss Prevention and Prosthetic Engineering, VA Puget Sound, Seattle, WA, USA
[2] Department of Orthopaedics, University of Washington, Seattle, WA, USA
[3] Department of Medicine, University of Washington, Seattle, WA, USA
[4] Epidemiologic Research and Information Center, Seattle, WA, USA
Email: wrledoux@u.washington.edu Web: rehabctr.vamc.washington.edu

INTRODUCTION

Foot type is an architectural concept; feet may be broadly classified as one of three foot types: neutrally aligned, pes planus (low arch) and pes cavus (high arch). The neutrally aligned foot type is asymptomatic, healthy and well aligned. A pes planus foot type has little or no arch, while a pes cavus foot type has an abnormally high arch, both of which are primarily sagittal plane deformities.

Although peripheral vascular disease has been associated with ulceration, it is now understood that the majority of foot ulcers are caused by mechanical trauma to an insensate foot (Cavanagh *et al.* 2001). High plantar pressure, a measure of the mechanical trauma the tissue is exposed to, is often associated with abnormal foot biomechanics (Ahroni *et al.* 1999). However, the relationship between aberrant foot structure and altered plantar pressure distributions is not well documented. Nor has the concept of foot type been conclusively defined. Thus, in order to further our understanding of the ulceration process as it is related to foot architecture and aberrant plantar pressures, we must first increase our knowledge of the differences between foot types.

METHODS

The data employed for this study were previously collected for the Seattle Diabetic Foot Study (SDFS) (Boyko *et al.* 1999). Subjects were included if their foot type was determined as neutrally aligned, pes cavus (high arch) or pes planus (low arch). Subjects with current ulcers were excluded. Several biomechanical parameters were measured on each subject, including: 1) ankle, subtalar and first metatarsophalangeal joint mobility, 2) presence of foot deformity (muscle atrophy, bony prominences, as well as toe and metatarsal head deformities) and 3) various radiographic measurements. This study will report on the differences in the measured variables between foot types.

Chi-square tests were used to test for an association between foot type and categorical biomechanical measures. For continuous variables, a one way ANOVA was used to test whether means were different by foot type. Helmert contrasts were used to determine the pattern of significance among individual foot types.

RESULTS

There were several significant relationships between biomechanical measures and foot type (see Table 1). For hallux dorsiflexion, pes cavus feet had increased motion and rigid pes planus had decreased motion. Pes cavus feet had lower hallux plantar flexion. For the deformity measures, the percent of subjects with intrinsic muscle atrophy and bony prominences is significantly lower for the neutrally aligned feet, while the differences in the percent of subjects with hallux valgus and hallux limitus was higher with the rigid pes planus feet. Pes cavus feet had significantly higher percentages of bony prominences. Neutrally aligned feet had less hammer/claw toes, while occurrence of this malady was significantly greater for pes cavus feet. The pes cavus feet also had greater amounts of prominent metatarsal heads. Additionally, the neutrally aligned feet had a smaller percentage of plantar calluses. The X-ray parameters demonstrated longer metatarsal heads, greater intermetatarsal (IM) angles and lower lateral talometatarsal angle for both pes planus groups. Finally, the pes planus feet had significantly larger talocalcaneal angles.

joint mobility (°)	neutrally aligned (n=1174)	pes cavus (n=493)	pes planus rigid (n=171)	pes planus flex (n=209)	p -value
dorsiflexion	8.1 ± 0.2 (760)	7.4 ± 0.4 (349)	9.0 ± 0.6 (107)	8.3 ± 0.5 (151)	0.063 [a]
calcaneal ever.	15.1 ± 0.6 (117)	17.5 ± 2.7 (28)	15.9 ± 1.3 (21)	15.4 ± 1.3 (34)	0.6 [a]
calcaneous inv.	18.2 ± 0.7 (117)	18.1 ± 1.4 (28)	18.7 ± 0.7 (21)	17.8 ± 1.5 (34)	1.0 [a]
hallux dorsi.	38.8 ± 0.4 (806)	44.6 ± 0.6 (372) [c]	36.0 ± 1.0 (118) [c]	39.1 ± 0.9 (168)	< 0.0001 [a]
hallux plan.	33.8 ± 0.4 (804)	27.8 ± 0.7 (370) [c]	32.8 ± 1.1 (118)	32.1 ± 1.0 (168)	< 0.0001 [a]
deformity (%), (n)					
int. mus. atrophy	49.0 (802) [c]	76.2 (370)	71.1 (121)	67.7 (164)	< 0.0001 [b]
bony prominences	48.7 (799) [c]	78.1 (370) [c]	74.4 (121)	65.7 (166)	< 0.0001 [b]
hallux valgus	28.7 (1170)	33.5 (490)	43.8 (169) [c]	32.7 (208)	0.0007 [b]
hallux limitus	29.2 (1167)	32.4 (491)	42.3 (168) [c]	21.2 (208)	0.0001 [b]
hammer/claw toes	60.4 (1171) [c]	86.4 (491) [c]	74.7 (170)	72.6 (208)	< 0.0001 [b]
prom. met. head	53.4 (1169)	86.2 (493) [c]	55.0 (171)	64.1 (206)	< 0.0001 [b]
plantar callus	52.0 (1173) [c]	59.6 (493)	57.3 (171)	57.9 (209)	0.022 [b]
X-ray measures					
met. length (mm)	4.01 ± 0.08 (455)	4.10 ± 0.11 (221)	4.64 ± 0.17 (86) [d]	4.76 ± 0.19 (91) [d]	< 0.0001 [a]
inter. met. ang. (°)	9.4 ± 0.1 (459)	9.2 ± 0.2 (221)	10.2 ± 0.4 (86) [d]	10.0 ± 0.3 (91) [d]	0.015 [a]
hal. valg. ang. (°)	14.2 ± 0.3 (453)	14.5 ± 0.4 (220)	14.7 ± 1.0 (86)	14.4 ± 0.8 (91)	0.9 [a]
5th met. angle (°)	11.5 ± 0.3 (455)	11.2 ± 0.5 (220)	11.9 ± 0.8 (86)	10.5 ± 0.6 (91)	0.6 [a]
lat. ta-calc. ang. (°)	45.8 ± 0.4 (459)	47.8 ± 0.4 (221) [c]	44.4 ± 0.8 (86)	44.7 ± 0.7 (91)	< 0.0001 [a]
lat. ta-met. ang. (°)	0.0 ± 0.5 (458)	-1.7 ± 0.6 (221)	9.8 ± 1.3 (86) [d]	5.6 ± 1.0 (91) [d]	< 0.0001 [a]

[a]ANOVA, [b]Chi-square, [c]significantly different from others, [d]significantly different from two others

Table 1: The differences between foot types for several biomechanical parameters.

DISCUSSION

A prospective study of the differences of several biomechanical parameters between neutrally aligned, pes cavus and pes planus feet was conducted. The data indicated that there were several interesting differences between the foot types. Pes cavus feet have abnormal first metatarsophalangeal joint ranges of motion (both in dorsiflexion and plantar flexion) as well as increased percentages of hammer/claw toes and prominent metatarsal heads. These findings are all indicative of aberrant metatarsophalangeal joint mechanics found with pes cavus feet (Green *et al.* 1987). Neutrally aligned feet have lower percentages of intrinsic muscle atrophy, bony prominences, hammer/claw toes and plantar calluses, all of which is consistent with neutrally aligned feet being asymptomatic. Additionally, rigid pes planus feet had higher percentages of hallux valgus and hallux limitus, a finding contradicted in the literature (Kilmartin and Wallace 1992), perhaps because that study dealt with children and did not differentiate between rigid and flexible feet. Finally, both rigid and flexible pes planus feet demonstrated differences in X-ray parameters that have been observed previously (Gould 1982). This study provides a further understanding of the relationship between foot structure and foot function in a large scale, prospective manner.

ACKNOWLEDGEMENT

This work was funded by The Seattle Epidemiologic Research and Information Center.

REFERENCES

Ahroni, J. H., E. J. Boyko, et al. (1999). *Diabetes Care* **22**(6): 965-72.

Boyko, E. J., J. H. Ahroni, et al. (1999). *Diabetes Care* **22**(7): 1036-42.

Cavanagh, P., J. S. Ulbrecht, et al. (2001). *The Diabetic Foot.* J. H. Bokwer and M. A. Pfeifer. St. Louis: 125 - 196.

Gould, N. (1982). *Foot Ankle* **2**(4): 213-9.

Green, D. R., G. M. Lepow, et al. (1987). *Comprehensive Textbook of Foot Surgery.* E. D. McGlamry. Baltimore, Williams and Wilkins. **1:** 287-323.

Kilmartin, T. E. and W. A. Wallace (1992). *Foot Ankle* **13**(2): 53-6.

A QUASI-LINEAR VISCOELASTIC MODEL OF FOOT-ANKLE LIGAMENTS

Chimba Mkandawire[1], William Ledoux[1,2], Bruce Sangeorzan[1,2] and Randal Ching[1,2]

[1]Center of Excellence for Limb Loss Prevention and Prosthetic Engineering, Puget Sound VA, Seattle, WA, USA
[2]Department of Orthopaedics, University of Washington, Seattle, WA, USA
E-mail: bluntme@u.washington.edu Web: http://rehabctr.vamc.washington.edu/

INTRODUCTION

We have developed a computational model of the foot and ankle (Ledoux 2000) to assist in the diagnosis and treatment of diabetic foot ulcers. The goal of this research was to investigate a quasi-linear viscoelastic (QLV) model of ankle and foot ligaments for future implementation into our computational model.

METHODS

Experimental Procedure. Five fresh-frozen lower-limb cadaver specimens were obtained, and the following bone-ligament-bone specimens were prepared: inferior calcaneonavicular (ICN), long plantar (LP), plantar first-cuneiform first-metatarsal (PFCFM), and posterior tibiotalar (PTT). The LP ligament was not harvested beyond its initial insertion into the cuboid. Ligaments were potted in polymethyl-methacrylate and tested on an MTS Materials Testing System (MTS Systems Corporation, Eden Prairie, MN). Specimens were preconditioned to maximum passive physiologic strain, defined by measuring ligament displacement from neutral position of cadaver limb to maximum passive eversion, inversion, planterflexion, dorsiflexion, internal rotation and external rotation.

After specimen preparation, stress relaxation experiments were conducted. A ramp and hold test was performed, where ligaments were deformed at 1 mm/s to the preconditioned strain, then held for 300 seconds. Data acquisition was performed at 1 kHz using TestStar2 software (MTS Systems Corporation, Eden Prairie, MN). Post-process filtering was performed at 10 Hz using DADiSP software (DSP Development Corporation, Newton, MA).

Quasi-linear Viscoelastic Model. Several variations of QLV have been used to model soft tissue, including ligaments (Funk 2000, Iatradis 1997, Kwan 1993, Woo 1981). The variant used for this study, shown in equations (1-4), has been previously described by Ledoux (1999). These relations are as follows.

$$\sigma(t) = \int_0^t G(t-\tau)\frac{\partial \sigma^e[\varepsilon(t)]}{\partial \tau} \quad (1)$$

$$\sigma(\varepsilon) = A\left(e^{B\varepsilon} - 1\right) \quad (2)$$

$$G(\tau) = \frac{1 + \int_0^\infty S(\tau)e^{-t/\tau}d\tau}{1 + \int_0^\infty S(\tau)d\tau} \quad (3)$$

$$S(\tau) = \begin{cases} \frac{C_1}{\tau} + \frac{C_2}{\tau^2}, \tau_1 \le \tau \le \tau_2 \\ 0, \tau < \tau_1 and \tau > \tau_2 \end{cases} \quad (4)$$

Nonlinear Curve Fit. The parameters *A, B,* C_1, C_2, and τ_1 were fit using the nonlinear Levenberg-Marquardt least-squares optimization routine of Igor Pro (WaveMetrics, Inc., Lake Oswego, OR). The parameter τ_2 was set to the final time-point. Due to the sensitivity of the coefficients, the stress relaxation data were averaged for each ligament before curve fitting.

RESULTS

Figure 1 illustrates a relaxation fit of the PFCFM ligament. This fit is representative of the other ligaments. Table 1 lists the parameters from the curve fit of all the ligaments, as well as the reduced chi-square Goodness of Fit value.

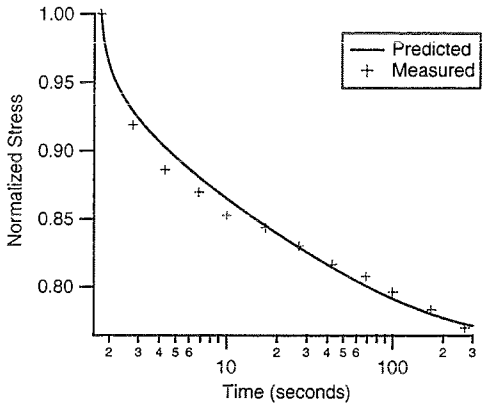

Figure 1: Typical decimated averaged ligament data and curve fit (PFCFM ligament). Note, all data used in curve fit.

DISCUSSION

The reduced chi-square values listed in Table 1 were all less than one, indicating successful fits with the QLV model. This study modeled ligaments as viscoelastic elements, whereas previous ligament material studies have considered ligaments as linear elastic elements (Siegler 1988). Previous QLV models of ligaments have only focused on ankle ligaments (Funk 2000). Future work will involve accommodation of greater ligament diversity within the foot-ankle complex, and the classification of ligaments based on area-length ratios. In addition, comparisons with two other nonlinear constitutive models for ligament behavior, the Weibull-based stress-stretch relationship developed by Hurschler (1997) and a nonlinear three-element model composed of a nonlinear spring in series with a nonlinear Voigt body will be made. Since the ligaments were ramped at only 1 mm/s, relaxation may have occurred during the ramp. Future tests will be conducted at faster loading rates.

REFERENCES

Funk J.R., Hall G.W. (2000). et al. *J Biomech Eng.* 122(1):15-22.

Hurschler, C., Loitz-Ramage B., et al. (1997). *J Biomech Eng.* **119**(4):392-399.

Iatradis J.C., Setton L.A., et al. (1997). *J Biomech.* 30(10):1005-1013.

Ledoux W.R., Meaney, D.F. et al. (1999). 23rd Annual Meeting, American Society of Biomechanics. Pittsburgh, PA.

Ledoux W.R., Camacho, D.L. et al. (2000). The World Congress on Medical Physics and Biomedical Engineering, Chicago, IL.

Kwan M.K., Lin T.H., et al. (1993). *J Biomech.* **26**(4-5):447-452.

Siegler S., Block J., et al. (1988). *Foot & Ankle.* **8**(5):234-242.

Woo S.L., Gomez M.A., et al. (1981). *J Biomech Eng.* **103**(4):293-298.

ACKNOWLEDGMENTS

This work was funded by the VA Rehabilitation Research & Development Service and a VA Pre-Doctoral Associated Health Rehabilitation Research Fellowship.

Table 1: Relaxation curve fit data

	C_1	C_2	τ_1	τ_2	A	B	N	reduced χ^2
ICN	4.06e-3	3.26e-2	6.10e-4	301.86	1.87e-3	1.53	4	5.43e-3
PTT	8.00e-2	1.00e-3	1.00e-3	303.3	1.26	10.0	5	1.14e-2
LP	3.50e-3	2.86e-2	3.88e-2	301.84	5.03e-2	5.47	5	2.69e-3
PFCFM	1.19e-3	1.00e-3	1.10e-3	301.78	3.76e-4	0.595	5	8.20e-4

SPATIAL DISTRIBUTION OF HIP CAPSULE STRUCTURAL AND MATERIAL PROPERTIES

Kristofer J. Stewart, Rohan Edmonds-Wilson, Richard A. Brand, and Thomas D. Brown

Orthopaedic Biomechanics Laboratory, 2181 Westlawn Building,
University of Iowa, Iowa City, IA 52242
E-mail: kristofer-stewart@uiowa.edu Web: poppy.obrl.uiowa.edu

INTRODUCTION

Contemporary computational models now allow the practical incorporation of the effects of a joint capsule on both motion and the loads transmitted to the other parts of the joint. However, to date, material properties have not been available to represent the hip capsule for this purpose (Scifert, 1999). The capsule is critical to the stability and proper function of the hip joint. Only recently have experimental studies begun to attempt to quantify the mechanical properties of hip capsule (Hewitt, 1999). We here report quantitative, structural and material properties of the hip capsule, obtained experimentally for the entire intact capsule structure, and for eight individual segments of the hip capsule.

METHODS

Both hip joints of fresh-frozen, non-diseased cadavers were procured from five donors (three females and two males) ranging from 68 to 89 years of age (average 82) at the time of death. All specimens were stored at –20 °C and thawed for twelve hours prior to dissection. After thawing, all exterior skin and musculature layers were dissected from each hemi-pelvis, care being taken to preserve the integrity of the capsule encasing the joint. Throughout storage, dissection, geometric measurements, and experimental testing stages, specimens were irrigated with physiologic saline solution to minimize tissue dehydration and degradation.

Whole joint distraction was initially performed to measure the overall structural stiffness of the capsule. The iliac crest, ischial tuberosity, and distal portion of the femur were individually potted in polymethylmethacrylate (PMMA) bone cement. The specimen was mounted in an MTS servo-hydraulic materials testing machine, with the longitudinal axis of the femoral neck (and hence the capsule) coincident with the direction of the applied tensile force. Each hemi-pelvis specimen was preconditioned by ramping from 20 N to 100 N at a rate of 0.4 mm/sec, and then loaded (nondestructively) to 750 N at a rate of 0.4 mm/sec.

Following the whole joint distraction test, the anatomical insertion points of the hip capsule at the anterior superior iliac spine (ASIS) and the lesser trochanter (LT) were tattooed with fiduciary marks. A complete capsulectomy was performed by cutting longitudinally between the two points, and then circumferentially around the acetabular and femoral insertions of the capsule. Once extracted from the joint, the arc-shaped capsule was photographed (Figure 1a). A specially constructed fixture (Figure 1b) was used to section the capsule into eight, approximately even sectors (Figure 1c).

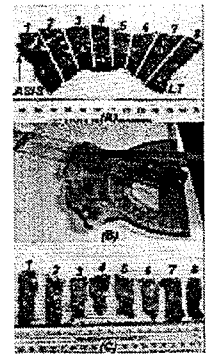

Figure 1

The individual sectors were fastened to a set of cyroclamps, mounted to the MTS machine, and straightened with a small tensile load (~1N). Digital vernier calipers were used to record the following geometric measurements: width and thickness at the proximal, medial, and distal ends of the clamped specimen; and initial clamp-to-clamp length.

The specimen was subjected to ten cycles of preconditioning to displacement of 1 mm (strain nominally 5%), followed by testing to failure at a strain rate of 0.8 sec^{-1} (distension rate of 4mm/sec). Stiffness was measured as the slope of the load-deformation plot in the region between the characteristic nonlinear "toe" region and the first sign of a failure as determined from the resulting load-deformation curve. Strain measurements were based on clamp-to-clamp displacements, normalized by initial length obtained with digital vernier calipers.

RESULTS AND DISCUSSION

The load-displacement data (as shown in Figure 2) reveal a non-linear response. The slope of the linear region represents the structural stiffness of the individual sectors.

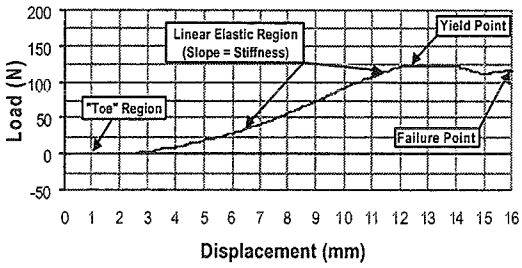

Figure 2: Representative load-deformation curve for an individual sector with four distinct regions: "toe", linear-elastic, yield, and failure.

Plotting the structural stiffness values for individual sectors illustrates the intrinsic specimen variability. Across-specimen averages were computed (overall average 36 N/mm) and reveal significantly lower ($p>0.01$) average stiffness values in posterior-inferior portion (sectors 3 to 6) of the capsule.

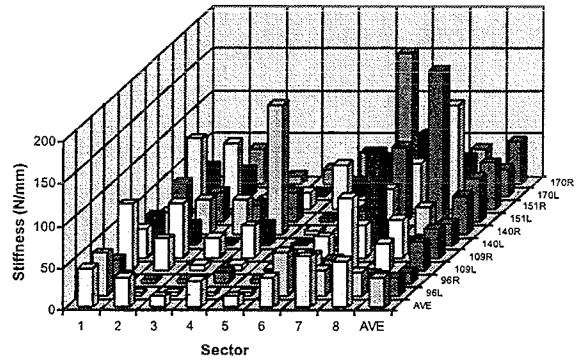

Figure 3: Absolute structural stiffness values with across-specimen and across-sector averages.

The results from this investigation for the first time map the full circumferential distribution of structural and material properties of hip capsule. Explorations of hip stability using numerical models can now be enhanced by incorporation of these experimental capsule data.

REFERENCES

Hewitt, J.D. et al. (1999). *45th Annual Meeting, Orthopaedic Research Society, Anaheim, California.*

Scifert, C.F. et al. (1999). *Computer Methods in Biomechanics and Biomedical Engineering,* **2**, 139-147.

ACKNOWLEDGEMENTS

This study was supported in part by NIH 46601. We wish to acknowledge the contributions of Dr. Anneliese Heiner, Dr. Douglas Pedersen, and Will Lack.

A Study of Tissue Vibration Transmissibility Using a Scanning Laser Vibrometer

W. Paul Smutz, Ren G. Dong, and Aaron W. Schopper
National Institute for Occupational Safety and Health, Morgantown, WV, USA

INTRODUCTION

Prolonged exposure to vibration has been associated with the development of hand-arm vibration syndrome (HAVS). While vibration is known to have adverse physiological effects on the tissues of the human hand, it is still unclear how these physiological effects are influenced by factors such as tissue thickness or vibration intensity, frequency, and duration. Understanding the response of the hand to vibration may be helpful in determining the mechanisms behind the development of HAVS. Dynamic response of the hand and arm to vibration has been studied by several investigators (Abrams and Suggs, 1966, Burstrom, 1990). However, these studies have concentrated on the overall impedance of the hand/arm system or have looked only at the vibration transmitted along the bones or on the surface of the hand or arm. The vibration transmissibility through individual tissues such as skin, fat, muscle, blood vessels, and nerves has not been investigated because of the difficulty in making these measurements in vivo. Computer models of the hand have been proposed as a solution to this problem. By using finite element modeling techniques, each tissue can be modeled separately and the vibration transmissibility at different tissue depths can be calculated. However, for these models to be truly useful, validation is necessary. As a first approximation to validate these models, transmissibility in skeletal muscle and fat was measured as a function of the tissue depth using a scanning Doppler laser vibrometer.

METHODS

The test system consisted of an electro-mechanical shaker, a power amplifier, an open loop controller, a scanning Doppler laser vibrometer, and a data acquisition and analysis system. The heart of the system was the scanning Doppler laser vibrometer (Polytech PSV 300). The vibrometer measures the Doppler shift of laser light that is reflected off of a vibrating object and determines the velocity of the object. The velocity of the vibrating object is then differentiated to obtain acceleration. The laser vibrometer has several advantages over accelerometers. First, because it is a non-contact device, no mass is added to the tissue which may alter the local properties of the mechanical system and thus affect the measured data. Second, because the vibrometer can scan several points quickly, a detailed pattern of the vibration can be obtained.

For this study bovine tissue was used because it was easier to obtain and safer to use than human cadaveric tissue. Samples of skeletal muscle and fat from a beef steak were cut into sections 25 mm square and of various thicknesses. Using cyanoacrylate, the samples were glued to an aluminum plate that was attached to the shaker. Care was taken to keep the samples moist. Tests were performed at room temperature. A sine wave that was repeatedly swept linearly from 1 to 1600 Hz over a 10 second period was input into the shaker. The laser vibrometer was then used to measure the acceleration of 9 points on the surface of the

sample and 2 points on the aluminum plate. The test was performed on each sample for acceleration amplitudes of 2, 4 and 8 g's (peak). Tissue transmissibility was calculated by dividing the acceleration at each point on the surface of the sample by the acceleration of the aluminum plate.

RESULTS AND DISCUSSION

Test results showed a marked difference in vibration transmissibility for muscle and fat. For skeletal muscle, a fundamental resonance was found between 50 and 200 Hz (Figure 1-3). Muscle thickness was found to influence vibration transmissibility as well as the frequency of the fundamental resonance. Fat was found to have a transmissibility close to unity for thicknesses of less than 6 mm and for frequencies between 1 and 1000 Hz.

The results from this study for the skeletal muscle are consistent with those of previous studies which report that resonant peaks for the hand and arm are in the frequency range of 80 to 200 Hz and that vibrations above 500 Hz are damped out quickly in the hand (Potts et al., 1983). This study showed that the laser vibrometer was capable of measuring the acceleration of soft tissues exposed to vibration. The muscle reflected sufficient light back to the laser vibrometer so that accurate measurements could consistently be made.

Future studies using the laser vibrometer will include measuring the vibration transmissibility of the soft tissues of the hand using cadaveric specimens. These values will then be compared to those predicted by finite element models of the finger that have been developed in our laboratory.

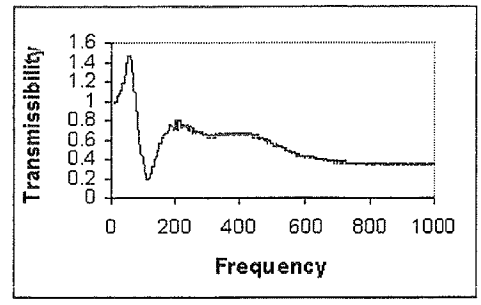

Figure 1. Muscle 8 g's 18.0 mm thick

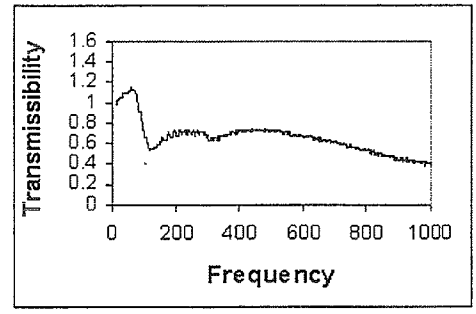

Figure 2. Muscle 8 g's 12.3 mm thick

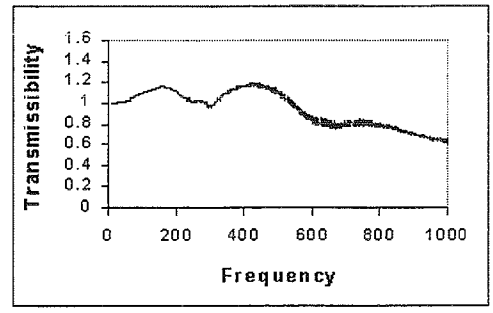

Figure 3. Muscle 8 g's 4.6 mm thick

REFERENCES

Abrams, C.F. and Suggs, C.W. (1966) *Transactions of ASAE*, 423-425

Burstrom, L. (1990) *In Arch Occup Environ Health*, 62(6):431-439

Potts, R.O. et al. (1983) *J Biomech*, 16(6):365-372

RESTRAINING FORCE FIELD OF THE GLENOHUMERAL CAPSULOLIGAMENTS

M. Makhsous[1,3], L.-Q. Zhang[1-4], and F. Lin[1,3]
[1]Sensory-Motor Performance Program, Rehabilitation Institute of Chicago; Depts. of
[2]Orthopaedic Surg., [3]Phys. Med. & Rehab., and [4]Biomed. Eng., Northwestern University
E-mail: m-makhsous2@nwu.edu

Introduction

Glenohumeral (GH) instabilities occur frequently in various shoulder injuries, manifested as excessive GH translations and rotations. Pathological conditions of the passive structures (joint capsule, ligaments, labrum, and the articular surfaces) are closely related to the GH instabilities. It is not very clear how different portions of the capsuloligamentous system contribute to GH stability. The objective of this study was to determine the restraining force field provided by the GH capsuloligamentous system under systematically varied humeral head translations and rotations relative to the glenoid.

Methods

Fresh-frozen shoulder specimens, positioned at 60° abduction (corresponding to 90° arm abduction) in the scapular plane, were used to evaluate passive restraining forces provided by the GH capsuloligamentous system. The scapula was mounted rigidly onto a Teflon plate with the glenoid surface oriented vertically (Fig. 1). The plate can be translated in the mediolateral and superior-inferior directions by an X-Y table controlled by two micrometers. A second X-Y table moved the humerus relative to the glenoid in the anterior-posterior and proximal-distal directions. The displacements of the two X-Y tables were measured by four linear potentiometers as well as by the micrometers built into the X-Y tables. The humeral abduction, flexion, and axial rotation were measured by three precision potentiometers. A six-axis force sensor (JR3 Inc.) was used to measure the

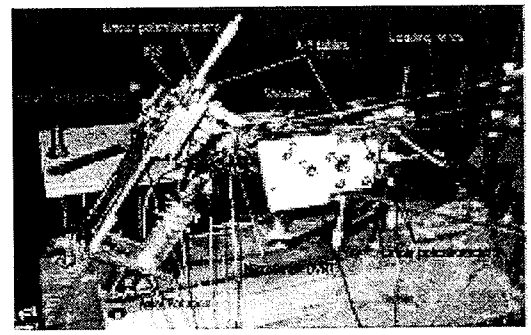

Fig 1. Experimental setup for testing GH-joint.

restoring forces and moments exerted onto the humerus induced by the passive translations and axial rotations of the humerus relative to the glenoid. Ropes were sutured to individual muscles (anterior, middle, and posterior deltoid, supraspinatus, upper and lower infraspinatus, upper, middle, and lower subscapularis, teres minor, and the long head of biceps) through fiberglass mesh, and multiple ropes and pulleys were used to load different portions of fan-shaped muscles like infraspinatus. The tests were repeated under eight loading conditions: No muscle load; 2% maximum muscle force (called physiological load: proportional to muscle PCSA[4]); ditto plus an extra 8% load on the supraspinatus, subscapularis, infraspinatus, teres minor, anterior & middle deltoid, or posterior deltoid (individual muscle loading, one at a time). At each condition, the humerus was translated in the anterior-posterior, superior-inferior and mediolateral directions, axially rotated from neutral rotation to maximal external and internal rotations. Work done by each force along the translation, which is the change of potential energy of the humeral head, was calculated by integrating the force along the translation.

Results

The GH capsuloligaments generated considerable resistance forces to the varied passive displacements, and the resistance force increased considerably when the capsuloligaments were stretched (Fig. 2). Furthermore, the resistance force increased more quickly with superior-inferior displacement than with anterior-posterior displacement, as shown by the contour lines (Fig. 2). For example, the force magnitude for a 10 mm posterior translation was almost twice as large when the humeral head was laterally translated 5 mm.

Physiologically loading the muscles made the GH joint more stable, as indicated by the shrinkage of the contour curves and the faster rise of the resisting forces with the displacements (comparing the right and left columns in Fig. 2). Results on individual muscle loading showed that the subscapularis provided the greatest degree of anterior stability for all superior-inferior humeral positions. Teres minor provided stability in inferior and anterior translations. The supraspinatus provide stability during posterior translations for all superior-inferior positions tested. The infraspinatus increased the resistance force considerably with posterior-superior humeral translation. Besides the cuff muscles, the anterior and middle deltoid contributes to anterior stability, and the posterior deltoid to inferior stability. Humeral axial rotation laxity decreased markedly when the muscles were loaded moderately at 2% maximal muscle force. The rotation laxity was further decreased when the supraspinatus was loaded at 10% of its maximal force.

Discussion

The study provides us quantitative information on the resistance force of the GH capsuloligaments and muscles as functions of anterior-posterior, superior-inferior, and mediolateral GH displacements. The information is useful in developing mathematical models of the GH-joint capsule as well as in analyzing capsuloligamentous function and injuries. Contribution of the rotator cuff was found to be important under anterior and inferior humeral translations. Our results are consistent with previous findings[1-3] that the subscapularis and teres minor were important in stabilizing the shoulder anteriorly with the arm in abduction and neutral rotation. Our results also showed that low-level muscle activity (2%), representing physiological muscle tone contraction, is important and effective in stabilizing the GH joint[4].

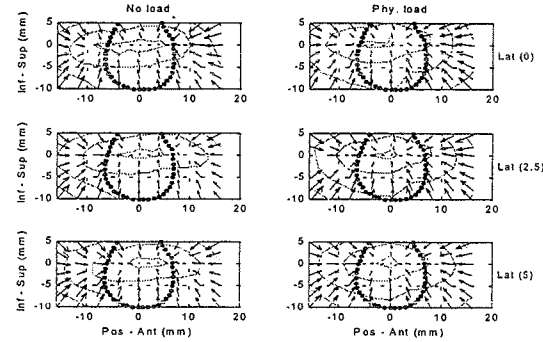

Fig. 2. Restoring force acting on the humeral head under two muscle loading configurations (No load & Phy. load) and three lateral translations (0, 2.5, 5 mm). The contour lines are given at 10, 20, 30, 40, ... N. The dots indicate the glenoid surface.
The origin in the force field corresponded to the neutral position where the glenoid and humeral head were aligned with each other. The arrows represent the resistance forces induced by the passive displacements. The length and direction of the arrows represent the magnitude and direction of the resistance force, respectively.

References

[1] O'Brien, S.J. et al. (1990). *Am J Sports Med*, **18**, 449-456. [2] R. Cain et al. (1987). *Am J Sports Med*, **15**, 44-148. [3] McKernan D. et al. (1990) *Orthop. Trans*. **14**, 237-238. [4] Makhsous, M., (1999). PhD Thesis, Chalmers Univ Tech, Göteborg, Sweden.

Acknowledgements

The study was supported in part by NIH (LZ) and Arthrex Inc (LZ).

CREEP RESPONSE OF THE TRANSVERSE CARPAL LIGAMENT IN CADAVERS: APPLICATION TO CARPAL TUNNEL SYNDROME

Richard N. Hinrichs[1], Benjamin M. Sucher[2], Robert W. Welcher[1], L. Diego Quiroz[1], and Bryan J. Morrison[1]

[1]Department of Exercise Science, Arizona State University, Tempe, AZ 85287-0404 USA
[2]Center for Carpal Tunnel Studies, Paradise Valley, AZ 85253 USA
E-mail: hinrichs@asu.edu

INTRODUCTION

Carpal tunnel release surgery involves cutting the transverse carpal ligament (TCL) in the wrist to relieve pressure on the median nerve in those suffering from Carpal Tunnel Syndrome (CTS). Sucher and Hinrichs (1998) have shown potential for non-surgical treatments for stretching the TCL rather than cutting it. Our initial study used very low static loads (2 N and 4 N) applied to the TCL of seven male cadavers over 8-12 hours to reach the asymptote in the ligament's creep response. In the current study we expanded the sample size to 20 limbs, included both male and female cadavers (10 each), and used higher tensile loads to achieve asymptotic creep over shorter time periods (10 N over 2-3 hours). The purpose of this study was to see how extensible the TCL is under 10 N loads and to see if the stretch remained after the weights were removed. A secondary purpose was to see if there was a gender difference in the ability of the TCL to stretch under load.

METHODS

Twenty fresh cadaver upper limb segments were tested, 10 males and 10 females. The mean age of the cadavers was 65 ± 9 years (males 63 ± 11 years, females 67 ± 8 years). All limbs were free from known injury or disease to the upper extremity. Surgical pins were drilled into the scaphoid, trapezium, pisiform, and hamate bones (palm up). 10 N loads were applied to each pin via hanging weights to create tensile loads on the TCL. Loads were applied until the asymptotic creep response was reached, at which time the loads were removed and the ligament allowed to recoil. When the asymptote of recoil was reached, the cycle was repeated once. Distances between pins at skin level were measured with precision calipers. Two video cameras recorded movements of 3 balls placed on each pin in 3D using the DLT algorithm. The movements of the pins were used to calculate actual ligament elongation by extrapolating below the skin using post-dissection measurements of skin height above the ligament. Measurements were taken for the proximal portion of the TCL (scaphoid to pisiform) and the distal portion (trapezium to hamate). Changes in ligament length were normalized by dividing by the original unloaded length (i.e., strain).

RESULTS AND DISCUSSION

Consistent with our previous research (Sucher & Hinrichs, 1998) we found that the distal portion of the TCL (trapezium to hamate) is much thicker and less extensible than the proximal portion (pisiform to scaphoid). Because of this we were interested primarily in the distal portion of the ligament.

Mean data over all 20 limbs showed that the application of 10 N static loads took approximately 2 hrs to reach an asymptotic creep response (see Figure 1). At the end of these 2 hrs, the distal portion of the ligament reached approximately 5.7% strain (males 5.5%, females 5.9%). After the weights were removed, the distal portion of the ligament recoiled back to approximately 2.0% strain (males 1.6%, females 2.5%) after 2 hrs. Upon re-application of weights, the ligaments stretched slightly further than during the first application of weights (5.9% strain overall, 5.3% males, 6.4% females). Finally upon second recoil, the ligament remained at 2.0% strain (1.5% males, 2.5% females). The data showed the tendency for females to respond to the weight loading with larger strains than males, however these differences were not statistically significant.

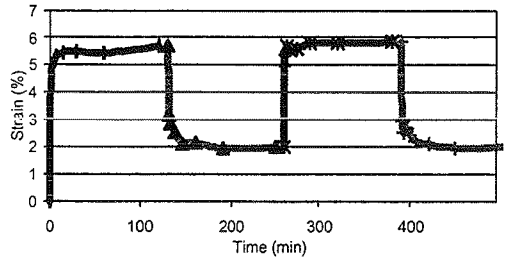

Figure 1: Mean creep response of the distal portion of the TCL across all limbs (two complete cycles of loading and unloading). Note residual strains of approximately 2% after weights were removed.

We do not know at this time if a residual 2% increase in length of the TCL is sufficient to relieve the pressure on the median nerve and reduce the symptoms in patients who suffer from CTS. We assume that the long-term results of such a stretching regimen will produce clinically relevant changes in ligament length. Perhaps they could even prevent some people from requiring CTR surgery. Sucher (1994) has demonstrated measurable benefits to a group of CTS patients who underwent repeated osteopathic manipulation (OM) to stretch the TCL. No study has yet quantified the effects of statically applied loads on a living TCL. The results of the present study are being used as design parameters for a dynamic orthosis (US Patent 5,468,220) that could apply similar tensile loads to a living TCL as a treatment or prevention for CTS (and an alternative to surgery).

SUMMARY

Static tensile loads were applied to the transverse carpal ligament in 20 cadaver limbs (10 male, 10 female) by way of four bone pins. These loads (10 N per pin) produced strains of approximately 6% over a 2-hour period with residual strains of approximately 2% when the loads were removed. Female limbs were found to respond to these loads with slightly greater strains than the males, but these differences were not statistically significant. The extensibility of the TCL under load provides hope for an effective non-surgical treatment for Carpal Tunnel Syndrome.

REFERENCES

Sucher B.M. 1994) *J. Am. Osteopath. Assn.* **94**, 647-663.

Sucher, B.M. & Hinrichs, R.N. (1998). *J. Am. Osteopath. Assn.*, **98**, 679-686.

ACKNOWLEDGEMENTS

This study was supported by a grant from the American Osteopathic Association.

PROJECT OF CAGES BASED ON A CARBON-CARBON COMPOSITE

Miroslav Sochor [1], Karel Balik [2], Petr Tichy [1], Miroslav Spaniel [1] and Jaroslav Vtipil [1]

[1] Department of Mechanics, Faculty of Mechanical Engineering, Czech Technical University in Prague, Prague, Czech Republic

[2] Institute of Rock Structure & Mechanics, Academy of Sciences of the Czech Republic, Prague, Czech Republic

E-mail: sochor@fsid.cvut.cz

INTRODUCTION

Osteosynthesis of the lumbar spine is currently treated by implants of anterior and posterior types. A project developing intervertebral implants based on a carbon-carbon composite was initiated by some extraordinary characteristics of this material. The C/C-composite shows very good bio-tolerance, has a lower modulus of elasticity than titanium and its alloys, is X-ray transparent, and stimulates both tissue and bone to grow well into them. A disadvantage of the C/C-composite, i.e., a loosening of carbon particles into the neighboring tissue, can be eliminated by impregnating and covering the C/C-composite by a compatible material (poly[2-hydroxyethyl methacrylate]). The project aims at applying the C/C-composite with a titanium mantle and without the mantle, to create T+C/C-, and C/C-cages, respectively.

MATERIALS AND METHODS

The samples used in this study were 2-D C/C-composites based on a plain-woven cloth (Torayca carbon fibers, T 800H, Japan) and UMAFORM LE phenolic resin (SYNPO Ltd., Pardubice, CR) as a matrix precursor. The cured samples were carbonized at 50^0C/hr up to 1000^0C in nitrogen. Three-step impregnation with a phenolic resin was used. Subsequently, HTT up to 2200^0C in argon was applied. Pyrolytic carbon was deposited from propane in the tumbling bed reactor, at ambient pressure, at the reaction temperature of 850^0C. Final values of the open porosity and apparent density of the samples were 6 % and 1.6 g/cm^3, respectively. The samples were infiltrated and covered with poly[2-hydroxyethyl methacrylate] in the autoclave under pressure.

Great attention was paid to computer simulations of the stress states in the intervertebral implants and the adjacent vertebrae by means of the finite element method (FEM). In the course of the project a number of computational models were worked on, and these provided valuable information about the stress distribution in implants of various concepts. Gradually, a relatively complicated contact model has been developed, consisting of lumbar vertebrae L_3 and L_4, a pair of implants of the PLIF type, and a pair of internal fixations. This model aims at assessing the stresses not only in the implants themselves but also in the adjacent vertebrae. The problem was analyzed with the use of ABAQUS software, version 5.8-15, The structure of the vertebrae was modeled from C3D8 8-node linear brick elements. The vertebra material was chosen to characterize the bone tissue as well as possible. The thin external layer of the vertebra, made up predominantly of

compacta, was treated as isotropic and linearly elastic. On the other hand, the spongy tissue inside the vertebra was modeled as anisotropic, and, besides, its elastic properties change in the direction from the vertebra center to its surface. This relatively complicated definition aims to respect the relation of the elastic modulus of the spongy bone to the trabecular density of the spongiosis. The posterior implants made of C/C-composite considered as orthotropic elastic were composed of C3D8 elements whose local coordinate systems were oriented to take into account the structure of the TORAYCA fabric. The whole model was stabilized by means of B31 structural beam elements of the BEAM type, which model the internal fixations applied in these types of operations. The internal fixations are screwed to the vertebrae by means of pedicle screws which were also modeled by B31 structural elements, but with a different definition of the cross-sectional characteristics. The material of the internal fixations and the pedicle screws was chosen isotropic and linearly elastic in order to correspond to the Ti6Al4V alloy. The whole FEM model comprises 72408 elements, including the contact elements which serve to define the contact surfaces.

RESULTS AND DISCUSSION

A microscopic examination showed that the poly[2-hydroxyethyl methacrylate] was present not only on the surface of the composite but also in its pores and cracks. The C/C-composite has been tested: i) *in vitro* (cell proliferation); ii) *in vivo* (by implanting into the femurs of pigs and by subcutaneous implantation into rats). The computional FE-models of the implants themselves provided a relatively good idea about the stress distribution and the sites of the maximum stress values in the implant. These models have also been used to verify results obtained when applying more complex contact models, which are still under development, due to great difficulties in formulating the boundary conditions. The stress distribution obtained by one of the contact models is shown in Fig.1

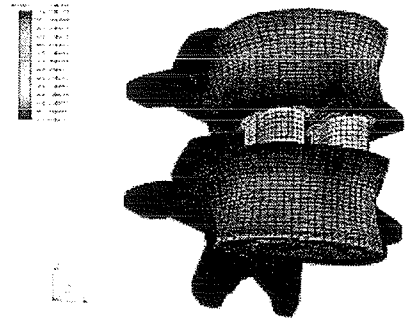

Figure 1: Von Mises stress distribution of a contact model of vertebrae L_3-L_4 with a pair of C/C-composite implants being vertically loaded.

SUMMARY

Cages based on a C/C-composite have been developed including: i) *in vivo* and *in vitro* material testing; ii) FEM-stress distribution computation.

REFERENCES

Balik, K., Sochor, M. et al. *Engineering of Biomaterials* 7, **8**, (1999), J. of UMM Cracow, Poland, 8-10.

Pesakova, V., Klezl, Z., Balik, K., Adam M. *Journal of Materials Science: Materials in Medicine,* **11** (2000), Kluwer Academic Publishers, 793-798.

ACKNOWLEDGEMENTS:

The project is part of the GACR project: Cages based on carbon-carbon composite, No. 106/00/1407; the Ministry of Education project: Transdisciplinary research in Biomedical Engineering, No. MSM 210000012.

MEASUREMENT OF RANGE OF MOTION FOR THE SPINE IN NORMAL INDIVIDUALS USING ELECTROMAGNETIC TRACKING DEVICE

Yi-Wen Chang[1], Chien-Jen Hsu[2], Hong-Wen Wu[3], Wei-Ning Chang[2], Wen-Ying Chou[4]
[1]Department of Physical Therapy, Foo-Yin Institute of Technology, Taiwan
[2]Orthopedic Section, Veterans General Hospital - Kaohsiung, Taiwan
[3]School of Physical Therapy, China Medical College, Taiwan
[4]Second Section of Anesthesia, Chang Gang Memorial Hospital - Kaohsiung, Taiwan
Email: sc092@mail.fy.edu.tw

INTRODUCTION

The spine may be considered as a structure composed of multiple motion segments connected in series. The movements of thoracic spine, lumbar spine and pelvis basically constitute the trunk motion. The measurement of range of motion (ROM) for the spine is common in clinics as a basis of the evaluation for the impairment of the spine. The tape measure and inclinometer are typically utilized in the noninvasive assessment. However, the traditional methods may not be easy to distinguish the hip from spinal motion and thoracic from lumbar motion. The electromagnetic tracking device can derive the movement pattern of multiple segments with simple sensor placement. Therefore, the purposes of this study were to measure the ROM of the spine for the normal subjects using the electromagnetic tracking device, and to analyze the relative contribution of thoracic spine, lumbar spine and pelvis to the trunk motion during the forward/backward bending, side bending and axial rotation.

MATERIALS AND METHODS

A three-dimensional kinematic model of trunk was established in this study. There were four coordinate systems, including thoracic spine, lumbar spine, pelvis and thigh. Since the standing position was chosen to measure the ROM of spine, a close chain exercise was investigated in this study. Thus, the relationship of a proximal coordinate system relative to a distal coordinate system was used to define the segmental movement of the spine. Euler angles were used to describe the movement of a proximal segment relative to a distal segment (An et al, 1984).

Eighteen normal male subjects participated in the study. The Flock of Birds electromagnetic tracking device (1999 Ascension Technology Corporation, Burlington, VT, USA) with four sensor units was used in this study. The locations of these sensors were on the spinous processes of the 7th cervical spine, the 12th thoracic spine and the 5th lumbar spine, and on the middle area of the right posterior thigh. After having obtained the subjects' informed consent, the anatomical position was first collected with the static standing, as a reference of the segmental movement computed from Euler angle. Then the trials of forward/backward bending, bilateral side bending and axial rotation of the trunk were performed for each subject. Three repetitions for each movement were collected in this study.

RESULTS

The ROM for different functions of trunk was shown in Table 1. Thoracic spine generated the greatest angle in axial rotation and the least angle in backward bending. Lumbar spine generated the greatest angle in forward bending and the least angle in axial

rotation. Pelvis generated the greatest angle in forward bending and the least angle in backward bending.

The contribution of each movement segment was computed as a percentage of total trunk motion (Figure 1). 40% of forward bending motion occurred at lumbar spine and 40% at pelvis. 60% of backward bending occurred at lumbar spine. 60% of axial rotation occurred at thoracic spine. 45% of side bending occurred at thoracic spine. The contribution of lumbar spine was substantial for forward and backward bending, but the thoracic spine was significant in the motion at the frontal and horizontal planes.

Table 1: ROM (mean ± standard deviation) for the trunk motion. (F: flexion; E: extension; LB: left bending; RB: right bending; LR: left rotation; RR: right rotation)

Degrees	Thoracic	Lumbar	Pelvis	Sum
F	26 ± 9	51 ± 12	58 ± 17	131 ± 23
E	17 ± 10	25 ± 15	8 ± 7	45 ± 13
LR	49 ± 9	7 ± 3	15 ± 5	56 ± 9
RR	42 ± 9	9 ± 4	25 ± 8	59 ± 8
LB	27 ± 6	19 ± 5	12 ± 4	66 ± 10
RB	26 ± 4	20 ± 5	16 ± 7	71 ± 12

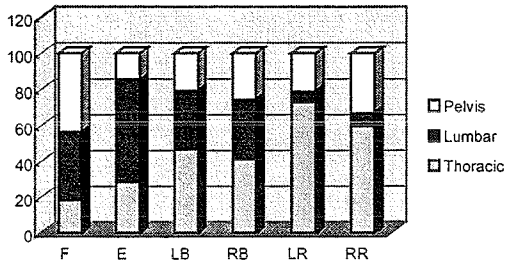

Figure 1: Contribution (%) for different spinal segments (F: flexion; E: extension; LB: left bending; RB: right bending; LR: left rotation; RR: right rotation)

DISCUSSION

A three-dimensional kinematic model of the spine has been developed in this study. Although the real movement unit of the spine is between two vertebrae connected in series, it is currently impractical to define the three-dimensional coordinate system in vivo for each vertebra using the motion analysis system. To minimize this difficulty, three movement segments of the spine were defined in this study, to evaluate the angle change for the different spine region.

Several noninvasive methods have been used in clinics to measure the ROM of the trunk, including the inclinometer and tape measure. However, these approaches can only measure static positions. Radiographic goniometry has also been used in vertebral measurement. However, it might have errors caused by the x-ray beam not rectangular to the plane of the spinal movement (Tulley et al, 1997). With the technique in this study, the dynamic pattern of the spine motion could be quantitatively evaluated. The model of the receiver placement isolated the pelvic motion from the lumbar motion, and lumbar motion from thoracic motion, and provided the in vivo information regarding the relationship between the movements of the adjacent spinal segments.

REFERENCES

An, K.N. et al (1984). *J Biomech Eng*, **106**, 364-7

Tully, E.A., Stillman, B.C. (1997). *Arch Phy Med Rehab*, **78**, 759-66

ACKNOWLEDGEMENTS

Supported by the Veterans General Hospital - Kaohsiung, Taiwan (VGHKS89-1)

BIOMECHANICAL ROLE OF LUMBAR SPINE LIGAMENTS IN FLEXION AND EXTENSION USING A PARALLEL LINKAGE ROBOTIC TESTING SYSTEM

Kevin A. Gillespie and James P. Dickey

Human Biology and Nutr. Sci., University of Guelph, Guelph, Ontario, CANADA
E-mail: jdickey@uoguelph.ca Web: www.uoguelph.ca/hb+ns/dickey.htm

INTRODUCTION

This *in vitro* study examined the functional mechanical characteristics of the spinal ligaments that resist flexion and the interaction between the supraspinous and interspinous ligaments. To accurately quantify the mechanical contribution of each ligament to the resistance of flexion, the kinematics from one trial must be repeated during subsequent trials (Woo et al., 1999). A parallel linkage robotic manipulator was developed to record and replicate the dynamic flexion-extension motion of the spine (Gillespie et al, 2000).

METHODS

Four porcine spinal specimens consisting of six lumbar vertebrae (L2- L7) were used. The spine segment was preflexed to 10 Nm, and the spinous processes of the three vertebrae at each end were bolted together. This allowed unconstrained movement at one motion segment while prestressing the supraspinous ligament, which spans multiple segments. The ends of the spine segment were fixed in pots by using dental plaster and mounted inside the robotic manipulator on top of the six degree of freedom load transducer (Figure 1).

The robotic manipulator was operated in load control to respond to the natural movement profile of the spine. A compressive force was first applied 15 cm anterior to the centre of the spine causing the spine segment to travel dynamically through to 10 Nm of flexion moment. Then a compressive force was applied 15 cm posterior to the centre of the spine caused the spine to travel dynamically into extension. Four cycles of the flexion-extension path of the spine were recorded by the robotic manipulator so that the kinematics could be precisely replicated during subsequent cycles. Data was extracted from the fourth cycle for analysis.

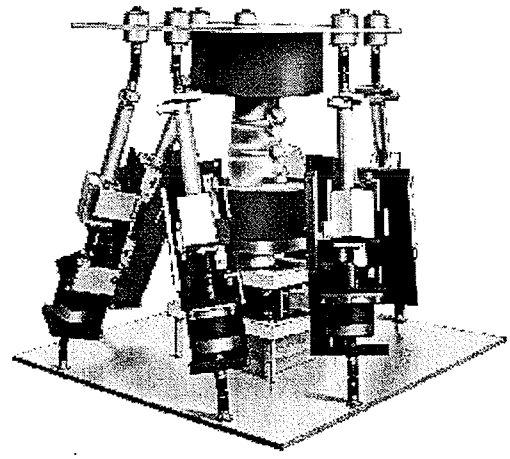

Figure 1: Porcine lumbar spine mounted within parallel linkage robotic manipulator

Repeated serial dissection tests were performed, which involved the intact spine, supraspinous-interspinous ligament interactions cut, supraspinous ligament (SSL) cut, interspinous ligament (ISL) cut, ligamentum flavum (LF) cut, and facet capsules (FJC) being removed, allowing 5 minutes rest between conditions. Stiffness was calculated from the linear portion of

each condition. A repeated measures ANOVA ($P<0.05$) with Tukey's post hoc test was used to assess statistical significance.

RESULTS AND DISCUSSION

A typical moment-angle curve for one specimen with six trials of serial dissection is shown in figure 2. The percent stiffness following each successive dissection is presented in figure 3.

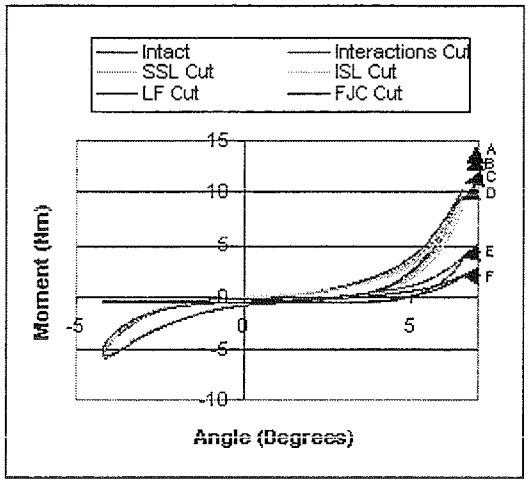

Figure 2: Representative moment-angle plot for a serial dissection involving an intact lumbar spine (A), supraspinous\interspinous interactions cut (B), supraspinous cut (C), interspinous cut (D), ligamentum flavum cut (E) and facet joints removed (F)

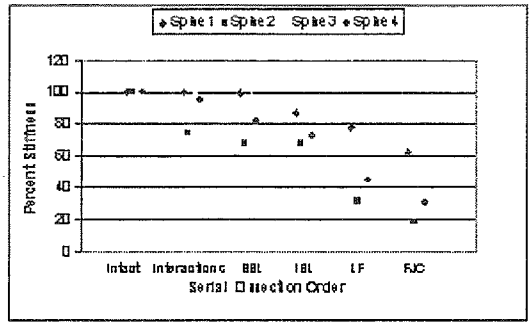

Figure 3: Plot of percent total stiffness for the six conditions of the serial dissection

The stiffness of the spine was not significantly changed by cutting the interactions between the supraspinous and interspinous ligaments, nor cutting the supraspinous and interspinous ligaments. Cutting the ligamentum flavum resulted in a significant decrease in stiffness, however, removing the facet joints did not further reduce the stiffness. The role of the facet joints does, however, seem to be important during extension. The stiffness of the spine in extension was significantly reduced after the facet joints were removed.

Although cutting the interactions between the supraspinous and interspinous ligaments did not significantly reduced the stiffness, the variability between specimens may indicate that these interactions make a contribution to the joint stiffness (Dumas et al., 1987). It is hypothesized that the location of the cut intended to sever the interactions is crucial

The results the present study are in agreement with previously published work, demonstrating the ligamentum flavum's large contribution to stiffness (Dumas et al., 1987), and the relatively small contribution of the supraspinous and interspinous ligaments (Abumi et al., 1990). The importance of maintaining the kinematics of a joint, while altering its structure, can not be over emphasized. The parallel linkage robotic manipulator used in this study is ideally suited for this purpose.

REFERENCES

Abumi, K. et al. (1990). *Spine*, **15**, 1142-7.

Dumas, G.A. et al. (1987). *J. Biomech.*, **20**, 301-310.

Gillespie, K.A. et al. (2000). *Archives of Phys. and Biochem.*, **108**, 106.

Woo, S.L-Y. et al. (1999). *J Sci. Med. Sport*, **2**, 283-297.

EVALUATION OF SWELLING KINEMATICS OF THE SPINE

David Reiter [1], Fadi Fathallah [1], Nesrin Sarigul-Klijn [2], Munish Gupta [3],

[1] Occupational Biomechanics Laboratory, University of California, Davis, CA, USA
[2] SMART Laboratory, University of California, Davis, CA, USA
[3] Orthopedic Research Laboratory, University of California, Davis, CA, USA
E-mail: dareiter@ucdavis.edu

INTRODUCTION

The spine changes in length and curvature when relieved of axial loading for extended durations, such as during space flight. Thornton reports that the pilot of Skylab experienced a height increase of two inches coupled with a loss in thoracolumbar curvature (Thornton et al. 1977). In a retrospective survey of 18 astronauts, Wing et al. reported 72% of the respondents experienced back pain with intensities ranging from low to severe (Wing et al. 1991). Previous studies provided insight into the mechanism that causes soft tissue like the intervertebral disc (IVD) to swell (Urban and McMullin 1985). However, there exists little work that examined the implications of this swelling mechanism on back pain and injury over extended periods when the spine is relieved of its axial load. Bed rest studies have indicated that 70% of the height increase from long-term unloading of the spine occurs in the first five hours with the temporal distribution of height increase following a logarithmic trend (Styf et al. 1997). Considering this logarithmic swelling behavior of soft tissue, the implications of spinal lengthening and changes in spinal curvature from bed rest could provide insight into injury and back pain in the general population. The objectives of this study were to investigate the effect of free swelling on the kinematics of spinal segments and develop a technique of monitoring nucleus movement *in vitro* using x-rays.

METHODS

The entire spine of a domestic pig was disarticulated into 13 functional spinal units (FSUs) with posterior elements removed. Each specimen was potted in dental plaster prior to testing. A 300 Newton load was applied for 15 minutes. An initial lateral radiograph was then captured.

Optical markers were fixed to the superior and inferior surfaces of the specimen and lateral digital images of the optical markers were captured. The specimen was then allowed to soak in a saline bath free of axial loads. The specimen was removed periodically in order to capture lateral images of the optical markers. After 24 hours of swelling, a final lateral digital image was captured along with a final lateral radiograph.

The digital images of the optical markers were analyzed using Scion Image. The angle of flexion/extension was determined for each specimen over the 24-hour period of swelling. The lateral radiographs were digitized and analyzed using Scion image as well. The density of exposure intensity was measured across the intervertebral disc of each specimen. The sagittal distribution of density was compared from initial to final radiographic images and was used to estimate anterior/posterior (a/p) position of the nucleus pulposus. A polynomial was fit to the spatial distribution of density. The

mean density was arbitrarily chosen as a boundary for the a/p nucleus position. The a/p location of the nucleus from the initial radiograph was then compared to the nucleus location of the final radiograph.

RESULTS AND DISCUSION

The cervical and upper thoracic spinal segments swelled in flexion and the lower thoracic and lumbar spinal segments swelled in extension. The results of this study further support the work of Yingling et al. (1999) for use of the porcine cervical spine as a surrogate experimental model for the human lumbar spine. The segments that swelled in flexion (n = 9) reached an average angle of flexion of 0.789° after 6 hours of swelling. This flexion angle is similar in magnitude to previous work of Andersson and Schultz (1979). Their results showed a mean flexion angle of 0.78° after injecting 6 human lumbar IVDs with saline.

Of the 13 FSUs, five specimens produced radiographic images that were suitable for the measurement of nucleus movement. A perfect correlation existed between nucleus movement and kinematic motion (see Table 1).

Table 1. Radiographic measurement of nucleus shift and sagittal motion.

Specimen (Level)	Nucleus movement	Kinematic motion
C5-6	Posterior	Flexion
T4-5	Posterior	Flexion
T12-13	Anterior	Extension
L1-2	Anterior	Extension
L3-4	Anterior	Extension

SUMMARY

Swelling kinematics of spinal segments was measurable *in vitro* using the optical techniques employed in this study.

Determination of a/p nucleus movement was measured using a radiographic method. The determination of nucleus movement from the radiographic data was possible through the use of a polynomial curve fit. More advanced models are currently being investigated in order to more accurately determine the a/p nucleus position of intervertebral discs *in vitro*.

Snook et al. (1998) have reported the reduction of low back pain through minimization of early morning lumbar flexion. Although increased hydration of the IVD is thought to be a cause of early-morning injury, other mechanisms associated with hydration, such as a/p nucleus shift, could be contributing to injury and pain. Further understanding of nucleus movement could provide better insight into temporal implications of spinal loading with respect to possible modes of disc injury and low back pain.

REFERENCES

Andersson, G. B. J. and A. B. Schultz (1979). *Journal of Biomechanics* **12**: 453-458.

Snook, S. H., B. S. Webster, et al. (1998). *Spine* **23**(23): 2601-2607.

Styf, J. R., R. E. Ballard, et al. (1997). *Aviation, Space, and Environmental Medicine* **68**(1): 24-29.

Thornton, W. E., G. W. Hoffler, et al. (1977). *Biomedical Results From Skylab, NASA*: 330-338.

Urban, J. P. G. and J. F. McMullin (1985). *Biorheology* **22**: 145-157.

Wing, P. C., I. K. Y. Tsang, et al. (1991). *Orthopedic Clinics of North America* **22**(2): 255-262.

Yingling, V. R., J. P. Callaghan, et al. (1999). *Journal of Spinal Disorders* **12**(5): 415-423.

ON THE RISK OF ZYGOMA FRACTURE FROM BASEBALL LOADING

Joel D. Stitzel[1], Paul F. Vinger[2], and Stefan M. Duma[1]

[1]Impact Biomechanics Laboratory, Mechanical Engineering, Virginia Tech
[2]Tufts University School of Medicine, New England Medical Center
Email: joel@vt.edu, Web: www.ibl.vt.edu

INTRODUCTION

It is estimated that 16 million children play some form of organized baseball in the US. Little league baseball is the world's largest sporting organization, with 190,000 teams in over 80 countries. From 1994-1998, the mean estimated yearly baseball related injury rate in children from 5-14 years of age was 103,731 (Yen, 2000). The most commonly injured body part was the face, followed by fingers, head, ankles, wrists, mouth, knees, and hands. Softer baseballs, with weight, liveliness, and surfaces similar to standard hard balls, have been designed to reduce these injuries. However, there is no data on the risk of fracture due to baseball loading in the literature with respect to younger children. The purpose of this study is to predict the risk of zygoma fracture from impact with a range of baseballs of varying hardness. In particular, this paper develops injury risk functions to predict the probability of fracture of the zygoma for children in the range from 9-11 and 12-14 years of age, and compares these to adult values.

METHODS

Existing research on the danger of fracture due to the type of impact loading that may be seen in a facial impact with a baseball is limited to three studies. Nahum *et al.* (1968), Schneider and Nahum (1972), and Hodgson (1967) quantified the peak force necessary to fracture the zygoma with a cylindrical impactor, for automobile safety. For this study, the peak force at fracture from these three studies was selected (28 tests resulting in failure from the three studies). Data was then mass scaled to a standard mass that would be expected for the two age groups of children. Average mass for the two age groups was based on actuarial data from the Metropolitan Life Insurance Company. Average mass for the adult population was based on 1985 Humanscale data for the US population. The mass used for the 9-11, 12-14, and adult age groups was 31.5, 50.4, and 73 kg, respectively. Mass scaling was performed using the technique developed by Eppinger *et al* (1984). This technique utilizes a scaling relationship that takes into account occupant mass and an assumed increase in bone size and strength that accompanies this mass. Known force values are scaled using the scaling relationship to obtain equivalent force values for the mass of interest.

The scaled data was used to obtain risk functions for the two age groups. Risk functions were established with the failure data using a logit formulation, where the probability of injury is related to the average of failure data and a function of the standard deviation of the data (Duma, 2000). The logit formulation was selected versus the normal distribution in order to produce a closed form solution. Given an impact force, these risk functions can be used to predict injury due to commonly used baseball types (Equation 1).

$$Risk = \frac{1}{1+e^{-\left(\frac{x-m}{b}\right)}}, \quad b = \frac{\sigma\sqrt{3}}{\pi} \qquad (1)$$

Where m is the mean of the failure data, b is a function of the standard deviation of the data, σ, and x is the peak force in Newtons. The peak force that might be seen on the zygoma due to a baseball impact was obtained from work performed by Vinger *et al.* (1999). This work correlated impact velocity of increasingly harder baseballs to peak orbital force. This orbital force was analyzed relative to the failure data for the zygoma and then again for the mass scaled failure data. Regression equations were used to determine the impact force on the orbit for two age groups, using pitch velocities of 35

and 55 mph for the 9-11 and 12-14 year age groups, respectively. These velocities were chosen because they are the average pitch speeds seen at these age levels (Vinger *et al.*, 1999).

RESULTS AND DISCUSSION

The risk functions established for the adult, the 9-11 year age group, and the 12-14 year age group demonstrate a notably increased risk of fracture due to baseball impact to the younger population (Figure 1, Equations 2-4). The 50th percentile of the risk function for 9-11 year olds is approximately half the force that is required for the adult age group, with 12-14 year olds falling about halfway between this (Figure 1). Using pitch velocities and average masses of children seen in the two age groups, large differences in risk are seen (Table 1). As ball hardness increases, risk of fracture of the zygoma also increases. In both categories, ball CD's above 35 result in scaled risks above 96%. It is only for adults subjected to lower velocity pitches (9-11 year category) that there is any risk below 50%, and this is only for the softest two types of balls tested. Baseball velocities likely to be thrown by little league pitchers posess a substantial risk of fracturing the zygoma should a direct impact occur. Mass scaling injury criteria using known cadaver failure data to a younger population demonstrates this increase. Even with the softest ball types now available, the maximum force imparted in a direct hit to the zygoma is sufficient for fracture. This risk of injury underscores the need for facial protection in little league baseball.

$$Risk_{9-11 years} = \frac{1}{1+e^{-\left(\frac{Peak\ Force-1020.83}{207.62}\right)}} \quad (2)$$

$$Risk_{12-14 years} = \frac{1}{1+e^{-\left(\frac{Peak\ Force-1394.8}{283.68}\right)}} \quad (3)$$

$$Risk_{Adult} = \frac{1}{1+e^{-\left(\frac{Peak\ Force-1786.77}{363.40}\right)}} \quad (4)$$

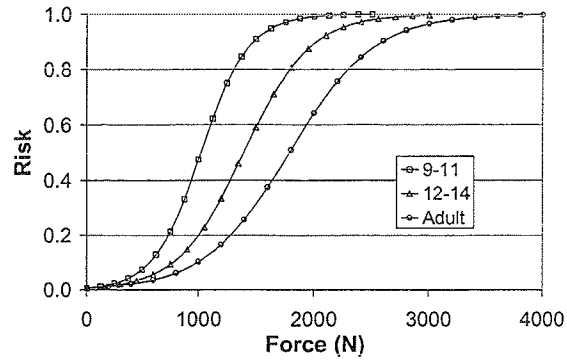

Figure 1. Risk of zygoma fracture versus peak baseball impact force for the adult, 9-11, and 12-14 year old populations

Table 1. Risk of zygoma fracture for the adult and two selected age groups

Adult mass = 73.0 kg	9-11 Years mass = 31.5 kg velocity = 35 mph			12-14 Years mass = 50.4 kg velocity = 55 mph		
Ball CD, lb	Force, adult, N	Risk, adult	Scaled Risk	Force, adult, N	Risk, adult	Scaled Risk
25	1104	0.13	0.60	2295	0.80	0.96
35	1674	0.42	0.96	3126	0.98	1.00
50	1915	0.59	0.99	3335	0.99	1.00
266	2034	0.66	0.99	3643	0.99	1.00
291	2163	0.74	1.00	3672	0.99	1.00
250	2288	0.80	1.00	3745	1.00	1.00

REFERENCES

Duma SM. (2000). *Injury Criteria for the Small Female Upper Extremity;* University of Virginia

Eppinger RH, Marcus JH, Morgan RM. (1984). *SAE Technical Publication no. 840885*

Hodgson VR. (1967). *American Journal of Anatomy*, **120**, 113.

Nahum AM, Gatts JD, Gadd CW, Danforth J. (1968). *Proceedings of the 12th Annual Stapp Car Crash Conference*, 302.

Schneider DC, Nahum AM. (1972). *Proceedings of the 16th Annual Stapp Car Crash Conference*, 186.

Vinger PF, Duma SM, Crandall J. (1999). **117**, 354.

Yen KL, Metzl JD. (2000). *Pediatr Emerg Care*, **16**, 215.

THE ACUTE EFFECTS OF PRIOR CYCLING CADENCE ON RUNNING PERFORMANCE AND KINEMATICS

Jinger S. Gottschall and Bradley M. Palmer

The Locomotion Laboratory, University of Colorado, Boulder, CO, USA
Email: gottscha@ucsu.colorado.edu

INTRODUCTION

The most arduous and strategic part of a triathlon is the transition from cycling to running. Authors of lay publications suggested various cycle to run methods to optimize this transition. For example, Brick (1996) recommended concluding the cycling stage with a low-resistance, fast cadence spin. In contrast, Friel (1998) advocated high-resistance, low cadence frequencies during the final moments of the cycling bout. However, these ideas remain controversial and are not based on scientific evidence.

Some research studies have investigated the effects of prior cycling on subsequent running. In a previous study, we compared running kinematics and performance during maximal run after high-intensity cycling versus after a high-intensity running bout (Gottschall and Palmer, 2000). We found that cycling prior to running elicited kinematic adaptations during the maximal run: stride frequency increased, stride length decreased, and efficiency increased. Yet, that study did not directly investigate how cycling affected running speed and running biomechanics.

It is plausible that cycling cadence could influence subsequent running frequency and hence, speed. Classic studies in neuroscience, by Brugger and Gardener (1994), have demonstrated that persons performing a rhythmic activity for an extended period of time will involuntary continue this movement pattern. This phenomenon is called perseveration.

The rationale for the present study was that cycling cadence might influence subsequent running speed via changes in stride frequency. We hypothesized that compared to the preferred cadence, a fast cycling cadence would increase subsequent running speed and a slow cycling cadence would decrease running speed.

METHODS

Thirteen male athletes of the University of Colorado triathlon team volunteered (24.8 $\pm$ 1.20 yr, 72.7 $\pm$ 1.42 kg, 1.80 $\pm$ 0.02 m, mean $\pm$ SD).

Each participant completed three sessions of testing. During the control condition (CC), each participant completed a 30-minute cycling bout immediately followed by a 3200 m running bout. Heart rate was recorded every two minutes so the participants could monitor and maintain similar intensities during the second and third sessions. During the fast condition (FC) and the slow condition (SC), each participant completed a 30-minute, high intensity cycling bout at a cadence 20% faster or 20% slower than the control condition. The cycling bout was immediately followed by a 3200 m run at the same heart rate intensity as during the control run.

RESULTS AND DISCUSSION

Our most important finding was that faster cadence cycling substantially increased the subsequent average running speed of the

3200-m race effort (Figure 1). During the fast condition, participants ran almost a minute faster than during the slow condition. This remarkable increase in running speed after cycling with a fast cadence occurred with heart rates matched to the values of the control condition during both the cycling and running bouts.

Figure 1.

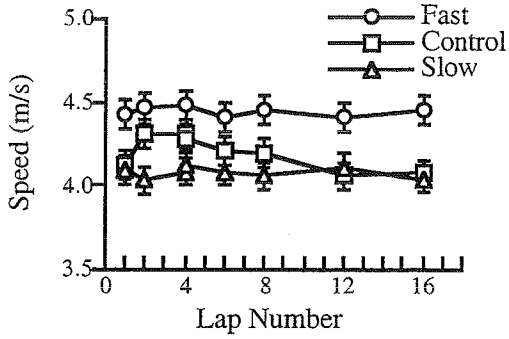

The participants ran faster primarily by increasing stride frequency (Figure 2). Immediately after each cycling bout, the participants ran with a stride frequency that reflected the prior cycling cadence.

Figure 2.

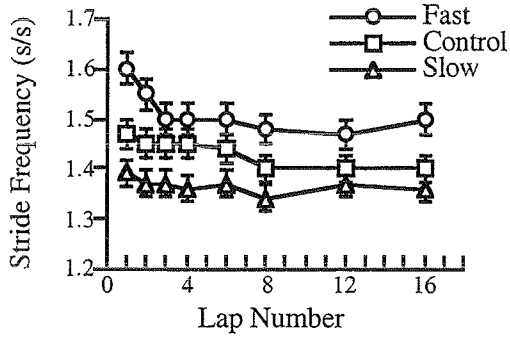

In contrast, there were no significant differences between conditions for stride length (Figure 3).

Figure 3.

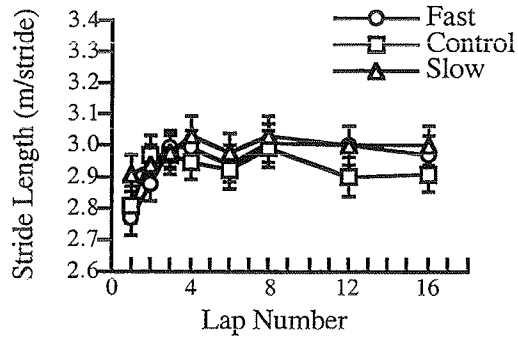

Perseveration is the most likely mechanism responsible for the elevated running stride frequency of the fast condition. Hudson (1968) determined that cycling and running depend on different neural firing rates due to the specific cyclic frequencies of each movement. It is possible that the neural firing rate after each cycling condition biased the firing rate used subsequently for running. For example, the high frequency firing rate during the fast cadence cycling bout appears to have translated into an increased SF during the running bout.

In conclusion, we found that cadence during a cycling bout immediately prior to a running bout influenced performance and stride kinematics. Maintaining an unusually high cadence while cycling resulted in substantially faster running speed. On a practical note, athletes may benefit from adapting an increased cycling cadence prior to the running segment of a triathlon.

REFERENCES

Brick, M. (1996). *Inside Triathlon*, **4**, 76.

Brugger, P., Gardener, M. (1994). *Percept. Mot. Skills*, **78**, 777-778.

Friel, J. (1998). *Inside Triathlon*, **4**, 21-23

Gottschall, J.S., Palmer, B.M. (2000). *J. Strength Cond Res*, **14**, 97-101.

Hudson, A.J. (1968). *Brain*. **91**, 571-582.

A REAL-TIME BIOMECHANICAL FEEDBACK SYSTEM FOR TRAINING ROWERS

Paul Page and David Hawkins

Human Performance Laboratory, University of California, Davis, CA, USA
E-mail: dahawkins@ucdavis.edu

INTRODUCTION

Successful competitive rowing requires cardiovascular fitness, anaerobic power, and proper technique to move the boat as rapidly as possible over the course of a race. Researchers have studied both rowing kinematics (Nelson and Widule, 1983) and kinetics (Macfarlane et al., 1997) on rowing ergometers. Recently, kinematic and kinetic analyses have been combined, but not in real-time (Torres-Moreno et al., 2000; Hawkins, 2000). While rowers can benefit from objective visual feedback during training (Henry et al., 1995), no system to-date provides real time kinematic and kinetic feedback.

An ergometer-based biomechanical feedback system was developed to provide integrated kinematic and kinetic data in real-time. While the athlete rows, a two-dimensional stick figure of the rower is displayed above the power profile produced during the drive (power-producing) portion of the stroke. Joint kinematic data are displayed and a file save and replay capability allows further stroke analysis following a training session.

METHODS

A Concept II Model C rowing ergometer was modified with the following hardware (Figure 1):
A) A 10-turn potentiometer coupled to the flywheel sprocket via a plastic chain and sprocket assembly to measure handle distance from the flywheel hub;
B) A spring-return linear position transducer mounted between the ergometer foot stretchers, and connected to the ergometer handle via a radial bearing;

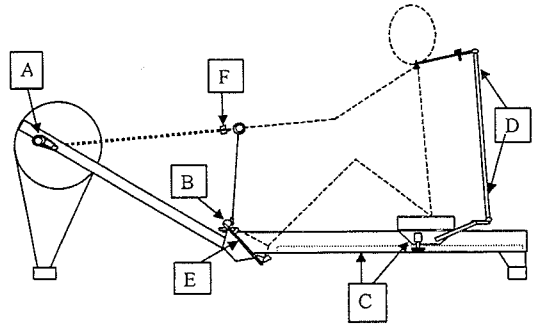

Figure 1. Modified rowing ergometer.

C) A 10-turn potentiometer mounted to the seat and coupled to the seat track via a rack and pinion mechanism;
D) A shoulder-position measurement system mounted to the seat and consisting of three single-turn potentiometers interconnected with aluminum bars;
E) A single-turn potentiometer mounted to the flexible foot stretcher;
F) A 2224 N load cell mounted in line with the ergometer handle.

The instrumentation was wired to a data acquisition computer via a National Instruments data acquisition card.

Two computer programs were written using National Instruments LabView™ software. The RowTrainer program provides real-time data collection and display. The ReRow program allows for replay and analysis of previously saved data. Calibration data for the system components are entered into the

RowTrainer program along with the rower's anthropometric data. Assuming simple hinge joints and motion in the sagittal plane, a real-time stick figure is generated while the athlete rows. Handle position data are numerically differentiated and combined with the load cell force to generate a power profile over the course of the stroke. Other parameters of interest, such as stroke rate, slide ratio (the ratio of time spent on the recovery phase to time spent during the power phase of the stroke), and hip and knee angles over the course of the stroke, are also provided in real-time. Data can be saved for subsequent detailed analysis using the ReRow program.

Static and dynamic error analyses were performed to determine the accuracy and limitations of the system. Static measurements compared joint locations predicted by the RowTrainer system with values measured directly. Three-dimensional motion analysis was utilized to perform both dynamic and static error analyses. Joint locations predicted by the RowTrainer system were compared to values determined using the video system.

RESULTS AND DISCUSSION

Average static joint position errors ranged from 0.2 cm to -2.5 cm, with a typical joint location error being 1 cm. Average dynamic joint errors ranged from ±0.1 cm to –4.4 cm, with typical errors on the order of ±1 cm. Joint position errors were more pronounced at the extremes of the stroke. Errors in joint positions resulted in average knee and hip joint angle errors of 9.6° and 5.8°, respectively. Additionally, the average handle horizontal velocity error during the drive phase was –1.8%. Figure 2 provides a visual comparison of the effect that the typical errors have on the RowTrainer stick figure (compared to videography). Two experienced rowing coaches evaluated the system and concluded that the accuracy was sufficient to provide beneficial feedback.

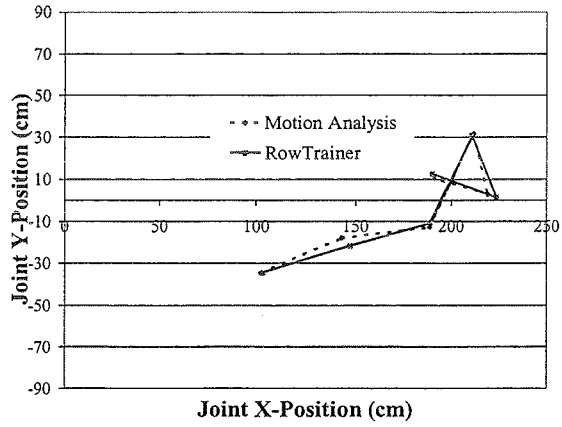

Figure 2. RowTrainer vs. Videography stick figures.

SUMMARY

A rowing ergometer biomechanical feedback system was developed to provide athletes and coaches with real-time kinematic and kinetic information during dry land training. While system accuracy is limited at the extremes of the stroke, coaches believe the system to be a useful training tool.

REFERENCES

Hawkins, D. (2000). *Journal of Biomechanics,* **33**, 241-245.

Henry, J.C. et al. (1995). *Journal of Sports Sciences*, **13**, 199-206.

Macfarlane, D.J. et al. (1997). *Journal of Sports Sciences*, **15**, 167-173.

Nelson, W.N., Widule, C.J. (1983). *Medicine and Science in Sports and Exercise*, **15**, 535-541.

Torres-Moreno, R. et al. (2000). *International Journal of Sports Medicine*, **21**, 41-44.

A Kinematic Analysis Between Triple and Quadruple Revolution Figure Skating Jump

Meris Johnson and Deborah L. King, Ph.D.

Biomechanics Laboratory, Montana State University, Bozeman, MT
Email: dking@montana.edu

INTRODUCTION

To remain internationally competitive in figure skating, US athletes must be able to perform jumps consistently and safely. Male skaters in particular must be able to perform quadruple revolution jumps. Thus, coaches are challenged to distinguish between particular elements of a triple jump that must be changed to perform the quadruple. Biomechanical analyses can assist coaches in this endeavor. In the past, much emphasis has been given to increasing jump height. However, it is not known that jump height is as critical as other factors, such as moment of inertia, angular momentum, or various segmental angles (Aleshinsky, 1988; King, et. al. 1994; King, 1999a). This study will compare successful quadruple jumps to successful triple jumps of the same type performed by the same athletes to determine the critical factors for completing quadruple jumps.

METHODS

Data were collected at the 2000 State Farm National Championships in Cleveland, OH. All participants signed a consent form giving written permission to participate in the study. Height, weight, and age were recorded at this time.

Data were taken during competition and selected on ice practices. Four high speed (120-pictures/second) pan and tilt cameras (Peak Performance Technologies, Inc.) were used to film the approach through landing of selected skills. The cameras were placed approximately 90 degrees apart in the stands, so that two cameras were on each side of the rink. The cameras on the same side of the rink were gen-locked. Eight survey poles were used for the calibration of the cameras. A calibration was taken before each day of competition to ensure accuracy.

All video data were manually digitized using Peak Motus Pan and Tilt software. Only two of the four camera views were used in the analysis of each jump. Due to the fact that there are only a limited number of skaters that can perform the quadruple jumps (4 skaters attempted quads at this competition), only five toe-loops and two Salchows were performed cleanly by three different skaters. Cleanly completed triple Salchows and triple toe-loops from these same three athletes were also analyzed. Custom software written in LabView (National Instruments, Inc.) was used to analyze the jumps

RESULTS AND DISCUSSION

In order to increase the revolutions of a jump, the skater must either jump higher or rotate faster or do both. The jump height and the air time did increase from the triple to quadruple Salchow jumps (Table 1). Additionally, angular velocity was higher at take off and in flight due to lower moments of inertia at takeoff and during flight for the quadruple Salchow as compared to the triple Salchow. Angular momentum was slightly less in the quadruple Salchow as compared to the triple Salchow.

Table 1. Basic Characteristics of Triple and Quad Salchows and Toe-Loops. Q = quadruple, T = triple, Vel = Velocity, Ang = Angular, TO = Take-off. Values are average ± SD, except the T Salchow where N = 1.

	Jump Height (m)	Time of Jump (sec)	Ang. Momentum @TO (kgm/s)	Moment of Inertia @ TO kgm^2	Moment of Inertia min kgm^2	Angular Vel @TO (rev/sec)	Max Angular Velocity (rev/sec)	Horizontal Vel @ TO (m/s)	Vertical Vel @TO (m/s)
Q Salchow	0.44±0.07	0.66±0.02	20.1±1.5	1.39±0.80	0.79±0.00	2.31±0.64	4.58±0.19	3.04±0.01	2.90±0.12
T Salchow	0.36	0.55	24.2	1.84	0.86	2.09	3.95	4.14	2.67
Q Toeloop	0.48±0.03	0.64±0.01	28.0±1.3	1.53±0.26	0.74±0.03	3.02±0.66	4.84±0.30	3.33±0.15	3.23±0.18
T Toeloop	0.47±0.01	0.62±0.0	26.1±0.9	1.64±0.45	0.90±0.18	2.60±1.10	4.58±0.08	4.25±0.59	3.24±0.21

For the toe-loop jumps, jump height and air time were very similar for both the triple and quadruple jumps. While angular momentum was slightly greater in the quadruple toe-loop as compared to the triple, the greatest difference in these jumps was the angular velocity. The angular velocity at take-off and maximum angular velocity during flight were greater for the quadruple toe loop as compared to the triple (Table 1). This was due to smaller moments of inertia at take-off and during flight. In the triple Salchow, positive vertical velocity was accompanied by rapid knee extension throughout the propulsive phase. However, in the quadruple Salchow, when the COM began to rise, the take-off leg was still flexing (Figure 1). Thus, the skater may have been utilizing the larger force producing capabilities of the quadriceps muscle during eccentric actions (whilst the knee was flexing) to generate larger ground reaction forces whilst the COM was already rising. Additionally, note that the greater vertical velocity was accompanied by a slower approach, as shown by the horizontal velocity at takeoff (Table 1).

CONCLUSION

To increase the revolutions of a toe-loop or a Salchow from a triple to a quadruple, angular velocity must be increased. Decreased moments of inertia permit this to happen. Angular momentum is needed to complete any level of jump; however, the trend shows that it is not increased from the triple to the quadruple. In the Salchow, vertical velocity was also increased from triple to quadruple. This lead to higher jump heights and longer flight times, allowing the extra revolution. A slower approach speed accompanied the greater vertical velocities, as did a different pattern of knee motion during propulsion. This may have allowed the skater to take advantage of eccentric muscle actions in the generation of positive vertical velocity.

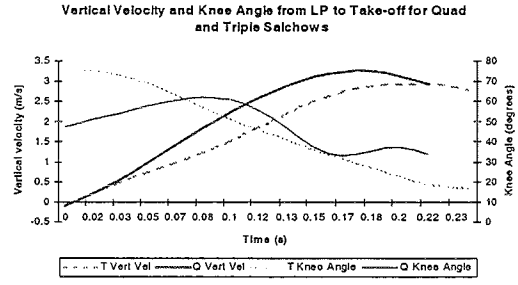

Figure 1. COM vertical velocity and take-off leg knee angle during propulsive phase of a quad and triple Salchow. Propulsion is from the lowest point of the COM (LP) to take-off.

REFERENCES

Aleshinsky SY (1988). *Proceedings from ASB annual meeting, 1988.*

King, et.al. (1994). *J Applied Biomechanics*, **10**, 51-56.

King, DL (1999). *Proceeding from Am. College of Sports Medicine,* 1999.

RUNNING SPEED ON CURVED PATHS IS LIMITED BY THE INSIDE LEG

Young-Hui Chang[1], Kelly Campbell[2] and Rodger Kram[3]

[1] Department of Physiology, Emory University, Atlanta, GA
[2] Department of Physics, University of California, Berkeley, CA
[3] Department of Kinesiology & Applied Physiology, University of Colorado, Boulder, CO
Email: younghui2k@yahoo.com Web: http://socrates.berkeley.edu/~hbbiomxl/YoungHui/

INTRODUCTION

In nature, animals rarely sprint along straight trajectories. Rather, prey species try to evade faster predators with high-speed small radius locomotor maneuvers (Alexander, 1982). Sprint performance along curves is also critical in many sports like baseball, soccer, and basketball. In track, it is well established that the radius of curvature of the lanes affects performance (Harrison and Ryan, 2000; Jain, 1980).

Greene (1985) proposed a model for curve running performance based on the assumption that the maximal effort leg extension force is a physiological upper limit to running speed. His data generally supported this theory. However, he noted a significant degree of scatter to [the] data, and thus it is...possible that other theoretical models can predict the data as successfully. Furthermore, Greene did not measure ground reaction forces to validate his assumption nor do these data currently exist.

The primary goal of this study was to test directly whether an upper limit to leg extension force limits sprint velocity along curved paths.

METHODS

Five recreationally fit men (29.4 – 5.2 yrs., 80.7 – 9.0 kg, mean – SD) gave informed consent to serve as subjects. They sprinted along a straight track and along circular tracks of 1, 2, 3, 4, and 6 m radii. Curve sprinting was performed normally and with a tether. The tether attached a harness worn about the waist to a vertical pole at the center of each track. Speeds were determined from high-speed video analysis. Ground reaction forces (GRFs) were recorded from a force platform mounted flush with the running surface. Tether forces were recorded from an in-line force transducer.

RESULTS AND DISCUSSION

Sprint velocity decreased with radius, but less so with the tether (Fig. 1). At the 3 m radius, velocity decreased by 42% for normal curve sprinting, but only 33% with the tether.

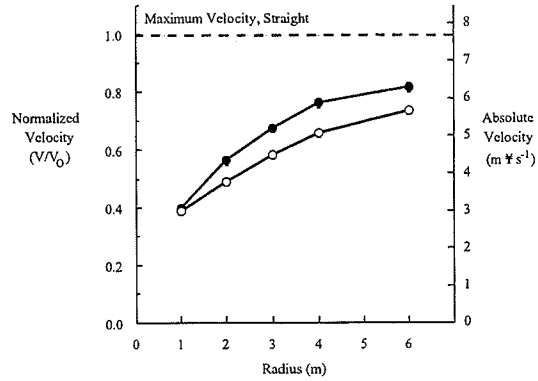

Figure 1. Maximum sprint velocity as a function of track radius for normal (unfilled circles) and tethered (filled circles) sprinting. Data are means – SE. Dashed line indicates average straight path maximum velocity – SE.

The outside leg produced significantly more force than the inside leg during normal curve sprinting (Fig. 2A). In contrast, outside and inside legs generated nearly the

same peak resultant GRFs during tethered curve sprinting (Fig. 2B).

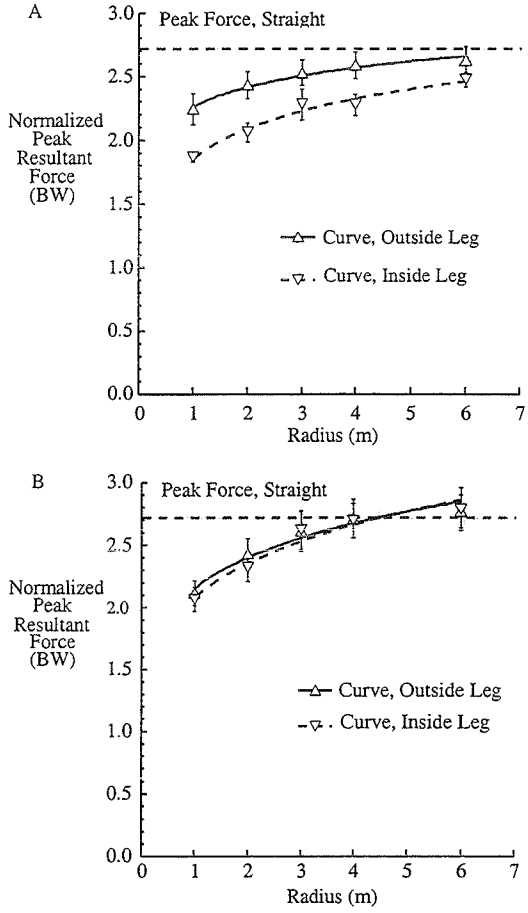

Figure 2. Normalized peak resultant GRFs for outside (triangles) and inside (inverted triangles) legs as a function of radius during (A) normal and (B) tethered curve sprinting. Data are means – SE. Dashed line indicates average straight path GRFs – SE.

Our direct measurements show that peak resultant GRFs decreased at smaller radii is strong evidence against Greene s primary assumption that the physiological limit of leg force is generated at all radii. We found that the tether provided approximately 50% of the needed centripetal force. According to Greene s hypothesis, supplying 50% of the centripetal force at a given radius is equivalent to normal curve sprinting at twice that radius, and velocities should thus also be equivalent. However, despite having the same peak resultant GRFs, velocities at the 2 and 3 m radii with the tether were significantly slower than velocities at 4 and 6 m radii without the tether, respectively.

An implicit assumption that Greene made was that the legs act symmetrically. In contrast, we found that the inside leg generates smaller peak resultant GRFs during curve sprinting. Weyand et al. (2000) recently correlated maximum straight path sprint velocity with GRFs. If this is the case, the inside leg appears be limiting the sprint speed on curved paths. This is consistent with data for cutting maneuvers (Ohtsuki et al., 1988).

Curve sprinting velocity is not determined by a general physiological leg extension force limit. Instead, we find that curve running performance is specifically limited by the ability of the inside leg to generate GRFs and thus change the direction of the momentum vector.

REFERENCES

Alexander, R. M. (1982). Locomotion of Animals. Blackie Press.

Greene, P. R. (1985). *Trans. ASME,* **107**, 96-103.

Harrison, A., Ryan, G. J. (2000). *12th Conf. Eur. Soc. Biomech,*. 358.

Jain, P. C. (1980). *Res. Quart. Exerc. Sport,* **51**, 432-436.

Ohtsuki, T., et al. (1988). *Biomechanics XI-B.* Free University Press.

Weyand, P. G., et al. (2000). *J. Appl. Physiol.* **89**, 1991-1999.

ACKNOWLEDGEMENTS

Supported by ASB Grant-in-Aid of Research (Y.-H.C.), McNair Scholarship (K.C.) and NIH AR44688 (R.K.).

SPECIFICITY OF STRENGTH TRAINING EXERCISES DURING CONCURRENT RESISTANCE AND SPRINT/JUMP TRAINING

Anthony J. Blazevich, Robert U. Newton and Roger Bronks

School of Exercise Science and Sport Management, Southern Cross University, Lismore, NSW, AUSTRALIA

Email: ablaze20@scu.edu.au Web:http://sessm.scu.edu.au/ablazevich

INTRODUCTION

Adaptations to resistance training (RT) are often shown to be specific to the movement patterns (Wilson et al., 1996) and velocities (Caiozzo et al., 1981) of the training exercises. However, in most studies RT has not been performed concurrently with other types of training (e.g. speed training). Moreover, in those studies where concurrent training has been performed, a comprehensive assessment of neuromuscular changes has not been presented. The purpose of this series of studies was ultimately to describe neuromuscular and performance adaptations to concurrent speed- and resistance training when RT exercises had either similar or dissimilar movement patterns to running and jumping tasks.

METHODS

The research consisted of two main studies and two reliability/validation studies. In the first study, 8 strength-trained men were filmed (200 Hz) while performing several variations of standing broad jump (BJ), countermovement vertical jump (VJ), 'traditional' squat (SQ), jump-squat (JSQ) and forward hack squat (FHS; Figure 1) tasks. Hip, knee and ankle joint angular displacements, velocities and accelerations were calculated after digitising joint markers from video using Peak Motus software (Peak Performance Technologies, USA).

In the second study, 15 men and 8 women were allocated to one of 3 training groups: 1) squat lift + sprint/jump (both twice a week), 2) FHS + sprint/jump (both twice a week) or 3) sprint/jump only (4 times a week). Before and after 5 weeks of training subjects' 20 m sprint, VJ, FHS (with load of 40 and 70% of predicted 1 RM) and SQ (with load of 30 and 60% of predicted 1 RM) performances were tested. Additional tests included isokinetic knee extensor torque (30 and $180^{\circ}.s^{-1}$), muscle thickness, pennation and fascicle length estimation of the vastus lateralis (VL) and rectus femoris (RF) muscles, and EMG quantification of 8 major lower limb muscles during the performance of sprint and VJ tasks.

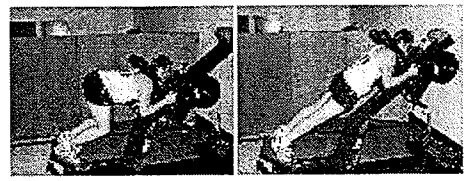

Figure 1: The forward hack squat (FHS) exercise.

In two further studies the reliability of the isometric SQ and FHS were examined (ICC > 0.97), as were correlations with their dynamic counterparts (1 RM: $r > 0.76$; $p<0.01$). They were deemed useful in predicting 1RM for the purposes of setting training loads. Reliability of the dynamic FHS at 70% ($ICC_{unilateral} = 0.90$; $ICC_{bilateral} = 0.95$) and 40% ($ICC_{unilateral} = 0.70$; $ICC_{bilateral}$ 0.64) of predicted 1 RM was also examined. Given the reliability of the FHS tests they could be used (with the SQ) in the second study (described above).

RESULTS AND DISCUSSION

The first study was designed to assess similarities and differences between several RT exercises and sporting tasks such as VJ and BJ. The kinematics of the VJ (with arms crossed over the chest) and JSQ (with a load of 60% bodyweight) were very similar. There was little similarity however between the 'traditional' SQ and VJ. The kinematics of the concentric phases of BJ and FHS were not similar, although the kinematics of the FHS appeared similar to those of the acceleration phase of the sprint run as reported by Jacobs & Ingen Schenau (1992). We concluded that the VJ & JSQ and sprint & FHS tasks had similar movement patterns.

The hypothesis of the second study was that subjects would improve most in tests (i.e. VJ or sprint) that had movement patterns similar to the RT exercises used in training (i.e. JSQ or FHS). Despite a collective improvement in many of the tests, there were no significant differences between the three training groups in their improvements in VJ, sprint, FHS or SQ tests. Given that subjects who performed JSQ and FHS training did not improve more in VJ and sprint tests respectively, we conclude that there was no significant movement pattern-specific training effect. There were also no differences between groups in torque produced at 30 & $180^{\circ}.s^{-1}$ in isokinetic knee extension suggesting that the addition of RT did not significantly affect velocity-specific strength. Thus specific adaptations did not occur as rapidly as in past studies where RT was performed by itself.

Despite these results, there was a trend toward JSQ subjects producing maximum knee extension torque at more closed knee angles than FHS subjects after the training. This might be explained by the differences in knee ROM during training. There was also some evidence that intermuscular coordination (EMG) differed between resistance and sprint/jump subjects after training, although only a small number of subjects were tested (N = 10). More significantly, subjects who performed JSQ or FHS training showed greater muscle pennation and shorter fascicle lengths in the VL while the opposite was true for subjects who only performed sprint/jump training. These changes are consistent with those presented in previous studies (i.e. higher force/lower velocity = larger pennation and shorter fascicles) and suggest that rapid muscle architecture adaptations specific to the speed of training can occur. While muscle thickness increased in RF, no significant pennation or fascicle length changes occurred. Given that length changes in RF are small the velocity of contraction might be important for architectural adaptations.

SUMMARY

There appeared to be no training-specific performance changes in subjects performing concurrent resistance and/or speed/jump training for 5 weeks. Significant muscle architecture changes, and small changes in EMG and angle-related knee extension torque suggest however that longer-term adaptations may be specific to the RT performed in concurrent training regimes.

REFERENCES

Caiozzo, J., Perrine, T., Edgerton, V.R. (1981). *J. Appl. Physiol.*, **51**, 750-754.
Jacobs, R.,Ingen Schenau, G.J van. (1992). *J. Biomech.*, **25(9)**, 953-965.
Wilson, G.J., Newton, R.U., Murphy, A.J., Humphries, B.J. (1993). *Med. Sci. Sports Ex.*, **25(11)**, 1279-1286.

ACKNOWLEDGEMENT

This research was partly supported by a grant from the ASB Grant-in-aid program (1998).

PREVALENCE OF JUMPING AND LANDING TECHNIQUES IN VOLLEYBALL: AN ANALYSIS OF ELITE FEMALE PLAYERS

Mark D. Tillman[1], Chris J. Hass[1], Denis Brunt[2], Janique Miller[1]

[1]Biomechanics Lab, University of Florida, Gainesville, Florida
[2]Department of Physical Therapy, University of Florida, Gainesville, Florida
Email: mtillman@hhp.ufl.edu Web: www.hhp.ufl.edu/ess/biomech

INTRODUCTION

Volleyball is a very popular sport with an estimated 800 million participants worldwide. The game involves many physical skills and successful performance is highly related with an individual's ability to propel themselves into the air during both offensive and defensive maneuvers. These ballistic activities often result in the creation of ground reaction forces on the order of five times body weight (Adrian & Laughlin, 1983). The deleterious effects of these forces may be compounded when one considers that a front row player may jump numerous times during a regulation match.

The jump landing sequence is the most common source of injury in volleyball (Briner & Kacmar, 1997). The majority (90%) of injuries occur in the lower extremity with the knee joint being particularly vulnerable. Injuries to the knee joint are especially important because they are associated with more lost time from sports participation than other injuries sites (Solgård, et al., 1995). Perhaps the most serious knee injury in volleyball involves rupture of the anterior cruciate ligament (ACL). The issue is further complicated because females are more likely to suffer an ACL injury than their male counterparts.

It has been hypothesized that the high number of jumps and the likelihood of losing balance due to deviations in jumping technique are the primary causes of injury during volleyball. However, little research exists regarding the prevalence of jumping and landing techniques in elite female volleyball. The purpose of this study was to quantify the number of jumps performed by elite female volleyball players in a competitive match and to determine the relative frequency of different jumping techniques.

PROCEDURES

A videotape recording of a match between two Division IA female volleyball teams was analyzed for this study. Both teams were considered elite (ranked in the top 10 nationally) at the time the match was played (fall of 2000). During the four game match, 593 jumps and landings were executed. Thirteen different front row players performed the jumping activities.

The videotape was played back at reduced speed in order to accurately observe several aspects of the jumping activity. Each activity was categorized by jump type (offensive spike or defensive block) and phase (jump or landing). Phase was further categorized by foot use patterns (right foot, left foot, or both feet). Each factor was scored in a categorical manner.

Four chi-square analyses were performed to determine whether jumping techniques occurred in disproportionate amounts relative to jump type, phase, and foot use patterns (α=0.05).

RESULTS AND DISCUSSION

All tests were statistically significant ($P<0.001$). The majority (86.5%) of offensive jumps were performed using both feet. Most (50%) offensive landings occurred with both feet, but 38.9% resulted in a left foot first landing, while 11.1% utilized a right foot first technique. Over 98% of defensive jumps used both feet. Defensive landings involving both feet were most prevalent (47.2%) followed by right foot landings (36.0%) and left foot landings (16.8%). The distribution of jumps and landings appears in Table 1.

The overwhelming majority of propulsive jumps (offensive and defensive) are performed using both feet. Jumping with both feet provides a wide base of support resulting in stable force production and allowing the forces to be generated by both limbs for maximal vertical performance. Although more landings are made with two feet than with one, the relative frequencies for landing are far more variable than for the jump phase. Approximately half of all landings in volleyball utilize only the right or left foot. Accordingly, the most frequent mechanism of knee injury in volleyball is landing from a jump (Ferretti, et al., 1992). The relatively high number of asymmetric footfalls during landing may lead to loss of balance and subsequent injury. Interestingly, 62.5% of right foot jumps result in right foot landings and 59.4% of left jumps end in left foot landings. Additionally, most jumps are made with two legs, but half of the associated landings are made with only one leg. Thus a single leg must dissipate the forces originally created by both legs. This situation could be quite detrimental.

SUMMARY

Volleyball is a high-risk sport relative to the knee joint and landing techniques appear to be quite variable. Further kinematic and kinetic analyses of these different landing techniques are required to fully quantify the biomechanical risks of performing these tasks.

ACKNOWLEDGEMENTS

The authors appreciate the assistance of Mary Wise and Laurie Doody.

REFERENCES

Adrian, M.J., Laughlin, C.K. (1983). *Biomechanics VIII-B*, 903-14.

Briner, W.W., Kacmar, L. (1997). *Sports Med*, **24(1)**, 65-71.

Ferretti, A., et al. (1992). *Am. J. Sports Med*, **20(2)**, 203-207.

Solgård, L. et al. (1995). *Br. J. Sports Med.* **29(3)**, 200-204.

Table 1: Distribution of jumps and landings.

Activity	Right foot	Left foot	Both feet	$\chi 2$
Offensive jump	8	32	256	377.97
Offensive landing	33	115	148	70.84
Defensive jump	2	2	293	570.2
Defensive landing	107	50	140	41.88

DYNAMIC CHANGES IN ANTERIOR/POSTERIOR TRANSLATION AND INTERNAL/EXTERNAL ROTATION OF THE KNEE DURING CYCLING

Ajit M. Chaudhari, Chris O. Dyrby, and Thomas P. Andriacchi

Stanford Biomotion Laboratory, Stanford University, Stanford, CA, USA
E-mail: chaudhari@stanford.edu Web: http://biomotion.stanford.edu

INTRODUCTION

Cycling is a very popular competitive sport, recreational activity, and rehabilitative therapy. For competitive athletes, the sport can be strenuous, and the intense training can lead to overuse injuries. For recreation and rehabilitation, on the other hand, the main benefits of cycling seem to be that it has minimal impact and can be well-controlled and gentle. However, overuse injuries at the knee have been reported during cycling (e.g. Ruby, 1992, Hannaford, 1986). In addition, cycling is used for rehabilitation following knee injury. Therefore, understanding the kinematics of the knee is particularly important since motions such as anterior/posterior (AP) translation and internal/external (IE) rotation can cause stress in soft tissue structures. While there are a number of important studies describing kinematic and kinetics during cycling (e.g. Ruby, 1992, Hannaford, 1986) due to technological limitations, very little work has been done to understand the relative motion of the femur and tibia. With the development of the point-cluster technique (PCT) (Andriacchi, 1998), it is now possible to collect highly accurate data which can shed light on the dynamic function of the soft-tissue structures of the knee during cycling. In particular, this study will focus on the dynamic envelope of knee motion.

Past studies have shown that dynamically, the knee operates in an envelope of motion between flexion and extension (Dyrby, 1999). For different activities, the same flexion angles produced an offset of secondary positions of the femur with respect to the tibia. These motions were dependent on the external forces and were shown to be different for dynamic activities such as walking and stair climbing as well as passive activities such as leg extension. Walking and stair climbing have complex loading patterns that include flexion/extension moments as well as IE rotational moments. This study used the PCT to determine secondary offsets during partial weight bearing seated cycling.

METHODOLOGY

An experienced cyclist with no history of musculoskeletal involvement was tested in the laboratory. Data was collected while pedaling on a professionally-fitted road cycle with clipless pedals (Look) using a stationary fixed-resistance trainer (Performance TravelTrac 2000). The subject's right leg was tested at multiple gear ratios and cadences. Motion was tracked using a four-camera optoelectronic digitizer (Qualisys). The PCT was used to obtain the six degree-of-freedom motion of the knee. The PCT uses 21 retro-reflective markers placed on the lower limb segments to create two cluster groups: one on the thigh and one on the shank. Motion is described in a fixed tibial reference system. Several five-second trials were collected.

A two-tailed T-test with unequal variances ($\alpha = 0.05$) was used to compare the AP

position of the femur with respect to the tibia during the push and pull phases at 78 degrees of knee flexion, the midpoint of knee motion for this subject.

RESULTS AND DISCUSSION

Ranges of motion were consistent throughout the trials. The results for one typical trial with a 42:15 gear ratio and a cadence of 62 rotations per minute are presented. Figure 1 shows the IE Rotation and AP Translation for 5 consecutive cycles. As shown in Figure 1, there is no hysteresis seen between the push and pull phases for IE rotation. There is, however, a significant offset shown for the AP translation ($p<0.001$). At 78° flexion the pull phase averaged 1.4 ± 0.06 cm., while the push phase averaged 0.9 ± 0.02 cm.

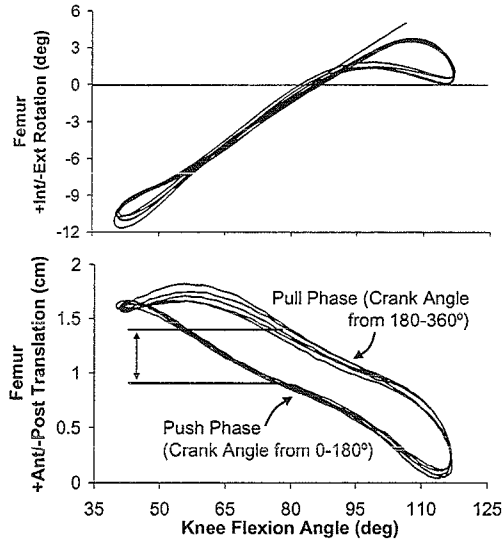

Figure 1. Motion of the femur relative to the tibia for 5 consecutive cycles. The significant offset in AP motion is noted by the arrows.

Using minimum knee flexion as a reference point, the knee internally rotated to a peak just after max knee flexion, then externally rotated as the knee continued to extend. Anterior translation was greatest at minimum knee flexion. The femur translated posteriorly with flexion, reaching greatest posterior translation when the knee was fully flexed.

CONCLUSION

This study demonstrated a dynamic offset in the AP motion of the knee between the push and pull phases of cycling. The femur is forward (tibia pulled back) during the pull phase (hamstrings contracting). During the push phase (quadriceps contracting) the tibia is forward relative to the pull phase. This is the first study to show a dynamic offset in the AP movement of the knee during cycling. This offset can influence soft tissue strains and should be considered for patients during rehabilitation.

This study presents new information to increase the understanding of knee kinematics during cycling. Using this method of analysis coupled with force data, researchers will be able to further determine the etiology of overuse injuries, develop more successful rehabilitation regimes, and improve coaching/training techniques.

REFERENCES

Andriacchi, T.P., Alexander, E.J., Toney, M.K. et al. (1998) *J. Biomech Eng*, **120**, 743-749.

Dyrby, C.O. and Andriacchi, T.P. (1999) Trans 45th ORS, **24**, 934.

Hannaford, D.R., Moran, G.T., Hlavac, H.F. (1986). *Clin Pod Med Surg*, **3**, 671-678.

Ruby, P., Hull, M.L., Hawkins, D. (1992). *J. Biomechanics*, **25**, 41-53.

PEAK GROUND REACTION FORCES AND BRAKING FORCES WHILE WALKING DOWNHILL WITH AND WITHOUT THE USE OF TREKKING POLES

Julianne Abendroth-Smith[1], Ed.D. and Michael Bohne[2]

[1]Willamette University, Salem OR;
[2]University of Northern Colorado, Greeley CO USA
Email: jabendro@willamette.edu

Introduction

As a recreational pursuit, hiking has become a popular pastime in America, as well as in many parts of the world, especially where mountains are a predominant part of the geographic area. In addition, many outdoor-based occupations require downhill walking as a component of the job. The purpose of this research project was to examine peak GRFs and peak braking forces (BF) of walking downhill at different gradients while hiking with or without trekking poles. Gradients included level ground, 15, 20 and 25 degrees, which are similar to common grades of mountain trails. Gender differences were also examined.

Manufacturers of trekking poles claim that using poles reduces forces on the body by as much as 21% (Sierra Trading Post Catalog, 1999). Schwameder et al. (1999) examined walking downhill, with and without the use of trekking poles, at a gradient of 25 degrees, and found a reduction in ground reaction forces with the use of the trekking poles. Knight and Caldwell (2000) examined the use of trekking poles while walking uphill at a five degree grade and concluded that pole use redistributed some of the load from backpacks, thus alleviating stress from the lower extremities. Willson et al (2001) examined the effects of walking poles on lower extremity gait mechanics for level walking only. Differences were noted for walking speed, vertical ground reaction forces, vertical knee joint reaction forces, and the knee support moment, depending on the poling condition used. Lastly, Abendroth-Smith and Bohne (in press) noted changes in gait patterns and ground reaction forces while hiking downhill (without pole use) as the angle of incline increased, with observed differences between men and women in their walking strategies on differing slopes. As women usually have a lower center of gravity and specific structural differences, hiking downhill may impact women differently.

Methods

Ten subjects were recruited on a volunteer basis, from a healthy, active adult population (5 men, 5 women). Participants were screened for any conflicting medical issues and signed informed consents. Procedures included a practice session which involved walking down a wooden ramp at all gradients to become familiar with each appropriate protocol, until participants felt natural in their gait patterns, and with pole use. The data collection consisted of 10 successful trials per condition. A predetermined counterbalanced order of conditions was used, due to the change-over time in adjusting the slope of the ramp. Force data was collected on a Bertec force plate at 500 Hz, mounted flush with the wooden ramp. Means and SD were calculated for the multiple trials of each condition. All force data was normalized to body mass (N/kg).

Results

Kinetic parameters of peak GRF and BF (N/kg) were examined for differences between gradient, gender and pole use. Significant differences between conditions were determined using a 3-way ANOVA. Statistically significant differences ($p<.05$) were noted for changes in GRFs between gradients, and for gender, but not for pole use (Figure 1). Peak GRFs were minimally less with pole use for level walking and at the 25 degree slope, which has been previously noted (Schwameder et al, 1999; Willson, et al, 2001). However, at the 15 and 20 degree slopes, pole use resulted in similar or higher GRFs than without pole use. Gender differences were similar in walking without poles to previous research (Abendroth & Bohne, in press) for women, but men demonstrated little or no decrease in peak GRFs at the higher slopes.

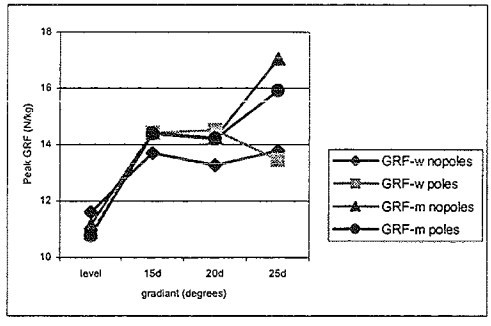

Figure 1. Peak GRF with and with pole use.

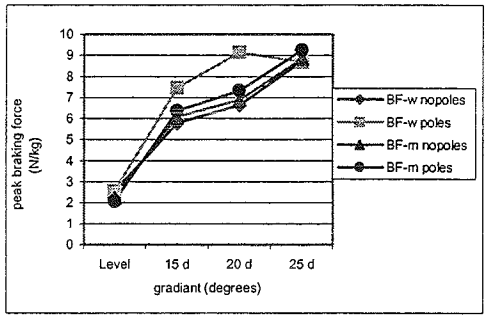

Figure 2. Peak BFs with and without pole use.

Statistically significant results for BFs were similar to GRF data, in that gradient and gender differences were noted overall, but with pole use, BFs were not statistically different (Figure 2). Again women demonstrated higher BFs with pole use than without at the middle gradients, while the men demonstrated similar BFs regardless of pole use.

Discussion and Conclusions

Pole use did not significantly reduce forces (GRF or BF) on the body at any of the measured gradients, even though previous research has documented differences. Of greater concern are the increased forces at the middle gradients, for women especially, with pole use. Though not statistically significant, these differences may indicate that either incorrect pole use can lead to greater forces acting on the body, or that pole use might hinder walking while hiking downhill at certain gradients. Differences were noted in normalized forces between men and women as well, indicating changes in walking strategies at the differing gradients. Recommendations include the examination of joint forces and moments with the use of poles at multiple gradients, and examination of medial/lateral forces to see if stability is enhanced with pole use. It is hoped these results might lead to useful information for both men and women in maintaining a healthy lifestyle, while providing gender specific recommendations for keeping individuals injury and pain free while hiking downhill.

References

Abendroth-Smith, et al. (in press).(Abstract) Med Sci Sp Ex.
Knight, et al. (2000) Med Sci Sp Ex. 32(12), 2093-2101.
Schwameder, et al, (1999) J Sport Sci 17, 969-978.
Willson et al. (2001) Med Sci Sp Ex 33(1). 142-147.
Sierra Trading Post Fall Catalog (1999).

A QUASI-STATIC METHOD FOR DETERMINING THE CHARACTERISTICS OF A MOTION CAPTURE CAMERA SYSTEM IN A "SPLIT-VOLUME" CONFIGURATION

Chris Miller [1], Ajitkumar Mulavara [1], and Jacob Bloomberg [2]

[1] Neurosciences Laboratory, Wyle Laboratories, Houston, TX, USA
[2] Neurosciences Laboratory, Johnson Space Center, Houston, TX, USA
E-mail: chris.miller1@jsc.nasa.gov

INTRODUCTION

To confidently report any data collected from a video-based motion capture system, its functional characteristics must be determined, namely accuracy, repeatability and resolution. Many researchers (Haggard and Wing, 1990; Klein and DeHaven, 1995; Thornton, et al., 1998; VanderLinden, et al., 1992) have examined these characteristics with motion capture systems, but they used only two cameras, positioned 90 degrees to each other. Everaert, et al. (1999) used 4 cameras, but all were aligned along major axes (two in x, one in y and z). Richards (1998) compared the characteristics of different commercially available systems set-up in practical configurations, but all cameras viewed a single calibration volume. The purpose of this study was to determine the accuracy, repeatability and resolution of a 6-camera Motion Analysis system in a split-volume configuration using a quasi-static methodology.

METHODS

Per our standard data collection protocol for treadmill walking, six Hi-Res Falcon cameras (Motion Analysis, Santa Rosa, CA) were setup in a split-volume configuration to enable whole-body kinematic measurements in a confined lab space. Three cameras were aimed to capture lower limb motion (i.e., waist-down); three cameras were aimed to capture upper body motion (i.e., waist-up). Each camera was positioned between 1.8 and 2.5 meters from the center of the calibration volume (size 0.75 x 0.50 x 1.77 meters), in a distribution that covered from "two o'clock" to "seven o'clock" in the xy-plane (with 12 o'clock being in the direction of progression).

A retroreflective marker (25 mm dia.) was fixed to a linearly translating table. The table was moved via a screw micrometer with a resolution of 0.001 inches (0.0254 mm). Retroreflective tape was wrapped around the end of the micrometer handle, such that the tape was hidden while the operator turned the handle. Data were collected on the marker's position as the table was moved from 0.000 to 1.000 inches (0 to 25.4mm) by increments of 0.001 inch. Each incremental (i.e., quasi-static) position was held for 2 seconds with the operator's hand away from the micrometer handle (i.e., not covering the handle tape).

The table was placed at each of five different heights, centered in the xy-plane of the calibration volume. The five heights corresponded to the following regions: head-level (upper); chest (mid-upper); waist (middle); mid-thigh (mid-lower), and shank (lower). Two data files for each region were collected on separate days.

The handle tape, when visible, was tracked as an indicator. A window of 31 frames was defined within each quasi-static position

(i.e., when the handle marker was visible), centered about its mid-frame point. Within each window, the mean and standard deviation (SD) of the displacements from the initial position were computed. Calculated displacements were subtracted from actual displacements (as measured by the micrometer position) to compute error.

To determine resolution, the mean displacements at each quasi-static position were analyzed with an ANOVA ($p < 0.01$) with a Tukey post-hoc test for significance. Differences between consecutive significantly different displacements were calculated, and the mean and SD of the differences were computed for each region. To determine the accuracy, the absolute values of the mean errors of the marker displacement for each position were calculated, and the mean and SD for each region were computed. Repeatability was determined by averaging the SDs for each position, and 99% confidence limits ($3*SD_{avg}$) were calculated for each region.

RESULTS AND DISCUSSION

The results are shown in Table 1. It should be noted that with the split-volume camera setup, the characteristic values were consistent across all regions. The actual resolution calculated was 0.06mm, but this was rounded up to 0.1mm for practical reporting. This resolution is approximately 0.40% of the marker size (25mm) and 0.02% of the shortest calibration volume dimension (502mm). Repeatability also was computed to 0.1mm, based on the 99% confidence limit definition. Regional means for accuracy ranged from 0.05mm to 0.16mm.

SUMMARY

The quasi-static method is an effective method for determining the characteristics of a motion capture system in a split-volume configuration. Values were consistent across all regions of the calibration volume. This method permits precise measurement over the entire body during treadmill locomotion within a confined lab space.

REFERENCES

Everaert, D.G., et al. (1999). *Arch Phys Med Rehabilitation,* **80**, 1082-9.

Haggard, P., Wing, A.M. (1990). *J. Motor Behavior,* **22**, 315-21.

Klein, P.J., DeHaven, J.J. (1995). *Arch Phys Med Rehabilitation*, **76**, 183-9.

Richards, J.G. (1998). *Proceedings of 5th International Symposium on the 3-D Analysis of Human Movement,* 1-9.

Thornton, M.J., et al. (1998). *Clinical Biomechanics*, **13**, 452-4.

Vander Linden, D.W., et al. (1992). *Physical Therapy*, **72**, 300-5.

Table 1: Resolution, accuracy (mean±SD) and repeatability (99% CL) statistics (in mm).

	Resolution		Accuracy		Repeatability	
Region	*Trial 1*	*Trial 2*	*Trial 1*	*Trial 2*	*Trial 1*	*Trial 2*
Upper	0.059 ± 0.020	0.062 ± 0.020	0.097 ± 0.078	0.103 ± 0.083	0.102	0.102
Mid-upper	0.055 ± 0.019	0.064 ± 0.014	0.054 ± 0.041	0.057 ± 0.035	0.087	0.125
Middle	0.055 ± 0.020	0.052 ± 0.018	0.093 ± 0.056	0.061 ± 0.069	0.082	0.086
Mid-lower	0.049 ± 0.013	0.058 ± 0.018	0.115 ± 0.075	0.163 ± 0.101	0.083	0.110
Lower	0.066 ± 0.026	0.069 ± 0.023	0.144 ± 0.076	0.101 ± 0.062	0.101	0.131

ACHILLES TENDON ADAPTATION DURING STRENGTH TRAINING IN YOUNG ADULTS

Alessandro Urlando & David Hawkins

Human Performance Laboratory University of California, Davis, CA, USA
E-mail: dahawkins@ucdavis.edu

INTRODUCTION

Skeletal muscle strength (Weiss, et al., 1988) and tendon properties (Józsa and Kannus, 1997) change in response to new physical demands. However, little is known about the interactions between muscle strength changes and tendon property changes in functional muscle-tendon units in-vivo. The purpose of this study was to investigate human muscle-tendon units in-vivo and to test the hypothesis that tendons adapt to muscle strength training to maintain strains within a preferred operating range.

METHODS

The Gastrocnemius/Soleus-Achilles tendon complexes of 11 male subjects, age 24.8 ± 3.2 years (mean ± SD), mass 78.5 ± 9.3 kg and height 177.7 ± 8.0 cm, were studied. Subjects performed an eight-week strength-training program consisting of three weekly sessions separated by at least one day of rest. The strength-training sessions consisted of three sets of ten heel-raising lifts involving 70% of the subject's maximum effort.

Subjects were tested before and at the end of the first, second, fourth, sixth and eighth week of the strength training program. Lower leg volume was measured by water immersion at the start of each testing session. Subjects kneeled on a custom bench and performed isometric plantar flexion efforts (Figure 1). Plantar flexion force was quantified using a load cell secured to the custom bench on one side and attached to a foot jig on the other. A Hitachi EUB 405 PLUS Ultrasound system, with a 64 mm-7.5 MHz linear probe was used to obtain images of the Achilles tendon, defined as the region between the calcaneus bone-Achilles tendon junction or notch and the Achilles tendon-soleus muscle junction (MTJ).

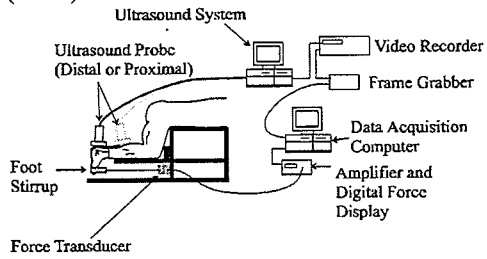

Figure 1. The basic setup used to quantify tendon length during isometric muscle efforts.

The ultrasound probe length limited the portion of Achilles tendon that could be imaged at one time to about 60 mm. A hollow one millimeter diameter plastic rod was secured to the subject's skin with tape and spray adhesive. Proximal and distal Achilles tendon images were obtained by placing the ultrasound probe between the calcaneus bone and the plastic rod (REF) and by placing the ultrasound probe between the plastic rod and the MTJ respectively (Figure 2). Subjects performed six isometric plantar flexion efforts ranging from rest to their maximum voluntary contraction. Each section of the Achilles tendon (i.e. proximal and distal) was imaged three times during the six isometric plantar flexion efforts.

Tendon length and strain were determined from the ultrasound images. Snappy™ 4.0 (by Play®) was used to capture and digitize ultrasound video images that corresponded to the specified effort levels. *Scion Image*, an image analysis program, was used to digitize these images and quantify Achilles tendon lengths and cross sectional areas. The lengths of the Achilles tendons during the various plantar flexion efforts were obtained by combining images of the proximal (D2) and distal (D1) sections (Figure 2). Strain was calculated from these lengths.

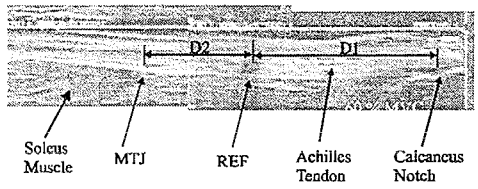

Figure 2. Longitudinal images of the Soleus muscle-Achilles tendon-Calcaneus bone created from proximal and distal ultrasound images.

RESULTS AND DISCUSSION

The group's average percent increase in maximum Achilles tendon force from baseline to the eighth week of training was statistically significant and equal to 22.4 %. The group's average percent increase in soleus volume from baseline to the eighth week of training was also statistically significant, equal to 7.7 %. Maximum Achilles tendon strain (ε_{max}) values ranged between 0.006 mm/mm and 0.135 mm/mm throughout the study. Six of the eleven subjects had an initial increase in ε_{max} followed by a return to baseline by week 8. The remaining five subjects had an initial decrease in ε_{max} followed by a return to baseline in two subjects. Average stress-strain curves were computed for the entire group (Figure 3). Stress-strain curves shifted to the left initially and then back to the right from week 6 to week 8. Alterations in the initial non-linear portion rather than alterations in tendon stiffness appear responsible for shifts in the stress-strain curves.

On average, tendons appeared to have preferred strain limits that were maintained as muscle strength increased supporting the study's hypothesis. The magnitude of these limits or "set-points" varied between individuals as did the initial tendon strain responses to strength training.

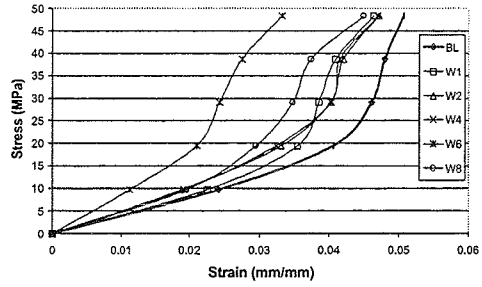

Figure 3. Average stress-strain curves showing the group's response to the strength-training program.

REFERECES

Józsa, L., P. Kannus (1997). Chp 5 in *Human Tendons. Anatomy, Physiology and Pathology*, Human Kinetics Publisher, Champaign, Il.

Weiss, L., F. Clark, D. Howard (1988). *Physical Therapy*. **68**(2): 208-213.

EFFECT OF SKIN MOVEMENT ON FIBEROPTIC TRANSDUCER MEASUREMENT OF TENDON FORCES

A. Erdemir[1,2], A. J. Hamel[1], S. J. Piazza[1,2,3] and N. A. Sharkey[1,2]

[1]The Center for Locomotion Studies and Departments of [2]Kinesiology and [3]Mechanical & Nuclear Engineering, The Pennsylvania State University, University Park, PA
Email: sjp12@psu.edu Web: www.celos.psu.edu

INTRODUCTION

Komi et al. (1996) described minimally invasive measurement of *in vivo* tendon forces using a fiberoptic transducer. This technique involves passing a fiberoptic cable transversely through the tendon and recording the intensity of light transmitted, which is modulated by the force in the tendon. A decrease in fiberoptic output signals an increase in tendon force, since compression of the fiberoptic cable results in decreased light power. The required instrumentation is inexpensive and easy to implement. However, an *in situ* calibration scheme is required to relate tendon force to transmitted light. Erdemir et al. quantified fiberoptic force measurement errors resulting from potential discrepancies between calibration and experiment conditions (load rate, cable movement), but the effect of skin movement relative to tendon on raw transducer output and on force predictions remains unclear. The aim of our study is to supply this information, which is necessary for reliable *in vivo* measurements.

METHODS

Three cadaver foot specimens were tested using the Dynamic Gait Simulator (DGS; Sharkey and Hamel, 1998). The DGS reproduces the movement of the foot and ground reaction forces during the stance phase by prescribing knee kinematics and applying muscle forces to the extrinsic tendons. A fiberoptic cable (dia. 0.5 mm, Toray Ind. Inc.) was passed through the Achilles tendon about 2 cm proximal to its calcaneal insertion (Finni et al., 2000) and attached to a transmitter-receiver unit (Agilent Tech. Inc.) as described by Komi et al. (1996). Fiberoptic transducer output and Achilles tendon force (ATF) were simultaneously collected for each walking trial. Each specimen was tested under two conditions: with the skin surrounding the insertion site intact and with skin dissected away (Figure 1). Four trials were completed for each condition.

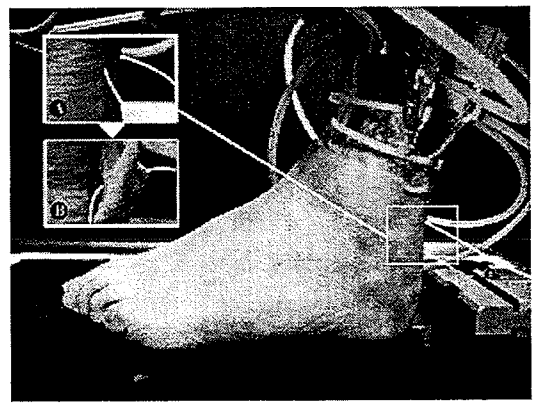

Figure 1. A foot specimen mounted in the DGS. The fiberoptic cable is highlighted for display purposes. Insertion site is magnified for (A) skin intact (B) after skin removal.

The influence of skin movement on tendon force predictions was assessed for one specimen by calculating calibration constants from calibration trials (0 N to 1000 N ramp loading-unloading of the Achilles tendon) and applying them to fiberoptic data of simulated walking. Four calibration trials were completed with the foot positioned at neutral and ~10° of dorsiflexion, before and after skin removal.

RESULTS AND DISCUSSION

Output ranges of the fiberoptic transducer were higher for all specimens when the skin was intact (Figure 2). This was likely due to relative movement between skin and tendon, which bent the cable and decreased the transmitted light intensity. Achilles tendon force estimations using the fiberoptic transducer showed that skin movement had a distorting rather than amplifying effect (Figure 3). Predictions using calibrations performed at different ankle angles were substantially different when the skin was intact. On the other hand, skin removal resulted in reasonably accurate and repeatable force estimates regardless of ankle joint angle during calibration.

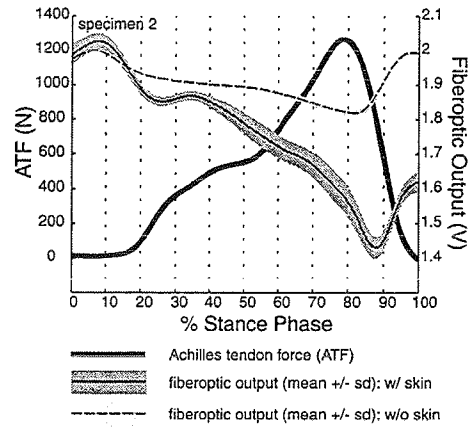

Figure 2. Fiberoptic output and Achilles tendon forces for a representative specimen. ATF was nearly identical within specimens.

Skin movement during *in vivo* tests may differ from that observed in cadaver specimens in this study. Nevertheless, the distorting effect of skin seems to be higher than the 2 % of peak forces reported by Finni et al. (2000). Ankle angle at which the calibration data was collected affected ATF predictions, indicating a coupling between skin movement and joint angle. It is therefore advisable to complete *in vivo* calibrations at different ankle angles and apply correction factors. The performance of the fiberoptic transducer on exposed tendon validates its utility as a tool for tendon force measurements when a direct force measurement is not feasible, and skin effects can be compensated for during calibration.

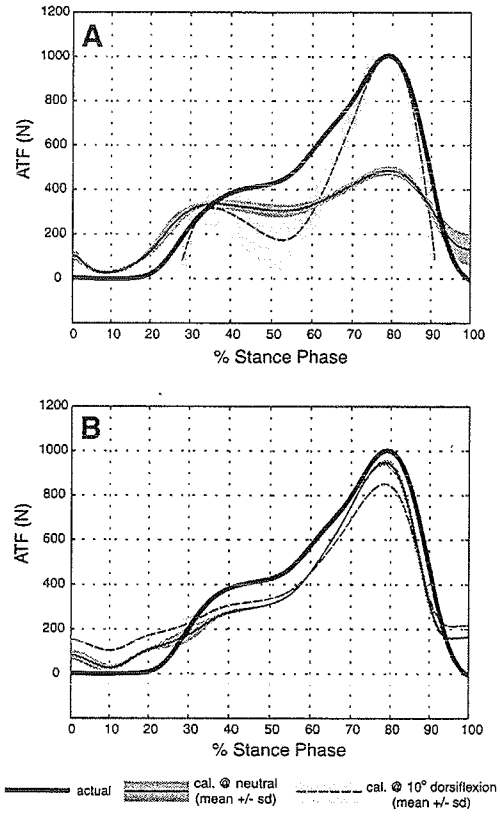

Figure 3. Achilles tendon force predictions for specimen 3: (A) w/ skin, and (B) w/o skin. Calculated forces are shown only for voltages within the calibration range.

REFERENCES

Erdemir A. et al., *J. Biomech.*, in review.

Finni, T. et al. (2000), *Eur. J. Appl. Physiol.*, **83**, 416-426.

Komi, P.V. et al. (1996), *Eur. J. Appl. Physiol.*, **72**, 278-280.

Sharkey, N.A., Hamel, A.J. (1998), *Clin. Biomech.*, **13**, 420-433.

ACKNOWLEDGEMENTS

ISB and Irma & Harold Zipser Fellowship.

EXAMINATION OF THE QUASI-STATIC ESTIMATION OF RESULTANT JOINT MOMENTS

John H. Challis

Biomechanics Laboratory, Department of Kinesiology, The Pennsylvania State University, University Park, Pennsylvania
Email: jhc10@psu.edu

INTRODUCTION

Resultant joint moments are frequently computed for the analysis of human movement. A complete inverse dynamics analysis of a movement requires the computation of segment center of mass accelerations and segment angular accelerations (dynamic approach). Computation of derivatives from inherently noisy displacement data is an ill-posed problem (Lanshammar, 1982), meaning the moments can be strongly influenced by errors in derivatives values. During the ground contact phase of a movement the moments at the joints can be estimated by ignoring the inertial contributions, and the weights of the segments. The moment is computed by taking the product of the magnitude of the ground reaction force vector and the perpendicular distance between the joints position and the ground reaction force vector originating from the center of pressure. This approach will be referred to as the static approach, it has been used for the analysis of human movement (e.g. Arborelius et al., 1992; Schultz et al., 1992).

Wells (1981) compared the dynamic with the static approach for computing moments during walking. The deficiency in this evaluation was that there were no criteria with which to compare the computed moments, they were only compared with one another. It was the purpose of this study to compare the accuracy of the static approach with the dynamic approach using criterion data generated from a simulation model.

METHOD

A simulation model of vertical jumping was developed. The model was planar and consisted of four segments linked by frictionless pin joints. The segments were the foot, shank, thigh, and the HAT (head, arms, and trunk). The inertial properties of these segments were determined for a male subject 1.85m in stature with a body mass of 85kg. The equations of motion of the four-link system were integrated forward in time to determine the motion of the segments given the moments acting at the joints. The integration step was 0.0001 seconds. The moments at the joints were provided by actuators crossing the joints, with muscle like properties. The sequence of the actuator activations was selected to provide a maximum vertical jump.

White noise was added to the model determined displacement data. To mirror typical experimental protocols the noisy data was low-pass filtered using either a Butterworth filter or a spline. For both filters the amount of filtering was automatically selected using either an autocorrelation based procedure (Challis, 1999), or dynamic programming (Dohrmann

and Busby, 1990). The filtered and differentiated data were used to compute the resultant joint moments. The percentage root mean squared difference (%RMSD) between the moments computed using either approach (dynamic and static) and the model produced moments were computed.

RESULTS

The kinematics and kinetics of the simulated jump were similar to those measured for experimental subjects (e.g. Challis, 1998). Quantitatively the results were similar whether the data had been filtered using the Butterworth filter or the spline so tables 1, 2 and 3 present only the results for the spline.

Table 1 - The %RMSD between the criterion moments and those computed using the dynamic approach.

Noise Level	*Ankle %RMSD*	*Knee %RMSD*	*Hip %RMSD*
σ=1.0mm	1.1	13.7	119.0
σ=2.5mm	1.7	15.8	118.6
σ=5.0mm	2.1	18.8	130.8

Table 2 - The %RMSD between the criterion moments and those computed using the static approach.

Noise Level	*Ankle %RMSD*	*Knee %RMSD*	*Hip %RMSD*
σ=1.0mm	4.2	6.0	20.4
σ=2.5mm	4.3	5.9	20.4
σ=5.0mm	4.3	5.9	20.5

Table 3 - The %RMSD between the moments computed using the dynamic and static approaches.

Noise Level	*Ankle %RMSD*	*Knee %RMSD*	*Hip %RMSD*
σ=1.0mm	4.1	14.7	61.4
σ=2.5mm	4.2	16.5	59.8
σ=5.0mm	4.1	14.7	61.4

DISCUSSION

For the ankle joint the dynamic approach was more accurate than the static approach, but for the other joints the static approach was more accurate. In effect ignoring the influence of the acceleration of the limbs on the joint moments was preferable to estimating them from noisy derivative data. Comparing static and dynamic moments is not a viable way of assessing the accuracy of the static approach (table 3).

A high-speed movement was selected to test the assumptions underlying the static approach, but it also served to highlight the problems in accurately estimating second derivatives for the dynamic approach. These results highlight the problems of accurately estimating resultant joint moments, and demonstrate that the static approach has some benefits. It should be anticipated that these results are most likely activity specific.

REFERENCES

Arborelius, U.P. et al. (1992). *Ergonomics.*, **35**, 1377-1391.

Challis, J.H. (1998). *Human Mov. Sci.*, **17**, 307-325.

Challis, J.H. (1999). *J.Appl.Biom.*, **15**, 303-317.

Dohrmann, C.R., Busby, H.R. (1990). In: *Biomechanics of Human Movement*, Bertc.

Lanshammar, H. (1982). *J. Biom.*, **15**, 459-470.

Schultz, A.B. et al. (1992). *J.Biom.*, **25**, 1383-1391.

Wells, R.P. (1981). *Bull. Pros. Res.*, **18**, 15-19.

ACKNOWLEDGEMENTS

This research was in part support by a grant from The Whitaker Foundation.

Reliability of Digitizing Anatomical Points from Knee MR Images for Establishing Reference Frames

[1]Bergron, K., [1]Houck, J., [1]Huson, M., [1]Keisling, B., [1]Mazer, L., [2]Boyd, K.

1. Ithaca College – Rochester Campus, 300 E. River Road, Rochester, NY
2. University of Rochester-River Campus, 215 Hopeman Rochester, NY

INTRODUCTION

Recent studies suggest the determination of anatomic axi of the femur and tibia from palpated surface landmarks are prone to errors (≈ 13 °) (Piazza, 2000). The result of incorrectly locating the flex/ext axis is cross talk or the expression of sagittal plane movement in the frontal and transverse planes. Recent advances in tracking skeletal motion in vivo propose merging anatomic points defined with magnetic resonance (MR) images and data obtained in a movement analysis laboratory(Andriacchi, 2000). Although improved consistency and accuracy are expected few studies have evaluated the consistency in determining points from MR images. The purpose of this study was to evaluate the reliability of determining points (x, y, z) from MR images used to establish anatomic reference frames and the effect of these inconsistencies on establishing tibiofemoral orientation.

METHODS

Four subjects were recruited for this study. The left knees of two subjects and both knees of two subjects were imaged, generating 6 sets of knee images. Each knee was imaged using a gradient recalled echo (GRE) sagittal, 3 minute sequence. The slice thickness was 1.5 to 1.7 mm. The in plane resolutions were either 0.5 x 0.5 mm or 0.7 x 0.7 mm. Sagittal and axial images were analyzed using NIH image software.

Figure 1. Anatomic Points

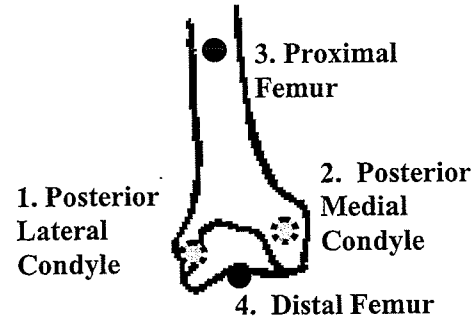

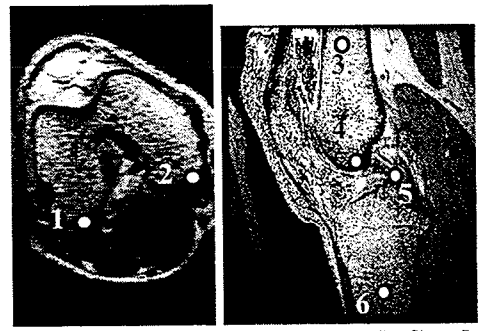

1. Post. Lat. Cond 2.Post. Med. Cond., 3. Prox. Fem., 4. Dist. Fem., 5. Med Tib Spine, 6. Dist. Tib.

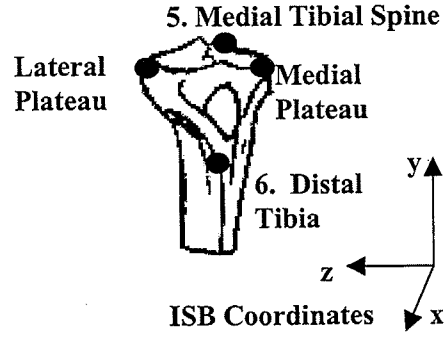

Using operational definitions for each point (Figure 1) 2 testers recorded the (x, y, z using the ISB standard) location 8 points two times, blinded to which image they were digitizing. For a right femur the M/L axis was the vector from the Post. Med. Cond. to the Post. Lat. Cond. The A/P axis was the cross between the vector from the dist. Fem. to the Prox. Fem. point and the M/L axis. The vertical axis was the cross between the M/L axis and A/P axis (Sheehan, 1998). The origin was the Dist. Fem. point. An analogous reference frame was established for the tibia.

RESULTS AND DISUCSSION

Pearson correlations for intra and inter rater reliability were above 0.9 except for the medial tibial spine. The root mean square (rms) differences between test 1 and test 2 were < 3 mm (≈ 4 pixels or 2 slices) (Table 1).

Table 1. RMS difference of the x, y, z coordinates between Test 1 and Test 2.

Anatomic Point	**Intra-rater Reliability Tester 1**	**Tester 2**
Tibia Points	**x,y,z(±mm)**	**x,y,z(±mm)**
Tibial Spine	0.9, 1.3, 0.7	2.6, 0.5, 0.9*
Dist Tibia	2.1, 1.3, **5.0**	0.7, 1.3, 0.9
Med Tibial Plateau	**3.7**, 0.2, **5.4**	1.4, 0.7, 0.7
Lat Tibial Plateau	2.0, 0.4, 0.3	1.4, 0.3, 1.5
Femur Points		
Dist Fem	1.1, 0.4, 1.5	0.5, 1.5, 3.0
Prox Fem	0.4, 1.4, 1.5	0.5, 1.2, 3.0
Med Cond	0.5, 0.2, 1.1	0.3, 0.3, 1.1
Lat Cond	0.7, 0.2, **5.3**	0.5, 0.3, 0.5

***One subject with a difference of 1 cm in the y and z coordinate is excluded.**

However, there were some exceptions. Tester 2 was inconsistent in identifying the medial tibial spine in one subject, in contrast to tester one, suggesting additional training is necessary to accurately identify this point. The errors correlated with identifying the lateral rather than the medial tibial spine.

The RMS differences led to between tester and within tester changes in axi alignment of < 3 °. However, a 10 mm difference in locating the A/P coordinate of the Med. Tib. Plat. in one subject resulted in a 7° transverse plane rotation of the tibia M/L axis. In contrast a 9 mm difference in locating the M/L coordinate of the Post. Lat. Fem. Cond. resulted in little change in the M/L axis (< 1°). The definition of the reference frames explains this result.

SUMMARY

The consistency of locating the axi of the tibia and femur appears with in a few (< 3°) degrees for most subjects (5 of 6). It's plausible that training and refinement of operational definitions may reduce peak differences (< 7 °), thereby improving the consistency of identifying anatomic points for establishing reference frames.

REFERENCES

Andriacchi, T. P., Alexander, E. J., (2000). *J Biomech*, **33**,1217-1224.

Sheehan, F. T., et al. (1998). *J Biomech*, **31**, 21-26.

Piazza, S. J., Cavanagh, P. R., (2000). *J Biomech*, **33**, 1029-1034.

ACKNOWLEDGEMENTS

The authors thank Dr. Lerner and Dr. Totterman.